DEVELOPMENT OF AN EFFICIENT FUTURE ENERGY STORAGE SYSTEM INCORPORATING FLUIDIZED BED OF MICRO-PARTICLES

By

Ibitoye Adebowale Adelusi

Student ID: 31435902

Supervisors

Dr Dawson and Dr Andrieux

Dissertation for the degree of Doctor of Philosophy

Lancaster University Engineering Department

06/06/2019

Declaration

This research work: numerical modeling and simulation and laboratory experiments and write-up of this thesis **DEVELOPMENT OF AN EFFICIENT FUTURE ENERGY STORAGE SYSTEM INCORPORATING FLUIDIZED BED OF MICRO-PARTICLES** was carried out by me.

I also confirm that the Lancaster university laboratory equipment's and numerical software's such as solidwork, ANSYS and COMSOL have been used to acquire all the results. In terms of the referencing, I have used Lancaster University library one search tools to access all the resources such as scientific journals that were related to the research work of this thesis.

Furthermore, I can confirm that: before or after submitting this dissertation, the following papers that are listed below will be published.

1. Practical Development of a ZnBr2 Flow Battery with a Fluidized Bed Anode Zinc-Electrode Journal of The Electrochemical Society, Volume 167, Number 5 Focus Issue, 2019 – **Published**.
2. Hybrid Zinc Based Redox Flow Batteries as a renewable energy source: an overview – **Pending**.
3. Simulation of Added Carbon Particles Within Fluidized Bed Anode Zinc-Electrode – **Pending**

Additionally, my supervisors, Dr Andrieux and Dr Dawson have checked every written word of this dissertation, supervised me during the research work and corrected and checked all my experimental work acquired results (numerical modelling and laboratory) and recommended to me most of the conferences and training that I had attended during this research work and close to completion. The zinc-bromine battery cell was fabricated by the engineering department of Lancaster University.

Acknowledgement

First and foremost, my appreciation goes to God almighty who has given me the gift of life to complete this research work in good health. Furthermore, many thanks to my project supervisors; Dr Andrieux and Dr Dawson for their guidelines and support during this PhD research work. I would also say to my wife, Elizabeth Adelusi and children a great thank you for their support and encouragement during this research work. Furthermore, I also thank Peter Jones, Andrew Gavriluk for their support whenever I need their help in terms of laboratory facilities and IT provisions. I pray that may the God almighty continue to bless you all amen.

Dr Andrieux and Dr Dawson had given me a great training on electrochemical techniques that had made it possible for this research work to be completed. These trainings that I have acquired from them had improved my engineering judgements, technical skills and managerial skills in terms of progress report writing and presentation skills and moving straight to the point etc. Once again, I am very grateful for their devoted time and all their effort.

Furthermore, I pray that Lancaster University will continue to progress on their research because this is a great University that has also given me the opportunity to complete this research work in terms of all their research facilities such as using the university chemical laboratories workshops especially on B-Floor etc.

Table of Contents

Declaration **2**

Acknowledgement **3**

Symbols and Nomenclature **12**

List of Abbreviations **13**

List of Figures **15**

List of Tables **21**

List of Equations **25**

Abstract **27**

1 Chapter 1 Introduction to Energy Storage **29**

1.1 Energy Storage Needs and Categories 29

1.2 Energy Storage Systems and Comparison 31

1.2.1 Compressed Air Energy Storage System (CAES) 32

1.2.2 Pumped Hydroeletric Storage (PHS) 33

1.2.3 Capacitor Storage (CS) 34

1.2.4 Thermal Energy Storage System (TES) 35

1.2.5 Flywheel Energy Storage (FES) 36

1.3 Electrochemical Energy Storage Technologies 36

1.3.1 Supercapacitor Energy Storage (SCES) 38

1.3.2 Reversible Fuel cell 39

1.4 Introduction to Redox Flow Batteries 41

1.4.1 History of Redox Flow Batteries 42

1.4.2 Classifications of Redox Flow Batteries 43

1.4.3 All Liquid Aqueous Flow Batteries 44

1.4.4 Iron-Chromium RFB 48

1.4.5 Polysulfide-Bromine RFB 49

1.4.6 Soluble Metal-Bromine RFB 51

1.4.7 Quinone/ hydroquinone RFB with Aqueous Electrolyte 51

1.4.8 Organic Regenerative Fuel Cells 53

1.4.9 All-Uranium/ All Neptunium 54

1.4.10 Nickle-Iron RFB 55

1.4.11 Cobalt-Iron RFB 56

1.4.12 All-Copper 56

1.4.13 Organic RFB 56

1.4.14 Other Inorganic Flow Batteries 57

1.4.15 Semisolid Flow Batteries 58

1.4.16 Hybrid RFB 58
1.5 Types of Zinc-Based Hybrid Flow Batteries 64
1.5.1 Zinc-Lead and Zinc-Nickel RFB 64
1.5.2 Zinc-chlorine RFB 64
1.5.3 Zinc-Iodide RFB 65
1.5.4 Zinc-Cerium RFB 65
1.5.5 Other Zinc-Based RFB 67
1.6 Zinc-Bromine RFB 67
1.7 Zinc Bromine Batteries Cells Advantages and Disadvantages 69
1.8 Zinc Bromine Batteries Cells Application and Systems Design 70
1.9 Components of Zinc Bromine Batteries Cells Systems 72
1.9.1 Ion-Exchange Membrane 73
1.9.2 Anode Zinc-Side FBR's Reactors 74
1.9.3 Cathode Bromine-Side Reactor 76
1.10 Safety and Hazard 77
1.10.1 Bromine Treatment 77
1.11 Zinc Electrodeposition Electrochemistry 79
1.12 Effect of Zinc Electrodeposits Morphologies on Hybrid Flow Batteries 82
1.13 Electrolyte additives to improve morphologies 84
1.14 Side Effects of Dendrites and Prevention 85
1.14.1 Different Phases 87
1.15 Fluidized Bed Zinc-Electrodes and Benefits 87
1.15.1 Metal Deposition 87
1.15.2 High Loading 88
1.16 Methods to Improve ZnBr2 Performance 89
1.16.1 Introduction to Fluidization Beds and Flows 89
1.17 Foundations of Fluid Mechanics with Applications 90
1.17.1 Liquid-Solid FBR's and Hydrodynamic Behaviour 90
1.17.2 Laminar (Streamline) and Turbulent Flow 91
1.17.3 Uniform Flow and Non-Uniform Flow 91
1.17.4 Steady Flow and Unsteady Flow 92
1.18 Real and Ideal Flow 92
1.18.1 Non-Compressible Flow 93
1.19 Fluidization 93
1.20 Non-Uniform Fluidization 94
1.21 Minimum Fluidization Velocity 94
1.21.1 Introduction 94
1.21.2 Calculating Fluidization Minimum Velocity 96
1.21.3 Gravitational Forces 98
1.21.4 Hydrodynamic Drag Forces 99

2 Chapter 2 Purpose of the Research 104
2.1.1 High Surface Area Electrodes 104
2.1.2 Electrodes Concepts 105
2.1.3 Incorporating Glass Beads and Carbon 109
2.1.4 Proposed Feeder Electrode Materials 110

3 Chapter 3 Hydrodynamic Evaluation, Umf and Ansys Fluent 112
3.1 Introduction 112
3.1.1 Calculating Fluidization Minimum Velocity 113
3.2 Fluidized Bed Lab Experiment 113
3.2.1 Introduction and Objectives 113
3.3 Experimental Procedures 114
3.3.1 Apparatus 116
3.4 Description OF Results – Investigated Glass Beads and Carbon Particles 116
3.5 ANSYS-Fluent 118
3.5.1 Introduction 118
3.5.2 Numerical Purpose and Design 118
3.5.3 The Designed Battery Cell Test Rig 120
3.6 Problem Description in Ansys Fluent 123
3.7 Preparation and Modelling of the Problem 123
3.7.1 Boundary and Initial Conditions 123
3.7.2 Mesh Preparation and Fluent Launcher 126
3.7.3 Eulerian and Lagrangian Approach 126
3.8 Results and Validation 127
3.8.1 Carbon and Glass Beads 127
3.9 Conclusions 129
3.9.1 Computational Experiment 129
3.9.2 Hydrodynamic Experiment 130

4 Chapter 4 Numerical Modelling in COMSOL 133
4.1 Particle Trajectories and Flow Cell Electrochemistry 133
4.2 Streamline of Flows 134
4.3 Pressure Contour and Velocity Magnitude 136
4.4 Description of the Battery Cell System 140
4.5 Description and Analysis of Results – Electrolyte Potential Vs Current (A) and Voltage (V). 143
4.6 Results and Conclusions on the Electrolyte Potential (EP) and Current (A) Vs Voltage (V) 145
4.7 Description of Results 145
4.7.1 Anode Zinc Concentration 145

4.8 Description of Analysis 147
4.8.1 Anode Zinc Concentration 147
4.9 Result Discussions and Conclusions 147
4.9.1 Anode Zinc Concentration 147
4.10 Description of Results 147
4.10.1 Cathode Bromide Concentration 147
4.10.2 Cathode Bromine Concentration 149
4.11 Description of Analysis 150
4.11.1 Cathode Bromide and Bromine Concentration 150
4.12 Result Discussions and Conclusions 150
4.12.1 Cathode Bromide Concentration 150
4.12.2 Cathode Bromine Concentration 151
4.13 Numerical Modelling & Results Conclusion 151
5 CHAPTER 5 Materials and Methods. 153
5.1 SEM Preparation and Method 153
5.2 Results Discussions and Conclusions 154
5.2.1 Examined Particles 154
5.3 Results Discussions and Conclusions 157
5.3.1 Identified Elements 157
Table 5. 1 Mapped Elements after Drying the Particles after Discharged 158
5.4 SEM Conclusions 160
5.5 UV-Vis Protocol and Details 161
5.6 Rig Design Bill of Materials and Components 162
5.7 Electrodes Substrates and Fittings 162
5.7.1 Carbon Feeder Electrodes Material 163
5.7.2 Nickel Feeder Electrode Material 163
5.7.3 Titanium Feeder Electrodes Materials 164
5.8 Measuring Techniques 167
5.8.1 Cyclic Voltammetry 168
5.8.2 Chronopotentiometry (Charge and Discharged) 168
5.8.3 Electrochemical Impedance Spectroscopy (EIS) 169
6 Chapter 6 Measuring Techniques. 171
6.1 Introduction and Experimental Condition 171
Charged rate and discharged rate (0.1 amps vs -0.01 amps) @ both 3600 secs 171
Three cycles of charged rate and discharged rate at (0.1 amps vs -0.1 amps) @ 3600 secs and 1800 secs 171
Three-cycles of charged rate and discharged rate at (0.4 amps and -0.4 amps) for 3600 secs and 1800 secs 172

The re-examined nickel and carbon materials at (a) charged rate of 0.1 amps for 3600 secs and (b) discharged rate of -0.1 amps for 1800 secs 172
3 cyclic voltammetry of 1 sweep @ 25 mV/sec 172
6.1.1 Examined Carbon Electrodes Materials 173
6.1.2 Materials and Methods – Carbon Feeder Electrodes 174
6.1.3 Instrumentations Methods and Operation - Carbon Feeder Electrodes 175
6.1.4 Error Bar Graphical Representations 177
6.1.5 Descriptions of Results 177
6.1.6 Description of Analysis - Carbon Feeder Electrodes 180
6.1.7 Observation and Comments - Carbon Feeder Electrodes 182
6.1.8 Conclusions - Carbon Feeder Electrodes 183

6.2 Recognition of Cu and Cell Reversion - Carbon Feeder Electrodes 183
6.2.1 Description of Results – Charged Passed Via Carbon Feeder Electrodes 184
6.2.2 Description of Analysis - Carbon Feeder Electrodes 186
6.2.3 Findings and Comments - Carbon Feeder Electrodes 187
6.2.4 Results Conclusions - Carbon Feeder Electrodes 191

6.3 Five Cycles of Chronopotentiometry - Carbon Feeder Electrodes 191
6.3.1 Description of Results - Carbon Feeder Electrodes 191
6.3.2 Findings and Comments - Carbon Feeder Electrodes 195
6.3.3 Overall Final Conclusions - Carbon Feeder Electrodes 196

6.4 Effects of Cleaning and Polishing Electrodes - Carbon Feeder Electrodes 196
6.4.1 Results Description - Carbon Feeder Electrodes 197
6.4.2 Analysis and Description - Carbon Feeder Electrodes 198
6.4.3 Findings and Conclusions - Carbon Feeder Electrodes 200
6.4.4 Conclusions Made on Investigated Carbon Electrodes 200

6.5 Materials and Method – Nickel vs Carbon and Nickel vs Titanium 204

6.6 Instrumentations Methods and Operation - Nickel vs Carbon and Nickel vs Titanium 204
Charged and discharged rate (0.1 amps vs -0.01 amps) @ both 3600 secs 206
Three -cycles of charged and discharged at (0.1 amps Vs -0.1 amps) @ 3600 secs and 1800 Secs 206
Three-cycles of charged and discharged at a rate of (0.4 amps and -0.4 amps) for 3600 secs and 1800 secs. 206
Re-examined nickel and carbon materials at (a) charged rate 0.1 amps for 3600 secs and (b) discharged rate -0.1 amps for 1800 secs 206

6.7 Description of Results – Nickel vs Carbon and Nickel vs Titanium 206

6.8 Analysis of Results – Nickel vs Carbon 208

6.9 Findings and Comments on Feeder Electrodes 210
6.9.1 Carbon Vs Nickel (0.1 Amps, -0.01 Amps for 3600 secs) 210
6.9.2 Titanium Vs Nickel (0.1 Amps for 3600 secs) 211

6.10 Conclusions 212
6.10.1 Carbon Vs Nickel (0.1 Amps, -0.01 Amps for 3600 secs) 212
6.10.2 Titanium Vs Nickel (0.1 Amps for 3600 secs) 213

6.11 Effects of Different Electrodes 213

6.11.1 Description of Results – Carbon vs Nickel Feeder Electrode and Titanium Vs Nickel Feeder Electrode 213

6.12 Description of Analysis for Carbon vs Nickel Feeder Electrode and Titanium vs Nickel Feeder Electrode 215

6.13 Findings and Comments 217
6.13.1 Carbon Vs Nickel at 0.1 Amps and -0.1 Amps: (Cycle-1) (3900 secs and 2000 secs), (Cycle-2). (3000 secs and 1600 secs), (Cycle-3). (2400 secs for only to charge) 217
6.13.2 Nickel Vs Titanium at 0.1 Amps and -0.1 Amps: (Cycle-1) (1800 secs and 900 secs), (Cycle-2). (1810 secs and 900 secs), (Cycle-3). (1705 secs and 900 secs) 218

6.14 Conclusions – Carbon vs Nickel and Nickel vs Titanium 219
6.14.1 Material Performance (Carbon Vs Nickel) 219
6.14.2 Material Performance (Nickel Vs Titanium) 220

6.15 Enhancement of Cycle Performances and Conditions. 221

6.16 Description of Results 222
6.16.1 Carbon Vs Nickel at a Current of 0.1 Amps and -0.1 Amps: (Cycle-1) for (4000 secs and 1900 secs), and (2), for (3100 secs and 2000 secs), and (3) for (3000 secs and 1900 secs). 222
6.16.2 Nickel Vs Titanium at a Current of 0.3 Amps and -0.3 Amps: (Cycle-1) for (1800 secs and 200 secs), and (2), for (1700 secs and 200 secs), and (3) for (1900 secs and 200 secs) 223

6.17 Description of Analysis 225

6.18 Findings and Comments 227
6.18.1 Carbon Vs Nickel at 0.1 Amps and -0.1 Amps: (Cycle-1) for (4000 secs and 1900 secs), and (2), for (3100 secs and 2000 secs), and (3) for (3000 secs and 1900 secs) 227
6.18.2 Nickel vs Titanium at 0.3 Amps and -0.3 Amps: (Cycle-1) for (1800 secs and 200 secs), and (2), for (1700 secs and 200 secs), and (3) for (1900 secs and 200 secs) 227

6.19 Conclusions on Results 227
6.19.1 Carbon vs Nickel at 0.1 Amps and -0.1 Amps: (Cycle-1) for (4000 secs and 1900 secs), and (2), for (3100 secs and 2000 secs), and (3) for (3000 secs and 1900 secs) 228
6.19.2 Nickel vs Titanium at 0.3 Amps and -0.3 Amps: (Cycle-1) for (1800 secs and 200 secs), and (2), for (1700 secs and 200 secs), and (3) for (1900 secs and 200 secs) 228

6.20 Encountered Problems (Non-Conductive Materials and Causes) 229
6.20.1 Description of Result 229

6.21 Description of Analysis 231
6.21.1 Carbon Vs Nickel Feeder Electrode and Titanium 231

6.22 Observations and Comments 234
6.22.1 Carbon Vs Nickel at 0.4 Amps and -0.4 Amps with these charge and discharge time steps: cycle-1, (3900 secs and 1100 secs), and (cycle-2), for (3700 secs and 1300 secs), and (cycle-3) for (3700 secs and 1200 secs). 234
6.22.2 Carbon Vs Nickel at 0.1 Amps and -0.1 Amps with these charge and discharge time steps: cycle-1 as (3600 secs, 500 secs), and cycle-2 for (1200 secs) before Interrupting the Battery Cell to Charge Further 236

6.22.3 Nickel Vs Titanium at 0.1 Amps and -0.1 Amps with these charge and discharge time steps: cycle-1 @ (1800 secs and 200 secs), cycle-2 @ (1900 secs and 100 secs) and cycle-3 @ (2000 secs and 300 secs) 236

6.23 Conclusions on Results 238

6.23.1 Carbon Vs Nickel at 0.4 Amps and -0.4 Amps at these charge and discharge time steps: cycle-1, (3900 secs and 1100 secs), and (cycle-2), for (3700 secs and 1300 secs), and (cycle-3) for (3700 secs and 1200 secs) 238

6.23.2 Carbon Vs Nickel at 0.1 Amps and -0.1 Amps at these charge and discharge time steps: cycle-1 as (3600 secs, 500 secs), and cycle-2 for (1200 secs) before Interrupting the Battery Cell. 238

6.23.3 Nickel Vs Titanium at 0.1 Amps and -0.1 Amps at these charge and discharge time steps: cycle-1 @ (1800 secs and 200 secs), cycle-2 @ (1900 secs and 100 secs) and cycle-3 @ (2000 secs and 300 secs) 239

7 Final Overall Conclusions on all Chapters 241

7.1 Dendrite Measurement and Assessments 241

7.1.1 Zinc-Based Metal-Anode RFB 242

7.1.2 Zinc Electrodeposition. 242

7.2 Challenges and Control 244

7.3 Assessment of Efficiencies Results 246

7.3.1 SEM (Scanning of Electrons Microscopy) 247

Charged and discharged rate (0.1 amps vs -0.01 amps) @ both 3600 secs 248

Three-cycles of charged and discharged at a current rate of (0.1 amps Vs -0.1 amps) @ 3600 secs and 1800 Secs 248

Three-cycles of charged and discharged at (0.4 amps and -0.4 amps) for 3600 secs and 1800 secs 248

Re-examined nickel and carbon materials at (a) charged rate 0.1 amps for 3600 secs and (b) Discharged rate -0.1 amps for 1800 secs 249

Three cyclic voltammetry of one sweep condition at 25 mV/ sec 249

7.4 Recommended Future Work 253

7.5 Other ZnBr2 Cells Systems Challenges 254

7.5.1 Chlorides in ZnBr2 Systems 254

7.6 Future Solutions 255

8 References 257

9 Appendix 294

9.1 Engineering Draft of Designed Components Incorporated to the Proposed Zinc-Bromine Battery Cell to be Fabricated. 294

9.1.1 Carbon Vs Nickel Cycle-1 (0.1 Amps Vs -0.1 Amps) @ (3900 Secs and 2000 Secs), (3600 Secs and 1600 Secs) and (2400 secs only to Charge) 305

9.1.2 Nickel Vs Titanium Cycle-1 (0.1 Amps Vs -0.1 Amps) @ (1800 Secs and 900 Secs), (1810 Secs and 900 Secs) and (1705 Secs and 900 Secs) 306

10 Attended Conferences and Meetings 314

Symbols and Nomenclature

Symbols	Meaning
A	Ampere
mA	Milliamperes
MV/ Sec	Millivolt Per Second
G	Grams
G/ CCm^3	Grams Per Cubic Centimetres
L/ Hr	Litres Per Hour
C	Coulombs
KWh	Kilowatt-Hour
Wh	Watt-Hour
Zn^{2+}	Zinc
Br2	Bromine
Br^-	Bromide
Cl^-	Chlorine
K^+	Potassium

List of Abbreviations

Abbreviation	Full Meaning
ZBBS	Zinc Bromine Battery System
ESS	Energy Storage System
CAES	Compressed Air Energy Storage
PHS	Pumped Hydroelectric Storage
CS	Capacitor Storage
TES	Thermal Energy Storage
CV	Cyclic Voltammetry
FES	Flywheel Energy Storage
EEST	Electrochemical Energy Storage Technologies
SES	Supercapacitor Energy Storage
EIS	Electrochemical Impedance Spectroscopy
RFC	Reversible Fuel cell
OCV	Open Circuit Voltage
SOC	State of Charge
BSC	Batteries State of Health
ZNBR2	Zinc Bromide

KCl	Potassium Bromide
ZnCl2	Zinc Chloride
KCl	Potassium Chloride
CE	Coulombic Efficiency
EE	Energy Efficiency
CE	Charge Efficiency
DE	Discharge Efficiency
ZBB	Zinc bromine Battery
jL	Limiting Current
∂N	Nernst Diffusion Layer
NSE	Navier Stokes Equation

List of Figures

Figure 1. 1 Schematic diagram of caes system [72] 33
Figure 1. 2 Pumped hydroelectric storage [76] 34
Figure 1. 3 Flow chart of the expanded plant with tes [85] 35
Figure 1. 4 Flywheel energy storage [89] 36
Figure 1. 5 Ragone plot of stationary electrodes from traditional batteries [101] 38
Figure 1. 6 In-lab grid electrochemical supercapacitors for energy storage system [102] 39
Figure 1. 7 A typical example of a redox flow battery 42
Figure 1. 8: Types of rfb, according to the nature of energy storage. energy is stored (a) in the electrolytes, (b) in the active material within the electrodes and (c) hybrid in both electrode and electrolyte phases) [108]. 44
Figure 1. 9: Schematic of the functioning of a vanadium redox flow battery (vrfb) system [139] 45
Figure 1. 10 (a) Schematic of an iron-chromium rfb [184] 49
Figure 1. 11:The principle of sodium polysulfide/bromine rfb [191] 51
Figure 1. 12 Identifies dissolved quinone species in 1 m h_2so_4, of a cell potential 0.7 v. with stored two electrons during charging with 2 h^+ been exchanged through a nafion membrane [196] 52
Figure 1. 13 Schematic diagram of a nonaqueous rfb [227] 57
Figure 1. 14 Regenerative hydrogen-chlorine fuel cell schematic [279]. 64
Figure 1. 15 Diagram of a divided zinc-cerium flow battery [292]. 66
Figure 1. 16 Schematic of a zinc-bromine rfb during charging (left) and discharging (right). [309]. 69
Figure 1. 17 Zinc bromine battery cell components [321] 72
Figure 1. 18 Pourbaix diagram for zinc different ph in water [350] 80
Figure 1. 19 Morphologies of zinc electrodepositions (heavy spongy, dendrite, boulder, layer-like and filamentous mossy) on electrode surface (electrodeposited through alkaline electrolytes). 84
Figure 1. 20 Half liquid-solid fbr [378] 85
Figure 1. 21 Turbulent and laminar flow [416] 91
Figure 1. 22 Pressure drop Δp in respect to superficial velocity 96
Figure 1. 23 Bed of particles with the force balance [437] 98

Figure 2. 1 Concept one and concept two 107
Figure 2. 2 Concept three and concept four 107
Figure 2. 3 Concept five and concept six 108
Figure 2. 4 Sketched diagram of the reactor 109

Figure 3. 1 Investigated glass beads 114
Figure 3. 2 Anode zinc-electrode 116
Figure 3. 3 Anode reactor with (a) fluidized glass beads and (b) carbon particles 117
Figure 3. 4 Anode-side reactor 119
Figure 3. 5 Zinc-bromine battery cell test rig isometric view 120
Figure 3. 6(a) The zbb labelled components and (b) a complete front view of the designed - zinc-bromine battery cell test rig showing the anode and the cathode 121
Figure 3.7(a) Side view cathode-cell compartment and (b) side view anode-cell compartment 122

Figure 3. 8 Investigated particles within the anode-reactor (254 microns to 354 microns) (a) non-uniformed glass beads (b) uniformed graphite particles. 131

Figure 4. 1 (a) The designed zbb reactor with flow path and (b) the mesh results using tetrahedron mesh method..... 133
Figure 4. 2 (a) Isometric view - streamline of flows with particle trajectories at 0.098 m/s and (b) side view - streamline of flows with particle trajectories at a velocity of 0.098 m/s 135
Figure 4. 3 (a) Pressure contour at 101325 pascals at the inlet and 101600 pascals at the outlet (b) velocity magnitude at 0.098 m/s at the inlet 137
Figure 4. 4 The designed zbb cell incorporating all the battery cell components: such as the gaskets, reactors, membrane, cell anode and cathode endplates and both the cathode side and anode-side incorporated feeder electrodes. 138
Figure 4. 5 The designed zbb cell components 139
Figure 4. 6 The zinc-bromine battery cell model 142
Figure 4. 7: Cell model electrolyte potential and current vs voltage (a) charged at 0.1 amps & -0.1 amps (b) mid-charged at 0.1 amps & -0.1 amps and (c) discharged at 0.1 amps & -0.1 amps all at 3600 secs. 144
Figure 4. 8: Cell model anode electrode zinc concentrations and graphs result plots (a) charged at 0.1 amps and -0.1 amps (b) mid-charged at 0.1 amps & -0.1 amps and (c) discharged at 0.1 amp & -0.1 amps all at 3600 secs. 146
Figure 4. 9: Cell model cathode electrode bromide concentrations and graphs result plots (a) charged at 0.1 amps & -0.1 amps (b) mid-charged at 0.1 amps & -0.1 amps and (c) discharged at 0.1 amps & -0.1 amps all at 3600 secs. 148
Figure 4. 10: Cell model cathode electrode bromide concentrations and graphs result plots (a) charged at 0.1 amps & -0.1 amps (b) mid-charged at 0.1 amps & -0.1 amps and (c) discharged at 0.1 amps & -0.1 amps all at 3600 secs. 150

Figure 5. 1 Lancaster university jeol jsm-601 oplus/la analytical scanning electron microscope machine 154
Figure 5. 2 Charged dried particle 155
Figure 5. 3: Discharged dried particles 156
Figure 5. 4: Copper deposits during charging and discharging 156
Figure 5. 5: Uv-vis spectroscopy device [483] 162

Figure 6. 1 Two carbon fibre materials incorporated to the anode-side and cathode-side of the znbr2 cell..... 173
Figure 6. 2: Charged and discharged result plot (ai) (0.1 amps at 3600 secs & -0.1 amps for 500 secs) and (aii) (0.2 amps @ 1500 secs &, -0.1 amps for 1300 secs) of 3 moles of kbr (535.51 grams), 1 mole of kcl (111.89 grams) as the cathode-side electrolyte solution and 3 moles of znbr2 (675g), 1 mole of $zncl_2$ (205 grams), and 1 mole of kcl (111.826 grams) as the anode electrolyte solution. 178
Figure (6. 3A) Zinc morphology (254 microns to 354 microns) appearances within the anode zinc reactor after reacting (b) cyclic voltammetry of the two-carbon electrodes feeder materials at 0.2 amps, and -0.1 amps for 3600 seconds for one sweep condition using 3 moles of kbr (535.51 grams), 1 mole of kcl (111.89 grams) as the cathode-side electrolyte solution and 3 moles of znbr2

(675 grams), 1 mole of $zncl_2$ (205 grams), and 1 mole of kcl (111.826 grams) as the anode electrolyte solution at a charge rate of (0.2 amps @ 1500 secs &, -0.1 amps for 1300 secs) and before completely losing the cell apart. 179
Figure 6. 4 Cell components after the explored two-chronopotentiometry 180
Figure 6. 5 Bar chart showing the compared energy efficiencies charge-(blue) and energy-(pink) at (1) 0.1 amps & -0.1 amps @ 3600 secs & 500 secs and (2) a charged rate of 0.2 amps & -0.1 amps for 1500 secs & 1300 secs 181
Figure 6. 6 Charge rate and discharge rate of (a) 0.1 amps for 3600 secs, -0.1 amps for 800 secs (b) 0.1 amps and -0.1 amps for 3600 secs and 200 secs (c) 0.25 amps and -0.25 amps for 3600 secs and 100 secs of 3 moles of kbr (535.51 grams), 1 mole of kcl (111.89 grams) of cathode electrolyte solution and 3 moles of znbr2 (675 grams), 1 moles of $zncl_2$ (205 grams), and 1 moles of kcl (111.826 grams) of anode electrolyte solution. 185
FIgure 6. 7 Charge-(blue) and energy-(pink) efficiencies of charge rates (1) 0.1 amps and -0.1 amps for 3600 secs and 800 secs (2) at 0.1 amps and -0.1 amps for 3500 secs and 200 secs (3) 0.25 amps for 3600 secs and -0.25 amps for 100 secs of 3 moles of kbr (535.51 grams), 1 mole of kcl (111.89 grams) of cathode electrolyte solution and 3 moles of znbr2 (675 grams), 1 mole of $zncl_2$ (205 grams), and 1 mole of kcl (111.826 grams) of anode electrolyte solution. 186
Figure 6. 8: Brown deposits identified as copper after charging the zbb battery cell at a charge rate of (1) 0.1 amps and -0.1 amps for 3600 secs and 800 secs (2) at 0.1 amps and -0.1 amps for 3500 secs and 200 secs and (3) at 0.25 amps for 3600 secs and -0.25 amps for 100 secs with 3 moles of kbr (535.51 grams), 1 mole of kcl (111.89 grams) as the cathode-side electrolyte solution and 3 moles of znbr2 (675 grams), 1 mole of $zncl_2$ (205 grams), and 1 mole of kcl (111.826 grams) as the anode electrolyte solution. 189
Figure 6. 9A: First identified peak showing the presence of copper at a wavelength of 740nm and b: second identified peak showing the presence of copper at a wavelength of 900nm with a uv-visible spectrophotometer device. 190
Figure 6. 10: Charge and discharge rates electrolyte solution: 3 moles of kbr (535.51 grams), 1 mole of kcl (111.89 grams) of cathode electrolyte solution and 3 moles of znbr2 (675 grams), 1 mole of $zncl_2$ (205 grams), and 1 mole of kcl (111.826 grams) of anode electrolyte solution at (a) 0.25 amps for 3600 secs, -0.25 amps for 400 secs (b) 0.1 amps for 3600 secs and -0.005 amps for 3500 secs (c) 0.25 amps for 3600 secs, and -0.01 amps for 3600 secs (d) 0.5 amps for 3600 secs, and -0.01 amps for 3600 secs. (e) 1 amp for 3600 secs, and -0.05 amps for 3500 secs. 193
Figure 6. 11: Charge-(blue) & energy-(pink) efficiencies: 3 mole of kbr (535.51 grams), 1 mole of kcl (111.89 grams) of cathode electrolyte solution and 3 mole of znbr2 (675 grams), 1 mole of $zncl_2$ (205 grams), and 1 mole of kcl (111.826 grams) of anode electrolyte solution at (1) at a charge rate and discharge rate of 0.25 amps and -0.25 amps @ 3600 secs and 400 secs (2) 0.1 amps and -0.005 amps @ 3600 secs and 3500 secs. (3) 0.25 amps and -0.01 amps @ both 3600 secs. (4) 0.5 amps and -0.01 amps @ both 3600 secs. (4) 1 amp and -0.05 amps @ both 3600 secs. 194
Figure 6. 12: (A) Unpolished cathode carbon electrode feeder (b) polished cathode carbon electrode feeder. 197
Figure 6. 13: Charge and discharge rate: 3 moles of kbr (535.51 grams), 1 mole of kcl (111.89 grams) of cathode electrolyte solution and 3 moles of znbr2 (675 grams), 1 mole of $zncl_2$ (205 grams), and 1 mole of kcl (111.826 grams) of anode electrolyte solution at (a) a charge rate and discharge rate of 0.1 amps, and -0.01 amps for 3600 secs and (b) cyclic voltammetry of 1 sweep @ 25mv/sec. 198
Figure 6. 14: Charge efficiency (blue colour) and energy efficiency (orange colour) 199

Figure 6. 15: The eleventh cell charge-(blue) and energy-(pink) efficiencies with the two-carbon electrodes (anode current collector and cathode current collector. 203
Figure 6. 16: (A) Nickel and carbon electrode feeder material (b) nickel and titanium electrode feeder material that were incorporated to the cell as the second and third set of electrode feeder materials 205
Figure 6. 17: The ZnBr2 cell polished electrode (nickel), and other materials..... 207
Figure 6. 18: (A) Carbon and nickel charge and discharge result at a current of 0.1 amps and -0.01 amps for both 3600 secs (b) the formation of bromine during charge through the two-carbon electrodes and (c) colourless anode electrolyte thru the two-carbon electrodes. 208
Figure 6. 19: 3D Pie chart of (blue colour) charge and (orange colour) energy efficiency at a charge rate and discharge rate of 0.1 amps and -0.01 amps for 3600 secs with 3 moles of kbr (535.51 grams), 1 mole of kcl (111.89 grams) as the cathode-side electrolyte and 3 moles of znbr2 (675 grams), 1 mole of $zncl_2$ (205 grams), and 1 mole of kcl (111.826 grams) as the anode electrolyte solution. 210
Figure 6. 20: Charge result of the nickel and titanium electrode at 0.1 amps for 3600 secs..... 212
Figure 6. 21: (A) 3-Cycles of charged and discharge at 0.1 amps and -0.1 amps for (3900 secs and 2000 secs), (3000 secs and 1600 secs), (2400 secs for only to charge) through the carbon vs nickel (b) 3-cycles of charged and discharge at 0.1 amps and -0.1 amps for (1800 secs and 900 secs), (1810 secs and 900 secs), and (1705 secs and 900 secs) through using the nickel vs titanium with 3 moles of kbr (535.51 grams), 1 mole of kcl (111.89 grams) as the cathode-side electrolyte and 3 moles of znbr2 (675 grams), 1 mole of $zncl_2$ (205 grams), and 1 mole of kcl (111.826 grams) as the anode electrolyte solution (c) cyclic voltammetry at 25 mv/ s taken after investigating the nickel and titanium electrode..... 214
Figure 6. 22: Bar chart of charge-(blue) and energy-(pink) efficiency at a current of 0.1 amps and -0.1 amps at (1). (3900 secs and 2000 secs), (2). (3000 secs and 1600 secs), (3). (2400 secs for only to charge) with 3 moles of kbr (535.51 grams), 1 mole of kcl (111.89 grams) as the cathode-side electrolyte and 3 moles of $znbr_2$ (675 grams), 1 mole of $zncl_2$ (205 grams), and 1 mole of kcl (111.826 grams) as the anode electrolyte solution. 216
Figure 6. 23: Bar chart of charge-(blue) and energy-(pink) efficiency (1). (1800 secs and 900 secs), (2). (1810 secs and 900 secs) and (3). (1705 secs and 900 secs) at 0.1 amps and -0.1 amps secs with 3 moles of kbr (535.51 grams), 1 mole of kcl (111.89 grams) as the cathode-side electrolyte and 3 moles of znbr2 (675 grams), 1 mole of $zncl_2$ (205 grams), and 1 moles of kcl (111.826 grams) as the anode electrolyte solution 217
Figure 6. 24: Overall bar chart of the charge-(blue) and energy-(pink) efficiency at 0.1 amps and -0.1 amps using the carbon and nickel electrode (1), for (3900 secs and 2000 secs), and (2), for (3000 secs and 1600 secs), and with the nickel and titanium electrode (3), for (1800 secs and 900 secs), (4), for (1810 secs and 900 secs) and (5), for (1705 secs and 900 secs) with 3 moles of kbr (535.51 grams), 1 moles of kcl (111.89 grams) as the cathode-side electrolyte and 3 moles of $znbr_2$ (675 grams), 1 mole of $zncl_2$ (205 grams), and 1 mole of kcl (111.826 grams) as the anode electrolyte solution..... 221
Figure 6. 25: (A) Carbon and nickel at 0.1 amps and -0.1 amps for (1), for (4000 secs and 1900 secs), and (2), for (3100 secs and 2000 secs), and (3) for (3000 secs and 1900 secs). (c) nickel and titanium at 0.3 amps and -0.3 amps for (1800 secs and 200 secs), and (2), for (1700 secs and 200 secs), and (3) for (1900 secs and 200 secs). 224
Figure 6. 26: Bar chart of charge-(blue) and energy-(pink) efficiency at 0.1 amps and -0.1 amps for (1), for (4000 secs and 1900 secs), and (2), for (3100 secs and 2000 secs), and (3) for (3000 secs and 1900 secs). with 3 moles of kbr (535.51 grams), 1 mole of kcl (111.89 grams) as the cathode-side

electrolyte and 3 moles of $znbr_2$ (675 grams), 1 mole of $zncl_2$ (205 grams), and 1 mole of kcl (111.826 grams) as the anode electrolyte solution. 225
Figure 6. 27: Bar chart of charge-(blue) and energy-(pink) efficiency at a current of 0.3 amps and -0.3 amps for (1800 secs and 200 secs), and (2), for (1700 secs and 200 secs), and (3) for (1900 secs and 200 secs) with 3 moles of kbr (535.51 grams), 1 mole of kcl (111.89 grams) as the cathode-side electrolyte and 3 mole of znbr2 (675 grams), 1 mole of $zncl_2$ (205 grams), and 1 mole of kcl (111.826 grams) as the anode electrolyte solution 226
Figure 6. 28: Overall bar chart of the charge-(blue) and energy-(pink) efficiency at 0.1 amps and -0.1 amps: (1) for (4000 secs and 1900 secs), and (2), for (3100 secs and 2000 secs), and (3) for (3000 secs and 1900 secs) with the c and nickel electrode and nickel vs titanium at a 0.3 amps and -0.3 amps: (4) for (1800 secs and 200 secs), and (5), for (1700 secs and 200 secs), and (6) for (1900 secs and 200 secs) 229
Figure 6. 29: (A) Cell chronopotentiometry plots at 0.4 amps and -0.4 amps cycle-1 (3900 secs and 1100 secs), and (cycle-2) for (3700 secs and 1300 secs), and (cycle-3) for (3700 secs and 1200 secs) with 3 moles of kbr (535.51 grams), 1 mole of kcl (111.89 grams) as the cathode electrolyte solution and 3 moles of $znbr_2$ (675 grams), 1 mole of $zncl_2$ (205 grams), and 1 mole of kcl (111.826 grams) as the anode electrolyte solution. (b) titanium and nickel electrode at a current range of 0.1 amps and -0.1 amps for cycle-1 (1800 secs and 200 secs), cycle-2 (1900 secs and 100 secs) and cycle-3 (2000 secs and 300 secs) for three cycles of charge and discharge with 3 moles of kbr (535.51 grams), 1 mole of kcl (111.89 grams) as the cathode electrolyte solution and 3 moles of znbr2 (675 grams), 1 mole of $zncl_2$ (205 grams), and 1 mole of kcl (111.826 grams) as the anode electrolyte solution. 230
Figure 6. 30: Bar chart of (charge-blue-1) and (energy-pink-2) efficiency with the carbon and nickel electrode at a charge rate and discharge rate of (a) 0.4 amps and -0.4 amps for cycle-1, (3900 secs and 1100 secs), and (cycle-2), for (3700 secs and 1300 secs), and (cycle-3) for (3700 secs and 1200 secs) with 3 moles of kbr (535.51 grams), 1m of kcl (111.89 grams) as the cathode-side electrolyte and 3 moles of $znbr_2$ (675 grams), 1 mole of $zncl_2$ (205 grams), and 1 mole of kcl (111.826 grams) as the anode electrolyte solution. 232
Figure 6. 31: Doughnut pie chart of (charge-blue-1) and (energy-pink-2) efficiency with the carbon and nickel electrode at a charge rate of (a) 0.1 amps and -0.1 amps for cycle-1: (3600 secs and 500 secs) and cycle-2 (1200 secs) with 3 moles of kbr (535.51 grams), 1 mole of kcl (111.89 grams) as the cathode-side electrolyte and 3 moles of znbr2 (675 grams), 1 mole of $zncl_2$ (205 grams), and 1 mole of kcl (111.826 grams) as the anode electrolyte solutions. 233
Figure 6. 32: Bar chart of (charge efficiency-blue) and (energy efficiency-pink) thru the titanium and nickel electrode at a current of 0.1 amps and -0.1 amps (1) @ (1800 secs and 200 secs), (2) @ (1900 secs and 100 secs) and (3) @ (2000 secs and 300 secs) with 3 moles of kbr (535.51 grams), 1 mole of kcl (111.89 grams) as the cathode-side electrolyte and 3 moles of $znbr_2$ (675 grams), 1 mole of $zncl_2$ (205 grams), and 1 mole of kcl (111.826 grams) as the anode electrolyte solution. 234
Figure 6. 33: Overall bar chart of (charge-blue colour) and (energy-pink colour) efficiency of (**a**) three cycles (1 to 3) of charge and discharge by incorporating a nickel and carbon electrode at a charge 0.4 amps and 0.4 amps at these time steps (3900 secs & 1100 secs), (3700 secs &1300 secs), (3700 secs & 1200 secs) (**b**) (4) by investigating further the same nickel and carbon electrode before it was interrupted at 0.1 amps and -0.1 amps with these time steps (3600 secs & 1800 secs) and (**c**) three cycles (5 to 7) of charge and discharge by investigating the titanium and nickel electrode at 0.1 amps and -0.1 amps at these time steps (1800 secs & 200 secs),(1900 secs & 100 secs),(2000 secs & 300 secs) with 3 moles of kbr (535.51 grams), 1 mole of kcl (111.89 grams) as the cathode-

side electrolyte and 3 moles of znbr2 (675 grams), 1 mole of $zncl_2$ (205 grams), and 1 mole of kcl (111.826 grams) as the anode electrolyte solution. 240

Figure 7. 1 The incorporated anode reactor to the cell anode side 242
Figure 7. 2 (a) Zinc system with solid phase reaction, (b) liquid state reaction, (c) and gaseous phase reaction [559]. 245
Figure 7. 3: Excellent (charge-blue) and (energy-pink) efficiencies through investigating (a) carbon-cathode versus carbon-anode at a charge rate of 0.2 amps and -0.1 amps (b) carbon-cathode versus nickel-anode a charge rate of 0.1 amps and -0.1 amps, and at a charge rate of 0.4 amps and -0.4 amps (c) titanium-cathode versus nickel-anode at a current rate of 0.4 amps and -0.4 amps. 247

Figure 9. 1: Zinc-bromine battery cell anode endplate 294
Figure 9. 2: Zinc-bromine battery cell cathode endplate 295
Figure 9. 3: Zinc-bromine battery cell anode gasket between anode endplate and anode reactor feeder 296
Figure 9. 4: Zinc-bromine battery cell anode gasket between the anode reactor and the membrane . 297
Figure 9. 5: Zinc-bromine battery cell cathode gasket between cathode endplate and cathode reactor feeder 298
Figure 9. 6: Zinc-bromine battery cell cathode gasket between the cathode reactor and membrane . 299
Figure 9. 7: Anode-side of the zinc-bromine battery cell electrode feeder 300
Figure 9. 8: Cathode-side of the zinc-bromine battery cell electrode feeder 301
Figure 9. 9: The zinc-bromine battery cell membrane 302
Figure 9. 10: Anode-side of the zinc-bromine battery cell engineering drafting 303
Figure 9. 11: Cathode-side of the zinc-bromine battery cell engineering drafting 304
Figure 9. 12: ZBB bom 313

List of Tables

Table 1. 1 Electrochemical energy storage technologies for stationary applications [97, 98] 37
Table 1. 2: Categories of zinc deposit morphology [365]. 83

Table 3. 1 Boundary and initial condition 124
Table 3. 2 Theoretical and experimental results 128

Table 4. 1 Charged and mid-charged and discharged concentrations 140

Table 5. 1 Mapped elements after drying the particles after charged 157
Table 5. 1 Mapped elements after drying the particles after discharged 158
Table 5. 1: Mapped elements of charged and discharged after copper deposits 159
Table 5. 4 Electrolyte chemical materials and suppliers 164
Table 5. 5 Anode and cathode components and suppliers. 165

Table 6. 1 Cycle-3: explored charged and discharged experiment at various charge rate via the three sets of electrode feeder materials carbon vs carbon, nickel vs carbon and nickel vs titanium with 3 moles of kbr (535.51 grams), 1 mole of kcl (111.89 grams) as the cathode-side electrolyte and 3 moles of znbr2 (675g), 1 mole of $zncl_2$ (205g), and 1 mole of kcl (111.826g) as the anode electrolyte solution. 171
Table 6. 2: Cycle-3: explored cyclic voltammetry experiment using the three feeder sets of electrode materials, carbon vs carbon, nickel vs carbon and nickel vs titanium with 3m of kbr (535.51 grams), 1m of kcl (111.89 grams) as the cathode-side electrolyte and 3m of znbr2 (675 grams), 1m of $zncl_2$ (205 grams), and 1m of kcl (111.826 grams) as the anode electrolyte solution 172
Table 6. 3: Anode and cathode electrolyte solution 174
Table 6. 4: Chronopotentiometry experimental current values on the investigated two-carbon materials with 3 moles of kbr (535.51 grams), 1 mole of kcl (111.89 grams) as the cathode-side electrolyte and 3 moles of znbr2 (675 grams), 1 mole of $zncl_2$ (205 grams), and 1m of kcl (111.826 grams) as the anode electrolyte solution. 175
Table 6. 5: Cyclic voltammetry experimental scan values on the investigated two-carbon materials with 3m of kbr (535.51g), 1m of kcl (111.89g) as the cathode-side electrolyte and 3m of znbr2 (675g), 1m of $zncl_2$ (205g), and 1m of kcl (111.826g) as the anode electrolyte solution. 176
Table 6. 6: Methods for the cell efficiencies 176
Table 6. 7: Experimental data of the investigated two-carbon materials with 3 moles of kbr (535.51 grams), 1 mole of kcl (111.89 grams) as the cathode-side electrolyte and 3 moles of znbr2 (675 grams), 1 mole of $zncl_2$ (205 grams), and 1 mole of kcl (111.826 grams) as the anode electrolyte solution. 180
Table 6. 8: Experimental data's of the investigated two-carbon materials with 3 moles of kbr (535.51 grams), 1 moles of kcl (111.89 grams) as the cathode-side electrolyte and 3 moles of znbr2 (675 grams), 1 moles of $zncl_2$ (205 grams), and 1 moles of kcl (111.826 grams) as the anode electrolyte solution. 186

Table 6. 9: Experimental data of the investigated two-carbon materials with 3 mole of kbr (535.51 grams), 1 mole of kcl (111.89 grams) as the cathode-side electrolyte and 3 mole of znbr2 (675 grams), 1 mole of $zncl_2$ (205 grams), and 1m of kcl (111.826 grams) as the anode electrolyte solution.....194
Table 6. 10: Experimental data's of the investigated two-carbon materials with 3 moles of kbr (535.51 grams), 1 mole of kcl (111.89 grams) as the cathode-side electrolyte and 3 moles of znbr2 (675 grams), 1 mole of $zncl_2$ (205 grams), and 1 mole of kcl (111.826 grams) as the anode electrolyte solution.....199
Table 6. 11: Cell explored experiments: carbon vs carbon charged and with 3 moles of kbr (535.51 grams), 1 mole of kcl (111.89 grams) as the cathode-side electrolyte and 3 moles of znbr2 (675 grams), 1 mole of $zncl_2$ (205 grams), and 1 mole of kcl (111.826 grams) as the anode electrolyte solution.....201
Table 6. 12: Cell experimental data's and evaluation: with 3m of kbr (535.51g), 1m of kcl (111.89g) as the cathode-side electrolyte and 3m of znbr2 (675g), 1m of $zncl_2$ (205g), and 1m of kcl (111.826g) as the anode electrolyte solution for the first sets of electrode feeder materials-carbon against carbon.....201
Table 6. 13 Chronopotentiometry experimental current values on the investigated carbon and nickel materials and nickel and titanium materials with 3 moles of kbr (535.51 grams), 1 mole of kcl (111.89 grams) as the cathode-side electrolyte and 3 moles of znbr2 (675 grams), 1 mole of $zncl_2$ (205 grams), and 1 mole of kcl (111.826 grams) as the anode electrolyte solution.....206
Table 6. 14 of (figure 6.18a) cell evaluation: carbon vs nickel charged and discharged experiment at a charge rate of 0.1 amps and discharge rate of -0.01 amps at both 3600 secs with 3 moles of kbr (535.51 grams), 1 mole of kcl (111.89 grams) as the cathode-side electrolyte and 3 moles of znbr2 (675 grams), 1 mole of $zncl_2$ (205 grams), and 1 mole of kcl (111.826 grams) as the anode electrolyte solution.....209
Table 6. 15: Experimental data of the investigated nickel and carbon materials consisting 3 moles of kbr (535.51 grams), 1 mole of kcl (111.89 grams) as the cathode-side electrolyte and 3 mole of znbr2 (675 grams), 1 mole of $zncl_2$ (205 grams), and 1 mole of kcl (111.826 grams) as the anode electrolyte solution.....209
Table 6. 16: Charge and energy efficiency of the investigated nickel and carbon materials of the 3-cycles of charge and discharge with 3 moles of kbr (535.51 grams), 1 mole of kcl (111.89 grams) as the cathode-side electrolyte and 3 moles of znbr2 (675 grams), 1 mole of $zncl_2$ (205 grams), and 1 mole of kcl (111.826 grams) as the anode electrolyte solution.....215
Table 6. 17 Charge and energy efficiency of the investigated nickel and titanium electrode of the 3-cycles of charge and discharge with 3 moles of kbr (535.51 grams), 1 mole of kcl (111.89 grams) as the cathode-side electrolyte and 3 moles of znbr2 (675 grams), 1 mole of $zncl_2$ (205 grams), and 1 mole of kcl (111.826 grams) as the anode electrolyte solution.....216
Table 6. 18: Experimental data of the charge and energy efficiency for the investigated nickel and carbon material with 3 moles of kbr (535.51 grams), 1 mole of kcl (111.89 grams) as the cathode-side electrolyte and 3 moles of $znbr_2$ (675 grams), 1 mole of $zncl_2$ (205 grams), and 1 mole of kcl (111.826 grams) as the anode electrolyte solution.....225
Table 6. 19: Experimental data such as the charge and energy efficiency of the investigated nickel and titanium materials with 3 moles of kbr (535.51 grams), 1 mole of kcl (111.89 grams) as the cathode-side electrolyte and 3 moles of $znbr_2$ (675 grams), 1 mole of $zncl_2$ (205 grams), and 1 mole of kcl (111.826 grams) as the anode electrolyte solution.....226
Table 6. 20: Cell efficiencies of the investigated nickel and carbon materials with 3 moles of kbr (535.51 grams), 1 mole of kcl (111.89 grams) as the cathode-side electrolyte and 3 moles of $znbr_2$ (675

grams), 1 mole of $zncl_2$ (205 grams), and 1 mole of kcl (111.826 grams) as the anode electrolyte solution.....231
Table 6. 21: Cell efficiencies of the investigated carbon and nickel materials with 3 moles of kbr (535.51 grams), 1 moles of kcl (111.89 grams) as the cathode-side electrolyte and 3 moles of znbr2 (675g), 1 moles of $zncl_2$ (205 grams), and 1 moles of kcl (111.826 grams) as the anode electrolyte solution. 232
Table 6. 22: Cell efficiencies of the investigated nickel and titanium materials with 3 moles of kbr (535.51 grams), 1 mole of kcl (111.89 grams) as the cathode-side electrolyte and 3 moles of $znbr_2$ (675 grams), 1 mole of $zncl_2$ (205 grams), and 1 mole of kcl (111.826 grams) as the anode electrolyte solution.....233
Table 6. 23: The cell efficiencies and other parameters of the investigated nickel and carbon electrode and the titanium and nickel electrode investigated in 3 moles of kbr (535.51 grams), 1 mole of kcl (111.89 grams) as the cathode-side electrolyte and 3 moles of znbr2 (675 grams), 1 mole of $zncl_2$ (205 grams), and 1 mole of kcl (111.826 grams) as the anode electrolyte solution.....237

Table 7. 1 Electrode feeder materials and current..... **ERROR! BOOKMARK NOT DEFINED.**
Table 7. 2: Cycle-3: applied charged and discharged amps to the three sets of electrode feeder materials carbon vs carbon, nickel vs carbon and nickel vs titanium with 3 moles of kbr (535.51 grams), 1 mole of kcl (111.89 grams) as the cathode-side electrolyte and 3 moles of znbr2 (675 grams), 1 mole of $zncl_2$ (205 grams), and 1 mole of kcl (111.826 grams) as the anode electrolyte solution. 248
Table 7. 3: Explored cyclic voltammetry after investigating the three sets of electrode feeder materials carbon vs carbon, nickel vs carbon and nickel vs titanium in a 3 moles of kbr (535.51 grams), 1 mole of kcl (111.89 grams) as the cathode-side electrolyte and 3 moles of $znbr_2$ (675 grams), 1 mole of $zncl_2$ (205 grams), and 1 mole of kcl (111.826 grams) as the anode electrolyte solution. 249
Table 7. 4: First investigated electrode materials: carbon-cathode vs carbon-anode experimental data with a 3 moles of kbr (535.51 grams), 1 mole of kcl (111.89 grams) as the cathode-side electrolyte and 3 mole of $znbr_2$ (675g), 1 mole of $zncl_2$ (205 grams), and 1 mole of kcl (111.826 grams) as the anode electrolyte solution 249
Table 7. 5: Experimental data of the second and third investigated electrodes materials: (carbon-cathode vs nickel-anode) & (titanium-cathode and nickel-anode) both with 3 moles of kbr (535.51 grams), 1 mole of kcl (111.89 grams) as the cathode-side electrolyte and 3 moles of $znbr_2$ (675 grams), 1 mole of $zncl_2$ (205 grams), and 1 mole of kcl (111.826 grams) as the anode electrolyte solution. 251

Table 9. 1: Cycle-1 to cycle-3 cell evaluation: carbon vs nickel charged and discharged experiment-1 @ 0.1 amps for 3900 secs and -0.1 amps (3900 secs and 2000 secs), (3000 secs and 1600 secs), (2400 secs for only to charge) with 3 moles of kbr (535.51 grams), 1 mole of kcl (111.89 grams) as the cathode-side electrolyte and 3 moles of znbr2 (675 grams), 1 mole of $zncl_2$ (205 grams), and 1 mole of kcl (111.826 grams) as the anode electrolyte solution.....305
Table 9. 2: Experimental data of the investigated nickel and titanium electrode for the 3-cycles of charge and discharge at 0.1 amps and -0.1amps for (1800 secs and 900 secs), (1810 secs and 900 secs) and (1705 secs and 900 secs) with 3 moles of kbr (535.51 grams), 1 mole of kcl (111.89 grams) as the cathode-side electrolyte and 3 moles of znbr2 (675 grams), 1mole of $zncl_2$ (205 grams), and 1 mole of kcl (111.826 grams) as the anode electrolyte solution.....306

Table 9. 3: Experimental data of the investigated carbon and nickel electrode for the 3-cycles of charge and discharge at a current rate of 0.1 amps and -0.1 amps for (cycle-1), (4000 secs and 1900 secs), and (cycle-2), for (3100 secs and 2000 secs), and (cycle-3) for (3000 secs and 1900 secs). with 3 moles of kbr (535.51 grams), 1 mole of kcl (111.89 grams) as the cathode-side electrolyte and 3 moles of znbr2 (675 grams), 1 mole of $zncl_2$ (205 grams), and 1 mole of kcl (111.826 grams) as the anode electrolyte solution. 307
Table 9. 4: Experimental data of the investigated nickel and titanium electrode for the 3-cycles of charge and discharge at 0.3 amps and -0.3 amps for (1800 secs and 200 secs), and (2), for (1700 secs and 200 secs), and (3) for (1900 secs and 200 secs) with 3 moles of kbr (535.51 grams), 1 mole of kcl (111.89 grams) as the cathode-side electrolyte and 3 moles of znbr2 (675 grams), 1 mole of $zncl_2$ (205 grams), and 1 mole of kcl (111.826 grams) as the anode electrolyte solution..... 308
Table 9. 5: Experimental data of the investigated carbon and nickel electrode for the 3-cycles of charge and discharge at a charge and discharge of 0.4 amps and -0.4 amps for cycle-1, (3900 secs and 1100 secs), and (cycle-2), for (3700 secs and 1300 secs), and (cycle-3) for (3700 secs and 1200 secs) with 3 moles of kbr (535.51 grams), 1 mole of kcl (111.89 grams) as the cathode-side electrolyte and 3 moles of znbr2 (675 grams), 1 mole of $zncl_2$ (205 grams), and 1 mole of kcl (111.826 grams) as the anode electrolyte solution..... 310
Table 9. 6: Experimental data of the investigated and interrupted 3-cycles of charge and discharge at 0.1 amps and -0.1 amps for cycle-1 (3600 secs, 500 secs), and cycle-2 for (1200 secs) incorporating the carbon and nickel electrode with 3 moles of kbr (535.51 grams), 1 mole of kcl (111.89 grams) as the cathode-side electrolyte and 3 moles of znbr2 (675 grams), 1 mole of $zncl_2$ (205 grams), and 1 mole of kcl (111.826 grams) as the anode electrolyte solution..... 311
Table 9. 7: Experimental data of the investigated titanium and nickel electrode for the 3-cycles of charge and discharge at 0.1 amps and -0.1 amps for cycle-1 @ (1800 secs and 200 secs), cycle-2 @ (1900 secs and 100 secs) and cycle-3 @ (2000 secs and 300 secs) with 3 moles of kbr (535.51 grams), 1 mole of kcl (111.89 grams) as the cathode-side electrolyte and 3 moles of znbr2 (675 grams), 1 mole of $zncl_2$ (205 grams), and 1 mole of kcl (111.826 grams) as the anode electrolyte solution. 311
Table 9. 8: The fabricated cell bill of materials 313

List of Equations

Equation 1: Regenerative fuel cell reverse function in hydrogen−air fuel cells, gaseous fuel and oxidant 40
Equation 2: Reaction of lithium metal with water and oxygen to generate a regenerated fuel cell of 3.0v 40
Equation 3: Lithium reaction with oxygen to form a lithium oxide regenerative fuel cell of 2.96v..... 40
Equation 4: Zinc reaction with oxygen to generate a zinc-oxide regenerative fuel cell of 1.59v 41
Equation 5: (Polysulfide-bromine chemistry) 49
Equation 6: Anodic reaction in an organic regenerative fuel cell 53
Equation 7: Full cell reaction with an air cathode utilizing oxygen. 54
Equation 8: All-uranium rfb chemical reaction nonaqueous solvents dimethylformamide 54
Equation 9: All-neptunium rfb in nonaqueous solvents propylene carbonate 54
Equation 10: All-iron rfb overall reaction (e_0 = 1.2 v) 59
Equation 11: All-lead acid rfb cells of classic lead-acid chemistry chemical reaction 61
Aquation 12: All-copper rfb aqueous solution of cucl in both cathode and anode 62
Equation 13: All-copper electrochemical second reaction 62
Equation 14: Solubility of zinc-oxide (inorganic compound) with water to lose an electron to form zinc with oxygen and hydrogen. 66
Equation 15: Zinc reduction process at the anode-side of a battery cell 75
Equation 16: Formation of bromide due to gain electron 77
Equation 17: Bromide reaction with quaternary ammonium bromides 77
Equation 18: Nernst equation for independent reaction on ph corresponding to a horizontal line at −0.763 v vs. she in the pourbaix diagram 81
Equation 19: First linear variation reaction of zinc electrodeposition routes within the negative gradients 81
Equation 20: Second linear variation reaction of zinc electrodeposition routes within the negative gradients 81
Equation 21: Third linear variation reaction of zinc electrodeposition routes within the negative gradients 81
Equation 22: The carman-kozeny equation used theoretically for calculating minimum fluidization velocity 96
Equation 23: Drag forces and gravitational forces on the particles 97
Equation 24: Bed of particles net gravitational forces 98
Equation 25: Voids calculation in bed particles 98
Equation 26: Calculating the total volume of particles within a fluidized bed 99
Equation 27: Occupying volume by particles within a fluidized bed. 99
Equation 28: Drag forces acting on bed of particles 99
Equation 29: Pressure drops across the bed of particles 100
Equation 30: Local pressure dropping ∇p through a bed based on the bed voidage, the particles details and the flow velocity with the fluid other properties 100
Equation 31: Calculating the drag forces on bed particles via multiplying the column cross-sectional area 101
Equation 32: Drag force or the pressure gradient depending on the velocity 101

Equation 33: Recognition of fluid viscosity using symbols (μ) and (re) for the voidage to adjust the use of a superficial velocity (u). 101
Equation 34: Derived form of an idealized model of a packed bed of particles 102
Equation 35: Ergun's theory 102
Equation 36: Hydrodynamic drag forces and gravitational forces 113
Equation 37: Function of the shape and distribution of the particles size 113

Abstract

This project focuses on the development of efficient energy storage systems by addressing problems commonly encountered in zinc bromide flow batteries. For example, the kinetics of charge, a discharge onto plane electrodes, can be slow, affecting the ability of such a cell to restitute energy quickly to an external load; zinc deposition is also prone to the formation of dendrites, which can become detached from the electrode substrate and reduce the storage capacity of the battery, while those dendrites can also be responsible for damage to the membrane, separating the anolyte and the catholyte. The project also incorporates both theoretical modelling and simulation two using different software packages (ANSYS and COMSOL).

In this project, we design a novel fluidized bed electrode for the zinc-bromine (ZnBr2) flow battery, particularly concentrating on its anode. This is achieved by

1. Simulating electrolyte flow to identify reactor shapes and flow parameters that allow large electrolyte volumes to be processed and to support the fluidization of particles.
2. Fabricating an experimental rig from the identified geometry.
3. Carrying out extensive electrochemical testing (cyclic voltammetry, Electrochemical Impedance Spectroscopy, chronopotentiometry) to validate the model.

The key component of the design is its use of a fluidized bed electrode where particles support the transfer of electron within the cell and provide a locus for electrodeposition of the zinc, improving the kinetics of electron transfer during the charging and discharging cycle. The particles used in the fluidized bed reactor possess intrinsic chemical resistance to the solution components and abrasion.

Chapter 1
Introduction to Energy Storage

1 Chapter 1 Introduction to Energy Storage

1.1 Energy Storage Needs and Categories

Energy storage is critically important to enable balancing power generation and consumption, especially in the context of renewable energy innovation, such as promoting energy distribution and management [1-24]. Many renewable energy sources rely on intermittent phenomena (wind, solar, etc.), which makes it difficult to predict and regulate the output to fit in with demand. Today's world is at a turning point because of low resources, increase in pollution, and changes to the climate. Before the next decade, we might have run out of fossil fuels and we are concerned to find alternatives that can guarantee our acquired wealth and further growth on a long-term basis.

Wind turbines, biomass plant and photovoltaic cells as modern technologies are already providing us with such alternatives. But these technologies have flaws compared to traditional power plants because they can only produce smaller amounts of electricity. The issue of irregularity during production is one of the major problems and there is huge demand of electricity globally. This continues to grow annually by approximately 3.6 percent [25]. But the sun and wind are not reliable. However, because of technical reasons and due to consumers, the quantity of electricity feeding into power grids must be levelled to avoid power failure and damage to the grid. It is important to balance out these flaws in a situation where there is higher production and high rate of consumption.

This is where energy storage technologies come into play as the key element that can balanced out these flaws by introducing standing renewable energy sources. Engineers and scientists are anxious toward enhancing the efficiencies and lowering these technologies cost. Yet, only one or two technologies seems to be available that are economical enough and efficient. Energy storage is not an easy task, as known by most of us. Our smartphones batteries can only last for about one day and laptops has only limited hours.

Electric cars ranges are limited to only little 100 kilometers and a few more. This are only examples for comparatively small devices. Now imagine the problem of storing energy at the level of hundreds to thousands of photovoltaic cells and wind turbines. Today, it works fine the way the fluctuating energy demand is been handled for now. But grids are changing as we

are approaching faster and faster the point of peak oil and when we try hard to replace a conventional plant with a regenerative source of energy. However, the demanding will remain about the same [26]. It is hard to predict a fluctuating production with renewable energy the way we can predict the weather for the next few days. But the weather forecast as we all know is not 100% accurate. Furthermore, the context of a national or even transnational power grid cannot be calculated within few days because it will not be enough, and this cannot guarantee a secure energy supply. Predicting the wind when it stops will not alter the required energy that can be provided by a wind turbine.

This shows that we need to look for way that can compensate this fluctuation; which will save energy when windy and sunny and utilize it during windless and cloudy days. There are existing technologies that are currently in use today that are not capable enough if we prepared to go green and sustainable. It is not possible to build more existing storage technologies due to each technology with different flaws [27, 28]. For instances, the developed different types of energy storage systems for various energy sources [29] have made it challenging and confusing to evaluate and stay within an energy storage system [30-36].

Several companies are now pursuing zinc−bromine redox flow batteries cells, and a review of zinc−bromine modelling efforts have also been published [37]. These companies include Redflow Ltd. (www.redflow.com), Primus Power (www. primuspower.com), ZBB Energy (www.zbbenergy.com) and have various field installations operating or under development. According to a recent report, the testing of zinc−bromine RFB at remote telecom sites carried out has shown that, when the electrical load is low for a broadly installed generation, there is the potential for significant fuel savings [38-40].

Since the discovery of electricity by Benjamin Franklin in 1752, various effective methods have been explored to store energy for use based on later demand. The technologies can serve multiple grids and function off grid for energy storage purposes. Their modes of response with time can be grouped in terms of demand, scale, and duration of discharge; this includes the capacity to supply, voltage control, regulation, and spinning reserve [41]. In order to assist with our understanding of the various strategies currently being employed to store energy around the world, energy storage technologies have been divided into the following main categories listed below:

1. Solid State Batteries - such as a series of electrochemical storage solutions with advanced chemistry batteries and capacitors [42]
2. Flow Batteries - batteries with quick response times, such as the fabricated ZnBr2 battery cell of this research report that stores energy directly for long periods of time in the electrolyte solution [43].
3. Flywheels - mechanical devices that provide immediate rotational energy to produce electricity [44].
4. Compressed Air Energy Storage - employing compressed air to create a prominent energy reserve [45].
5. Thermal - generating power on demand from captured heat and cold [46].
6. Pumped Hydro Power - producing energy from large-scale reservoirs with water [47].

Worldwide electrical power generation will not stop undergoing significant changes due to the depletion of fossil fuels to reduce greenhouse gas emissions. For instance, by 2050 in the United States, 40% of all energy consumed in 2012 will be doubled, based on worldwide demand [7, 48-51]. The global amount of energy generated by solar and wind energy are the most environmental and irregular energy is 12% and considered as a small fraction compared to the amount produced by other renewable energy sources, such as hydroelectric, biomass, and geothermal power.

The capacities of installed solar power and wind turbines, growing at a rate of 60% and 20% every year throughout the world, are necessary to drive and reduce carbon emissions respectively. Recently, fossil fuel has been surpassed by installing renewable energy systems as the new capacity to generate electricity. In the United States alone, the goal of most states is to reach at least 20% of the total electricity production from renewables by 2020 and even higher than the 12% target set in Europe. Energy storage systems, such as electrochemical, mechanical or thermal are necessary to store energy from these fastest growing energy generation sources such as wind and solar power helping to balance demand and supply [4, 52-60]. The development of novel electrical energy storage technologies competent to resolve these challenges is essential [38-40].

1.2 Energy Storage Systems and Comparison

Electrical energy storage technologies, such as superconducting magnetic energy storage (SMES), flywheel electrical energy storage, high power density batteries such as lithium-ion, and supercapacitors are mainly for high-power applications like power quality and frequency regulation [61]. Pumped hydro storage, Compressed air energy storage, Thermal energy storage, and some batteries that manage energy applications are competing with flow batteries [62] for the longer time constant grid storage market. Pumped hydrostatic energy storage technology (PHES) and compressed air energy storage systems (CAES) are taking the lion's share of current grid-scale storage capacity at >99% and >0.35%, respectively [63]. These two technologies are the least expensive and most economical to use at large scale but are restricted to some geographical environments such as the compulsory underground cavern (hole) needed for the presence of compressed air energy storage systems (CAES).

Thermal energy storage systems (TES) are comparable with compressed air energy storage systems (CAES) systems concerning installed capacities, suitable for peak shaving, and usually connected with solar power plants. TES have a low energy density, between 10−50 Wh/kg, and require high capital costs. All these technologies need substantial capital investments, have a large footprint, and are not flexible. In contrast, electrochemical energy storage systems technologies are of better flexibility because of their higher energy density and modular designs. Furthermore, there is also an increase in demand for vehicle electrification, and powertrain also requires onboard energy storage of high energy density including the capacity of the 40−120 kilowatt-hour range.

Zinc-bromine redox flow batteries (ZnBr2), among other alternatives for storing energy are recommended and reliable to use for storing energy from renewable energy sources; such as wind and solar because of their significant benefits above conventional technologies. These include high energy densities, low costs, high efficiencies and power rating, long life cycles of more than 2000 sequences and, the capacity to operate these batteries with different applications in a wide range of various environments [30, 52].

1.2.1 Compressed Air Energy Storage System (CAES)

Figure 1.1 shows a CAES system - The basic concept of compressed air energy storage systems (CAES) is rather simple. These systems store energy when charged by using an electrically

driven compressor that changes electrical energy into potential energy of the pressurized gas. compressed air energy storage systems (CAES) draws electricity from the grid when demand is low as power is sufficient and compresses air into geological features such as salt caverns hundreds of meter underground. Air is released to regenerate the electricity when needed from the cavern. Gas can be stored for decades in a salt cave as the salt seals to prevent any cracks and pressure loss [64-71].

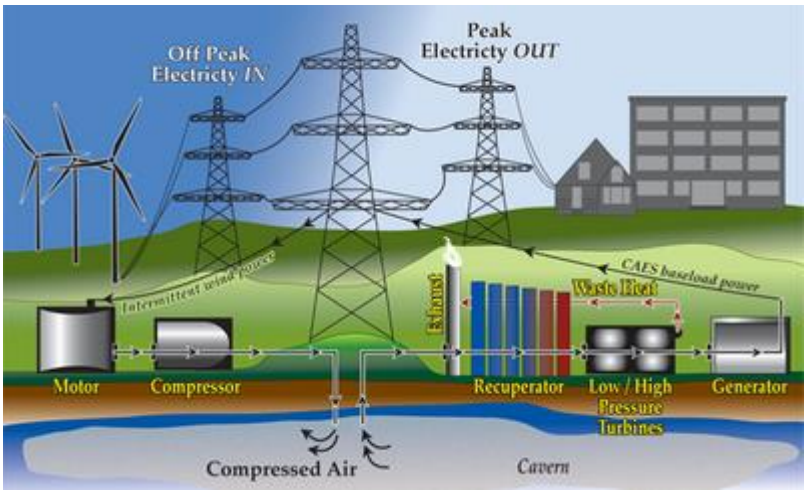

Figure 1. 1 Schematic Diagram of CAES System [72]

1.2.2 **Pumped Hydroeletric Storage (PHS)**

In figure 1.2, Pumped hydro energy storage systems are the most efficient solution that allow the storing of substantial quantities of electrical energy by using a turbine operation. In the United States (USA), more than 22GW of Pumped hydrostatic energy storage technology (PHES) systems has been installed and now the most extensive storage system. Nevertheless, most pumped hydrostatic energy storage systems projects plans are suspended due to the high cost of these devices. These devices plants mainly require two reservoirs at different elevations. Water is pumped into an upper reservoir tank when supply is more than demand as energy is stored. The system operates in the opposite direction by releasing water when demand exceeds supply. Released water generates electricity by running downhill via turbines into the lower reservoir [3, 73-75].

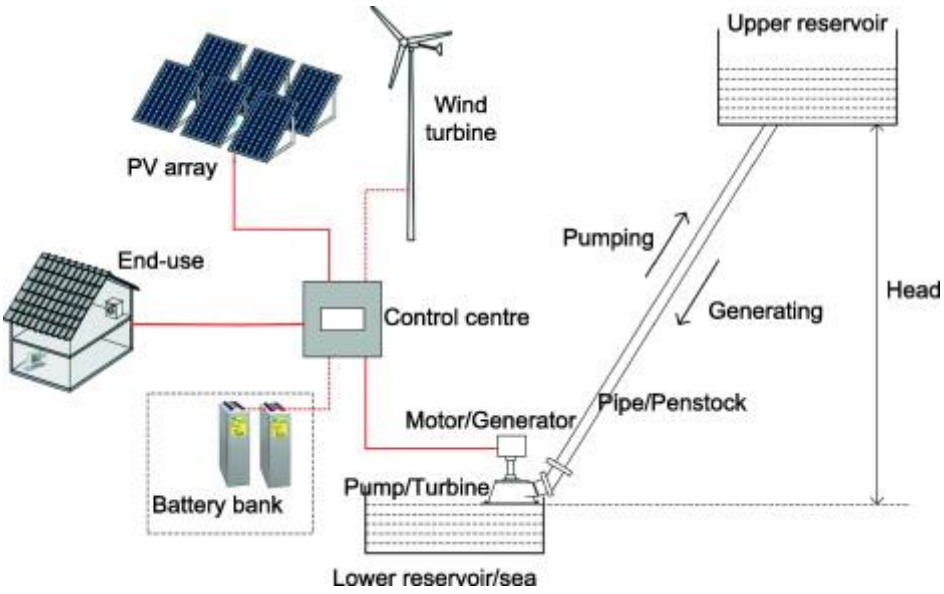

Figure 1. 2 Pumped hydroelectric storage [76]

1.2.3 **Capacitor Storage (CS)**

Coupled capacitor storage systems are devices that can store energy in an electric vehicle. Capacitors have many advantages such as the flexibility of the circuit for broad current ranges, voltage recovery for work development [77, 78]. Capacitors can store electrical energy on their plates in the form of electrical charge. Capacitors can be connected to a power source to accumulate energy and release it as soon as the capacitor is disengaged from the charging source. This process makes them to be like batteries. Batteries electrochemical processes are used for storing energy compare to capacitors that are simply for storing charge which make them to be different. However, stored energy can be released by capacitors at higher rate compare to batteries because of more required time for the chemical process to take place.

1.2.4 **Thermal Energy Storage System (TES)**

According to figure 1.3, TES are grouped as thermal chemical energy storage, sensible heat storage, and latent heat storage and also have the waste application potential for recovering heat, energy saved in houses, solar energy utilization and to manage electronic devices [59, 60, 79-81]. Thermal storage generates electricity via energy from the sun when shining or not. The device can store heat from the sun and store it in molten salts, water or other fluid and later use them when needed. These technologies have been proposed and currently operated in Nevada, California and Arizona. A typical example in Blythe, California is the Rice Solar Energy Project; where molten salt storage provides energy to roughly 68,000 homes with a concentrating solar tower. These technologies are operated by freezing water at night when electricity demand is less (off-peak). The stored cold energy is thereby released from the ice to improve air conditioning throughout the day [82-84].

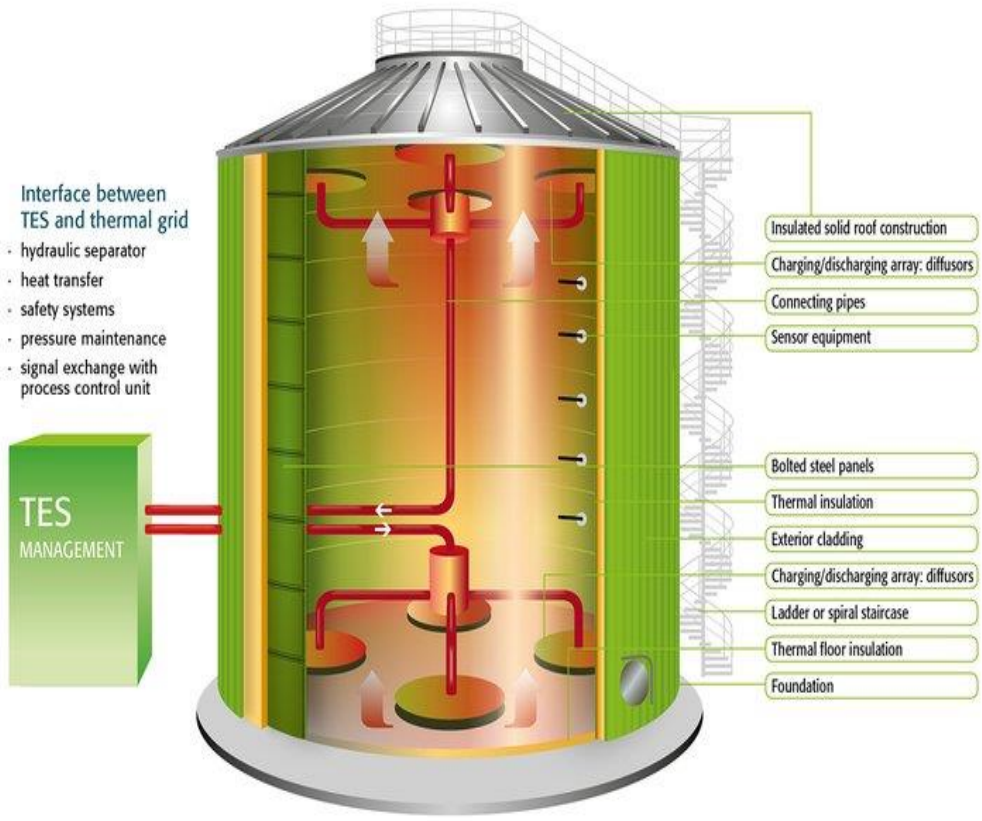

Figure 1. 3 Flow chart of the expanded plant with TES [85]

1.2.5 Flywheel Energy Storage (FES)

Figure 1.4 shows a FES system. Flywheel energy storage systems discharge timescale is short (milliseconds to minutes) and are suited to power quality and frequency regulation. It is a device that stores energy as the kinetic energy of a large rotor spinning at high speed [86] [87]. Out of all the developed energy storage technologies to store an additional AC power to be used later, flywheel energy storage technologies have been considered as the next option [88].

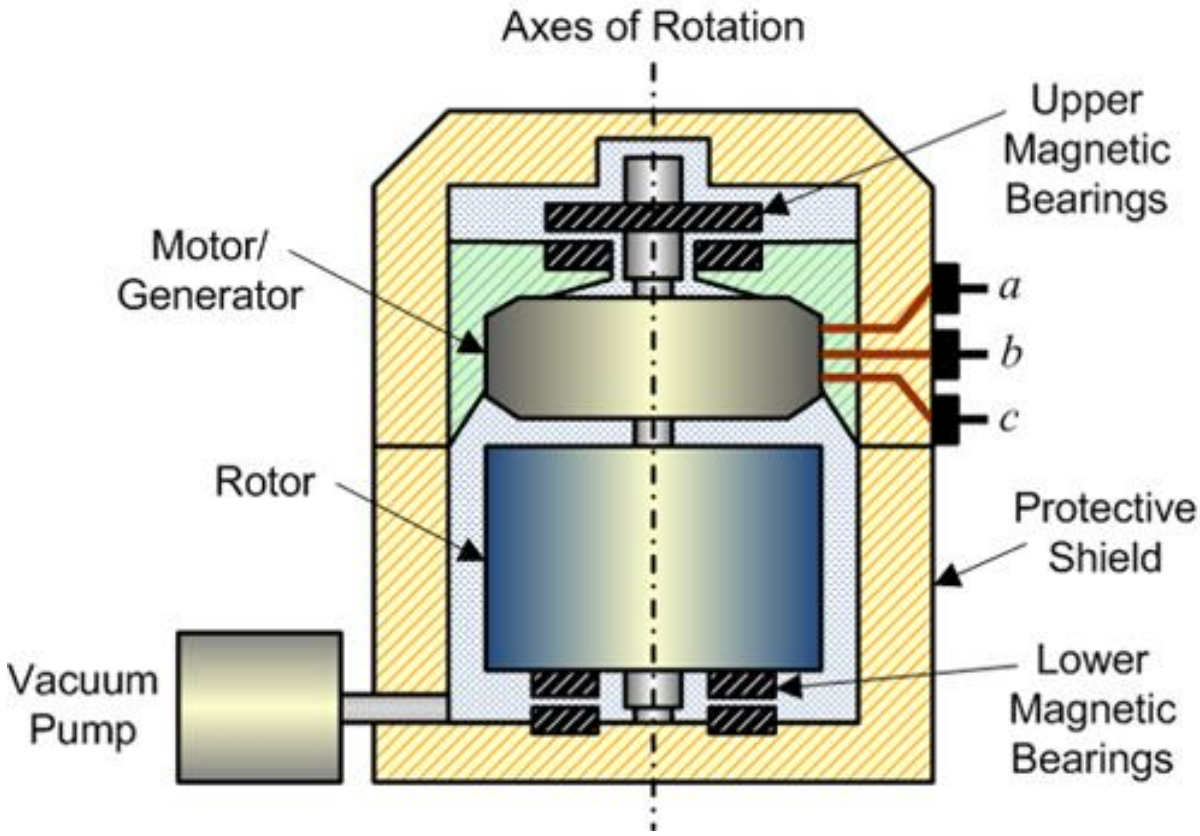

Figure 1. 4 Flywheel Energy Storage [89]

1.3 Electrochemical Energy Storage Technologies

Electrochemical energy storage includes all categories of secondary batteries; such as, stationary batteries, supercapacitors, regenerative fuel cells and rechargeable metal−air batteries. Various studies have been published that compared these different options of electrochemical energy storage systems [21, 31, 52, 90-96]. See table 1.1 for the analysis of these commercially available electrochemical energy storage options.

Chemical Reviews						
Technology	Typical Power (MW)	Discharge Time	Storage Capacity Cost ($/kWh)	Lifetime (Cycle/Years)	Efficiency (%)	Drawbacks
Supercapacitors	0.25	<1 min	500−3000	500000/20	>90	Explosion hazard, low energy density, and cost
Regenerative Fuel Cells with Hydrogen Storage	10[a]	>5 h		2010/13	40−50	Low-density storage, high cost, and safety
Lead-Acid Batteries	0.5−20	3−5 h	65−120	1000−1200/3−4	70−80	Low energy density, short lifetime, and temperature sensitive
Li-ion batteries		1−5 h	400−600	750−3000/6−8	80−90	Cost, safety, short lifetime, self-discharge, temperature sensitive
NAS battery Sodium–sulfur battery	0.25−1	6−8 h	360−500	2500−4500/6−12	87	Cost, high-temperature operation, and safety
Vanadium Redox Flow Battery	0.5−12	10 h	150−2500	500−2000/10	70	Low energy density

Table 1. 1 Electrochemical Energy Storage Technologies for Stationary Applications [97, 98]

Supercapacitors have excellent efficiency, power capability, including cycle life but of very low energy density and costly. Through electrostatic interaction, a charge can be stored in electric double layer and supercapacitors capacitors, at electrodes interfaces and within the double layer of highly porous carbon material and nonaqueous or aqueous electrolyte. Additionally, electrochemically active species may be observed on electrodes such as metal oxides, of fast reversible redox transformations [99]. The most advanced and broad categories

of electrochemical energy storage systems are the secondary batteries of electroactive materials with stationary electrodes. See figure 1.5. Secondary batteries that are widely used are the nickel–metal hydride battery, Sodium–sulfur battery, the nickel-cadmium battery, lithium-ion polymer battery, lead-acid battery, and lithium-ion battery [100]. These batteries have disadvantages such as safety issue, high cost, and short lifetime.

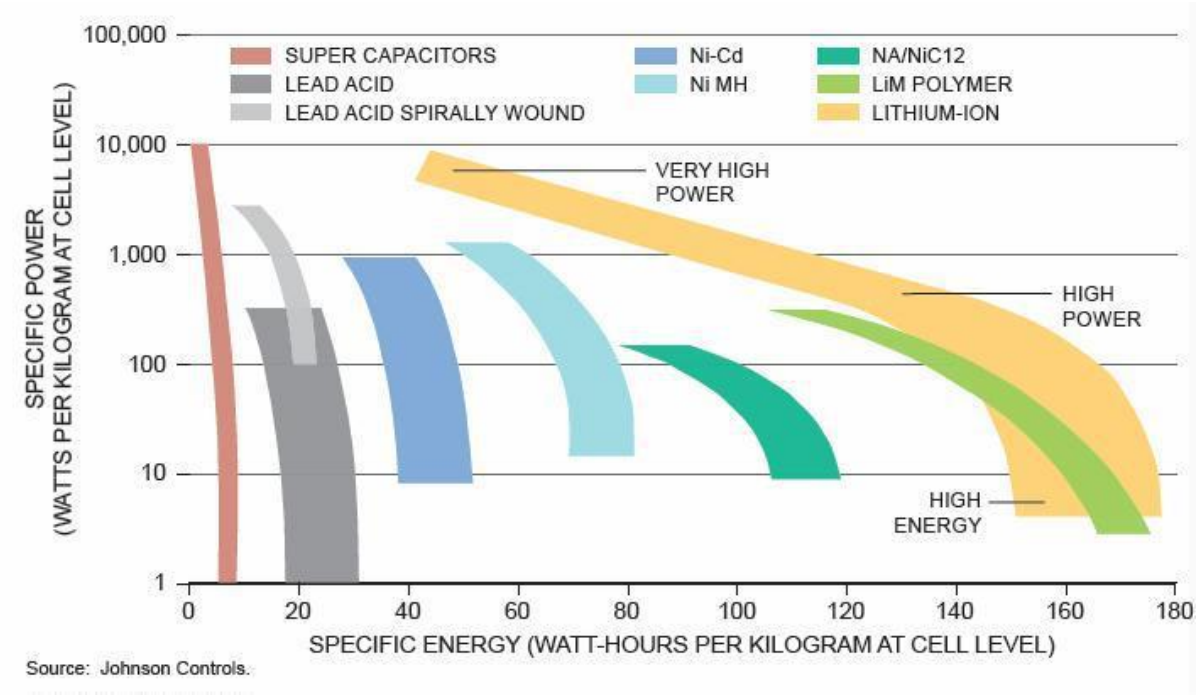

Figure 1. 5 Ragone Plot of Stationary Electrodes from Traditional Batteries [101]

1.3.1 Supercapacitor Energy Storage (SCES)

Figure 1.6 shows how SCES (supercapacitors energy storage) are used in batteries cells and the charge and discharge voltage that can be expected from these devices. Energy storage elements such as supercapacitors are used widely in high-power applications. Electrochemical capacitors of the double layer (EDLC) are known as ultracapacitors or supercapacitors. supercapacitor as energy storage devices can be integrated and used in conjunction with other storing energy devices for enhancing the stability of grids. An overall higher energy rating can be produced by charging supercapacitors energy storage systems instead of discharging the

system. This can make both the capacitance with the derating coefficient to improve during charge.

Figure 1. 6 In-Lab Grid Electrochemical Supercapacitors for Energy Storage System [102]

1.3.2 **Reversible Fuel cell**

As expressed in equation 1 (regenerative fuel cell reverse function), in hydrogen−air fuel cells, gaseous fuel and oxidant are consumed individually at the anode and cathode respectively to generate electricity. A reversible fuel cell; such as a regenerative fuel cell, is where water can be reconverted back into reactants (hydrogen and oxygen) via one possible methods; such as; thermal, chemical, and electrical for energy storage applications [103]. Compared to batteries, regenerative fuel cells have higher energy density but lower round-trip efficiency and higher cost. Notwithstanding, regenerative fuel cells become more cost-effective than stationary batteries as the storage time exceeds three days.

Equation 1: regenerative fuel cell reverse function in hydrogen−air fuel cells, gaseous fuel and oxidant

	$H_2 + 1/2O_2 \rightleftarrows H_2O\ (E^0 = 1.23V)$	(1)

A rechargeable lithium or zinc metal-air battery can be considered as a regenerated fuel cell if the anode has solid active materials and of an aqueous liquid as described in equation 2: the reaction of lithium metal with water and oxygen to generate a regenerated fuel cell of 3.0V) and equation 3: Lithium reaction with oxygen to form a lithium oxide regenerative fuel cell of 2.96V or nonaqueous electrolyte respectively as presented in equation 4: zinc reaction with oxygen to generate a zinc-oxide regenerative fuel cell of 1.59V.

Despite that lithium-air and zinc-air batteries energy densities are (1700 Wh/kg) and (700 Wh/kg), the values are still remarkably less by comparing them to the theoretical energy density of Li-O2 coupled and compared to that of gasoline (12.2 kW/Kg) [104-107]. Moreover, the values are still higher than the required energy density for Li-ion batteries. Notwithstanding, all electrochemical cells with oxygen cathode suffer from inactive kinetics, which results in high cell overpotentials and low energy efficiency. Besides, metal−air batteries suffer from low lifetime and poisoning of the electrolyte with CO_2 from air.

Equation 2: Reaction of lithium metal with water and oxygen to generate a regenerated fuel cell of 3.0V

$4Li + 6H_2O + O_2 \rightleftarrows 4(LiOH.H_2O)$ $(E^0 = 3.0V \text{ in } LiOH)$	(2)

Equation 3: Lithium reaction with oxygen to form a lithium oxide regenerative fuel cell of 2.96V

$2Li + O_2 \rightleftarrows Li_2O_2\ (E^0 = 2.96V)$	(3)

Equation 4: Zinc reaction with oxygen to generate a zinc-oxide regenerative fuel cell of 1.59V

$2Zn + O_2 \rightleftarrows 2ZnO\ (E^0 = 1.59V)$	(4)

1.4 Introduction to Redox Flow Batteries

Figure 1.7 represents a schematic diagram of a redox flow battery system. Redox flow batteries are energy storage technology with efficient potentials to store chemical energy into electrical energy by converting it and releasing it in a controlled way when needed to generate electricity. Redox flow batteries have a membrane and two electrodes, and their electrolytes are stored in separate tanks and flow into the cell stack with the help of pumps on the anode-side and cathode-side. To acquire more energy storage capacity for a redox battery system the electroactive species concentration or the volume of the electrolyte can be increased. This serves as a significant advantage over other battery-based energy storage systems. Issues of cost per kWh stored is the primary driver for electrochemical energy storage. Because currently, all electrochemical energy storage systems are costly to implement on a large-scale for major automotive and stationary applications [108].

As with all batteries, in redox flow batteries, the reduction process during charge occurs at the cell anode-sides incorporating negative electrodes where transferring of electrons from the cell cathode-side occurs via the external circuit. Ions complete the circuit in the cell via the electrolyte, which may contain a microporous or ion conducting membrane. The oxidation process occurs at the cathode-side during charge, completing the full cell reaction. During discharge the reactions are reversed. One of the redox flow batteries electroactive materials may be a flowing gas. Some batteries are connected in series using a bipolar electrode designs or parallel, forming a pack.

Essentially, redox flow batteries can be considered to be regenerative fuel cells because these batteries systems are similar to fuel cells due to both cases fuel and oxidant that are stored externally and supplies to such electrochemical cells on demand [109]. Redox flow batteries are relatively new technologies compared to other more well-developed technologies such as lead-acid batteries, nickel-cadmium batteries, and Li-ion secondary batteries [110]. Redox flow batteries are not considered to be suitable for mobile applications due since these batteries' cells have low energy density. This is despite some of their advantages decoupling of storage and conversion, power sizes, energy, and the possibility of rapid mechanical charging (for example by refilling electrodes with granular metal or fresh electrolyte) [111].

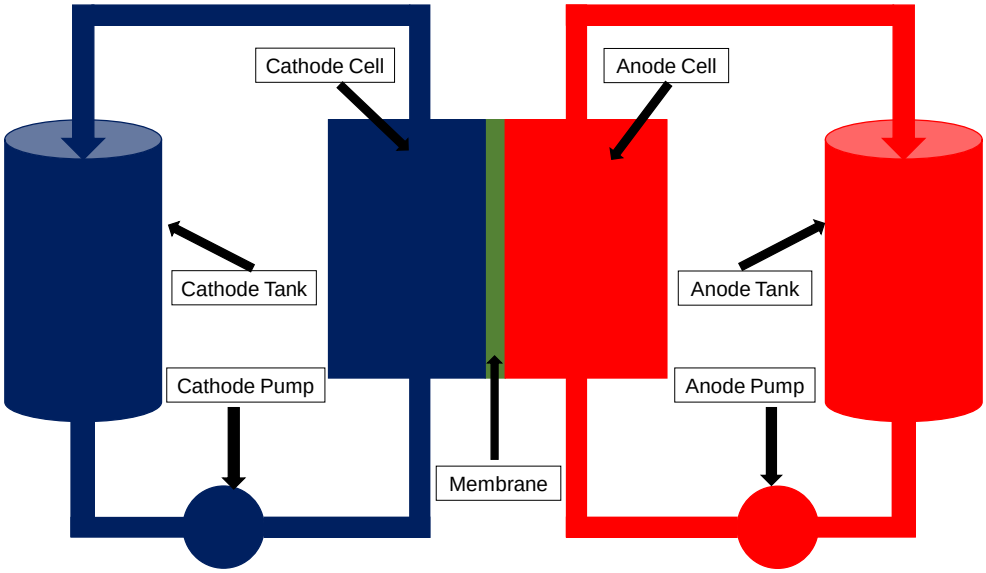

Figure 1. 7 A typical example of a Redox Flow Battery

1.4.1 History of Redox Flow Batteries

Roughly 60 years back before 1950's, the first flow cell concept that was proposed by Posner on the Sn^{II}/Sn^{IV} (metal Stannous compounds) couple in combination with Br^{-}/Br_2 and later the Fe^{II}/Fe^{III} couple as the cathode. The invented flow cell was disregarded for many years and later reconsidered between 1950's and 1970's. Around the same time, Oei reported, regarding

a cell using VO_2^+/VO^{2+} at the cathode but with alternative couples at the anodes (Sn^{II}/Sn^{IV}, Fe^{II}/Fe^{III}, and Cu^0/Cu^{II} redox couples) [112]. From this cell, the maximum power output was 8.1 mW/cm^3 on graphite felt electrode [113]. Thaller later invented the first practical flow battery using Cr^{II}/Cr^{III} and Fe^{II}/Fe^{III} redox couples. The battery cell was the most common all liquid flow battery type [95, 114].

1.4.2 Classifications of Redox Flow Batteries

Redox flow batteries can be classified according to the electrode and electrolyte phases as numbered and explained below. Fig. 1.8 illustrates the reactions of the electrodes of these three illustrative examples: (a) all-vanadium, (b) lead-lead-dioxide and (c) hybrid zinc-cerium redox flow batteries (RFB)s [115-121]. The first dissolved group of electrolyte solution has reactants and products as their redox couples in solution; and the second redox couples group consists of both solid species when charged. While at one half-cell, some hybrid RFB couples involve solid (zinc, Fe, metal oxide such as PbO_2) or gaseous species that are involved in one of the electrode reactions [122-131].

1. The standard (or true) redox flow batteries (e.g., the all-vanadium redox flow batteries). On these kind of batteries electrodes, there will be no changes to the phases and no solubility of the electroactive species. The incorporated electrodes electrocatalytic surfaces are effective and the energy is stored in the electrolyte. The batteries kinetic is sluggish and the cross mixing of the half-cell electrolyte with the issue of instability of reactants are also the additional common problem.
2. Regarding the type 1 hybrid redox flow batteries, some of the electroactive species phase are in a solid or gaseous state based on the electrode reactions. The storage capacity can be limited in the process of electrodeposition at an electrode; regardless of their well demonstrated feasibility by the commercial Zn-Br redox flow batteries [132] The detachment of solid-dendrites can make these kinds of systems to be prone to blockage and due to the inlet and exit effects and edge effect of incorporated electrodes [133]. Hybrid systems such as Zn-Ce and Zn-Br can encounter slow self-discharge due to deposit corrosion. Furthermore, achieving compact deposit can be difficult in the event of mixing and in the condition of mass transport This category includes half-

fuel redox flow batteries of half-cell and membrane blockage that can be suffering from diffusion of liquid to the gas [134, 135].

3. The type 2 hybrid Redox flow batteries (soluble lead RFB) can encounter phase change at both electrodes surface in the cell during charge and or discharge. At the positive electrode, Lead ions are reversibly in an acidic solution and can be converted to lead-oxide (PbO2) during charge including encountering metallic lead at the negative electrode. Stored energy is stored in the two electrodes as deposits with limiting the capacity due to the inter-electrode volume [133].

Other classifications can be based on the cell design, the composition of electrolytes (aqueous or non-aqueous) and other features such as electrolytes phases and types of membranes.

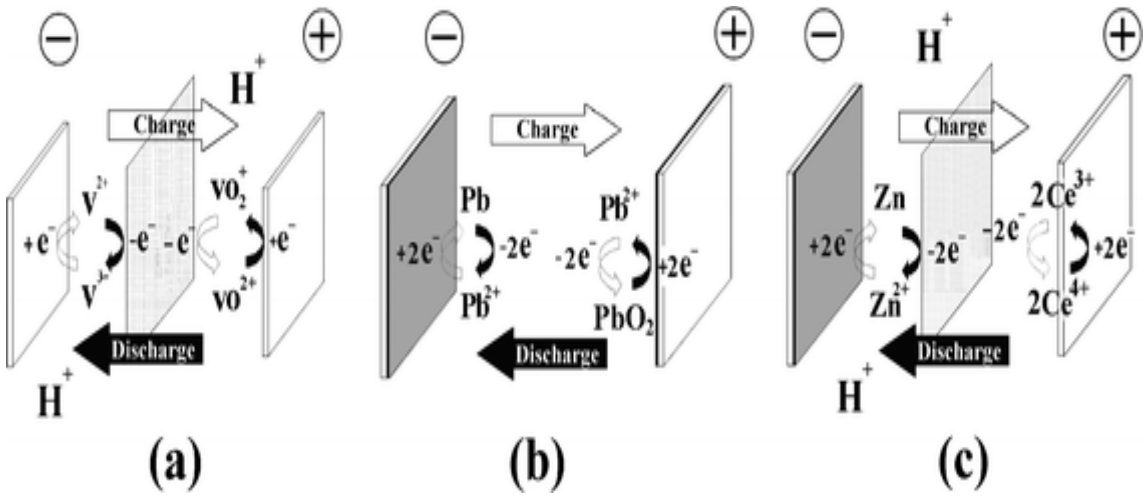

Figure 1. 8: Types of RFB, according to the nature of energy storage. Energy is stored (a) in the electrolytes, (b) in the active material within the electrodes and (c) hybrid in both electrode and electrolyte phases) [108].

1.4.3 All Liquid Aqueous Flow Batteries

1.4.3.1 All-Vanadium Redox Flow Battery

Figure 1.9 has presented a vanadium redox flow battery with its redox reaction. The most advanced and studied RFB is the all-vanadium redox battery (VRFB). It was invented by

Skyllas-Kazacos et al.; at the University of New South Wales (Australia) in 1986 [136-138]. The chemistries of these batteries are highly reversible and facile. They are based on the cell anode-side and cathode-side as Vanadium^{II}/ Vanadium^{III} and Vanadium^{IV}/ Vanadium^{V} respectively. Vanadium flow batteries use the multiple valence states of just vanadium to store and release charges. The loss of one electron in vanadium three can be produce with an electrochemical cell (Ecell) of -0.255 volts. Vanadium can exist as several ions of different charges in solution, V($^{2+}$,$^{3+}$,$^{4+}$,$^{5+}$), each having different numbers of electrons around the nucleus.

Fewer electrons gives a higher positive charge. Energy is stored by providing electrons making V ($^{2+}$,$^{3+}$), and energy is released by losing electrons to form V($^{4+}$,$^{5+}$). In vanadium batteries cells, sulfuric acid boosts performance and maintains the pH values required. The concentration of the acid is up to four molar, very conductive and leads to the reaction at the cathode being mix-controlled for charge transfer and diffusion steps.

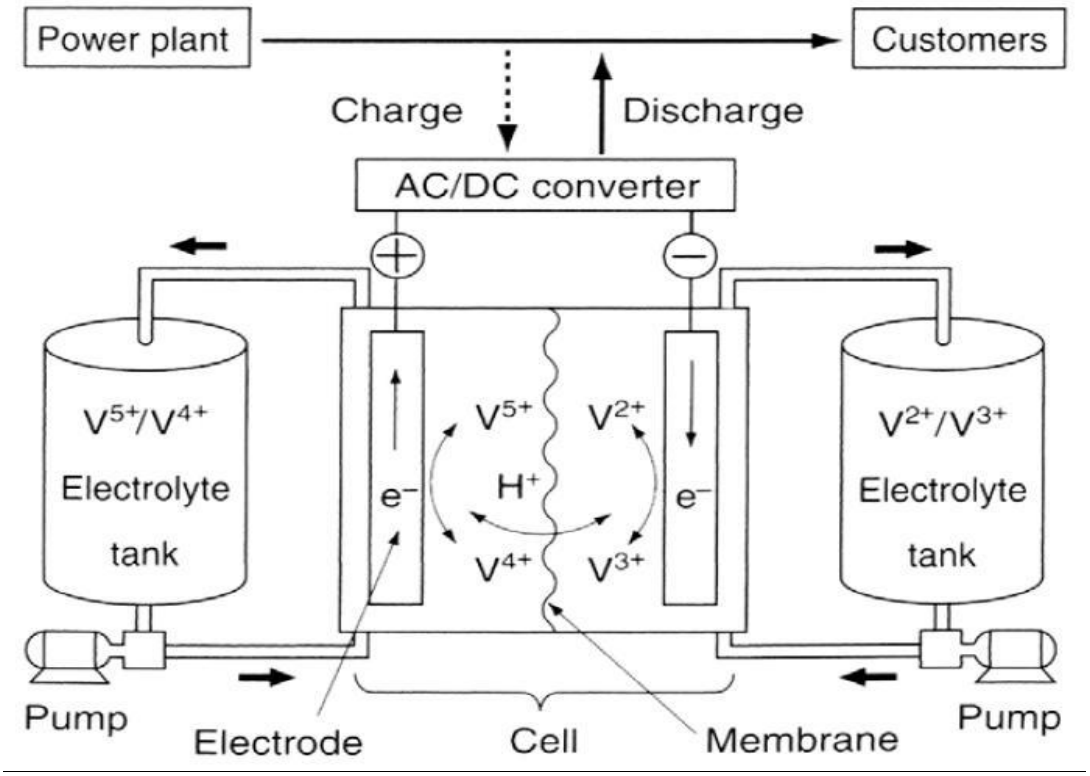

Figure 1. 9: Schematic of the functioning of a Vanadium Redox Flow Battery (VRFB) system [139].

The solubility of the vanadium species determines the theoretical energy density of the battery cell (60.5 Wh/kg). To enhance the charge transfer reactions and active electrode surface area of all-vanadium RFB, material such as carbon electrodes, various electrocatalysts like platinum group of metals (PGM metal catalysts), such as $CuPt_3$, non-PGM oxides like Mn_3O_4 and WO_3 have been proposed [140-145]. All-vanadium redox flow batteries cells are prone to precipitation of V_2O_5 at high temperatures; which limits their energy density and operating range. In all-vanadium cells, maintaining the cathodic concentration is possible at a temperature below 40°C with a level of 3 M in 6 M sulphate/ bisulphate (sodium bisulphate). The potential solution to the problem of precipitation of oxide could be stabilized efficiently in all the four vanadium ion (V^{2+}, V^{3+}, VO^{2+}), and VO_2^+ and could be stabilized efficiently with a mixture of poly (acrylic acid) and methanesulfonic in 1.8 moles of an electrolyte solutions [146].

Vanadium cells electrolyte can be preserved, by adding various additives; such as ammonium oxalate [147]. The combination of mixed acids such as (H_2SO_4 and HCl) has been previously used to promote the solubility of a vanadium cathode-side electrolyte and its thermal stability. By using DFT, (density functional theory) to model [148] Vanadium and [149] Chlorine, NMR can show vanadium(V) cation at higher concentrations (≥1.75 M) and existence as a di-nuclear, chlorine-bonded $(V_2O_3Cl_2\cdot\ 6H_2O)^{2+}$ complex by assuming that such complex is resistant to deprotonation reaction. In V_2O_5 precipitation, this serves as the initial step [150]. Therefore, introducing sulfate−chloride (NaCl) to mix electrolytes will improve vanadium (V) solubility up to 2.5 M, increasing the energy capacity to 70% over the pure sulfate system and expanding the operational temperature range to −5 to +50°C [151].

The use of advanced electrode materials and improving electrodes design can be used to enhanced significantly (all-vanadium) redox flow batteries. For example microwave treatments at 400 °C can be used to treat graphite felt electrode to improve the efficiency, electrocatalytic activity and increase the concentration of hydrophilic OH-groups improving wetting [140]. The cathode surface area can be made flexible and increased to around 350 cm^2/cm^3 with carbon nanofibers compared to commonly used carbon felt [152]. Flow fields can be added to vanadium redox flow batteries to increase the voltage discharge, and increase the energy efficiency by 5% and the pressure drop by 5% [153]. Improving a cell design has been shown to increase the peak power and density up to 500 mW/cm^2 [154]. These improvements can be used in electrode and cell design for different flow batteries cells chemistries. The crossover of

electrochemically active species can reduce a cell efficiency and may require replacement of the electrolyte periodically. Therefore, the development of a selective ionically conductive membrane; is of great importance. Sol−gel-derived Nafion/ SiO_2 hybrid membrane lowers vanadium ions permeability and increases Coulombic and energy efficiencies compared to pure Nafion membrane [155].

RFBs can achieve a Coulombic efficiency of 97% by using the number of silica gels inside the pores to control the poly (ether sulfone) (PES)/silica composite porous membranes and the pore size distribution [156]. Higher efficiency with high mechanical strength can be achieved via graphene embedded membranes of sulfonated poly ether-ether ketone (SPEEK) or by using short carboxylic acid group functionalised multiwalled carbon nanotubes [157]. This has been shown to result in having 4-7% higher Coulombic efficiency and mechanical strength whilst demonstrating a decreased permeability of vanadium ions. Similar effect can be achieved if carboxylic acid groups are grafted to the Sulfonated poly (ether ether ketone) (**SPEEK**) backbone [158]. In vanadium redox flow batteries, a porous polytetrafluoroethylene (PTFE) substrate with pores filled with a Sulfonated poly (ether ether ketone) **SPEEK**−graphene oxide composite has demonstrated stable performance for 1200 cycles [159]. The use of a double layer membrane made of ultrathin Nafion film on the PES/ SPEEK porous membranes have been shown to support very high ion selectivity and energy efficiency (86.5% at 80 mA/cm^2) [160]. A further option is to use an anion exchange membrane. These are typically made of quaternary ammonium-functionalized poly (fluorenyl ether) and can be seen to increase VRFB coulombic efficiency to near 100% since the permeation of VO^{2+} is shown to be extremely low [161, 162]. This however, requires low current densities (<60 mA/cm^2) to achieve this [163-169].The model results can serve as a guideline to design and optimize practical VRFB and apply the technique to other RFB types. Many tests that have been carried out on VRFBs in the past and it is still encouraging that the following companies listed below are active in the field.

1. Sumitomo Electric,
2. American Vanadium (http://www. americanvanadium.com),
3. UniEnergy Technologies (www.uetechnologies.com),
4. Cellenium (www.vanadiumbattery.com),
5. Ashlawn Energy (http://www.ashlawnenergy.com),
6. Prudent Energy (former VRB Power Systems) (www.pdenergy.com),

7. REDT (http://www.redtenergy.com),
8. Gildemeister AG (http://energy. gildemeister.com),
9. WattJoule (www.wattjoule. com), and
10. The developed novel technology at PNNL that was licensed to Imergy, formerly known as Deeya (www.imergypower.com) [108, 170].

Presently, Sumitomo Electric Industries in Japan are still planning to carry out an installation of a 60MWh VRFB plant. This is in addition to those currently installed from tens of kilowatt-hour to seven megawatt hour [171]. The issues of high costs are the major problem the commercial uptake for VRFB cells systems. A cost analysis of a 300-kWh unit showed that the vanadium-related electrolyte cost is approximately 62% of the total cost [172]. Vanadium as an expensive metal has high requirement for its purity; which has made the material cost to be very high [173]. It has been shown that the operating temperature range of the VRFB and the cost can be improved by changing the cathode chemistry to an alternative. PNNL (pacific North-western National Lab) demonstrated that the Fe(II)/Fe(III) was a suitable option though this reduces the cell voltage [174-176].

1.4.4 **Iron-Chromium RFB**

In 1970, Thaller introduced the iron−chromium flow batteries chemistries in (figure 1.10) [177] and National Aeronautics and Space Administration (NASA) later improved the battery cell in the 1980s [178, 179] with the University of Alicante in the 1990s [94, 180]. These redox couples; Fe^{II}/Fe^{III} and Cr^{II}/Cr^{III}, are the positive and negative electrode reaction respectively which take place in hydrochloric acid. An ion-selective membrane is required to pass either protons (and small cations) or anions. However, cross-contamination will never be prevented and represents a loss in performance. The open circuit voltage (OCV) changes along with the state of charge (SoC), because of the differences between the Cr(III) as the hydrated complexes of Cr(III) during various stages [181].

The development of catalysts to enhance the electrode performance is still a research topic since particularly the chromium reaction has slow kinetics. Promising catalysts include bismuth-lead and bismuth [182]. The addition of (ethylenediaminetetra-acetic acid, EDTA, to chromium electrolytes aids the chromium anolyte stability, but reduces the anodic kinetics of

such cells [183]. The addition of bismuth to either solution reduces the polarization of the cell by almost a factor of 2. The need for these additions can be seen as a disadvantage to this battery type compared to others including the cell studied in this work. In California, EnerVault (http://enervault.com) have recently installed a 250 kW/1MWh battery base on this chemistry, and Imergy another commercial developer, had started developing iron-chromium systems of 5 kW/ 30 kWh RFB, but the company have recently diverted their attention towards developing VRFB systems.

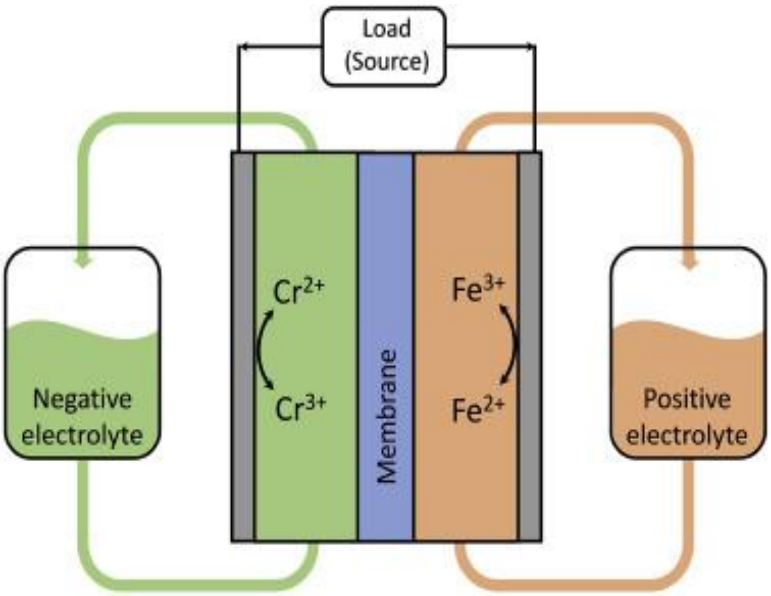

Figure 1. 10 (a) Schematic of an iron-chromium RFB [184]

1.4.5 **Polysulfide-Bromine RFB**

Polysulfide-Bromine RFB (PSRFB) was invented in 1984 as shown in figure 1.11 with the chemistry as described in equation 5. [185]. The chemistry is the oxidation of bromide to bromine and the reduction of polysulfides during charge of a bromine-based cathode and a polysulfide-based anode. There is a particular interest in this type of battery for the work reported in this thesis as the cathode has reasonable similarity.

Equation 5: (Polysulfide-Bromine Chemistry)

	$2NaBr + (x-1)Na_2S_x \rightleftarrows Br_2 + xNa_2S_{x-1}$	(5)

In this flow cell, the cathode-side contains bromine in the form of polybromide anions $Br^-_{(2n+1)}$ where $n =$ 1-6 [186] Because anode and cathode hold separate species, polysulfide-Bromine RFB cells suffer from active species crossing over via the ion-exchange membrane. In PSBFB as with all flow batteries electrode surface area and stability are important, it has been shown that by replacing open pore nickel foam with a carbon in the anode increases the energy efficiency of the cell by 77% at 40 mA/ cm^2. For the cathode the use of carbon felt has showed a promising result and when coupled with a nickel anode increases the coulombic and voltage efficiency. However, self-discharge due to precipitating sulfur building up within micro-pores of the Nafion membrane was a problem. [187].

To aid the electrode kinetics, tungsten disulfide, (WS_2) has been recommended as an electrocatalyst for PSBFB processes in aqueous alkaline solutions for improving the cell efficiency [188]. The fabrication of practical Polysulphide-Bromine flow batteries (PSBFB) was piloted by the United Kingdom, the company had a demonstration plant, with an energy storage capacity of 120 megawatt-hours at a discharge time of 8 hours. However, in 2003, the project was stopped before completion by the owner of RWE, a German utilities group. The modelling of a PSRFB system by Scamman et al according to research, [189, 190] have demonstrated that the current state of art in the electrode design and associated kinetics on how PSRFB are unlikely to be economically viable without significant improvements [190].

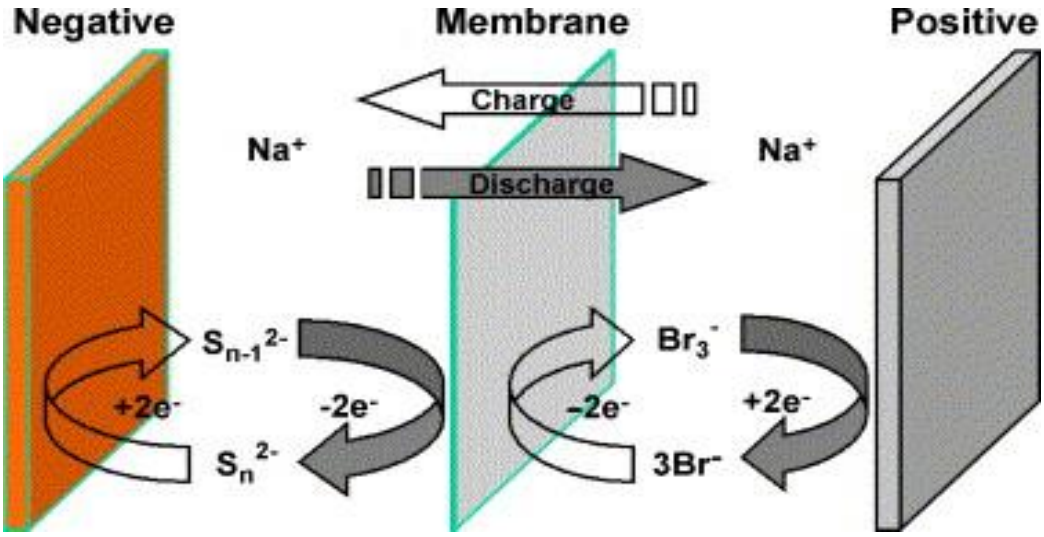

Figure 1. 11:The principle of sodium polysulfide/bromine RFB [191]

1.4.6 Soluble Metal-Bromine RFB

The vanadium polyhalide RFB employing VCl_2 and VCl_3 as the anode-couple and $Br^-/ClBr_2$ has been demonstrated. This cell which uses a Nafion membrane was able to achieve coulombic and voltage efficiencies of 83% and 80%, respectively [192]. The titanium polyhalide cell which replaces the V with Ti on the anode-side has been investigated. Which was attractive due to a significant reduction to the cost of Ti compared to the vanadium cost. However, the voltage efficiency of the cell are low because of ohmic losses and there are stability issues with the anode species by forming insoluble precipitates [193]. A chromium−bromine RFB with an acidic chloride-based anode, and a polybromide cathode has been patented [194]. In the patent, it is claimed that the cell voltage and energy density of the invented cell can be increased up to 24 Wh/L by adding phosphoric acid, citric acid, and EDTA (Ethylenediaminetetraacetic acid) to the anode electrolyte for the formation of chromium chelate complexes of more negative redox potentials (up to −1.0 V vs NHE) [195].

1.4.7 Quinone/ hydroquinone RFB with Aqueous Electrolyte

Organic electroactive materials in RFB can possibly offer low-cost, low crossover and higher solubility in electrolytes. Figure 1.12 illustrates the quinone/ hydroquinone cell as an example of an organic RFB which utilizes an aqueous electrolyte.

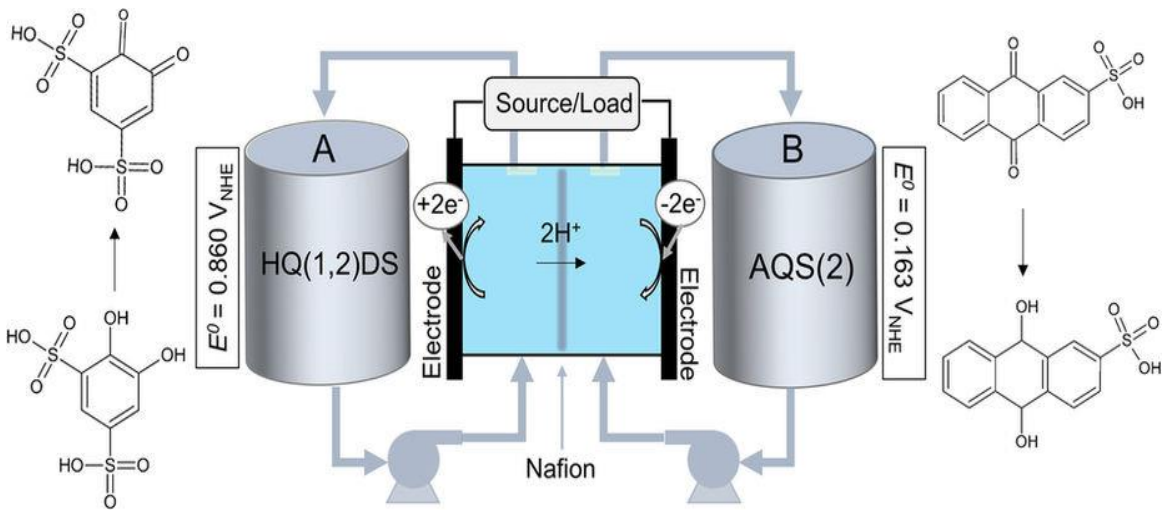

Figure 1. 12 Identifies dissolved Quinone species in 1 M H_2SO_4, of a cell potential 0.7 V. with stored two electrons During charging with 2 H^+ been exchanged through a Nafion membrane [196]

The reversible quinone/ hydroquinone couples were initially investigated as anolyte material for redox mediated fuel cells and a catholyte material for rechargeable lithium batteries [197-199]. Currently, redox couples such as quinones are being considered for RFB; as promising active materials for both catholyte and anolyte. The materials can demonstrate two sequential one electron reductions in an aprotic solvent (solvent containing a labile H^+). In aqueous solutions they undergo a fast two-electron reduction with or without transferring of the proton though this is dependent on the pH of the solution [200].

A single-flow RFB cell utilizing water plus insoluble tetrachloro-pbenzoquinone (chloranil) as the catholyte material, Cd/ $CdSO_4$ as the anolyte material and with an H_2SO_4–$(NH_4)_2SO_4$–$CdSO_4$ electrolyte have been reported. The observed average coulombic efficiency was 99% and energy efficiency of 82% when running the battery cell for over 100 cycles at 10 mA/cm^2 current density [201]. In later work the authors achieved cells with a voltage of 0.7V to 1.0V by combining soluble sulfonated quinones; such as tiron (5,6 dioxocyclohexa-1,3-diene-1,3-disulfonic acid disodium salt) in H_2SO_4 as the catholyte and Pb/ $PbSO_4$ as the anode. They reported energy efficiencies of 70% with a small capacity loss during 100 cycles at 10 mA/cm^2[202]. An aqueous RFB of bromine/ bromide as the catholyte and an organic anolyte of sulfonated anthraquinones has been demonstrated to give very high-power densities, that can be up to 0.6 W/cm^2 at 1.3 A/cm^2. [203].

Authors who investigate these classes of RFB cells with fast-redox reactions based on both anolyte and catholyte state that the cells do not require an electrocatalyst if a kinetic rate constant; of k_0 9,10-anthraquinone-2,7-disulfonic acid (AQDS) reduction in the acidic media can be 7.2×10^{-3} cm/s; which is higher than other redox active species used in RFB [203], [96]. If this is possible it is a great benefit as it can reduce significantly the cost of the RFB. Authors investigating anthraquinone-2-sulfonic acid (AQS) for the anode and 1,2-benzoquinone-3,5, -disulfonic acid (BQDS) for the cathode demonstrated this. This is partly attributed to the formation of intramolecular hydrogen bonds [204].

Generally, it has been shown that these RFBs can be cycled for fifty cycles and still have a retention capacity of approximately 99% per cycle. The crossover of bulky and negatively charged salt or ester should be minimal, however depending on the cathode chemistry, the issue of cross over can still be an issue [205]. The power density of these cells can decrease considerably below 50% SoC however the use of organic redox materials to increase the solubility and tuning the electrochemical properties can help improve this [205].

1.4.8 Organic Regenerative Fuel Cells

An organic regenerative fuel cell was developed at the National Institute of Advanced Industrial Science and Technology (NIAIST) [206]. The direct use of organic hydrides as an anode active material in RFB was then proposed and then studied by DOE-funded GE-led Energy Frontier Research Center for Electrocatalysis, Transport Phenomena, and materials [207, 208]. Hydrocarbons and alcohol serve as organic hydrides, hydrogen carriers, creator of stable protons, organic molecules which constitute the anode part of the RFB. See equation 6 for the anodic reaction in an organic regenerative fuel cells and equation 7 for the full cell reaction with an air cathode utilizing oxygen.

Equation 6: Anodic reaction in an organic regenerative fuel cell

	$LH_n \rightleftarrows L + nH^+ + ne^-$	(6)

Equation 7: Full cell reaction with an air cathode utilizing oxygen.

	$\mathrm{LH_n} + \frac{\mathrm{n}}{4} O_2 \rightleftarrows \mathrm{L} + \frac{n}{2} \mathrm{H_2O}$	(7)

Organic regenerative fuel cell's energy density can be lower than that of traditional fuel cells due to the mass of the organic components in the anode side. Theoretically, the energy densities for practical variants are between 1600 to 2200 Wh/L, compared to liquid hydrogen fuel cells (2540 Wh/L). However, the organic fuel cells theoretical efficiency; which are higher than hydrogen fuel cells energy efficiency (93% to 95% against 83%); and so, can later result to higher round-trip efficiency compared to a reversible hydrogen / oxygen fuel cell [209].

1.4.9 **All-Uranium/ All Neptunium**

Yamamura et al proposed all-uranium [210-212] and all-neptunium [213-215]. Redox flow batteries (RFB) based on (equation 8 and equation 9) are of nonaqueous solvents (dimethylformamide (DMF) and propylene carbonate). The all-uranium RFB chemical reaction in nonaqueous solvents dimethylformamide (DMF) is displayed in equation 8 and equation 9 has displayed the all-neptunium RFB in nonaqueous solvents propylene carbonate. Uranium and neptunium cations can both be stabilized by β-diketonate, and polyketonate ions and their solubility can be up to 0.8 M for MVI and 0.4 M for MIV. The open circuit voltage of such cell is usually approximated to be 1V, whereas in aqueous solutions the open circuit voltage will be much lower (0.68 V for U)

Equation 8: All-uranium RFB chemical reaction nonaqueous solvents dimethylformamide

	$\mathrm{MO_2^{2+}} + \mathrm{e^-} \rightleftarrows \mathrm{MO_2^+}\ (\mathrm{M = U, N_p})$	(8)

Equation 9: All-neptunium RFB in nonaqueous solvents propylene carbonate

	$M^{4+} + e^- \rightleftarrows M^{3+}\ (M = U, N_p)$	(9)

Uranyl cations that are identical in structures support a fast transfer of electron in the cathode-side. [174]. The redox reaction of neptunium on a plastic-formed carbon electrode is approximately two orders of magnitude faster than the similar reactions of vanadium ions [215]. However, such reaction will make both uranium and neptunium RFB energy efficiency to be 98% and 99% respectively at 70 mA/cm^2; and remarkably higher than that for the all chemical VRFB [108, 214] Unfortunately, these RFB are not feasible due to the obvious hazard and expense of using radioactive materials in batteries.

Regarding a single-metal RFB using vanadium (III) acetylacetonate in acetonitrile with NEt_4BF_4 as a supporting electrolyte has been proposed [216]. This can achieve high cell voltage of 2.2 V but a low coulombic efficiency of 50% [217]. The degradation of the non-aqueous acetylacetonate vanadium RFB due to an inert surface layer was formed of oxovanadium species and thereby coating the cathode [218]. Better solubility of active materials in the electrolyte solution can be achieved if it has a low molar volume and a high Hansen polarity for conductivity [219]. Acetonitrile (CH_3CN), can demonstrate the best conductivity but it has high volatility and it is moderately toxic which make its use more complex.

1.4.10 **Nickle-Iron RFB**

It is possible that redox flow batteries (RFB) can show a stable performance during the first 100 cycles and a stabilized performance by running these cells with propylene carbonate solutions of tris (2,2′bipyridine) nickel (II) tetrafluoroborate in anolyte, and tris (2,2′bipyridine) iron(II) tetrafluoroborate in catholyte. Such cells under these operating conditions can show a cell voltage of 2.2V, first Coulombic and energy efficiencies of 81.8% and 90.4% respectively [220]. The replacement of bipyridyl ions in these complexes by phenanthroline and of the solvent with gamma-butyrolactone has been shown to increase the cell OCV to 2.4 V and yield an average energy efficiency of 81.6% [221]. Ni-complex (nickel (II) complexes) with multidentate ions, (nickel (II)-1,4,8,11-tetracyclo-tetradecane, (Ni(cyclam)$^{2+}$) have shown promise in terms of reversibility. Adding a phosphoric ester polymer to the Ni and Fe based

electrolytes forms complexes that increase the metal ion solubility by 14%−24% in propylene carbonate [222].

1.4.11 **Cobalt-Iron RFB**

In this redox flow batteries (RFB), $(Co(bpy)_3)^{+/2+}$ (anode) and $(Fe(bpy)_3)^{2+/3+}$ (cathode) redox couples in solutions of NEt_4BF_4 in propylene carbonate using carbon-coated Ni-FeCrAl and Cu metal foam electrodes have exhibited a practical operating voltage higher than 2.1volts with 85% energy efficiency. These cells have demonstrated promising stability with no observable loss of energy efficiency of over 300 cycles [186]. Combinations of $Co(bpy)_3(BF_4)_2/Fe(TMPO)_5(BF_4)_2$ and $Ni(TMPO)_3BF_4/Fe(bpy)_3(BF_4)_2$ as anolyte/ catholyte have been shown to produce an open circuit voltage of 1.95 and 1.12 V, an energy efficiency of 89.5%, and respectively to have theoretical energy densities of 25 and 29 Wh/kg [223].

1.4.12 **All-Copper**

All-copper RFB's that were developed utilises copper chloride anions in a mixture of choline-chloride, and ethylene glycol as electrolyte. The ratio can be (1:2), and be fast [216]. The authors demonstrated a small cell with an open circuit voltage of 0.75V and a low energy efficiency of 52% at 10 mA/cm^2 will make such cell to be ineffective.

1.4.13 **Organic RFB**

Figure 1.13 is a nonaqueous RFB which has been predicted to be one of the emerging large-scale energy storage systems that may overcome the limitation of low energy density due to water break down in aqueous RFB at high voltage [224]. Anthraquinone ($C_{14}H_8O_2$) can be used in a nonaqueous solvent (propylene carbonate) incorporating a lithium metal anode at the cathode-side. This achieves two discharge/charge plateaus of 2.40V and 2.20V, that can be observed as two redox events in cyclic voltammetry [225].

This can be beneficial in understanding the state of charge. Another lithium-based RFB which utilizes organic solutions of such as naphtalene or anthracene in an organic solvent for the anode-side and a quinone of high redox potential such as dichlorodicyanoquinodimethane at the cathode has been demonstrated [226]. A solid Li-ion conductor; such as LISICON can be used as the ion-exchange membrane with the possibility to have high active species concentration up to 10M as the anolyte; that will lead to a theoretical energy density of 1800 Wh/kg [226].

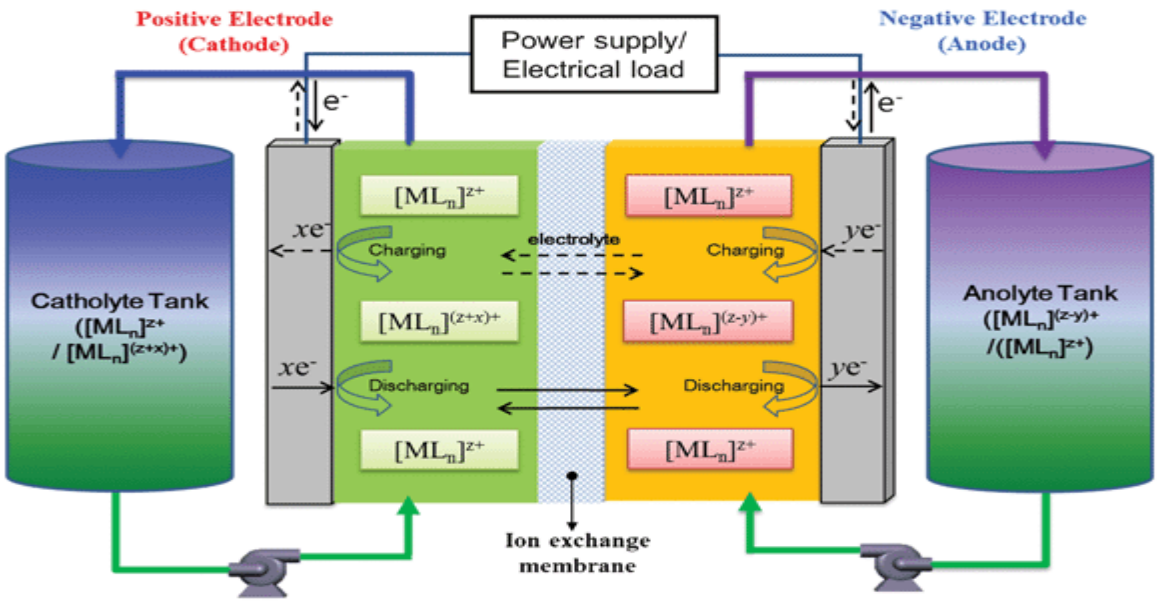

Figure 1. 13 Schematic diagram of a nonaqueous RFB [227]

1.4.14 **Other Inorganic Flow Batteries**

Anderson et al., at Sandia National Laboratory have attempted in the past to combine active materials with a solvent in the form of an electroactive ionic liquid [228, 229]. Anderson et al., observed that it is possible to maintain metal complexes carrying copper and iron cations and other metal with ethanolamine or diethanolamine, and ethyl hexanoate or triflate anions as liquids at ambient temperature. However, this showed in some cases an irreversible electrochemical behaviour as these metal complexes resulted in poor reversibility [228, 229]. Ionic liquids of high molecular weight present an opportunity as RFB electrolytes. Particularly ones based on diethanolamine have proven to be stable but have thus far led only to a single-

digit Wh/kg energy density. The sheer range of options for ionic liquids does present a potentially rich area of research for RFBs but membrane selection, solubility of active species and cost will always be a problem.

1.4.15 **Semisolid Flow Batteries**

Chiang and co-workers proposed the first concept of semisolid RFB that use suspended active materials of flowable conducting suspension as electrolyte [230]. Semisolid RFB's cells are designed to make charged and discharged insoluble active materials possible. This is to overcome the solubility constraint of the active materials. Semisolid RFB of cathode solids like $LiFePO_4/LiPF_6$ in ethylene carbonate−dimethyl carbonate (EC-DMC)/Li with a percentage volume of 12.6% can demonstrate a power density of 328 mW/cm^2, more than the observing Li-ion batteries of stationary electrodes, and energy densities up to 50Wh/kg (67Wh/L). [231]. This is largely due to the enhanced Li ion transport rates in the pumped slurry compared to the static electrode / electrolyte interfaces in the regular Li-ion battery.

An alternative slurry cathode has been demonstrated using $LiTi_2(PO_4)_3$−$LiFePO_4$ [232, 233]**.** Unfortunately these cells so far show high capacity fade and have shown 40% capacity fade in 100 cycles [234]. A nonaqueous lithium Polysulfide RFB of a 1.5% volume Ketjen Black carbon suspension in a 2.5 M lithium polysulfides per 0.5 M LiTFSI catholyte have been shown to be feasible [232, 233]. Generally, all semisolid designs encounter high pump losses due to high viscosity of slurries. This can be improved via using plug flow systems, and an intermittent flow of electrolyte. [234-236].

1.4.16 **Hybrid RFB**

Zinc–bromine batteries are hybrid flow batteries. Zinc bromide solutions is stored in two separate tanks. The batteries solutions are pumped via a reactor and back into the tank as these batteries charge and discharge. Further detail regarding these batteries are provided in section 1.6. However, some single metal flow batteries with metallic anodes are briefly discussed in some section here.

1.4.16.1 Single-Metal Flow Batteries with metallic anodes

In single-metal RFB, a metal during the charging process is electrodeposited on the anode and with the possibility to use of a single electrolyte in both cells. The issue of crossing over via a membrane can be significantly reduced by incorporating the same metal in both anode and cathode. One of the main disadvantages of a single metal redox flow battery (RFB) is the depositing of metals such as zinc on a current collector. Such deposition can result to a limited capacity due to an incomplete discharge. This can possibly be improved by a movable slurry electrolyte for metal electroplating or a fluidized bed (discussed in chapter two). Iron-based, lead-based, and copper-based systems are currently in progress.

1.4.16.2 All-Iron RFB

Hruska and Savinell, proposed in 1981 all-iron RFB overall reaction at 50% SoC with an Ecell of 1.2V. The cell overall reaction, E_0 = 1.2 V is as expressed in equation 10. High theoretical energy density of 76 Wh/L is possible to achieve by introducing chloride salts due to their high solubility. Nevertheless, at a high concentration of iron (II) chloride and iron (III) chloride, the solution electrical resistivity grows sharply, which will limit the practical concentrations. Introducing NH_4Cl and KCl can decrease the electrolyte resistivity [160].

Cells such as the all-iron RFB can perform better if the anodic pH can be adjusted to a value of around one, and the cathode pH is between 3 and 4. The pH difference is possible to maintain by utilizing an AEM that is coupled with $FeCl_4^-$ions. All-iron RFB cells can show coulombic efficiencies of 90%; but with discharge power density of 50 mW/cm^2, at low energy efficiencies of 50% and with the possibility to note during cycling imbalances in the electrolyte that may be hydrogen evolution [237].

Equation 10: All-Iron RFB Overall Reaction (E_0 = 1.2 V)

$3Fe^{2+} \rightleftarrows 2Fe^{3+} + Fe^0$	(10)

The problematic hydrogen evolution will occur at higher cell voltages, and as the anolyte pH rises and leads to precipitation of iron (II) hydroxide, $Fe(OH)_2$. This is a significant issue and represents a loss reaction. In Fe^{II}/ Fe^{III} couple, attempting to improve the electrode kinetics and increase the iron solubility on a broader pH range will require evaluating several ions; such as organic diacids (an organic compound containing two carboxyl functional groups), polyhydric alcohols, amino acids, and dimethylsulfoxide (colourless liquid). [238].

The plating efficiency of iron in all-iron RFB can be increased by adding boric acid or glycerol [239]. For the electrodes bonded and non-bonded conductive and non-conductive porous media, in different electrode configurations has been investigated to observe and confirm the plating capacity and voltaic efficiency [240]. A good plating capacity can be accomplished using a bonded configured carbon felt/ non-conductive felt with a good voltaic efficiency. Some authors have investigated particles such as carbon and metal slurry electrodes; which have shown a shear thinning behaviour, and resulted in small parasitic pumping losses less than 0.5 percent [241].

1.4.16.3 All-Lead RFB

In 2004, Pletcher and co-workers proposed and implemented the all-lead acid RFB cells of classic lead-acid chemistry with the chemical reaction presented in equation 11. The proposed batteries cell employed a single methane sulfonic acid electrolyte, in which lead (II) was highly soluble. The cell demonstrated a current density of 60 mA/cm^2 with a coulombic efficiency of 85%. [242, 243]. The problem of dendrite formation was identified in the beginning, and different additives, such as Sodium Lignosulfonate (molecular Formula = $C_{20}H_{24}O_{10}Na_2S_2$, molecular weight = 534.52) and polyethylene glycol (PEG), were successfully used to smoothen the surface of electrodeposits [244].

In all-lead redox flow batteries (RFB), polarization is reduced due to a decreasing pH; but will increase the side reaction by producing oxygen and hydrogen. This corrodes the electrodes and leads to stress increase within the deposit causing cracking and stripping [245]. The evolution of oxygen reaction can be suppressed by increasing the PbII concentration above 0.9 M but this reduces the voltage efficiency. [246]. Addition of nickel(II) will lessen the overpotential of lead oxide (PbO_2) deposition [244]. However, the coulombic efficiency is limited by all these additives [244].

Equation 11: All-lead acid RFB cells of classic lead-acid chemistry chemical reaction

$2Pb^{2+} + 2H_2O \rightleftarrows Pb + PbO_2 + 4H^+$	(11)

Excess lead (Pb) formed on electrodes from the chemical combination of Pb and PbO_2 is considered as the problem of soluble lead RFB due to imbalances in the coulombic efficiency during the electroplating process [247]. The use of H_2O_2 (Hydrogen peroxide) cyclic addition can be used to redress the issue of imbalance in Coulombic efficiency via oxidation of oxygen at open circuit [248], [249]. Graphite material can be replaced with stainless steel as negative electrodes in the all-lead RFB, and using TaC (tantalum carbides) as positive electrodes to allow an average coulombic efficiency greater than 96%; and an energy efficiency of 80.2% at the current density of 10 mA/cm^2 and a coulombic efficiency higher than 70% at the current density of 20 mA/cm^2 [250].

The morphology and phase composition of lead-dioxide (α-PbO_2 vs β-PbO_2) depositing at the positive electrode can play a significant role in cyclability, and further the optimization of the deposition conditions which can increase the cycle life of the battery to 2000 cycles at 79% energy efficiency [251]. All-lead RFB can demonstrate the power of 160 mW/cm^2. The significant failure modes; such as the formation of dendrites (Pb) with creeping and sludging of PbO_2 [252] are the potential problems in all RFBs that deposit solids. The soluble lead RFB has a better charge efficiency, but has lowered discharge efficiency than the conventional lead-acid battery, but of the same overall energy efficiency and with the possibility that the battery could recover its performance after a single charge and discharge cycle [253].

1.4.16.4 All-Copper RFB

The proposed all-copper RFB use an aqueous solution of CuCl in both cathode and anode [254] See equation 12 for all-copper electrochemical first reaction and equation 13 for All-copper electrochemical second reaction. High concentration of copper (3 moles) can be achieved in these batteries' cells due to the addition of HCl and $CaCl_2$ (4 moles) which partially

compensates the relatively low cell open circuit potential of 0.6 volt by allowing a reasonable capacity of 20 Wh/L.

Electroplating of copper on different materials can increase the Coulombic efficiency of batteries cells such as all-copper RFB's according to the order; graphite < stainless steel < titanium. A non-optimized cell with a nanoporous composite poly (vinyl chloride) (PVC)/ silica separator can also demonstrate an energy efficiency of 90% but can be at a very low current density of (5 mA/cm^2). The current density has been demonstrated to increase to or above 20 mA/cm^2, but sharply reduces the energy efficiency and capacity of the cell. [254].

Equation 12: All-copper RFB aqueous solution of CuCl in both cathode and anode

$\mathrm{Cu^+} \rightleftarrows \mathrm{Cu^{2+}} + \mathrm{e^-}\ (\mathrm{E^0} = -0.15\mathrm{V})$	(12)

Equation 13: All-copper electrochemical second reaction

$\mathrm{Cu^+} + \mathrm{e^-} \rightleftarrows \mathrm{Cu^0}(\mathrm{E^0} = +0.52\mathrm{V})$	(13)

Other types of flow batteries hydrogen anode are the regenerative hydrogen−oxygen fuel cells, hydrogen chlorine and Hydrogen−vanadium redox flow batteries etc. In a regenerative hydrogen−oxygen fuel cell, these redox flow batteries (RFB) utilize hydrogen stored often as compressed gas at (350 or 700) bar or as other hydrogen storage alternatives. These can be; liquid H_2, chemical hydrides and metal hydrides, however, they are usually more expensive, suffer irreversibility or have low capacity [255-257]. Hydrogen−halogen redox flow batteries (RFB) show much similarity with hydrogen−oxygen regenerative fuel cells particularly when the halogen is produced and stored in gaseous form. For the simplest hydrogen-chlorine cell, the cathodic reaction is extremely fast and an electrocatalyst is not required [258] which is clearly advantageous though the use of chlorine due to its toxicity and oxidising power is challenging.

Hydrogen−chloride and hydrogen−bromide cells have high open circuit voltage and theoretical energy density of 353 and 993 Wh/kg, respectively and are consequently appealing for energy storage [259-271]. Hydrogen−VRFB use the same V^{IV}/ V^{V} cathode redox couple as the all-VRFB. These batteries can show excellent reversibility and can reach a peak power density of 114 mW/ cm^2 [272]. Hydrogen−iron RFB are based on the Fe^{II}/Fe^{III} redox couple in a sulfuric acid electrolyte [273].

These cells have demonstrated excellent coulombic efficiencies up to 96% and energy efficiencies of 85% at 200 mA/cm^2 with a power density of 71 mW/cm^2 [274].

Air cathodes are most notably coupled to metal anodes; such as in zinc-air cells. RFB sizes and weights can be minimized by applying air (oxygen) to the catholyte. These batteries had similar features related to regenerative fuel cells and vanadium−air RFB's were patented in the year 1994 [275, 276]. For example, redox flow cells operating with 1.2 M $V_2(SO_4)_3$ in 2 M H_2SO_4 as the anolyte and IrO_2-based catalyst as a bidirectional cathode has shown an initial energy efficiency of 41.6% and decreases along with the number of cycles. Irreversible degradation of voltage and Coulombic efficiencies have been attributed to the loss of active material by corrosion and crossover [277, 278].

Figure 1.14 has described the electrolytic mode, or the charging process of how hydrochloric acid will be electrolyzed to produce hydrogen and chlorine via electrical energy from an external source.

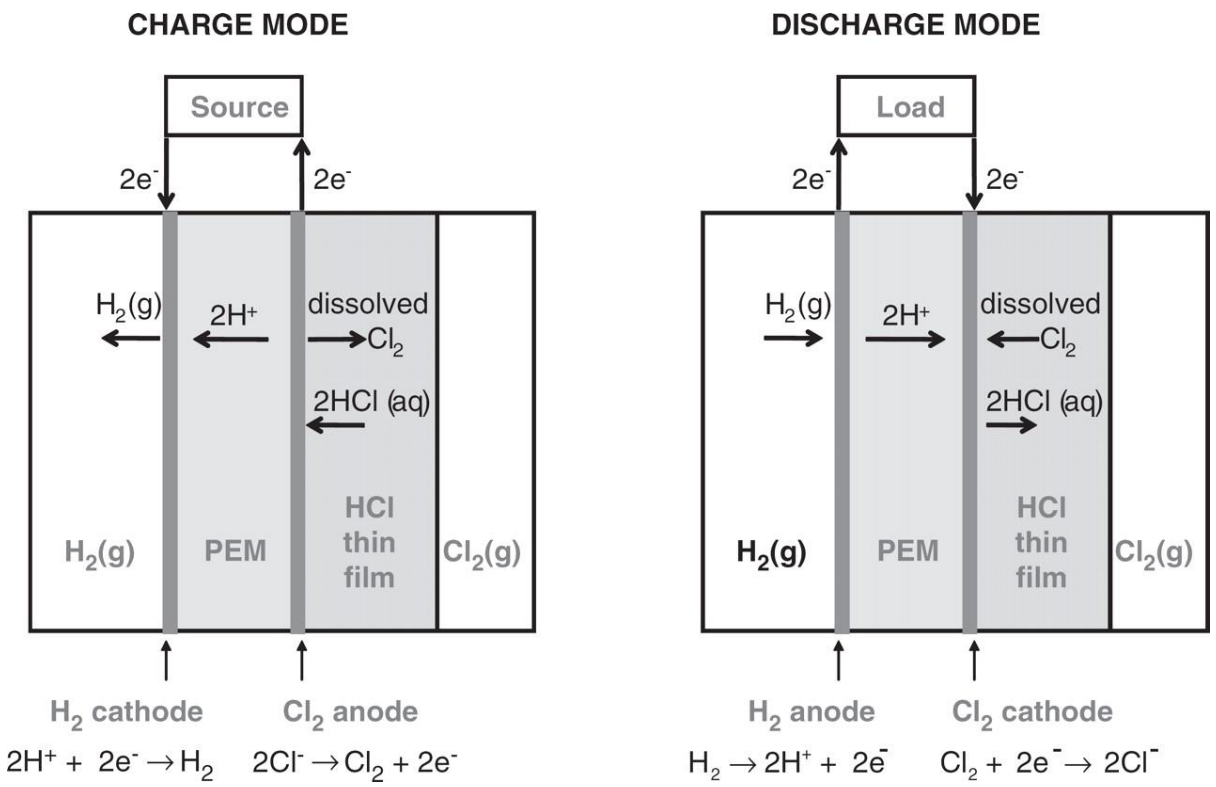

Figure 1. 14 Regenerative Hydrogen-Chlorine Fuel Cell schematic [279].

1.5 Types of Zinc-Based Hybrid Flow Batteries

1.5.1 Zinc-Lead and Zinc-Nickel RFB

Zinc-nickel and zinc-lead-dioxide cells can be of single-flow membraneless design since the positive redox couples involves solid phase active materials [280]. This means the electrolyte can include soluble zinc (II) species and serve as primary electrolytes for both half-cell reactions which allows for significant cost saving and system simplicity [242]. However, the capacity is limited by the all solid phase cathode [281, 282].

1.5.2 Zinc-chlorine RFB

Charles Renard, a French scientist, invented the very first zinc-chlorine RFB (435kg) and used it to power an airship in 1884. In 1921, a cell that uses zinc anode and at the cathode-side, and a chlorine-liquid was also developed [283]. However, a zinc-chlorine RFB that used a solid

chlorine hydrate as Cl_2 storage in the cathodic tank emerged only in the 1980's [201, 284]. This represented a safer means of chlorine storage but still represented a significant hazard.

1.5.3 Zinc-Iodide RFB

It is possible to replace bromide/ bromine catholyte with iodide/triiodide of the same equivalent to achieve a zinc-polyiodide cell with an OCV of 1.299 volt [285]. RFB based of these chemistries will have the same theoretical energy density due to the high solubility of ZnI_2 (~7 M). Lately it was reported that, a single electrolyte flow cell of 3.5 M ZnI_2 (zinc iodide), incorporating a Nafion 115 as a membrane can demonstrate a stable performance for forty cycles at 10 mA/cm^2 with an energy density of 125 Wh/L [286]. The formation zinc dendrites can be suppressed with increasing the solubility of Zn species by adding alcohols like (ethyl alcohol, C_2H_6O) EtOH. [286]. A zinc-polyiodide RFB of this type with (5 M ZnI_2) electrolyte that showed an impressive energy density of 167 Wh/L have recently been demonstrated [287].

1.5.4 Zinc-Cerium RFB

The patented zinc−cerium RFB by Plurion can operate in aqueous methanesulfonic acid CH_3SO_3H (MSA) See figure 1.15. These batteries have the highest open circuit cell voltage (Ecell = 2.4 volts) of all RFB with similar pH in the anode and cathode. [252, 288]. Cells such as zinc−cerium RFB during charge can have high coulombic efficiencies of approximately 90%; independent of charge duration (10 min to 4 hours). Electrolytes typical consist of 2.5 M Zn^{II} in 1.5 M MSA (negative side) and 0.59 M Ce^{IV}/0.8 M Ce^{III} in 3.5 M MSA (positive side) and the cell runs at 45−55 °C. [261, 289]. Adding sulfuric acid to the MSA solutions in the ratio 1:4 can improve the electrolyte conductivity and does not decrease cerium solubility. However, overall the solubility of cerium sulphates in H_2SO_4 is poor, which result to an energy efficiency of 85−87% [290]. Potential increase and depletion of Ce^{III} will occur at a higher current density due to parasitic oxygen evolution and yield a relatively low cycle life; such as twenty-five cycles [122]. Remarkably it is possible that a high cell voltage of 3.08 V at OCV can be achieved with double ion-exchange membranes, complex flow cells structures plus an additional electrolyte in the middle [291].

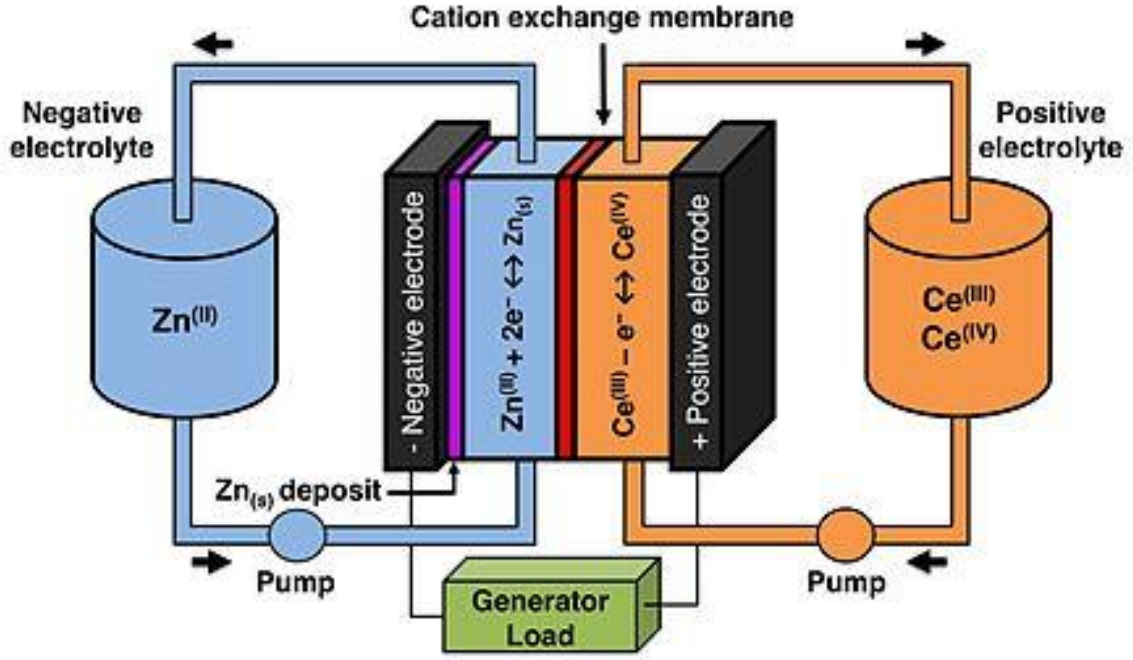

Figure 1. 15 Diagram of a divided Zinc-Cerium Flow Battery [292].

In an alternative version of the Zinc-cerium RFB, the anode redox couple is $(Zn\ (OH)_4)^{2-}/Zn$ ($E^0 = -1.21$ V), and an acidic cerium Ce_2O^{6+}/Ce^{3+} as the cathode couple ($E^0 = +1.87$ V). The two sides are separated by cation exchange membrane (CEM) and an anion exchange membrane (AEM), with the electrolyte in between containing an electrochemically inactive salt MZ. This is a Zincate species (any salt formally derived from zinc-oxide or hydroxide) in small quantities that are soluble in an alkaline phase, and then converted into zinc-oxide (ZnO) precipitate based on most of the discharged material. See equation 14 for the solubility of zinc-oxide (inorganic compound) with water to lose an electron to form zinc with oxygen and hydrogen.

Equation 14: Solubility of zinc-oxide (inorganic compound) with water to lose an electron to form zinc with oxygen and hydrogen.

$ZnO + H_2O + 2_e^- \rightleftarrows Zn + 2OH^-$	(14)

Zinc-cerium RFB cells electrical when charged can be balanced, and the average electrolyte concentration can be reduced when cations M^+ and anions X^- are transported separately via CEM and AEM. Furthermore, as the cell starts to discharge, the processes will continue to occur in the opposite direction. [293]. These cells can demonstrate a stable performance during a cycling test, without capacity fade at voltage efficiencies of (91%), coulombic efficiencies of 98 % and current densities of 5mA/cm^2 [293]. It is suggested that double-membranes can be applied to any batteries cells chemistries coupled with anion-anion and cation-cation. Furthermore, some authors have proposed and demonstrated such concepts with a sulfur-iron cell S_4^{2-}/ S_2^{2-} in 1M NaOH/ 3M NaCl|Fe^{3+}/Fe^{2+} in 1M HCl, and showed a stable OCV of 1.4 volts (theoretical value 1.22 volts) and an energy efficiency of 70% at 5mA/cm^2 [293].

1.5.5 Other Zinc-Based RFB

There are a number of other Zn anode-based chemistries that have been researched, a selection which show some promises are summarized below;

- Alkaline zinc/ ferricyanide rechargeable batteries can charge at cell voltages of 1.94 volts, discharge at 1.78 volts and at a current density of 35 mA/cm^2 including energy efficiencies of 84%. [294, 295].
- Currently, ViZn Energy (formerly zinc-air, http://www.viznenergy.com) is developing an alkaline zinc-iron RFB module (80 kW/160 kWh) that is housed in a 20-foot shipping container for grid-scale application; however, they do not disclose any formal information of the chemistry used [296].

1.6 Zinc-Bromine RFB

The zinc-bromine battery was first patented in 1885 and developed as a hybrid flow battery by Exxon, Gould and the NASA in the 1970s [123, 297-299]. These cells among other zinc-based hybrid flow batteries are one of the most promising systems for large-scale energy storage applications due to some advantages regarding cost, cell voltage and energy density. Further details regarding the advantages and disadvantages will be provided in section 1.7. Zinc-bromine batteries rely on zinc electrodeposition in flowing electrolytes as the negative

electrode reaction, which is usually coupled with organic or inorganic positive active bromine in the cathode. The specific energies of most commercial systems are still limited to between 60-85 Wh kg^{1}; which is considered as just 20% of the theoretical value [300].

The zinc-bromine ($Zn–Br_2$) redox battery has been extensively investigated for energy storage, commercialized and installed by several companies with the scaleup of this system to multi-kW scales as facilitated by modular designs. These batteries cells have high theoretical specific energy (~440 Wh kg^{-1}) and relatively high energy efficiencies (<80%) [301]. See figure 1.16 which shows basic diagram for the cell during charge and discharge.

Zinc-bromine batteries cells have good cell voltages ranging from 1.3V to 2.05 volts and have a two-electron transfer in the anode reaction. The average voltage of a zinc−bromine RFB is (1.67volts). These properties both aid the high theoretical energy density which are the highest energy density among flow batteries. In addition to the high specific energy, the use of zinc is suitable as a negative electrode for batteries because of its excellent and electrochemical kinetic properties. [18, 79, 302-304].

Therefore, in a zinc-bromine cell regardless of any current collector material, ohmic resistance is the main factors that restrict a cell voltage in operation. This is demonstrated by electrochemical impedance spectroscopy (EIS), which can be used to determine the charge transfer resistance and ohmic resistance at each electrode of each component. [305].

However, bromine materials are expensive, and the cathode bromine species are highly toxic through inhalation and skin contact. Therefore, a sequestering agent is needed to contain bromine in a zinc bromide cell, to avoid any evolution of such volatile bromine species. Furthermore, continuous plating of zinc metals on the negative electrode can form dendrites which can puncture the membrane and / or short out the cell (short circuit). Therefore, when designing a zinc-bromine cell, the mode of operating, discharging and charging need careful consideration to achieve reliable operation [306-308]. However, even with these complexities the high specific energy, power and relative low cost compared to other RFBs makes zinc–bromine an attractive option for energy storage.

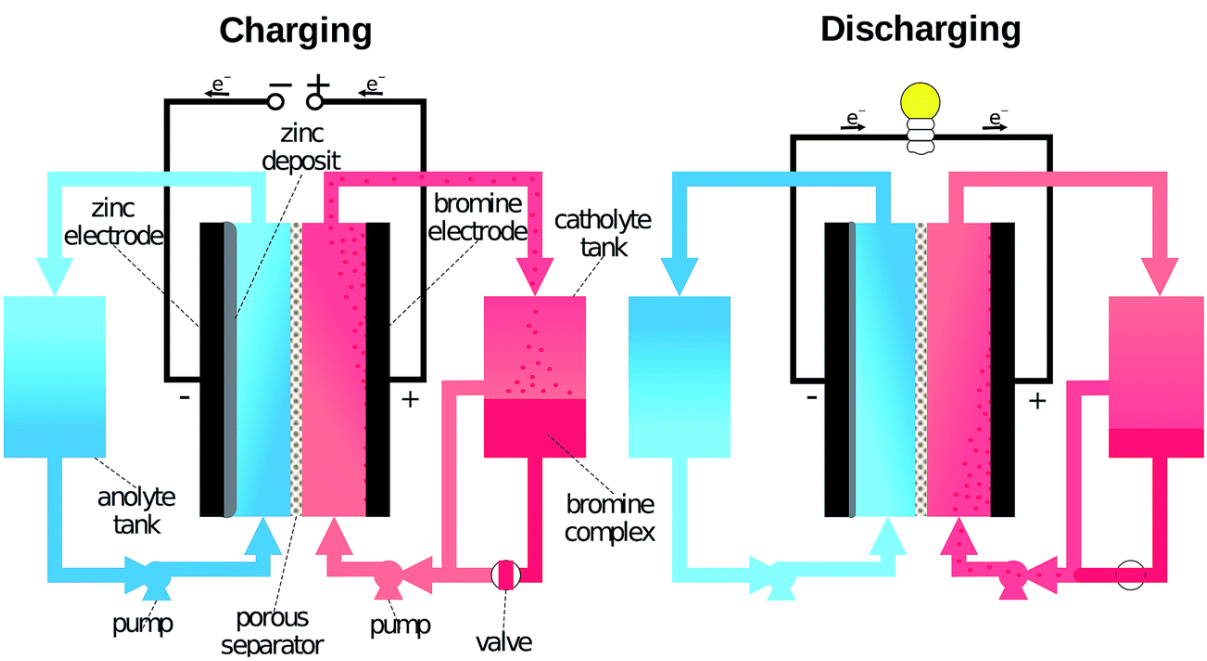

Figure 1. 16 Schematic of a zinc-bromine RFB during charging (left) and discharging (right). [309].

1.7 Zinc Bromine Batteries Cells Advantages and Disadvantages

	ADVANTAGES	DISADVANTAGES
1	Circulating electrolyte always made it easy for ease of thermal management and having a uniformed reactant when supplied to each cell.	1.To control the temperature, a supporting system is required.
2	Exceptional specific energy in between 34.4W.h/kg to 54W.h/kg	2. For all batteries, there must be an ensured safety for a system design.
3	Incomparable energy efficiency of 65-75%	3. When shut down, an initial high self-discharge rate occurred while charged.
4	Low cost materials readily available materials and low environmental impact.	4. Further developments may be required to moderate power capability

	The components can be recycled and re-used via conventional manufacturing techniques.	
5	Overall flexible system design	
6	Ambient-temperature operation in between 20ºC to 50ºC	
7	The power density is suitable for most application	
8	Capable of charge rapidly	
9	The battery cells cannot be damage when discharge 100%.	

1.8 Zinc Bromine Batteries Cells Application and Systems Design

The demonstration of a minimal-architecture zinc-bromine battery cell can be fabricated to replace expensive traditional components of zinc-bromine batteries systems by using free membranes and a single-chamber; which can operate with a coulombic efficiency higher than 90% and 60% for over 1000 cycles and with a cost of <$100 per kilowatt-hour at a scale of nearly 9 Watt-hour/liter.

Different experimental test on a 2 kW and 10 kWh zinc-bromine batteries cells have been carried out with new carbon/ PVDF bipolar electrodes in a polybromide aqueous zinc-bromine electrolyte and circulated the electrolyte through the cell stalks before a turn-around efficiency of 65-70% was achieved [203, 255, 297, 310-312]. The system was less complex, reliable and has high efficiency. Furthermore, through such explored experimental test, it was possible for the (25 amperes) hour single cell to complete 400 cycles (100% depth-of-discharge), and to achieve over 75% energy efficiency as the total return and made the technology to be attractive and extremely good as an application to supply power to remote-area.

The total capacity of energy stored in the system depends on the two-stack size (electrode area) and the size of the reservoir tank storing the electrolyte. As such, zinc-bromine flow batteries rating power and energy are not sufficiently decoupling.

For some utility-scale applications, the test carried out on an integrated zinc-bromine battery energy storage system on a transportable trailer was up to 1 MW/3MWh. Furthermore, research have also showed that multiple sizes of such zinc-bromine battery are possible to be connected

in parallel for use for much more extensive applications. Based on the further explored research, on such zinc-bromine battery system at community energy storage and based on Zn/Br supplied at the (5-kW/20-kWh), the battery has also been operating in Australia by utilities [313]

Zinc-bromine redox flow batteries (ZBRFB) produce good stabilities during cycling tests and perform excellently when graphite felt electrodes are thermally treated; because such approach improves the electrochemical activities in $ZnBr_2$ cells. However, this has already been observed and confirmed by introducing (KCl and 4 moles of NH4Cl) to observe the ionic conductivity and how the electrolyte resistance is minimized. These tested (KCl and 4 moles of NH4Cl) supporting electrolytes can improve ZBFB cells energy efficiencies to a value of 74.3% at a current density of 40 mA cm^{-2} from an energy efficiency of 60.4% of no supporting electrolyte.

The energy efficiency of ZBB cells can also be increased to 81.8% with a similar current density of 40 mA cm^{-2}. Therefore this experimental work has demonstrated that Zinc-bromine redox flow batteries (ZBRFB) cells can be operating at higher current frequencies of 80 mA cm^{-2} and each cell with their energy efficiencies as 70%; by introducing a thermal treatment and those mentioned supporting electrolyte to a positive electrode [123]

The mechanism behind self-discharge in secondary battery cells attributes to the aqueous bromine action occurring on the bromine-side of the cell, moving to the electrode zinc-side of the battery and subsequently oxidizing the zinc electroplating. Therefore, self-discharge is usually caused due to this effect [314]. Thermodynamically for zinc, bromine is an effective corrosion on zinc-bromine battery cells systems due to several encountering problems that required addressing them but without attendance [315].

To avoid this, using an independent circulation of electrolytes for the zinc bromide cell on both sides on the cell of the bipolar electrode stack and a microporous separator or film is the only solution [316]. Research has proposed using two possibilities for explaining the principles behind diffusion of bromine through an ion-exchange membrane as summarized. (1) The complexes of bromine action soaks the ion-exchange membrane and this makes provision for a pathway for bromine as an element to be diffusing through and (2) The equilibrium existing between the bromine in the liquid phase diffusing through the ion-exchange membrane and the quantity of it in the prepared electrolyte [134].

Efficient bipolar plates are used to store the obtained electric power from renewable energy systems (RES) since a polypropylene material is suitable for such plates [317]. The level of conductivity can be achieved by loading it up to (80 wt. % graphite); which will prevent the compound to later break and to ensure that the remains are easy to process. Furthermore, the method to improve the impact strength with elastomers is currently under development. It is also possible to use bipolar electrodes in zinc-bromine batteries cells where one of the electrodes is for the positive side, and the other electrode is on the negative side of the battery [318-320].

1.9 Components of Zinc Bromine Batteries Cells Systems

Some of the components of a zinc-bromine battery cell are presented figure 1.17 and more further discussions about the components in sub-sections 1.9.1 to 1.9.3.

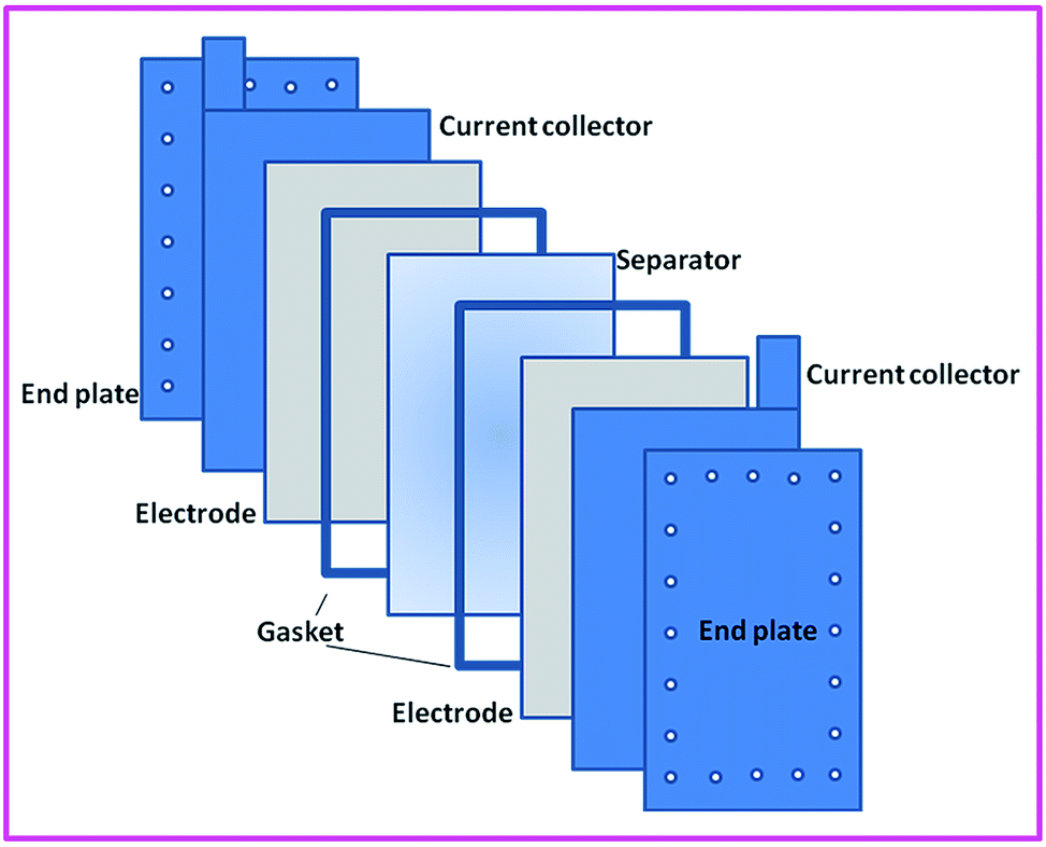

Figure 1. 17 Zinc Bromine Battery Cell Components [321]

1.9.1 **Ion-Exchange Membrane**

The ion-exchange membrane of a zinc-bromine battery cell is an integral component because of its service regarding standing as a barrier preventing the electrochemical cross-contamination of active species within the cell system and creating a possible reduction of the electrical contact through anode and cathode electrodes.

The electrochemical system requirement is to reduce the bromine diffusion to the electroplated zinc (Zn) as much as possible in a reasonable way to prevent self-discharge in the zinc-bromine battery cell; when charged and left unused for a longer period. Self-discharge occurrence in a zinc-bromine battery cell would lead to the system having a lower coulomb efficiency. Further studies comparing different separator has revealed that diffusion coefficient of bromine consists of values with a wide range between (1.44×10^{-10} to 3.74×10^{-10} cm^2 s^{-1}) [134] and (1.52×10^{-8} to 2.28×10^{-8} cm^2 s^{-1}) [322]. According to research and observation in one set of studies, the rate of diffusion of bromine through the ion-exchange membrane in a complex presence and aqueous phases could be doubled and high due to the presence of a liquid phase alone. Therefore, due to the description made from the start on bromine diffusion, the requirements for ion-exchange membrane are demanding and strict due to a high degree of selection which is necessary between bromide and zinc ion; which should usually be permitted to pass across.

Ion-exchange membranes in zinc bromide cell battery also serve as a barrier to bromine migration to the anode zinc side of the battery cell whether in the form of elemental or complexed with QBr (bromine sequestering agent). Therefore, due to its interaction with different species, ion-exchange membranes must be chemically inert as possible and not be participating in undesirable side reaction concerning electrolyte degradation and promotion. Membranes used in zinc-bromine batteries cells should be able to withstand the harsh operating environment as this is important for the reasonable duration of time.

Therefore, durability is an important aspect to be considered when picking the appropriate membrane to be used in a zinc-bromine battery cell. In zinc-bromine batteries, different materials of specific properties are put into practice for use and ion- microporous plastic exchange membrane known as polyolefin Daramic®. Research has been carried out on some other membranes apart from cation exchange Nafion® membrane of which the stability and

high cost are undergoing testing. These include coated and uncoated composite separators made from plastic-silica and fluorine membranes treated with Asahi SF-600 [323]

These two materials have shown that composite ion-exchange membrane of higher silica levels has lower-resistivity and fluorine-treated Asahi SF-600 membrane brings improvement regarding bromine diffusion. While plastic-silica composite ion-exchange membrane contributes consequently to improve coulombic and energy efficiencies. In accordance to studies, the cation exchange Nafion® membrane is found to be suitable in terms of high effectiveness and ability of the membrane to reduce bromine when transporting it across the separator compare to their microporous counterpart's due to bromide species that occur mostly as Br_3 – and Br_5 – complexes [323, 324].

The success of such separator (cation exchange Nafion® membrane) has encouraged a recent review [325] and instigated more work for incorporating multiple membranes like this into a single working unit to be used in RFB [326]. Sulfonated Polysulfone is known as another category of functionalized ion-exchanged membrane demonstrated and observed to be better than those made with grafting of organic substrates [327]. Ion-exchange membranes made from zeolites materials have also been examined in research of vanadium-based system and observed to be a suitable material according to the onion size concerning high degree selectivity leading to moving of wasted space and leaving aside others [328].

Nafion membranes and less costly Daramic microporous membranes can deliver similar comparable energy efficiencies; While Nafion membranes will only allow a higher Coulombic efficiency and lower voltaic efficiency. During seventy cycles, cells incorporating these membranes can have an energy efficiency of 82% at 20 mA/cm^2 during seventy cycles and demonstrate a stable performance. The use of a composite Nafion/PTFE (porous polytetrafluoroethylene) membrane can as well support constant cycling. Dendrites formation and resistance at the anodic-side of zinc-bromine RFB cells can affect the charging of these cells [307, 308].

1.9.2 Anode Zinc-Side FBR's Reactors

Mostly, and according to [329], zinc half-cell of zinc-bromine batteries cells can be expected to behave hugely like an electroplating system if incorporated with zinc-electrodes to improve

them. Furthermore, zinc-electrodes have been examined in rechargeable zinc-air batteries of an outer frame and a porous foam electrode of supporting structures; to address the formation of zinc dendrites on external surfaces of which the outer casing has a pathway where the electrolyte circulates to the treated zinc coated porous foam.

Ordinarily, cationic zinc comes out during the charging process from the aqueous solution to electroplate zinc onto negative-sides of bipolar electrodes in a $ZnBr_2$ battery cell; as shown in equation 15 for zinc reduction process at the anode-side of a battery cell. Besides, Adams had observed such reaction via the electrical discharge process at the cell anode-side, cathode-side and during the battery cell charge cycle of the reversible condition that produces soluble reaction products which are transported in the electrolyte to the respective external storage tanks as the battery capacity increases [295]. However, Jacoby further observed such reaction and reported it in a newspaper article on how abundant exploitation of zinc in the next generation of batteries would be a useful approach; by preparing zinc-electrodes in the form of a structure that has a porous sponge-like. The anticipated novel idea will therefore make batteries cells of such sponge-like electrodes to have denser energy, be naturally safe and make batteries cells to last longer as per the study [330].

Equation 15: zinc reduction process at the anode-side of a battery cell

$\mathrm{Zn^{2+}} + 2\mathrm{e^-} \rightarrow \mathrm{Zn}, \mathrm{E^0} = -0.76\mathrm{V}$ versus SHE	(15)

Furthermore, and before Jacoby [330] reported the next novel batteries that will be produced, Kim and other researcher like Jeong, Park and Sohn, had initially carried out an experimental research on inventing secondary batteries of metallic anodes for the next generation [331]. However, in between year 2013 and 2017, Higashi, was able to use a numerical software (COMSOL) for the estimation of an electrolyte current density distribution on a copper electrode surface and developed a backside-plating arrangement to prevent the undergoing short circuits problems in batteries cells due to the formation of zinc metal dendrites on the anode-side electrode [332].

The Ni-Zn (nickel-zinc) full cell battery demonstrated a charge and discharge cycles of 800 cycles at a high rate of (20 mA cm^{-2}) by using 6 M of potassium hydroxide (KOH) of zincate aqueous solution for the backside of the plating configuration. Furthermore, it was concluded that the electrolyte solution needs a specific thickness due to the backside-plating configured arrangement that was beyond the plating substrate (observed chemical species in the chemical reaction) for a homogenous plating of Zn throughout the substrate.

Liang, Jing, Gheytani and Lee, experimentally quoted quinones as reliable anode materials in the same year as (Jacoby, 2017) after testing them in aqueous solution and exploiting them structurally as stable anode materials based on their stability as good ion-coordinator of charge storage mechanism and chemical inertness towards aqueous electrolytes [333]. Nevertheless, three systems were into demonstration towards selecting and designing these quinone structures rationally before coupling them and establishing them industrially to the cathodes and electrolytes to exhibit extended cycle life that was up to 3,000 cycles/3,500 h.

Furthermore, the anode materials are and of fast kinetics less than and equal to ≤ 20C. Other features include having high anode specific capacity that was up to 200–395 mAh g^{-1}. Further highlights, are the state-of-the-art of the specific energy density (up to 76–92 Wh kg−1/ 161–208 Wh l−1) for various operational pH values (−1 to 15), charge carrier species (H^+, Li^+, Na^+, K^+, Mg^{2+}), temperature (−35 to 25 °C), and atmosphere with and without O_2; to make them as universal anode materials for aqueous batteries technologies.

1.9.3 Cathode Bromine-Side Reactor

Quaternary ammonium bromides (QBr) can be stored safely and considered as a separate liquid phase [334]. Bromide anions are converted during charge to bromine which is subsequently complexed. See equation 16: for the formation of bromide due to gain electron and equation 17: for bromide reaction with quaternary ammonium bromides. Kemira [335], carried out a similar experimental work related to Dey, Dhar, and Kalita experimental work [336, 337] by producing quaternary ammonium compounds thru selecting anion during the reaction of a trialkylamine with an alkyl bromide to form a quaternary tetraalkylammonium bromide salt. Furthermore, the quaternary tetraalkylammonium bromide salt was converted to a quaternary tetraalkylammonium hydroxide salt via an ion-exchange resin by converting the quaternary

tetraalkylammonium hydroxide salt to quaternary tetraalkylammonium salt of the selected anion [312, 338, 339].

Equation 16: Formation of bromide due to gain electron

$2Br^{-} \rightarrow Br_2 + 2e^{-}, E^0 = +1.065\ \text{V versus SHE}$	(16)

Equation 17: Bromide reaction with quaternary ammonium bromides

$Br_2 + QBr \rightarrow Br_2 - QBr\ \text{complex}$	(17)

During charge, zinc-bromine batteries cells electrolyte should be circulated continuously according to research to remove QBr-polybromide complex from the vicinity of the electrode surface. Similarly, the circulation of electrolyte via the cell stack can be used for transporting the complex from the reservoirs tank to the surface of the electrode for the occurrence of charge transfer. In addition, monobromide ions and its reaction with aqueous bromine will forms tribromide ions during charge and higher polybromides as shown below [186].

Bromine (Br_2) reaction with bromide (Br) can form polybromide (Br_3^-)., more bromine element (Br_5^-)., can further be formed when polybromide reacts with bromide. The formation of more bromine elements with bromine as follows: $(Br_5^-) + (Br_2)$ can lead to (Br_7^-) etc. Bromine (Br_2) can dissociate during charge from the QBr complex and become limited to the anionic bromide form as follows: $Br_2 - QBr\ \text{complex} \rightarrow Br_2 + QBr$.

1.10 Safety and Hazard

1.10.1 Bromine Treatment

Bromine emission is possible by eliminating a cathode-side storage tank and the associated pump; which can improve the performance like conventional batteries cell at a lower weight and as a novel zinc-bromine RFB. Positive electrodes fabricated of carbon felt, soaked with

$ZnBr_2$, and with a bromine complexing agent such as N-methyl−ethylmorpholinium can be separated from a liquid anolyte with a microporous membrane.

Most recently, some researchers reported a proposed test by introducing and adding the following acid (9,10-anthraquinone-2,7-disulphonic), to RFB system. These chemical compounds were the organic system and inorganic metal free based system of bromine–bromide (Br/ Br2) redox couple. The test carried out by these researchers was to screen and study in order and the promising molecules.

Bromine as an elemental (Br_2) substance exist in different forms; such as pentabromide, tribromide, monobromide or higher when charged within an electrolyte solution as soon as charge and discharge cycle on a zinc bromide cell system is occurring. Among all listed elements, solvent elemental bromine is hazardous and dangerous as a gas when escaping to the external environment. However, it can be prevented by isolating the bromine into a complex liquid phase by introducing an appropriate QBr to lower the pressure of the vapour and any route for escaping. Furthermore, bromine vapour is very toxic with inhalation. Additional information regarding the chemical element can be found in the material safety data sheet (MSDS) [340].

Bromine concentration and vapour pressure can both be decreased via using the complexation of quaternary ammonium bromides such as a quaternary bromide salt (QBr), like N-methyl N-ethyl pyrrolidinium bromide (MEP) or N-methyl N-ethyl morpholinium bromide (MEM) [341]. It is possible that quaternary ammonium polybromides will form a separate liquid dense phase [342-346] which can aid practical system design. The addition of surfactants as a compounds to lower a two liquids surface tension, connecting gas and a liquid, or separating a liquid and solid; such as sodium dodecyl sulphate can be used to improve the phase separation and decrease any adverse microporous separator interaction between the fluid and solid phases [347]. Quaternary bromide additives does not only reduce bromine pressure but also reduces cells resistance based on the adsorption of polybromide complexes on the bromine-side electrode surface [308]. Fourier transforms infrared spectroscopy (FTIR) can be used to follow the formation of the polybromide complexes from the electrochemically generated bromine [348].

1.11 Zinc Electrodeposition Electrochemistry

Generally, in acidic and alkaline media respectively, zinc has a standard electrode potential of −0.76 volt, and −1.29 volt; with the electrode potential equilibrium separating both the oxidized and reduced phases on a phase diagram; but depending on the chemical activities of the thermodynamic parameters. It is possible to have a non-stabilized electrostatically aqueous suspensions of zinc oxide if there is a suspended decreasing pH in the region between (7.2 and 12) based on transforming colloidal $Zn(OH)_2(S)$ particles to $Zn(OH)_2(aq)$ ions as confirmed via investigating commercially the surface charge on some available zinc oxide powders in aqueous solution [349].

Figure 1.18 shows a pourbaix diagram plotting the equilibrium potential against pH in aqueous electrolytes. The description is based on dissolved zinc ion of low concentration (e.g. 10^{-6} M). The diagram at a given potential and pH is used to determine species that can be stable thermodynamically but cannot provide information about a reaction kinetics.

From this diagram, it is important to note;

1. The simple Zn^{2+} ion is only stable in the acidic pH range
2. Between a pH just below 9 and about 12.5 an insoluble Zn hydroxide species is likely to be formed.
3. At high pH above about 11 soluble Zn oxy / hydroxyl species are formed.

However, the exact pH ranges at which species are formed will depend on species activities and that local pH changes at electrode, electrolyte interfaces can lead to unexpected reactions.

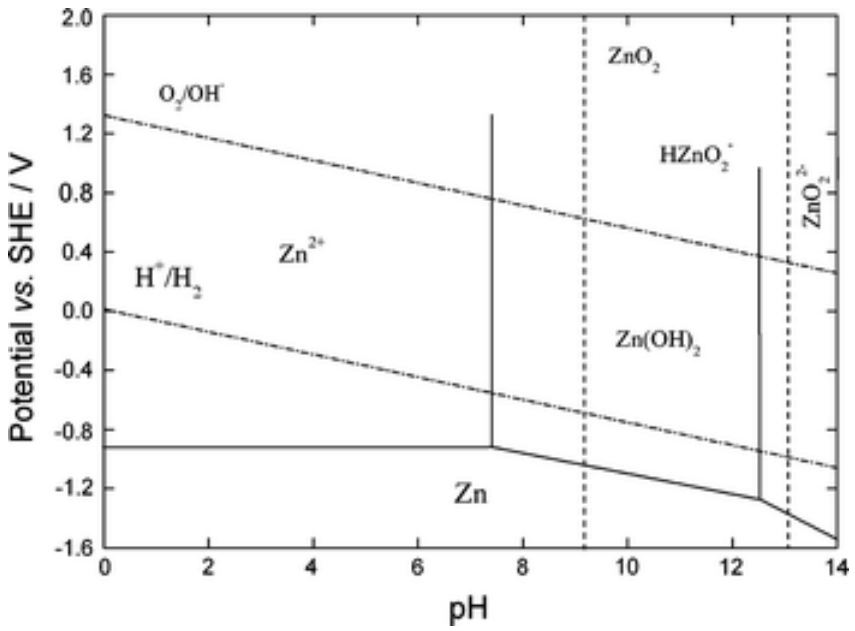

Figure 1. 18 Pourbaix diagram for zinc different pH in water [350]

Pourbaix diagrams can focus on electrolyte and temperature variance and are presented by several authors [351, 352]. According to figure 1.18, metallic zinc can be electrodeposited from solution through three different routes with their reactants in the forms of Zn^{2+}, $HZnO_2^-$ and ZnO_2^{2-}. The formation of $HZnO_2^-$ and ZnO_2^{2-} are possible via Zn^{2+} hydrolysis; should the pH of the aqueous electrolyte change. In most definitions of battery chemistry, the species represented by $HZnO_2^-$ and ZnO_2^{2-} also include further hydrolysed zinc complexes of Zn $(OH)_3^-$ and Zn $(OH)_4^{2-}$. The lines representing the charge transfer reactions on the Pourbaix diagram can be defined with the Nernst equation.

Equation 18 is the Nernst equation for independent reaction on pH corresponding to a horizontal line at −0.763 V *vs.* SHE in the Pourbaix diagram. Equation 19, is the first linear variation reaction of the electrodeposition routes of the negative gradients.

The second linear variation reaction of the electrodeposition routes of the negative gradients is displayed in equation 20 and the second and third linear variation reaction of the electrodeposition routes of the negative gradients in equation 21. The vertical lines between the four regions are independent of electrode potential and represent chemical reactions without charge transfer. These can be determined by considering the equilibrium constants for the reactions [353, 354].

Equation 18: Nernst equation for independent reaction on pH corresponding to a horizontal line at −0.763 V vs. SHE in the Pourbaix diagram

$$Zn^{2+} + 2e^- \rightleftharpoons Zn$$ $$E_e = -0.763 + 0.0295\log(Zn^{2+})$$	(18)

Equation 19: First linear variation reaction of zinc electrodeposition routes within the negative gradients

$$Zn(OH)_2 + 2H^+ + 2e^- \rightleftharpoons Zn + 2H_2O$$ $$E_e = -0.439 - 0.0591pH$$	(19)

Equation 20: Second linear variation reaction of zinc electrodeposition routes within the negative gradients

$$HZnO^{2-} + 3H^+ + 2e^- \leftrightarrow Zn + 2H_2O$$ $$E_e = 0.54V - 0.0886pH + 0.0295\log(HZnO^{2-})$$	(20)

Equation 21: Third linear variation reaction of zinc electrodeposition routes within the negative gradients

$$ZnO_2^{2-} + 4H^+ + 2e^- \leftrightarrow Zn + 2H_2OE_e$$ $$= 0.441V - 0.1182pH + 0.0295\log(ZnO_2^{2-})$$	(21)

There are also irreversible processes due to hydrogen evolution or oxidation and compete with the zinc electrodeposition/dissolution processes leading to reduced current efficiency. Furthermore, zinc or other metals exposed to electrolytes that contain protons/acid and an

oxidizing agent (e.g. dissolved oxygen) could suffer corrosion particularly at open circuit voltage by yielding a mixed potential at the electrode and a cell voltage lower than expected [135]. This is exacerbated in membraneless systems which exhibit slow dissolution of zinc in the presence of active species at low concentration (<0.5 M) when the dissolution of zinc is taking place only at open circuit or during the discharge process [355-358].

For the electrode substrate material, carbon-based materials are suitable as they can withstand negative electrode potentials and when there is excess hydrogen evolution. However, carbon can also corrode during oxidation reactions via evolving carbon dioxide; though this is not typically an issue at potentials used for the anode [359, 360]. There are problems associated with carbons low electronic conductivity compared to metallic conductors which can be worsen due to the need for nonconductive binders to yield electrodes in a physically usable form. [361, 362], [362-364]. Zinc flow batteries cathodic potential can vary, but such variation will depend on the composition of the electrolyte and particularly on the concentration of anion and pH.

1.12 Effect of Zinc Electrodeposits Morphologies on Hybrid Flow Batteries

Long-term cycle life depends on how zinc electrodeposit morphologies change. Dendritic growth is an undesirable feature of zinc electrodeposition and usually develops from mossy to pyramidal/ acicular form as summarized in table 1.2 with scanning electrons micrograph obtained from alkaline electrolytes in figure 1.19 [365]. It leads to risk of damage to the separator and possibly an electrical short-circuit or self-discharge.

The diffusion process influenced dendrites formation, and the overall growth is complex [366-368]. The two primary sources of convection and diffusion are usually from the local forced convection due to the evolution of hydrogen bubbles, shedding and density differences in the electrolyte as local compositions change. The use of appropriate operating conditions is essential to obtain some favourable electrodeposits morphologies by flowing electrolytes and electrolyte species [369]. Active zinc species can be uniformly distributed via using a flowing liquid electrolyte, which can decrease the thickness of Nernst diffusion layer (dN).

Therefore, the corresponding limiting current (jL) during zinc deposition can enhanced reducing risk of dendrite growth as dendritic morphologies can develop at limiting current densities; particularly if there is non-uniform concentration. Hence, an enough flow of

electrolyte can be applied as observed on zinc-based rechargeable batteries [370-372]. Moseley reported that it is possible to start finding dendritic growth in static electrolytes with any zinc ion concentration if the current density is approximately 8 mA cm^{-2}.

Whereas dendritic problem can be prevented if it possible to achieve circulating electrolyte current densities in between 20 and 40 mA cm^{-2} [373], though this will depend on the exact operating conditions. However, the use of a linear flow velocity around 2cm s^{-1} was reported to prevent such occurrences within the electrode stack. Furthermore, dendritic growth under a prolonged operating condition was difficult to avoid even with a flowing electrolyte [374].

Categories of zinc deposit morphology					
Property	Heavy Spongy	Dendritic	Boulder	Layer-like	Mossy
Appearance	Black powder	Metallic crystal	Grey metal	Reflective metal	Black powder
Microstructure (under microscope)	Agglomerate	Fern, leaf, hexagon	Granular boulder	Ridge, layer-like	Filament, whisker
Adherence	Non-adherent	Non-adherent	Adherent	Adherent	Non-adherent
porosity	Dispersed	Dispersed	Compact non-porous	Compact non-porous	Highly porous
Crystallinity	Anisotropically	Isotopically oriented	Anisotropically oriented	Epitaxial oriented	Isotopically oriented
Growth current density	highest	Very high	Moderate	Low	Lowest
Nucleation site selectivity	Non-selective	Non-selective	Selective	Non-selective	Highly selective

Table 1. 2: Categories of zinc deposit morphology [365].

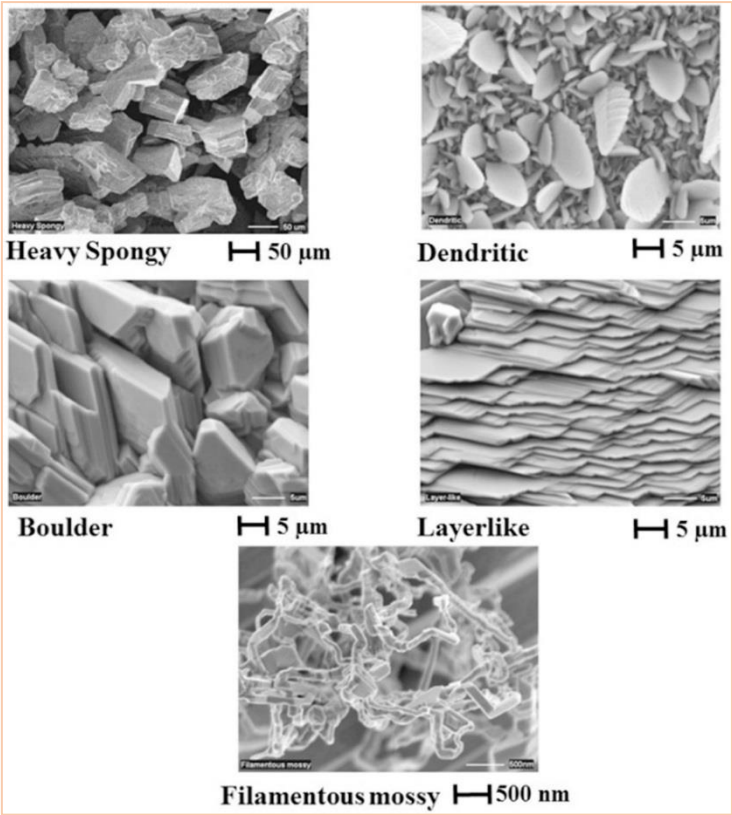

Figure 1. 19 Morphologies of zinc electrodepositions (heavy spongy, dendrite, boulder, layer-like and filamentous mossy) on electrode surface (electrodeposited through alkaline electrolytes).

1.13 Electrolyte additives to improve morphologies

Electrolyte additives are used in zinc electroplating industries to obtain brighter electrodeposits and more desirable grain sizes [375]. According to previous studies these additives can promote the 2-dimensional growth of the crystallites and achieve a faster nucleation rate and finer crystal grain sizes due to higher deposition overpotential [376, 377]. The use of large organic molecules, such as surfactants can be used to lower the surface tension and improving the surface wetting. It can also increase the deposition overpotential if the electrode surface is partially covered to prevent further grain from growing and to promote nucleation.

1.14 Side Effects of Dendrites and Prevention

Regular charging of zinc-bromine batteries cells is necessary to prevent dendrites formation in such technology systems. This is important because dendrites accumulation is the drawback in zinc bromide cells systems. Additionally, dendrites can puncture a zinc-bromine battery cell separator and run down the cell system. Such as facing cut off voltage, having inefficient efficiency and shut down a battery cell system. Dendrites formation on zinc-bromine batteries cells electrodes required addressing such a problem by introducing fluidized beds zinc-electrodes to these cells systems. Figure 1.20 is a typical example of a half liquid solid FBR biological nutrient removal system device.

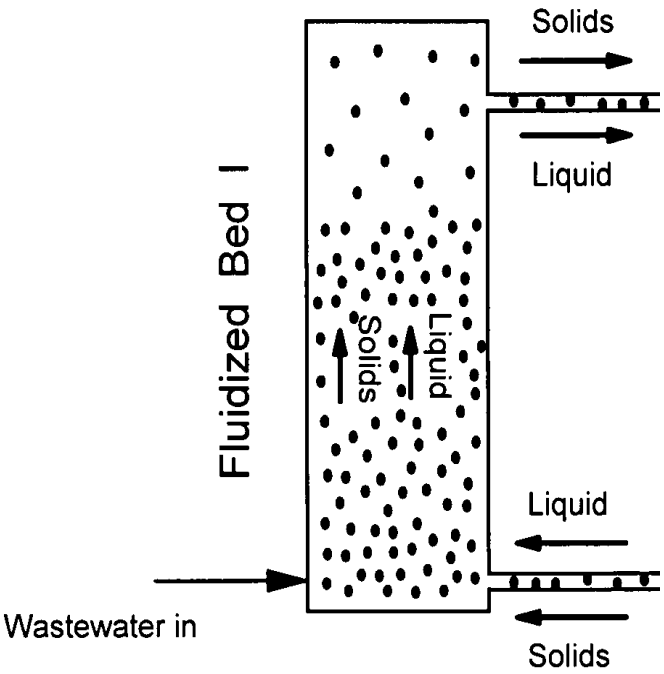

Figure 1. 20 Half Liquid-Solid FBR [378]

Generally, minimum fluidization velocity plays an essential role in fluidized beds because of the particulate solid floating and behaving in the state of the liquid [379, 380]. The physical methods concerning fluidization include granulation, coating, heat exchange, solidification, drying, and gases purification with the adsorbent [381, 382]. However, there will be more discussions regarding the general ideas in further section, about the relationship between

viscosity, minimum fluidization velocity, importance of thickness, when developing any applications like fluidized bed reactors. Such discussions are important since there are fluid flows in these technologies fluidized bed reactors (FBR).

Fluidized beds technologies are used in several areas; such as for gasification, drying, and combustion [383]. The words (fluidized beds reactor, fluidized anode zinc-electrode and fluidization) are three different things entirely that may look strange to people who are unfamiliar to them regarding where, how and what people are deriving from them. The term fluidization has several significant advantages related to fluidized bed reactors and fluidized bed zinc-electrode and has different definitions according to research.

1. Fluidization occurs when fluid is transferred to a porous reactor and injected particles in such reactor start to behave in the state of the liquid (electrolyte) [384] by using minimum fluidization velocity to reach a steady state. To design the best and have high efficiency beds, a good knowledge of an inverse fluidized bed and fluid hydrodynamic is essential according to research.
2. Fluidization is a method of converting a bed of smooth particulate materials into the state of liquid by running liquid or gas through beds of particles or the contact between a bed of solid and a flow of fluid. Moreso, this makes the solid particles to behave in the state of the liquid which can be applied to various purposes [385, 386].

Many definitions have further been given to fluidized bed reactors [387, 388] and fluidized bed zinc-electrodes [389]. Some researchers like Masayuki and Sawsan, regarded fluidized bed reactors as the most powerful device and technique for handling different types of solid, rugged materials in chemical industries apart from using it to provide a significant interfacial area, a high degree of mixing and temperature uniformity [390-392]. Kunni as a researcher also defined the device an alternative technique offering solutions to problems for meeting environmental requirement set out by any agency concerned and mainly for multiphase purposes and used for proper mixing of catalysts [393-395].

However, a section in this chapter will be providing a detailed discussion regarding the benefits that can be derived from fluidized bed zinc-electrodes as the only electroplating machines that can address and prevent dendrites formation within zinc-bromine batteries cells.

1.14.1 **Different Phases**

Different porosities can be expected if poly-disperse particles are simulated in fluidised bed systems and within reactors of monodisperse particles beds [396]. Impurities in zinc during an electrowinning process (electrodeposition of metals) are very sensitive [397] as their side effect had been observed during the deposition of zinc (50 g/1) from an acidic sulphate (100 g/1 H2SO4) solutions. This was observed in a fluidized bed cathode electrode used to determine the effect of current density, zinc concentration, acid concentration on current efficiency, specific energy consumption and the cell voltage of such pure solution [398].

Transport occurrence in fluidized beds zinc-electrodes could have various challenging process and some benefits in different processes. The electroplating machine could have different phases such as (solid, liquid and gas) that can be simulated and experimented together depending on the problem [399]. The fabricated anode zinc-electrode of this research work can be used as a typical example and the one used by Li [400] and Gao [401] to observed the contribution of heat and mass transfer to a dense and bubbling phase via the effects of air flow velocity on the electrical conductivity of the bed.

Water and air with glass beads (5mm-6mm-diameter) in a 90mm diameter column were used to achieve various degrees of a uniform distributor and non-uniform distribution of gas to investigate the different location of each test hole in the fluidized bed reactor. See section 2.13 for further discussions regarding these three phases (solid, liquid and gas).

1.15 Fluidized Bed Zinc-Electrodes and Benefits

1.15.1 **Metal Deposition**

Zinc-electrode electroplating devices are the subject of various investigations in terms of metal deposition from aqueous solution and offers several benefits regarding capital costs and as high surface area electroplating machines with the ability to reduce electrical energy consumption [402]. In terms of storing energy, these high surface area electroplating devices can be storing energy without excessive parasitic losses due to over-voltages. Fluidized bed zinc-electrode has high mass transfer rate and capable of fast electron exchange in the charge and discharge

cycle. Lately Savaskan and Evans were able to develop a rechargeable zinc-air battery engaging particulate packed bed anode that recharges mechanically. Towards the end of the discharge, residual particles and electrolyte were removed from the battery and replaced with new electrolyte and particles after regenerating them electrochemically in the regional facility from the cell discharge products. In the zinc-air battery application, it was only possible and would be a crucial step to use a large electrochemical reactor like a fluidized bed zinc electrode to generate directly new zinc particles from the strong alkaline solution [403].

Savaskan and Evans observed that via fluidized bed zinc electrodeposition, a 45% potassium hydroxide zincate solution was successfully performed and the regenerating of zinc particles via fluidized bed electrodeposition and without any operating problems.

1.15.2 **High Loading**

Zinc bed electrode incorporation to zinc-bromine batteries cells have been tested for high loading to establish high performance proficiently, steady charge, and discharge cycling over more extensive SoC ranges [404]. Particles of different microns on fluidized bed anode zinc-electrodes can only be suspended and expanded if a relatively low degree of the bed enlargement can be maintained to increase the current capacity [394].

Langde had further experimented Zambo's experimental observation and conclusion to this that was explored in the year 1980 by using a specific minimum fluidization velocity to fluidize some injected micron size of particles tested with silical gel to observe the different level of sound of pressure and frequencies [405]. Based on the result, the added particles fluidized smoothly with a low sound frequency but decreased the minimum fluidization velocity as the sound frequency was increased and further and continue to improve the pressure at the same level of sound [404].

The discovered result also showed that the two signals between particles and electrolyte potentials within a fluidized bed zinc-electrode can be measured instantaneously for their overpotentials. The experiment was carried out on copper beds particles of cathodic deposition from beds of zinc coated particles and acidified sulphate solution that is both passing through zinc deposition and dissolution with an alkaline zincate electrolyte. The potentials of copper

particles injected into the fluidized electrode showed both excellent band noise and low frequency compared to that of zinc-coated polymer particles. According to Mehrabi, bed porosities can increase by adding more particles sizes, decrease due to vertical velocities and make the fluid viscosities to rise [406].

1.16 Methods to Improve ZnBr2 Performance

1.16.1 Introduction to Fluidization Beds and Flows

As highlighted in section 1.15, formation of dendrites is a significant problem for Zinc based flow batteries. To address this problem, developing a fluidized zinc-reactor can be used to improve the cycling stability and prevent dendrites within these cells. Before developing this design, one needs to understand the nature of fluid flow. Different kind of fluid flow can be encountered in fluidized beds zinc-reactors when trying to improve zinc-bromine batteries cells performances and preventing dendrites problems. But this depend on the applied flow rate and the shape of such fluidized bed reactor. However, not all these flows (uniform and non-uniform flow, steady and unsteady flow and laminar and turbulent flow) are suitable for a fluidized bed reactor. Nevertheless, one important thing that should be considered when investigating various kinds of problem-related to a fluid is to know the kind of flow that is on ground and to have an idea of the problem and equation that should be applied [407]. Most importantly, “It is not simply the water quantity flowing in a river that is essential, but the entire environmental flow regime; as this will provide a quality flow, frequency, duration, timing, and the volume [408].

Fluid flow in porous media with the term deformation have been an enormous interest in various engineering disciplines especially in water resources, mining and petroleum engineering [409]. To be able to control turbulence flow, it is important to understand ways to achieve drag sub-laminar level of high Reynolds number since multiphase flows usually happen with turbulence in a technological application and nature [410]. Turbulence multiphase flows can make the direct numerical simulation in large timescales and length scales range of microscale coordination that is hard to be controllable for several applications. Large eddy simulation systematic approach can be used for dispersing multiphase flow beginning from microscale model.

1.17 Foundations of Fluid Mechanics with Applications

Fluid mechanics is a branch of science that deals with flow investigation about continuous external forces. Which deals with liquids, gases, and plasmas. The study of fluid mechanics is critical regarding predicting drags on airplanes and cars, rainfall, ocean currents and engines design. Fluid mechanics is also impressive when considering it from the mathematical perspective based on the nonlinear nature of its equations [411].

1.17.1 Liquid-Solid FBR's and Hydrodynamic Behaviour

In a suspension, velocity and volumetric concentration and their general relation are found to have the same sedimentation between velocity and particles concentration. Hydrodynamically, the similarity of liquid and solid systems in a fluidized bed makes particles to undergo no net movement and their maintenance in suspension by liquid flowing upward. Whereas, this description of performance is different in the sedimentation of particles suspension due to the particles moving downwards and liquid flowing upward as displayed by the settling particles. In a viscous solution, circulating fluidization regime begins earlier due to a liquid viscosity. Such process decreases in critical translational velocity and the onset of particles holding up and increasing due to rise in liquid viscosity for glass beads and sand as reported in a work of literature during fluid movement in a liquid-solid circulating fluidized bed of various viscous liquid together with injected particles [412-414].

The operating parameters effects studied are the primary flow rate of the liquid, different density, and size of the particles in the riser and the auxiliary flow rate of liquid and total liquid flow rate with the liquid viscosity. The particles circulation rate also increases based on the total and auxiliary velocity and increase in viscosity. However, such experimental result is in a literature entitled circulating liquid solid FBR. The report showed average particles holding up in an axial direction in a fluidized bed riser was investigated using liquids of different viscosities and considering the operating effects of the primary, secondary and the accumulative velocity parameters of the particle's diameter and the density.

This approach supported axial uniform mixing of the solid holding up in the viscous liquids in the riser by increasing the auxiliary velocity and therefore making the average solid holding up

in the riser to be decreasing [415]. Flow structure in two-phase (solid liquid) could exist by measuring and applying a particle tracking velocimetry. Therefore, further evaluation of both phases can be downward and upward flow in a pipe to show the effect of fluid flowing direction on the particles during motion.

1.17.2 Laminar (Streamline) and Turbulent Flow

Figure 1.21 presents laminar and turbulent flow. Turbulent flow is the kind of flow in which the fluid particles move in a highly disorganized manner leading to the rapid mixing.

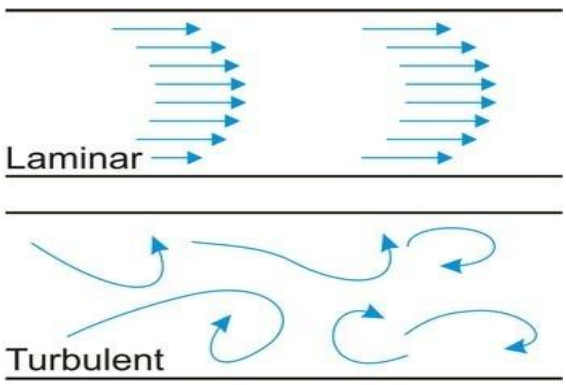

Figure 1. 21 Turbulent and Laminar Flow [416]

1.17.3 Uniform Flow and Non-Uniform Flow

The flow field of a uniform flow along any of the streamlines, magnitude, direction and velocity will not change from one point to another. However, it is mandatory for the velocity and area of a flow to be the same at every cross-section during a uniform flow, with the parallel streamlines and in straight manner. There can only be a change in the flow direction supposing the streamlines are not straight and if a change occur in the flow magnitude. Furthermore, this will only happen if there are no parallel streamlines. But the velocity can change in non-uniform flow streamlines from point to point.

1.17.4 **Steady Flow and Unsteady Flow**

With respect to time, steady flow in the flow field is the velocity at any point that does not change. But overtime, a change to the velocity at a point will make the flow as unsteady. A common example is the discharge constant rate that can be found via a pipe. The flow can only be steady and uniform if the pipe has a constant diameter. Flow from a nozzle can be regarded as non-uniform and unsteady since these flows happens at the same time and due to discharges rates. Regarding a steady uniform flow, in this kind of flow, with time or position, the conditions cannot change, and the cross-sectional area will be the same at each cross-section with the velocity of the fluid stream. A uniform flow of liquid via a pipe at full at a constant velocity can be a typical example.

The flow conditions in a steady non-uniform flow can change but not with time except from point to point. There can be variation between the cross-sectional area, the velocity of the stream and between the two cross-sections. But, for the two cross-sections, they cannot differ with time; e.g. liquid flowing via a tapered pipe at a constant rate and running totally full. The velocity in unsteady uniform flow is the same at every point and at a given instant of time. But there can be a change to the velocity with time e.g. liquid flow accelerating via a pipe of uniform bore running full, that can occur when a during starting a pump. From point to point; in unsteady non-uniform flow, the cross-sectional area and velocity can vary and change with time; e.g. a travelling wave along a channel.

1.18 Real and Ideal Flow

Travelling fluid can be in contact immediately with the boundary and have the same velocity at the boundary; while the fluid layers can increase when moving away from the boundary due to velocity. Shear stress can develop between fluid layers due to different viscosities and velocities in boundary layers. Boundary layers and its thickness can be equal to 99% due to free stream velocity and distances. It is possible to ignore the effect of shear stress outside boundary layers and treat the fluid ideally. High and low viscosity can create a thin boundary

layer based on the velocity of the fluid. Furthermore, treating a real fluid ideally is an assumption that simplify that a flow analysis can still leads to a useful result.

1.18.1 Non-Compressible Flow

Today, different computational approaches are available for solving incompressible flow problems [417]. The computational methods for solving (NSE) Navier-Stokes equation are generally within two groups but only incompressible flow will be discussed in this section [418]. Incompressible fluid flow is regarded as a change in fluid density when subjected to elevated pressure gradients or as a ways of transmitting forces across fluid [419, 420]. The primary differentiation between compressible and incompressible flow is the flow velocity. But incompressible flow density can be constant as fluid flows.

1.19 Fluidization

Fluidized beds of fine particles are formed more quickly and fluidized well compare to those of coarse particles. Surface-related forces tend to be compatible with smooth particles. Although fine particles are sometimes tricky to fluidize as there is the tendency for fine particles to develop large stable agglomerates that would remove virtually and by-passed the gas or liquid. In small diameter beds, in some extreme cases, the entire particulate mass may rise as a solid. The uniformity of a fluidized bed and its characteristic is often influenced critically by the support of the bed and gas or liquid distributor [421].

Additionally, the distribution of fine mesh is usually preferred with the category of nozzles at the base of the bed, even when the former is more difficult. Proper distribution of liquid or gas over a bed cross-section may sometimes be difficult to achieve if the pressure drop is not ensuring the broad distribution in a bed of large particles. Increase of flowrate can improve gas or liquid distribution to the pressure dropped across the bed during fluidization and based on independent flowrate. Increase in pressure drop across the distributor depends on the square of flow rate. Therefore, drop in the total pressure and fraction occurring across the distributor can increase rapidly when the flow rate increases. Low fluidizing velocity usually causes Non-uniformities and similar behaviour of gas-solid and liquid-solid fluidized beds. Fluidized beds

at low gas and liquid rate commonly exhibit a natural expansion when the flow rate increases with the relation between voidage and fluidizing velocity [29, 422-424].

1.20 Non-Uniform Fluidization

Non-uniformities majorly happen in deep beds with tiny particles. These beds types have a similar comparison to tapered fluidized bed enclosed with a different characteristic; in such a way that their capabilities are different towards handling particles of various sizes and properties for acquiring extensive mixing of particles [425, 426]. Usually, fluidized bed consisting of particles of different particles sizes can be incredibly complicated when dealing with them. Referring to section 1.14 in this (chapter 1), general fluidization happens when solid microparticles suspends in a fluid moving in an upward direction and behaves in the state of the fluid. Reactions in various fluidized beds are demonstrated using Kunni-Levenspiel fluidized bubbling bed model as presented earlier in Figure 1.20 also of section 1.14.

Once the reactant gases are formed and moves up while bubbling, mass transfers begins to happen as they move in and out of the dense mass particles. This process therefore allow the electrochemical reaction to take place [427]. The fluidization of particles with a liquid does not always bring regular and even expansion of beds that is mainly for solids with high densities. The separation in beds of particles of mixed sizes can have particles consisting of the significant sizes range. Beds voidage formation are due to occur in layers having the most significant particles coordinating a bed of reduced voidage. However, this is usually near the bottom, while the smallest particles can be establishing a bed of high voidage near the top.

1.21 Minimum Fluidization Velocity

1.21.1 Introduction

Many studies have been discussing the effect of fluidized bed materials and using minimum fluidization velocity (U_{mf}) for mixing and separating two different phases. Minimum fluidization velocity is a free-falling velocity of particles dwelling in the fluid. Concerning falling speed of particles, a single particle in an infinitely dilute suspension under gravity would

be falling quickly and accelerating for the time it accomplishes a steady state velocity. See also figure 1.22 for a pressure drop in respect to an applied superficial velocity.

Most studies continue to indicate that fluidization behaviour changes due to the complexity of the bed material. However, it has been difficult to provide a complete insight information due to these results not using adequate materials in burning process [428].

The expansion of bed is an essential aspect of studying for specifying fluidized bed height. The increase usually takes place due to the formation of bubbles, and this begins when it is beyond minimum fluidization velocity [429]. Another aspect to consider include the applied initial parameter and effect, inlet and particles temperature and the velocity of temperature, changes to solid particles and outlet [430]. Minimum fluidization velocity reduces with pressure increase.

Moreover, its influence on pressure is determined by the minimum fluidization velocities and encourages fluidization for bigger particles compared to particles that are smaller [431]. Various studies have been carried out to know the minimum fluidization velocities for biomass particles, and research has also revealed that minimum fluidization velocities work in conjunction with the bed height, and increases as the bed particles density are increased [432]. Increase in upward velocity of fluid flowing across a uniform packed bed of sphere particles results to incipient fluidization.

In a fluidized bed, there can be a pressure drop as fluid passes over the packed bed. Pressure drop within a fluidized bed is therefore roughly proportional to the applied velocity. Consequently, depth (l) in a bed of unit cross-sectional area and porosity (e) and the additional bed pressure available to the layout weight of the particles

In any fluidization operation, a crucial parameter is needed to achieve the required minimum velocity for a packed bed of particles to fluidize. A minimum velocity depends on some number of factors, e.g.; density of particles, shape, size, and the particles polydispersity. Acting net gravitational forces on particles can be altered directly by density, and later the velocity, minimum drag force before lifting a particle. The properties of the packed fixed bed can be altered along with the shape, the relationship between the velocity and drag forces and the connected void spaces and the fluid velocity through them.

Theoretical and experimental approaches can be introduced to know a minimum fluidizing velocity, Umf. In this research work, how a flow rate can be calculated to achieve a fluidized

bed will be described. This will be used to review the necessary designs governing the behaviour of a packed bed of particles before describing the procedure that can be used to estimate from experimental measurements a minimum velocity.

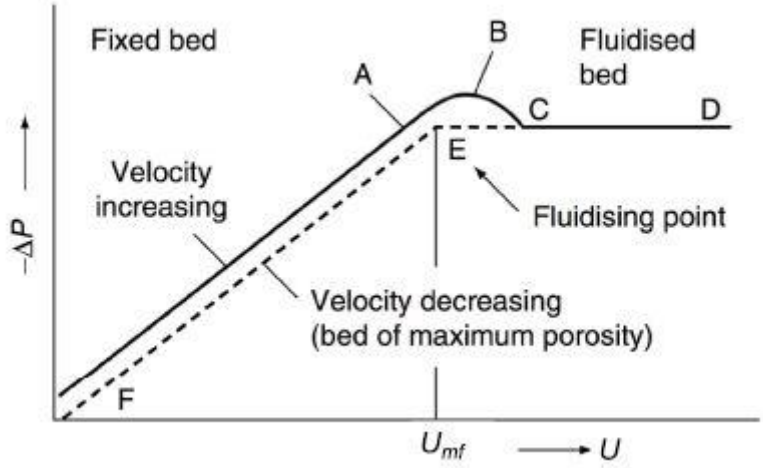

Figure 1. 22 Pressure drop ΔP in respect to superficial velocity

1.21.2 **Calculating Fluidization Minimum Velocity**

The Carman-Kozeny equation can be used theoretically for calculating minimum fluidization velocity as presented in equation 22. In this equation, the function of the shape and distribution of the particles size are identified as (d^2), the diameter, (ρ_s) is the density of the particles and (ρ) as the density of water.

Equation 22: The Carman-Kozeny equation used theoretically for calculating minimum fluidization velocity

$$\left(1.75\frac{\rho_f}{D_p\varepsilon_0^3}\right)u_0^2+\left(\frac{150(1-\varepsilon_0)\mu}{D_p^2\varepsilon^0}\right)u_0+\left(-g\left(\rho_s-\rho_f\right)\right)=0 \qquad (22)$$

The initial point at which the fluid, or gas flow will make a bed of particles to expand before lifting into a vertical column. With a minimum fluidization velocity (Umf), the particles will experience hydrodynamic drag forces (F_d) because of the fluid or gas flowing via particles of the packed bed and matches or surpasses the net gravitational forces (F_g). See equation 23 for the drag forces and gravitational forces on the particles.

Equation 23: Drag forces and gravitational forces on the particles

$$0 = F_g + F_d \tag{23}$$

Several similarities can be used to calculate and evaluate the terminal velocity of a particle. Packed beds of particles can also be balanced in the direction of gravity as presented in figure 1.23. Terminal settling is the final velocity to display the highest useful superficial velocity that is reachable in fluidized bed reactors [433, 434]. Though, fluid characterization is extensive and complex than what is usually our expectation. But, for the system of this research work, Newtonian fluids will be considered. A typical example of Newtonian is water and organic solvent but depending on temperature [435]. In the majority of fluidized beds, a Newtonian system can be satisfactory and have good interaction for the prediction of minimum fluidization velocities as reported in a present investigation [436].

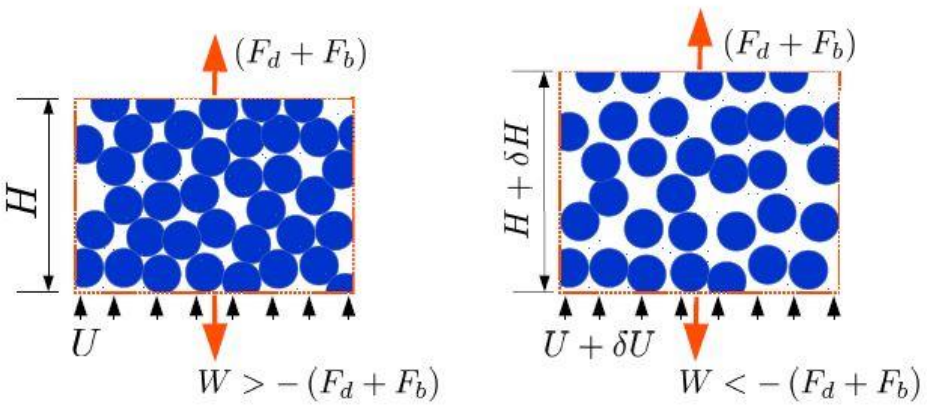

Figure 1. 23 Bed of particles with the force balance [437]

Particles are expected to be fixed in place when their weight (W) are exceeding the drag forces (Fd) with the buoyancy forces (Fb) based on the fluid velocity (U). The minimum fluidization velocity (U) can then be considered if the velocity (δU) increases slightly and make the bed to expand via a small amount of δH above the original height (H)

1.21.3 **Gravitational Forces**

Bed of particles net gravitational forces must consider the weight (W) of the buoyancy forces Fb, acting on these particles. See equation 24 for the physics.

Equation 24: Bed of particles net gravitational forces

$F_g = W - F_b$ $(P_P - P_f)gV_p$	(24)

Where (P_p) is the particles density, (P_f) is the fluid density, (g) is the gravitational acceleration constant, and (V_p) as the particles total volume inside a fluidized bed, (A), is the column cross-section area of the two-electrodes, and (V_t) is the velocity time. For a lower density fluid, the buoyancy force can be represented by a small correction to the net gravitational force. The equation of drag forces and a bed voidage can be similar and the gravity force but the definition for a bed is different. A bed voidage (ξ) can be define as the volume of fraction of voids in bed particles. See equation 25 for voids calculation in bed particles. A bed voidage, (ξ), is one of the key parameters that should be measured independently. Also see equation 26 for the total volume of the bed and equation 27 for further elucidation.

Equation 25: Voids calculation in bed particles

$$\xi = \frac{V_t - V_p}{V_t}$$	(25)

Equation 26: Calculating the total volume of particles within a fluidized bed

$$V_t = AH$$	(26)

In equation 26, a fluidized bed cross-sectional area can be represented by A and H as the bed height of the particles before fluidization. Therefore, the occupying volume by particles can then be written as presented in equation 27.

Equation 27: Occupying volume by particles within a fluidized bed.

$$V_p = AH(1 - \xi)$$	(27)

1.21.4 **Hydrodynamic Drag Forces**

Drag forces acting on bed of particles in this research work can be presented as showed below. See equation 28.

Equation 28: Drag forces acting on bed of particles

$$F_d = \Delta PA$$	(28)

(A), can be used as the column cross-section area of the two-electrodes and (ΔP) can be the pressure drop across the bed particles. The pressure drops across the bed of particles can then be calculated as described in equation 29.

Equation 29: Pressure drops across the bed of particles

$$\Delta \mathrm{P} = \int_0^{\mathrm{H}} \nabla \mathrm{P}(z)\mathrm{d}z \qquad (29)$$

In equation 30, the local pressure drops ∇P through the bed will be related a bed voidage, the particles details and the flow velocity with the fluid other properties. The fluid volumetric flowrate can be identified by (U), or as the superficial velocity that will be normalized by the cross-sectional area of the column. Added spherical particles sizes, details and shapes; can be accounted for via an equivalent sphericity factor (ϕ_s) and the corresponding volume diameter (D_e) . The sphericity of a particle can be equal to one. The equivalent diameter can simply be the diameter of these spheres [438].

Equation 30: Relation of a Local pressure dropping ∇P through a bed based on the bed voidage, the particles details and the flow velocity with the fluid other properties

$$\nabla \mathrm{P} = \mathrm{f}(\xi, \mathrm{U}, \mathrm{D_e}, \phi_\mathrm{s}) \qquad (30)$$

In homogeneous bed of uniform particles sizes, the voidage (ξ) can be the same on the bed. In this research work, the gradient of the pressure (∇P) may be the same throughout the bed and mixing. (Equation 28) of (∇P) over the bed of particles can yields ΔP = ∇P H. The bed particles drag forces can be calculated via multiplying the column cross-sectional area (A) as presented in equation 31.

Equation 31: Calculating the drag forces on bed particles via multiplying the column cross-sectional area

$$F_d = \nabla PAH$$	(31)

As presented in equation 32, either the drag force or the pressure gradient can depend on the velocity. But in a non-simplistic way. However, in the same way to other flow types. The pressure drops across the fluidized bed can also be related to the flow velocity through the coefficient of the friction (fp), Furthermore, according to equation 32, before the drag force can be obtained, the friction coefficient (fp) must be determined. The (fp) value will now depend on the flow regime, exactly like the drag force acting on a single particle. Reynolds number can be the best method to define the flow regime.

Equation 32: Drag force or the pressure gradient depending on the velocity

$$\nabla P = pff_p \frac{U^2(1-\xi)}{\xi^3}$$	(32)

In equation 33, a fluid viscosity can be recognized by (μ) and (R_e) for the voidage to adjust the use of a superficial velocity (U). (f_p) can be inversely proportional to Re_p. A flow can also be considered as inertialess when the $Re_p \leq 10$. But a flow within the inviscid Newton region and (f_p) can be independent of Re_p at a very high Reynolds number of values ($Re_p \geq 1000$). In an inertialess or viscous regime, the connection between the pressure drop and flow can be linear in relation to a Carman-Kozeny equation [439, 440].

Equation 33: Recognition of fluid viscosity using symbols (μ) and (R_e) for the voidage to adjust the use of a superficial velocity (U).

$$\mathrm{Re_p} = \frac{\mathrm{DU_{pf}}}{(1-\xi)\mu'}$$	(33)

Equation 34 is the derived form of an idealized model of a packed bed of particles like the proposed type of this research work. (d), represent the diameter and (ξ), is the bed voidage. In this equation, it is possible that (f_p) can be equal to $\left({}^{180}/_{Re_p}\right)$ which correspond to the surrounded variables of the frictional factors of Reynold number particles of a packed beds. Furthermore, according to the Burke-Plummer equation, it is possible that $f_p = 1.75$ [441].

Equation 34: derived form of an idealized model of a packed bed of particles

$$\nabla \mathrm{P} = 180\frac{\mu \mathrm{U}}{\mathrm{D}^2}\frac{(1-\xi)^2}{\xi^3}$$	(34)

To bridge the hole between the Burke-Plummer equations and Carman-Kozney equation, the proposed Ergun's theory in equation 35 can be applied and written as showed below. Equation 35 is the combination of a linear viscous and inviscid relations where the viscosity will be equal to zero. The modified constant value (150 instead of 180), was given by Carman and Kozney [442]. This value had been widely used and will be introduced to our experimental work in chapter 3 and chapter 6 of this research work to describe the flow via the anode zinc-electrode and cathode-electrode [443]. The value can fit any experimental data and is dependable in relation to variety of Reynold numbers.

Equation 35: Ergun's theory

$$\mathrm{f_p} = \frac{150}{\mathrm{Re_p}} + 1.75$$	(35)

Chapter 2
Purpose of the Research

2 Chapter 2 Purpose of the Research

The interest of this project is based on using $ZnBr_2$ battery cells to store energy and to address problems that are been encountered by these cells particularly on dendrite formation. Zinc bromine batteries cell materials can be expensive compare to other redox flow batteries cells; but ZnBr2 batteries cells systems has high cell voltage (1.828 volts) and highly oxidative element (bromine), demand cell electrodes, membranes, and fluid handling components that can withstand the chemical conditions. Regarding all these benefits has made zinc-bromine redox flow batteries as promising technologies for electrochemical energy storage.

Dendritic growth during cycling in ZnBr2 cells is the main limitation of zinc-bromine batteries cells because it does not only lead to perforation of the membrane but can short-circuit the cell and enhances hydrogen evolution and electrode passivation (corroded). Hydrogen evolution during charge at the low potentials required for the deposition reaction is a significant challenge. The presence of excess zinc ions can prevent this and improve zinc plating at all states of charges. The addition of zinc chloride ($ZnCl_2$) or zinc fluoride (ZnF_2) to an electrolyte solution for higher zinc concentration instead of the bromide formed can also suppress the evolution of hydrogen, with these optimal compositions; 2 moles $ZnBr_2$, 1 mole $ZnCl_2$, and 0.5 M NH_4Br. [444, 445].

Presently as discussed in section 1.16, introducing fluidized bed zinc-electrodes are the only option to prevent dendrite formation within zinc-bromine batteries cells [330]. Furthermore, since the fundamental reason for this research work is to address encountering problems on zinc-bromine batteries cells majorly on plating and dissolution of zinc ions onto the zinc electrode causing the electrode to deteriorate and shortening the cell life span via mechanical abrasion, some efficient and compulsory techniques can be introduced to solve these problems so that deposition of nano-structured zinc can be prevented from the electrode surface to retain the good performances and efficiency of the cell.

2.1.1 High Surface Area Electrodes

Fabricating different high surface area fluidized bed zinc-electrodes and carrying out separately numerical modelling on them to observe their capability for fast electron transfer during the

charge and discharge cycles would be good for fast deposition and dissolution of zinc-ions. Fluidized beds zinc-electrode can provide high mass and transferring of heat features, particles flowability, temperature, high solid and liquid mixing rates and uniformity [446-450] [451]. These proposed fluidized bed anode reactors can be injected with large zinc particles instead of using smaller particles. This is because particle sizes of three different fractions investigated in the past were based on these values (meters) (0.00012–0.00016 metre, 0.00012–0.0003 metre, and 0.00025–0.0003 metre) and within the liquid phase, where the issue of dispersion will be reduced by using particles sizes of wide distribution [452].

These reactors will initially be numerically modelled separately to demonstrate the flow of electrolyte before the proposed carbon particles will be added to one out of the modelled and suitable anode-reactors. Furthermore, the selected reactor is expected to be charged with some added carbon particles and glass beads and particularly to observe the formation of zinc morphologies on the anode-reactor and have a good contact with the anode-current collector. These reactors to be modelled separately are expected to have a fluidization region of 50 mm*50 mm*12 mm where current is expected to be collected within the anode fluidized bed reactors.

2.1.2 Electrodes Concepts

Six fluidized bed reactors (concept 1 to concept 6) were initially designed and investigated to observe their performances as listed below.

- Capturing of flows during charge
- Support fluidization during charge
- To support fast transportation of ions

1. Concept 1 was modelled in Ansys and not selected as the best candidate because the designed inlet and outlet were both positioned in the opposite direction. The results from the numerical experiment are presented in figure 2.1. The same conclusion was given to concept 2. Therefore, these geometries were not the appropriate reactors that should be incorporated to the anode cell-side due to the outlet and inlet position
2. Concept 3 and 4 required a long computational time and not selected because the generated cells exceeded 512 cells despite using different mesh types (multizone, cut

cell, tetrahedron and quadrilateral mesh methods). The generated meshes were also above the cells available from research license despite slashing the geometry as presented in. figure 2.2 Additionally, due to the shape of these geometries, they were not the appropriate reactors that should be incorporated to the anode cell-side.

3. Concept 5 and concept 6 were the best candidate that supported fluidization, capturing of flows, and the only geometry that could be suitable for the kinetic at the electrode, diffusion and the convection process. See figure 2.3 of the Ansys fluent result.

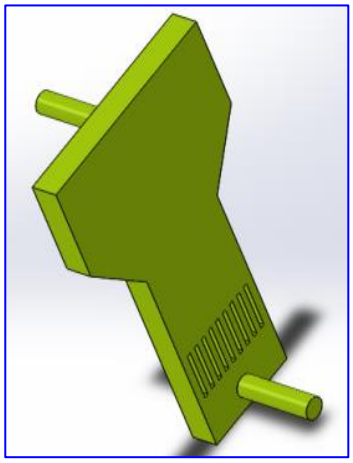

Concept 1

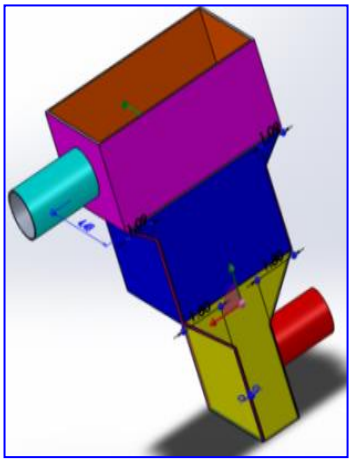

Concept 2

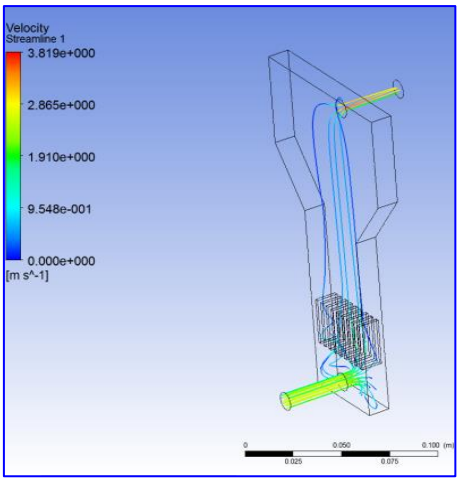

Concept 1 Electrolyte Potential - Ansys Fluent

Figure 2. 1 Concept one and Concept two

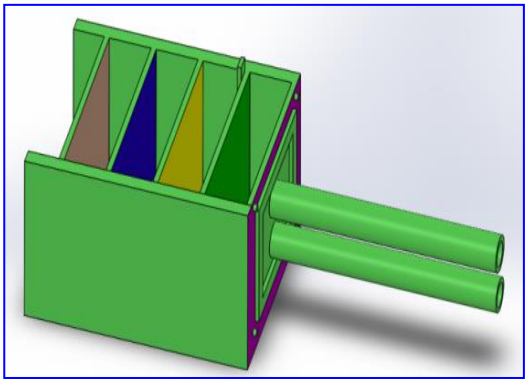

Concept 3

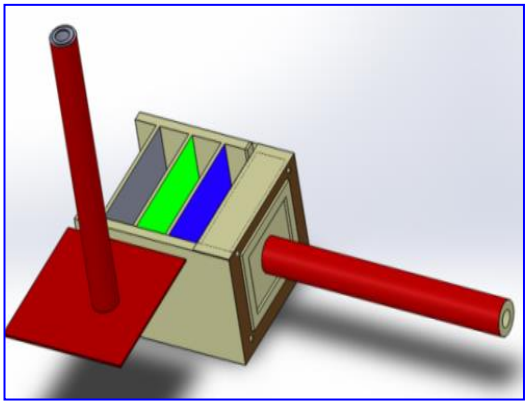

Concept 4

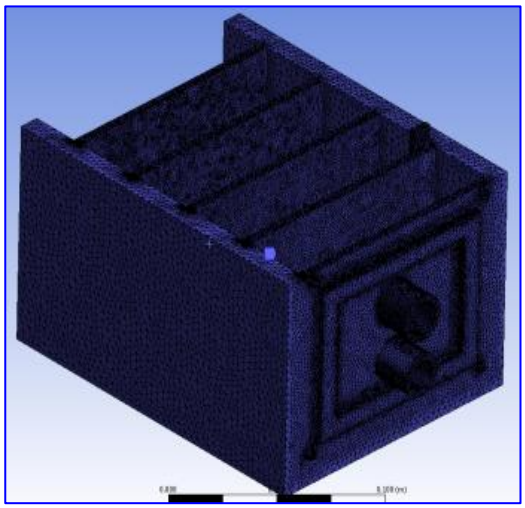

Concept 3 Mesh result – Ansys Fluent

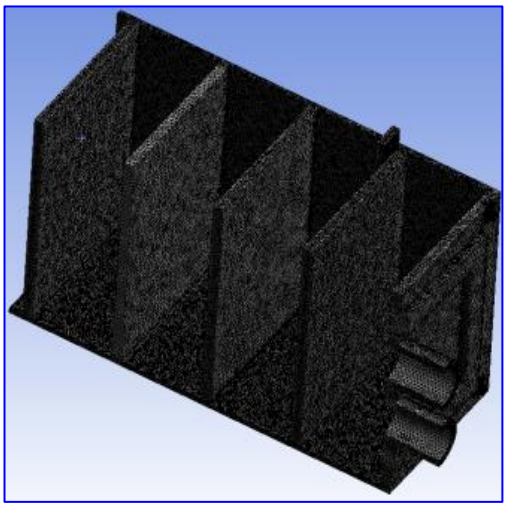

Concept 4 Mesh Result – Ansys Fluent

Figure 2. 2 Concept three and Concept four

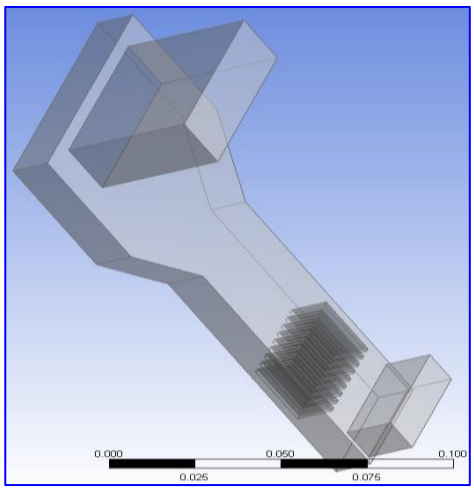

Concept 5

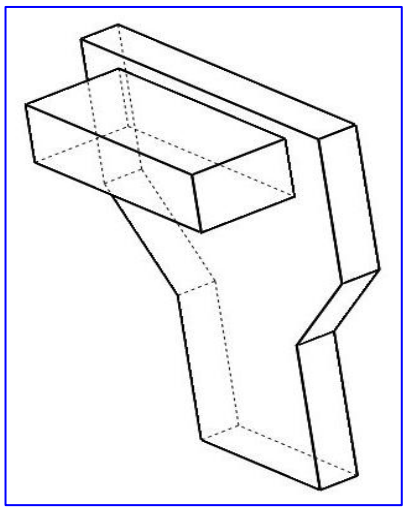

Concept 6

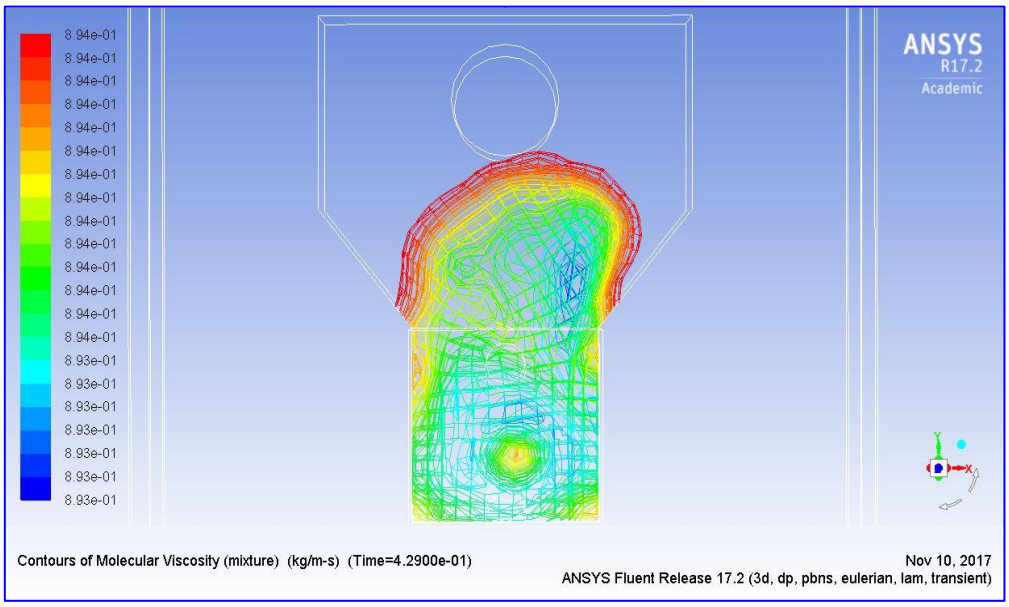

Concept 6 Front View of the Contour of Diameter (Phase-2)

Figure 2. 3 Concept five and Concept six

2.1.3 **Incorporating Glass Beads and Carbon**

Now that the six concept was the suitable reactor among others, and as the best candidate that will be further investigated, before adding some carbon particles to the anode-electrode for studying, it would be good and interesting to investigate first some glass beads within this proposed anode-reactor that will be fabricated. The proposed fluidized bed reactor measurements will be made as 100 mm*130 mm*12 mm and the proposed zinc bromine battery cell as 190 mm*190 mm*12 mm. Through this idea, there is possibility to observe the behaviour of these added glass beads whether they will be fluidized and behave in the state of the liquid at the point where a fluidization state can be reached when a minimum fluidization velocity value is applied. However, this minimum fluidization velocity is expected to be known during the laboratory experiment, possibly through using a flow metre that will be coupled to the anode-side of the cell to regulate the flow. See figure 2.4 for a sketched diagram of the selected concept 6 reactor.

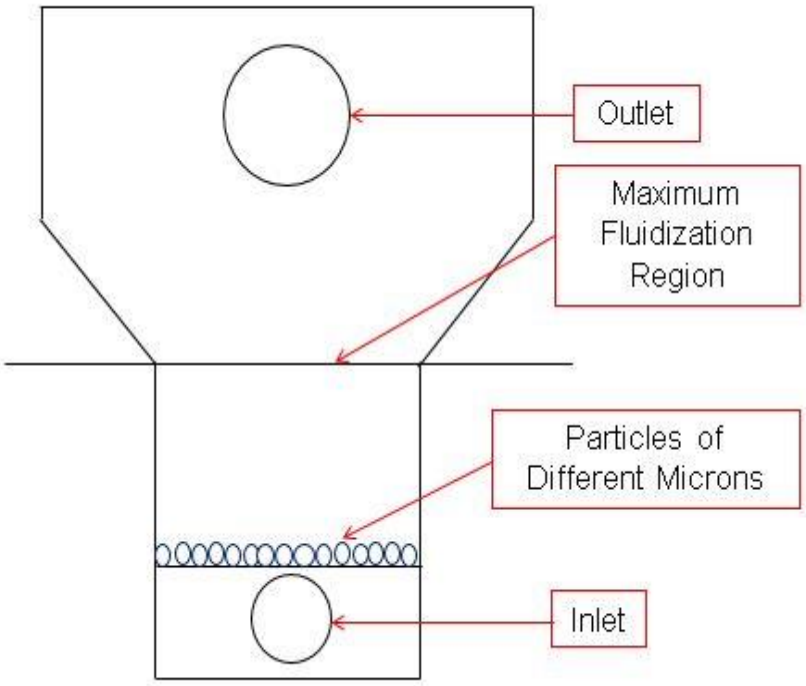

Figure 2. 4 Sketched Diagram of the Reactor

Regarding the suitable reactor (concept six), the maximum fluidization region, inlet and outlet of the proposed anode-reactor that will be fabricated and experimented in the laboratory are also labelled on the diagram. In addition, the fluidization region, 50 mm*50 mm*12 mm is where current is expected to be collected within the anode FBR reactors.

- THE ENGINEERING DRAFT OF THE DESIGNED AND FABRICATED ZINC BROMINE BATTERY CELLS COMPONENTS CREATED IN SOLIDWORK ARE PRESENTED IN THE APPENDIX (CHAPTER 9). THESE COMPONENTS INCLUDE THE GASKETS, MEMBRANE, THE TWO REACTORS ETC.

2.1.4 Proposed Feeder Electrode Materials

Carrying out further numerical modelling in ANSYS fluent and COMSOL would be interesting, and hydrodynamic experiment on the anode reactor. However, since it is believed and necessary to fabricate a complete zinc bromine battery cell apart from the anode-reactor that will added and charged with carbon particles and incorporated to the cell anode-side, investigating these electrode materials; carbon, nickel and titanium as current collectors would be also be exciting; by coupling them to the proposed zinc-bromine battery cells that will be fabricated. Also, it is assumed that studying these suggested electrode materials would be a good idea that can be used to observe their level of conductivity of these materials by charging the cell after incorporating these feeder electrode materials separately to the anode-side and cathode-side of the cell. In addition, the feeder electrode materials to be incorporated to the cell anode-side are expected to have a good contact with the proposed anode-reactor to be added with carbon particles and charged to see zinc deposition and morphology. These feeder electrodes materials can be coupled to the cell-side as numbered below.

1. Carbon electrode materials can be investigated as the cell cathode-side and anode-side current collector.
2. Carbon and nickel electrode material as the cathode-side and anode-side current collector
3. Titanium and nickel electrode material as the cathode-side and anode-side current collector.

Chapter 3

Hydrodynamic Evaluation, Umf and Ansys Fluent

3 Chapter 3 Hydrodynamic Evaluation, Umf and Ansys Fluent

3.1 Introduction

According to figure 1.21.2 of chapter 1, the pressure drops across a bed of particles can be used to measure and identify a minimum velocity of fluidization. The pressure drop in the reactor of this research work can continue to increase with the flow rate until the bed expands and the porosity is increased as displayed on (point A). The pressure drops within the reactor in this experiment with the specific velocity applied may not be linear because of the range of the Reynold number. As the velocity is increased, a maximum pressure drop can be attained.

Between the two points on the graph plot, (A and B) as presented earlier in figure 1.22 of chapter 1, the particles may be rearranged due to the frictional drag force; which can alter the voidage. The negative sign $(-\Delta P)$ on the (y-axis) on the graph can be used to indicate the drag force and its opposition to the velocity (U). Fluidization will occur at (point E) due to the minimum velocity that can be applied.

As a result, the pressure drop can decrease and (point B) and can rise beyond (point C). (Point U), can also increase above (point C) and the pressure drop will remain constant until it reaches (point D) if there is no further increase to a velocity greater than (point C). Furthermore, if the process is steadily reversed and lowered, the velocity (U) and (point E) can be found as an alternative instead of (point B) because of the different voidage. This can lead to re-arranging the particles and make the line (EF) as the process to reform the fixed bed of particles.

The theoretical diagram in figure 1.22 provides the (U_{mf}) basis for the experimental determination. (Point E), can be identified by increasing the fluid velocity to the maximum point until the pressure goes up and then ceased to change. The techniques can be used to define the (CD) line. This can be followed by reducing the fluid flow and be reduced to the line (EF). The minimum fluidization velocity can be represented where the two lines has intercepted and (point E) can be resolved by decreasing the velocity. The curve in figure 1.22 of chapter 1 can be identified as a steady-state flow by gradually increasing the velocity (U) with enough time to equilibrate the pressure drop. However, minimum fluidization velocity, U_{mf} can be subjected to an error until it is compared to the calculated values in (section 3.1.1 of this chapter 3). See equation 36 for the hydrodynamic drag forces and gravitational forces.

Equation 36: Hydrodynamic drag forces and gravitational forces.

$$0 = F_g + F_d$$	(36)

Where, F_g is the gravitational forces and F_d as the hydrodynamic drag forces

3.1.1 Calculating Fluidization Minimum Velocity

In this section of the research work, the previous Carman-Kozeny equation presented for calculating minimum fluidization velocity in section 1.21.2 was used here to calculate the glass beads minimum fluidization (0.001 m/s) and the added zinc minimum fluidization (0.001 m/s) See equation 37. In this equation, the function of the shape and distribution of the particles size. (d^2) is the diameter, (ρ_s) is the density of the particles and (ρ) as the density of water.

Equation 37: Function of the shape and distribution of the particles size

$$\left(1.75\frac{\rho_f}{D_p\varepsilon_0^3}\right)u_0^2 + \left(\frac{150(1-\varepsilon_0)\mu}{D_p^2\varepsilon^0}\right)u_0 + \left(-g\left(\rho_s - \rho_f\right)\right) = 0$$	(37)

3.2 Fluidized Bed Lab Experiment

3.2.1 Introduction and Objectives

As previously mentioned in section 1.22.2, the proposed flow has now been chosen and used for the explored hydrodynamic work in this section, concentrating on the laboratory fluidization experiments of the investigated glass beads and carbon-particles that were examined separately within the fabricated anode-reactor before incorporating this feeding electrode to the anode-side of the fabricated zinc-bromine battery cell and running it under a

set of operating condition via this suitable chosen flow rate from 0.001 m/s to 0.009 m/s for the added and investigated glass beads and carbon particles.

Figure 3.1 has showed some glass beads that were added and experimented separately within the anode reactor apart from the carbon particles before incorporating the fabricated anode reactor to the cell anode side. By carrying out a hydrodynamic laboratory and numerical modelling and simulation experiments on the glass beads and carbon particles will enabled the below listed objectives to be determined:

1. Observing the pressure drops and expansion via the fixed fluidized bed.
2. The verification of the Ergun equation (1952) theoretically for the laboratory experiment [453], Wen & Yu equation (1966) [454] for the numerical simulation thru using DDPM and DEM model in Ansys Fluent and Baeyens & Geldart equation (1977) [455, 456].
3. To observe the beginning of fluidization during the laboratory experiment

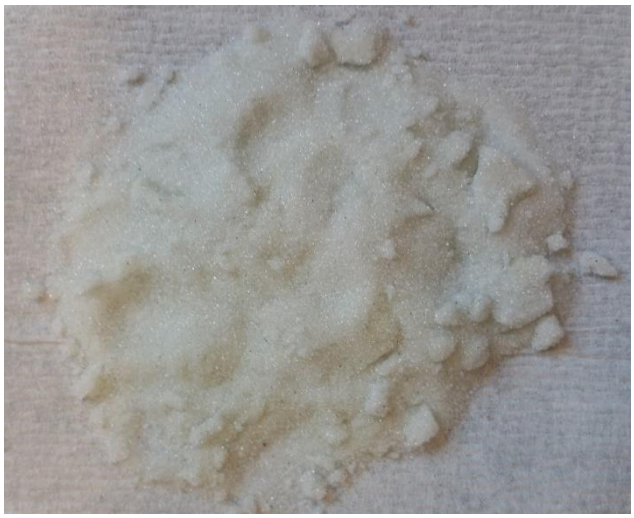

Figure 3. 1 Investigated Glass Beads

3.3 Experimental Procedures

At the cell anode-side, the incorporated anode reactor was separately filled up with some quantity of carbon particles and glass beads to a height of 35 mm and both carbon and glass

beads particles were examined discretely one after the other. Both glass beads and injected carbon particles fluidized as expected and behave in the state of the fluid. At 0.0046 m/s, the glass beads had gained its steady state and at 0.0047 m/s, the investigated carbon particles had also gained its steady state. Through the experiment, the applied minimum fluidization velocity was maintained for the glass beads and carbon particles to prevent the pressure from dropping drastically. Alone, some glass beads were initially investigated in a flowmeter reactor experimented again within the anode-zinc electrode apart from the carbon particles that was just examined in the fabricated anode-reactor. The fabricated reactor is presented in figure 3.2 under sub-section 3.3.1. The examined carbon particles and glass beads results will later be offered in section 3.4. Furthermore, a DC power supply was used to control the current and a small centrifugal pump for transferring the fluid. The small centrifugal pump was coupled with the used flow meter reactor added with some quantity of glass beads before re-introducing them to the fabricated anode zinc electrode (reactor). But the glass beads quantity was not measured and the carbon particles. The final applied flow rate was 166.7 cm^3 min^{-1}as it was gradually increased from 1 cm^3 min^{-1}. This flow rate was approximately 0.0046 m/s and 0.0047 m/s by converting the values to cubic meter per second m^3/s and to m/s as summarized below

0.05 m*0.05 m*0.012 m*166.7 cubic meter per minute = 0.005 m/s

The apparatus (test tube flowmeter and fluidized bed anode-reactor) used for this experiment were carefully checked to know their condition or else they might affect the experimental data.

1. The carbon particles were filled within the anode-reactor up to a height of 35 mm and examined. The same height applies to the added and examined glass beads. But only the carbon-particles were between 254 microns to 354 microns.
2. Zinc nano-particles density is usually 7140 kg/m^3. However, the zinc particles are expected to increase during charge and the glass beads particles density was not measured but appeared very tiny compared to the carbon particles.
3. This was followed by operating the centrifugal pump at a constant flow rate of 166.7 cm^3/min. Theoretically, the minimum fluidization velocity for both glass beads and zinc-graphite were 0.001m/s respectively. These values were calculated through the available minimum fluidization velocity equation in equation 37 of section 3.1.1 of this chapter 3.

4. The bed expansion and reading of the injected glass beads and carbon particles were based on the fluidization level and the state of the bed when the flowrate was increased.
5. The glass-beads and carbon-particles experimental data were both carried out within the anode-reactor for easier observations. The viscosity of added distilled water with the glass beads was also measured and repeated twice using a Ubbelohde viscometer device [457, 458].

3.3.1 Apparatus

Figure 3.2 is the fabricated anode reactor where the glass beads and carbon particles were separately investigated.

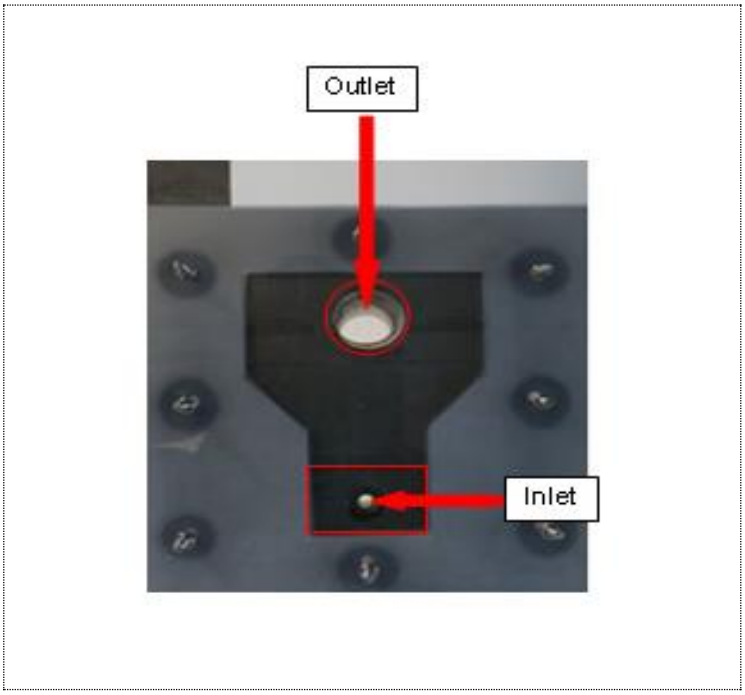

Figure 3. 2 Anode Zinc-Electrode

3.4 Description OF Results – Investigated Glass Beads and Carbon Particles

Figure 3.3 presents (a) the fluidization state of the investigated fluidized glass beads and (b) the carbon particles. A flow rate of 166.7 cm^{-3} per min was separately applied to the

investigated glass beads and carbon particles within the anode-reactor to fluidize these particles. These two different particles were filter with a nickel sieve mesh to obtain precisely particles sizes between 254 microns and 354 microns for the carbon particles alone.

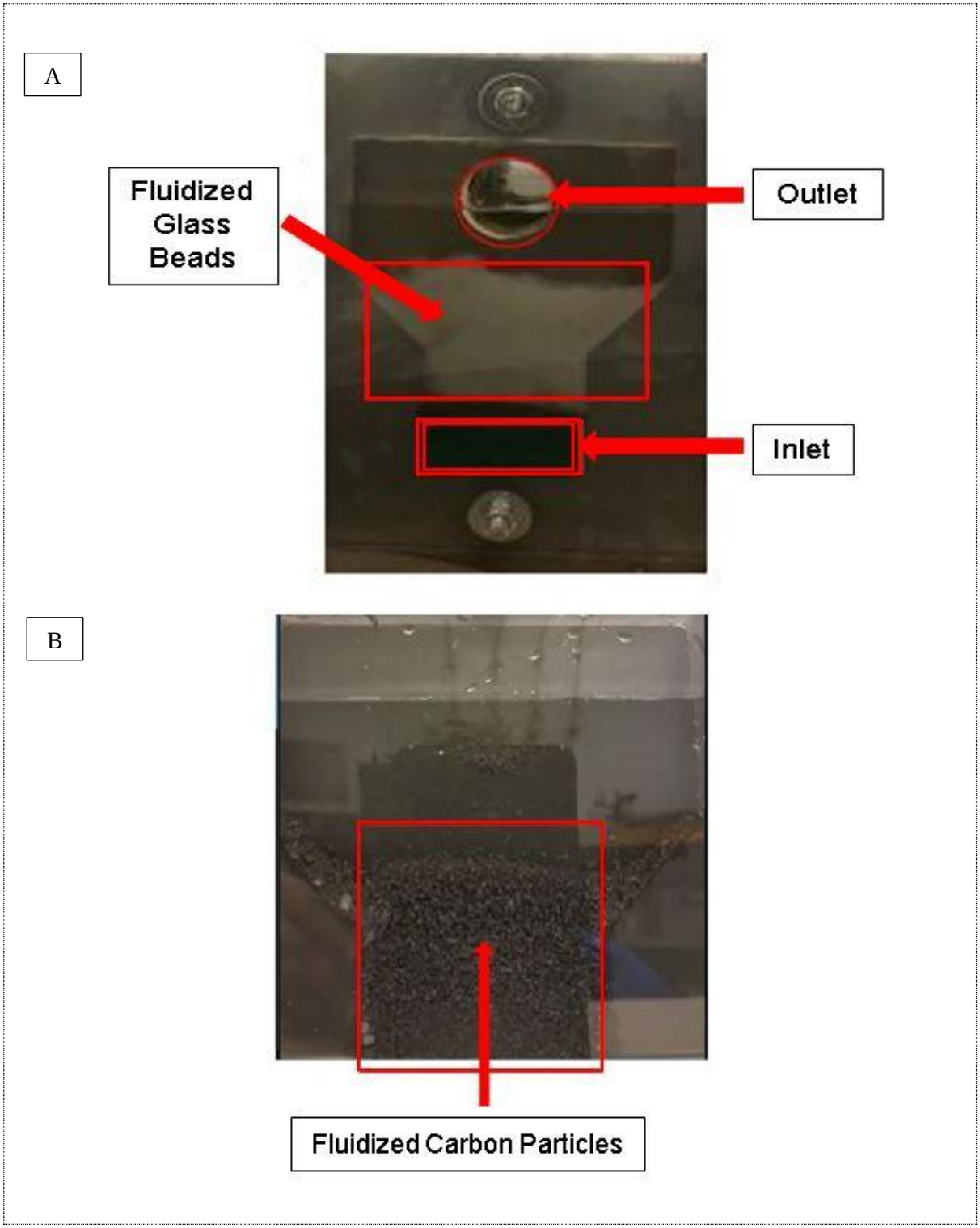

Figure 3. 3 Anode Reactor with (a) Fluidized Glass Beads and (b) Carbon Particles

3.5 ANSYS-Fluent

3.5.1 Introduction

Numerical modelling in academia and industry is quite common. Various physical systems can be understood via a numerical approach. Approaches such as Discrete Element Modelling (DEM), and dense discrete phase model (DDPM) in Computational Fluid Dynamics (CFD), Finite Element Analysis (FEA) are used globally [459]. Their popularity still grows, increase and the demand for computationally simulations still runs and highly accepted. Fluidized beds are common in industry but can be difficult to simulate because the device does not depend only on the pressure drop across the bed [460]. This is because it usually contains added particles, which can make the modelling to be complex due to the interactions of the fluid and particles.

Computer fluid dynamics, CFD packages are very suitable for modelling pressure drops in fluidized bed reactors but except for the particles presence that can be large in number [461]. The DDPM+DEM model in Ansys fluent during fluidized beds modelling can handle the interaction of complex particles and their collisions calculations [462]. This section examines the flow of electrolyte through (1) a packed bed of glass beads and (2) via some added carbon particles for results validation under a minimum fluidization condition within a fluidized bed zinc-electrode that was incorporated to the anode-side of a fabricated zinc-bromine battery cell system.

3.5.2 Numerical Purpose and Design

To determine the flow regime required to provide good fluidization. The chosen reactor geometry that was designed for the cell anode-side is represented in Figure 3.4. The anode-reactor was separately used to investigate the carbon particles and glass beads. This designed anode-reactor would be used to carry out the modelling work and to study the fluidization of particles within the half cell. Therefore, this required setting up the boundary conditions to the model, including the physical boundaries of the cells that was achieved by producing a solidwork model of the cell. This was then imported into Ansys fluent and for fluidization studies. It was necessary to carry out a fluidization experiment within the designed fluidized

bed reactor at the cell anode-side to observe the electroplating behaviour of the added carbon particles. This is in form of a parallel projection, in which all the projection lines are orthogonal to the projection plane.

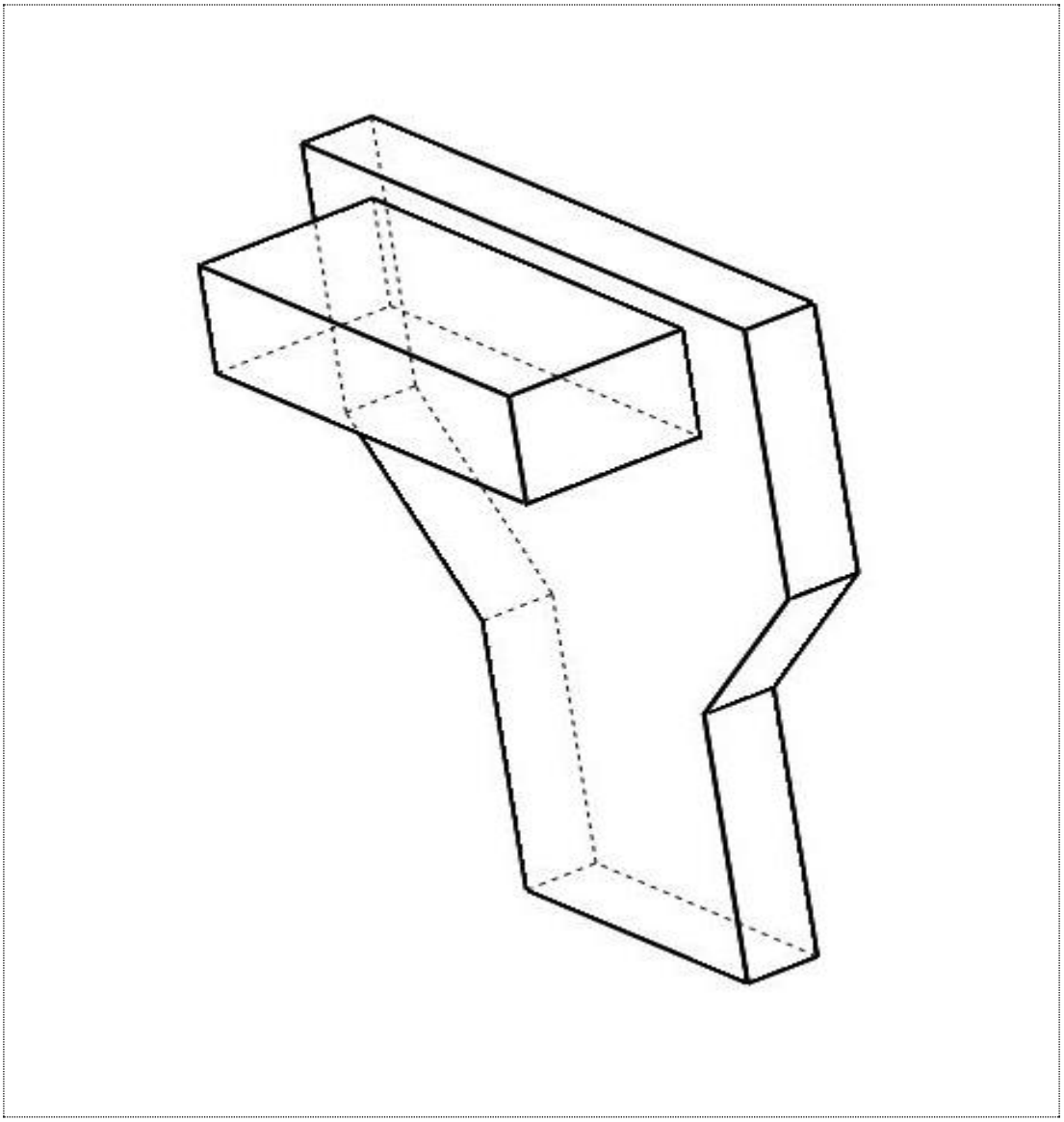

Figure 3. 4 Anode-Side Reactor

3.5.3 **The Designed Battery Cell Test Rig**

To design the complete zinc bromine battery cell test rig was also important to show where the whole laboratory experiment will be explored. The orthographic view of the designed battery cell test rig was presented differently in multiple views. All the engineering drawings of the battery cell components and the two incorporated reactors (anode and cathode) are presented in this thesis appendix in (chapter 9). See Figure 3.5, figure 3.6a and b and figure 3.7a and b for other presented components.

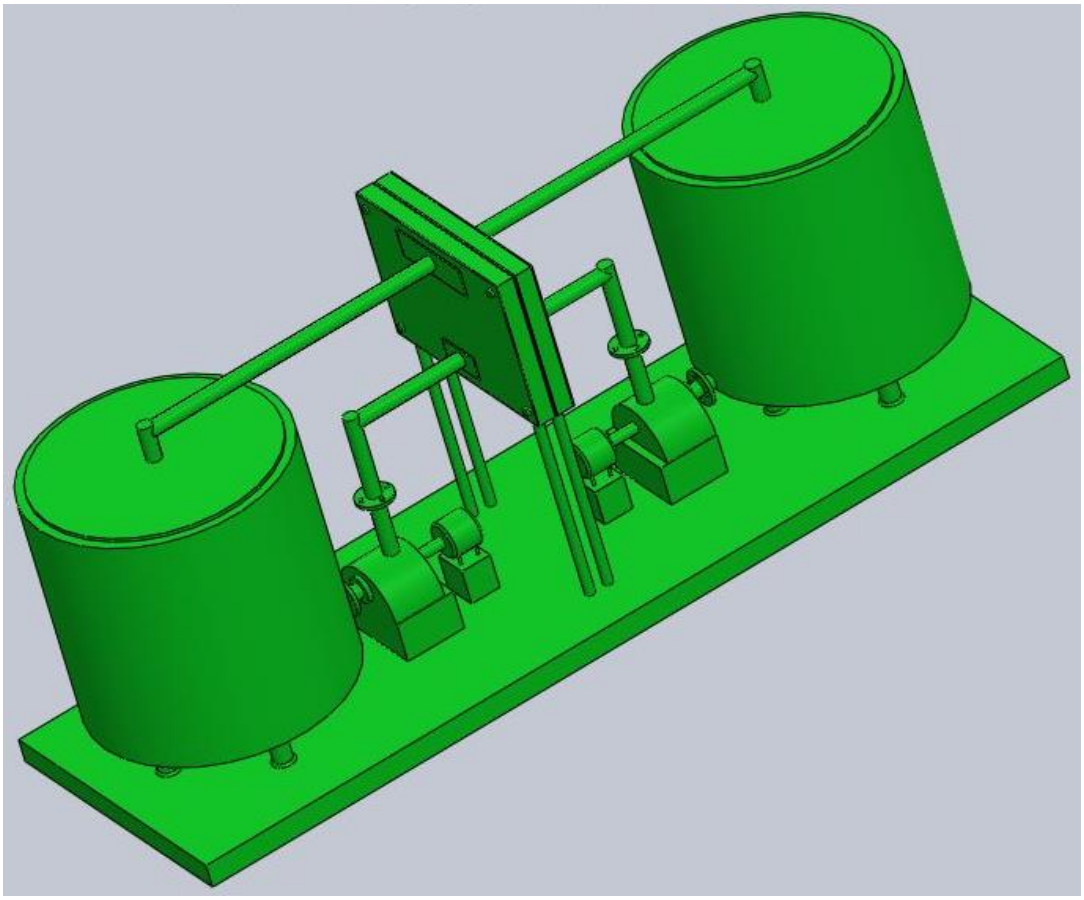

Figure 3. 5 Zinc-Bromine Battery Cell Test Rig Isometric View

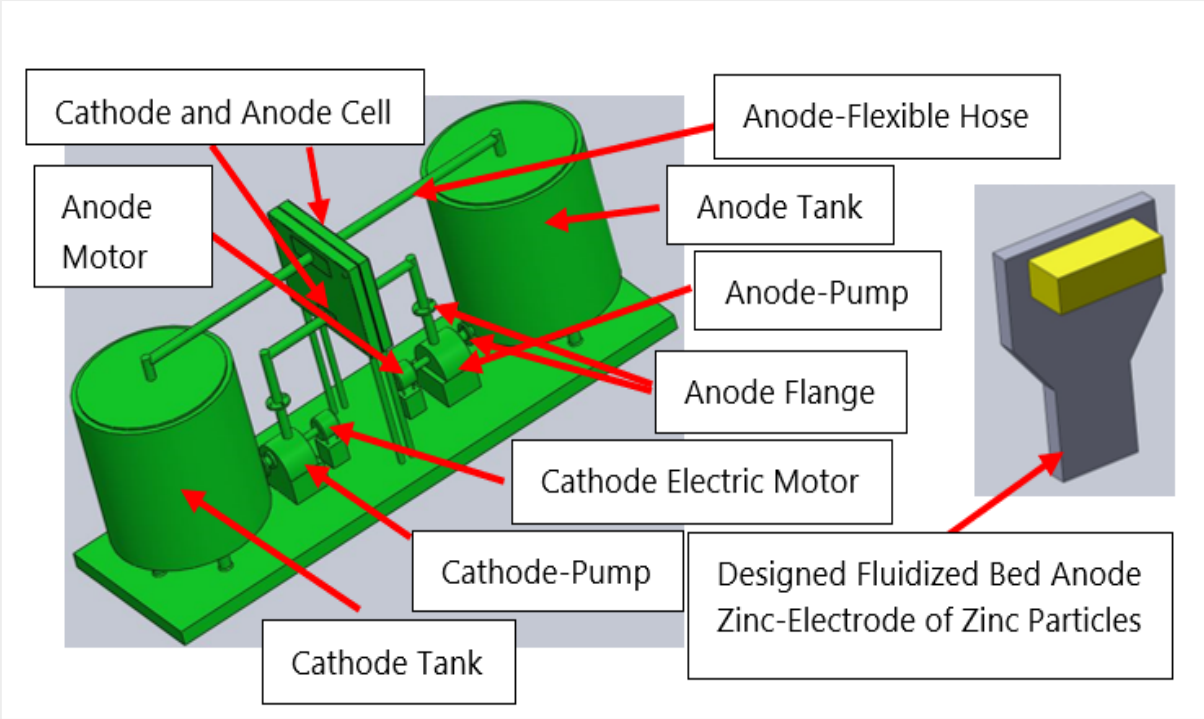

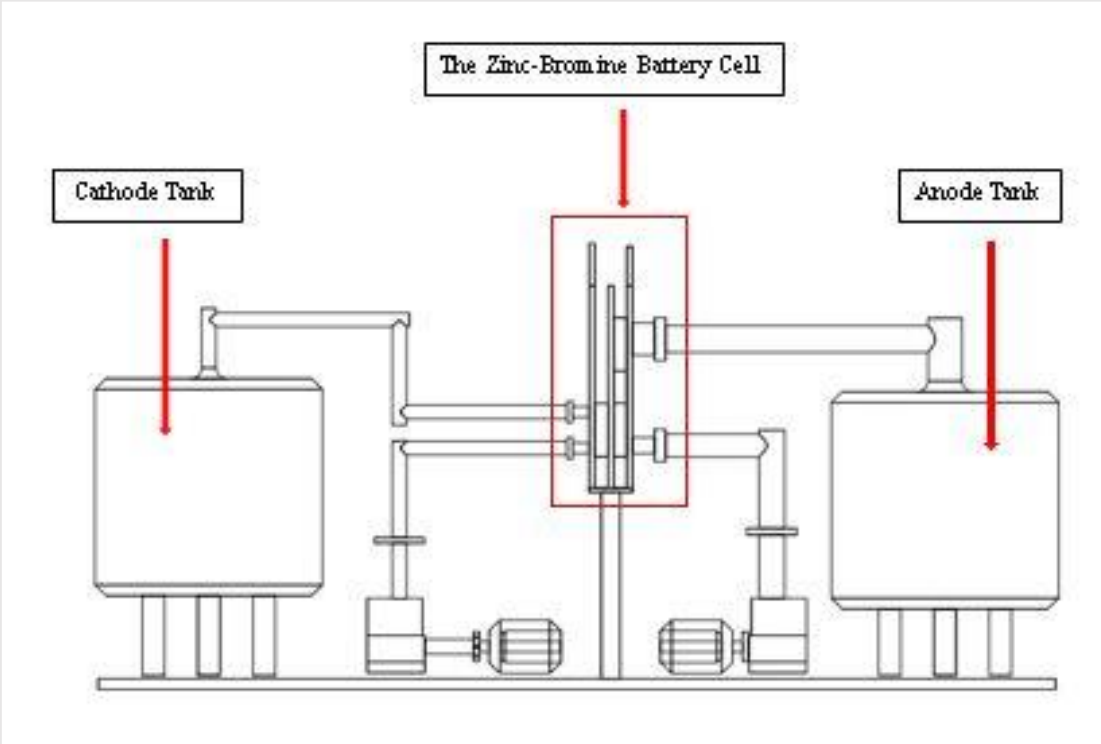

Figure 3. 6 (a) The ZBB labelled components and (b) a complete Front View of the Designed - Zinc-Bromine Battery Cell Test Rig showing the anode and the cathode

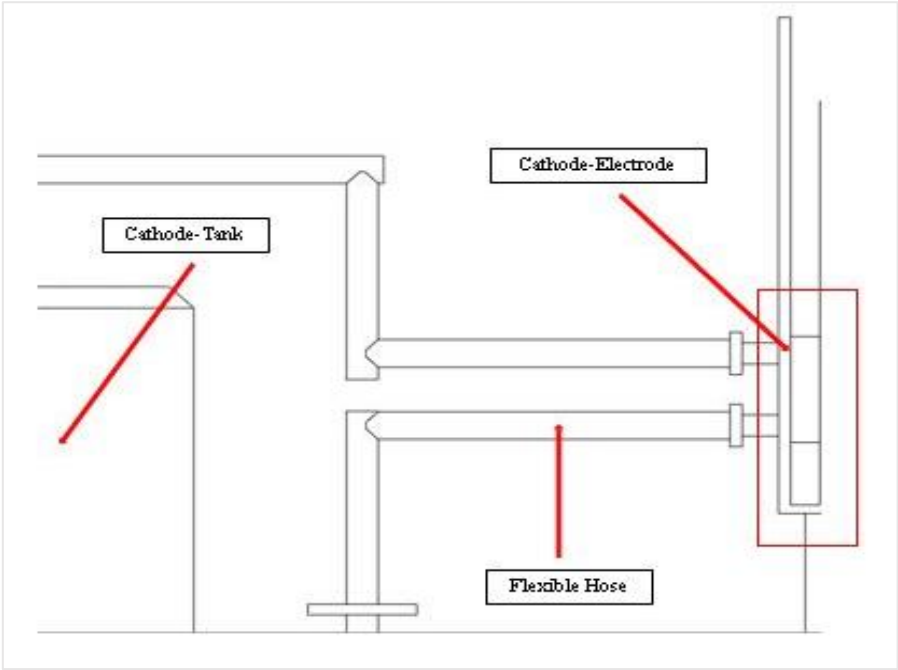

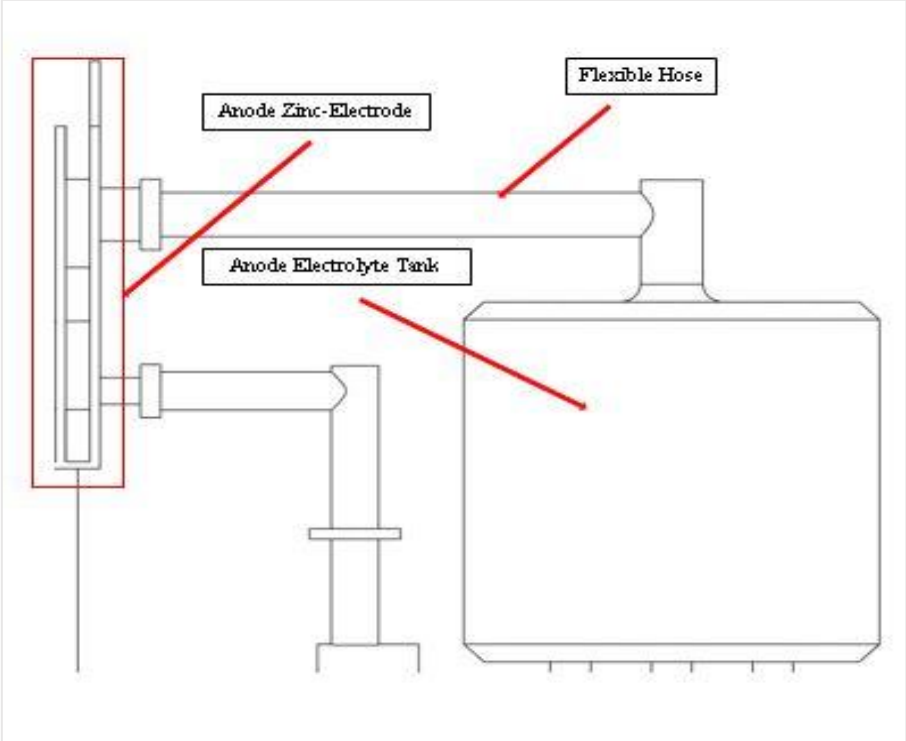

Figure 3.7(a) Side View Cathode-Cell Compartment and (b) Side View Anode-Cell Compartment

3.6 Problem Description in Ansys Fluent

The fluent version in ANSYS 17.2 was used for the modelling and simulation. The application of the used models is described in this section. The fluidized bed zinc-electrode was modelled by using the dense discrete phase model and discrete element method approach in Ansys. These models are widely used for the simulation of powder systems and suitable to determine complex phenomena based on flowing particles. Dense discrete phase model is suitable to model dense particulate flows and accounts for particles blockages and their effect on the primary phase solution [463].

The fluidising behaviour of carbon particles and glass beads investigated within the anode zinc-electrode were studied via the DEM model and collisions of these particles with the Dense discrete phase model (DDPM model) [464, 465]. The anode-side and cathode-side electrode of this research work were both designed to suite the required standard by considering their thickness due to the impact and importance of what these developed reactors (electrodes) will provide regarding their electrolyte feeding mode and performances of the flow rate as reported in works of literature especially on redox flow batteries (RFB) [466].

Besides, the electrode can be modified in agreement to some works of literature by adjusting electrodes of some fluidized bed reactors with their performances. In addition, the electrodes of this research work are specially made because of their contribution to cell voltage loss during charge transfer and ohmic resistances as reported again in some pieces of literature [467, 468].

3.7 Preparation and Modelling of the Problem

3.7.1 Boundary and Initial Conditions

The anode-side reactor was initially modelled and simulated with some amount of added glass beads and was later modelled separately with graphite particles in ANSYS as a 3D fluidized bed zinc-electrode. Investigated velocity were between 0.001 m/s to 0.098 m/s for the glass beads and zinc-particles. The bubbling fluidized bed zinc-electrode was modelled and simulated in Ansys fluent by using these approaches (Huilin-Gidaspow, Schiller-Naumann,

Wen-Yu, and Syamlal-Obrien model and finally selected the Wen-Yu model [465]. The values for the initial and boundary conditions presented in Table 3.1 were fed into the system (reactor).

Table 3. 1 Boundary and Initial Condition

ANSYS FLUENT DDPM + DEM MODEL		
Names	Glass Beads	Zinc Particles
Primary Phase	Liquid	Liquid
Secondary Phase	Solid Density (2520 kg/m^3)	Solid density (7140kg/m^3)
Mesh Type	Multizone	Multizone
Inlet Liquid Temperature	293K	293K
Inlet Pressure	101325 Pascals	101325 Pascals
Outlet Pressure	101600 Pascals	101600 Pascals
Inlet Velocity Magnitude	0.003 m/s	0.003 m/s
Total Flow Rate	0.00408 (Kg/ s)	0.00408 (Kg/ s)
Minimum Particle Sizes	0.00038 (m)	0.00038 (m)
Maximum Particle Sizes	0.00042 (m)	0.00042 (m)
Physical Model	Wen-Yu	Wen-Yu

Particle Time-Step Size	0.0002	0.0002
Particles travel velocity	0-50 m/s	0-50 m/s

These used parameters and boundary conditions has assisted to carry out successfully the (3D) modelled fluidized bed. The fabricated reactor of size (100 mm*130 mm*12 mm) was initially charged with carbon particles and with a chosen speed of (0.098 m/s) and a flow rate of (0.00408 kg/ s^{-1}) equivalent to 245.049g/min due to the calculated anode-side electrolyte density (1.47 g/ cm^{-3}).

The use of multizone mesh simulation for particle tracking results has the highest particle tracking number and a good pressure drop at the outlet compared to other mesh methods. Furthermore, the three essential aspects that were considered before choosing the hybrid initialization method were because of this approach solver enhancement for convergence robustness, improvement rate and particularly on the computational fluid dynamics simulations [469].

Referring to most of the standard fluidization curve with kinds of literature, the superficial velocity applied to the fluid inlet was gradually increased and made the bed to fluidize by using a minimum fluidization velocity. Apart from the expansion behaviour of added carbon particles to the fluidized bed zinc-electrode (reactor), the use of minimum fluidization velocity also assisted during the numerical simulation as an essential approach for specifying the height of the fluidized bed zinc-electrode, and seeing the particles not escaping.

The interaction of added carbon particles on the zinc-electrode would further address problems with the current state-of-art; such as the speed of charging and discharging onto planar surfaces shortening the lifespan of the cell due to poorly controlled deposition of zinc in other parts of the cell such as dendrite formation within the membrane. The use of a minimum fluidization velocity is significant because applying a small superficial velocity will not make the bed to fluidized and behave like a packed bed. The fluidization curve has been used as one of the classical phenomena methods for understanding fluidization [470-472].

The pressure applied in pumping the fluid through the anode and cathode reactors were both studied as a function of the superficial velocity. There was a linear increase under the packed bed (injected carbon particles) condition when the velocity increases gradually with the pressure as the superficial velocity increases.

Furthermore, the increase tapers off (diminished gradually) when the state of initial fluidization was achieved, and when a constant value of the pressure was reached. It was noticed that the condition of a continuous fluidization with pressure force is enough to maintain the weight of the bed and its buoyancy (floating or rise) as observed and shown below.

$$< \mathrm{P} >_{\mathrm{Inlet}} \times A_{inlet} = \text{ Buoyant weight of bed}$$

3.7.2 Mesh Preparation and Fluent Launcher

The dimension was interactively specified in Ansys fluent, displayed, processed and as another alternative in the Fluent Launcher. Ansys fluent was used to performed different checks on the mesh, and all progress was reported in the console. The minimum volume published in the console was noted, and transient solver was also enabled from the time list. Furthermore, both the Eulerian multiphase model and Dense Discrete Phase model were allowed and in the discrete phase model and acknowledged the updating of DPM sources at every flow iteration. The injected carbon particles were tracked with the electrolyte at a flow time step of (0.0002) and for the carbon particles time step size(s).

3.7.3 Eulerian and Lagrangian Approach

The cartesian coordinate system specifies uniquely each point in a plane of differential coordinates of signed distances from perpendicular two-point direct lines that are measured in the same unit of length. The Eulerian and the Lagrangian approach are the two general

coordinate systems that have been extensively used in the computational fluid dynamics of this research work.

The use of a unified Eulerian coordinate method was introduced to the computational fluid dynamics and multiphase numerical simulation of this research work to prevent and resolve any occurring flow discontinuities [473]. The enabled discrete element method was allowed due to its suitability for granular matter simulating such as the bead of several materials, coal, and gravel.

The simulation carried out in this research work are characterized by particles of high-volume fraction where electrolyte interaction with particles is essential. To define many injections and differentiate between them during the modelling of the fluidized bed, some procedures were introduced for describing the injection of these particles so that no problems will be encountered during the modelling and simulation as it is in most industrial applications [474].

The modelling and simulation conducted in this research work to examine injected particles can also be used as another kind of measurement in particle systems due to science development which enables researchers to have deep insight in particle system so that the detailed behaviour of the particles can be obtained [475]. The chosen materials for the particles were created in Ansys fluent based on the electrochemical compounds of mixtures anode and cathode electrolyte and using the appropriate density and viscosity of this substance.

3.8 Results and Validation

3.8.1 Carbon and Glass Beads

The presented validated results in table 3.2 were explored experimentally, numerically and theoretically. These include the minimum fluidization velocity (U_{mf}) and the pressure drop of the investigated added glass beads and carbon particles with water within the anode reactor. However, the pressure drop was not explored theoretically and during the laboratory experiment but only numerically on Ansys. Theoretically, the minimum fluidization velocity was in good agreement with the Ansys numerical value. Experimentally, theoretically and numerically, a lesser flow resistance was observed within the anode-reactor when added with

glass beads compared to the carbon particles. This was due to the similarities between their densities and mass.

Table 3. 2 Theoretical and Experimental Results

Parameters	Minimum Fluidization (U_{mf})	Change in Pressure ΔP (Pascal)
Glass Beads + Water		
Theory	0.001 m/s	Not Calculated
Ansys	0.003 m/s	0.0995218
Experiment	0.0046 m/s	Not Measured
Carbon Particles + Water		
Parameters	Minimum Fluidization (U_{mf})	Change in Pressure ΔP (Pascal)
Theory	0.001 m/s	Not Calculated
Ansys	0.003 m/s	0.07493255
Experiment	0.0047 m/s	Not Measured

3.9 Conclusions

3.9.1 Computational Experiment

Numerically, both the experimented (a) glass beads and (b) graphite particle residence time (mixture) seconds are displayed in Figure 3.8. The simulation time of the experimented glass beads was for a short period to prevent the particles from escaping from the anode-reactor's outlet compare to the added zinc-particles. The added glass beads were not uniformed within the reactor unlike the zinc-particles during the numerical simulation. These two particles densities carbon and glass beads could have resulted to such discrepancy. For instances, the glass beads density was (2520 kg/m^3) and the zinc particles solid density was (7140 kg/m^3). Furthermore, these has affected the spherical shapes of these two investigated particles which have also contributed to the outcome of the result.

Specifying different parameters had assisted through the numerical simulation and the used of rosin-rammler particles distribution in the setting the injection properties in Fluent as an addition to the initial velocity applied at the zinc-bromine battery cell anode inlet, temperature and total flow rate. During the experimental numerical modelling and simulation as reported in several literatures, the use of particle sizes in between (380 microns to 420 microns) had assisted to know the challenges that were encountered; such as particles disappearing, terminating, and escaping from the outlet of the anode reactor. However, just the investigated zinc-particles fluidized as expected during the experiment.

By importing the anode-zinc-electrode geometry into the Ansys workbench and simulating it was to generate a physical working model of the cell and validate simulations results experimentally and to demonstrate laminar flow on the cell.

Furthermore, and to investigate the electroplating and dissolution of the zinc during charge and discharge events. The designed reactor during the modelling and simulation showed that it has the capability of producing an electrode that reduces losses during charge and discharge and can create enough mass transport of zinc ions. The reactor was capable of quick exchanging of electrons based on the speed of charging and discharging onto plane surfaces according to the observations made in Ansys CFD Fluent by running at 0.001 m/s.

Multizone simulation result had been considered among different simulation results because of the RMSE value and the generated cell numbers in Ansys CFD Fluent compared to others mesh methods like hexahedral, automatic, cut cell, and tetrahedron. Israt as a researcher has also observed and reported similar advantages of this mesh approach in an experiment of a research paper on the importance of mesh convergence due to its strength in achieving a quick solution and having a good result [476].

The used engineering judgement and numerical simulation has revealed that using multizone mesh method was suitable to address the problem of this numerical problem; due to the number of generated element and flow capturing and to achieve a residual continuity equation value of $1*10^3$. Furthermore, having an accurate mesh and boundary conditions has predicted having a precise convergence and to achieve faster convergence by requiring a better mesh quality which guarantees a solution that is accurate.

The convergence of this research simulation is defined by looking at the residual values ($1*10^3$). Nevertheless, this has clarified the validity of the solution and having the possibility to have values closed to 1% [477]. Chapter 4 will particularly be focusing on the electrochemistry aspect of the research work via using COMSOL.

3.9.2 Hydrodynamic Experiment

Experimentally, during the hydrodynamic experiments with the glass beads and water, a minimum fluidization velocity was achieved in between (55.56 cm^3/ min^{-1}) to (146.7 cm^3/ min^{-1}) and in between (70.56 cm^3/ min^{-1}) and (166.7 cm^3/ min^{-1}) for the carbon particles and water. Therefore, due to these observed results, it was confirmed that the comparative carbon particles sizes would fluidize as expected within the anode zinc electrode when incorporated to the anode-side of the fabricated zinc-bromine battery cell during the charge and discharge state.

A

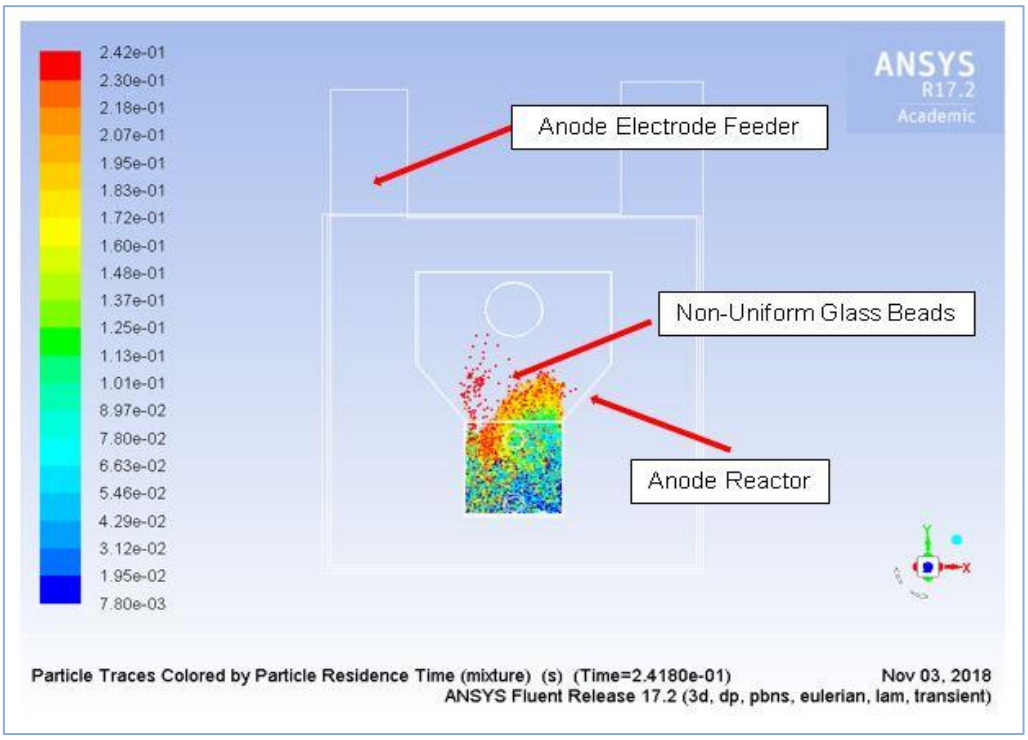

B

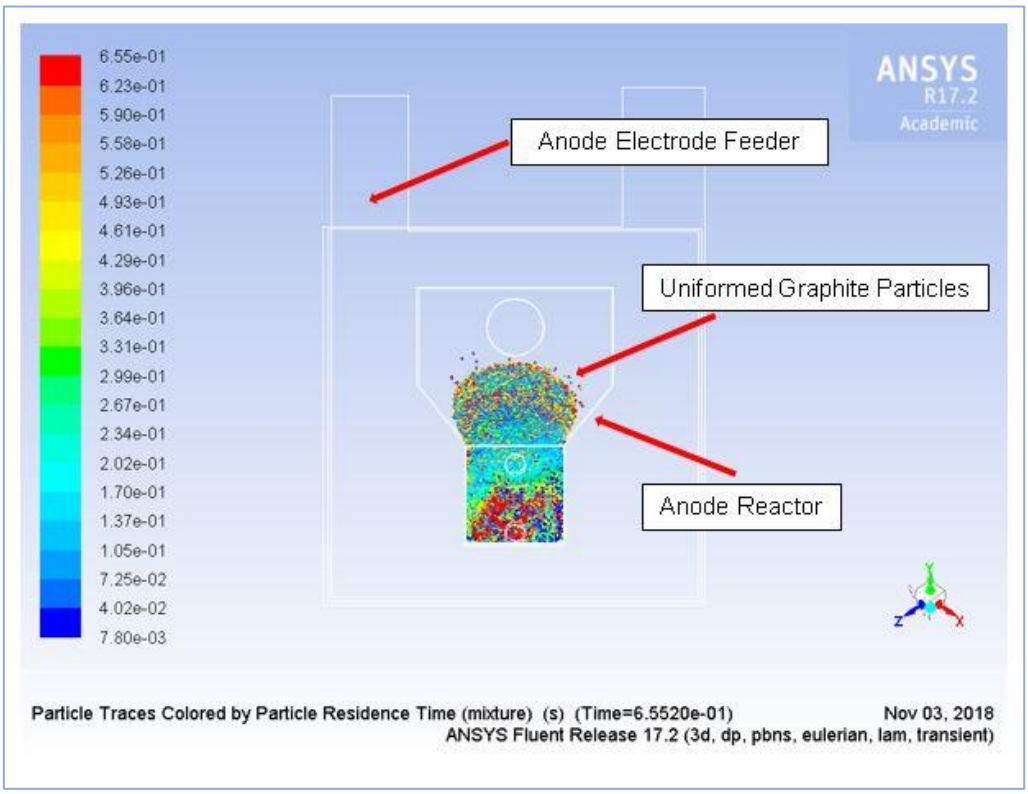

Figure 3. 8 Investigated Particles within the Anode-Reactor (254 microns to 354 microns) (A) Non-uniformed Glass Beads (B) Uniformed Graphite Particles.

CHAPTER 4

Numerical Modelling in COMSOL

4 Chapter 4 Numerical Modelling in COMSOL

4.1 Particle Trajectories and Flow Cell Electrochemistry

Before proceeding to the electrochemistry aspect of the research work with COMSOL 5.3a, the concept 5 reactor with added flow path that was previously discussed and presented in figure 2.3 of section 2.12 will be modelled in this chapter (4) also with COMSOL 5.3a to observe the interaction of the carbon particles and if the added flow path will have an impact on the direction of the electrolyte flow within the fluidized bed reactor when charging the cell and to compare it to the Ansys numerical modelling that was explored before choosing the suitable reactor and slashing away the flow path. The meshed geometry displayed in figure 4.1b was carried out to know the element number before progressing to the numerical modelling and simulation. See figure 4.1a for the represented geometry. Tetrahedron mesh was the applied method.

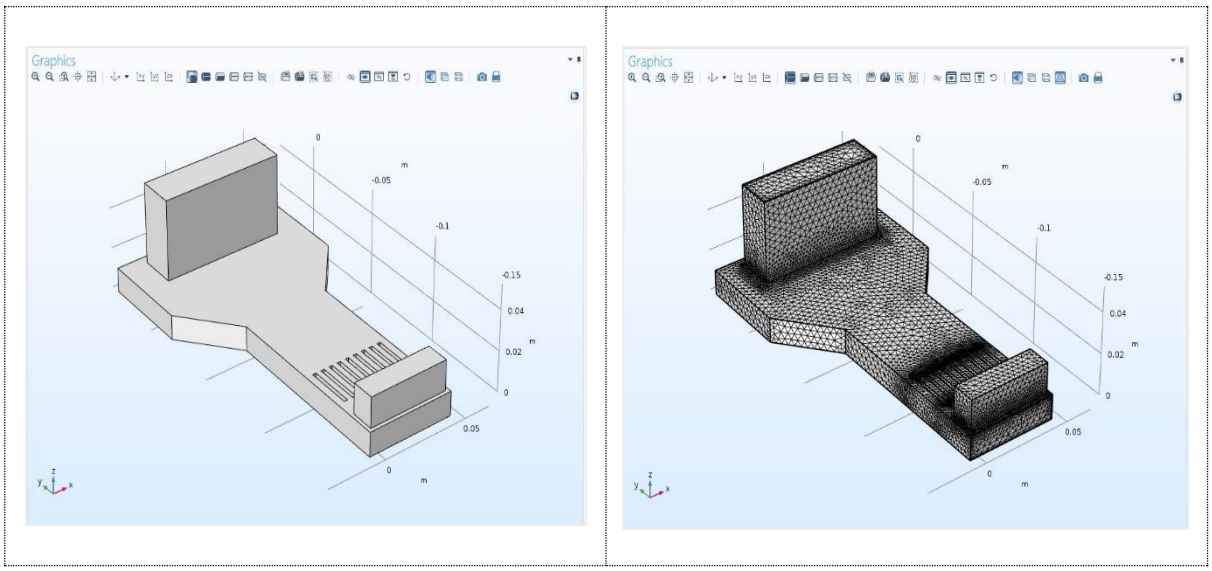

Figure 4. 1 (a) The Designed ZBB Reactor with Flow Path and (b) The Mesh Results using tetrahedron mesh method

4.2 Streamline of Flows

Figure 4.2a and 4.2b has presented the interaction of the numerically modelled injected carbon particles and electrolyte within the designed and chosen fluidized bed reactor, Figure 4.2a is the isometric view of the of streamline flow and figure 4.2b has also displayed the side view. The reactor encountered a bit of turbulence at the bottom of the reactor during the numerical simulation and the particle trajectories were not the same. All injected particles were not expected to reach the outlet of the reactor during the numerical modelling and simulation.

The idea of using the particle trajectories approach in COMSOL Multiphysics as mentioned earlier was to study the interaction of these injected particles with the electrolyte before proceeding to model the fluidized bed reactor in 2D; which was due to the multiscale 3D packed bed reactor license that was not available at Lancaster University. Furthermore, and to compare the result with the explored fluidized bed 3D modelling in Ansys results. The two displayed numerical results (isometric and side view) has shown that some of the injected zinc particles were grounded (stacked) in the anode reactor and at the wall.

By using a transmission probability technique on COMSOL, it was possible to define the number of particles and the ratio of these particles that successfully made it to the outlet by dividing them by the released number of particles. Out of the injected 3000 particles, 95% of these particles were grounded. The static mixer modelling approach on COMSOL has showed a good result. Apart that exploring a 2D model will also reduce the computational times compared to a 3D model, the achieved result has also supported carrying out a 2D model for the electrochemistry aspect of the research work.

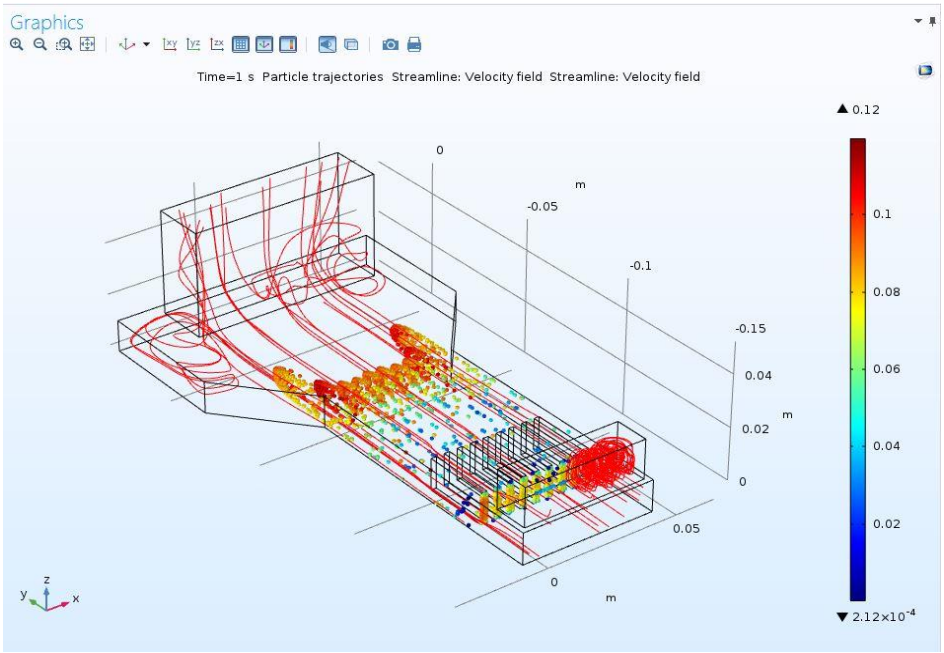

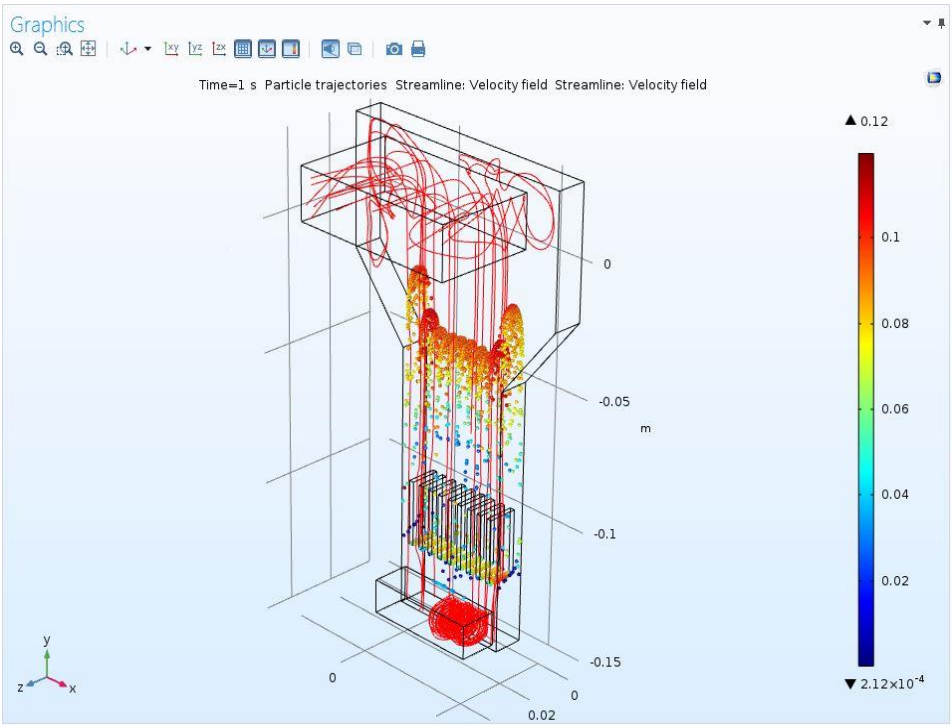

Figure 4. 2 (a) Isometric View - Streamline of Flows with Particle Trajectories at 0.098 m/s and (b) Side View - Streamline of Flows with Particle Trajectories at a velocity of 0.098 m/s

4.3 Pressure Contour and Velocity Magnitude

According to figure 4.3a, the pressure contour within the fluidized bed reactor had increased due to a change in velocity Initially, the applied velocity was 0.003 m/s before it was increased to 0.098 m/s for further observation. The minimum gradient was (-1.07 pascals) at (0.003 m/s) and (26.54 pascals) as the maximum gradient. Figure 4.3b is the slice velocity magnitude that was used as the cross-sectional surface of the anode-reactor and sometimes on all the geometry to show changes in the specific area of the plot.

The reactor's radius was measured to the 65 mm and 130 mm as the length. As observed in figure 4.3b and based on the gradient, the minimum applied flow rate for modelling the particles trajectories and velocity magnitude facilitated a uniformed flow. High pressure contour was observed as displayed in figure 4.3a at the bottom of the reactor was reduced thereafter from the inlet to the reactor's outlet.

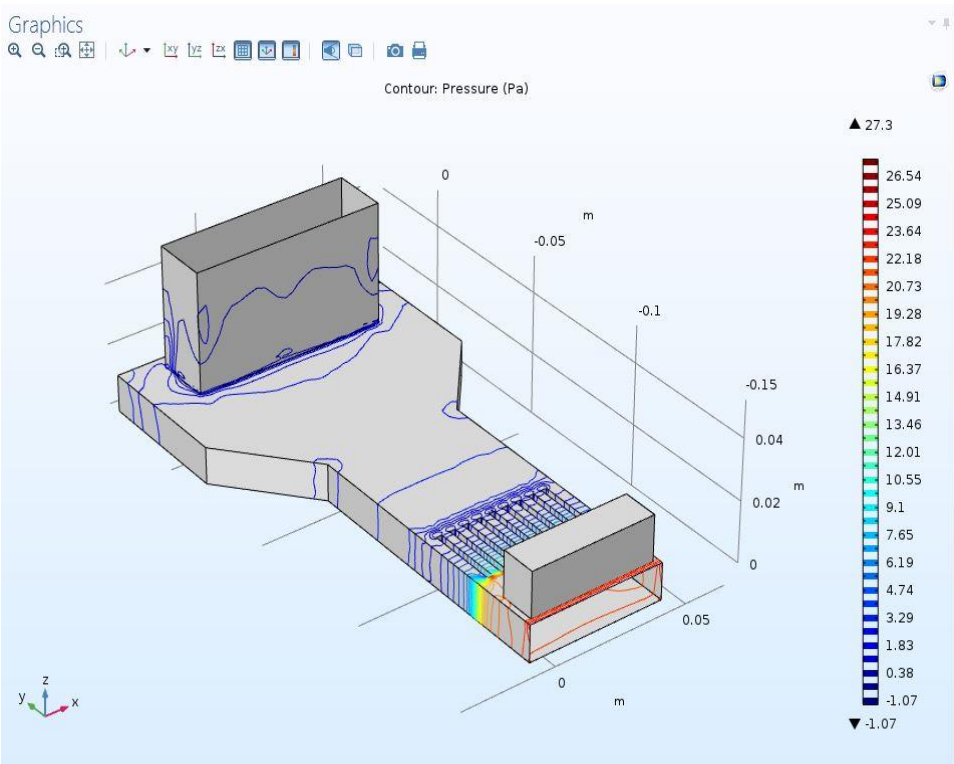

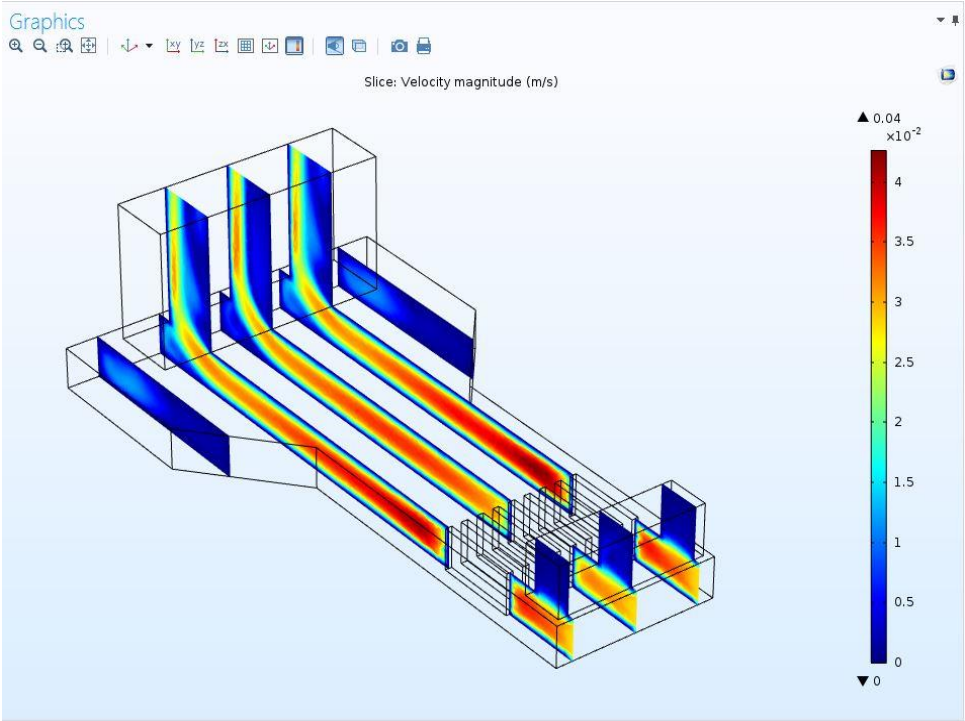

Figure 4. 3 (a) Pressure Contour at 101325 pascals at the inlet and 101600 pascals at the outlet (b) Velocity Magnitude at 0.098 m/s at the inlet

Figure 4.4 is the zinc-bromine battery cell (ZBB) completed designed that was modelled in Ansys with Fluent with all the incorporated components in (figure 4.5). (See No 1 to No 13) Particle size within this ranges (0.00012–0.00016 metre, 0.00012–0.0003 metre, and 0.00025–0.0003 metre) were investigated in chapter 3 by using the dense discrete phase model (DDPM) and discrete element method (DEM) model in Ansys fluent [478, 479] purposely because DDPM model are fast during computations due to larger time steps and stores smaller amount of information compare to a DEM model. Still, developing further a computational model within COMSOL can be of good idea to study the cell by operating the entire zinc-bromine battery cell after incorporating the fluidized bed anode-zinc reactor to the cell anode-side. COMSOL will be good for the electrochemistry aspect of the research work to understand and optimize the electrochemical systems via a precise simulation.

To help design the experiments described in chapter 4, it was necessary to model the electrochemical behaviour of the cell during charge, discharge in three key states: (i) fully

charge, (ii) mid-charge and (iii) fully discharge, in order to predict the current generated, potential differences between the electrodes, the current vs voltage response, and the changes in concentrations of key electrolyte composition. By modelling the cell system can be used to reduce the required time of the experiment via programming some values on COMSOL because it will point out the independent and experimental designed parameters and how they can be modified to better the performance of the model. Numerically, ZnBr2 model electrolytes compositions can be programmed separately on COMSOL to charge, discharge and partially-charge. Batteries cells anodic and cathodic electrolyte concentrations like the $ZnBr_2$ electrolyte model of this research work were treated on COMSOL chemically as elements; but in a compound form during the laboratory experiments.

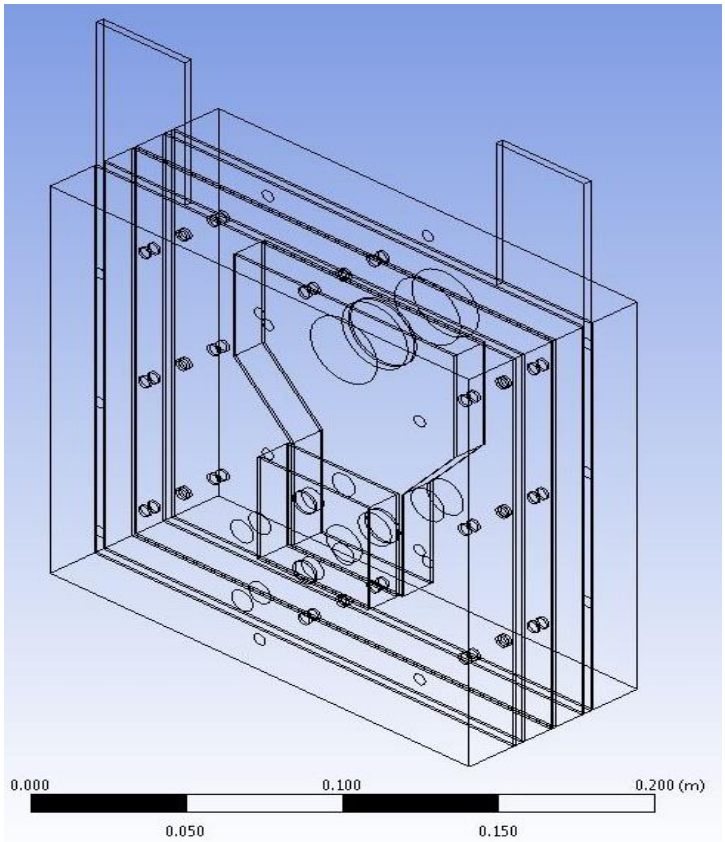

Figure 4. 4 The designed ZBB cell incorporating all the battery cell components: such as the gaskets, reactors, membrane, cell anode and cathode endplates and both the cathode side and anode-side incorporated feeder electrodes.

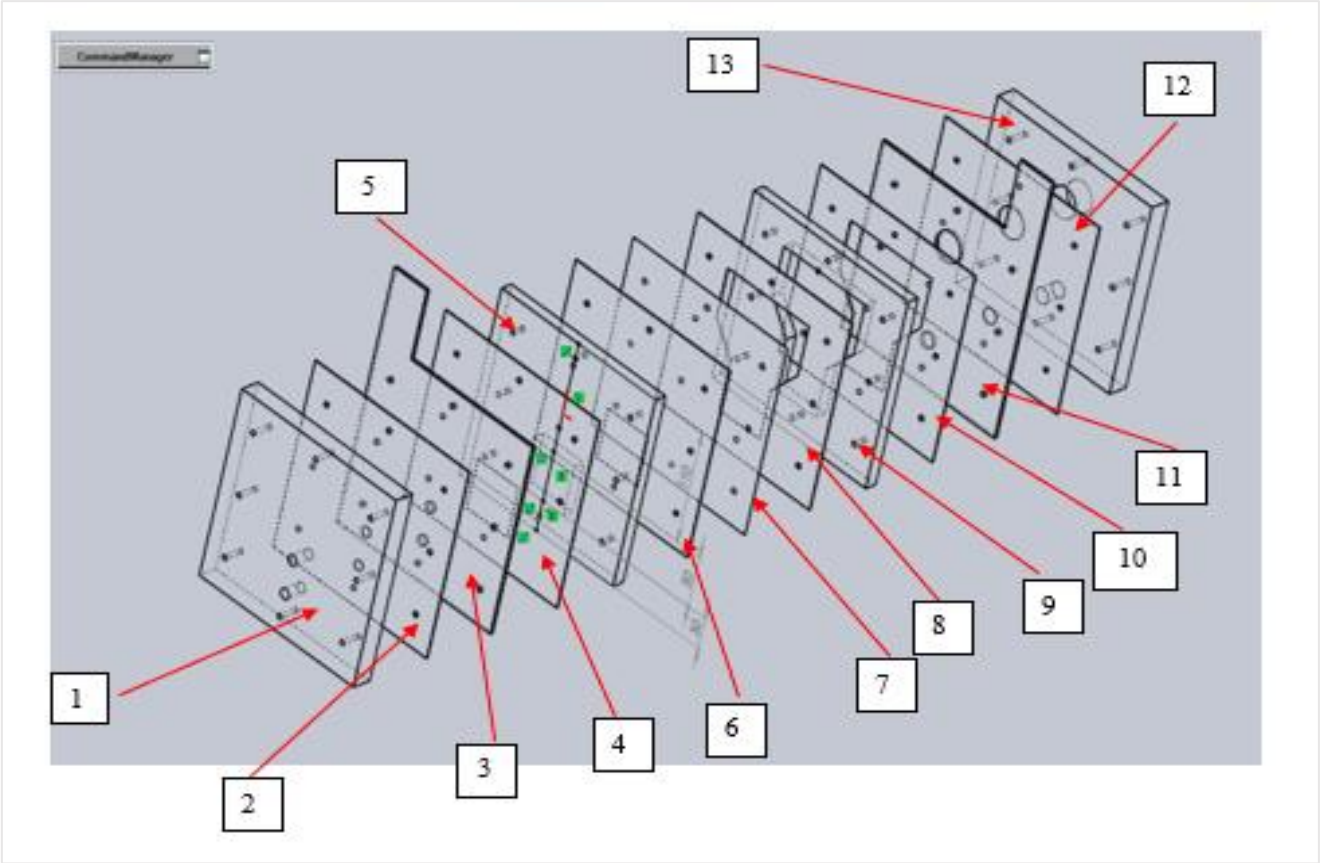

Figure 4. 5 The Designed ZBB Cell Components

1. Cathode Endplate
2. Cathode Gasket
3. Cathode Feeder Electrode
4. Cathode Gasket
5. Cathode Reactor
6. Cathode Gasket
7. Nafion Membrane
8. Anode Gasket
9. Anode Reactor
10. Anode Gasket
11. Anode Feeder Electrode
12. Anode Gasket
13. Anode Endplate

4.4 Description of the Battery Cell System

In this section, the two-dimensional (2D model) $ZnBr_2$ model geometry consists of five different layers as showed in Figure 4.6. This includes (a) the anode feeder electrode (b) anode-side reactor (b) Nafion ion-exchange membrane, (c) cathode-side reactor and (e) cathode feeder electrode. The anode and cathode feeder electrodes provide the electrical connection externally to the system. The Nafion membrane separates the two-electrolytes from mixing together. The anode-side reactor is injected with un-measured added zinc particles. The composition of the anode-side and cathode-side electrolytes are given in table 4.1. The system was simulated using COMOL Multiphysics® 5.3a and no additional program modules.

Table 4. 1 Charged and Mid-charged and Discharged Concentrations

ANOLYTE COMPOSITION INPUT			
Elements	Charge	Mid-Charge	Discharge
Zinc ($Zn2^+$)	2.5 moles	3.25 moles	4 moles
Bromide (Br^-)	6 moles	6 moles	6 moles
Chlorine (Cl^-)	3 moles	3 moles	3 moles
Potassium (K^+)	1 mole	1 mole	1 mole
Hydrogen (H^+)	0.00316 mole	0.00316 mole	0.00316 mole
Water (H2O)	55.555 moles	55.555 moles	55.555 moles
CATHOLYTE COMPOSITION INPUT			
Elements	Charge	Mid-Charge	Discharge

Bromide (Br^-)	0.01 mole	1.5 moles	3 moles
Chlorine (Cl^-)	1 mole	1 mole	1 mole
Potassium (K^+)	4 moles	1 mole	4 moles
Bromine (Br_2)	1.5 moles	0.75 mole	0.01 mole
Water (H2O)	55.555 moles	55.555 moles	55.555 moles

Before simulating the model to charge (see figure 4.6), the known anode-electrolyte density (1.48 g/cm^{-3}) was multiplied with the inlet velocity (0.098 m/s) and programmed in COMSOL. The specified inlet velocity was for the charge, discharge and mid-charge as programmed in COMSOL 5.3a. These velocity inlets were chosen to increase the flow running through the investigated two reactors (anode and cathode). Based on the anode and cathode electrolyte concentrations, the cathode electrolyte density was not measured but compared and evaluated with the anode electrolyte density before agreeing on a possible value of 1.46 g/cm^{-3}.

The ZnBr2 cell has the following measurements: cathode-side reactor (50 mm length*50 mm breadth*50 mm high and 12 mm thick), ion-exchange membrane width (0.001 m) and the anode-side reactor (50 mm length*50 mm breadth*130 mm high and 12 mm thick). To reduce computation times, the behaviour of the cell was simulated in 2 dimensions through the cross section cutting perpendicularly through each of the layers detailed above and as shown in figure 4.6.

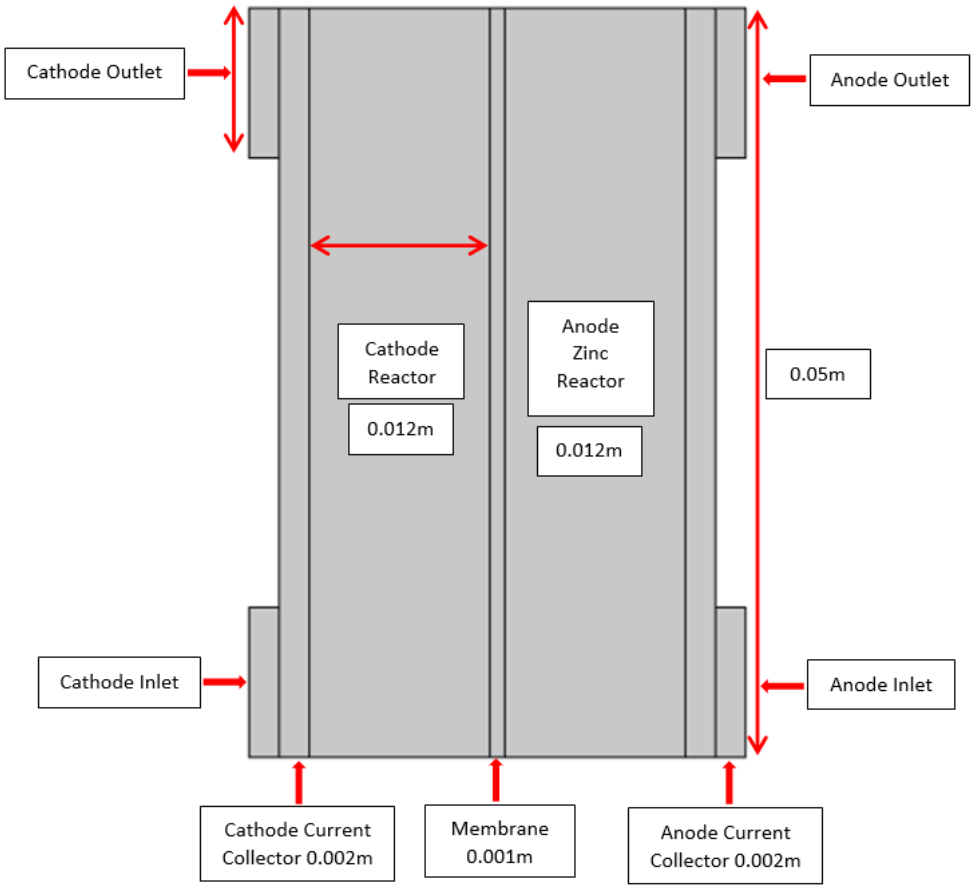

Figure 4. 6 The Zinc-Bromine Battery cell Model

The current was collected on the cell using COMSOL through the secondary current distribution interface and the electrolyte current distribution and density were further solved in COMSOL, via Ohms law since the ZnBr2 model was established as a closed-circuit system. However, after several numerical investigations and due to some accumulated reasons as stated below, two options were carefully and numerically explored further.

Such as the electric potential and the electrode potential (Evsref) option and specifying the electric reference potential. The electric potential option was preferred to be chosen in COMSOL as the boundary conditions for the anode and cathode electrodes rather than using the grounded approach to know the current that can be generated by the cell, and to observe possible potential differences and changes to the electrolyte composition.

The grounded approach can be programmed in COMSOL by setting one of the two electrodes boundary condition as electric potential and the other boundary condition to the total current. But the cell charged, and discharged electrolyte potential were very high (100 volts) despite that one of the current collectors (anode) was grounded (Not to carry electricity) and the other electrode (cathode) was programmed to a cell potential of 1.9 volts to comply with the total current condition.

The two reactors domain were both selected and cannot be neglected because of the chemical reaction. The model was further extended by modelling for the diffusion, convection and migration of ions through the use of transport of diluted species in porous medium on COMSOL and using a time dependent simulation (0, 60 and 3600 seconds). The cell was programmed to partially charge, charge and discharge at a current in between 0.1 Amp and -0.1 Amp. The cell was extended to model the (diffusion, convection and migration) because of the expected charged transfer of particles (ion) within the cell during the numerical and physical experimental work. The diffusion process is the movement of ions from a region of higher concentration to a region of lower concentration. The convection process is the mass transportation of ions and the term migration as the movements of ions due to an externally applied electrostatic field.

4.5 Description and Analysis of Results – Electrolyte Potential Vs Current (A) and Voltage (V).

The predicted electrolyte potential and current versus time by the model are presented in figure 4.7. These predicted results are for the charge state, partially charged state and discharge state. The electrolyte potentials presented in Figure 4.7 were observed after running the model under a set of operating condition at a steady state. Mathematically, the model was computerized under a constant temperature of 293.15 (K) with current flowing in the $ZnBr_2$ cell. The cell was set to first charge at a charge rate of 0.1 amps and -0.1 amps and discharged at -0.1 amps after charging at 0.1 amps at the same time. The mid-charge was programmed up at 0.1 amps and -0.1 amps for the cell to store energy and to predict the cell electrolyte potential when partially charged.

(A). CHARGED STATE ELECTROLYTE POTENTIAL AND CURRENT VS VOLTAGE

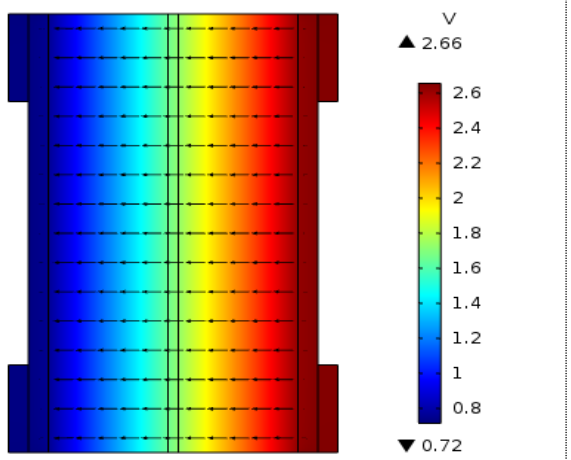

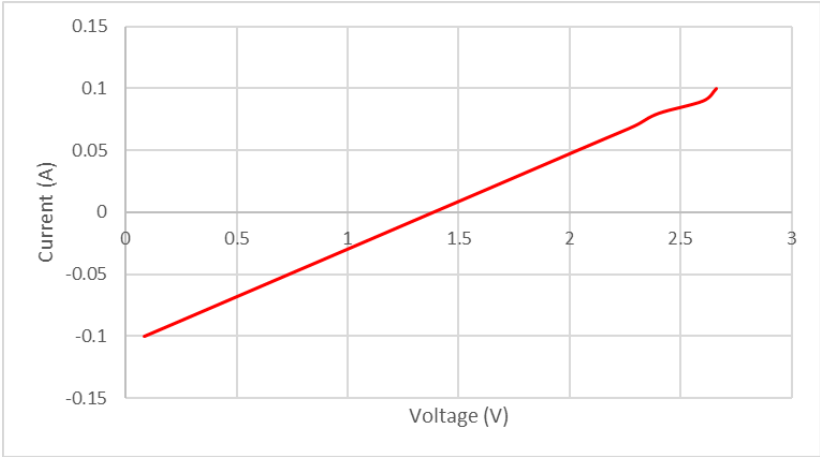

(B) MID-CHARGED STATE ELECTROLYTE POTENTIAL AND CURRENT VS VOLTAGE

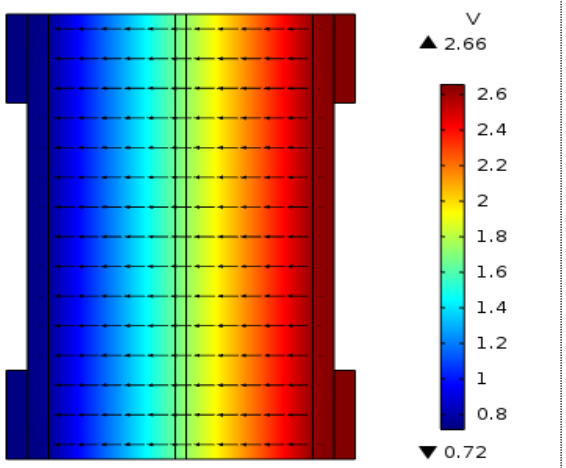

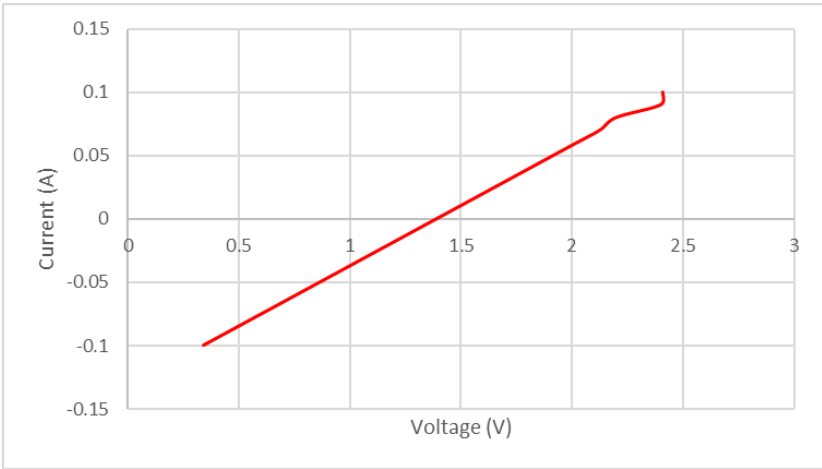

(C) DISCHARGED STATE ELECTROLYTE POTENTIAL AND CURRENT VS VOLTAGE

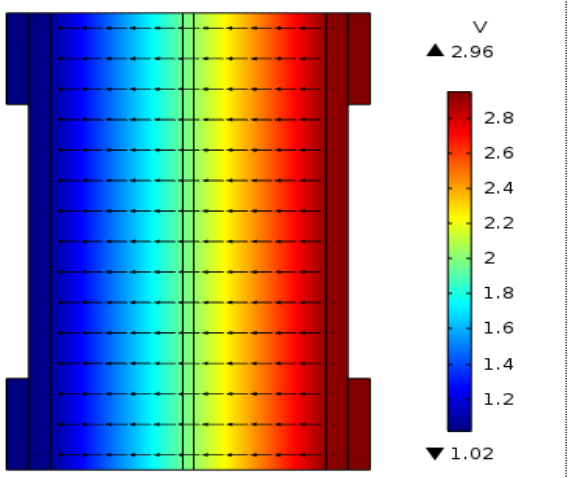

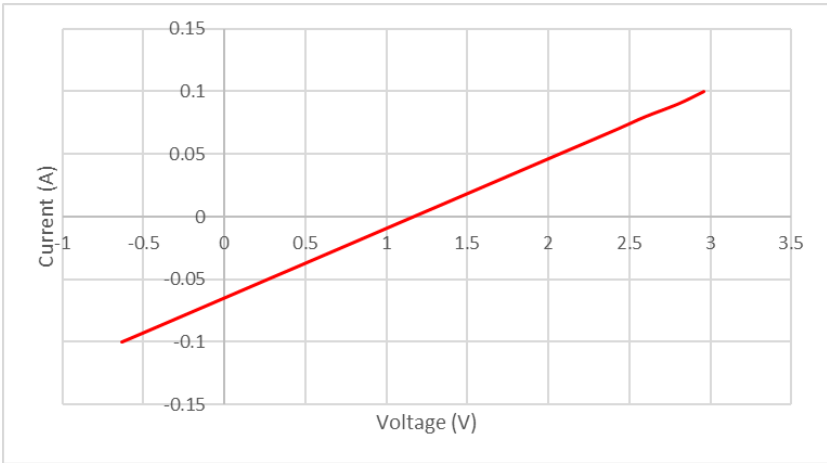

Figure 4. 7: Cell model electrolyte potential and current vs voltage (a) charged at 0.1 amps & -0.1 amps (b) mid-charged at 0.1 amps & -0.1 amps and (c) discharged at 0.1 amps & -0.1 amps all at 3600 secs.

4.6 Results and Conclusions on the Electrolyte Potential (EP) and Current (A) Vs Voltage (V)

The red mapped colour on the modelled geometry at the anode zinc-electrode identifies charged zinc. The model predicted the expected electrolyte potentials for the charged, mid-charged and discharge. These values corresponded with the explored laboratory experiment. The programmed current was at 0.1 amps and -0.1 amps before it was possible to observe what current the modelled cell can store and discharge at these programmed current rates.

The model did not predict a current that can be detrimental to the health of the cell in real life via the modelled $ZnBr_2$ cell. Flowing of electrons were identified by the black arrows from the anode zinc-electrode to the cathode-electrode. The predicted voltages by the model were in good agreement with the explored laboratory experiments based on the observed negative voltages. Before the bed could be more conductive, the model was re-designed to be thin.

This idea supported the resistivity of the cell. The cell voltage during charge, mid-charge and discharge at these current 0.1 amps and -0.1 amps were (2.6 volts, 2.4 volts and 2.9 volts) and (-0.1 volts, -0.4 volts and -0 volt). The model demonstrated the highest voltage during the discharge state followed by the charge state. The highest voltage predicted by the model during mid-charged was low compared to others. The differences between these voltages could have happened because of the variations in the electrolyte compositions. However, none of the predicted voltages can be detrimental to the state of health (SOH) of the real battery cell.

4.7 Description of Results

4.7.1 Anode Zinc Concentration

Only the added zinc concentrations results were presented in this section. See figure 4.8. Furthermore, not all the result of the concentration that were fed into the system were presented in this section; since the area of interest focusses on zinc depleted, bromine formed and the amount of bromide concentration at the cell anode-side and cathode-side.

(A). ANODE ZINC CONCENTRATION VERSUS CURRENT OF THE CHARGED STATE

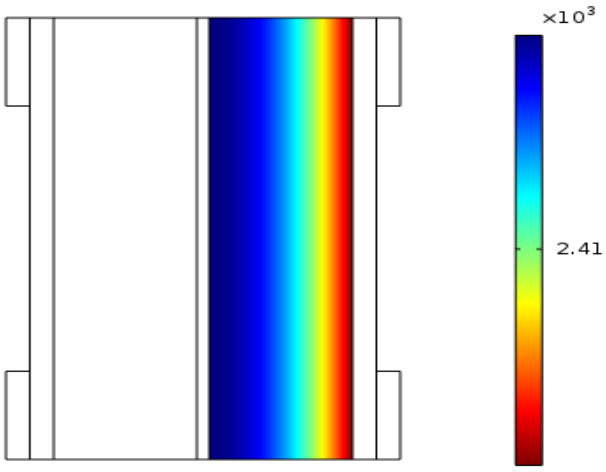

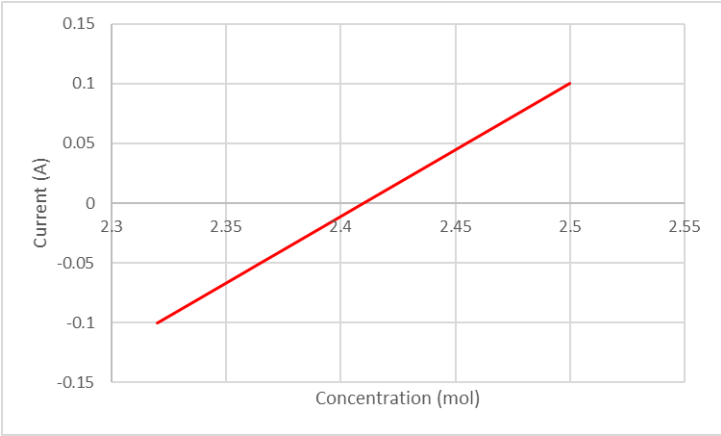

(B) ANODE ZINC CONCENTRATION VERSUS CURRENT OF THE MID-CHARGED STATE

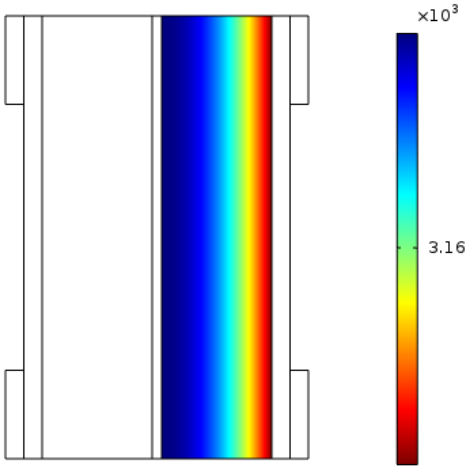

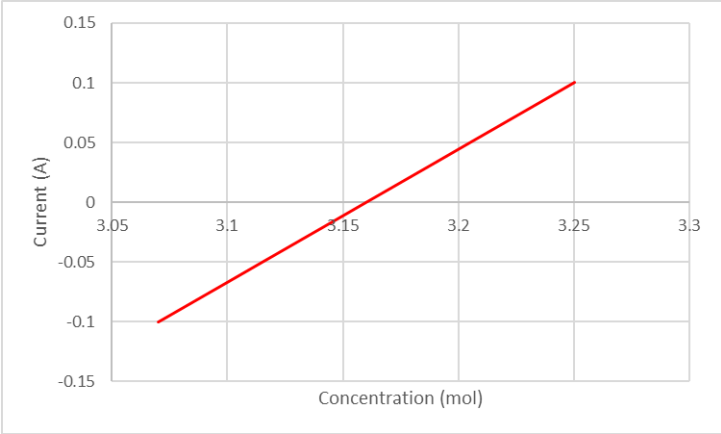

(C) ANODE ZINC CONCENTRATION VERSUS CURRENT OF THE DISCHARGED STATE

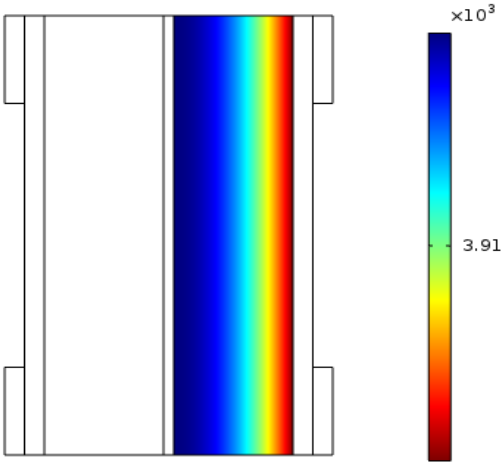

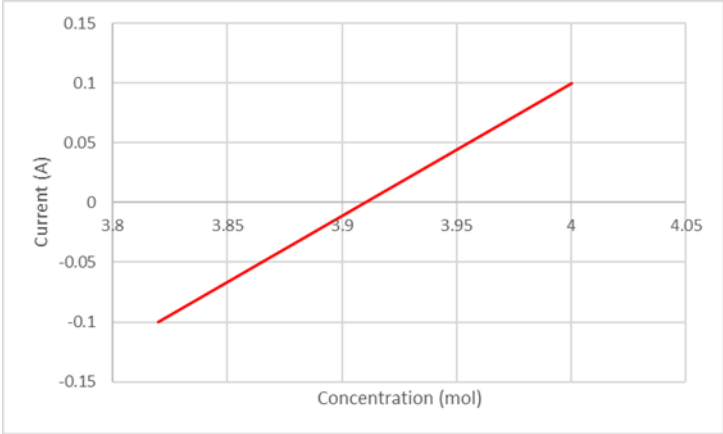

Figure 4. 8: Cell model anode electrode zinc concentrations and graphs result plots (a) charged at 0.1 amps and -0.1 amps (b) mid-charged at 0.1 amps & -0.1 amps and (c) discharged at 0.1 amp & -0.1 amps all at 3600 secs.

4.8 Description of Analysis

4.8.1 Anode Zinc Concentration

The anode zinc-electrode zinc concentrations were (2.5 moles), before charge, at a charge in between -0.1 amps and 0.1 amps and was (3.25 moles) for the mid-charged and (4 moles) for the discharged. The discharge current was also in between -0.1 amps and 0.1 amps and -0.1 amps and 0.1 amps as the mid-charge.

4.9 Result Discussions and Conclusions

4.9.1 Anode Zinc Concentration

On figure 4.8a, at 0.1 amps, more zinc was used at charge, by depleting from (2.5 moles to 2.41 moles) than at a charge of -0.1 amps (2.4 moles and 2.32 moles). According to figure (3.8b), the depleted zinc during mid-charge was (3.25 moles and 3.16 mol) at 0.1 amps and between (3.1 mol and 3.07 mol) at -0.1 amps. In figure (4.8c) it was between (4 mol and 3.9 mol) at 0.1 amps and (3.9 mol and 3.82 mol) at -0.1 amps for the discharge. These predictions were all in good agreement with the laboratory experimental work.

4.10 Description of Results

4.10.1 Cathode Bromide Concentration

The results in Figure 4.9a, b and c are the concentration of the bromide (Br) added to the cathode electrolyte.

(A). BROMIDE CONCENTRATION VERSUS CURRENT OF THE CHARGED STATE

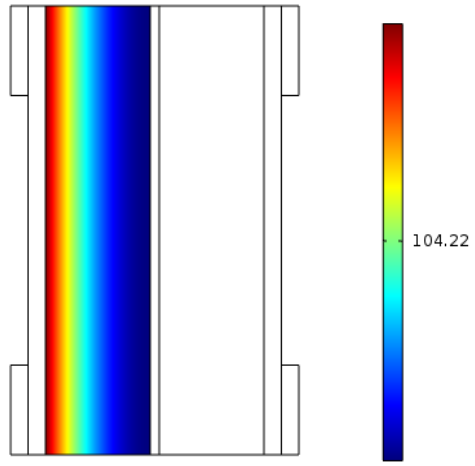

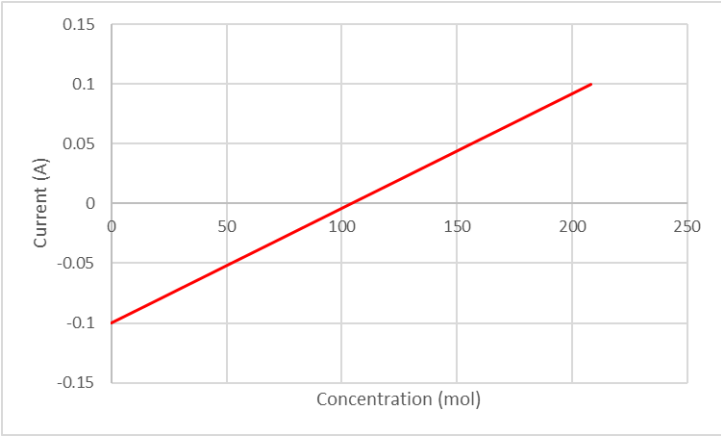

(B) BROMIDE CONCENTRATION VERSUS CURRENT OF THE MID-CHARGED STATE

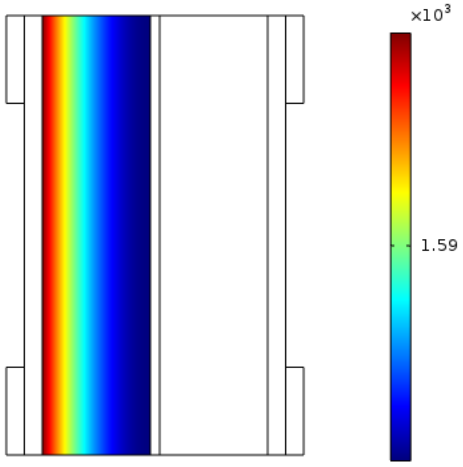

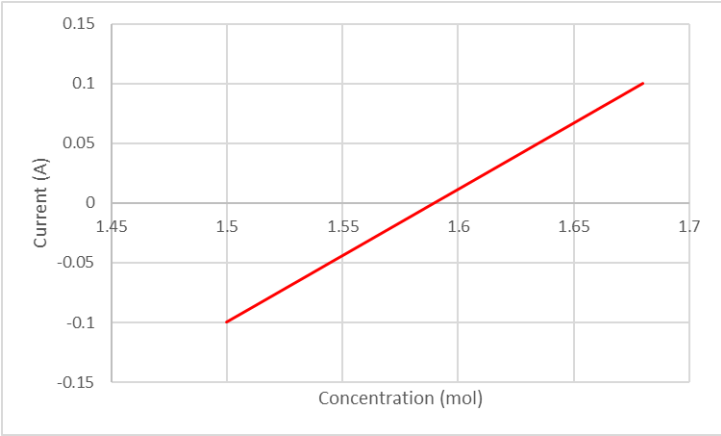

(C) BROMIDE CONCENTRATION VERSUS CURRENT OF THE DISCHARGED STATE

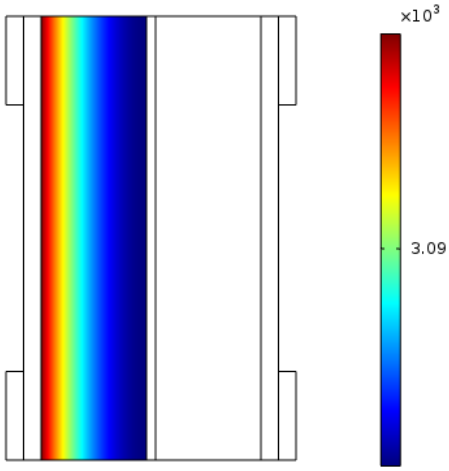

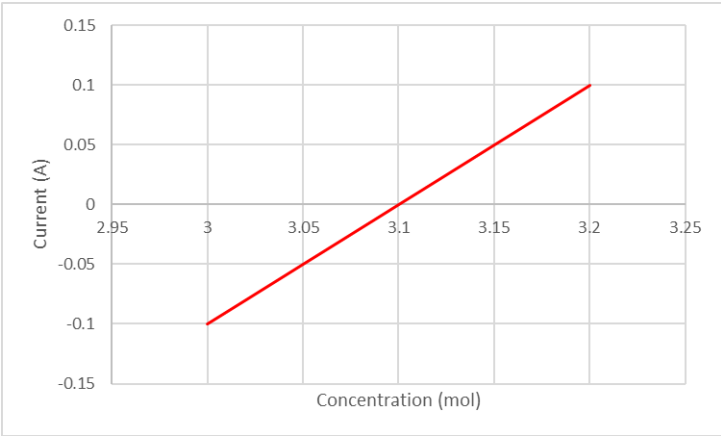

Figure 4. 9: Cell model cathode electrode bromide concentrations and graphs result plots (a) charged at 0.1 amps & -0.1 amps (b) mid-charged at 0.1 amps & -0.1 amps and (c) discharged at 0.1 amps & -0.1 amps all at 3600 secs.

4.10.2 **Cathode Bromine Concentration**

The results in Figure 4.10a, b and c are the concentration of the bromine (Br_2) programmed to the cathode electrolyte.

(A). BROMINE CONCENTRATION VERSUS CURRENT OF THE CHARGED STATE

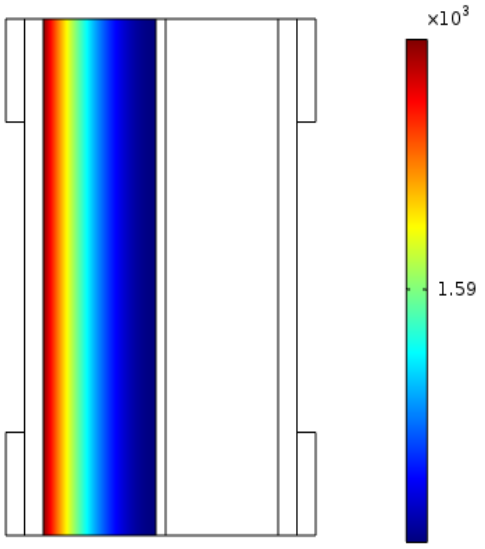

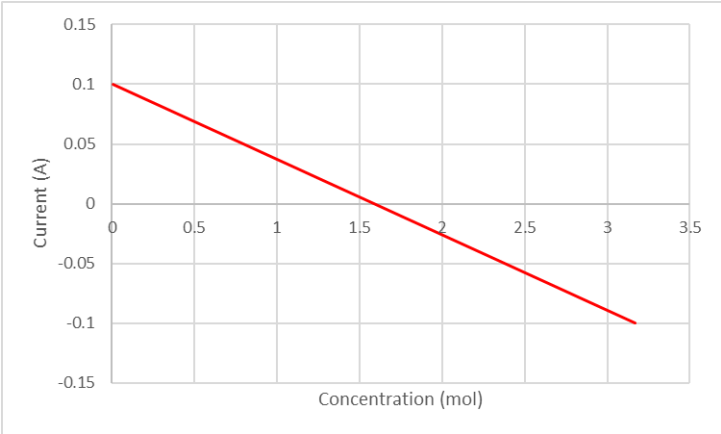

(B) BROMINE CONCENTRATION VERSUS CURRENT OF THE MID-CHARGED STATE

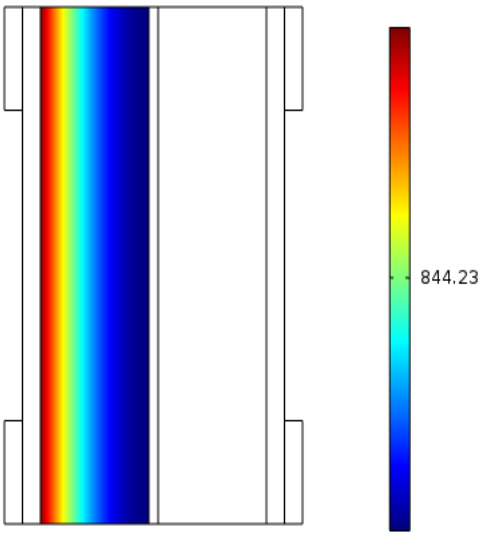

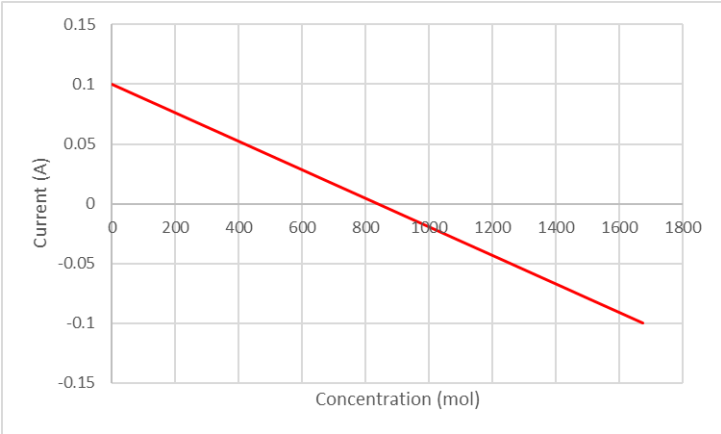

(C) BROMINE CONCENTRATION VERSUS CURRENT OF THE DISCHARGED STATE

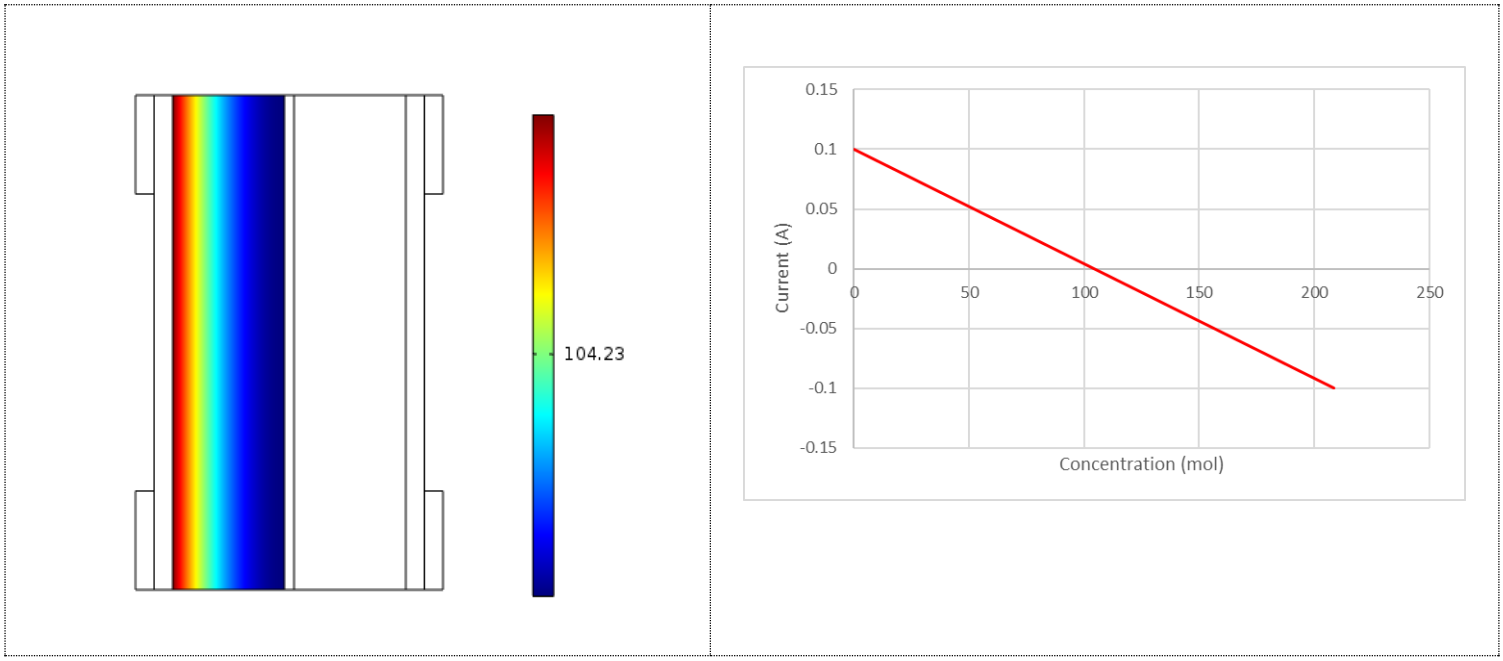

Figure 4. 10: Cell Model Cathode Electrode Bromide Concentrations and Graphs Result Plots (a) Charged at 0.1 amps & -0.1 amps (b) Mid-Charged at 0.1 amps & -0.1 amps and (c) Discharged at 0.1 amps & -0.1 amps all at 3600 secs.

4.11 Description of Analysis

4.11.1 Cathode Bromide and Bromine Concentration

The model was programmed to charge to observe the current that can be stored by running the simulation in between 0.1 amps and -0.1 amps, and for the discharged and mid-charged. This applies to the bromide and bromine concentration. The programmed bromide (Br) concentration for the charge was 0.01 mole, and 1.5 moles for the mid-charge and 3 moles for discharge and the bromine (Br_2) concentration for the charge was 1.5 moles, and 0.75 moles for the mid-charge and 0.01 moles for discharge.

4.12 Result Discussions and Conclusions

4.12.1 Cathode Bromide Concentration

The same bromide concentration was formed at charge (0.01 mole to 93.718 moles at 0.1 amps) and at -0.1 amps it was (114.542 moles and 208.25 moles). For the mid-charge, it was also increased by 0.08 mol (1.5 mol and 1.58 mol at 0.1 amps) and by 0.09 mol (1.59 moles and 1.68 moles at -0.1 amps). It was (3.01 moles and 3.09 moles) at 0.1A and (3.11 moles and 3.2 moles) at -0.1 amps for the discharge. See Figure 4.9a, b and c. The bromide concentration during the real experiment might have increased during the laboratory experiment. Numerically, the model has showed that the original ZnBr2 solution can be reformed during discharge. The simulation outcomes showed that the numerical modelling and experimental data were compatible and in good agreement.

4.12.2 Cathode Bromine Concentration

In Figure 4.10a, b and c, the model predicted a change to the discharge concentrations (0.01 mole). More bromine was formed during charge by 0.09 mole. Both the mid-charge and discharge concentrations elevated separately by 0.094 mole. At the cell cathode-side, the model has showed that more bromine will be formed during charge. On the graph (see figure 3.10a, b and c) at charge the concentration was between was between (0.16 mole to 1.4 moles at 0.1 amps) and (1.7 moles and 3.17 moles at -0.1 amps). For the mid-charge it was (84.3 moles and 753.1 moles at 0.1 amps) and (920 moles and 1672.7 moles at -0.1 amps). And (10.4 moles and 93.8 moles at 0.1 amps) and (114.6 moles and 208.4 moles at -0.1 amps) for the discharge.

4.13 Numerical Modelling & Results Conclusion

Since the electrochemistry aspect of the research work is completed and some results have been observed, such as the concentration of the added elements in terms of the condition of the programmed zinc, bromide and bromine, proceeding to the laboratory experimental aspect of the research work would be necessary since the model has demonstrated the expected voltages at charge, discharge and mid-charge at this current rate (0.1 amps to -0.1 amps). Furthermore, the performances of the modelled cell have been validated with the charge and discharged curve of zinc-bromine batteries cells and showed a good agreement between these two models based on the expected behaviour of the cell during the physical laboratory experiments.

Chapter 5
Materials and Methods

5 CHAPTER 5 Materials and Methods.

5.1 SEM Preparation and Method

Before measuring and adding separately the purchased anode and cathode chemical reactants and mixing them in a 250 mL glass bottle, 5% of a 250 mL DECON soap was used to wash all the beakers that were used in the laboratory to carry out the experiments. These beakers were rinsed adequately with the deionized water from the Lancaster university purified water dispensing machine and through using a deionized water bottle. However, the temperature of the fluid was not measured. DECON soap was also used to clean a 10 mL beaker flask before measuring (1.5 liters) of deionized water in this beaker flask and added it to the catalysts (chemicals) and for an appropriately mixing.

By exploring scanning of electrons microscopy (SEM) on charged particles collected from the anode zinc reactor was to discover all the present various elements after charging and discharging the zinc bromine battery cell at different charge rates. Before exploring the SEM, the charged and deposited zinc morphology collected from the anode reactor were dried in an oven to prevent any agglomeration of these particles. These particles were of different microns in sizes (254 microns to 354 microns). Some of the particles collected from the anode-side zinc-electrode after charging the cell were viewed at different microns (100 microns, 50 microns, 10 microns and 5 microns) by using the JEOL JSM-6010 PLUS/LA (SEM) scanning electron microscope machine. The SEM characterization of the zinc electrodeposits were examined after charging the cell at a charge rate of 0.27 amps and 0.3 amps.

The anode-electrolyte composition includes 3 moles of ZnBr2 (675 grams) Solution, 1 mole of $ZnCl_2$ (205 grams), and 1 mole of KCl (111.826 grams). The cathode electrolyte solution includes 3 moles of KBr (535 grams) and 1 mole of KCl (111.897 grams). The anode electrolyte solution density was 1.47gcm^{-3} which was used to gauge the cathode-electrolyte. A flow rate of (166.7 cm^3/min) was maintained throughout the experiment. The used JSM-6010LA/JSM-6010LV equipment for the scanning process is a compact mobile SEMs device with high performance and suitable for research use. (see figure 5.1) The surface structures are observed by secondary electrons, the distribution of materials in a specimen is observed by backscattering the electrons and analysing the elements by EDS (energy dispersive X-ray analyser). All the necessary functions are available in the all-in-one mobile multi-touch-panel SEM.

The use of (SEM) scanning electron microscopes can take advantage of the electron's properties and dispersive and will not deeply penetrate the sample. SEM basic parts are the electron source, the sources of electrons and encountering high voltage across them, electrons accelerating toward the sample, electromagnetic lenses and focus on electrons, temperature, detector and data system collections. Backscattered electrons can be collected through standard SEM as samples are diffracted off at high incidence angles. On a 2θ angle and within the user interface, SEM does not rely, but acts more slightly and similar to a light microscope. Some SEM can be equipped to count, detect, analyze off scattered x-rays from a sample. Such type of detector can determine the samples elemental composition is possible.

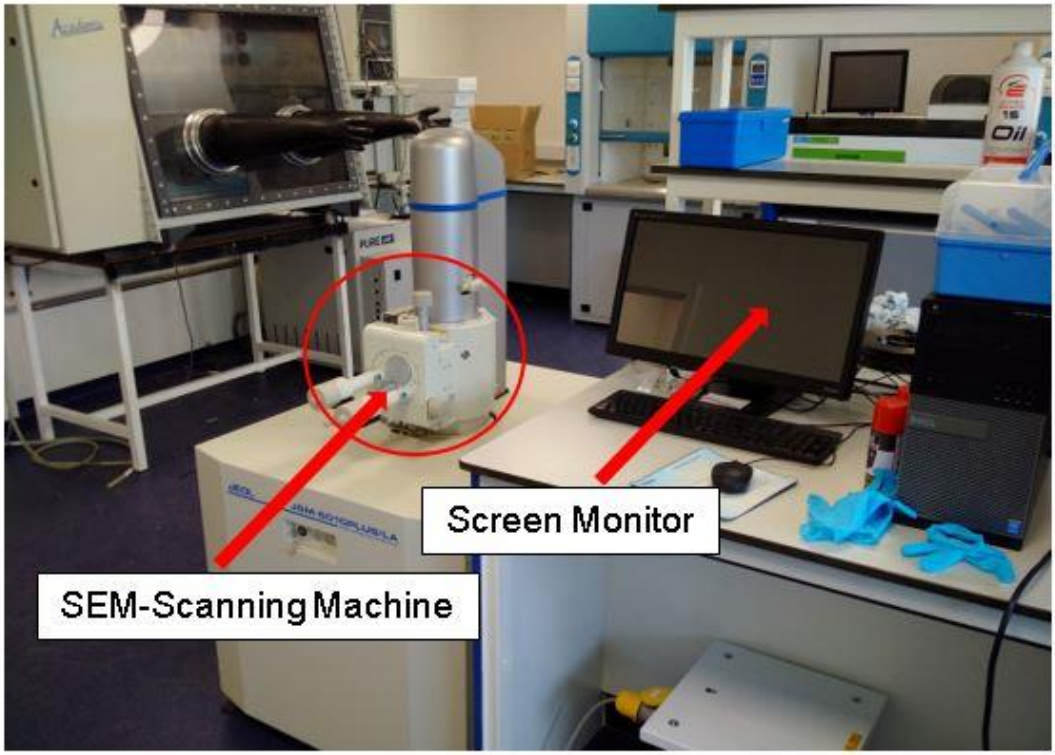

Figure 5. 1 Lancaster University JEOL JSM-601 OPLUS/LA analytical scanning electron microscope machine

5.2 Results Discussions and Conclusions

5.2.1 Examined Particles

From the lab, it was found that some white edges were present on the collected particles when examined via the SEI process (scanning of electrons image) after the charge and discharge experiments. This was observed during the colour mapping process. Furthermore, there was degasification (removal of dissolved gases from both electrolyte solutions) during the experimental test regarding some formed bubbles on the solid-liquid interfaces; which might have occurred due to some of the particles that were not properly dried before the SEM analysis. However, this has made them to behave strangely and created some changes to the zinc morphology concerning the shape and structure of these particles.

Figure 5.2, figure 5.3 and figure 5.4 were the observed different zinc morphologies during the three SEM characterization of the zinc electrodeposits after charging and discharging the stored energy by the ZnBr2 cell and after observing copper deposits at the cathode-side electrolyte due to the brass fittings that were not chemically resistance that initially changed the battery to a copper-zinc RFB cell before it was reverted back to a zinc-bromine battery cell by changing some of the materials.

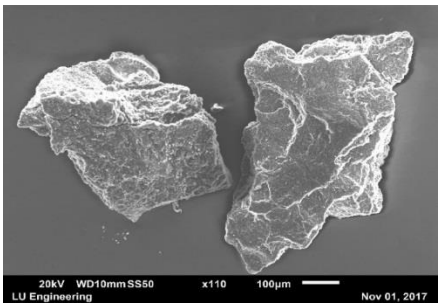

Picture 1: 100 Microns

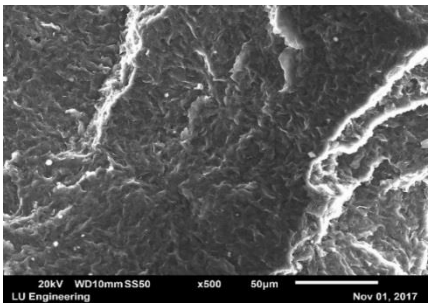

Picture 2: 50 Microns

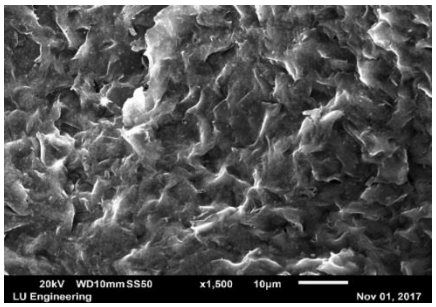

Picture 3: 10 Microns

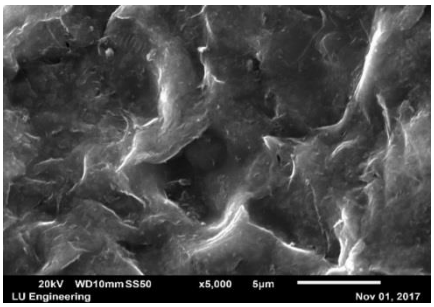

Picture 4: 5 Microns

Figure 5. 2 Charged Dried Particle

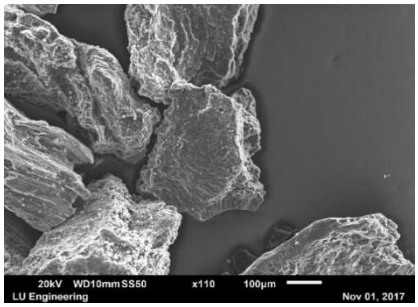

Picture 5: 100 Microns

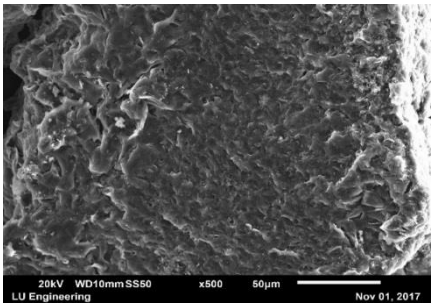

Picture 6: 50 Microns

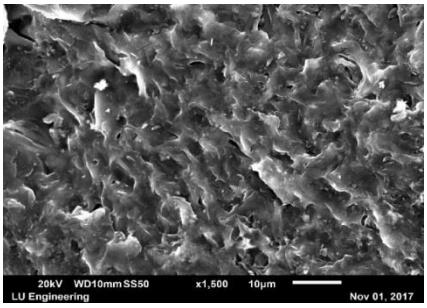

Picture 7: 10 Microns

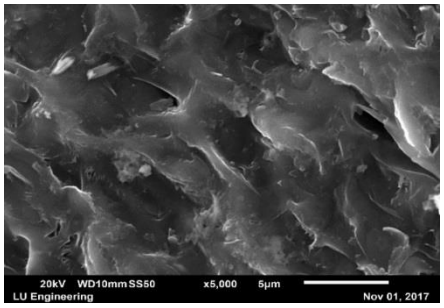

Picture 8: 5 Microns

Figure 5. 3: Discharged Dried Particles

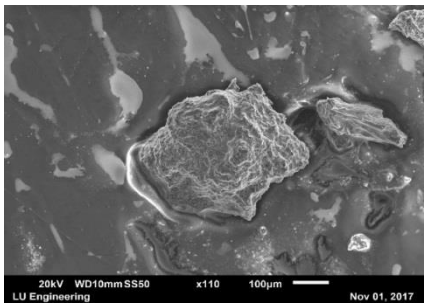

Picture 9: 100 Microns

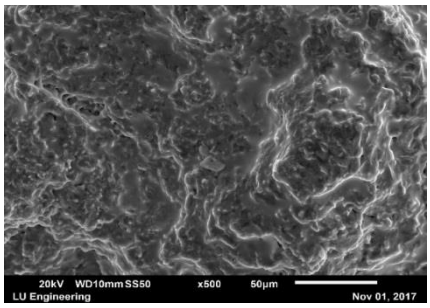

Picture 10: 50 Microns

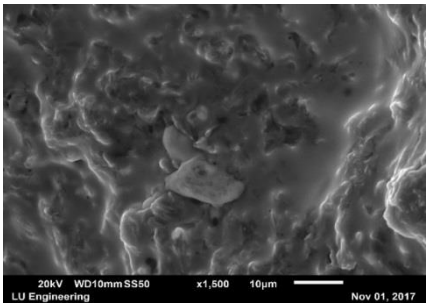

Picture 11: 10 Microns

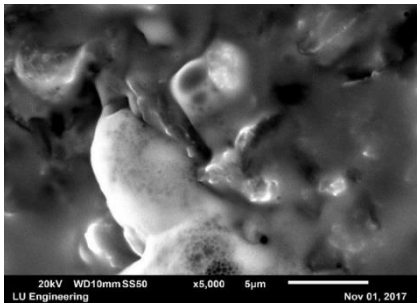

Picture 12: 5 Microns

Figure 5. 4: Copper Deposits During Charging and Discharging

5.3 Results Discussions and Conclusions

5.3.1 Identified Elements

Subsequently, after the explored charged and discharged experiments, no hydrogen traces were observed during the SEI, scanning of electrons image as observed on the mapped elements images. See Table 5.1, Table 5.2, and Table 5.3. This identified a good electrochemical performance as observed via the measured cyclic voltammetry. The identified sharped peaks, Zn-Br_2 (3M) has showed the regularity of the electroplated zinc and (Br) for the bromine formation. The identified copper (Cu) deposits was due to the coupled brass fittings. The presence of oxygen (O_2) was agreed to have occurred because the cell was exposed before coupling it and due to the presence of H_2O. Silicon has originated due to the applied adhesive glue to prevent leakages. Chromium (Cr), Iron (Fe) and carbon (C) were both produced due to the coupled anode-inlet and anode-outlet pipe steel materials and brass fittings that were not chemical resistance.

The anode and cathode inlets and outlets brass fittings materials had supported the origination of the identified selenium element during the chemical reaction. Selenium as non-metallic chemical elements in the group xvi of the periodic table could conducts electricity better in the light than in the dark and used in photocells. It wasn't peculiar by identifying some potassium elements during the SEM since the cell electrolytes consists some added salt.

Table 5. 1 Mapped Elements after Drying the Particles after charged

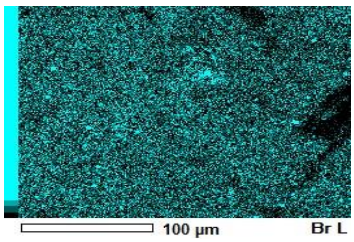 Bromine	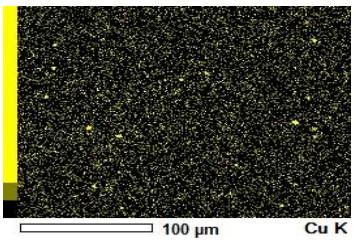 Copper	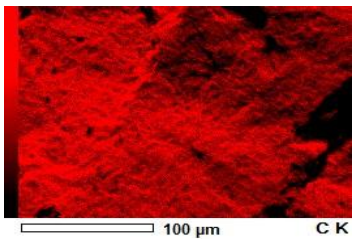 Carbon

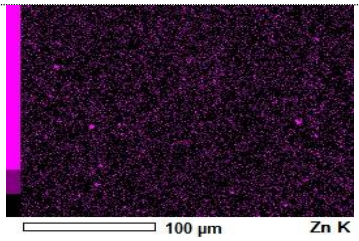

Zinc

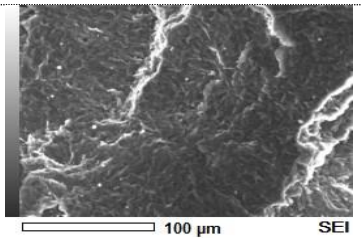

Silicon

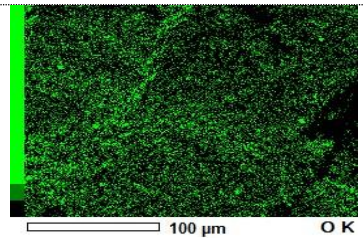

Oxygen

Formula	mass%	Atom%	Sigma	Net	K ratio	Line
C	96.04	97.48	0.01	2454302	0.5030845	K
O*	3.11	2.37	0.02	18513	0.0128878	K
Cu*	0.34	0.06	0.01	6154	0.0089637	K
Zn*	0.34	0.06	0.01	5262	0.0090137	K
Br*	0.17	0.03	0.01	10681	0.0047418	L
Total	100.00	100.00				

Elements Properties

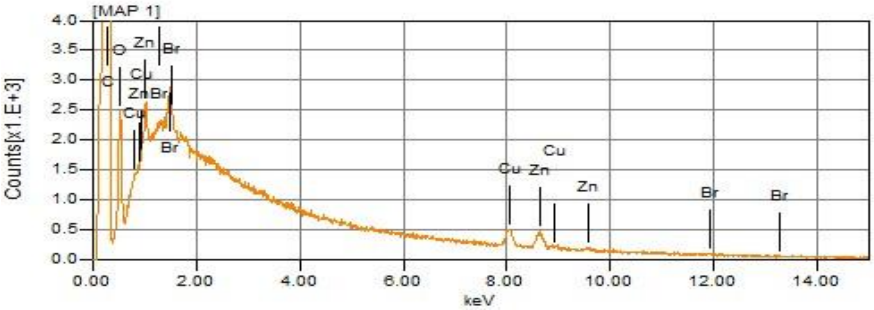

Map Counts

Table 5. 2 Mapped Elements after Drying the Particles after Discharged

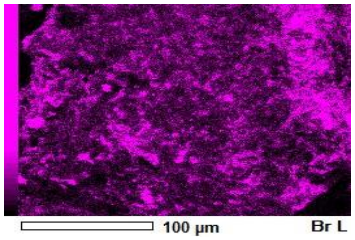

Bromine

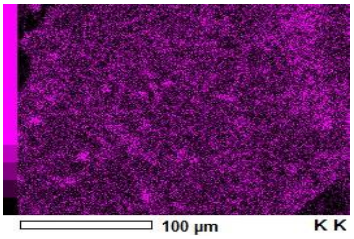

Potassium

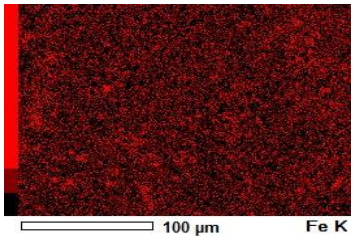

Iron

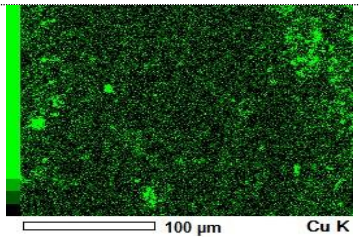

Copper

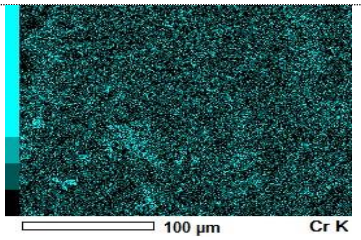

Chromium

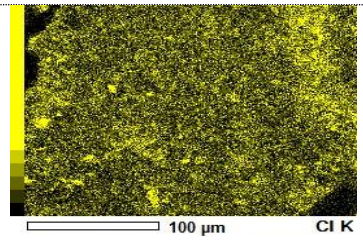

Chlorine

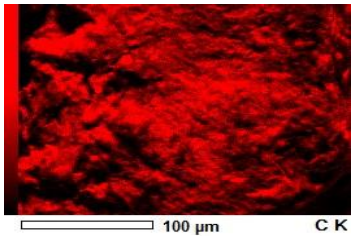

Carbon

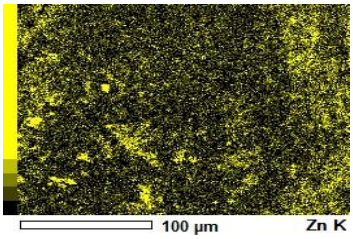

Zinc

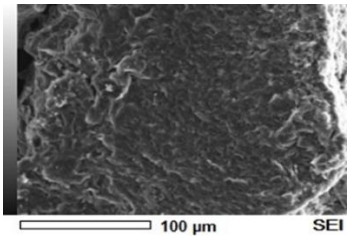

Silicon

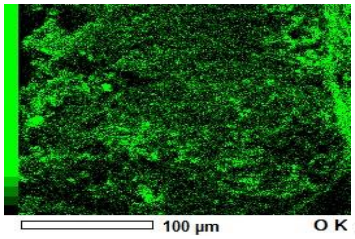

Oxygen

Formula	mass%	Atom%	Sigma	Net	K ratio	Line
C	88.10	94.51	0.01	1956419	0.4010615	K
O*	5.19	4.18	0.02	45690	0.0318090	K
Cl	0.33	0.12	0.00	42781	0.0141327	K
K*	0.16	0.05	0.00	18229	0.0070554	K
Cr*	0.09	0.02	0.01	5536	0.0036824	K
Fe*	0.08	0.02	0.01	3483	0.0031057	K
Cu*	0.78	0.16	0.01	20071	0.0292386	K
Zn	2.42	0.48	0.02	53916	0.0923618	K
Br	2.86	0.46	0.01	231046	0.1025811	L
Total	100.00	100.00				

Element Properties

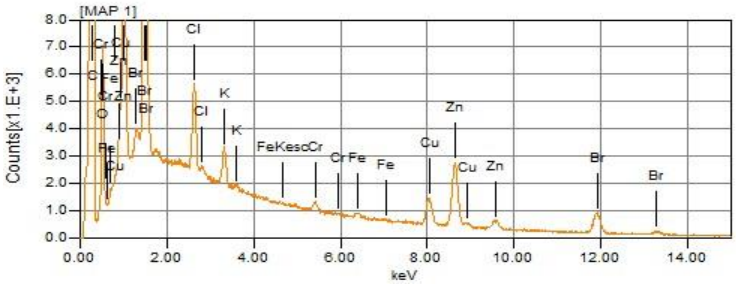

Elements Map Counts

Table 5. 3: Mapped Elements of Charged and Discharged After Copper Deposits

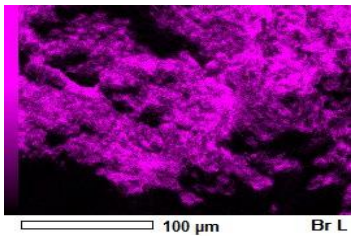

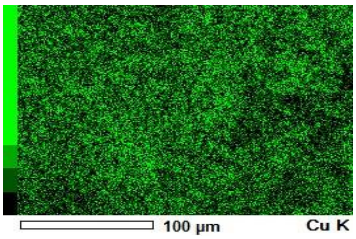

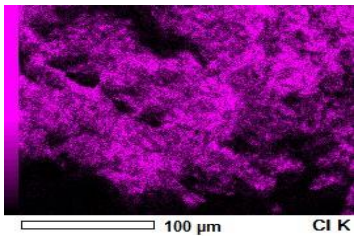

Bromine	Copper	Chlorine
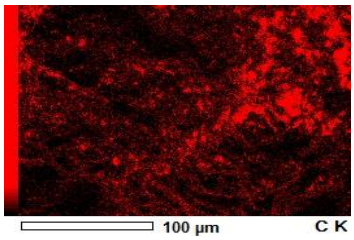 Carbon	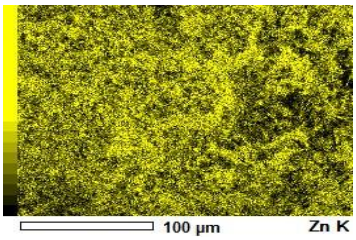 Zinc	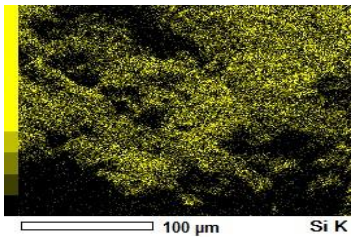 Silicon
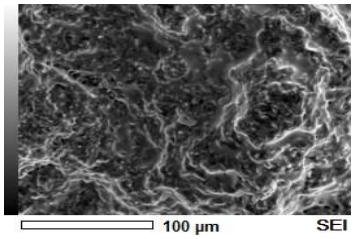 Selenium	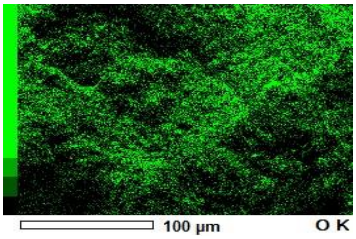 Oxygen	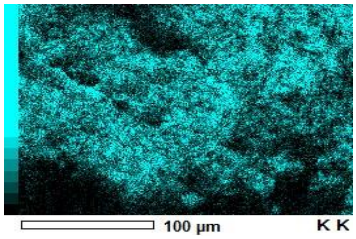 Potassium

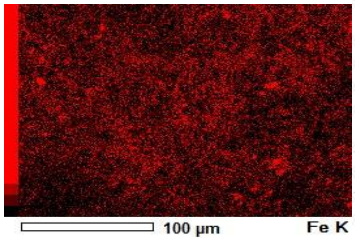

Iron

Formula	mass%	Atom%	Sigma	Net	K ratio	Line
C	40.09	75.21	0.03	88864	0.0182154	K
O*	3.39	4.78	0.02	23631	0.0164505	K
Si*	0.05	0.04	0.01	2202	0.0005507	K
Cl	5.56	3.53	0.01	307391	0.1015378	K
K	2.23	1.29	0.01	118667	0.0459243	K
Fe*	0.19	0.08	0.01	4808	0.0042868	K
Cu	1.80	0.64	0.02	27284	0.0397436	K
Zn	20.26	6.98	0.06	270830	0.4639136	K
Br	26.42	7.45	0.06	871135	0.3867394	L
Total	100.00	100.00				

Elements Properties

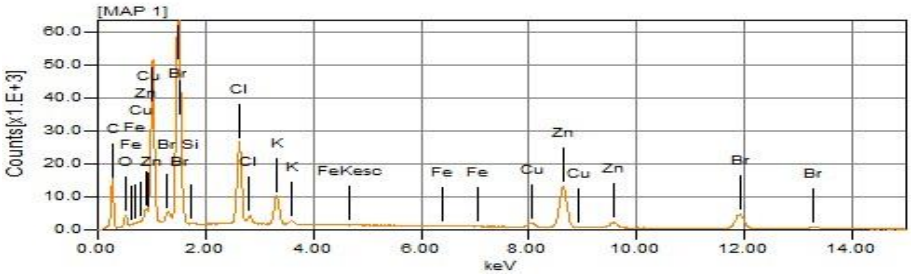

Map Counts

5.4 SEM Conclusions

Picture 1, observed as 100 microns has a sedimentary rock shape, photo 3, viewed in 10 microns has highly mossy deposits that look like zinc clusters. Picture 2 of 50 microns resemble silt sand that was sticky together, and photo 4, was observed in 5 microns.

Particles collected after discharging the stored energy by the battery cell were like the charged particles examined via the SEM machine. Furthermore, the carbon fibre feeder electrode materials also contributed to the low current in between (-300 mA to 300 mA) that was observed continuously when the fabricated battery cell was charged and throughout its mode of operation. In the past, a similar magnificently SEM results have been achieved despite using the appropriate working electrodes materials, primary and secondary supporting electrolyte which also enhanced a good electrochemical behaviour [480].

5.5 UV-Vis Protocol and Details

A UV-Vis Spectroscopy laboratory device is a simple, quick and not expensive measurable technique for measuring the amount of light absorbs by a chemical substance**.** This process can be carried out by gaging the light intensity passing through a sample in relation to the light intensity through a blank reference or sample. Multiple techniques can measure types of multiple sample; either in thin film, glass, liquids, or solids. UV-Vis Spectroscopy as a measuring device is suitable to know the transmitting, absorption and the functioning reflection of a material wavelength in the range of 190 nanometers to 1,100 manometers [481, 482]. See section 6.33 of chapter 6, for the analyzed results

With a UV-Vis spectroscopy device, it was possible the observed brown deposits within the cathode electrolyte solution as copper by collecting some of this electrolyte solution in a small glass bottle after passing these charges to the cell: (1) 0.1 amps and -0.1 amps for 3600 secs and 800 secs (2) At 0.1 amps and -0.1 amps for 3500 secs and 200 secs and (3) At 0.25 amps for 3600 secs and -0.25 amps for 100 secs with 3 moles of KBr (535.51 grams), 1 mole of KCl (111.89 grams) as the cathode-side electrolyte solution and 3 moles of ZnBr2 (675 grams), 1M of $ZnCl_2$ (205 grams), and 1 mole of KCl (111.826 grams) as the anode electrolyte solution.

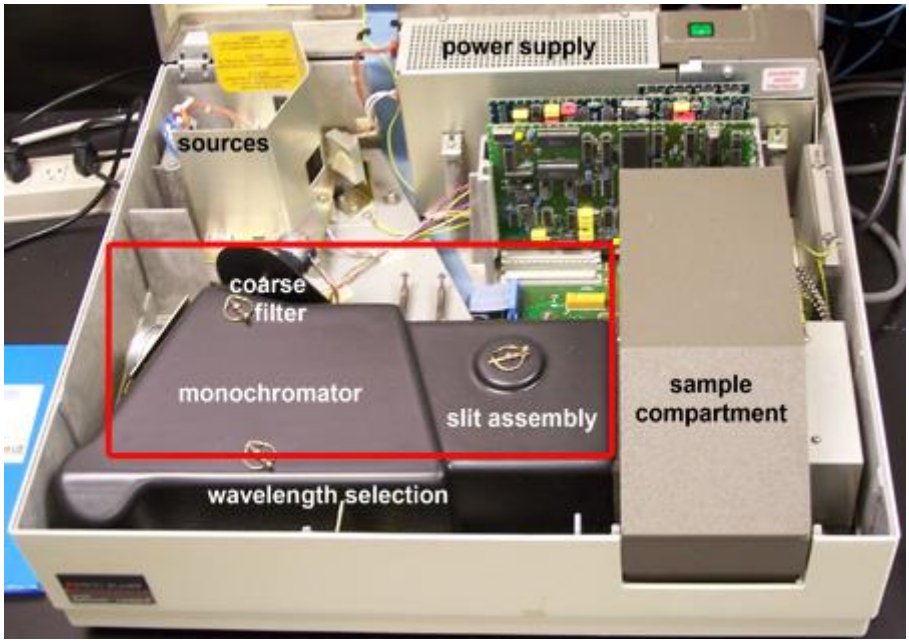

Figure 5. 5: UV-Vis spectroscopy device [483]

5.6 Rig Design Bill of Materials and Components

Section 4.3 of chapter 4, has presented earlier the zinc bromine cell test rig and all the enclosed components within the battery cell. These components are the anode and cathode endplates, anode and cathode gaskets the anode and cathode two fabricated reactors etc. Table 9.8 in chapter 9 of the appendix has provided the battery cell components without the bill of materials. This was due to the default settings of the Lancaster university solidwork software not allowing to select the BOM top level button. See figure 9.12 for further details.

5.7 Electrodes Substrates and Fittings

The three feeder electrodes (carbon-anode vs carbon-cathode) (nickel-anode vs carbon-cathode) and (nickel-anode vs titanium-cathode) investigated in chapter 6 were fabricated to the same size by using the Lancaster University automated CNC machine, shaping machine and some handy tools machines for cutting these feeder electrodes into the appropriate shapes. Table 5.1 has further presented the purchased electrolyte materials and name of the suppliers. Table 5.2 has also showed all the anode and cathode components and suppliers. Before the real laboratory experimental work in chapter 6, some pre-analysis calculations were explored to

know the transferring liters of electrolyte within the anode and cathode reservoir tank to the anode and cathode fabricated reactors of the ZnBr2 cell. Therefore, to know the electrolyte volume entering these reactors, the following approaches were considered: These includes (i) knowing the anode-side (100 mm) and cathode-side (50 mm) reactors length (ii) The two reactors breadth for the anode-side (130 mm) and cathode-side (50 mm) (iii) The electrodes thickness anode-side (12mm) and cathode-side (12 mm) (iv) Both electrodes hose fittings length anode-side (70 mm) and cathode-side (70 mm). (v) Both electrodes flexible tubing's height, anode-side (130 mm) and cathode-side (50 mm) and (vi) Electrodes flexible tubing radius anode-side (65 mm) and cathode-side (25 mm). These measurements were used for the fabricated anode reactor in section 3.3.1 and the battery cell test rig in section 3.5.3.

5.7.1 Carbon Feeder Electrodes Material

In microscale chemistry, a developed and modified carbon electrode can offer an inexpensive method for electrochemical investigations of encountered small quantities of compounds. The method involves transferring the analyte to the modified graphite electrode working surface, via abrasion from a solid target compound or by deposited evaporating from organic solutions. Pyrolytic carbon can be offering access to wide anodic potentials ranges, low electrical resistances, low residual currents, and the electrode surface reproducible structure and available in morphological variation as graphite pastes. This made it suitable for use in the microscale laboratory [484]. Carbon electrodes modification with waxes and oils can provide a suitable lipophilic surface for electrochemistry of water [485].

5.7.2 Nickel Feeder Electrode Material

Nickel is corrosively resistance as electrode feeders but can still have problems in halide conditions. Various temperature range (750–1100 °C) in fused NaCl–KCl, LiCl, $CaCl_2$, and LiF mixtures containing REE an Hastelloy G-35 and VDM® Alloy 625 nickel alloys corrosion resistance have been investigated with the materials corrosion and mechanisms with the interaction between alloys and melts and processes [486]. Another corrosion test on a redox system has influenced using nickel in this experimental work. The investigation was based on

a performed corrosion test concerning some nickel-based alloys samples of natural circulation and of a maximum melting temperature up to 700ºC [487].

Nickel supports electroplating. Electroplating is the process by which a thin layer of one metal is laid down on top of a second metal. Electroplating is used to make metal products with very specific qualities. Steel is strong but tend to easily corrode. Nickel does not corrode as fast as steel. Steel can be prevented from corrosion via using a thin layer of nickel on top of it. Nickel has become a very valuable metal and classified as a transition metal. The most common use is in stainless steel production, as a strong material that does not rust. It is used in hundreds of industrial and consumers applications. Nickel is also used in manufacturing several other alloys. Melting and mixing two or more metals can makes an alloy. The mixture has different properties from other individual metals and closely related to iron, cobalt copper and zinc.

5.7.3 Titanium Feeder Electrodes Materials

The electrochemical reaction of titanium has been studied as an excellent non-ferrous metal with good corrosion resistance, good fatigue properties, and with higher weight and strength and [488]. Titanium's excellent corrosion properties include using it for electrochemical processes such as electroplating, electrophoresis, electrodeposition, electroforming, electro-hydrolysis, electro chlorination, electrofluorination, and electrolysis. Within the earth crust, titanium as a strong metal is the tenth most commonly occurring element, light, naturally resistance to marine, chlorine corrosion and has the highest strength compare to the weight ratio of any metal. Titanium is around 45% lighter, strong as some steels with high melting point. From other elements, additional quantities of element are present in titanium alloys. These include vanadium and aluminium. These elements can further enhance the mechanical properties and corrosion resistance. Titanium is used for architectural applications by applying it as exterior panels and in the nuclear, oil and chemical industries where it is used for pipes, etc due to its corrosion resistance.

Table 5. 4 Electrolyte Chemical Materials and Suppliers

ANODE

Purchased Chemicals	Comment	The Suppliers
2 mol per liter of $Znbr_2$ (zinc bromide) weighed as 675 grams was the main target to be used. 574.5 grams of $Znbr_2$ was measured initially using the PRECISA ES220M measuring device before pouring it into a 250 mL glass bottle and further weighing 101 grams of $Znbr_2$ that was added and made the $Znbr_2$ quantity to be 676 grams.	(1) Zinc Bromide, Anhydrous 98+%, ACROS Organics™ is a colourless salt (2) $ZnBr_2$ is the linear chemical formula and the Molecular weight is 225.20 (3) Zinc Bromide, $ZnBr_2$ has different properties with zinc chloride such as highly soluble in water (H_20) (4) $ZnBr_2$ form acidic solutions and it is soluble in organic solvents.	Sigma-Aldrich Chemicals Company
205 grams of $Zncl_2$ was added to the anode electrolyte solution and weighed on the laboratory PRECISA ES220M measuring device.	(1). Zinc chloride, 98+%, extra pure, ACROS Organics™ (2). Anhydrous, beads, amorphous, −10 mesh, 99.99% trace metals basis with chemical compounds formula $ZnCl_2$ and its hydrates. (3). $ZnCl_2$ are highly soluble in water, white and colorless. (4). $ZnCl_2$ is the chemical formula, of molar mass (136.286 g/mol) and density of (2.91 g/cm³).	Sigma-Aldrich Chemicals Company
The added electrolyte solution was 111.1 grams of (KCl) and weighed accordingly by using the laboratory PRECISA ES220M measuring device.	(1). Potassium Chloride (KCl) is a metal halide salt, odourless, colourless or white in crystal appearance. (2). KCl as a solid substance dissolve readily in water and has a molar mass of 74.5513 g/mol, melting point 770 °C and density of 1.98 g/cm³.	Fisher Scientific
Bromoacetic acid, 98+% (250 grams) and Sodium bromoacetate, 98% (25 grams)	Chemical substances added to the cathode and anode electrolyte solution to balance the pH level to 2.5 and 3	Alfa Aesar
	CATHODE	
Two different supporting chemical compounds as electrolytes were added to the ZBB cell cathode-side. This include 395.625 grams of (KBr, purchased from Fishers Scientific, 99%) was first measured and added, 141.842 grams of KBr from the same supplier was also measured and added again. Further addition includes,112.644 grams (KCl, from Fishers Scientific, 99%). These chemical compositions were mixed in 1.5 liters of de-ionized water to avoid contamination.		

Table 5. 5 Anode and Cathode Components and Suppliers.

PURCHASED MATERIALS FOR THE ANODE AND CATHODE COMPARTMENT

Purchased Chemicals	Comment	The Suppliers
Graphite powder, -20+80 mesh, 99.9% (metals basis) 1kg	Graphite powder was added to the anode reactor and charged for the electrodeposition of zinc morphology.	Alfa Aesar
Azlon™ Square HDPE Carboys with Stopcock 5L	Cathode and anode reservoir tank	Fisher Scientific
Black Neoprene Rubber Sheets 1000 mm x 2000 mm x 1.5 mm	Rubber material was enclosed as gaskets (190mm*190mm*0.1mm) to the cell avoid unwanted leakage.	RS Components
RS Pro HDPE Laboratory Bottle with Narrow Neck, 5L	Material was purchased to replace the damaged cathode tank because of bromine formation.	RS Components
Gear Wrench 8 x 10 mm Offset Ring Spanner 185 mm length	Sprouted socket spanners mounted on the cell for tightening the bolts and nuts	RS Components
Nafion™ Membrane N324, Teflon Fabric Reinforced Gewebeverstärkt	Materials was purchased to prevent the anode and cathode electrolyte from mixing.	Ion Power, Uber uns, AGB, Datenschutzbestimmungen
RS Pro PET, PVC transparent Flexible Tube 25m, Long Reinforced, 60mm Bend Radius, Application, various	Material was purchased and coupled to the cell to transfer electrolyte into the anode and cathode reactor.	RS Components
Carbon Fibre Sheet, 300 mm x 300 mm x 0.75 mm (Carbon anode and cathode)	The first invested feeder electrode. The material was fabricated to this size: 190 mm*190 mm*0.1 mm.	RS Components
Carbon Fibre Sheet, 300 mm x 300 mm x 0.75 mm as the cathode feeder electrode Nickel Material as the anode feeder electrode	The anode coupled nickel material size was (190 mm*190 mm*0.1 mm) and the carbon feeder electrode was enclosed as the cathode feeder electrode	The carbon fibre sheet was purchased from RS component and the nickel material was supplied by Lancaster university supervisor.
Nickel Material as the anode feeder electrode Titanium Material as the cathode feeder electrode.	The anode coupled nickel material size was (190 mm*190 mm*0.1 mm) and the titanium feeder electrode was enclosed as the cathode feeder electrode.	PV3 technologies was the supplier of the titanium sample. The nickel feeder electrode was supplied by Lancaster university supervisor.
RS Pro Plain Nylon Threaded Bar, M8, 1m	The threaded bar carries the weight of the battery cell.	RS Components
Nylon, Hex Nut Natural, M8	The material was mounted on the purchased treaded bar and tightened to prevent leakages.	RS Components

M8 Plain Nylon Sealing Washer, 2 mm Thickness	The material was mounted on the cell before the purchased treaded bar was mounted and tightened.	RS Components
Klinger Statite 2000 x 1000 mm 1.5 mm Thick Beige, Gasket Sheet, Statite, Maximum of +120 °C	The material was purchased to replace the initial fabricated rubber gaskets that can't prevent leakages.	RS Components

5.8 Measuring Techniques

A potentiostat can be used to observe the battery cell performances via carrying out these electrochemical measurements: cyclic voltammetry (CV), chronopotentiometry (charging and discharging), measuring the impedances and proceeding to the scanning of electrons image via the scanning of electrons microscopy (SEM) after the electrochemical measurement. Since one ampere (1A), was the potentiostat capacity, there this will be used during the experiment to measure the resulted current from the cell with the applied potential. A direct current, DC via the potentiostat will be measured and expected to produce a maintained accurate potential, determine, allowed and draw different current into the system without any changes to the voltage.

Any resulting current, to a voltage converter can be measured and a data acquisition system will produce the voltammogram results. The potentiostat will be connected to the electrochemical cell in a different way because it is a two-electrode experiments. These are the simplest cell setups and the whole cell electrochemical results can be observed by using a two-cell electrode. Sometimes, with the corresponded analysis, their results can be complex. A connected physical setup is possible with a two-electrode mode and connect the current and sense leads. Measuring a complete voltage dropped is possible thru a two-electrode setup, via the working electrode by the current across the whole electrochemical cell, electrolyte, and counter electrode.

A two-electrodes cell in electrochemical set-up is one out of the approaches that are commonly used in electrochemistry and applied with electrodes roles. In a two-electrodes cell setup, counter electrode (CE) and reference electrode (RE) are shorted on one of the electrodes while

the working electrode (WE) and (S-connector) are shorted on the opposite electrode before the potential across a complete cell and measured.

This includes contributions from the counter electrode (CE/electrolyte) interface and the electrolyte itself. The two-electrode configuration can be used whenever a precise interfacial potential control across the working electrode (WE) electrochemical interface is not critical, and the whole system behaviour is under investigation. Concerning conversion devices like fuel cells, batteries, photovoltaic panels etc., this setup is typically used.

5.8.1 Cyclic Voltammetry

The introduced potentiostat in this research work will support carrying out a cyclic voltammetry technique to characterize the current that develops within the fabricated zinc-bromine battery redox system against the voltage and because it has many other advantages. [489, 490]. Between one to five cycles (1-5) will be the applied multiple cycles at a sweep condition of 25mV/sec. Cyclic voltammetry technique advantages includes using it to investigate aqueous solutions redox reactions, adsorption and zinc deposition onto electrode surfaces and for kinetic studies [491-493]. Others include for heterogenous and homogeneous calculation via the numerical packages such as COMSOL. During the experiments, the potential axis will be chosen as x-axis to show the voltammogram corresponding relationship in the result panel [494-502]

5.8.2 Chronopotentiometry (Charge and Discharged)

Additionally, a potentiostat is needed to carry out chronopotentiometry electrochemical characterization method that will measure the electric potential response of the cell system to an imposed current. Compared to other dynamic characterization methods, i.e. electric impedance spectroscopy or cyclic voltammetry (CV), chronopotentiometry (CP) allows a direct access to the voltage contributions in different states of the solution membrane system. Compared to a steady state voltage or current sweeps, more detailed information can be obtained by a chronopotentiometry technique because the dynamic voltage response is quick in time and can be analyzed. This is why chronopotentiometry is used in electrochemical

science to investigate transport processes and reactions in electrolyte solutions, at electrodes [503-517].

5.8.3 Electrochemical Impedance Spectroscopy (EIS)

Electrochemical impedance spectroscopy (EIS) will be used to measure the response of the fabricated electrochemical systems (ZnBr2) based on the applied potential [518, 519]. Electrochemical impedance is usually measured by applying an alternative current (AC) potential to an electrochemical cell and then measuring the current through the cell. Electrochemical impedance is normally measured using a small excitation signal. This is done so that the cell's response is pseudo-linear. In a linear (or pseudo-linear) system, the current response to a sinusoidal potential will be a sinusoid at the same frequency but shifted in phase

Chapter 6
Measuring Techniques

6 Chapter 6 Measuring Techniques.

6.1 Introduction and Experimental Condition

The presented charge and discharge rate and time in table 6.1 of this chapter, were the programmed conditions of the chronopotentiometry experiments that were explored in this research work by using the three feeder electrodes materials. Furthermore, the cyclic voltammetry's sweep condition presented in table 6.2 were explored after charging and discharging the stored current by the fabricated zinc-bromine battery cell at those various programmed rates in table 6.2. The cell impedances will later be discussed somewhere in this chapter 6. However, the scanning electron microscopy (SEM) outcome were already presented in chapter 5 and discussed.

Table 6. 1 Cycle-3: Explored charged and discharged experiment at various charge rate via the three sets of electrode feeder materials carbon vs carbon, nickel vs carbon and nickel vs titanium with 3 moles of KBr (535.51 grams), 1 mole of KCl (111.89 grams) as the cathode-side electrolyte and 3 moles of ZnBr2 (675g), 1 mole of $ZnCl_2$ (205g), and 1 mole of KCl (111.826g) as the anode electrolyte solution.

Charge and Discharged Experiments			
Experiments	Carbon & Carbon	Nickel & Carbon	Nickel & Titanium
1	(a) Charge rate and discharge rate (0.2 amps and -0.1 amps @ 1500 secs & 1300 secs) (b) (0.1 amps and -0.1 amps @ 3600 secs & 500 secs).	Charged rate and discharged rate (0.1 amps vs -0.01 amps) @ both 3600 secs	Charged @ 0.1 amps for 3600 secs
2	(a) Charged rate at (0.1 amps, 0.1 amps, and 0.25 amps) @ 3600 secs, 3500 secs & 3600 secs (b) Discharged rate (-0.1 amps, -0.1 amps, and -0.25 amps) @ 800 secs, 200 secs & 100 secs	Three-cycles of charged and discharged rate of 0.1 amps and -0.1 amps @ 3600 secs and 1800 secs	First Charged and discharged rate of 0.1 amps for 1800 secs and at -0.1 amps for 900 secs
3	(a) Charge and discharge rate of (0.25 amps, 0.1 amps, 0.25 Amp, 0.5 amps and 1 amps) @ 3600 secs and (b) Discharged	Three cycles of charged rate and discharged rate at (0.1 amps vs -0.1 amps) @ 3600 secs and 1800 secs	Charge and discharge rate of 0.1 amps for 1800 secs and at -0.1 amps for 900 secs.

	rate (-0.25 amps, -0.005 amps, -0.01 amps, -0.01 amps and -0.05 amps) @ 400 secs, 3500 secs, 3600 secs, 3600 secs & 3600 secs		
4	The re-examined two-carbon electrodes at (a) charged rate of 0.1 amps for 3600 secs and discharged rate of -0.01 amps for 3600 secs. (b) charge rate and discharge rate at 0.1 amps and -0.1 amps at both for 3600 secs	Three-cycles of charged rate and discharged rate at (0.4 amps and -0.4 amps) for 3600 secs and 1800 secs	Three cycles of charged rate and discharged rate of (0.1 amps vs -0.1 amps) for 1800 secs and 900 secs
		The re-examined nickel and carbon materials at (a) charged rate of 0.1 amps for 3600 secs and (b) discharged rate of -0.1 amps for 1800 secs	Charged rate and discharge rate at 0.3 amps for 1800 secs and at -0.3 amps for 900 secs
			Charge rate and discharge rate at 0.1 amps for 1800 secs and at -0.1 amps for 900 secs

Table 6. 2: Cycle-3: Explored cyclic voltammetry experiment using the three feeder sets of electrode materials, carbon vs carbon, nickel vs carbon and nickel vs titanium with 3M of KBr (535.51 grams), 1M of KCl (111.89 grams) as the cathode-side electrolyte and 3M of ZnBr2 (675 grams), 1M of $ZnCl_2$ (205 grams), and 1M of KCl (111.826 grams) as the anode electrolyte solution

Cyclic Voltammetry Experiments at one sweep for each set of conditions			
Experiments	Carbon & Carbon	Nickel & Carbon	Nickel & Titanium
	15 cyclic voltammetry of 1 sweep @ 25 mV/sec	3 cyclic voltammetry of 1 sweep @ 25 mV/sec	5 cyclic voltammetry of 1 sweep @ 25 mV/sec
1	6 cyclic voltammetry of 5 sweeps @ 20 mV/sec		
2	2 cyclic voltammetry of 5 sweeps @ 50 mV/sec		

By exploring various electrochemical measurements using different charged and discharged rates and techniques will allow to know the most conductive electrode materials that can be recommended in future to fabricated zinc-bromine batteries cells. Some of these techniques as discussed earlier include the cyclic voltammetry, chronopotentiometry, electrochemical impedance spectroscopy and apart from the scanning electrons microscopy (SEM) to identify elements surrounding the charged carbon particles. These electrode feeder materials (two-carbon materials, nickel versus carbon materials and titanium versus nickel materials.) were incorporated separately and investigated within the cell (anode-side and cathode-side). See Figure 6.1 as the first investigated feeder electrode.

6.1.1 Examined Carbon Electrodes Materials

INVESTIGATED ANODE ELECTRODES FEEDER MATERIALS IN THE ZBB BATTERY CELL SYSTEM	INVESTIGATED CATHODE ELECTRODE FEEDER MATERIAL IN THE ZBB BATTERY CELL SYSTEM
A material portion of 190 mm*190 mm* 0.75 mm was cut out of the carbon fiber sheet, of 300 mm x 300 mm x 0.75 mm purchased from RS components	A material portion of 190 mm*190 mm* 0.75 mm was cut out of the carbon fiber sheet, of 300 mm x 300 mm x 0.75 mm purchased from RS components

Figure 6. 1 Two Carbon Fibre Materials Incorporated to the Anode-Side and Cathode-Side of the ZnBr2 Cell

6.1.2 **Materials and Methods – Carbon Feeder Electrodes**

The battery cell was programmed to charge and discharge using a chronopotentiometry charge and discharge rates up to 1 amp and -1 amps and at different time up to 10800 seconds. The impedance was constantly measured after the charge and discharged amperes at (0.1 amps, 0.4 amps, 0.7 amps, 1 amps) and at (-0.1 amps, -0.4 amps, -0.7 amps, -1 amps). Cyclic voltammetry was performed on the cell at sweep conditions: 20 mV/s, 25 mV/s, and 50 mV/s by setting the maximum volt to 3.500 volts and minimum volt to 0.200 volts.

Between 1 sweep and 5 sweeps condition was applied to the cell. The anode and cathode electrolyte solution were prepared and weighed on a PRECISA ES220M balance measuring device before they were transferred into two different glass bottles (250 mL) and later mixed with 1.5 liters of de-ionized water from the laboratory Lancaster university dispensing machine to avoid any contamination. See table 6.3 for these chemical quantities. These chemicals, 99.999% trace metals basis were purchased from these different suppliers (Sigma-Aldrich and Fisher Scientific).

The anode electrolyte density was 1.47 gcm^{-3}. This density was used to gauge the cathode-electrolyte solution. The used direct current (DC) power supply was between (0-30 volts) and (2.5 Amp) was used to regulate the flow rate of the flow meter (166.7 cm^3/min) and the two-different coupled self-priming centrifugal pump with a flow rate capacity of 2100 L/ Hr.

Table 6. 3: Anode and Cathode Electrolyte Solution

	Electrolyte Solutions	
Items	Anode	Cathode
1	3 moles of ZnBr2 (675 grams)	3 moles of KBr (535 grams)
2	1 mole of $ZnCl_2$ (205 grams)	1 mole of KCl (111.897 grams)
3	1 mole of KCl (111.826 grams).	

6.1.3 Instrumentations Methods and Operation - Carbon Feeder Electrodes

The explored chronopotentiometry and cyclic voltammetry on the fabricated zinc-bromide cell were explored using the available set conditions in table 6.4 and in table 6.5 for the two-carbon electrode materials. The introduced potentiostat can supply a current up to (1 amps) for charges and discharges rates. The carbon material purchased from RS Components (300 mmx300 mm x 0.75 mm) was re-shaped to 190 mm x190 mm x 0.75 mm. The two-carbon current collector were rinsed with de-ionized water and the zinc electrodeposition area was fixed as (50 mm x 50 mm x 12 mm). The added carbon before charge and the anode-carbon electrode feeder were positioned closely to have a good contact. The electrodeposition was carried out at ambient temperature (25 ^{0}C). Some particles were collected as a sample after the deposition process and dried at a room temperature of (25 ^{0}C) before the SEM. The solutions were all weighed on the PRECISA ES22OM laboratory balance.

Table 6. 4: Chronopotentiometry experimental current values on the investigated two-carbon materials with 3 moles of KBr (535.51 grams), 1 mole of KCl (111.89 grams) as the cathode-side electrolyte and 3 moles of ZnBr2 (675 grams), 1 mole of $ZnCl_2$ (205 grams), and 1M of KCl (111.826 grams) as the anode electrolyte solution.

Chronopotentiometry Experiments	
Experiments	Investigated first sets of electrode feeder materials carbon at the anode-side and cathode-side
1	(a) Charge and discharge experiment at a rate of (0.2 amps and -0.1 amps @ 1500 secs and 1300 secs) (b) (0.1 amps and -0.1 amps @ 3600 secs & 500 secs).
3	(a) Charged condition at (0.1 amps, 0.1 amps, and 0.25 amps) @ 3600 secs (b) Discharged rate (-0.1 amps, -0.1 amps, and -0.25 amps,) @ 3600 secs
5	(a) Charge & discharge rate of (0.25 amps for 3600 secs, 0.1 amps for 3600 secs, 0.25 amps for 3600 secs, 0.5 amps for 3600 secs and 1 amps for 3600 secs) and (b) Discharged rates at (-0.25 amps for 400 secs, -0.005 amps for 3500 secs, -0.01 amps for 3600 secs, -0.01 amps for 3600 secs and -0.05 amps for 3600 secs).

6	The re-investigated two-carbon electrodes at a current of (a) Charge at 0.1 amps for 3600 secs and discharge at -0.01 amps for 3600 secs.

Table 6. 5: Cyclic Voltammetry experimental scan values on the investigated two-carbon materials with 3M of KBr (535.51g), 1M of KCl (111.89g) as the cathode-side electrolyte and 3M of ZnBr2 (675g), 1M of $ZnCl_2$ (205g), and 1M of KCl (111.826g) as the anode electrolyte solution.

Cyclic Voltammetry Experiments	
Experiments	Investigated First Sets of Electrode Feeder materials Carbon at the Anode-Side and Cathode-Side
1	Five cyclic voltammetry of 1 sweep condition @ 25mV/sec

The charged and discharge amperes were compared with the those predicted by the model in COMSOL. Chronopotentiometry (CP) technique was used because it was suitable for analytical purposes. Chronopotentiometry has a standard and accurate measurements in between four to five percent. Extracted data from the battery cell were used to calculate the charge and energy efficiencies after the charge and discharge rates by introducing the presented formula in the table 6.6. The specified zinc-bromine battery cell charge and energy efficiencies were generally assessed using the following three efficiencies: voltage efficiency (VE), coulombic efficiency (CE), and energy efficiency (EE).

Table 6. 6: Methods for the Cell Efficiencies

Charged State		
1	Charged Passed During Charging	Current (A)*Charge time (secs) = Coulombs (C)
Discharged State		
2	Charged Passed During Discharging	-Current (A)*Charge time (secs) = -Coulombs (C)
3	Charge Efficiency (CE) $\frac{\text{Charged Recovered (Discharge)}}{\text{Charged Input (Charge)}} * 100\%$	$\frac{\text{Discharged (C)}}{\text{Charged (C)}} * 100\% = \%$

4	Energy Efficiency (EE) $\frac{\text{Energy Recovered (Discharge)}}{\text{Energy Input (Charge)}} * 100\%$	$\frac{\text{Charge Recovered} * \text{Average Voltage During Discharge}}{\text{Charge Input} * \text{Average Voltage During Charge}} * 100\%$ $\frac{\text{Discharged (C)} * \text{Average Voltage During Discharge}}{\text{Charged (C)} * \text{AverageVoltage During Charge}} * 100\% = \%$

6.1.4 **Error Bar Graphical Representations**

All the calculated charge and energy efficiencies that will be extracted from the fabricated zinc-bromine battery cell with the investigated three feeder electrodes materials (carbon, nickel and titanium) will graphically be presented on bar charts with their attached error bars. Error bars as graphical representations demonstrate the variations among all graphically used data and will be used to indicate any uncertainty or errors that are reported in this electrochemical measurement. Error bars provides a true precise measurement and generally the differences from all the reported values.

6.1.5 **Descriptions of Results**

The two different results presented in (Figure 6.2ai) and (Figure 6.2aii) were the chronopotentiometry results. The presented aggregated zinc particles in figure 6.3 were the charged particles. Figure 6.4 is the displayed cell components that showed all the incorporated materials existing in the cell. These materials were incorporated to the cell before it was possible to carry out the chronopotentiometry, cyclic voltammetry in (figure 6.3b) and the electrochemical impedance spectroscopy measurement that were explored on the cell. For instance, to measure the resistances of the battery cells.

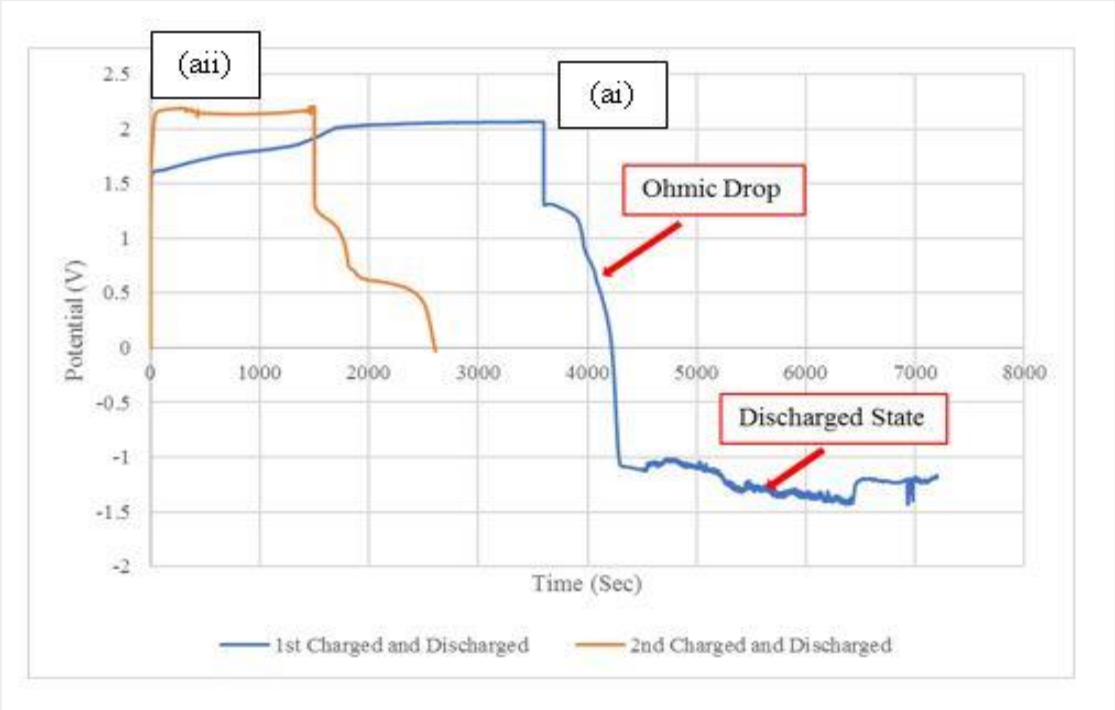

Figure 6. 2: Charged and discharged result plot (ai) (0.1 amps at 3600 secs & -0.1 amps for 500 secs) and (aii) (0.2 amps @ 1500 secs &, -0.1 amps for 1300 secs) of 3 moles of KBr (535.51 grams), 1 mole of KCl (111.89 grams) as the cathode-side electrolyte solution and 3 moles of ZnBr2 (675g), 1 mole of $ZnCl_2$ (205 grams), and 1 mole of KCl (111.826 grams) as the anode electrolyte solution.

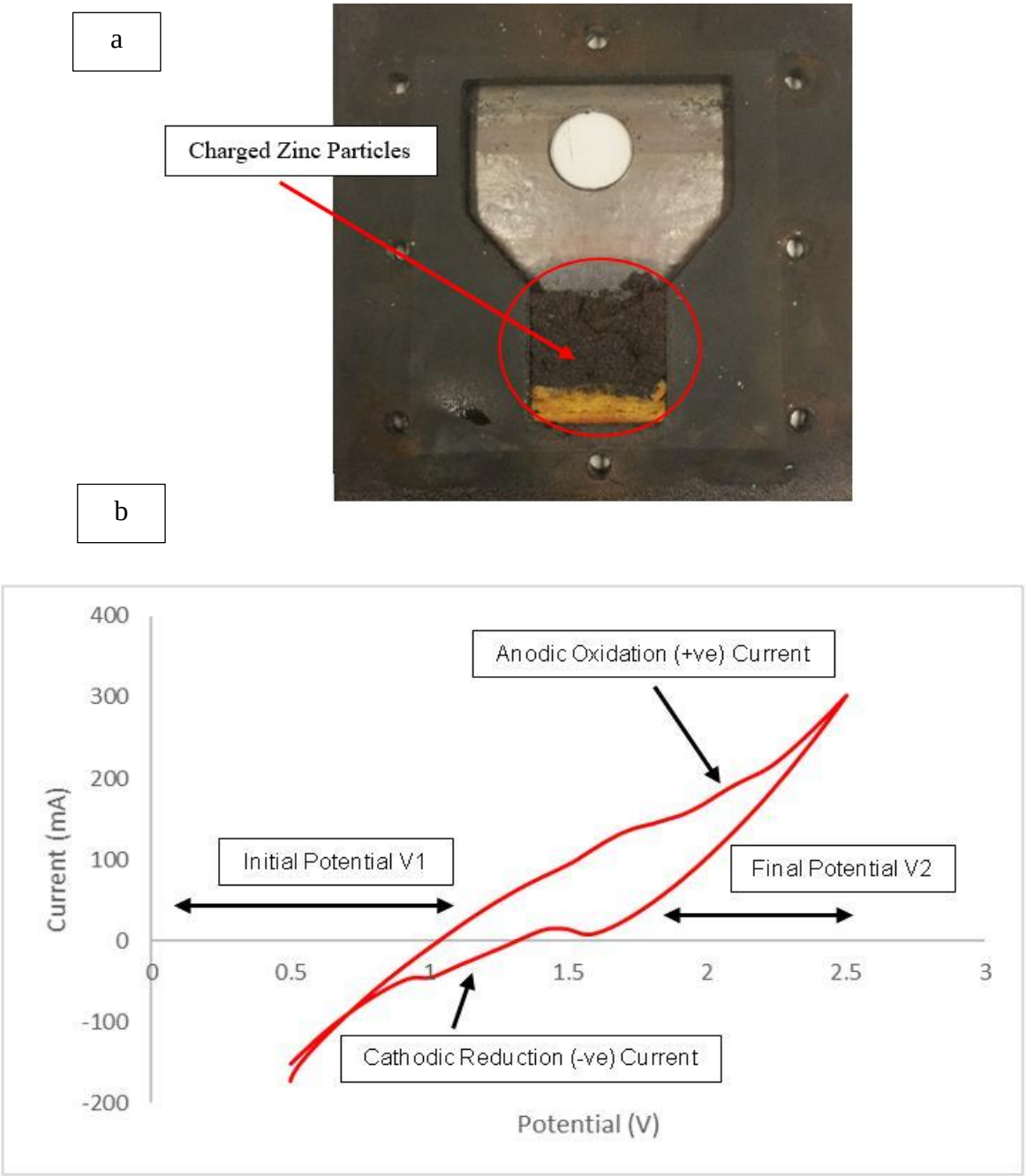

Figure (6. 3a) Zinc morphology (254 microns to 354 microns) appearances within the anode zinc reactor after reacting (b) Cyclic voltammetry of the two-carbon electrodes feeder materials at 0.2 amps, and -0.1 amps for 3600 seconds for one sweep condition using 3 moles of KBr (535.51 grams), 1 mole of KCl (111.89 grams) as the cathode-side electrolyte solution and 3 moles of ZnBr2 (675 grams), 1 mole of $ZnCl_2$ (205 grams), and 1 mole of KCl (111.826 grams) as the anode electrolyte solution at a charge rate of (0.2 amps @ 1500 secs &, -0.1 amps for 1300 secs) and before completely losing the cell apart.

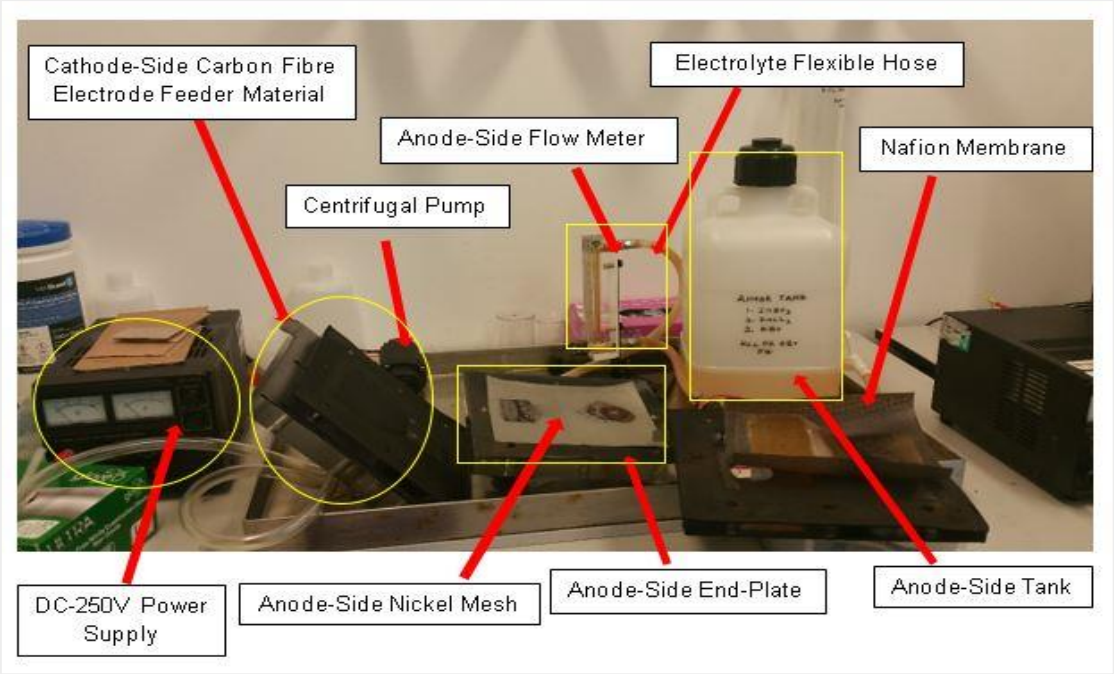

Figure 6. 4 Cell Components after the Explored Two-Chronopotentiometry

6.1.6 **Description of Analysis - Carbon Feeder Electrodes**

To acquire some information on the cell, such as the charge and energy efficiencies and performances of the incorporated current collectors, etc., it was necessary to allow the battery cell at a charge rate of (0.2 amps and -0.1 amps) and at (0.1 amps and -0.1 amps) to charge and discharge under one hr condition. See table 6.7 for more detailed information. Data's that were gathered through the applied chronopotentiometry technique were used to generate the two graph curves in figure 6.2ai, and in figure 6.2ii.

Figure 6.4 has showed the cell components. To draw a conclusion, these obtained data were used graphically and compared with the experiments since statistical charts are used to examine and summarize a range of data values [520]. See (figure 6.5: bar chart) for the cell efficiencies.

Table 6. 7: Experimental Data of the investigated two-carbon materials with 3 moles of KBr (535.51 grams), 1 mole of KCl (111.89 grams) as the cathode-side electrolyte and 3 moles of ZnBr2 (675 grams), 1 mole of $ZnCl_2$ (205 grams), and 1 mole of KCl (111.826 grams) as the anode electrolyte solution.

No	BATTERY CELL DATA'S CHARGE AND DISCHARGE	CHARGE STATE			DISCHARGE STATE			RESULTS	
		TIME STEP (SEC)	ENERGY (W. HR)	VOLTAGE (V)	TIME STEP (SEC)	ENERGY (W. HR)	VOLTAGE (V)	CHARGE EFF %	ENERGY EFF %
TWO CHARGE AND DISCHARGE EXPERIMENTS									
Ai	0.1 A & -0.1 A	3600	2	2	500	1.1	1.1	13.8	N/A
Aii	0.2 A & -0.1 A	1500	2.1	2.1	1300	1.3	1.3	43.3	15.63

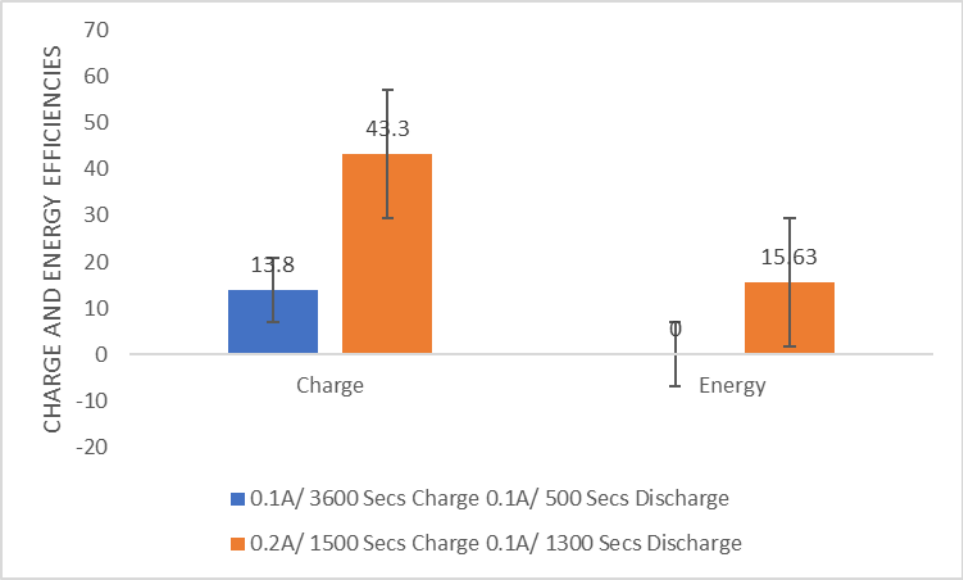

Figure 6. 5 Bar chart showing the compared energy efficiencies charge-(blue) and energy-(pink) at (1) 0.1 amps & -0.1 amps @ 3600 secs & 500 secs and (2) A charged rate of 0.2 amps & -0.1 amps for 1500 secs & 1300 secs.

Error bar can show the discrepancies between batteries life cycle, composition and average cycle life though their data. These batteries material formulation could include super P, (carbon black) and graphitic carbon [521]. In figure 6.5, the 13.8% CE is 100% conclusive due to no overlapping with the other CE bar. The 43.3% EE extracted data is 100% conclusive. The 15.63% EE is 71% conclusive due a data similarity of 29% with the 43.3% EE. In conclusion, during the charge passed, oxygen growing within the cell when coupling it back could have affected the performances and efficiencies as observed during the recharge condition in a zinc-air battery [522].

6.1.7 Observation and Comments - Carbon Feeder Electrodes

6.1.7.1 Chronopotentiometry @ (0.1 Amps & -0.1 Amps) @ (3600 Secs & 500 Secs)

In figure 6.2ai, only the cell charge efficiency was calculated, but very low compare to the charge efficiency of the experimental result in (aii). The cell showed a negative potential of 1.1 volts and a charge voltage of 2 volts. The cell completed its charged and discharged cycle at the actual programmed rates (0.1 amps, and -0.1 amps) and within 3600 seconds and 500 seconds but with a strange voltage. During charge the cell watt was 0. 2 watt.hr (0. 0002 kilowatt.hr) and 0. 11 watt.hr (0. 0001 kilowatt.hr) during discharge.

The cell stored 360 coulombs at 3600 seconds and discharged the stored current at the expected 500 seconds. Carrying out a deep discharge on the cell at a charge and discharge rate of 0.1 amps and -0.1 amps can stress the battery cell if a partial discharge (500 secs) on the cell can result to a negative voltage. Furthermore, this could have affected the cell charge and energy efficiencies (CE and EE). Therefore, it is not advisable to partially or completely discharge current stored by the cell rather than programming the cell to store more current and programming the cell to discharge at a proper discharge time and currents. The cell was able to reverse back its polarity after it was fully discharged. This was confirmed via other chronopotentiometry measurements that was later carried out on the cell which indicated that the cell was not damaged and required no replacement.

6.1.7.2 Chronopotentiometry @ (0.2 Amps & -0.1 Amps) @ 1500 Secs & 1300 Secs

At 2.1 volts, from the graph plot in figure 6.2aii, the cell energy was 0.42 watt. hr with the following efficiencies: (CE, 43.3%, and EE, 15.63%). See the bar chart in figure 4.5 for further elucidation. The cell demonstrated a voltage of 1.3 volts at discharged. The battery cell was unable to store the expected 720 coulombs due to loss of energy and failed to discharge the programmed (-360 coulombs) of energy. The cell was fully charged at 1500 secs but could only store 300 coulombs out of the anticipated 720 coulombs. Therefore, 460 coulombs of energy were lost, and the cell still has 2300 secs to complete its charged. Additionally, the cell was able to discharge -130 coulombs at 1300 secs out of the expected 360 coulombs and lost -210 coulombs.

6.1.7.3 Cyclic Voltammetry @ 25mV/Sec - Carbon Feeder Electrodes

The presented cyclic voltammetry result in figure 6.3a had showed that the cell encountered high resistance during charge. The occurred high resistance contributed to the low current and low zinc depletion (non-conductive bed). The high slope on the cyclic voltammetry shape indicated a high resistance of about 5 ohms. Applying a slow scan rate to the explored cyclic voltammetry experiment was to observe a fast-chemical reaction. The reduction voltage occurred at 1.1 volts and a reduction current peak at -30 mA. Zinc depletion (Oxidation) continued until 2.3 volts with the oxidation current peak in between 200 mA and 300 mA.

6.1.8 Conclusions - Carbon Feeder Electrodes

Unanticipated side reaction could be occurring by charging and discharging the cell at 0.1 amps and -0.1 amps instead of charging and discharging it at a rate of 0.2 amps and -0.1 amps. Therefore, the electrodeposition of zinc is better at these rates: 0.2 amps and -0.1 amps; as this favours the Zn reaction. Similar current could be repeated to later to observe if the cell resistance will be reduced. The energy efficiency was calculated for charged passed at 0.1 amps and -0.1 amps (See table 6.7) but not recorded due to a negative discharge voltage.

The battery cell required dismantling it and cleaned to improve the efficiency and examine it methodically to prevent any future fault. The lost current might have gone into the added zinc particles or via wiping or leakage. From the bar chart in figure 6.5 (charge and discharge), the cell performed better at a current rate of 0.2 amps for 1500 secs and at -0.1 amps at 1300 secs. The system electrochemical design required checking it.

This include the zinc-electrode and cathode-electrode and the composition of the electrolyte. The high resistance on the zinc-bromide cell can also be reduced by lowering the salts concentration. Furthermore, placing the two electrodes more closely to each other and firmly can also be of help and reducing the thickness of the gasket demarcating these two electrodes for a more closed intact.

6.2 Recognition of Cu and Cell Reversion - Carbon Feeder Electrodes

Batteries cells capacities can be reduced, and the resistances can be increased, when different charges conditions are passed to them. This can be expected always based on different combination and decomposition of chemical reactions concerning the active materials. Therefore, this has instigated the different charge rates carried out in this section on the experimented zinc-bromine battery cell. This is because it has been reported in previous studies and based on the earlier charged passed on the cell in this research work.

Many research studies has also confirmed how the addition of active compound, and many other elements existing in batteries cells can give rise to undesirable chemical reactions [523]. In this section, the battery cell was charged and discharge at different acceleration voltages and programmed to charge and discharge at some different rates to observe the electrodeposited metallic zinc elements via using scanning the electron image with the SEM device (JSM-6010LA/JSM-6010LV).

6.2.1 Description of Results – Charged Passed Via Carbon Feeder Electrodes

A charge was passed twice at these charged rates conditions (0.1 amps and -0.1 amps) to confirm if the strange electrochemical noise was actually from the centrifugal pump and for further elucidation on what percentage of efficiency that can be derived from the cell. This has made the current results in this section as three different chronopotentiometry measurements at these current (0.1 amps, 0.1 amps, and 0.25 amps) and (-0.1 amps, -0.1 amps, and -0.25 amps) and three cyclic voltammetry results. See (Figure 6.6a-c) for the chronopotentiometry measurements. All the experimental cyclic voltammetry (CV) results in this section were similar to the first (CV) that was not displayed but were not reliable to be presented.

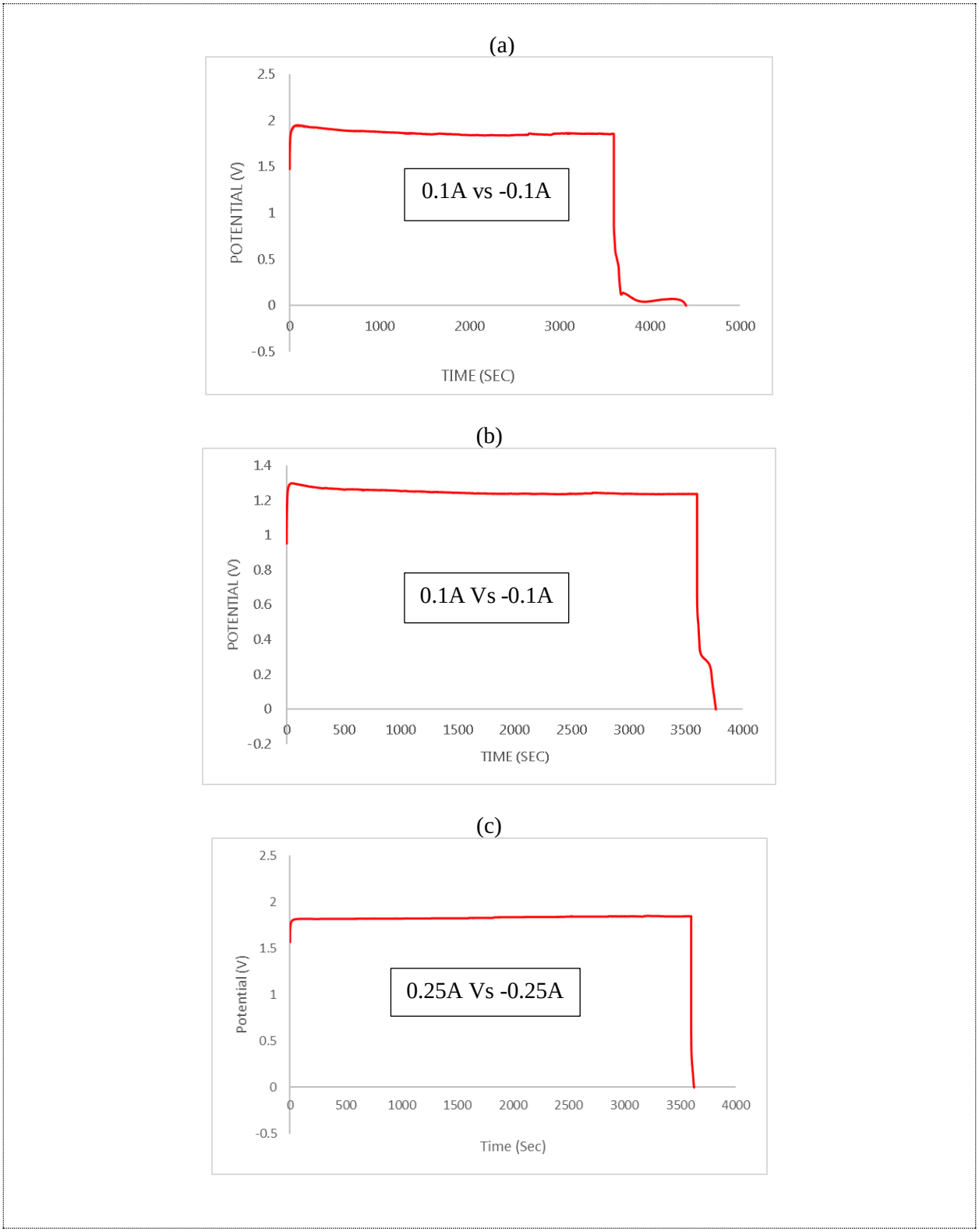

Figure 6. 6 Charge rate and discharge rate of (a) 0.1 amps for 3600 secs, -0.1 amps for 800 secs (b) 0.1 amps and -0.1 amps for 3600 secs and 200 secs (c) 0.25 amps and -0.25 amps for 3600 secs and 100 secs of 3 moles of KBr (535.51 grams), 1 mole of KCl (111.89 grams) of cathode electrolyte solution and 3 moles of ZnBr2 (675 grams), 1 moles of $ZnCl_2$ (205 grams), and 1 moles of KCl (111.826 grams) of anode electrolyte solution.

6.2.2 Description of Analysis - Carbon Feeder Electrodes

The presented bar charts in figure 6.7 with the error bars were explored after programming the battery cell to charge and discharge at different ampere conditions and time. The retrieved data from the cell supported each part of the hypothesis and gathered conclusions from the introduced and presented bar charts in Figure 6.7 and Table 6.8 for further analysis.

Table 6. 8: Experimental Data's of the investigated two-carbon materials with 3 moles of KBr (535.51 grams), 1 moles of KCl (111.89 grams) as the cathode-side electrolyte and 3 moles of ZnBr2 (675 grams), 1 moles of $ZnCl_2$ (205 grams), and 1 moles of KCl (111.826 grams) as the anode electrolyte solution.

THREE CHARGE AND DISCHARGE RATE EXPERIMENT									
10	0.1 A & -0.1 A	3600	0.19	1.9	800	0.7	0.07	22.22	5.90
11	0.1 A & -0.1 A	3500	0.13	1.3	200	0.03	0.3	5.71	2
12	0.25 A & -0.25 A	3600	0.45	1.8	100	0.025	0.5	2.77	1.07

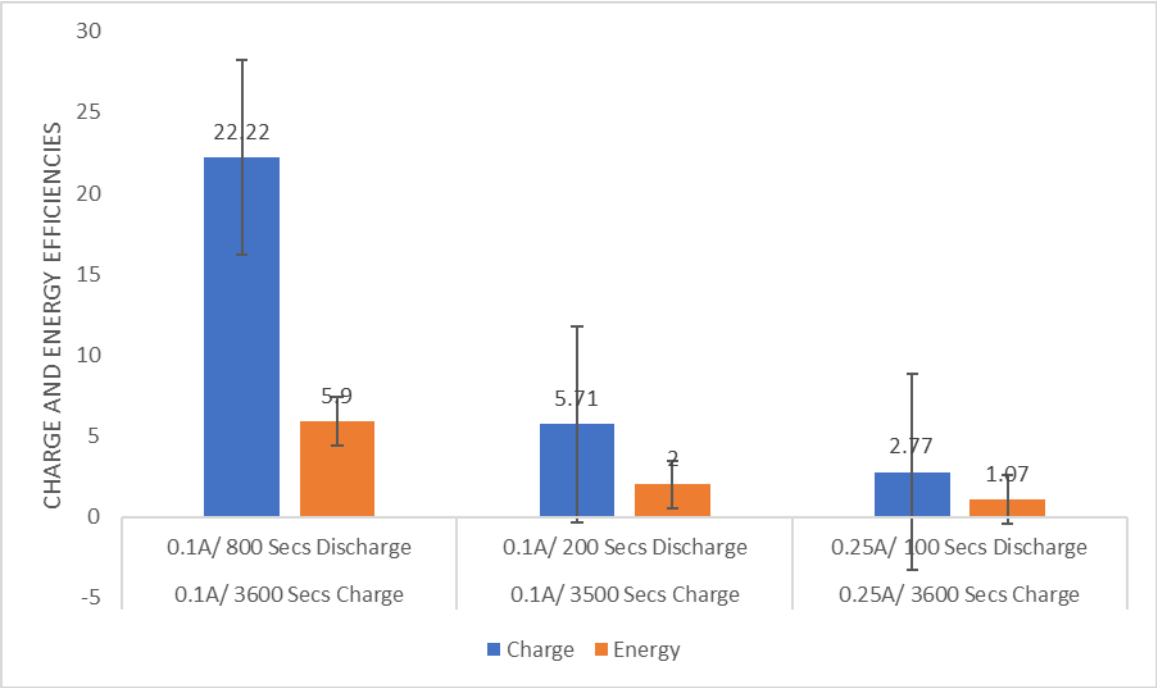

Figure 6. 7 Charge-(blue) and energy-(pink) efficiencies of charge rates (1) 0.1 amps and -0.1 amps for 3600 secs and 800 secs (2) At 0.1 amps and -0.1 amps for 3500 secs and 200 secs (3) 0.25 amps for 3600 secs and -0.25 amps for 100 secs of 3 moles of KBr (535.51 grams), 1 mole of KCl (111.89 grams)

of cathode electrolyte solution and 3 moles of ZnBr2 (675 grams), 1 mole of $ZnCl_2$ (205 grams), and 1 mole of KCl (111.826 grams) of anode electrolyte solution.

Originality of data and differences can be known using error bar as used to know the behaviour of a cathode material (olivine-type lithium manganese phosphate) (LiMnPO4) in a saturated aqueous lithium hydroxide electrolyte [524, 525]. From the charge efficiency in figure 6.7, charged passed at these rates of (0.1 amps for 3600, and at -0.1 amps for 800 secs) was 100% conclusive.

Other charged efficiencies at (0.1 amps, 0.25 amps) and at (-0.1 amps, -0.25 amps) were 100% conclusive since part of the error bar held large portion of collected data by 10.22% and 13.22%. However, the data of energy efficiency at (0.1 amps for 3600 secs, 3500 secs and at -0.1 amps for 800 secs, 200 secs) were conclusive excluding for the energy efficiency at 0.25 amps for 3600 secs and -0.25 amps and 100 secs).

6.2.3 Findings and Comments - Carbon Feeder Electrodes

6.2.3.1 The Three Charge and Discharge Experiments

Charged passed to the cell at these low current (0.1 amps, 0.1 amps, and 0.25 amps) and (-0.1 amps, -0.1 amps, and -0.25 amps) might have increased the resistances or may be the bed was not conductive as expected to fluidize and charge the added carbon particles and result to zinc electrodeposition. The presented bar charts supported each part of the data. See the three charge rates conditions in figure 6.7. Furthermore, the cell temperature was raised unexpectedly without any problem of short circuited. The charge and energy efficiencies might have reduced due to the secondary reaction; like the redox reaction within the cell.

Some parameters of the battery cell need to be monitored; such as the voltage, temperature and current during passing charges. These parameters are important so that the cell can be kept in a good operating condition. Other areas that required concentration is the electrolyte depletion and preventing the cell from overcharging. The electrolyte should be change as this can be degrading slowly. This can make the voltage to fluctuate, have low coulombic efficiency in relation to the discharge capacity and charge capacity and can lead to a non-uniformed

electrodeposition of zinc like dendrite formation [526]. But the incorporated high surface area anode-reactor will certainly prevent dendrite problems.

Brown deposit identified as copper were also observed within the cathode-side electrolyte during those explored charged passed and on the electrodeposited zinc within the anode-reactor (See figure 6.8). Such observed results impelled interrupting the cell from operating further and led to pulling the cell components apart for a proper cleaning and introducing a separation technique to sieve the cathode electrolyte solution and the anode electrolyte from these escaped zinc-particles.

Fitting materials that were not chemically resistance had contributed to such deposition. Furthermore, the cathode electrolyte also suddenly turned to a dark green colour during the charge rates and discharge rate. As previously mentioned in section 5.2 of chapter 5, the observed brown deposit which had converted the zinc-bromine batteries cell to a copper-zinc battery cell and later reverted back to a zinc-bromide cell had instigated carrying out a filtration process and repeatedly to separate the sediments observed from the anode and cathode electrolyte solution.

The UV-visible spectrophotometer device was introduced to detect why the cathode-side electrolyte did not change to a red colour during the charge rate and discharged rate before identifying a dark green coloured electrolyte as copper at a wavelength of 900nm and with two peaks. See figure 6.9a and b. The battery cell was able to establish a good redox reaction after these processes and according to the electrochemical results and from the experimental observation.

However, the cell efficiencies were too low due to internal losses, and some of the energy were assumed and agreed that they might have been converted into heat. See the bar chart in figure 6.7 for the different charged rates condition. The cell metallic bolts and nuts must be changed to first avoid the transferring of current onto them. The opening charge and discharged initially showed a voltage of 2 volts and dropped to 1.9 volts. The second and third charge and discharged voltage was 1.3 volts and 1.9 volts at the same current rates and programmed time. The last charged and discharged rate of 0.25 amps and -0.25 amps for 3600 seconds showed 1.8 volts.

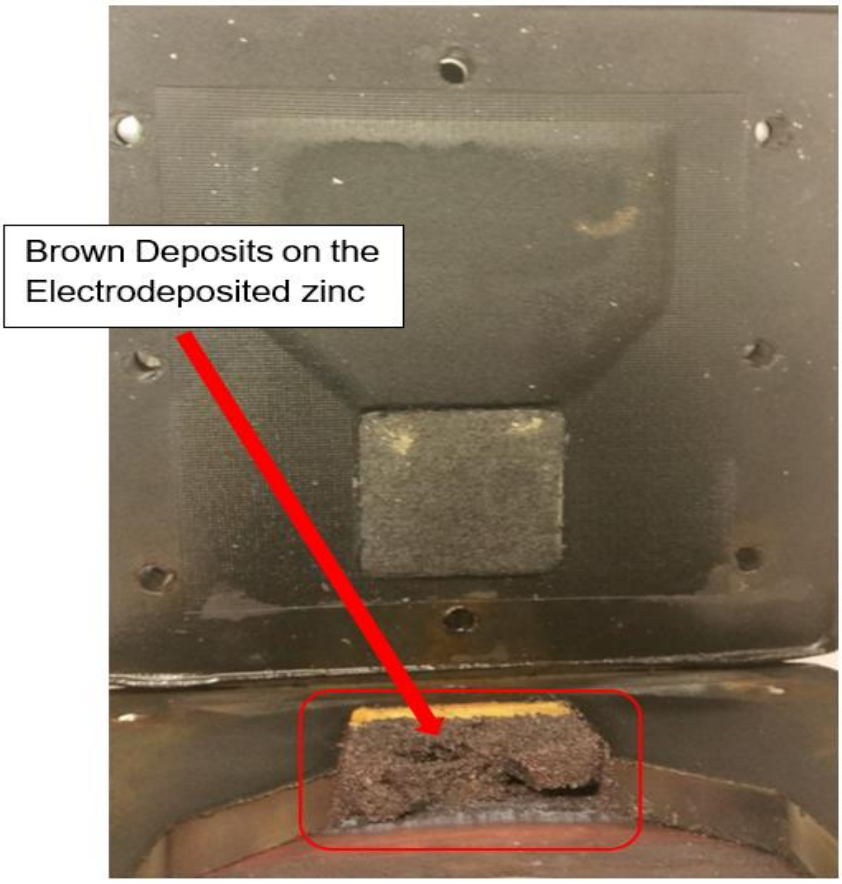

Figure 6. 8: Brown deposits identified as copper after charging the ZBB battery cell at a charge rate of (1) 0.1 amps and -0.1 amps for 3600 secs and 800 secs (2) At 0.1 amps and -0.1 amps for 3500 secs and 200 secs and (3) At 0.25 amps for 3600 secs and -0.25 amps for 100 secs with 3 moles of KBr (535.51 grams), 1 mole of KCl (111.89 grams) as the cathode-side electrolyte solution and 3 moles of ZnBr2 (675 grams), 1 mole of $ZnCl_2$ (205 grams), and 1 mole of KCl (111.826 grams) as the anode electrolyte solution.

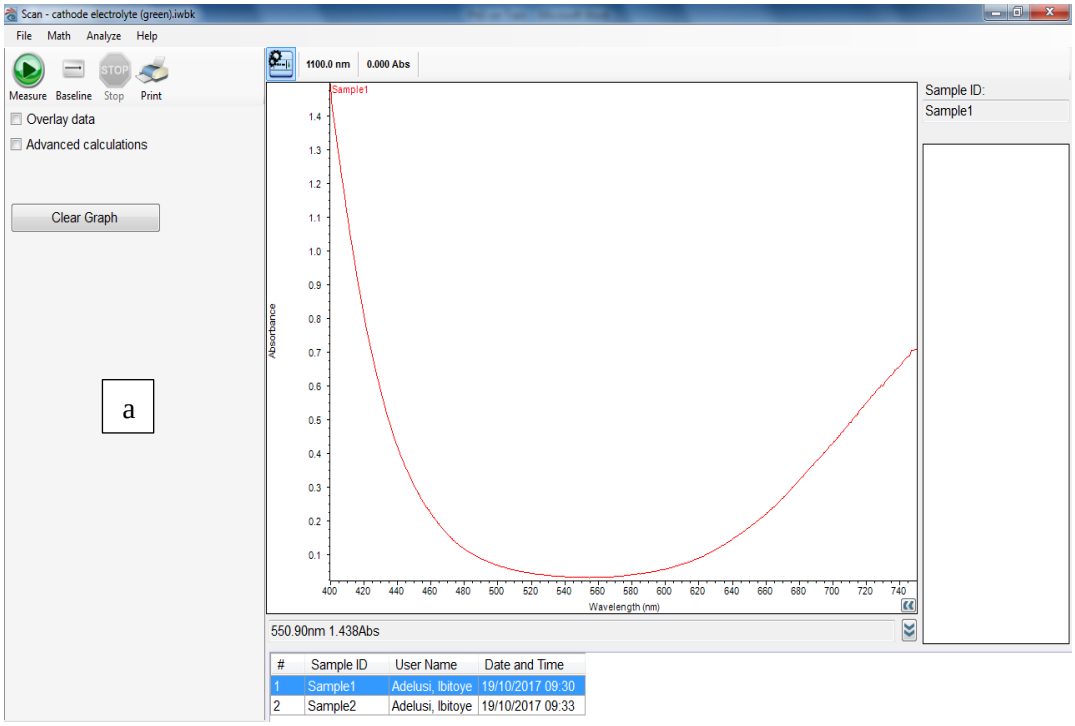

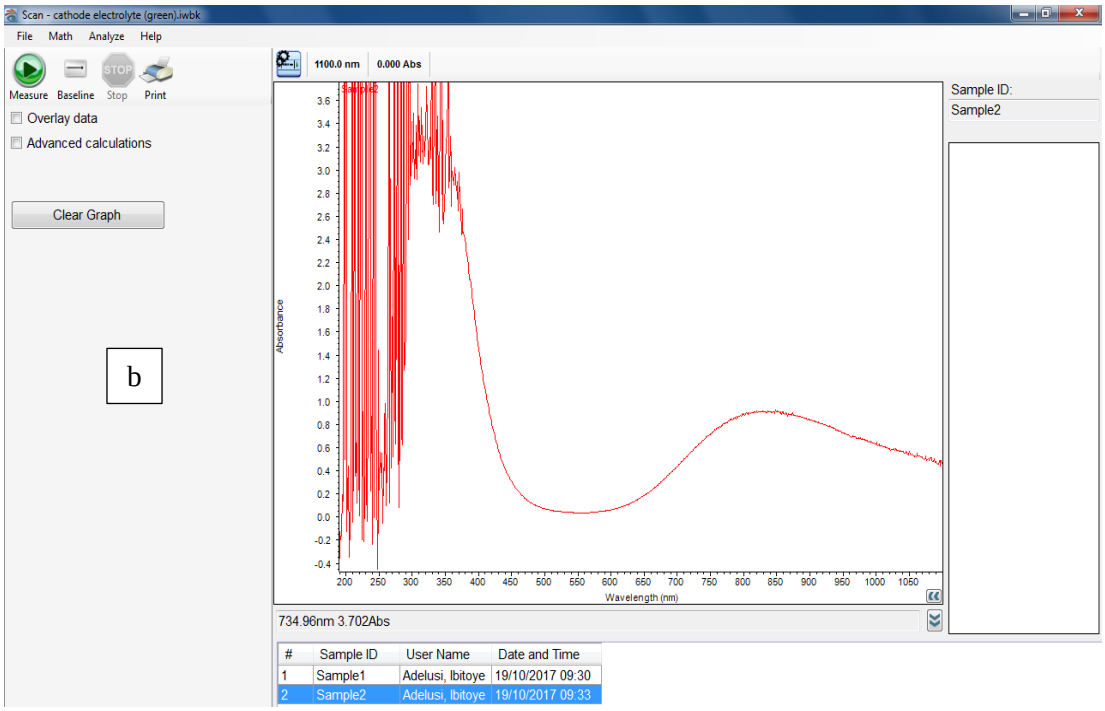

Figure 6. 9a: First identified peak showing the presence of copper at a wavelength of 740nm and b: Second identified peak showing the presence of copper at a wavelength of 900nm with a UV-visible spectrophotometer device.

6.2.4 Results Conclusions - Carbon Feeder Electrodes

Different energy efficiencies were established by the cell through the passed charged and due to the internal losses and heat that was encountered and suffered by the cell as presented with the bar chart in figure 6.7. Although these efficiencies were not good as desired; but still the best efficiency can be given to the 1st chronopotentiometry measurement at a current of (0.1 amps, -0.1 amps at 3600 secs and 800 secs) because of the observed charge efficiency of 22.22%, and energy efficiency of 5.90%.

6.3 Five Cycles of Chronopotentiometry - Carbon Feeder Electrodes

As mentioned earlier in section 6.2.3.1, to compare the cell energy efficiencies, the cell was further charged at these current (0.25 amps, 0.1 amps, 0.25 amps, 0.5 amps and 1 amps) and discharge at (-0.25 amps, -0.005 amps, -0.01 amps, -0.01 amps and -0.05 amps) at various seconds. See figure 6.10. The cathode electrolyte solution contains 3 moles of potassium bromide (KBr) (535.51 grams) and 1 mole of potassium chloride (KCl) (111.89 grams). The anode-side electrolyte also includes the following chemicals solution: 3 moles of zinc-bromide ($ZnBr_2$) (675 grams) Solution, 1 mole of zinc chloride ($ZnCl_2$) (205 grams), and 1 mole of potassium chloride (KCl) (111.826 grams). The anode electrolyte density was 1.47 g/ cm^{-3}.

6.3.1 Description of Results - Carbon Feeder Electrodes

Table 6.9 has provided further details in this section regarding the chronopotentiometry results. By charging the battery cell at those current stated in section 6.3 was to observe the current condition that can rapidly make the battery cell to have more better charge and energy efficiency of approximately 90% compared the previous results. The charged passed at 0.25 amps for 3600 secs and -0.25 amps for 400 secs has made the battery cell to stored 900 coulombs at 3600 secs during charge but lost (-700 coulombs) in between 3600 secs to 4000 secs and only stored 100 coulombs at 400 secs from the charge passed to discharge.

The charged voltage was 1.9 volts with 0.475 watt. hr (0. 000475 kilowatt.hr) and 0.5 volt as the discharged with 0.125 watt. hr (0.000125 kilowatt. hr). In between (0.1 amps and -0.005

Amp), at 3600 secs to 7100 secs, the stored current from the charged passed was -17.5 coulombs instead of -18 coulombs and 360 coulombs for the charged at exactly 3600 secs. The lost charge passed during discharge was -0.5 coulombs. the cell voltage was 1.5 volts during charge with 0.15 watt. hr (0.00015kilowatt. hr). The discharged voltage was 0.7 volt and demonstrated 0.0035 watt. hr (0.0000035 kilowatt. hr.).

During the charged passed at 0.25 Amp and -0.01 amps for both 3600 secs, the cell stored 900 coulombs at 3600 secs and lost -1 coulomb in between 3600 secs and 7100 secs during discharge but could discharged -35 coulombs at exactly 3500 secs. The cell charge voltage was 1.9 volts during charge and 1.0 volt for the discharged. the cell showed 0.475 watt. hr (0.000475 kilowatt. hr) for the charged and 0.01 watt. hr (0.00001 kilowatt. hr.) for the discharged.

The charged passed during charge and discharged at 0.5 amps and -0.01 amps for 3600 secs were 1800 coulombs and -35 coulombs. The voltage was 2.6 volts for the charge and 1.4 volts for the discharge. The charged passed made the cell to established 1.3 watt. hr (0.0013 kilowatt. hr) for the charge and 0.014 watt. hr (0.000014 kilowatt. hr) for the discharged. At exactly 3500 secs the cell could also discharge -35 coulombs of energy. Both the charge and energy efficiencies were low due to the poor performances.

At 1 amp and -0.05 amps for 3600 secs, the cell established 4 volts, 4 watts. hr (0.004 kilowatt. hr) during charge and 1.3 volts, 0.065 watt. hr (0.000065 kilowatt. hr) during discharged. The lost current was 5 coulombs out of 175 coulombs. The discharged current accumulated within (7100 secs) to (3600 secs). The charge passed during charge was 3600 coulombs and none of the charge passed throughout the charge period was recorded.

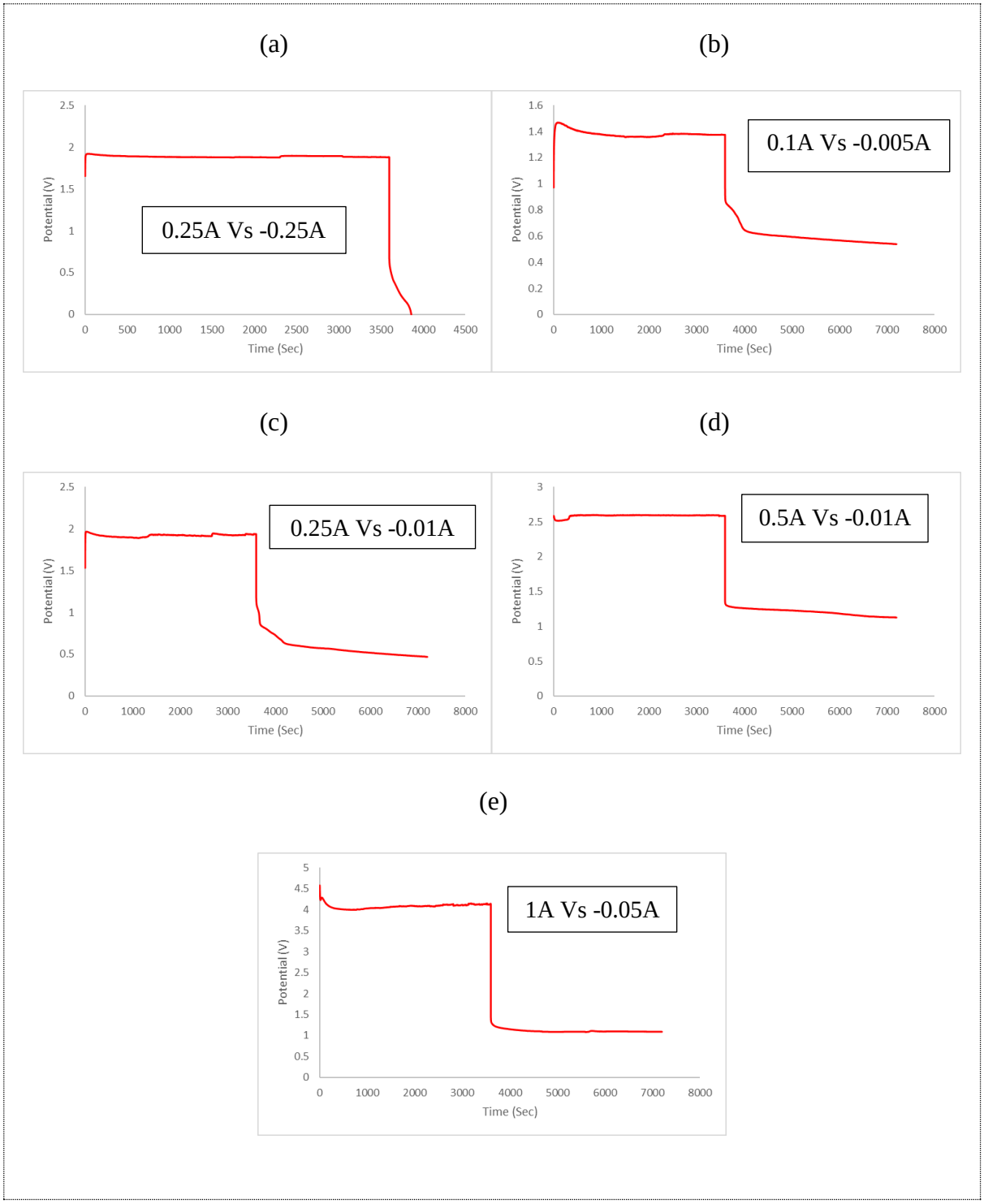

Figure 6. 10: Charge and discharge rates electrolyte solution: 3 moles of KBr (535.51 grams), 1 mole of KCl (111.89 grams) of cathode electrolyte solution and 3 moles of ZnBr2 (675 grams), 1 mole of $ZnCl_2$ (205 grams), and 1 mole of KCl (111.826 grams) of anode electrolyte solution at (a) 0.25 amps for 3600 secs, -0.25 amps for 400 secs (b) 0.1 amps for 3600 secs and -0.005 amps for 3500 secs (c) 0.25 amps for 3600 secs, and -0.01 amps for 3600 secs (d) 0.5 amps for 3600 secs, and -0.01 amps for 3600 secs. (e) 1 amp for 3600 secs, and -0.05 amps for 3500 secs.

Table 6. 9: Experimental data of the investigated two-carbon materials with 3 mole of KBr (535.51 grams), 1 mole of KCl (111.89 grams) as the cathode-side electrolyte and 3 mole of ZnBr2 (675 grams), 1 mole of $ZnCl_2$ (205 grams), and 1M of KCl (111.826 grams) as the anode electrolyte solution.

No	BATTERY CELL DATA'S CHARGE AND DISCHARGE	CHARGE STATE			DISCHARGE STATE			RESULTS	
		TIME STEP (SEC)	ENERGY (W. HR)	VOLTAGE (V)	TIME STEP (SEC)	ENERGY (W. HR)	VOLTAGE (V)	CHARGE EFF %	ENERGY EFF %
FIVE CHARGE AND DISCHARGE EXPERIMENTS									
1	0.25 A & -0.25 A	3600	0.475	1.9	400	0.0125	0.5	11.1	5.48
2	0.1 A & -0.005 A	3600	0.15	1.5	3500	0.0035	0.7	4.86	2.94
3	0.25 A & -0.01 A	3600	0.475	1.9	3600	0.01	1	3.88	1.81
4	0.5 A & -0.01 A	3600	1.3	2.6	3600	0.014	1.4	1.94	1.25
5	1 A & -0.05 A	3600	4	4	3600	0.065	1.3	4.86	2.21

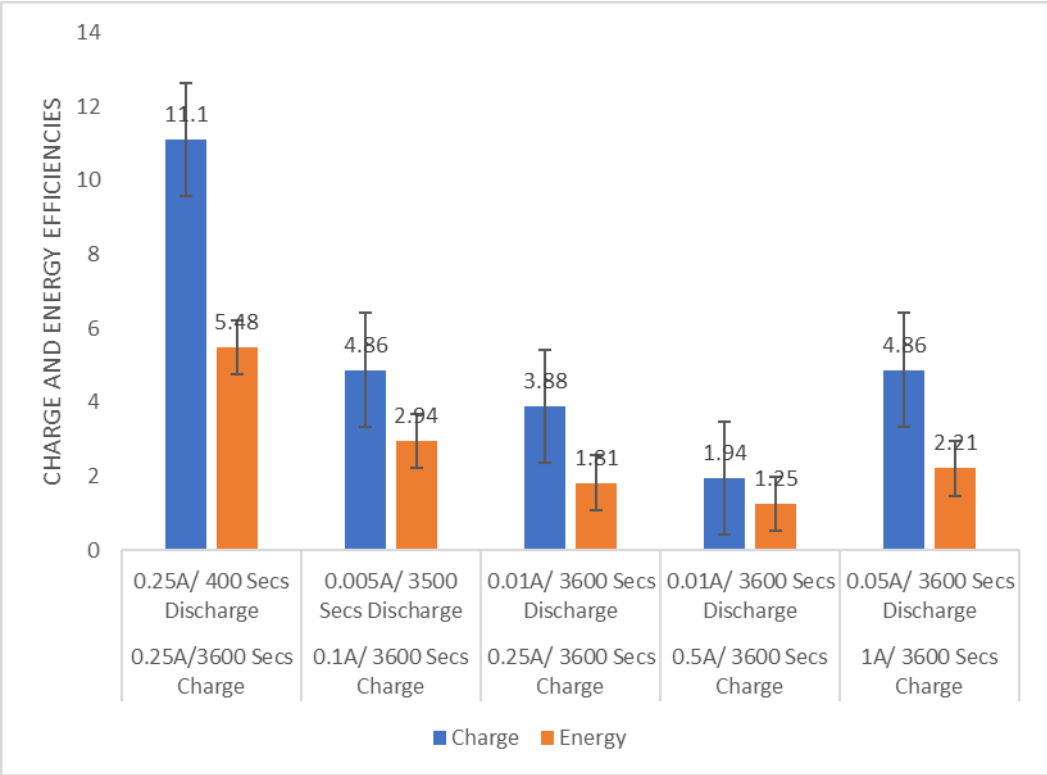

Figure 6. 11: Charge-(blue) & energy-(pink) efficiencies: 3 mole of KBr (535.51 grams), 1 mole of KCl (111.89 grams) of cathode electrolyte solution and 3 mole of ZnBr2 (675 grams), 1 mole of $ZnCl_2$ (205 grams), and 1 mole of KCl (111.826 grams) of anode electrolyte solution at (1) At a charge rate and discharge rate of 0.25 amps and -0.25 amps @ 3600 secs and 400 secs (2) 0.1 amps and -0.005 amps @ 3600 secs and 3500 secs. (3) 0.25 amps and -0.01 amps @ both 3600 secs. (4) 0.5 amps and -0.01 amps @ both 3600 secs. (4) 1 amp and -0.05 amps @ both 3600 secs.

In figure 6.11, CE (11.1%) is (100%) conclusive with the highest percentage since it did not overlap with the other bar charge efficiencies. These two charge efficiencies (4.86%) has a similarity of 6% with the 11.1% charge efficiency (94% conclusive). The 3.88% CE was 93.6% accurate due to a data similarity of 6.4% with the 11.1% CE. The 1.94% CE shared 91.6% data similarity 11.1% CE. The CE of 4.86% is 94% conclusive due to a similarity of 5.9%. For the EE, 5.48% has the highest value and 2.94% has 98% data similarity from it. EE of 1.81% has 3.8% data similarity with the 5.48% EE. So, it is 96% conclusive. EE of 1.25% has 4% data similarity (96% conclusive). EE of 2.21% with the 5.48% has 3% data similarity (97% conclusive).

6.3.2 Findings and Comments - Carbon Feeder Electrodes

From table 6.9, the cell demonstrated a very detrimental voltage (4 volts) at a charge and discharge rate of 1 amp and -0.05 amps and at 7000 secs. Passing a charge at 0.5 amps and -0.01 amps, the cell showed a voltage of 2.6 volts at 7000 secs. The cell voltage was low (1.5 volts) at a current of 0.25 amps and -0.01 amps. At 0.1 amps and -0.005 amps, the cell voltage was 2 volts. The cell further showed a very low voltage at a current of 0.25 amps and -0.25 amps. The cell demonstrated a good redox reaction during the charge state and according to the graph results, but the materials were not electrically conductive as expected. It was assumed that the entire cell energy efficiency was affected due to the problem.

The membrane can be re-boiled to be more conductive and the pH level of the two-electrolytes should be frequently checked since they determine the number of protons at the battery cell anode-side. Flow batteries cells electrolytes must not be ionically conductive alone to have higher efficiency, but also to be chemically stable, be conductive under a wide range of conditions, and be good mechanically [527, 528].

The anode electrode feeder must be changed to a better material that can be more conductive. Different coulombs (c) of charge were lost by charging the cell at different current and discharges conditions. The battery cell is so resistive, charging it at high current should be avoided but to discharge at a much lower condition. But not quite sure if the charges passed can be retrieved back from the cell at a lower current since the cell did not reached a point where the voltage collapsed. However, running the cell longer could have been a good idea for comparison of results.

6.3.3 **Overall Final Conclusions - Carbon Feeder Electrodes**

The bar chart confirmed each part of the data. See figure 6.11. The charge efficiency (CE) was better than the energy efficiency (EE). The cell demonstrated different results that cannot be presented due to the following indicated energy efficiencies: 11.1% as the 1st charge efficiency (CE), 4.86% as the 2nd charge efficiency (CE), 3.88% for the 3rd charge efficiency (CE), 1.94% for the 4th CE efficiency and 4.86% for the 5th CE efficiency. These observed results showed that the charge that was passed into the cell system were not completely recovered and none of these experiments can be recommended as a good zinc-bromine battery. The result also showed that almost 88.9% of the efficiency were lost.

6.4 Effects of Cleaning and Polishing Electrodes - Carbon Feeder Electrodes

Several electrochemical measurements were explored in this chapter 6 with the anode and cathode carbon electrode. However, after pulling apart the cell, the condition of the cathode current collector required cleaning it. See figure 6.12a before polishing the feeder electrode and in Figure 6.12b after polishing it. The results in figure 6.13a and b were the outcome of the re-used anode and cathode electrolyte solution after polishing the cell to remove any hidden contaminated substances and to be more conductive. Also see figure 6.14 and table 6.10.

Additionally, both the new cathode-side and anode-side electrolyte has the same chemical compounds as the old electrolyte solution. The only difference was the sequestering agent (Tetrabutylammonium bromide) with a chemical formula of $C_{16}H_{36}BrN$ that was added to the new cathode-side electrolyte solution instead of a MEP sequestering agent. Tetra-n-butylammonium bromide as a quaternary ammonium salt with a (Br) bromide concentration counterion is usually used as a catalyst for a quick phase transfer. The ammonium salt can also be used to prepare several other tetrabutylammonium salts through salt metathesis reactions. The cell was programmed to different current rates per hours to charge and discharge.

Experimentally, despite that the cell was able to comply and produce the expected programmed current during the charged and discharged, none of the produced result can be presented and endorsed as a good zinc-bromine battery cell. These include the efficiencies, watt. hr of the cell for the charge and discharge and other presented information's in table 6.10 etc.

CATHODE CURRENT COLLECTOR BEFORE POLISHING - A	CATHODE CURRENT COLLECTOR AFTER POLISHING - B
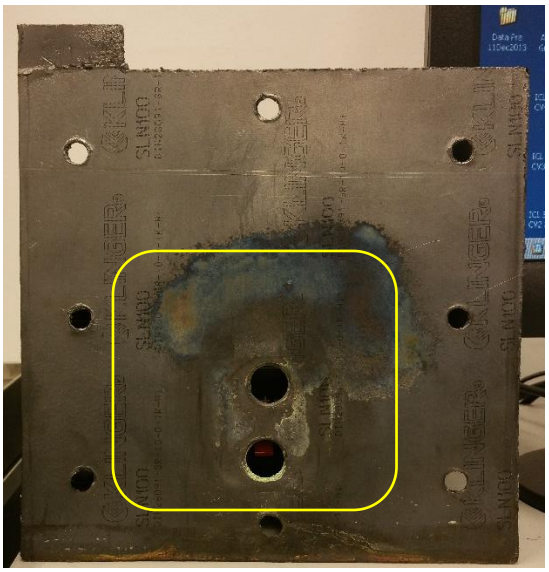	

Figure 6. 12: (a) Unpolished Cathode Carbon Electrode Feeder (b) Polished Cathode Carbon Electrode Feeder.

The cathode electrolyte solution consists of 3 mole of KBr (535.51 grams), 1 mole of KCl (111.89 grams) and 3 moles of ZnBr2 (675 grams), 1 mole of $ZnCl_2$ (205 grams), and 1 mole of KCl (111.826 grams) as the anode electrolyte solution at a current of 0.1 amps for 3600 seconds and to discharge at -0.01 amps for 3600 seconds.

6.4.1 **Results Description - Carbon Feeder Electrodes**

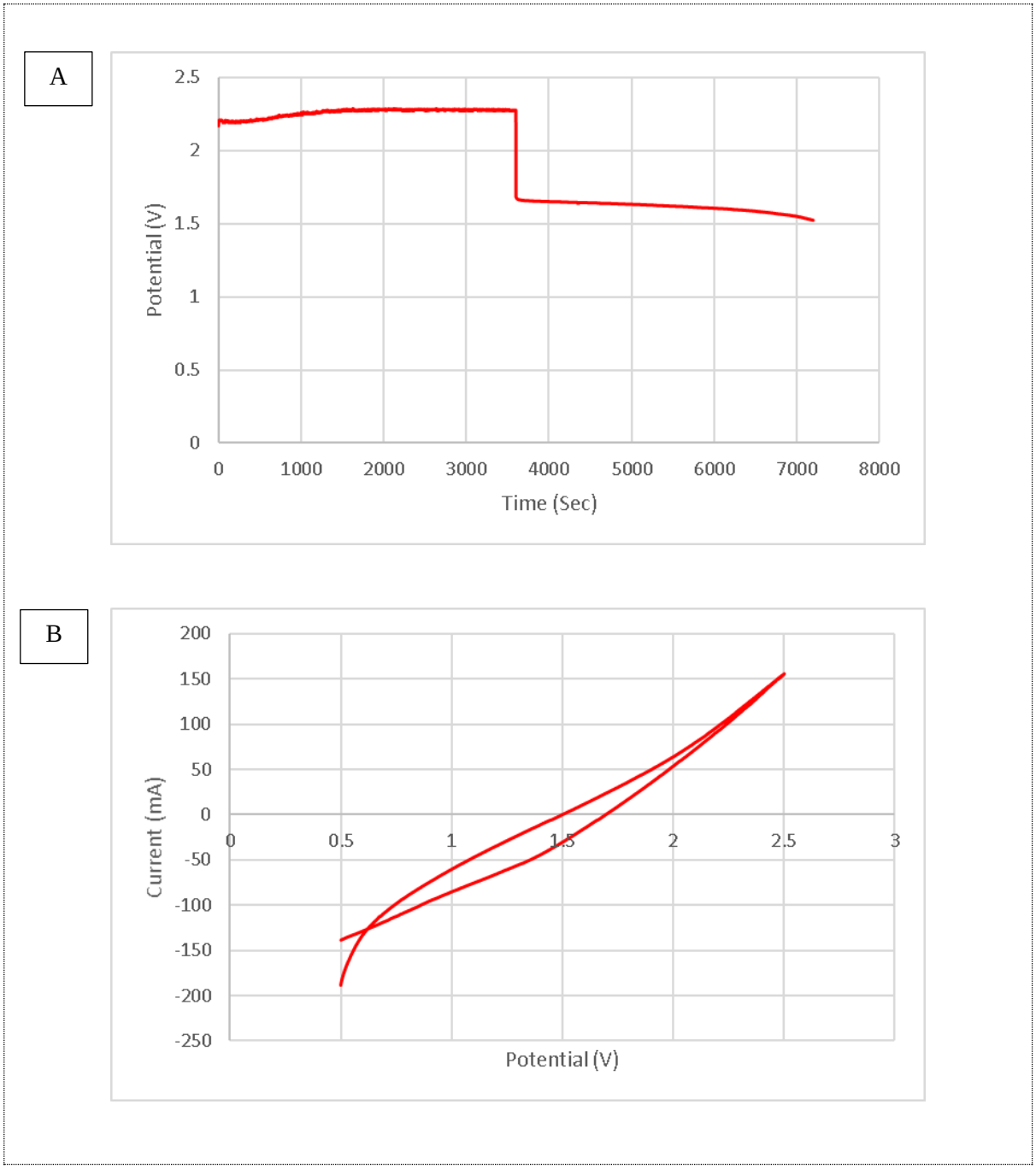

Figure 6. 13: Charge and discharge rate: 3 moles of KBr (535.51 grams), 1 mole of KCl (111.89 grams) of cathode electrolyte solution and 3 moles of ZnBr2 (675 grams), 1 mole of $ZnCl_2$ (205 grams), and 1 mole of KCl (111.826 grams) of anode electrolyte solution at (a) a charge rate and discharge rate of 0.1 amps, and -0.01 amps for 3600 secs and (b) cyclic voltammetry of 1 sweep @ 25mV/sec.

6.4.2 **Analysis and Description - Carbon Feeder Electrodes**

The cell demonstrated a low charge and energy efficiency of (10% and 8.085%), stored 360 coulombs at exactly 3600 seconds, and discharged 36 coulombs within 3600 seconds. The cell voltage was 2.4 volts during charge, and 0.24 watts. hr (0.00024 kilowatt. hr) as the power. The discharge voltage was 1.4 volts and the cell watt for the discharge was 0.014 watt. hr (0.000014kilowatt. hr). Table 6.10 has further presented additional information regarding the cell. The ZnBr2 cell was programmed to charge for 0.1 amps for 3600 seconds and discharge at -0.01 amps for 3600 seconds. In figure 6.13b, the cyclic voltammetry showed 0.15 amps at 2.5 volts. The zinc depleted until 2.5 volts. The results were agreed not to be presented because the cell produced a very high impedance which has affected the result after the charge and discharge experiment at a charge and discharge rate of 0.1 amps and -0.01 amps.

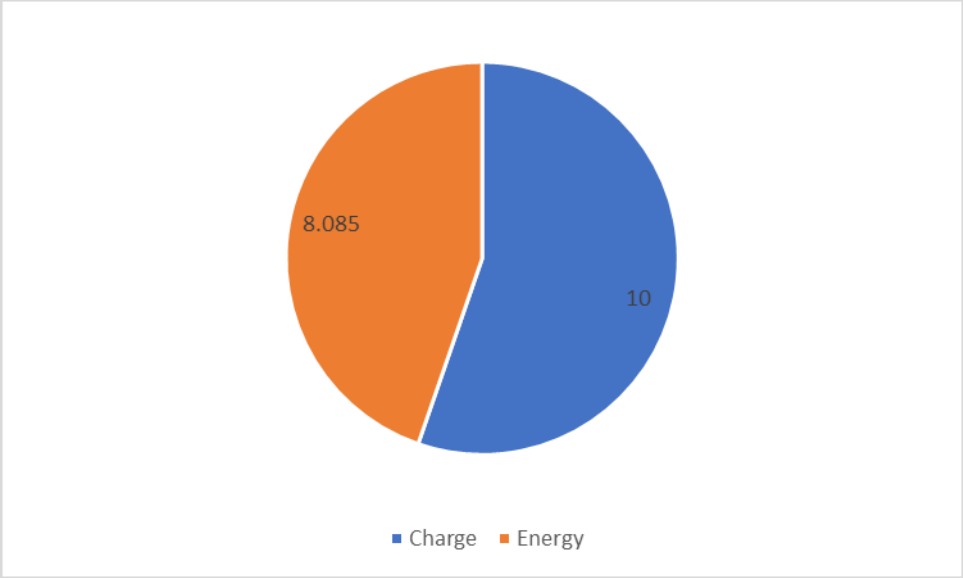

Figure 6. 14: Charge efficiency (blue colour) and energy efficiency (orange colour)

Table 6. 10: Experimental Data's of the investigated two-carbon materials with 3 moles of KBr (535.51 grams), 1 mole of KCl (111.89 grams) as the cathode-side electrolyte and 3 moles of ZnBr2 (675 grams), 1 mole of $ZnCl_2$ (205 grams), and 1 mole of KCl (111.826 grams) as the anode electrolyte solution.

No	BATTERY CELL DATA'S CHARGE AND DISCHARGE	CHARGE STATE			DISCHARGE STATE			RESULTS	
		TIME STEP (SEC)	ENERGY (W. HR)	VOLTAGE (V)	TIME STEP (SEC)	ENERGY (W. HR)	VOLTAGE (V)	CHARGE EFF %	ENERGY EFF %
ONE CHARGE AND DISCHARGE EXPERIMENTS									
1	0.1 A & -0.01 A	3600	0.24	2.4	3600	0.014	1.4	10	8.085

6.4.3 Findings and Conclusions - Carbon Feeder Electrodes

Still, the cell performance was not impressive despite polishing the cathode carbon electrode feeder's surface. However, it might worth it changing the anode and cathode electrolyte and prepare a new electrolyte before passing any charge to the cell again. Furthermore, re-boiling the membrane would be a good idea because this suggestion was previously explored somewhere in a section of this chapter 6.

6.4.4 Conclusions Made on Investigated Carbon Electrodes

The cell established different efficiencies, (charge and energy) apart from the high impedances (EIS). Throughout the experiment, the impedances were observed to be high because of the encountered high resistances within the two cell reactors and based on the incorporated materials. However, the information that was gathered on the cell by using the first feeder electrode materials (carbon versus carbon) are presented in table 6.11. Furthermore, all the existed elements attached to the zinc-graphite were identified through using the scanning of electrons microscopy, SEM.

The reason behind why most of these elements occurred have been explained and detailed in some sections of this chapter 6. The outcome of the investigated second and third sets feeder electrode (carbon versus nickel) and (nickel and titanium) are further presented starting from sections 6.10 of this (chapter 6) in this research work.

However, for the time being, among all the explored experiments in this section, the two carbon materials as the first investigated electrodes at a charge and discharge rate of 0.2 amps and -

0.1 amps has favoured the electrodeposition of zinc, showed the best charge and energy efficiency and produced a good current as highlighted in yellow and presented in table 6.12 on the second row in (Aii).

Table 6. 11: Cell explored experiments: carbon vs carbon charged and with 3 moles of KBr (535.51 grams), 1 mole of KCl (111.89 grams) as the cathode-side electrolyte and 3 moles of ZnBr2 (675 grams), 1 mole of $ZnCl_2$ (205 grams), and 1 mole of KCl (111.826 grams) as the anode electrolyte solution.

Chronopotentiometry Experiments	
Experiments	Investigated First Sets of Electrode Feeder materials Carbon at the Anode-Side and Cathode-Side
1	(a) Charge and discharge experiment at a charge and discharge rate of (0.2 amps and -0.1 amps @ 1500 secs and 1300 secs) (b) (0.1 amps and -0.1 amps @ 3600 secs & 500 secs).
3	(a) Charged rate at (0.1 amps, 0.1 amps, and 0.25 amps) @ 3600 secs (b) Discharged rate (-0.1 amps, -0.1 amps, and -0.25 amps) @ 3600 secs
5	(a) Charge rates of (0.25 amps for 3600 secs, 0.1 amps for 3600 secs, 0.25 amps for 3600 secs, 0.5 amps for 3600 secs and 1 amp for 3600 secs) and (b) Discharged rates at (-0.25 amps for 400 secs, -0.005 amps for 3500 secs, -0.01 amps for 3600 secs, -0.01 amps for 3600 secs and -0.05 amps for 3600 secs).
6	The re-investigated two-carbon electrodes at a charge rate and discharge rate of (a) Charge at 0.1 amps for 3600 secs and discharge at -0.01 amps for 3600 secs.

Table 6. 12: Cell Experimental Data's and evaluation: with 3M of KBr (535.51g), 1M of KCl (111.89g) as the cathode-side electrolyte and 3M of ZnBr2 (675g), 1M of $ZnCl_2$ (205g), and 1M of KCl (111.826g) as the anode electrolyte solution for the first sets of electrode feeder materials-carbon against carbon.

No	BATTERY CELL DATA'S CHARGE AND DISCHARGE	CHARGE STATE			DISCHARGE STATE			RESULTS	
		TIME STEP (SEC)	ENERGY (W. HR)	VOLTAGE (V)	TIME STEP (SEC)	ENERGY (W. HR)	VOLTAGE (V)	CHARGE EFF %	ENERGY EFF %
TWO CHARGE AND DISCHARGE EXPERIMENTS									
Ai	0.1 A & -0.1 A	3600	2	2	500	1.1	1.1	13.8	N/A
Aii	0.2 A & -0.1 A	1500	2.1	2.1	1300	1.3	1.3	43.3	15.63
No	BATTERY CELL DATA'S CHARGE AND DISCHARGE	CHARGE STATE			DISCHARGE STATE			RESULTS	
		TIME STEP (SEC)	ENERGY (W. HR)	VOLTAGE (V)	TIME STEP (SEC)	ENERGY (W. HR)	VOLTAGE (V)	CHARGE EFF %	ENERGY EFF %
THREE CHARGE AND DISCHARGE EXPERIMENT									
10	0.1 A & -0.1 A	3600	0.19	1.9	800	0.7	0.07	22.22	5.90
11	0.1 A & -0.1 A	3500	0.13	1.3	200	0.03	0.3	5.71	2
12	0.25 A & -0.25 A	3600	0.45	1.8	100	0.025	0.5	2.77	1.07
No	BATTERY CELL DATA'S CHARGE AND DISCHARGE	CHARGE STATE			DISCHARGE STATE			RESULTS	
		TIME STEP (SEC)	ENERGY (W. HR)	VOLTAGE (V)	TIME STEP (SEC)	ENERGY (W. HR)	VOLTAGE (V)	CHARGE EFF %	ENERGY EFF %
FIVE CHARGE AND DISCHARGE EXPERIMENTS									
1	0.25 A & -0.25 A	3600	0.475	1.9	400	0.0125	0.5	11.1	5.48
2	0.1 A & -0.005 A	3600	0.15	1.5	3500	0.0035	0.7	4.86	2.94
3	0.25 A & -0.01 A	3600	0.475	1.9	3600	0.01	1	3.88	1.81
4	0.5 A & -0.01 A	3600	1.3	2.6	3600	0.014	1.4	1.94	1.25
5	1 A & -0.05 A	3600	4	4	3600	0.065	1.3	4.86	2.21
No	BATTERY CELL DATA'S CHARGE AND DISCHARGE	CHARGE STATE			DISCHARGE STATE			RESULTS	
		TIME STEP (SEC)	ENERGY (W. HR)	VOLTAGE (V)	TIME STEP (SEC)	ENERGY (W. HR)	VOLTAGE (V)	CHARGE EFF %	ENERGY EFF %
ONE CHARGE AND DISCHARGE EXPERIMENTS									
1	0.1 A & -0.01 A	3600	0.24	2.4	3600	0.014	1.4	10	8.085

The presented bar chart in figure 6.15, has showed all the charge and energy efficiencies after exploring different charge rates and discharge rates by the incorporated carbon-anode and carbon-cathode feeder electrode to the battery cell in chapter 6. However, five-charged rates experimental results and another two-discharged experimental result were not discussed in this thesis and presented on the bar chart since their charge and energy efficiencies cannot be calculated; since these mentioned experiments were only programmed to charge and to discharge.

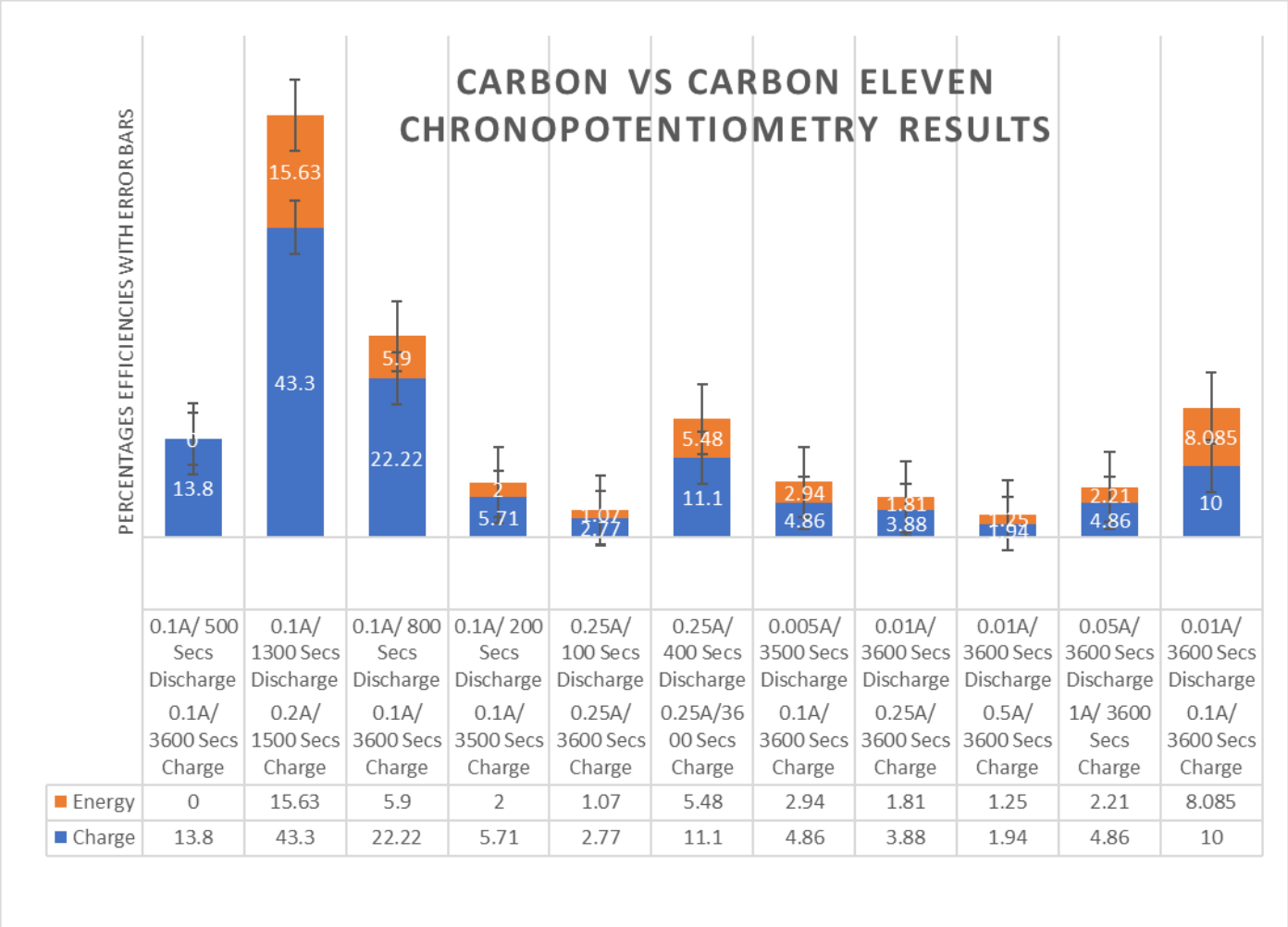

FIGURE 6. 15: THE ELEVENTH CELL CHARGE-(BLUE) AND ENERGY-(PINK) EFFICIENCIES WITH THE TWO-CARBON ELECTRODES (ANODE CURRENT COLLECTOR AND CATHODE CURRENT COLLECTOR.

6.5 Materials and Method – Nickel vs Carbon and Nickel vs Titanium

The cell was programmed to charge and discharge with the 2nd and 3rd set of electrodes (nickel and carbon electrode) and (nickel and titanium electrodes) to know if these materials were excellent conductors of electricity and compared them with the investigated two-carbon 1st feeder electrodes that were first examined. See figure 6.16a and b. Furthermore, and to observe if a zinc-bromine battery cell can be achieved by using these feeder electrodes materials. The potentiostat (1 amps) determines the cell capacity. Different charge rates were explored on the cell up to 1 amps and to -1 amps at different time up to 3600seconds.

The impedance was measured at these charge rates (0.1 amps, 0.4 amps, 0.7 amps, 1 amps) and discharge rates at (-0.1 amps, -0.4 amps, -0.7 amps, -1 amps) and a cyclic voltammetry was performed on the zinc-bromine battery cell at these scan rates: 20 mV/ s, 25 mV/ s, and 50 mV/ s. The measured cyclic voltammetry results were also similar to the previous results. The anode electrolyte contains 3 moles of $ZnBr_2$ (675 grams) Solution, 1 mole of $ZnCl_2$ (205 grams), and 1 mole of KCl (111.826 grams). The cathode electrolyte was made up of 3 moles of KBr (535 grams) and 1 mole of KCl (111.897 grams). The anode electrolyte density was 1.47 g/ cm^{-3} and this density was used to gauge the cathode-electrolyte solution. A constant flow rate of (166.7 cm^3/ min) was maintained throughout the experiment with two-different coupled self-priming centrifugal pump.

6.6 Instrumentations Methods and Operation - Nickel vs Carbon and Nickel vs Titanium

The explored chronopotentiometry measurement were performed by incorporating a (carbon electrode to the cell cathode-side and nickel to the cell anode-side) and (Nickel to the anode-side and titanium to the cathode-side) of the fabricated zinc-bromide cell. Three cyclic voltammetry's of 1 sweep @ 25 mV/ sec were also explored. See Table 6.13 for all the explored chronopotentiometry measurements.

(A) SECOND SET ELECTRODES	
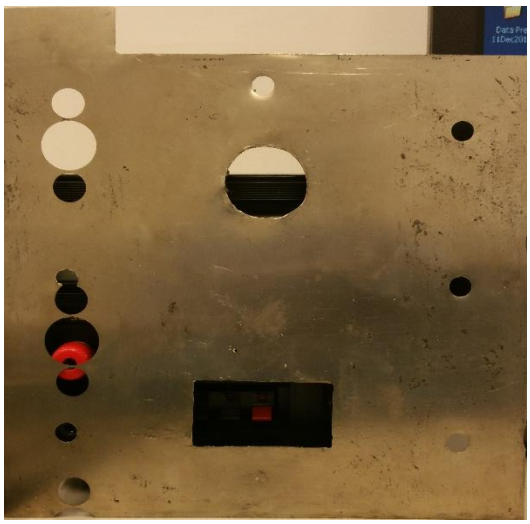 Nickel-Anode	 Carbon-Cathode
(B) THIRD SET ELECTRODES	
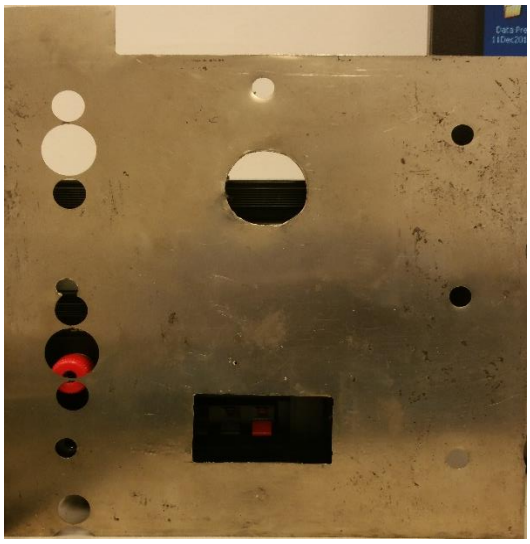 Nickel-Anode	 Titanium-Cathode The titanium electrode feeder incorporated to the cell cathode-side as the third investigated current collector has a specific electrocatalyst coating on it for the evolution and reduction of Bromine (Br_2).

Figure 6. 16: (a) Nickel and carbon electrode feeder material (b) Nickel and titanium electrode feeder material that were incorporated to the cell as the second and third set of electrode feeder materials

Table 6. 13 Chronopotentiometry experimental current values on the investigated carbon and nickel materials and nickel and titanium materials with 3 moles of KBr (535.51 grams), 1 mole of KCl (111.89 grams) as the cathode-side electrolyte and 3 moles of ZnBr2 (675 grams), 1 mole of $ZnCl_2$ (205 grams), and 1 mole of KCl (111.826 grams) as the anode electrolyte solution.

Charge and Discharged Experiments		
Experiments	Nickel & Carbon	Nickel & Titanium
1	Charged and discharged rate (0.1 amps vs -0.01 amps) @ both 3600 secs	Charged @ 0.1 amps for 3600secs
2	Three-cycles of charged rate and discharged rate at 0.1 amps and -0.1 amps @ 3600 secs and 1800 secs	First charged and discharged rate at 0.1 amps for 1800 secs and at -0.1 amps for 900 secs
3	Three -cycles of charged and discharged at (0.1 amps Vs -0.1 amps) @ 3600 secs and 1800 Secs	Charge rate and discharge rate at 0.1 amps for 1800 secs and at -0.1 amps for 900 secs.
4	Three-cycles of charged and discharged at a rate of (0.4 amps and -0.4 amps) for 3600 secs and 1800 secs.	Three cycles of charged and discharged at a rate of (0.1 amps vs -0.1 amps) for 1800 Secs and 900 Secs.
5	Re-examined nickel and carbon materials at (a) charged rate 0.1 amps for 3600 secs and (b) discharged rate -0.1 amps for 1800 secs	Charged and discharge at 0.3 amps for 1800 secs and at -0.3 amps for 900 secs
6		Charge and discharge at a rate of 0.1 amps for 1800 secs and at -0.1 amps for 900 secs

6.7 Description of Results – Nickel vs Carbon and Nickel vs Titanium

The picture in figure 6.17a and b are the cell pictures after polishing the two-electrode materials to remove any contaminated hidden substances and to be more conductive. The old electrolyte solution was also examined on the cell with the first and second sets electrodes (**nickel and carbon**) and (**carbon on both sides**). Additionally, both the new cathode-side and anode-side electrolyte has the same chemical compounds as the old electrolyte solution. The only

difference was the sequestering agent (tetrabutylammonium bromide) that was added to the new cathode-side electrolyte solution instead of a MEP sequestering agent. The cell was programmed to charge and discharge at various amperes and hours. The presented chronopotentiometry results in figure 6.18a (charge and discharge) were achieved through incorporating the carbon and nickel electrode at a charge rate and discharge of 0.1 amps and -0.01 amps for 3600 secs with the two electrolyte images (bromine formation and colourless (zinc) in figure 6.18b and 6.18c. Another two graph results were obtained through using the titanium and nickel electrodes materials but only one of them will be discussed and presented later in section 6.9.2.

The cathode reactor and anode reactor have a rectangular shape with porous inlet and outlet.

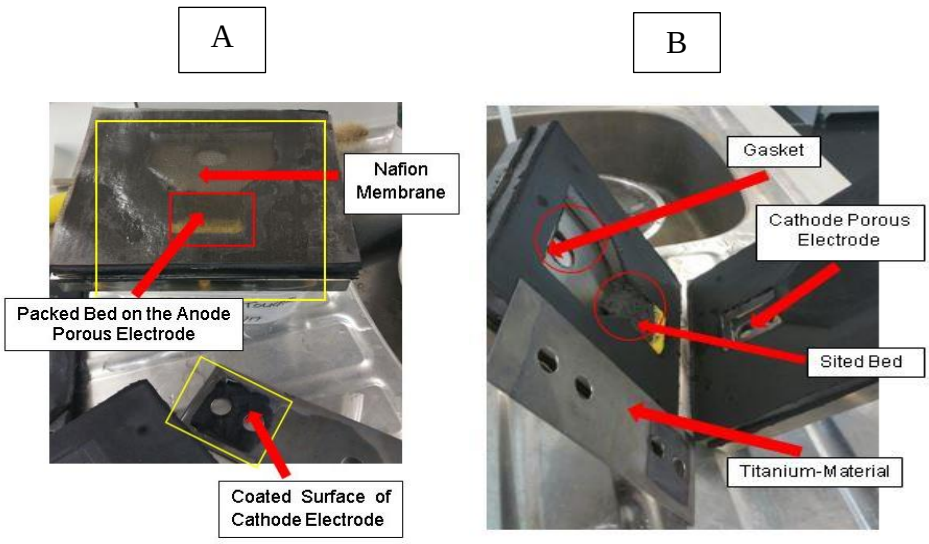

Figure 6. 17: The ZnBr2 Cell Polished Electrode (Nickel), and other Materials

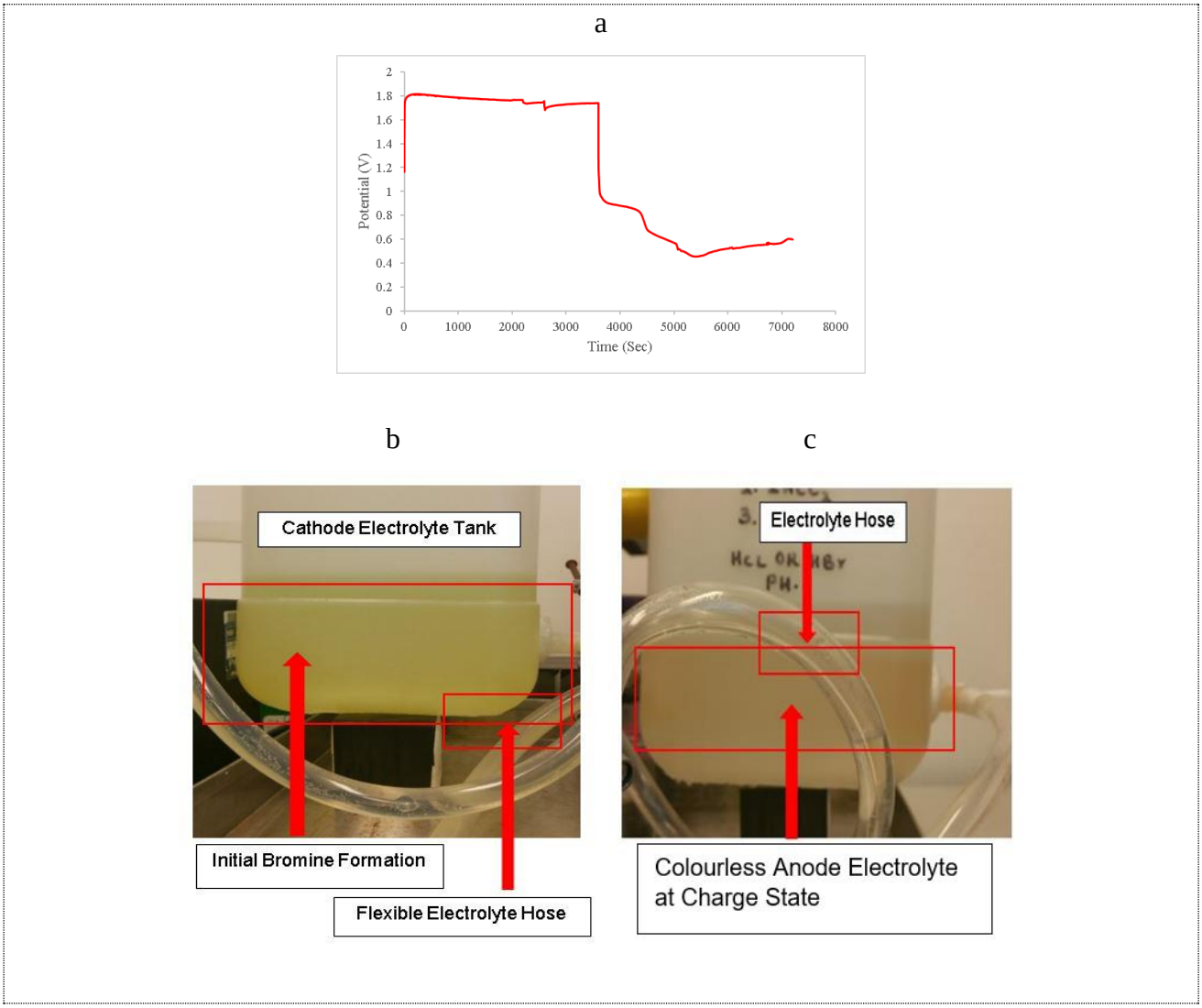

Figure 6. 18: (a) Carbon and Nickel charge and discharge result at a current of 0.1 amps and -0.01 amps for both 3600 secs (b) The formation of Bromine during charge through the two-carbon electrodes and (c) Colourless anode electrolyte thru the two-carbon electrodes.

6.8 Analysis of Results – Nickel vs Carbon

The zinc-bromide cell was programmed to charge and discharge to retrieve some data from the cell and used these data to draw some conclusions statistically. See table 6.14 for the calculated charge and energy efficiencies and table 6.15 for other data's and the 3D pie chart in figure 6.19 that presented the charge and energy efficiencies.

Table 6. 14 of (figure 6.18a) cell evaluation: carbon vs nickel charged and discharged experiment at a charge rate of 0.1 amps and discharge rate of -0.01 amps at both 3600 secs with 3 moles of KBr (535.51 grams), 1 mole of KCl (111.89 grams) as the cathode-side electrolyte and 3 moles of ZnBr2 (675 grams), 1 mole of $ZnCl_2$ (205 grams), and 1 mole of KCl (111.826 grams) as the anode electrolyte solution.

Charged State		
1	Charged Passed During Charging	0.1 amps*3600 secs = 360C
Discharged State		
2	Charged Passed During Discharging	-0.01 amps*3600 secs = -36C
3	Charge Efficiency (CE) $\frac{\text{Charged Recovered (Discharge)}}{\text{Charged Input (Charge)}} * 100\%$	$\frac{36}{360} * 100\% = 10\%$
4	Energy Efficiency (EE) $\frac{\text{Energy Recovered (Discharge)}}{\text{Energy Input (Charge)}} * 100\%$	$\frac{\text{Charge Recovered} * \text{Average Voltage During Discharge}}{\text{Charge Input} * \text{Average Voltage During Charge}} * 100\%$ $\frac{36 * 0.737}{360 * 1.509} * 100\% = 4.88\%$

Table 6. 15: Experimental data of the investigated nickel and carbon materials consisting 3 moles of KBr (535.51 grams), 1 mole of KCl (111.89 grams) as the cathode-side electrolyte and 3 mole of ZnBr2 (675 grams), 1 mole of $ZnCl_2$ (205 grams), and 1 mole of KCl (111.826 grams) as the anode electrolyte solution.

No	BATTERY CELL DATA'S CHARGE AND DISCHARGE	CHARGE STATE			DISCHARGE STATE			RESULTS	
		TIME STEP (SEC)	ENERGY (W. HR)	VOLTAGE (V)	TIME STEP (SEC)	ENERGY (W. HR)	VOLTAGE (V)	CHARGE EFF %	ENERGY EFF %
CHARGE AND DISCHARGE									
1	0.1 A & -0.01 A	3600	0.18	1.8	3600	0.01	1	10	4.88

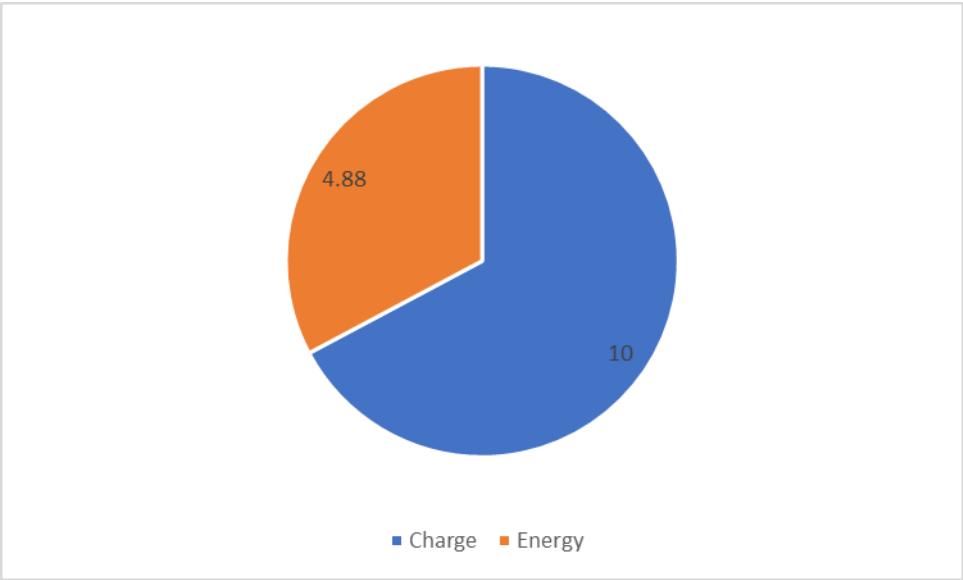

Figure 6. 19: 3D pie chart of (blue colour) charge and (orange colour) energy efficiency at a charge rate and discharge rate of 0.1 amps and -0.01 amps for 3600 secs with 3 moles of KBr (535.51 grams), 1 mole of KCl (111.89 grams) as the cathode-side electrolyte and 3 moles of ZnBr2 (675 grams), 1 mole of $ZnCl_2$ (205 grams), and 1 mole of KCl (111.826 grams) as the anode electrolyte solution.

6.9 Findings and Comments on Feeder Electrodes

6.9.1 Carbon Vs Nickel (0.1 Amps, -0.01 Amps for 3600 secs)

At a charge rate and discharge rate of (0.1 amps and -0.01 amps) for 3600 secs as shown in figure 6.18a, the cell energy was 0.18 watt.hr (0. 00018 kilowatt.hr) and 0.01 watt.hr (0. 00001 kilowatt.hr). The voltage was 1.8 volts during charge and 1 volt during discharge. At exactly 3500 secs, the charged passed during discharged was 35 coulombs and 360 coulombs during the charge passed. The final discharge voltage was 0.456 volt. The cyclic voltammetry, CV showed a minimum voltage of 0.5 volt and a maximum voltage of 2.5 volts.

Significant amount of zinc (Zn species) was reduced within the zinc-electrode (oxidation) due to the recorded negative currents. This resulted to a longer reduction reaction. The resistances on the cell was too high due to some incorporated materials within the cell; but better than the cyclic voltammetry (CV) result from first investigated electrode feeder (Carbon-Anode Vs Carbon-Cathode) that was not better enough to be presented. Most of the cyclic voltammetry (CV's) results demonstrated the same high current.

With the two investigated feeder electrodes (nickel and carbon), a zinc-bromide cell was achieved. By re-boiling the Nafion membrane up to three hours on a hotplate has made it to be more conductive and cleaning the cell with distilled water to remove any hidden contamination. Despite that the cell efficiency was very low during this experiment, it was still better compared to the previous experiments where it wasn't possible to achieve a zinc bromide cell through the first investigated electrode feeder (carbon-anode vs carbon-cathode).

The performances of the cell had improved due to some changed materials: like the brass fittings that were initially interrupting the cell performance by depositing brown residues (copper) to the cathode-side electrolyte. Normally, from onset and due to the electrolyte composition, a small amount of hydrogen gas concentration was expected which could have contaminated the cell and greatly contributed to the cell efficiencies that had previously decreased apart from the current efficiencies in this chapter 6. The cell was less resistive here and better than the experimental work of the first investigated electrode feeder (carbon-anode vs carbon-cathode).

6.9.2 **Titanium Vs Nickel (0.1 Amps for 3600 secs)**

The charged passed during charge was 360 coulombs at 3600 secs. the cell was not programmed to discharge. the cell energy was 0.6205 watts. hr (0.000625 kilowatt. hr) at a very detrimental voltage of 6.205 volts (See figure 6.20). Regarding the nickel and titanium material, the cell did not charge as expected by using the new cathode electrolyte solution containing (tetrabutylammonium bromide). The cell was programmed to charge at a current of 0.1 amps for 1800 seconds and to discharged at -0.1 amps for 900 seconds. The chronopotentiometry measurement on the cell demonstrated a voltage of 6 volts by charging it at 100 milliamperes (mA) for 3600 secs with the nickel and titanium material as the third sets of feeder electrodes.

These materials (nickel and titanium) initially demonstrated a high voltage of 6.3 volts and showed a discharged curve that was not programmed and expected. Furthermore, by encountering such problem on the cell has instigated re-introducing briefly the first and second set of electrodes feeder materials due to the cell negative response after charging it with the third sets of electrode feeder materials (nickel and titanium) that demonstrated a high voltage

and again to identify the root of the problem before considering again the third sets feeder electrodes materials (nickel and titanium materials).

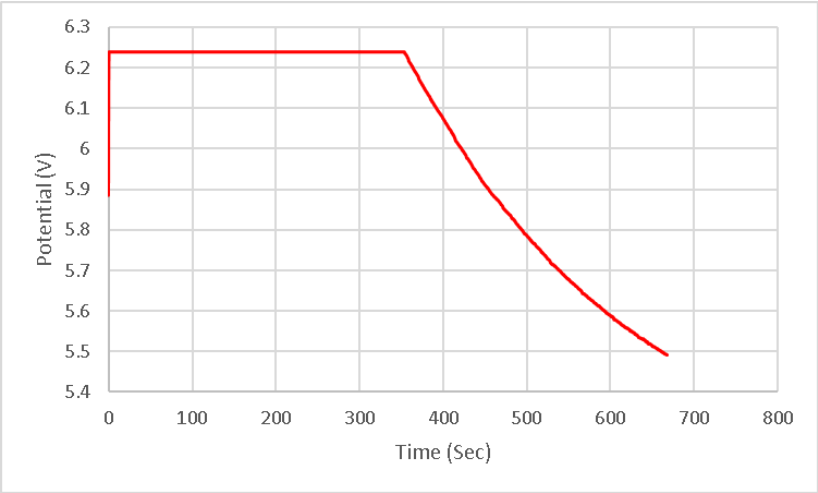

Figure 6. 20: Charge result of the nickel and titanium electrode at 0.1 amps for 3600 secs

6.10 Conclusions

6.10.1 Carbon Vs Nickel (0.1 Amps, -0.01 Amps for 3600 secs)

High resistance in between 95 ohms and 30 ohms was initially measured on the cell with the carbon and nickel material compared to the measured 8.3 ohms with the first investigated carbon materials; which might have happened due to some of the incorporated materials that were resisting the flow of current. This measurement was explored with the carbon and nickel feeder electrode. Furthermore, and later, it was believed that the odd measurement electrochemical impedance spectroscopy (EIS) might have happened because of the investigated new sequestering agent (tetrabutylammonium bromide). From the anode-zinc electrode, such high resistance wasn't expected likewise from the cathode-side electrode. Later, the two feeder electrodes, carbon and nickel were both conductive after cleaning the cell. By incorporating these two-materials, a zinc-bromide cell was achieved. The anode-electrolyte was able to turn colourless and the cathode-electrolyte was yellow in colour. Under normal condition, the observed colourless could have come from the dissociation of zinc salt and its transformed to a zinc ion to form $Zn(OH)_2$.

However, the electrolyte solution contained salt and was expected in excess during charge. Furthermore, the cell demonstrated a low energy efficiency of 4.88 percent. Between 63 percent to 75 percent was the expected energy efficiency for a typical redox battery cell. By programming the cell to charge and discharge at a current (0.1 amps and -0.01 amps) was to stay within the capacity of the potentiostat (1 amps) and to prevent the cell electrode materials from damaging.

6.10.2 Titanium Vs Nickel (0.1 Amps for 3600 secs)

By polishing the cell electrodes surface and cleaning the cell with distilled water before re-introducing them separately to the cell with the three-electrolyte solution has assisted during the experiment to identify the new sequestering agent (tetrabutylammonium bromide) as the cause of the problem. Furthermore, this observation has enabled to confirmed that the nickel and titanium are both conductive and in good condition.

6.11 Effects of Different Electrodes

6.11.1 Description of Results – Carbon vs Nickel Feeder Electrode and Titanium Vs Nickel Feeder Electrode

The result presented in figure 6.21a, were for the explored 3-cycles of charge and discharge at different amperes conditions. By incorporating the carbon and nickel electrode to the anode and cathode-side of the cell, charges passed during the 1st cycle was at (0.1 amps / 3900 secs and -0.1 amps / 2000 secs), 2nd cycle (0.1 amps/ 3000 secs and 0.1 amps / 1600 secs) and during 3rd cycle (0.1 amps for 2400 secs before the cell was interrupted from discharging due to leakage). In figure 6.21b, the charge passed by incorporating the titanium and nickel electrode to the anode-side and cathode-side of the cell were at 0.1 amps and -0.1 amps for (1800 secs and 900 secs), (1810 secs and 900 secs) and (1705 secs and 900 secs).

These charges were for the 1st, 2nd, and 3rd cycles of charge and discharge. The presented cyclic voltammetry in figure 6.21c was at a sweep rate of 25mV/sec for 1 cycle through the incorporated nickel and titanium electrode.

The resistance was also planned to be measured at 0.1 amps and -0.1 amps after the three cycles of charge and discharge to observe if the cause of the high resistance was not just from the incorporated materials; in connection to the observed chronopotentiometry voltage (6.3 volts) that was previously explored in figure 6.20 of sub-section 6.9.2 that demonstrated an odd charge and discharge result.

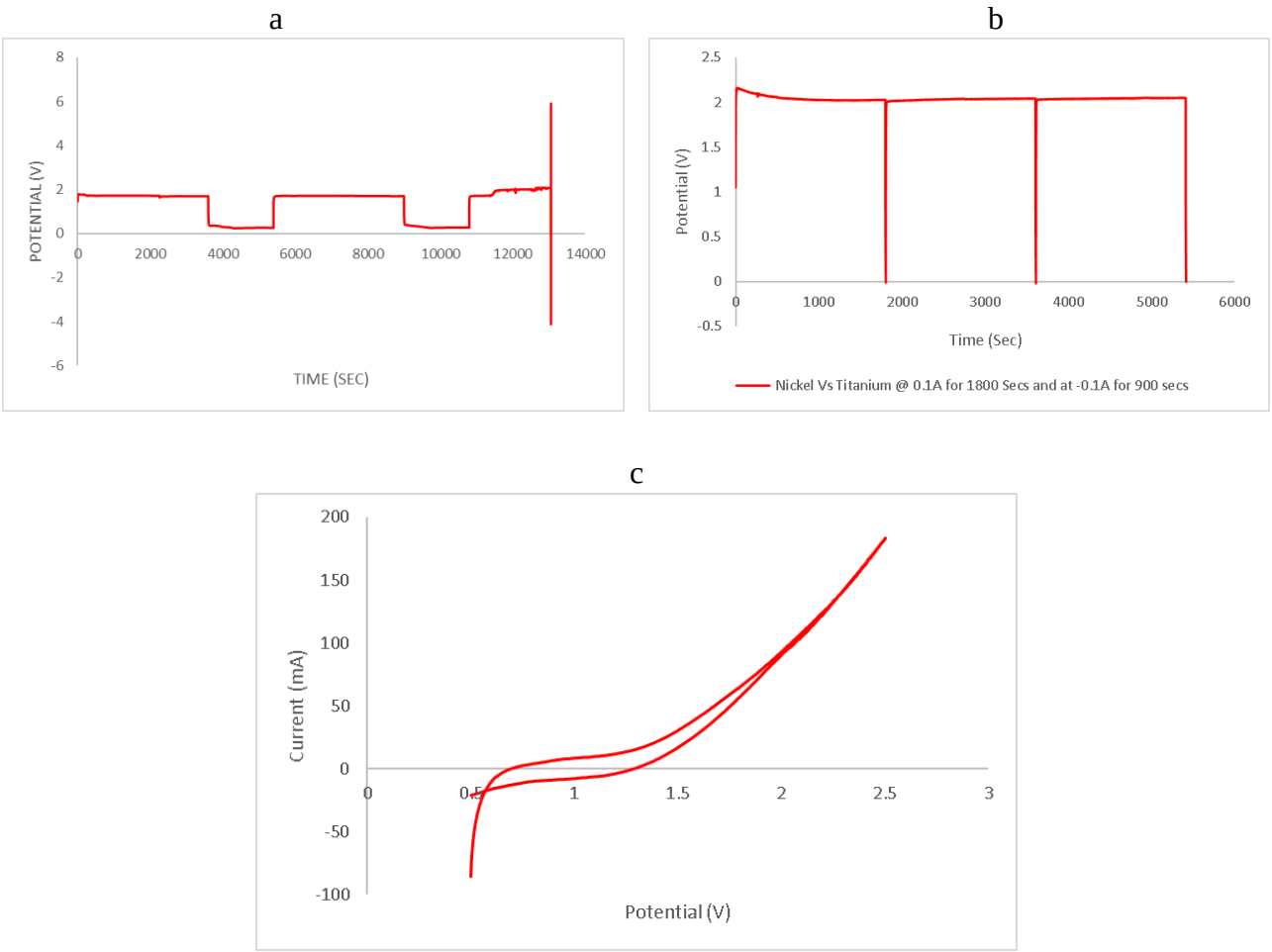

Figure 6. 21: (a) 3-cycles of charged and discharge at 0.1 amps and -0.1 amps for (3900 secs and 2000 secs), (3000 secs and 1600 secs), (2400 secs for only to charge) through the carbon vs nickel (b) 3-cycles of charged and discharge at 0.1 amps and -0.1 amps for (1800 secs and 900 secs), (1810 secs and 900 secs), and (1705 secs and 900 secs) through using the nickel vs titanium with 3 moles of KBr (535.51 grams), 1 mole of KCl (111.89 grams) as the cathode-side electrolyte and 3 moles of ZnBr2 (675 grams), 1 mole of $ZnCl_2$ (205 grams), and 1 mole of KCl (111.826 grams) as the anode electrolyte solution (c) cyclic voltammetry at 25 mV/ s taken after investigating the nickel and titanium electrode.

6.12 Description of Analysis for Carbon vs Nickel Feeder Electrode and Titanium vs Nickel Feeder Electrode

1. Charged passed in the table within section 9.1.1 (see the appendix chapter 9) were explored using the nickel and the carbon feeder electrode at: 0.1 amps and at -0.01 amps for (3900 secs and 2000 secs), (3000 secs and 1600 secs), and (2400 secs for only to charge). See table 6.16 and figure 6.22 for further detailed information in this chapter 6.
2. The information that was gathered from the investigated nickel and titanium feeder electrode are also presented in table of section 9.1.2 (See the Appendix in chapter 9), and table 6.17 and figure 6.23 for the bar chart presenting the energy and charge efficiencies. These electrodes nickel and titanium were examined on the cell at 0.1 amps and -0.01 amps at (1800 secs and 900 secs), (1810 secs and 900 secs), and (1705 secs and 900 secs)

Table 6. 16: Charge and energy efficiency of the investigated nickel and carbon materials of the 3-cycles of charge and discharge with 3 moles of KBr (535.51 grams), 1 mole of KCl (111.89 grams) as the cathode-side electrolyte and 3 moles of ZnBr2 (675 grams), 1 mole of $ZnCl_2$ (205 grams), and 1 mole of KCl (111.826 grams) as the anode electrolyte solution.

No	BATTERY CELL DATA'S CHARGE AND DISCHARGE	CHARGE STATE			DISCHARGE STATE			RESULTS	
		TIME STEP (SEC)	ENERGY (W. HR)	VOLTAGE (V)	TIME STEP (SEC)	ENERGY (W. HR)	VOLTAGE (V)	CHARGE EFF %	ENERGY EFF %
THREE CYCLES OF CHARGE AND DISCHARGE									
1	0.1 A & -0.1 A	3900	0.2	2	2000	0.1	1	51.3	12.77
2	0.1 A & -0.1 A	3000	0.2	2	1600	0.1	1	53.3	13.29
3	0.1 A & -0.1 A	2400	0.2	2	NONE	NONE	NONE	NONE	NONE

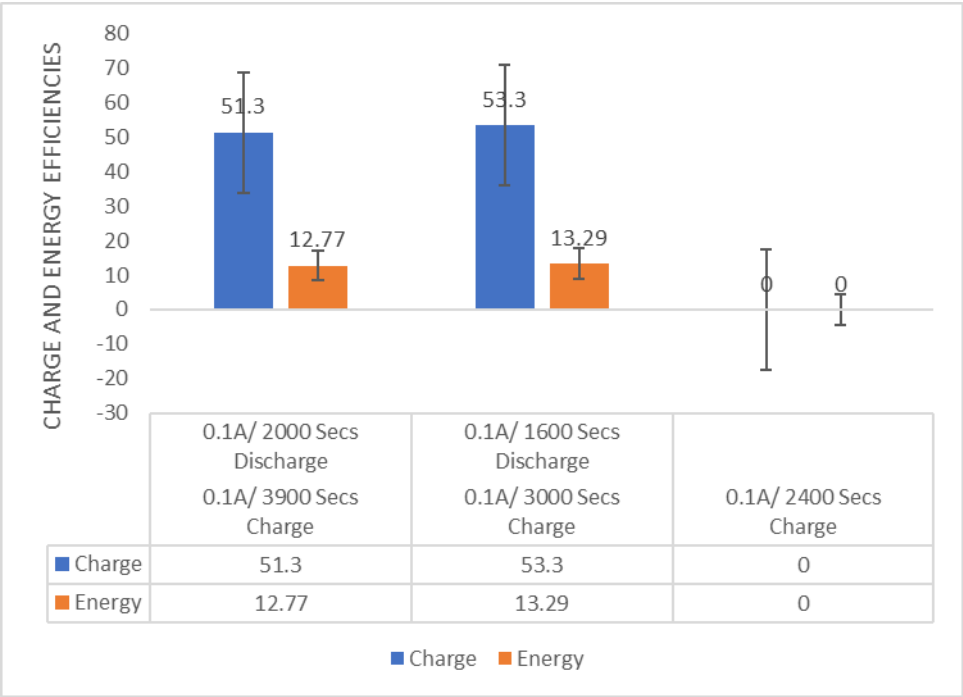

Figure 6. 22: Bar chart of charge-(blue) and energy-(pink) efficiency at a current of 0.1 amps and -0.1 amps at (1). (3900 secs and 2000 secs), (2). (3000 secs and 1600 secs), (3). (2400 secs for only to charge) with 3 moles of KBr (535.51 grams), 1 mole of KCl (111.89 grams) as the cathode-side electrolyte and 3 moles of $ZnBr_2$ (675 grams), 1 mole of $ZnCl_2$ (205 grams), and 1 mole of KCl (111.826 grams) as the anode electrolyte solution.

Charge efficiency, CE 51.3% and 53.3% are 62% and 63% conclusive based on a data similarity of 38% and 39%. These energy efficiency, EE 12.77% and 13.29% data are 91% and 92% accurate.

Table 6. 17 Charge and energy efficiency of the investigated nickel and titanium electrode of the 3-cycles of charge and discharge with 3 moles of KBr (535.51 grams), 1 mole of KCl (111.89 grams) as the cathode-side electrolyte and 3 moles of ZnBr2 (675 grams), 1 mole of $ZnCl_2$ (205 grams), and 1 mole of KCl (111.826 grams) as the anode electrolyte solution.

No	BATTERY CELL DATA'S CHARGE AND DISCHARGE	CHARGE STATE			DISCHARGE STATE			RESULTS	
		TIME STEP (SEC)	ENERGY (W. HR)	VOLTAGE (V)	TIME STEP (SEC)	ENERGY (W. HR)	VOLTAGE (V)	CHARGE EFF %	ENERGY EFF %
THREE CYCLES OF CHARGE AND DISCHARGE									

1	0.1 A & -0.1 A	1800	0.2	2	900	0.1	1	50	24.39
2	0.1 A & -0.1 A	1810	0.2	2	900	0.1	1	49.72	24.25
3	0.1 A & -0.1 A	1705	0.2	2	900	NONE	NONE	52.78	25.75

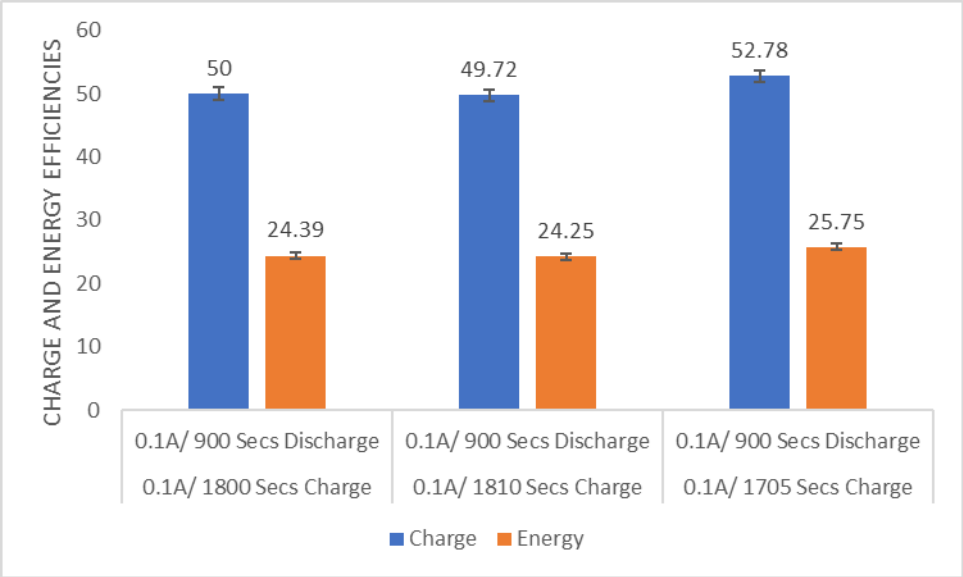

Figure 6. 23: Bar chart of charge-(blue) and energy-(pink) efficiency (1). (1800 secs and 900 secs), (2). (1810 secs and 900 secs) and (3). (1705 secs and 900 secs) at 0.1 amps and -0.1 amps secs with 3 moles of KBr (535.51 grams), 1 mole of KCl (111.89 grams) as the cathode-side electrolyte and 3 moles of ZnBr2 (675 grams), 1 mole of $ZnCl_2$ (205 grams), and 1 moles of KCl (111.826 grams) as the anode electrolyte solution.

The 50% CE and 49.72% CE were both 99% accurate. The similarity between these two CE's was 1%. The 52.78% is 100% conclusive. The 24.39% EE has data similarity of 3% with the 24.25% EE and 5% data similarity with the 25.75% EE. The 25.75% EE is 100% accurate.

6.13 Findings and Comments

6.13.1 Carbon Vs Nickel at 0.1 Amps and -0.1 Amps: (Cycle-1) (3900 secs and 2000 secs), (Cycle-2). (3000 secs and 1600 secs), (Cycle-3). (2400 secs for only to charge)

On the result graph (figure 6.21a), the cell voltage was 2 volts throughout the 3 cycles of charge and discharge but diminished to 1.04 volts as it begins to discharge immediately after the ohmic drop. The cell was interrupted from completing the third cycles to charge completely and discharged further due to some unexpected leakage. A total current of 1280 amps was stored

by the fabricated zinc-bromine battery cell for the whole three cycles and including when it was interrupted.

Through the incorporated carbon and nickel electrode, the charged passed during the 1st cycle was exactly 390 coulombs instead of 360 coulombs without any loss during 2 volts at 0. 2 watt.hr (0. 0002 kilowatt.hr). This happened due to an overflowing of electrons. For the charged passed during discharge at 1 volt, 200 coulombs were the charged passed for the discharged instead of 180 coulombs in between 3900 secs to 5900 secs. The cell watt was 0. 1 watt.hr (0. 0001kilowatt.hr). The replaced charged passed during the 2nd cycle was 300 coulombs as a substitute to 360 coulombs.

The cell voltage was 2 volts during charged and 1 volt at discharged. In between (9000 secs) and (10600 secs), the calculated charge was 160 coulombs and 20 coulombs as the lost charge. The cell was interrupted during the 3rd cycle due to some leakages and lost 120 coulombs out of the passed charged. The expected charge passed was 1440 coulombs for the 3-cycles of charges and discharges. The differences between the lost charge and stored charges was 160 coulombs; which was due to the abrupt leakages outside the cell. The cell experienced leakages due to the plastic threaded bars and fittings bolts that cannot continue to resist the weight of the cell and the enclosed components.

All the previous experiments were successful without any leakage since the plastic threaded bars and bolts were still able to tolerate the weight of the cell's components. The new cell configuration with the G-clamps were attached to prevent any further occurrence before carrying out any other electrochemical measurements on the cell. Furthermore, it was assumed that the battery cell might be leaking due to the chemical reactions within the cell; which might could happen because of the over-reaction process. Which might have led to the production of hydrogen gas within the cell. Though, leaks may also be happening on battery cells during discharge or gradual self-discharge.

6.13.2 Nickel Vs Titanium at 0.1 Amps and -0.1 Amps: (Cycle-1) (1800 secs and 900 secs), (Cycle-2). (1810 secs and 900 secs), (Cycle-3). (1705 secs and 900 secs)

The result in Figure 6.21b has showed that the old electrolyte performed outstandingly. But the cell could only charge at 100 mA, 200 mA, and 300 mA for 1800 seconds when it was expected

to charge up to 1000 mA. The cell also discharged at these current rates (-100 mA), (-200 mA), and (-300 mA) for 900 seconds and elevated from 1.3 volts to 2.2 volts. However, the new electrolyte solution and its reaction within the cell could not make the cell to charge. No leakage was also encountered on the cell during the experiment.

The cell abnormal performance was due to the added sequestering agent (Tetrabutylammonium bromide) in the cathode-side electrolyte solution. The old cathode-electrolyte with the new anode-electrolyte was also compatible to charge the cell at 100 mA for 1800 seconds and discharge at a current rate of -100 mA for 900 seconds before stopping. No peaks were observed for the nickel and titanium electrode feeder (See the cyclic voltammetry result in figure 6.21c). In between 1800 secs to 1890 secs, the charged passed during discharge was 90 coulombs during the first cycle and 180 coulombs at 1800 secs for the charge.

The cell voltage at the first cycle during charge was 2.2 volts at 0.22 watt. hr. (0.00022 kilowatt. hr). For the second cycle of charge and discharged, the charged voltage was also 2.2 volts and the charged passed was 181 coulombs in between 1890 secs to 3700 secs. Furthermore, the charge passed during discharge was 90 coulombs in between 3700 secs to 3790 secs. The charged passed during the third cycle of charge and discharge was 170.5 coulombs in between 3790 secs to 5495 secs instead of 180 coulombs; but for the discharged, 90 coulombs were the charged passed in between (5495 secs) and (5585 secs) at approximately 90 secs.

6.14 Conclusions – Carbon vs Nickel and Nickel vs Titanium

6.14.1 Material Performance (Carbon Vs Nickel)

Because the cell leaks, it was difficult to have the completed electrochemical measurement of the 3rd chronopotentiometry measurement and the energy efficiency for the carbon and nickel electrode material. Furthermore, these issues have affected the performance of the electrochemical cell and has encouraged it to function in a very strange way.

Additionally, since the first and second chronopotentiometry measurement were completed before the problem developed, the first and second experiments can be recommended as a good battery cell because of the presented outcome of the cell efficiencies in table 6.16. Furthermore,

these observed efficiencies can still be improved for a healthier result if the cell can be prevented from losing energy.

6.14.2 **Material Performance (Nickel Vs Titanium)**

Each cycle (1. 2 and 3) has showed that the cell was fully discharged up to (0 volt) during the 3-cycles of charge and discharge. Furthermore, cycle 1 and cycle 2 has a charge and efficiency of 50% and 52.78% compare to chronopotentiometry-3 that has a charge efficiency of 49.72%. (See the table in section 9.1.2 within the Appendix in chapter 9). Both Cycle-1 and cycle-2 charge efficiencies were similar except that the charge efficiency in cycle-1 was a bit higher than the charge efficiency in cycle-2 by 15%. Cycle-3 further has an energy efficiency that was also a bit higher than that of cycle-1 and cycle-2 efficiencies by 0.86% and 1%.

The battery cell did not lose any energy but gained additional energy (2%) at the end of the third cycle after charging it at a current of 0.1 amps and -0.1 amps secs of different cycles. (cycle-1) for (1800 secs and 900 secs), (cycle-2) for (1810 secs and 900 secs) and (cycle-3) for (1705 secs and 900 secs). Therefore, the three cycles of charge and discharge has good efficiencies and can be recommended as good zinc-bromine batteries cells.

The efficiency of battery cell during the third cycles has a good redox reaction with overflowing electrons compare to the other cycles. On the presented bar chart, the charge and energy efficiency of the 3rd cycles by using the carbon and nickel electrode feeder were not included since the cell was interrupted due to leakage. Therefore, just the 1st and 2nd cycle was presented. However, both the titanium versus nickel electrode during the lifetime cycles for the 1st, 2nd and 3rd cycles were completed and presented. See the bar chart in figure 6.23.

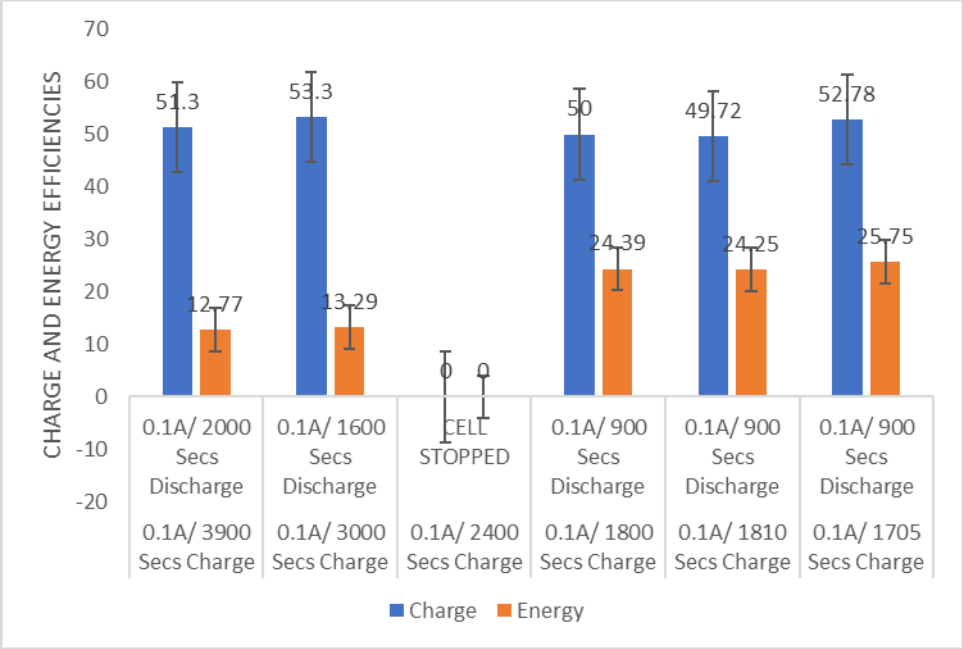

Figure 6. 24: Overall bar chart of the charge-(blue) and energy-(pink) efficiency at 0.1 amps and -0.1 amps using the carbon and nickel electrode (1), for (3900 secs and 2000 secs), and (2), for (3000 secs and 1600 secs), and with the nickel and titanium electrode (3), for (1800 secs and 900 secs), (4), for (1810 secs and 900 secs) and (5), for (1705 secs and 900 secs) with 3 moles of KBr (535.51 grams), 1 moles of KCl (111.89 grams) as the cathode-side electrolyte and 3 moles of $ZnBr_2$ (675 grams), 1 mole of $ZnCl_2$ (205 grams), and 1 mole of KCl (111.826 grams) as the anode electrolyte solution.

The presented bar in figure 6.24, showed that the 51.3%, 53.3%, 50%, 49.72% and 52.78% CE were 100% conclusive but shared collectively some significant portion of data by overlapping with each other. The shared similarities percentages were 19%, 20%, and 18%; meaning that the collected data can only be trusted up to 80% and 82%. For the energy efficiency, most of the data were not 100% accurate since they overlapped each other. For instances, the 12.77% EE has 11.1% similarity with other (88.9% conclusive), 13.29% EE is 91% conclusive (9% similarity), and 90% conclusive for the 24.39%, 24.25% and 25.75% EE.

6.15 Enhancement of Cycle Performances and Conditions.

By exploring further charges through carrying out another three cycles of charge and discharge, it was observed that the battery cell had performed better (charge and energy efficiency) by charging it at these current 0.1 amps and -0.1 amps at (1), for (4000 secs and 1900 secs), and (2), for (3100 secs and 2000 secs), and (3) for (3000 secs and 1900 secs) with the carbon and nickel

electrode. The condition of the cell through the incorporated nickel and titanium electrode were not as good compare to the carbon and nickel electrode despite that the cell was programmed to charge at a better current rate, (0.3 amps & -0.3 amps) at (1), for (1800 secs and 200 secs), and (2), for (1700 secs and 200 secs), and (3) for (1900 secs and 200 secs) with nickel and titanium electrode.

The established results were odd since titanium materials are conductive on their own; even apart from the surface of the coated and used titanium feeder electrode in this research work. High electrochemical impedances spectroscopy (EIS) was observed despite that these measurements were carried out constantly on the cell after the explored charge and discharge cycles at these current conditions (0.1 amps, 0.4 amps, 0.7 amps, 1 amps) and at (-0.1 amps, -0.4 amps, -0.7 amps, -1 amps) and all performed cyclic voltammetry at these sweep conditions: 20 mV/s, 25 mV/s, and 50 mV/s.

The cyclic voltammetry (cv) shape that was explored showed high resistance throughout the explored measurements. This has instigated not choosing to present the results since the experimented electrochemical impedances spectroscopy (EIS) results were not meaningful. Further details regarding these results may be provided in the next section or not.

6.16 Description of Results

6.16.1 Carbon Vs Nickel at a Current of 0.1 Amps and -0.1 Amps: (Cycle-1) for (4000 secs and 1900 secs), and (2), for (3100 secs and 2000 secs), and (3) for (3000 secs and 1900 secs).

During charge, the cell power was 0.18 watt.hr (0.00018 kilowatt. hr.) and 0.04 watt.hr (0.00004 kilowatt. hr) during discharge. (See figure 6.25a), (table 6.18) and (figure 6.26). The charged passed increased by 40 coulombs during the 1st cycle of charge in between 3600 secs to 4000 secs and during discharged by an additional 10 coulombs in between 4000 secs to 5900 secs. The cell demonstrated 1.8 volts during charge and 0.4 volts during discharged throughout the charged passed for the charge and discharge.

Less charge passed was recovered back (310 coulombs) in between (5900 secs to 9000 secs) during the 2nd cycle instead of having 360 coulombs. The lost charge passed was 50 coulombs. But during the discharge, 200 coulombs in between (900 secs to 1100 secs) was the charge retrieved when 180 coulombs was expected. Charged passed during the 3rd cycle was 300

coulombs in between 1100 secs to 14200 secs instead of 360 coulombs. The lost charged was 60 coulombs during charge and gained 10 coulombs in between 143000 secs to 16200 secs from the charge passed. But the expected coulombs from the charge passed was 180 coulombs.

The battery cell was able to complete the three cycles of charges and discharges at the exact programmed time and at a current of (0.1 amps, -0.1 amps). The current measured through the cyclic voltammetry at a scan rate of 25 mV/sec demonstrated a current of 0.27 amps. The measured resistance was high at 0.1 amps and -0.1 amps after the three cycles of charge and discharge, but the result was ignored and not appropriate for presentation.

The frequency was in between 50 hertz. No leakage was observed compared other explored measurements. The resistance was measured after charge at a rate of 0.1 amps and at -0.1 amps for the discharge to avoid high resistances due to the previous values. However, the impedance resistance was still high at the measured current (0.1 amps and -0.1 amps). The carbon and nickel current collectors showed a large reduction process during the forward scan and a peak during the reverse scan from a voltage of 2.4 volts to 1.6 volts. The result was similar to the previous ones and not therefore presented.

6.16.2 Nickel Vs Titanium at a Current of 0.3 Amps and -0.3 Amps: (Cycle-1) for (1800 secs and 200 secs), and (2), for (1700 secs and 200 secs), and (3) for (1900 secs and 200 secs)

In figure 6.25b, at 1800 secs, 540C was the charged passed during the 1st cycle. During discharged, in between 1800 secs and 2000 secs, 60C was recovered from the charged passed out of the expected 270 coulombs. The lost charged passed was 210 coulombs and 150 coulombs during discharge as the differences between the recovered charge passed and the lost charge. In between 200 secs to 3800 secs, 540 coulombs were the charged passed during the 2nd cycle.

During discharged, and in between 3800 secs and 4000 secs, 60 coulombs was recovered from the charged passed out of the expected 270 coulombs. (See also table 6.19, and figure 6.27). The lost charged passed was 210 coulombs and 150 coulombs during discharge as the differences between the recovered charge passed and the lost charge. During the 3rd cycle, 60 coulombs was the charge passed in between 5800 secs to 6000 secs and 210 coulombs lost

from the charge passed and a difference of 150 coulombs as the differences between the charged passed during discharge and charge lost during discharge.

a

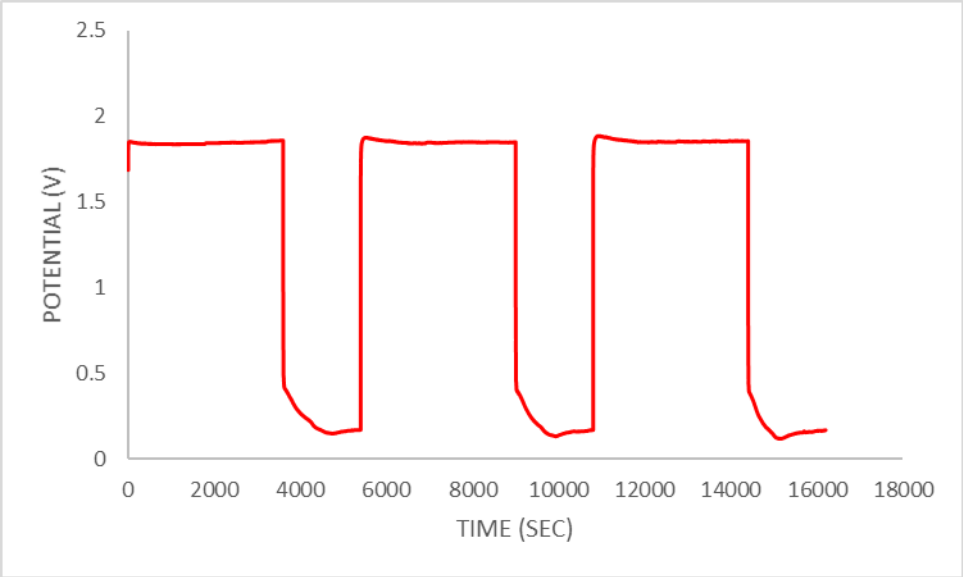

b

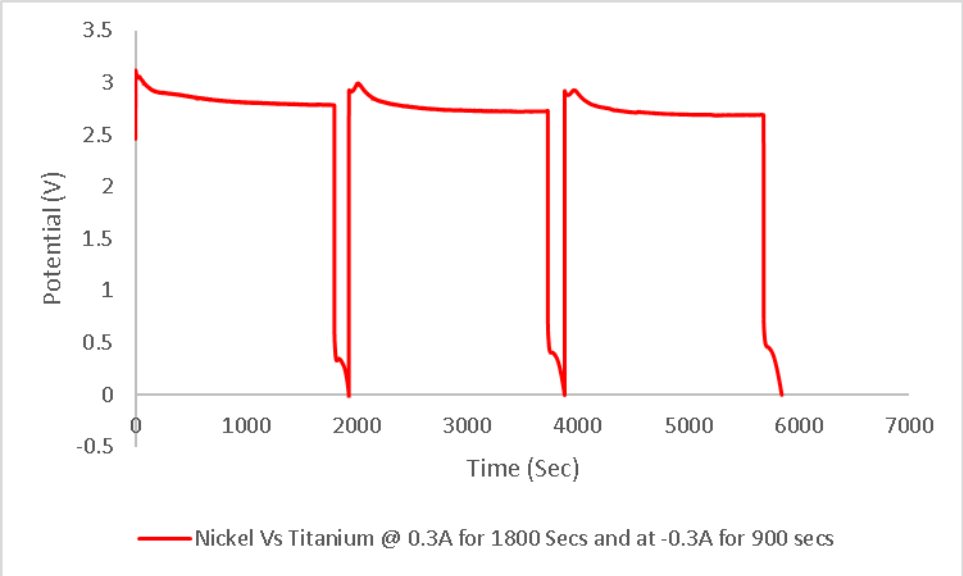

Figure 6. 25: (a) Carbon and nickel at 0.1 amps and -0.1 amps for (1), for (4000 secs and 1900 secs), and (2), for (3100 secs and 2000 secs), and (3) for (3000 secs and 1900 secs). (c) nickel and titanium at 0.3 amps and -0.3 amps for (1800 secs and 200 secs), and (2), for (1700 secs and 200 secs), and (3) for (1900 secs and 200 secs).

6.17 Description of Analysis

In table 6.18 and table 6.19, further details were provided regarding the incorporated carbon and nickel electrode. See the calculated charge and energy efficiencies in section 9.12 of chapter 9 (appendix). The calculated efficiencies for the carbon/ nickel and nickel/ titanium electrodes are further provided in table 6.18, table 6.19, figure 6.26 and in figure 6.27.

Table 6. 18: Experimental data of the charge and energy efficiency for the investigated nickel and carbon material with 3 moles of KBr (535.51 grams), 1 mole of KCl (111.89 grams) as the cathode-side electrolyte and 3 moles of $ZnBr_2$ (675 grams), 1 mole of $ZnCl_2$ (205 grams), and 1 mole of KCl (111.826 grams) as the anode electrolyte solution.

No	BATTERY CELL DATA'S CHARGE AND DISCHARGE	CHARGE STATE			DISCHARGE STATE			RESULTS	
		TIME STEP (SEC)	ENERGY (W. HR)	VOLTAGE (V)	TIME STEP (SEC)	ENERGY (W. HR)	VOLTAGE (V)	CHARGE EFF %	ENERGY EFF %
THREE CYCLES OF CHARGE AND DISCHARGE									
1	0.1 A & -0.1 A	4000	0.18	1.8	1900	0.04	0.4	47.5	13.97
2	0.1 A & -0.1 A	3100	0.18	1.8	2000	0.04	0.4	64.5	18.9
3	0.1 A & -0.1 A	3000	0.18	1.8	1900	0.04	0.4	63.3	18.6

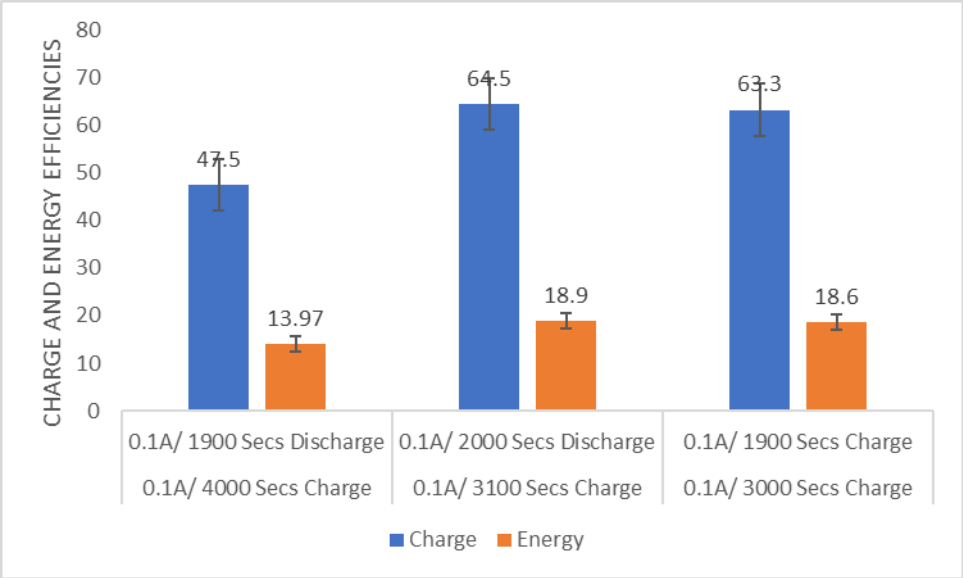

Figure 6. 26: Bar chart of charge-(blue) and energy-(pink) efficiency at 0.1 amps and -0.1 amps for (1), for (4000 secs and 1900 secs), and (2), for (3100 secs and 2000 secs), and (3) for (3000 secs and 1900 secs). with 3 moles of KBr (535.51 grams), 1 mole of KCl (111.89 grams) as the cathode-side electrolyte

and 3 moles of $ZnBr_2$ (675 grams), 1 mole of $ZnCl_2$ (205 grams), and 1 mole of KCl (111.826 grams) as the anode electrolyte solution.

Data from the 64.5% CE, 63.3% CE and 47.5% CE were not 100% different. They have 10% similarity. (Therefore, data were 90% to 91% conclusive). The 13.9% EE shared 4.9% data similarity with the 18.9% EE and 18.6% EE. Therefore, 95.1% of the data were true. The 18.9% EE and 18.6% EE has 0.2% similarity (99.8% conclusive).

Table 6. 19: Experimental data such as the charge and energy efficiency of the investigated nickel and titanium materials with 3 moles of KBr (535.51 grams), 1 mole of KCl (111.89 grams) as the cathode-side electrolyte and 3 moles of $ZnBr_2$ (675 grams), 1 mole of $ZnCl_2$ (205 grams), and 1 mole of KCl (111.826 grams) as the anode electrolyte solution.

No	BATTERY CELL DATA'S CHARGE AND DISCHARGE	CHARGE STATE			DISCHARGE STATE			RESULTS	
		TIME STEP (SEC)	ENERGY (W. HR)	VOLTAGE (V)	TIME STEP (SEC)	ENERGY (W. HR)	VOLTAGE (V)	CHARGE EFF %	ENERGY EFF %
THREE CYCLES OF CHARGE AND DISCHARGE									
1	0.3 A & -0.3 A	1800	0.9	3	200	0.12	0.4	11.11	2.26
2	0.3 A & -0.3 A	1700	0.9	3	200	0.12	0.4	11.76	2.39
3	0.3 A & -0.3 A	1900	0.9	3	200	0.12	0.4	11.11	2.26

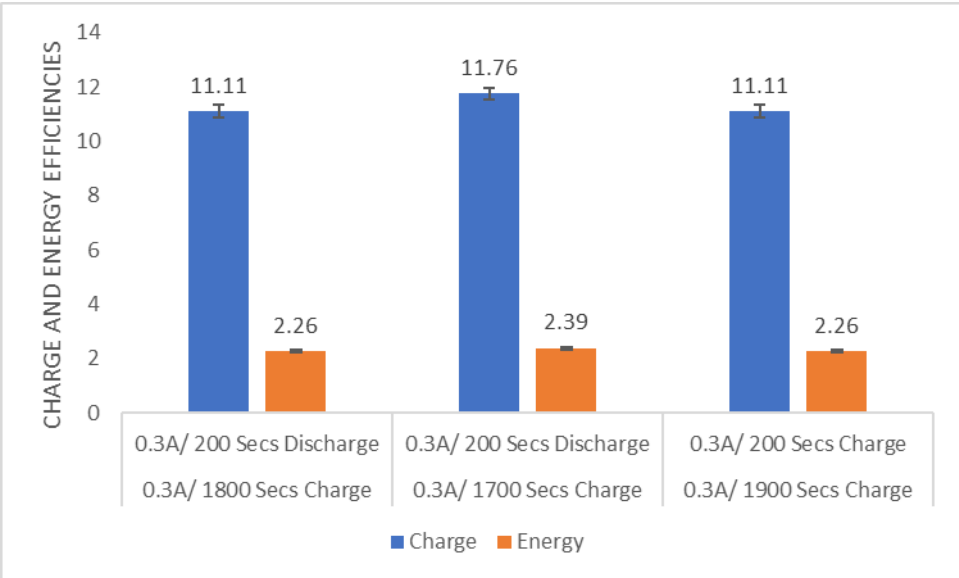

Figure 6. 27: Bar chart of charge-(blue) and energy-(pink) efficiency at a current of 0.3 amps and -0.3 amps for (1800 secs and 200 secs), and (2), for (1700 secs and 200 secs), and (3) for (1900 secs and 200 secs) with 3 moles of KBr (535.51 grams), 1 mole of KCl (111.89 grams) as the cathode-side

electrolyte and 3 mole of ZnBr2 (675 grams), 1 mole of $ZnCl_2$ (205 grams), and 1 mole of KCl (111.826 grams) as the anode electrolyte solution.

The CE of 11.76% is the highest and shared no data with other CE's. Therefore it's 100% conclusive. Both the two CE's (11.1%) also shared a data similarity of 1.6% (98.4% conclusive). Furthermore, the two EE, 2.26% bar overlapped each other. These efficiencies shared significant amount of data excluding an EE of 2.39% which was the highest.

6.18 Findings and Comments

6.18.1 Carbon Vs Nickel at 0.1 Amps and -0.1 Amps: (Cycle-1) for (4000 secs and 1900 secs), and (2), for (3100 secs and 2000 secs), and (3) for (3000 secs and 1900 secs)

The cell demonstrated a good redox reaction and good energy efficiencies through the compared values presented on the bar chart in figure 6.26. The anode-pump demonstrated a bit of electrochemical noise which could be the plating of the zinc.

6.18.2 Nickel vs Titanium at 0.3 Amps and -0.3 Amps: (Cycle-1) for (1800 secs and 200 secs), and (2), for (1700 secs and 200 secs), and (3) for (1900 secs and 200 secs)

The battery efficiency through the 3-cycles of charges and discharges were poor but the cell voltage was 3.01 volts during these processes and 0.4 volts during discharge. This has indicated a good flow of electrons (redox reaction). However, based on the cell efficiency (11.11%), the membrane was assumed not to be conductive and the pH level might be very low. High resistance was observed on the cell by using the nickel and titanium material which has resulted to a lower energy efficiency and for the cell to produce lower current compare to what was expected. The cell potential differences were 1.5 volts throughout the charge and discharge process. Further information regarding the cell are produced in table 6.19 regarding the efficiency of the cell.

6.19 Conclusions on Results

6.19.1 Carbon vs Nickel at 0.1 Amps and -0.1 Amps: (Cycle-1) for (4000 secs and 1900 secs), and (2), for (3100 secs and 2000 secs), and (3) for (3000 secs and 1900 secs)

Result demonstrated from the explored three chronopotentiometry cycles were good results that can be recommended as a better zinc-bromine battery cell due to their efficiencies. See figure 6.28 for the presented results on the bar chart. The cell efficiency from the first experiment was 47.5%. The cell also stored and discharge more current during the 1st cycle excluding the 2nd and 3rd cycle of charge and discharge. The second experiment demonstrated an efficiency of 64.4%. The cell efficiency was 63.3% for the 3rd cycle. The second charge and discharge had the best performances, followed by the third experiment and lastly the 1st chronopotentiometry experiment. See figure 6.28.

6.19.2 Nickel vs Titanium at 0.3 Amps and -0.3 Amps: (Cycle-1) for (1800 secs and 200 secs), and (2), for (1700 secs and 200 secs), and (3) for (1900 secs and 200 secs)

None of the energy efficiencies for the three cycles of charge and discharge were presentable and will not make the cell to be recommended as an efficient zinc-bromine battery cell. See figure 6.28 from results 4 to 6 (Charge and energy). This is because of the efficiency for the first charge and discharged that had demonstrated a value of 11.1% with the second cycle and third cycle that also demonstrated (11.1%) efficiency.

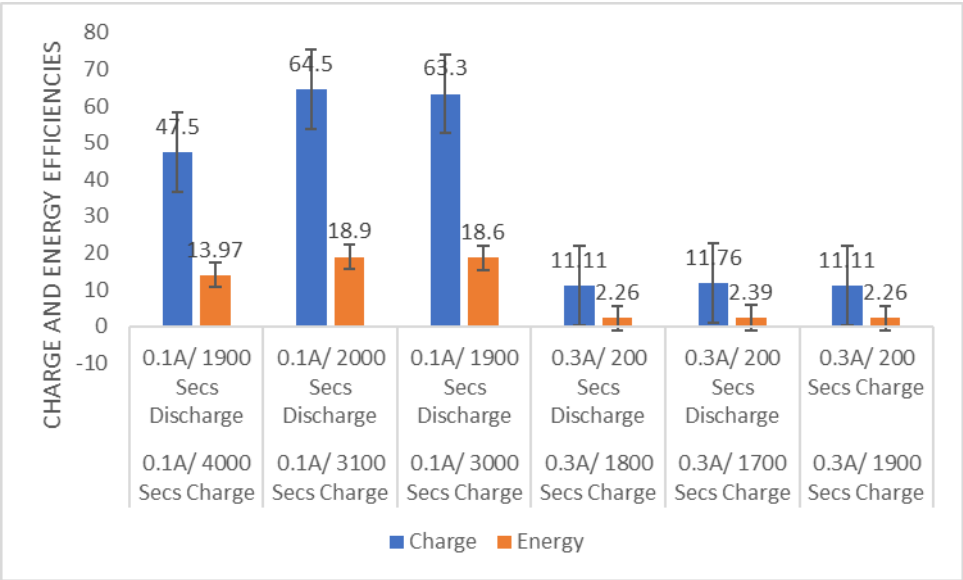

Figure 6. 28: Overall bar chart of the charge-(blue) and energy-(pink) efficiency at 0.1 amps and -0.1 amps: (1) for (4000 secs and 1900 secs), and (2), for (3100 secs and 2000 secs), and (3) for (3000 secs and 1900 secs) with the c and nickel electrode and nickel vs titanium at a 0.3 amps and -0.3 amps: (4) for (1800 secs and 200 secs), and (5), for (1700 secs and 200 secs), and (6) for (1900 secs and 200 secs)

As jointly presented in figure 6.28, not all the collected data used to process the charge efficiencies, CE and energy efficiencies, EE were 100% conclusive due to the overlapping of bars within the chart. This has identified some shared significant similarities of data used to worked out calculated efficiencies. See figure 6.26 and figure 6.27 for elucidation. Only the 11.76% CE from the presented bar chart in figure 6.27 was 100% different and true.

6.20 Encountered Problems (Non-Conductive Materials and Causes)

6.20.1 Description of Result

With the carbon and nickel feeder electrode, the charged passed at a current of 0.4 amps and -0.4 amps for (3900 secs and 1100 secs), and (2), for (3700 secs and 1300 secs), and (3) for (3700 secs and 1200 secs) was to complete a three cycles of charge and discharge. (See figure 6.29a). The cell later encountered some internal problem at 0.7 amps for 3600 seconds and at -0.7 amps for 1800 seconds as displayed through the chronopotentiometry plot. The cyclic voltammetry was measured at a scan rate of 25 mV/sec for one sweep set of conditions that was employed but not presented.

The resistance was measured at 0.1 amps and -0.1 amps after the three cycles of charge and discharge. The electrochemical impedance spectroscopy, (EIS) was not presented due to the encountered high resistance. The cathode electrolyte solution consists of 3 moles of KBr (535.51 grams), and 1 mole of KCl (111.89 grams). The anode electrolyte solution consists of 3 moles of ZnBr2 (675 grams), 1 mole of $ZnCl_2$ (205 grams), and 1 mole of KCl (111.826 grams). The cell was also interrupted during another three cycles of charges and discharges at 0.1 amps and at -0.1 amps for cycle-1 for (3600 secs, 500 secs), and cycle-2 for (1200 secs) before stopping the battery cell to charge further with the carbon and nickel electrode.

The result in figure 6.29b was also achieved through the incorporated nickel and titanium electrode at a current range of 0.1 amps at -0.1 amps for cycle-1 (1800 secs and 200 secs), cycle-2 (1900 secs and 100 secs) and cycle-3 (2000 secs and 300 secs) and another the cyclic

voltammetry plot not presented at a scan rate of 25mV/sec for one sweep set of conditions. The cause of the problem was the sequestering agent (tetrabutylammonium bromide) that was added to the new cathode-side electrolyte solution instead of a MEP sequestering agent.

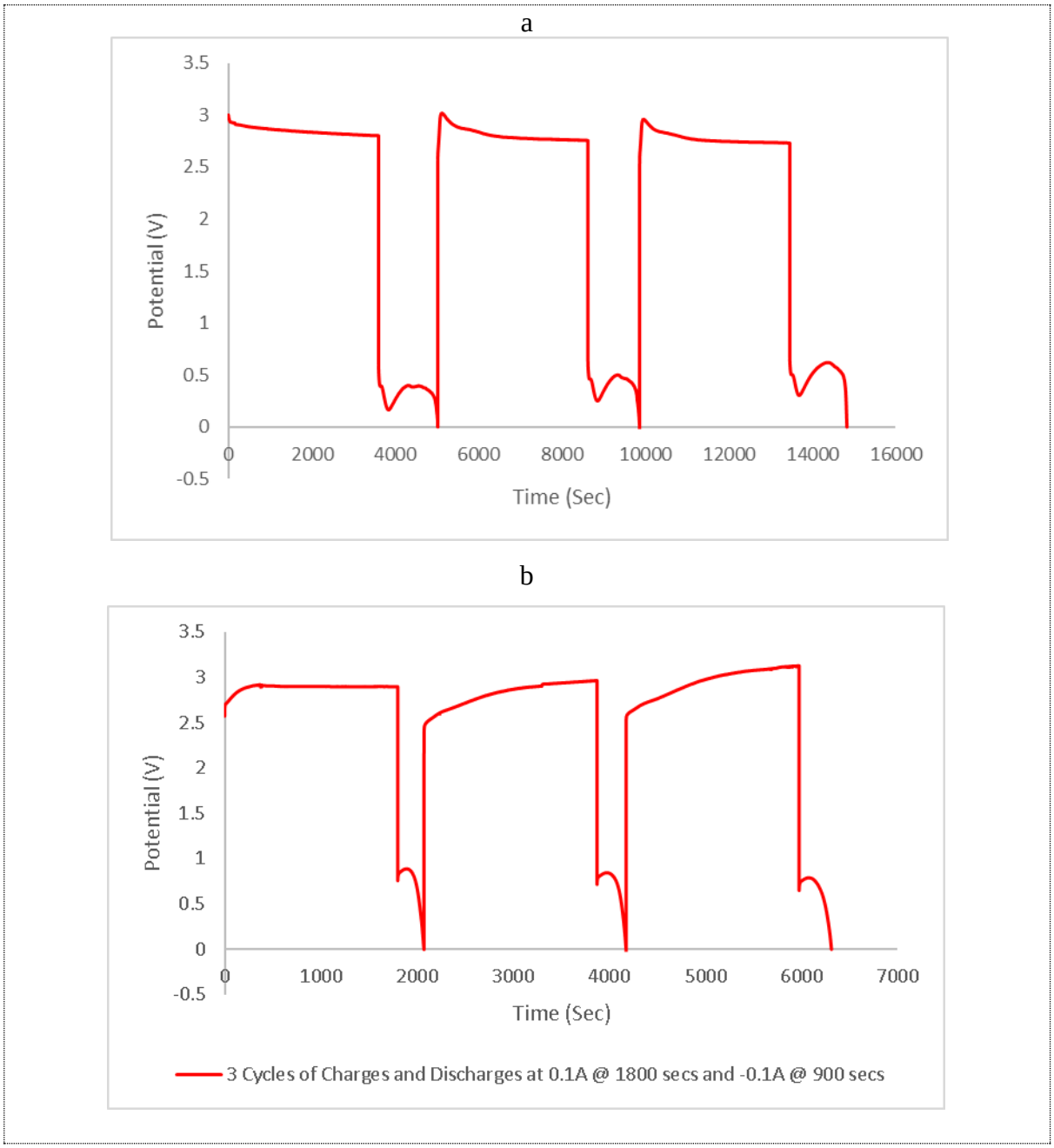

Figure 6. 29: (a) Cell chronopotentiometry plots at 0.4 amps and -0.4 amps cycle-1 (3900 secs and 1100 secs), and (cycle-2) for (3700 secs and 1300 secs), and (cycle-3) for (3700 secs and 1200 secs) with 3 moles of KBr (535.51 grams), 1 mole of KCl (111.89 grams) as the cathode electrolyte solution and 3 moles of $ZnBr_2$ (675 grams), 1 mole of $ZnCl_2$ (205 grams), and 1 mole of KCl (111.826 grams) as the anode electrolyte solution. (b) titanium and nickel electrode at a current range of 0.1 amps and -0.1 amps for cycle-1 (1800 secs and 200 secs), cycle-2 (1900 secs and 100 secs) and cycle-3 (2000 secs

and 300 secs) for three cycles of charge and discharge with 3 moles of KBr (535.51 grams), 1 mole of KCl (111.89 grams) as the cathode electrolyte solution and 3 moles of ZnBr2 (675 grams), 1 mole of $ZnCl_2$ (205 grams), and 1 mole of KCl (111.826 grams) as the anode electrolyte solution.

6.21 Description of Analysis

6.21.1 Carbon Vs Nickel Feeder Electrode and Titanium

The disclosed table in 6.20 were the programmed charge amperes and explored calculations on the cell before it was possible to collect some data from the cell and used them statistically to generate the bar chart in figure 6.30, the presented table in 6.21 and the doughnut pie chart in figure 6.31. Further results from the nickel and titanium feeder electrode are also showed in table 6.22 and in figure 6.32.

Table 6. 20: Cell efficiencies of the investigated nickel and carbon materials with 3 moles of KBr (535.51 grams), 1 mole of KCl (111.89 grams) as the cathode-side electrolyte and 3 moles of $ZnBr_2$ (675 grams), 1 mole of $ZnCl_2$ (205 grams), and 1 mole of KCl (111.826 grams) as the anode electrolyte solution.

No	BATTERY CELL DATA'S CHARGE AND DISCHARGE	CHARGE STATE			DISCHARGE STATE			RESULTS	
		TIME STEP (SEC)	ENERGY (W. HR)	VOLTAGE (V)	TIME STEP (SEC)	ENERGY (W. HR)	VOLTAGE (V)	CHARGE EFF %	ENERGY EFF %
THREE CYCLES OF CHARGE AND DISCHARGE									
1	0.4 A & -0.4 A	3900	1.2	3	1100	0.16	-0.4	28.20	9.54
2	0.4 A & -0.4 A	3700	1.2	3	1300	0.2	-0.5	35.1	11.88
3	0.4 A & -0.4 A	3700	1.2	3	1200	0.24	-0.6	32.4	11.27

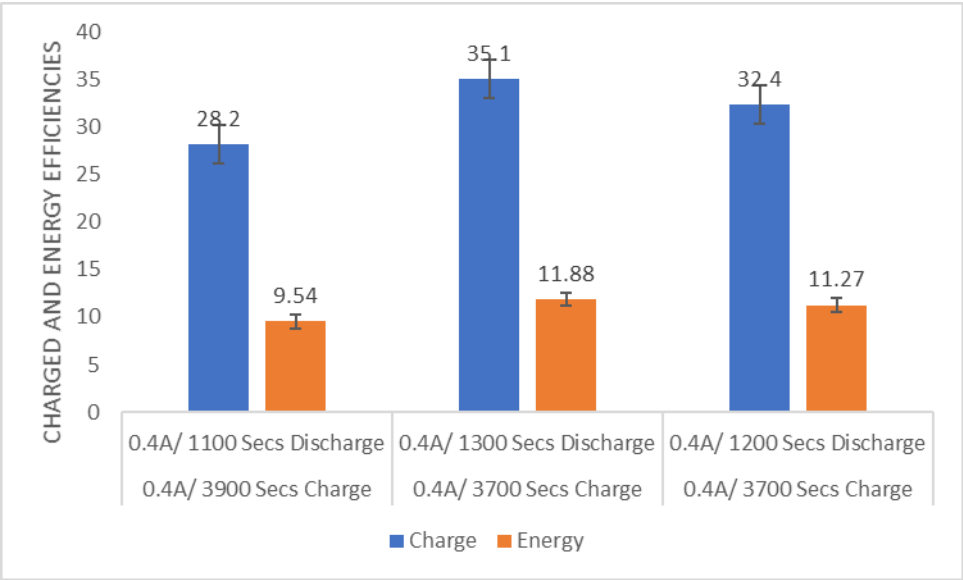

Figure 6. 30: Bar chart of (charge-blue-1) and (energy-pink-2) efficiency with the carbon and nickel electrode at a charge rate and discharge rate of (a) 0.4 amps and -0.4 amps for cycle-1, (3900 secs and 1100 secs), and (cycle-2), for (3700 secs and 1300 secs), and (cycle-3) for (3700 secs and 1200 secs) with 3 moles of KBr (535.51 grams), 1M of KCl (111.89 grams) as the cathode-side electrolyte and 3 moles of $ZnBr_2$ (675 grams), 1 mole of $ZnCl_2$ (205 grams), and 1 mole of KCl (111.826 grams) as the anode electrolyte solution.

The 35.1% CE data was 100% true. None of the data is related to the other CE's. However, the 28.2% CE and 32.1% CE were inconclusive. The 28.2% CE and 32.4% CE were only 95% conclusive. The 9.54% EE and 11.27% EE also shared significant portion of data with the 11.88% EE by 1% out of 100%. Therefore, both not 100% conclusive except the 11.88% EE.

Table 6. 21: Cell efficiencies of the investigated carbon and nickel materials with 3 moles of KBr (535.51 grams), 1 moles of KCl (111.89 grams) as the cathode-side electrolyte and 3 moles of ZnBr2 (675g), 1 moles of $ZnCl_2$ (205 grams), and 1 moles of KCl (111.826 grams) as the anode electrolyte solution.

No	BATTERY CELL DATA'S CHARGE AND DISCHARGE	CHARGE STATE			DISCHARGE STATE			RESULTS	
		TIME STEP (SEC)	ENERGY (W. HR)	VOLTAGE (V)	TIME STEP (SEC)	ENERGY (W. HR)	VOLTAGE (V)	CHARGE EFF %	ENERGY EFF %
THREE CYCLES OF CHARGE AND DISCHARGE									
1	0.1 A & -0.1 A	3600	0.23	2.3	500	0.11	-1.1	13.9	6.25
3	CELL INTERRUPTED DUE TO LEAKAGES								

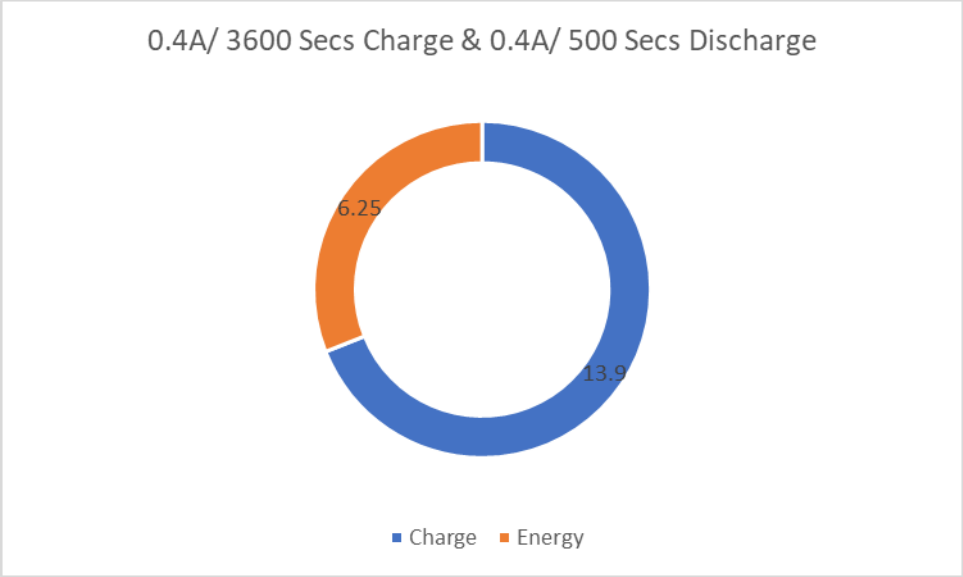

Figure 6. 31: Doughnut pie chart of (charge-blue-1) and (energy-pink-2) efficiency with the carbon and nickel electrode at a charge rate of (a) 0.1 amps and -0.1 amps for cycle-1: (3600 secs and 500 secs) and cycle-2 (1200 secs) with 3 moles of KBr (535.51 grams), 1 mole of KCl (111.89 grams) as the cathode-side electrolyte and 3 moles of ZnBr2 (675 grams), 1 mole of $ZnCl_2$ (205 grams), and 1 mole of KCl (111.826 grams) as the anode electrolyte solutions.

Table 6. 22: Cell efficiencies of the investigated nickel and titanium materials with 3 moles of KBr (535.51 grams), 1 mole of KCl (111.89 grams) as the cathode-side electrolyte and 3 moles of $ZnBr_2$ (675 grams), 1 mole of $ZnCl_2$ (205 grams), and 1 mole of KCl (111.826 grams) as the anode electrolyte solution.

No	BATTERY CELL DATA'S CHARGE AND DISCHARGE	CHARGE STATE			DISCHARGE STATE			RESULTS	
		TIME STEP (SEC)	ENERGY (W. HR)	VOLTAGE (V)	TIME STEP (SEC)	ENERGY (W. HR)	VOLTAGE (V)	CHARGE EFF %	ENERGY EFF %
THREE CYCLES OF CHARGE AND DISCHARGE									
1	0.1 A & -0.1 A	1800	0.29	2.9	200	0.07	-0.7	11.1	3.71
2	0.1 A & -0.1 A	1900	0.29	2.9	100	0.07	-0.7	5.26	1.76
3	0.1 A & -0.1 A	2000	0.3	3	300	0.07	-0.7	15	5.02

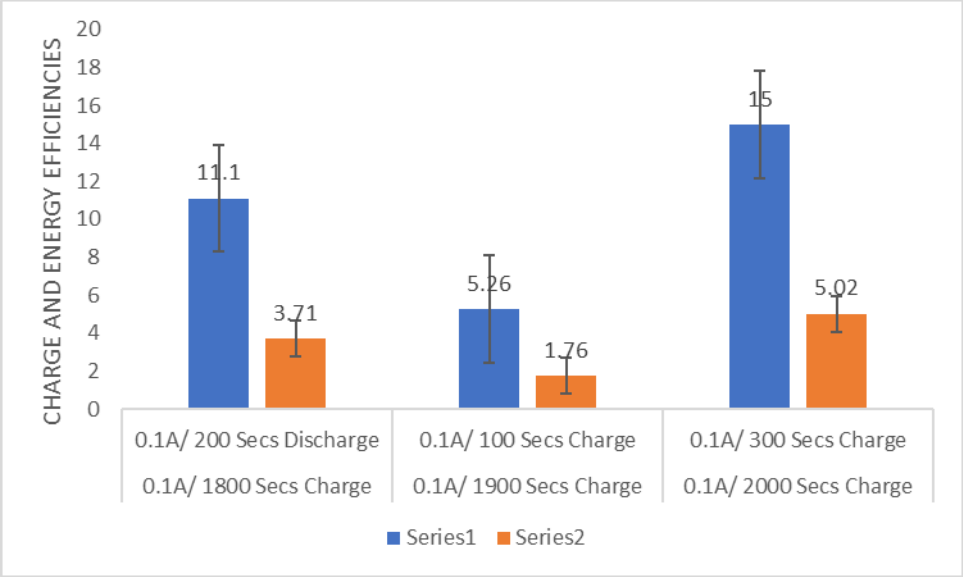

Figure 6. 32: Bar chart of (charge efficiency-blue) and (energy efficiency-pink) thru the titanium and nickel electrode at a current of 0.1 amps and -0.1 amps (1) @ (1800 secs and 200 secs), (2) @ (1900 secs and 100 secs) and (3) @ (2000 secs and 300 secs) with 3 moles of KBr (535.51 grams), 1 mole of KCl (111.89 grams) as the cathode-side electrolyte and 3 moles of $ZnBr_2$ (675 grams), 1 mole of $ZnCl_2$ (205 grams), and 1 mole of KCl (111.826 grams) as the anode electrolyte solution.

The 15% CE data is 100% conclusive. The 11.1% CE is inconclusive. It is 97% conclusive. Not all the data are different. Some were shared with the 15% CE. The 5.26% CE data was 94% true. The 5.02% EE is 100% conclusive. The 3.71% EE is 98% conclusive (2% data similarity with the 5.02% EE). The 3.71% EE is also 98% true.

6.22 Observations and Comments

6.22.1 Carbon Vs Nickel at 0.4 Amps and -0.4 Amps with these charge and discharge time steps: cycle-1, (3900 secs and 1100 secs), and (cycle-2), for (3700 secs and 1300 secs), and (cycle-3) for (3700 secs and 1200 secs).

Through the carbon and nickel electrode, the zinc-bromine battery cell completed three cycles of charges and discharges at the specific planned time; which was 3600 seconds and 1800 second and at 0.4 amps and -0.4 amps. The cyclic voltammetry showed a current of 0.3A via the IviumSoft potentiostat. The cell efficiency and other parameters are presented all together table 6.23. The anode-side and cathode-side electrolyte solution becomes more stronger in

colour by charging the cell at 400 milliamperes for 3600 seconds and to discharge at -400 milliamperes for 1800 seconds. Which has identified a more formation of bromine at the cathode-electrolyte and colourless zinc deposition at the anode-side and sign of a good redox reaction.

On the electrochemical impedance spectroscopy, EIS plot, a high frequency value of 40 Hz was observed from the cell positive-side and a low frequency of 30 Hz at the cell negative-side. These values were considered as high resistance and not presented. Most of the measured impedances on the cell were constant throughout the whole experiments; which were not expected. However, by using some other electrons conducting materials can reduce and correct the problem. Furthermore, the cell encountered an internal problem and behave strangely by charging it at 0.7 amps and up to 1 amp which was confirmed through pulling the cell apart.

The nickel and carbon electrodes feeder generated a large reduction and peak for the reversed sweep that was employed in between 2.5 volts to 1 volt. However, the result was not presented. According to (no-1 to no-3) in table 6.19, the cell demonstrated a potential of 3 volts during charge and -0.4 volts for the 1st cycle. The 2nd cycle showed a potential of 3 volts and -0.5 volts.

The 3rd cycle established -0.6 volts for the discharge and 3 volts for the charge. The charge passed during the 1st cycle was 1560 coulombs at 3900 secs instead of 1440 coulombs. The charge gained was 120 coulombs. For the discharge, the lost charge was 280 coulombs but gained 440 coulombs in between 3900 secs to 5000 secs.

The cell power was 1.2 watt.hr. (0.0012 kilowatt.hr.) during charge and 0.16 watt. hr. (0.00016 kilowatt. hr.) during discharge. The 2nd cycle demonstrated the same voltage as the 1st voltage except for the discharge voltage that was -0.5 volts. The expected charged was 1440 coulombs at 3600 secs but more current was discharged (1480 coulombs) in between (5000 secs and 5000 secs). The lost charge was 40 coulombs during charge and 200 coulombs during discharge.

The expected charged at 1800 secs was 720 coulombs but 520 coulombs were recorded in between 8700 secs to 10000 secs. The lost charge was 320 coulombs (520 coulombs minus 200 coulombs). the cell power was 1.2 watts. hr. (0.0012 kilowatt. hr.) during charge and 0.2 watt. hr. (0.0002 kilowatt. hr) during discharge. the charge passed during charge for the 3rd cycle was 1480 coulombs in between 10000 secs and 13700 secs.

More charge was also stored by the cell (1440 coulombs). the gained charged was 40 coulombs. the charge passed during discharge was 720 coulombs but lost 240 coulombs and stored 480

coulombs in between 13700 secs to 14900 secs. the cell watt was 1.2 watts. hr. (0.0012 kilowatt. hr.) and 0.24 watt. hr. (0.00024 kilowatt. hr.) during discharge.

6.22.2 Carbon Vs Nickel at 0.1 Amps and -0.1 Amps with these charge and discharge time steps: cycle-1 as (3600 secs, 500 secs), and cycle-2 for (1200 secs) before Interrupting the Battery Cell to Charge Further.

Before the cell was interrupted, the charge passed was 360 coulombs during charge. Furthermore, in between 3600 secs to 4100 secs, the charge passed was 50 coulombs during discharge in the 1st cycle. The lost charge was -130 coulombs and -80 coulombs as the differences between the charged passed during discharge and the lost charge. The cell watt was 0.23 watt. hr (0.00023 kilowatt. hr) during charge and 11 watts. hr (0.00011 kilowatt. hr) for the discharge. The 2nd cycle demonstrated 120 coulombs as the charge passed out of the expected 360 coulombs in between 4100 secs to 5300 secs. the cell confirmed 0.23 watts. hr (0.00023 kilowatt. hr) during charge.

6.22.3 Nickel Vs Titanium at 0.1 Amps and -0.1 Amps with these charge and discharge time steps: cycle-1 @ (1800 secs and 200 secs), cycle-2 @ (1900 secs and 100 secs) and cycle-3 @ (2000 secs and 300 secs)

The anticipated and observed charged passed during charge was 180 coulombs at 1800 secs. Furthermore in between 1800 secs and 200 secs, a charge passed of 20 coulombs was only recorded instead of 90 coulombs at 900 secs. The cell suffered huge loss during this process.

The charge loss was 70 coulombs and -50 coulombs as the difference between the charge gained and charge lost. The charge efficiency and energy efficiency were both low as presented in table 6.20. The cell watts and other essential parameters are also presented in table 6.22 for further elucidation. During the 2nd and 3rd cycle of charge and discharge, the cell demonstrated 2.9 volts during the first cycle of charge and discharge, second cycle of charge and discharge and 3 volts during the 3rd cycle. Furthermore, the cell stored an additional 20 coulombs of charge during the 2nd cycle in between 4000 secs to 6000 secs.

The opening charged passed was 180 coulombs, which later developed to 200 coulombs. For the discharge, 60 coulombs were expected but 30 coulombs were recovered in between 600 secs to 6300 secs and the charge efficiency was reduced by 85%. During the 2nd cycle of charge,

an additional charge passed of 10 coulombs was added to the expected 180 coulombs and for the discharge, out of the charge passed, 80 coulombs was lost, and 10 coulombs was gained out of the expected 90 coulombs.

The surface of the nickel and titanium electrode feeder should be polished again to remove any contaminated substances. The cell efficiency in this experiment has showed that the titanium and nickel current collector were compatible to produce a good current, but the problem might be from the electrolyte. This could have prevented these materials to establish the best efficiencies that can be recommended as a good $ZnBr_2$ battery cell as confirmed through the completed three cycles of charge and discharge. Table 6.23 has more detailed explanation regarding the accomplished results.

The electrolyte pH should also be checked constantly before operating the cell. To conclude, if an electrolyte pH rises beyond what is expected in an experiment, a pipette can be used to draw a small amount of hydrobromic acid and add it to both electrolyte solution to reduce the two-solvent pH values to a required value that is between (2.5 to 3). Furthermore, to elevate the pH of the two-electrolytes, some KOH pellet can be added.

Table 6. 23: The cell efficiencies and other parameters of the investigated nickel and carbon electrode and the titanium and nickel electrode investigated in 3 moles of KBr (535.51 grams), 1 mole of KCl (111.89 grams) as the cathode-side electrolyte and 3 moles of ZnBr2 (675 grams), 1 mole of $ZnCl_2$ (205 grams), and 1 mole of KCl (111.826 grams) as the anode electrolyte solution.

No	BATTERY CELL DATA'S CHARGE AND DISCHARGE	CHARGE STATE			DISCHARGE STATE			RESULTS	
		TIME STEP (SEC)	ENERGY (W. HR)	VOLTAGE (V)	TIME STEP (SEC)	ENERGY (W. HR)	VOLTAGE (V)	CHARGE EFF %	ENERGY EFF %
THREE CYCLES OF CHARGE AND DISCHARGE WITH THE CARBON AND NICKEL ELECTRODE									
1	0.4 A & -0.4 A	3900	1.2	3	1100	0.16	-0.4	28.20	9.54
2	0.4 A & -0.4 A	3700	1.2	3	1300	0.2	-0.5	35.1	11.88
3	0.4 A & -0.4 A	3700	1.2	3	1200	0.24	-0.6	32.4	11.27
THREE CYCLES OF CHARGE AND DISCHARGE WITH THE CARBON AND NICKEL ELECTRODE									
4	0.1 A & -0.1 A	3600	0.23	2.3	500	0.11	-1.1	13.9	6.25
5	CELL INTERRUPTED DUE TO LEAKAGES								
THREE CYCLES OF CHARGE AND DISCHARGE WITH THE NICKEL AND TITANIUM ELECTRODE									
6	0.1 A & -0.1 A	1800	0.29	2.9	200	0.07	-0.7	11.1	3.71

7	0.1 A & -0.1 A	1900	0.29	2.9	100	0.07	-0.7	5.26	1.76
8	0.1 A & -0.1 A	2000	0.3	3	300	0.07	-0.7	15	5.02

6.23 Conclusions on Results

6.23.1 Carbon Vs Nickel at 0.4 Amps and -0.4 Amps at these charge and discharge time steps: cycle-1, (3900 secs and 1100 secs), and (cycle-2), for (3700 secs and 1300 secs), and (cycle-3) for (3700 secs and 1200 secs)

From the presented bar chart in figure 6.33, the charge efficiency (CE), and energy efficiency (EE) were quite low compare and other efficiencies, CE and EE. The cell performed better during the first cycle compare to cycle-2 and cycle-3. During cycle-1 a CE loss of 71.8% and EE loss of 90.46% was recorded. The 2nd cycle established CE loss of 64.9% and an EE loss of 88.12%. The lost CE was 67.6% and 88.73% as the EE loss during the 3rd cycle.

The cell should not be operated up to 1000 milliamperes with the nickel and carbon electrodes to prevent some incorporated materials within the cell from destroying and will cause the zinc-particles to escape from the zinc-electrode and contaminate the two-electrolyte solution. Furthermore, this will require separating the solutions from these particles through a filtration process. Therefore, it would be advisable to stay within some specific amperes rates within 0.1 amps to 0.6 amps; but based on the capacity of the potentiostat and used materials and their resistances.

6.23.2 Carbon Vs Nickel at 0.1 Amps and -0.1 Amps at these charge and discharge time steps: cycle-1 as (3600 secs, 500 secs), and cycle-2 for (1200 secs) before Interrupting the Battery Cell.

Through further experimentation on the carbon and nickel electrode, the cell was able to store 360 coulombs of energy within 3600 secs with the re-introduced current collectors (nickel and carbon) at 0.1 amps and discharge 60 coulombs of energy at a current rate of -0.1 amps within 600 seconds before it was interrupted at 5500 secs. However, the cell could still store 140 coulombs of energy. The lost energy by the cell was 130 coulombs.

The outstanding lost energy that was not discharged was assumed to have entered the into the zinc-particles since there was no leakages from the cell. The cell charged efficiency, CE was

reduced by 86.1% and by 93.75% for the (EE) energy efficiency and charged at 2.3 volts. Through the polished surface electrodes and cleaned with de-ionized water before they were re-incorporated separately with the three-different electrolyte solution has assisted to identify the new sequestering agent (tetrabutylammonium bromide) as the cause of the problem. Furthermore, this has confirmed that the carbon and nickel electrode materials are in good condition and conductive.

6.23.3 Nickel Vs Titanium at 0.1 Amps and -0.1 Amps at these charge and discharge time steps: cycle-1 @ (1800 secs and 200 secs), cycle-2 @ (1900 secs and 100 secs) and cycle-3 @ (2000 secs and 300 secs)

The charge passed through the cell and current collected with the nickel and titanium electrode feeder material has discovered their conductivity level. During the experiment, these incorporated electrodes were not very conductive since they have been contaminated as observed through the three chronopotentiometry cycles.

Out of all the experimental work of this section, the third cycle of charge and discharge was better than the first and second cycle. But none of these results can be presented as a good zinc-bromine battery cell due to their efficiencies. Furthermore, lots of energy was lost during the discharge compared to what was expected from the cell.

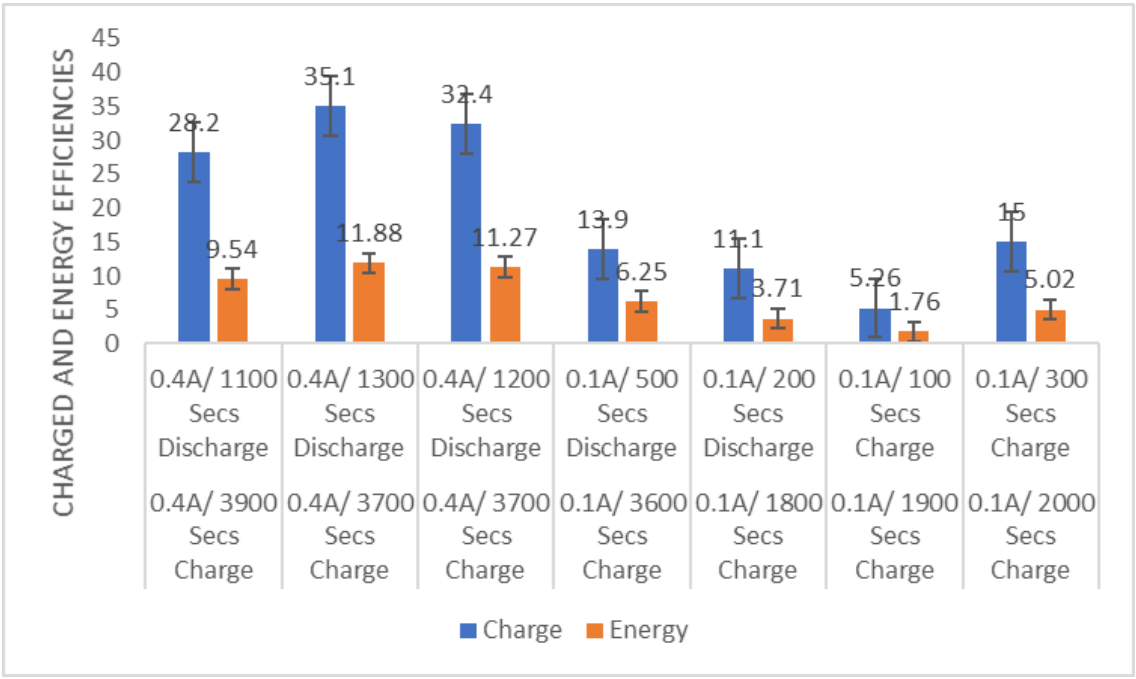

Figure 6. 33: Overall bar chart of (charge-blue colour) and (energy-pink colour) efficiency of (**a**) three cycles (1 to 3) of charge and discharge by incorporating a nickel and carbon electrode at a charge 0.4 amps and 0.4 amps at these time steps (3900 secs & 1100 secs), (3700 secs &1300 secs), (3700 secs & 1200 secs) (**b**) (4) by investigating further the same nickel and carbon electrode before it was interrupted at 0.1 amps and -0.1 amps with these time steps (3600 secs & 1800 secs) and (**c**) three cycles (5 to 7) of charge and discharge by investigating the titanium and nickel electrode at 0.1 amps and -0.1 amps at these time steps (1800 secs & 200 secs),(1900 secs & 100 secs),(2000 secs & 300 secs) with 3 moles of KBr (535.51 grams), 1 mole of KCl (111.89 grams) as the cathode-side electrolyte and 3 moles of ZnBr2 (675 grams), 1 mole of $ZnCl_2$ (205 grams), and 1 mole of KCl (111.826 grams) as the anode electrolyte solution.

Data from the 35% CE were 100% accurate. Other CE's data were not 100% conclusive as discussed earlier on their bar chart in this chapter. They all overlapped each other. All the collected data for the calculated EE's were not 100% conclusive as also discussed form onset.

7 Final Overall Conclusions on all Chapters

7.1 Dendrite Measurement and Assessments

The experimented fluidised bed electrode in this research has been shown to successfully prevent the problem of dendrites formation, produce sufficiently high mass transport of zinc during charging and discharging and supported the chemical reactions.

The explored charged amps and discharged amps on the battery cell has showed that the fabricated and incorporated anode reactor has magnificently and effectively suppressed the formation of zinc dendrite within the incorporated zinc reactor without degradation by running the cell up to 3hrs through using 3 moles of KBr (535.51 grams), 1 mole of KCl (111.89 grams) as the cathode-side electrolyte and 3 moles of ZnBr2 (675 grams), 1 mole of $ZnCl_2$ (205 grams), and 1 mole of KCl (111.826 grams) as the anode electrolyte solution [444]. Some of the advantages that were observed by experimenting the fluidized bed anode reactor are listed below. See also figure 7.1 for the experimented and discussed anode reactor. Similar image has been presented as figure 6.2 in section 6.2.3.

- The fluidized bed electrode was capable of fast electron exchange in the charge and discharge cycle because of the high surface area.
- The designed system was capable of fast deposition and dissolution of the metal at low over potential forming part of the electrolyte due to the use of small particles
- Numerically, the modelled and experimented fluidized bed electrode was highly electronically conductive. It also minimises ohmic losses (high efficiency cell) during charging and discharging; except for the high internal resistance constantly encountered within the cell. This was due to the cell size and enclosed materials; such as the reactors, gaskets, Nation membrane etc., which inhibited the production of higher charges and energy efficiencies.
- The high internal resistance observed during most of the electrochemical measurements had contributed to the discrepancies among all the charge and energy efficiencies.
- Despite the fact that carbon materials are good as current collectors, but they can corrode during the oxidation process when there is excess hydrogen evolution.

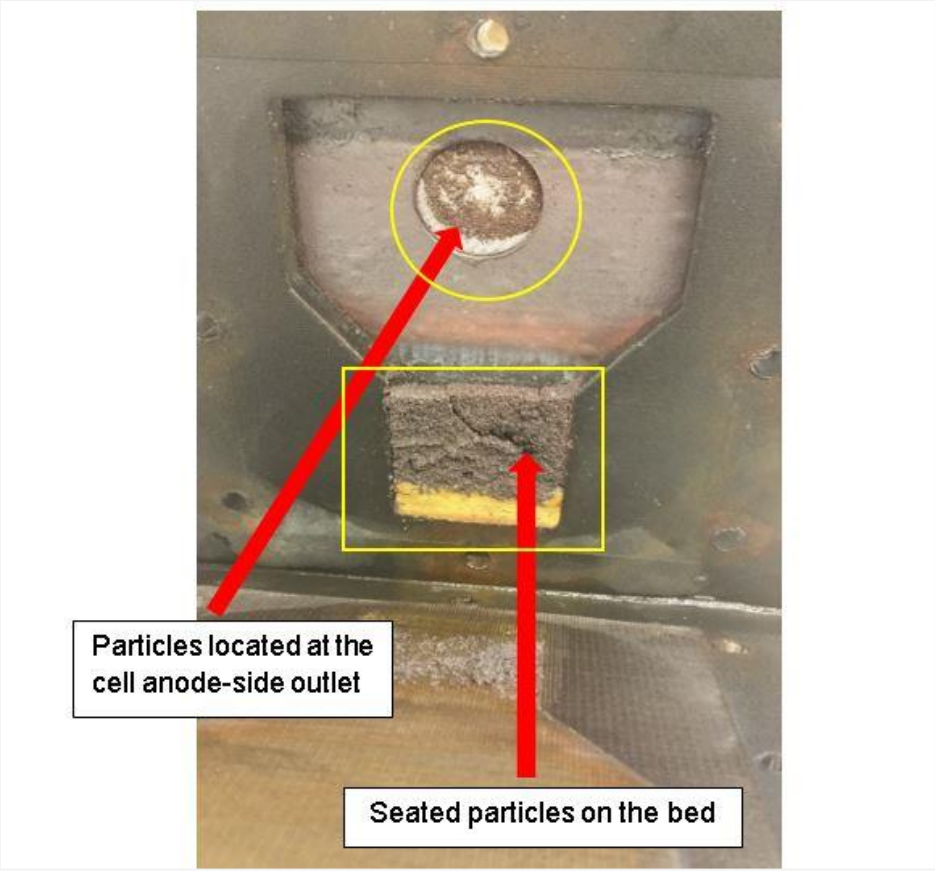

Figure 7. 1 The incorporated anode reactor to the cell anode side

7.1.1 Zinc-Based Metal-Anode RFB

Based on past studies and apart from the investigated feeder electrodes materials (carbon, nickel and titanium) in this research work, zinc deposition and dissolution during the charge and discharge stages, respectively, must be balanced to achieve extended lifetime and maximum efficiency of zinc bromine flow batteries cells [321]. Zinc-based redox flow batteries are suitable for various medium to large scale storage applications among other batteries; such as the all-vanadium systems [529, 530]. The reaction of positive electrodes in zinc-based metal-anode flow batteries can either be in solid, liquid or gaseous phase with inorganic or organic materials [531] as presented in figure 7.2.

7.1.2 Zinc Electrodeposition.

The reaction of negative electrodes in all systems relies on zinc electrodeposition from a flowing electrolyte containing dissolved zinc species. Therefore, the process of zinc electrodeposition to obtain a suitable deposit morphology for long-term cycles is critical. In redox/ hybrid flow batteries applications, the choice of low-cost metals (<USD$ 4 kg^{-1}) is still limited to lead, zinc, manganese, iron, chromium and cadmium.

The annual production of these metals exceeded to four million tons in 2016; as they are highly abundant in the earth's crust, higher than ten parts per million (ppm) which makes them attractive for large-scale energy storage purposes [17]. Zinc metal among other elements has large volumetric capacity (5.85 Ah cm^{-3}), highest energy content and high negative electrode potential in aqueous media (acidic: −0.76 V vs SHE; alkaline: −1.29 V vs SHE) [132, 532].

Zinc electrodeposition in both acidic and alkaline aqueous electrolytes on inert substrates can be a relatively efficient process with current efficiencies of over 90%; loss reaction attributable to the evolution of hydrogen. The use of zinc electrodeposition in industries such as automotive has been substantially investigated largely for corrosion protection [533-537].
Presently, zincate (alkaline), and sulphate (acid), and chloride (acid) in electroplating industries are still the main conventional baths for zinc electrodeposition [538-548].

In contrast, other electrodeposition of electronegative metals such as aluminum, lithium, and sodium are not possible in aqueous electrolytes but possible in nonaqueous solvents or in ionic liquids room-temperature [549]. These solvents in large-scale energy storage devices, such as RFB present problems due to low ionic conductivity (10^{-8}–10^{-10} S cm^{-1} without salts) and high cost. [550] Also, most organic solvent-based electrolytes for lithium and sodium are flammable and raise concerns regarding safety when combined with the reactive metal anodes [551-553].

Therefore, zinc is still one of the most common anodic materials for primary and secondary batteries. The early development of zinc anode primary systems such as zinc-manganese dioxide, originated in 1866; with various portable devices still using these zinc-alkaline dry cells [532, 554]. These cells and other primary zinc batteries such as zinc-carbon are often associated with one-time use, but rechargeable versions are available. The mode of cycling in zinc-alkaline dry cells and zinc-carbon have poor reversibility for both the anodic and cathodic materials [555, 556].

7.2 Challenges and Control

The issue of limiting current densities and non-uniform concentration gradients leads to anodic zinc dendritic morphologies in conventional static systems [370]. However, convection processes in the electrolyte can be used to control such problem and extend the battery life. Changing the shape of negative electrodes can aid this and make the cell less affected by dendrites or corrosion processes [370, 375].

Furthermore, separators or membranes are used in many of these systems to stop the crossing of active species preventing 'electrochemical' as well as electronic shorts. In zinc-based batteries systems, the involvement of at least one solid phase electrode reaction with zinc electrodeposition will provide the possibility to have a membraneless configuration, [124, 141, 373, 557-559].

Nevertheless, most zinc-based systems are still encountering the problem of self-discharge, and other failures due to dendrite formation. These problems must be addressed to prolong cell cycle life to improve their performance aided by mathematical modelling of new cell architectures and operating regimes and validated by experimental laboratory approaches. [21, 79, 108, 227, 550, 560-562].

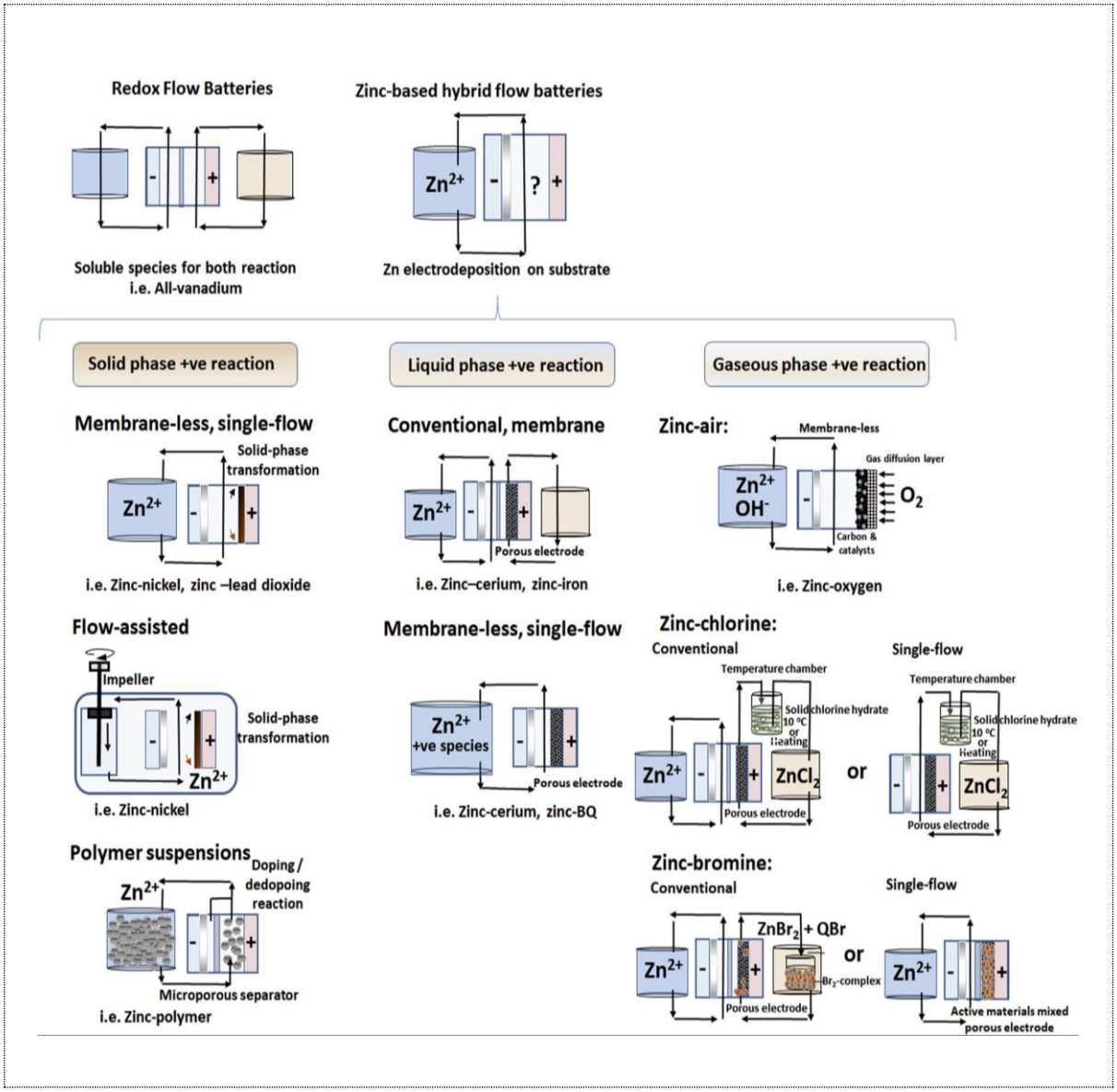

Figure 7. 2 (a) Zinc system with solid phase reaction, (b) liquid state reaction, (c) and gaseous phase reaction [563].

Furthermore, the regulated flow rate (166.7 cm^3 per min) had stopped a turbulence flow from occurring within the reactors and a laminar flow occurred instead. This model has demonstrated factors such as: Concentrations, Potential differences (PD) and Electrolyte potential (EP). These factors have been validated with the laboratory experiment. Additionally, the three sets of electrodes feeder materials have been investigated on the cell by charging and discharging it under a set of operating condition before measuring the impedances and cyclic voltammetry's.

7.3 Assessment of Efficiencies Results

Out of all the explored electrochemical measurement on the investigated feeder electrodes materials, the best results were only selected. The (carbon-cathode and nickel-anode) feeder electrode materials had the best performances. Then, the (nickel-anode and titanium-cathode). The carbon-anode versus carbon-cathode had a woeful performance.

The titanium versus nickel feeder electrode could have performed better than the carbon versus nickel feeder electrode supposing if these electrode materials were further charged at higher current rates. Nevertheless, the titanium versus nickel feeder electrodes were the last investigated materials that encountered series of electrolyte sequestering agent problems before the cell could be put back to normal. Therefore, such complications contributed towards not running the cell further.

The suggested and introduced analytical procedure were used in this research to know these investigated feeder electrodes performances. This procedure has enabled to recognize the good, better and best charge and energy efficiency via the introduced different sets of feeder electrodes materials as summarized below and presented on the bar chart in figure 7.3

1. Carbon-cathode and carbon-anode at 0.2 amps and -0.1 amps demonstrated a charge and energy efficiency of (43.3% and 15.63%).
2. Carbon-cathode and nickel-anode at 0.1 amps and -0.1 amps demonstrated a charge efficiency, CE of (51.3%, 53.3%) and energy efficiency, EE of (12.77% and 13.29%). These results were for 2-cycles of charge and discharge before the cell was interrupted.
3. Furthermore, at 0.1 amps and 0.1 amps, the carbon and nickel feeder electrode at 3-cycles of charge and discharge further demonstrated charge efficiency, CE of (47.5%, 64.5% and 63.3%) and energy efficiency, EE of (13.97%, 18.9%. and 18.6%).
4. At 0.4 amps and -0.4 amps, the carbon and nickel feeder electrode at 3-cycles of charge and discharge established these charge efficiencies, CE of (28.2%, 35.1% and 32.4%) and energy efficiencies, EE of (9.54%, 11.8%. and 11.27%).
5. Titanium and nickel at 3-cycles of charge and discharge at 0.1 amps and -0.1 amps established a charge efficiency, CE of (50%, 49.72% and 52.78%) and energy efficiency, EE of (24.39%, 24.25%. and 25.75%).

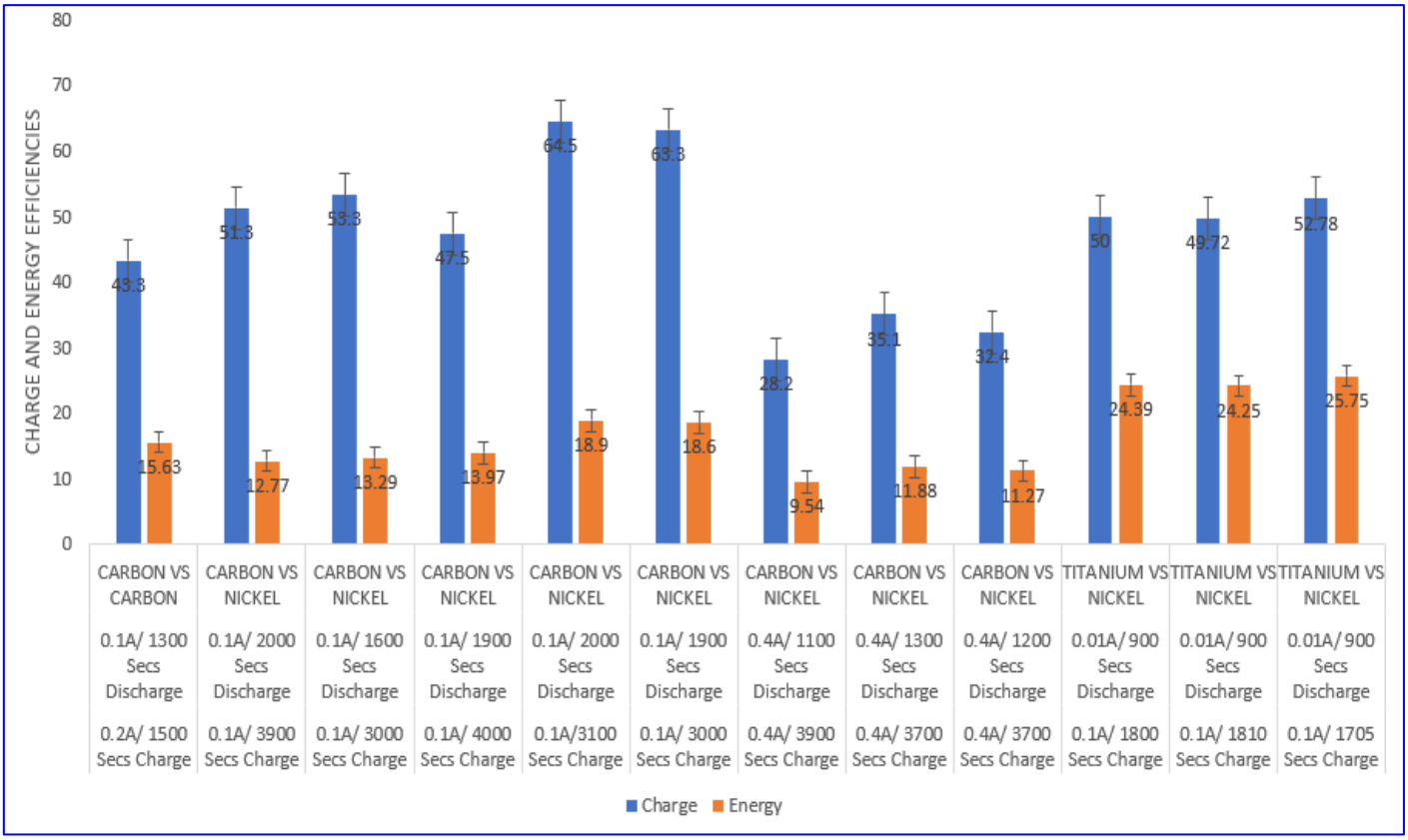

Figure 7. 3: Excellent (Charge-blue) and (Energy-pink) efficiencies through investigating (a) carbon-cathode versus carbon-anode at a charge rate of 0.2 amps and -0.1 amps (b) carbon-cathode versus nickel-anode a charge rate of 0.1 amps and -0.1 amps, and At a charge rate of 0.4 amps and -0.4 amps (c) titanium-cathode versus nickel-anode at a current rate of 0.4 amps and -0.4 amps.

7.3.1 **SEM (Scanning of Electrons Microscopy)**

The SEM has showed all entrapped elements within the charged zinc particles, similarities between all the observed elements and why some of the coupled materials to the cell were changed to achieve a zinc bromide cell. Collected current from the cathode and anode zinc-electrode during charge were possible by using the three feeder electrode materials. Before the SEM, the explored cyclic voltammetry using these investigated feeder electrodes showed their performances and chemical reaction with the anode zinc-electrode and cathode electrode with the electrolyte at a sweep condition of 25 mV/ sec. Furthermore, through a slow sweep rate, there was enough time for the electrochemical species and product reaction during the forward

reaction for a proper chemical reaction. Table 7.1 to table 7.4 has further presented the explored charge amps, sweep conditions, and outcome of the best feeder electrodes through exploring various charge rates.

Table 7. 1: Cycle-3: Applied charged and discharged amps to the three sets of electrode feeder materials carbon vs carbon, nickel vs carbon and nickel vs titanium with 3 moles of KBr (535.51 grams), 1 mole of KCl (111.89 grams) as the cathode-side electrolyte and 3 moles of ZnBr2 (675 grams), 1 mole of $ZnCl_2$ (205 grams), and 1 mole of KCl (111.826 grams) as the anode electrolyte solution.

Charge and Discharged Experiments			
Experiments	Carbon & Carbon	Nickel & Carbon	Nickel & Titanium
1	(a) Charge and discharge rate (0.2 amps and -0.1 amps @ both 3600 secs) (b) (0.1 amps and -0.1 amps @ both 3600 secs).	Charged and discharged rate (0.1 amps vs -0.01 amps) @ both 3600 secs	Charged @ 0.1A amps for 3600secs
2	Five-charged cycles @ 0.1 amps for 3600 secs	Three-cycles of charged and discharged at a current rates of 0.1 amps and -0.1 amps @ 3600 secs and 1800 secs	First Charged and discharged at a current rate of 0.1 amps for 1800 secs and at -0.1 amps for 900 secs
3	(a) Charged rate at (0.1 amps, 0.1 amps, 0.1 amps and 0.25 amps) @ 3600 secs (b) Discharged rate (-0.1 amps, -0.1 amps, -0.1 amps, and -0.25 amps) @ 3600 secs	Three-cycles of charged and discharged at a current rate of (0.1 amps Vs -0.1 amps) @ 3600 secs and 1800 Secs	Charge and discharge at a current rate of 0.1 amps for 1800 secs and at -0.1 amps for 900 secs.
4	(a) Charge and discharge at (0.25 amps, 0.1 amps, 0.25 amps, 0.5 amps and 1 amps) @ 3600 secs and (b) Discharged rate (-0.25 amps, -0.005 amps, -0.01 amps, -0.01 amps and -0.05 amps) @ 3600 secs	Three-cycles of charged and discharged at (0.4 amps and -0.4 amps) for 3600 secs and 1800 secs	Three cycles of charged and discharged at (0.1 amps vs -0.1 amps) for 1800 Secs and 900 Secs

5	Re-investigated two-carbon electrodes at (a) Charged at 0.1 amps for 3600 secs and discharged at -0.01 amps for 3600 secs. (b) Charge and discharge at 0.1 amps and -0.1 amps at both for 3600 secs	Re-examined nickel and carbon materials at (a) charged rate 0.1 amps for 3600 secs and (b) Discharged rate -0.1 amps for 1800 secs	Charged and discharge at 0.3 amps for 1800 secs and at -0.3 amps for 900 secs
6			Charge and discharge at 0.1 amps for 1800 secs and at -0.1 amps for 900 secs

Table 7. 2: Explored cyclic voltammetry after investigating the three sets of electrode feeder materials carbon vs carbon, nickel vs carbon and nickel vs titanium in a 3 moles of KBR (535.51 grams), 1 mole of KCl (111.89 grams) as the cathode-side electrolyte and 3 moles of $ZnBr_2$ (675 grams), 1 mole of $ZnCl_2$ (205 grams), and 1 mole of KCl (111.826 grams) as the anode electrolyte solution.

Cyclic Voltammetry Experiments			
Experiments	Carbon & Carbon	Nickel & Carbon	Nickel & Titanium
	Fifteen cyclic voltammetry of one sweep condition at 25 mV/ sec	Three cyclic voltammetry of one sweep condition at 25 mV/ sec	Five cyclic voltammetry of one sweep condition at 25 mV/ sec
1	Six cyclic voltammetry of one sweep condition at 20 mV/ sec		
2	Two cyclic voltammetry of one sweep condition at 50 mV/ sec		

Table 7. 3: First investigated electrode materials: carbon-cathode vs carbon-anode experimental data with a 3 moles of KBr (535.51 grams), 1 mole of KCl (111.89 grams) as the cathode-side electrolyte and 3 mole of $ZnBr_2$ (675G), 1 mole of $ZnCl_2$ (205 grams), and 1 mole OF KCl (111.826 grams) as the anode electrolyte solution

EXPLORED CHARGE AND DISCHARGE EXPERIMENTS WITH THE INVESTIGATED CARBON (CATHODE) AND CARBON (ANODE) ELECTRODE									
No	BATTERY CELL DATA'S CHARGE AND DISCHARGE	CHARGE STATE			DISCHARGE STATE			RESULTS	
		TIME STEP (SEC)	ENERGY (W. HR)	VOLTAGE (V)	TIME STEP (SEC)	ENERGY (W. HR)	VOLTAGE (V)	CHARGE EFF %	ENERGY EFF %
TWO CHARGE AND DISCHARGE EXPERIMENTS									
Ai	0.1 A & -0.1 A	3600	2	2	500	1.1	1.1	13.8	N/A
Aii	0.2 A & -0.1 A	1500	2.1	2.1	1300	1.3	1.3	43.3	15.63
No	BATTERY CELL DATA'S CHARGE AND DISCHARGE	CHARGE STATE			DISCHARGE STATE			RESULTS	
		TIME STEP (SEC)	ENERGY (W. HR)	VOLTAGE (V)	TIME STEP (SEC)	ENERGY (W. HR)	VOLTAGE (V)	CHARGE EFF %	ENERGY EFF %
THREE CHARGE AND DISCHARGE EXPERIMENT									
10	0.1 A & -0.1 A	3600	0.19	1.9	800	0.7	0.07	22.22	5.90
11	0.1 A & -0.1 A	3500	0.13	1.3	200	0.03	0.3	5.71	2
12	0.25A & -0.25A	3600	0.45	1.8	100	0.025	0.5	2.77	1.07
No	BATTERY CELL DATA'S CHARGE AND DISCHARGE	CHARGE STATE			DISCHARGE STATE			RESULTS	
		TIME STEP (SEC)	ENERGY (W. HR)	VOLTAGE (V)	TIME STEP (SEC)	ENERGY (W. HR)	VOLTAGE (V)	CHARGE EFF %	ENERGY EFF %
FIVE CHARGE AND DISCHARGE EXPERIMENTS									
1	0.25 A & -0.25 A	3600	0.475	1.9	400	0.0125	0.5	11.1	5.48
2	0.1 A & -0.005 A	3600	0.15	1.5	3500	0.0035	0.7	4.86	2.94
3	0.25 A & -0.01 A	3600	0.475	1.9	3600	0.01	1	3.88	1.81
4	0.5 A & -0.01 A	3600	1.3	2.6	3600	0.014	1.4	1.94	1.25
5	1 A & -0.05 A	3600	4	4	3600	0.065	1.3	4.86	2.21
No	BATTERY CELL DATA'S CHARGE AND DISCHARGE	CHARGE STATE			DISCHARGE STATE			RESULTS	
		TIME STEP (SEC)	ENERGY (W. HR)	VOLTAGE (V)	TIME STEP (SEC)	ENERGY (W. HR)	VOLTAGE (V)	CHARGE EFF %	ENERGY EFF %
ONE CHARGE AND DISCHARGE EXPERIMENTS									

1	0.1 A & -0.01 A	3600	0.24	2.4	3600	0.014	1.4	10	8.085

Table 7. 4: Experimental data of the second and third investigated electrodes materials: (carbon-cathode vs nickel-anode) & (titanium-cathode and nickel-anode) both with 3 moles of KBr (535.51 grams), 1 mole of KCl (111.89 grams) as the cathode-side electrolyte and 3 moles of $ZnBr_2$ (675 grams), 1 mole of $ZnCl_2$ (205 grams), and 1 mole of KCl (111.826 grams) as the anode electrolyte solution.

EXPLORED CHARGE AND DISCHARGE EXPERIMENTS WITH THE INVESTIGATED CARBON (CATHODE) AND NICKEL (ANODE) ELECTRODE									
No	BATTERY CELL DATA'S CHARGE AND DISCHARGE	CHARGE STATE			DISCHARGE STATE			RESULTS	
		TIME STEP (SEC)	ENERGY (W. HR)	VOLTAGE (V)	TIME STEP (SEC)	ENERGY (W. HR)	VOLTAGE (V)	CHARGE EFF %	ENERGY EFF %
CHARGE AND DISCHARGE									
1	0.1 A & -0.01 A	3600	0.18	1.8	3600	0.01	1	10	4.88
No	BATTERY CELL DATA'S CHARGE AND DISCHARGE	CHARGE STATE			DISCHARGE STATE			RESULTS	
		TIME STEP (SEC)	ENERGY (W. HR)	VOLTAGE (V)	TIME STEP (SEC)	ENERGY (W. HR)	VOLTAGE (V)	CHARGE EFF %	ENERGY EFF %
THREE CYCLES OF CHARGE AND DISCHARGE									
1	0.1A & -0.1 A	3900	0.2	2	2000	0.1	1	51.3	12.77
2	0.1A & -0.1A	3000	0.2	2	1600	0.1	1	53.3	13.29
3	0.1A & -0.1A	2400	0.2	2	NONE	NONE	NONE	NONE	NONE
No	BATTERY CELL DATA'S CHARGE AND DISCHARGE	CHARGE STATE			DISCHARGE STATE			RESULTS	
		TIME STEP (SEC)	ENERGY (W. HR)	VOLTAGE (V)	TIME STEP (SEC)	ENERGY (W. HR)	VOLTAGE (V)	CHARGE EFF %	ENERGY EFF %
THREE CYCLES OF CHARGE AND DISCHARGE									
1	0.1A & -0.1A	4000	0.18	1.8	1900	0.04	0.4	47.5	13.97
2	0.1A & -0.1A	3100	0.18	1.8	2000	0.04	0.4	64.5	18.9
3	0.1A & -0.1A	3000	0.18	1.8	1900	0.04	0.4	63.3	18.6
No	BATTERY CELL DATA'S	CHARGE STATE			DISCHARGE STATE			RESULTS	
		TIME	ENERGY	VOLTAGE	TIME	ENERGY	VOLTAGE		ENERGY

	CHARGE AND DISCHARGE	STEP (SEC)	(W. HR)	(V)	STEP (SEC)	(W. HR)	(V)	CHARGE EFF %	EFF %
THREE CYCLES OF CHARGE AND DISCHARGE									
1	0.4 A & -0.4 A	3900	1.2	3	1100	0.16	-0.4	28.20	9.54
2	0.4 A & -0.4 A	3700	1.2	3	1300	0.2	-0.5	35.1	11.88
3	0.4 A & -0.4 A	3700	1.2	3	1200	0.24	-0.6	32.4	11.27
No	BATTERY CELL DATA'S CHARGE AND DISCHARGE	CHARGE STATE			DISCHARGE STATE			RESULTS	
		TIME STEP (SEC)	ENERGY (W. HR)	VOLTAGE (V)	TIME STEP (SEC)	ENERGY (W. HR)	VOLTAGE (V)	CHARGE EFF %	ENERGY EFF %
THREE CYCLES OF CHARGE AND DISCHARGE									
1	0.1 A & -0.1 A	3600	0.23	2.3	500	0.11	-1.1	13.9	6.25
3	CELL INTERRUPTED DUE TO LEAKAGES								

EXPLORED CHARGE AND DISCHARGE EXPERIMENTS WITH THE INVESTIGATED TITANIUM (CATHODE) AND NICKEL (ANODE) ELECTRODE

No	BATTERY CELL DATA'S CHARGE AND DISCHARGE	CHARGE STATE			DISCHARGE STATE			RESULTS	
		TIME STEP (SEC)	ENERGY (W. HR)	VOLTAGE (V)	TIME STEP (SEC)	ENERGY (W. HR)	VOLTAGE (V)	CHARGE EFF %	ENERGY EFF %
THREE CYCLES OF CHARGE AND DISCHARGE									
1	0.1 A & -0.1 A	1800	0.2	2	900	0.1	1	50	24.39
2	0.1 A & -0.1 A	1810	0.2	2	900	0.1	1	49.72	24.25
3	0.1 A & -0.1A	1705	0.2	2	900	NONE	NONE	52.78	25.75
No	BATTERY CELL DATA'S CHARGE AND DISCHARGE	CHARGE STATE			DISCHARGE STATE			RESULTS	
		TIME STEP (SEC)	ENERGY (W. HR)	VOLTAGE (V)	TIME STEP (SEC)	ENERGY (W. HR)	VOLTAGE (V)	CHARGE EFF %	ENERGY EFF %
THREE CYCLES OF CHARGE AND DISCHARGE									
1	0.3 A & -0.3 A	1800	0.9	3	200	0.12	0.4	11.11	2.26
2	0.3 A & -0.3 A	1700	0.9	3	200	0.12	0.4	11.76	2.39
3	0.3 A & -0.3 A	1900	0.9	3	200	0.12	0.4	11.11	2.26
No	BATTERY CELL DATA'S CHARGE AND DISCHARGE	CHARGE STATE			DISCHARGE STATE			RESULTS	
		TIME STEP	ENERGY (W. HR)	VOLTAGE (V)	TIME STEP	ENERGY (W. HR)	VOLTAGE (V)	CHARGE EFF %	ENERGY EFF %

		(SEC)			(SEC)				
THREE CYCLES OF CHARGE AND DISCHARGE									
1	0.1 A & -0.1 A	1800	0.29	2.9	200	0.07	-0.7	11.1	3.71
2	0.1 A & -0.1 A	1900	0.29	2.9	100	0.07	-0.7	5.26	1.76
3	0.1 A & -0.1 A	2000	0.3	3	300	0.07	-0.7	15	5.02

7.4 Recommended Future Work

Research should also continue by implementing more novel techniques to address dendrite formation within zinc-bromine batteries cells; apart from the incorporated FBR anode zinc-electrode of this research work and via using mathematical modelling for simulating the performance of these batteries cells to address dendrites issue. Furthermore, research should include how low impedances resistances can be achieved on zinc-bromine batteries cells.

The architectures of $ZnBr_2$ batteries cells should concentrate on materials that can be chemically resistance. This will prevent unwanted corrosion and make incorporated current collectors to batteries cells to be extremely conductive. The pH values of ZnBr2 batteries cells should be checked constantly either before or after running a cell since it improves cells efficiencies due to the number of protons. Batteries cells storage capacities can be extended to improve having some more uniform electrodeposits.

Batteries cells electrochemistry modelling should be carried out with ANSYS and not only COMSOL for the comparison of results. Despite that to improve energy densities of redox flow cells is a pressing issue, it is also obvious that zinc-bromine batteries cells have better energy densities than other redox flow cells. The fabricated and incorporated high surface area electrode that was numerically modelled with ANSYS, has demonstrated fast capacity of electron exchange in the charge and discharge cycles with fast deposition and metal dissolution. This has been observed via the hydrodynamic behaviour of the added glass beads and carbon particles. Furthermore, as stated below,

1. Before charge, after and apart from the fabricated zinc-bromine battery cells of this research work, all other hybrid redox flow batteries cells pH values must be checked as they determine the number of protons.

2. Other different feeder electrodes materials, such as platinum can be coupled and investigated with the feeder electrodes of this research work to see if the charge and energy efficiency of zinc bromine batteries cells can be improved.

3. The same amps (charge and discharge) should be passed to ZnBr2 future fabricated batteries cells for a proper comparison instead of investigating the feeder electrodes at various current rates.

4. Since the sizes and watts of the ZnBr2 cell in this research had contributed to the high internal resistance (IR) within the cell of this research work, it would be advisable to fabricate in future the sizes of $ZnBr_2$ batteries cells to 1/3 of the cell size used in this research work (190mm*190mm*12mm).

5. Salt Concentrations should be minimised to prevent excess hydrogen gas. Although it can be totally prevented as numerically and experimentally observed.

6. Particles should be well dried before presenting them for scanning of electrons microscopy (SEM) to avoid degasification. Feeder electrodes surfaces should be polished with alumina after an experiment and before the experimental work. Through these, any anomalies can be prevented. Batteries cells should be programmed to charge and discharge at the same ampere. Through such procedure, the performances of the feeder electrodes can be compared accurately.

7. Although some of techniques recommended in number six has contributed much differences to the explored work carried out in this thesis; but such recommendation can further assist to know if there would be any differences. To conclude, apart from the three sets of investigated electrode feeder materials of this research work, some other materials such as platinum can be investigated to see their level of conductivity. These may include coupling platinum with nickel and platinum with carbon.

7.5 Other ZnBr2 Cells Systems Challenges

7.5.1 Chlorides in ZnBr2 Systems

Investigating further the effects of chlorides and influences on zinc deposition on an electrode in zinc-bromine cells systems will be interesting because of the corrosive nature. To continue developing a suitable alternatives according to researchers by considering the use of perchlorates (salts) within zinc bromide cells will be promising since the energy held in the external tanks of RFB systems can be converted when required in the conversion unit [564] [565]. Inconsistency with studies, sulphates effects on zinc plating should likewise continue to be examined because it could also be a benefit in zinc-bromine batteries cell electrolytes.

7.6 Future Solutions

Optimizing the properties and types of zinc-bromine batteries cells would be of interest in future. This can be done by making supporting electrolyte of zinc-bromine batteries for improving the performance and the uptake of systems for the utility-scale electrical storage system [538, 566-568]. Efficient electrodeposition can be promoted in a zinc-bromine battery by stripping of zinc during charging and discharging process[569].

There are benefits to promote the electrodeposition process and make it efficient to improve the system coulombic efficiency. An additional improvement would occur using this approach by reducing unwanted side-reactions in the cell system causing coulombic losses.

As a substrate material for the deposition zinc, the use of anchored carbon nanotubes to a carbon felt have the possibility to exhibit a better efficiency and strengthened it if used as bromine electrodes [570]. Furthermore, it is possible after 200 cycles, to achieve a higher electrocatalytic activity via using single-walled carbon nanotubes compared to the attribution of multiwalled carbon nanotubes to a more substantial number of basal planes for better energy efficiencies retention (98%); which can make it an assuring cathode material [570].

The combination of a $Br^-/ClBr_2^-$ and Zn/Zn^{2+} as anodic redox couple can separately increase both the energy density of a positive and negative half-cell. The battery performance can also be evaluated by carrying out a cycle test and using a charge and discharge method to achieve a high energy efficiency of 81%; based on a coulombic efficiency and voltage efficiency of (96% and 84%) [571].

In addition,

(1) The use of special membranes (Nafion) between positive and negative electrodes to act as a physical barrier to prevent short-circuiting [572].

(2) By modifying directly the active materials as recommended by Parker et al via using a three-dimensional structure of zinc that could be trapping dissolving zinc species such as zincate ions ($Zn(OH)_4^{2-}$) near the electrode upon discharge as this approach will minimize the redistribution of Zinc ions and shape change [573].

(3) By dividing the electrolyte additives into metallic and organic additives [574, 575]. Organic additives such as tetrabutylammonium bromide [576] tetra-alkyl ammonium hydroxides [577] triethanolamine [578]. Triton X-100 [579] or poly (ethylene glycol) [580] can prevent dendrite formation by slowing down diffusional mass transport and limiting the enhanced growth at specific sites.

(4) The electrochemical approach in the late 1980s and early 1990s, were several studies in which the shape change in zinc (Zn) metal anodes was proposed to be mitigated by applying a direct current (DC) pulses or alternating current (AC) charging protocols [581-583].

8 References

[1] M. J. Wu, C. Y. Huang, and Y. H. Hung, "Capabilities-Driven Curriculum Design for Hydrogen and Fuel Cell Technologies," in 2011 IEEE Green Technologies Conference (IEEE-Green), 14-15 April 2011 2011, pp. 1-6, doi: 10.1109/GREEN.2011.5754853.

[2] M. Yekini Suberu, M. Wazir Mustafa, and N. Bashir, "Energy storage systems for renewable energy power sector integration and mitigation of intermittency," Renewable and Sustainable Energy Reviews, vol. 35, pp. 499-514, 7// 2014, doi: http://dx.doi.org/10.1016/j.rser.2014.04.009.

[3] V. A. Boicea, "Energy Storage Technologies: The Past and the Present," Proceedings of the IEEE, vol. 102, no. 11, pp. 1777-1794, 2014, doi: 10.1109/JPROC.2014.2359545.

[4] X. Luo, J. Wang, M. Dooner, and J. Clarke, "Overview of current development in electrical energy storage technologies and the application potential in power system operation," Applied Energy, vol. 137, pp. 511-536, 1/1/ 2015, doi: http://dx.doi.org/10.1016/j.apenergy.2014.09.081.

[5] B. Zakeri and S. Syri, "Electrical energy storage systems: A comparative life cycle cost analysis," Renewable and Sustainable Energy Reviews, vol. 42, pp. 569-596, 2// 2015, doi: http://dx.doi.org/10.1016/j.rser.2014.10.011.

[6] C. Spanos, D. E. Turney, and V. Fthenakis, "Life-cycle analysis of flow-assisted nickel zinc-, manganese dioxide-, and valve-regulated lead-acid batteries designed for demand-charge reduction," Renewable and Sustainable Energy Reviews, vol. 43, pp. 478-494, 3// 2015, doi: http://dx.doi.org/10.1016/j.rser.2014.10.072.

[7] D. Larcher and J. M. Tarascon, "Towards greener and more sustainable batteries for electrical energy storage," Nat Chem, Review vol. 7, no. 1, pp. 19-29, 01//print 2015, doi: 10.1038/nchem.2085.

[8] D. O. Akinyele and R. K. Rayudu, "Review of energy storage technologies for sustainable power networks," Sustainable Energy Technologies and Assessments, vol. 8, pp. 74-91, 12// 2014, doi: http://dx.doi.org/10.1016/j.seta.2014.07.004.

[9] M. D. Charles J. Barnhart, Adam R. Brandt and Sally M. Benson, "The energetic implications of curtailing versus storing solar- and wind-generated electricity," Energy & Environmental Science, vol. 6, pp. 2804-2810, 2013

[10] M.-J. Kim and H. Peng, "Power management and design optimization of fuel cell/battery hybrid vehicles," Journal of Power Sources, vol. 165, no. 2, pp. 819-832, 3/20/ 2007, doi: http://dx.doi.org/10.1016/j.jpowsour.2006.12.038.

[11] L. Stuntz, "Bottling Electricity: Storage as a Strategic Tool for Managing Variability and Capacity Concerns in the Modern Grid ", United States, 2008. [Online]. Available: https://energy.gov/sites/prod/files/oeprod/DocumentsandMedia/final-energy-storage_12-16-08.pdf

[12] J. Kondoh et al., "Electrical energy storage systems for energy networks," Energy Conversion and Management, vol. 41, no. 17, pp. 1863-1874, 2000/11/01/ 2000, doi: http://dx.doi.org/10.1016/S0196-8904(00)00028-5.

[13] B. P. Roberts and C. Sandberg, "The Role of Energy Storage in Development of Smart Grids," Proceedings of the IEEE, vol. 99, no. 6, pp. 1139-1144, 2011, doi: 10.1109/JPROC.2011.2116752.

[14] P. Alotto, M. Guarnieri, and F. Moro, "Redox flow batteries for the storage of renewable energy: A review," Renewable and Sustainable Energy Reviews, vol. 29, pp. 325-335, 1// 2014, doi: http://dx.doi.org/10.1016/j.rser.2013.08.001.

[15] W. Wang, Q. Luo, B. Li, X. Wei, L. Li, and Z. Yang, "Recent Progress in Redox Flow Battery Research and Development," Advanced Functional Materials, vol. 23, no. 8, pp. 970-986, 2013, doi: 10.1002/adfm.201200694.

[16] T. M. I. Mahlia, T. J. Saktisahdan, A. Jannifar, M. H. Hasan, and H. S. C. Matseelar, "A review of available methods and development on energy storage; technology update," Renewable and Sustainable Energy Reviews, vol. 33, pp. 532-545, 5// 2014, doi: http://dx.doi.org/10.1016/j.rser.2014.01.068.

[17] B. R. Chalamala, T. Soundappan, G. R. Fisher, M. R. Anstey, V. V. Viswanathan, and M. L. Perry, "Redox Flow Batteries: An Engineering Perspective," Proceedings of the IEEE, vol. 102, no. 6, pp. 976-999, 2014, doi: 10.1109/JPROC.2014.2320317.

[18] B. Dunn, H. Kamath, and J.-M. Tarascon, "Electrical Energy Storage for the Grid: A Battery of Choices," Science, vol. 334, no. 6058, pp. 928-935, 2011, doi: 10.1126/science.1212741.

[19] A. Z. Weber, M. M. Mench, J. P. Meyers, P. N. Ross, J. T. Gostick, and Q. Liu, "Redox flow batteries: a review," Journal of Applied Electrochemistry, journal article vol. 41, no. 10, p. 1137, 2011, doi: 10.1007/s10800-011-0348-2.

[20] L. M. S. Moro, "Trends in redox flow battery technology and project REDOX2015," in 2013 International Conference on New Concepts in Smart Cities: Fostering Public and Private Alliances (SmartMILE), 11-13 Dec. 2013 2013, pp. 1-4, doi: 10.1109/SmartMILE.2013.6708218.

[21] M. Skyllas-Kazacos, M. H. Chakrabarti, S. A. Hajimolana, F. S. Mjalli, and M. Saleem, "Progress in Flow Battery Research and Development," Journal of The Electrochemical Society, vol. 158, no. 8, pp. R55-R79, August 1, 2011 2011, doi: 10.1149/1.3599565.

[22] H. M. Cheng, "Development of graphene-based materials for energy storage," in 2010 8th International Vacuum Electron Sources Conference and Nanocarbon, 14-16 Oct. 2010 2010, pp. 49-49, doi: 10.1109/IVESC.2010.5644354.

[23] G. Coppez, S. Chowdhury, and S. P. Chowdhury, "The importance of energy storage in renewable power generation: A review," ed, 2010, p. <xocs:firstpage xmlns:xocs=""/>.

[24] R. Fioravanti and Kema, "The importance of energy storage for system regulation," POWERGRID International, vol. 14, no. 10, p. 54, 2009.

[25] M. B. a. D. Roos. "How Power Grids Works." https://science.howstuffworks.com/environmental/energy/power.htm (accessed 30/10, 2018).

[26] S. Koohi-Kamali, V. V. Tyagi, N. A. Rahim, N. L. Panwar, and H. Mokhlis, "Emergence of energy storage technologies as the solution for reliable operation of smart power systems: A review," Renewable and Sustainable Energy Reviews, vol. 25, no. C, pp. 135-165, 2013, doi: 10.1016/j.rser.2013.03.056.

[27] M. Yazdanie, M. Densing, and A. Wokaun, "The role of decentralized generation and storage technologies in future energy systems planning for a rural agglomeration in Switzerland.(Special Section: On the Renewable and Nuclear Electricity: Opportunities, Challenges and Policy Recommendations)," Energy Policy, vol. 96, pp. 432-445, 2016.

[28] B. Zohuri. "Energy Storage Technologies and Their Role in Renewable Integration." https://www.geni.org/globalenergy/research/energy-storage-technologies/Energy-Storage-Technologies.pdf (accessed 30/10, 2018).

[29] C. Liu, F. Li, L.-P. Ma, and H.-M. Cheng, "Advanced Materials for Energy Storage," Advanced Materials, vol. 22, no. 8, pp. E28-E62, 2010, doi: 10.1002/adma.200903328.

[30] J. I. M. Skea and S. Nishioka, "Policies and practices for a low-carbon society," Climate Policy, vol. 8, no. sup1, pp. S5-S16, 2008/01/01 2008, doi: 10.3763/cpol.2008.0487.

[31] H. Ibrahim, A. Ilinca, and J. Perron, "Energy storage systems—Characteristics and comparisons," Renewable and Sustainable Energy Reviews, vol. 12, no. 5, pp. 1221-1250, 2008/06/01/ 2008, doi: http://dx.doi.org/10.1016/j.rser.2007.01.023.

[32] N. W. David Mackay, "The future role for energy storage in the UK Main Report," LONDON, 2011. Accessed: 09/08/2017. [Online]. Available: http://erpuk.org/wp-content/uploads/2014/10/52990-ERP-Energy-Storage-Report-v3.pdf

[33] E. J. Coster, J. M. A. Myrzik, B. Kruimer, and W. L. Kling, "Integration Issues of Distributed Generation in Distribution Grids," Proceedings of the IEEE, vol. 99, no. 1, pp. 28-39, 2011, doi: 10.1109/JPROC.2010.2052776.

[34] M. Świerczyński, R. Teodorescu, C. N. Rasmussen, P. Rodriguez, and H. Vikelgaard, "Overview of the energy storage systems for wind power integration enhancement," in Industrial Electronics (ISIE), 2010 IEEE International Symposium on, 2010: IEEE, pp. 3749-3756.

[35] S. Vazquez, S. Lukic, E. Galvan, L. G. Franquelo, J. M. Carrasco, and J. I. Leon, "Recent advances on Energy Storage Systems," in IECON 2011 - 37th Annual Conference of the IEEE Industrial Electronics Society, 7-10 Nov. 2011 2011, pp. 4636-4640, doi: 10.1109/IECON.2011.6120075.

[36] S. Manzetti and F. Mariasiu, "Electric vehicle battery technologies: From present state to future systems," Renewable and Sustainable Energy Reviews, vol. 51, pp. 1004-1012, 2015, doi: 10.1016/j.rser.2015.07.010.

[37] T. I. Evans and R. E. White, "A Review of Mathematical Modeling of the Zinc/Bromine Flow Cell and Battery," Journal of the Electrochemical Society, vol. 134, no. 11, pp. 2725-2733, 1987, doi: 10.1149/1.2100277.

[38] A. G. Boulanger, A. C. Chu, S. Maxx, and D. L. Waltz, "Vehicle Electrification: Status and Issues," Proceedings of the IEEE, vol. 99, no. 6, pp. 1116-1138, 2011, doi: 10.1109/JPROC.2011.2112750.

[39] P. Taylor, P. Butler, and W. Nerbun, "Lead/acid batteries in systems to improve power quality," Journal of Power Sources, vol. 67, no. 1, pp. 187-191, 1997, doi: 10.1016/S0378-7753(97)02548-2.

[40] N. S. Caetano, T. M. Mata, A. A. Martins, and M. C. Felgueiras, "New Trends in Energy Production and Utilization," Energy Procedia, vol. 107, pp. 7-14, 2017, doi: 10.1016/j.egypro.2016.12.122.

[41] X. Chen, W. Yu, D. Griffith, N. Golmie, and G. Xu, "On cascading failures and countermeasures based on energy storage in the smart grid," ed, 2014, pp. 291-296.

[42] J. G. Kim et al., "A review of lithium and non-lithium based solid state batteries," Journal of Power Sources, vol. 282, pp. 299-322, 2015, doi: 10.1016/j.jpowsour.2015.02.054.

[43] H. Roby, "flow batteries," 1 ed. ed: Oxford University Press, 2013.

[44] S. Wicki and E. G. Hansen, "Clean energy storage technology in the making: An innovation systems perspective on flywheel energy storage," Journal of Cleaner Production, vol. 162, pp. 1118-1134, 2017, doi: 10.1016/j.jclepro.2017.05.132.

[45] Y. Zhang, K. Yang, X. Li, and J. Xu, "The thermodynamic effect of thermal energy storage on compressed air energy storage system," Renewable Energy, vol. 50, pp. 227-235, 2013, doi: 10.1016/j.renene.2012.06.052.

[46] G. Alva, Y. Lin, and G. Fang, "An overview of thermal energy storage systems," Energy, vol. 144, pp. 341-378, 2018, doi: 10.1016/j.energy.2017.12.037.

[47] L. Zhencheng, L. Yu, and W. Hua, "The operation optimization model of pumped-hydro power storage station based on approximate dynamic programming," ed, 2014, pp. 215-220.

[48] S. Boehmer-Christiansen, "Fuel for Thought: Early June — Mid August 2012," Energy & Environment, vol. 23, no. 6-7, pp. 1105-1190, 2012, doi: 10.1260/0958-305X.23.6-7.1105.

[49] D. Elliott, Renewables : a review of sustainable energy supply options (Review of sustainable energy supply options). 2013.

[50] A. Price, "Storage technology and future developments," in Energy Storage: What's Next for the Grid?, 4-4 June 20155 2015, pp. 1-23, doi: 10.1049/ic.2015.0074.

[51] C. Imhoff, "Grid 2050: shaping system transformation," Public Utilities Fortnightly (1994), vol. 149, no. 8, p. 28, 2011.

[52] H. Chen, T. N. Cong, W. Yang, C. Tan, Y. Li, and Y. Ding, "Progress in electrical energy storage system: A critical review," Progress in Natural Science, vol. 19, no. 3, pp. 291-312, 3/10/ 2009, doi: http://dx.doi.org/10.1016/j.pnsc.2008.07.014.

[53] D. Zafirakis, "Modern Energy Storage Applications," in Handbook of Clean Energy Systems: John Wiley & Sons, Ltd, 2015.

[54] M. Farhadi and O. Mohammed, "Energy storage systems for high power applications," in 2015 IEEE Industry Applications Society Annual Meeting, 18-22 Oct. 2015 2015, pp. 1-7, doi: 10.1109/IAS.2015.7356787.

[55] S. Vazquez, S. M. Lukic, E. Galvan, L. G. Franquelo, and J. M. Carrasco, "Energy Storage Systems for Transport and Grid Applications," IEEE Transactions on Industrial Electronics, vol. 57, no. 12, pp. 3881-3895, 2010, doi: 10.1109/TIE.2010.2076414.

[56] K. C. Divya and J. Østergaard, "Battery energy storage technology for power systems—An overview," Electric Power Systems Research, vol. 79, no. 4, pp. 511-520, 4// 2009, doi: http://dx.doi.org/10.1016/j.epsr.2008.09.017.

[57] J. H. Teng, S. W. Luan, D. J. Lee, and Y. Q. Huang, "Optimal Charging/Discharging Scheduling of Battery Storage Systems for Distribution Systems Interconnected With Sizeable PV Generation Systems," IEEE Transactions on Power Systems, vol. 28, no. 2, pp. 1425-1433, 2013, doi: 10.1109/TPWRS.2012.2230276.

[58] A. Gabash and P. Li, "Active-Reactive Optimal Power Flow in Distribution Networks With Embedded Generation and Battery Storage," IEEE Transactions on Power Systems, vol. 27, no. 4, pp. 2026-2035, 2012, doi: 10.1109/TPWRS.2012.2187315.

[59] A. Sternberg and A. Bardow, "Power-to-What? - Environmental assessment of energy storage systems," Energy & Environmental Science, 10.1039/C4EE03051F vol. 8, no. 2, pp. 389-400, 2015, doi: 10.1039/C4EE03051F.

[60] M. Carbajales-Dale, C. J. Barnhart, and S. M. Benson, "Can we afford storage? A dynamic net energy analysis of renewable electricity generation supported by energy storage," Energy & Environmental Science, 10.1039/C3EE42125B vol. 7, no. 5, pp. 1538-1544, 2014, doi: 10.1039/C3EE42125B.

[61] M. Aneke and M. Wang, "Energy storage technologies and real life applications – A state of the art review," Applied Energy, vol. 179, pp. 350-377, 2016, doi: 10.1016/j.apenergy.2016.06.097.

[62] P. W. Parfomak, "EnergyStorage for Power Grids and Electric Transportation: A Technology Assessment," **Congressional Research Service**, pp. 1-146, 2012.

[63] M. Berre. "The Energy Storage Landscape in Japan." EU-JAPAN CENTRE FOR INDUSTRIAL COOPERATION.

https://www.eubusinessinjapan.eu/sites/default/files/energy_storage_landscape_in_japan.pdf (accessed 07/10, 2018).

[64] M. Budt, D. Wolf, R. Span, and J. Yan, "Compressed Air Energy Storage – An Option for Medium to Large Scale Electrical-energy Storage," Energy Procedia, vol. 88, pp. 698-702, 2016/06/01/ 2016, doi: http://dx.doi.org/10.1016/j.egypro.2016.06.046.

[65] R. B. Schainker and M. Nakhamkin, "Compressed -Air Energy Storage (CAES): Overview, Performance and Cost Data for 25MW to 220MW Plants," IEEE Transactions on Power Apparatus and Systems, vol. PAS-104, no. 4, pp. 790-795, 1985, doi: 10.1109/TPAS.1985.319075.

[66] J. Taylor and A. Halnes, "Analysis Of compressed air energy storage," in PCIC Europe 2010, 15-17 June 2010 2010, pp. 1-5.

[67] A. Rogers, A. Henderson, X. Wang, and M. Negnevitsky, "Compressed air energy storage: Thermodynamic and economic review," in 2014 IEEE PES General Meeting | Conference & Exposition, 27-31 July 2014 2014, pp. 1-5, doi: 10.1109/PESGM.2014.6939098.

[68] A. Moallemi, L. Machado, R. N. N. Koury, and F. J. P. Pujatti, "The effect of energy efficiency increase on a PV plant with a non-conventional energy storage system income," in 2016 7th Power Electronics and Drive Systems Technologies Conference (PEDSTC), 16-18 Feb. 2016 2016, pp. 457-463, doi: 10.1109/PEDSTC.2016.7556904.

[69] R. Madlener and J. Latz, "Economics of centralized and decentralized compressed air energy storage for enhanced grid integration of wind power," Applied Energy, vol. 101, pp. 299-309, 2013, doi: 10.1016/j.apenergy.2011.09.033.

[70] A. Cavallo, "Controllable and affordable utility-scale electricity from intermittent wind resources and compressed air energy storage (CAES)," Energy, vol. 32, no. 2, pp. 120-127, 2007, doi: 10.1016/j.energy.2006.03.018.

[71] WindSoHy. "Wind/CAES." WindSoHy's global engineering partner, Burns & McDonnell. http://windsohy.com/index.php?option=com_content&task=view&id=42&Itemid=24 (accessed 26/02, 2018).

[72] P. Li. "A Compressed Air Energy Storage (CAES) System for Wind Turbines." https://contest.techbriefs.com/2015/entries/sustainable-technologies/6164 (accessed 01/03, 2018).

[73] N. Gnanapragasam, D. Ryland, and S. Suppiah, "Status of energy storage options for electricity from nuclear power plants," in 2013 IEEE International Conference on Smart Energy Grid Engineering (SEGE), 28-30 Aug. 2013 2013, pp. 1-11, doi: 10.1109/SEGE.2013.6707910.

[74] D. Tarlock, "Hydro Law and the Future of Hydroelectric Power Generation in the United States," Vanderbilt Law Review, vol. 65, no. 6, pp. 1723-1767, 2012.

[75] A. H. Slocum, M. N. Haji, A. Z. Trimble, M. Ferrara, and S. J. Ghaemsaidi, "Integrated Pumped Hydro Reverse Osmosis systems," Sustainable Energy Technologies and Assessments, vol. 18, pp. 80-99, 2016, doi: 10.1016/j.seta.2016.09.003.

[76] T. Ma, H. Yang, and L. Lu, "Feasibility study and economic analysis of pumped hydro storage and battery storage for a renewable energy powered island," Energy Conversion and Management, vol. 79, no. C, pp. 387-397, 2014, doi: 10.1016/j.enconman.2013.12.047.

[77] D. Q. Hung and N. Mithulananthan, "Community energy storage and capacitor allocation in distribution systems," in AUPEC 2011, 25-28 Sept. 2011 2011, pp. 1-6.

[78] R. E. Voshall and A. Lee, "Capacitor Energy Storage Synthetic Testing of H.V.D.C. Circuit Breakers," Power Delivery, IEEE Transactions on, vol. 1, no. 1, pp. 185-190, 1986, doi: 10.1109/TPWRD.1986.4307906.

[79] A. F. ı.-F. C. Ponce de Le´on, J. Gonz´alez-Garc´ıa, D.A. Sz´anto, F.C. Walsh, "Redox flow cells for energy conversion," Journal of Power Sources, vol. 160, pp. 716–732, 2006.

[80] P. Zhao, H. Zhang, H. Zhou, J. Chen, S. Gao, and B. Yi, "Characteristics and performance of 10 kW class all-vanadium redox-flow battery stack," Journal of Power Sources, vol. 162, no. 2, pp. 1416-1420, 11/22/ 2006, doi: http://dx.doi.org/10.1016/j.jpowsour.2006.08.016.

[81] A. F. Regin, S. C. Solanki, and J. S. Saini, "Heat transfer characteristics of thermal energy storage system using PCM capsules: A review," Renewable and Sustainable Energy Reviews, vol. 12, no. 9, pp. 2438-2458, 2008/12/01/ 2008, doi: http://dx.doi.org/10.1016/j.rser.2007.06.009.

[82] Anonymous, "SolarReserve Moving Ahead on Southern California Solar Thermal Project," ed. Jacksonville, 2010.

[83] Anonymous, "SolarReserve Receives Final Licensing Decision for 150-Megawatt Rice Solar Energy Project in California," vol. 23, ed. Ontario, 2011, p. 3.

[84] M. Lanahan and P. C. Tabares-Velasco, "Seasonal Thermal-Energy Storage: A Critical Review on BTES Systems, Modeling, and System Design for Higher System Efficiency," in Energies vol. 10, ed, 2017.

[85] DELTASTORE. "J**anuary issue of BiogasJournal reports on integration of thermal storage systems into biogas plant heat circuits**." DELTASTORE Systems. http://archiv.farmatic.com/en/news/news/artikel/deltastore-thermal-energy-storage-in-the-news.html (accessed 02/03, 2018).

[86] S. Shili, A. Hijazi, A. Sari, X. Lin-Shi, and P. Venet, "Balancing Circuit New Control for Supercapacitor Storage System Lifetime Maximization," IEEE Transactions on Power Electronics, vol. 32, no. 6, pp. 4939-4948, 2017, doi: 10.1109/TPEL.2016.2602393.

[87] R. Sebastián and R. Peña-Alzola, "Control and simulation of a flywheel energy storage for a wind diesel power system," International Journal of Electrical Power and Energy Systems, vol. 64, pp. 1049-1056, 2015, doi: 10.1016/j.ijepes.2014.08.017.

[88] H. J. Bornemann and M. Sander, "Conceptual system design of a 5 MWh/100 MW superconducting flywheel energy storage plant for power utility applications," Applied Superconductivity, IEEE Transactions on, vol. 7, no. 2, pp. 398-401, 1997, doi: 10.1109/77.614513.

[89] KEELYNET. " **New flywheel energy storage system**." http://www.keelynet.com/news/080316j.html (accessed 02/03, 2018).

[90] O. Haas and E. J. Cairns, "Electrochemical energy storage," Annual Reports on the Progress of Chemistry - Section C, vol. 95, pp. 163-197, 1999.

[91] F. Beck and P. Rüetschi, "Rechargeable batteries with aqueous electrolytes," Electrochimica Acta, vol. 45, no. 15, pp. 2467-2482, 2000, doi: 10.1016/S0013-4686(00)00344-3.

[92] C. Ponce de Leon, A. Frias-Ferrer, J. Gonzalez-Garcia, D. A. Szanto, and F. C. Walsh, "Redox flow cells for energy conversion," Journal of Power Sources, vol. 160, no. 1, pp. 716-732, 2006.

[93] A. Oudalov, T. Buehler, and D. Chartouni, "Utility Scale Applications of Energy Storage," ed, 2008, pp. 1-7.

[94] G. L. Soloveichik, "Battery Technologies for Large-Scale Stationary Energy Storage," Annu. Rev. Chem. Biomol. Eng., vol. 2, pp. 503-527, 2011, doi: 10.1146/annurev-chembioeng-061010-114116.

[95] M. Bartolozzi, "Development of redox flow batteries. A historical bibliography," Journal of Power Sources, vol. 27, no. 3, pp. 219-234, 1989, doi: 10.1016/0378-7753(89)80037-0.

[96] A. Z. Weber, M. M. Mench, J. P. Meyers, P. N. Ross, J. T. Gostick, and Q. Liu, "Redox flow batteries: a review," Journal of Applied Electrochemistry, journal article vol. 41, no. 10, pp. 1137-1164, 2011, doi: 10.1007/s10800-011-0348-2.

[97] G. Soloveichik, "Flow Batteries: Current Status and Trends," in Chem. Rev. vol. 115, ed, 2015, pp. 11533-11558.

[98] F. Mitlitsky, B. Myers, and A. H. Weisberg, "Regenerative Fuel Cell Systems," Energy & Fuels, vol. 12, no. 1, pp. 56-71, 1998/01/01 1998, doi: 10.1021/ef970151w.

[99] S. Okashy, M. Noked, T. Zimrin, and D. Aurbach, "The study of activated carbon/CNT/MoO 3 electrodes for aqueous pseudo-capacitors," Journal of the Electrochemical Society, vol. 160, no. 9, pp. A1489-A1496, 2013, doi: 10.1149/2.084309jes.

[100] H. D. Yoo, E. Markevich, G. Salitra, D. Sharon, and D. Aurbach, "On the challenge of developing advanced technologies for electrochemical energy storage and conversion," Materials Today, vol. 17, no. 3, pp. 110-121, 2014, doi: 10.1016/j.mattod.2014.02.014.

[101] S. De-Leon. "High Power Rechargeable Lithium Battery Market." http://energyskeptic.com/2015/electric-vehicle-overview/ (accessed 25/08, 2018).

[102] A. Bostrom, A. Von Jouanne, T. K. A. Brekken, and A. Yokochi, "Supercapacitor energy storage systems for voltage and power flow stabilization," ed, 2013, pp. 230-237.

[103] F. Mitlitsky, B. Myers, and A. H. Weisberg, "Regenerative fuel cell systems," Energy and Fuels, vol. 12, no. 1, pp. 56-71, 1998, doi: 10.1021/ef970151w.

[104] J. Lu, L. Li, J. Park, Y. Sun, F. Wu, and K. Amine, "Aprotic and Aqueous Li-O-2 Batteries," in Chem. Rev. vol. 114, ed, 2014, pp. 5611-5640.

[105] J. Lee et al., "Metal-Air Batteries with High Energy Density: Li-Air versus Zn-Air," in Adv. Energy Mater. vol. 1, ed, 2011, pp. 34-50.

[106] J. Christensen et al., "A Critical Review of Li/Air Batteries," in J. Electrochem. Soc. vol. 159, ed, 2012, pp. R1-R30.

[107] L. Yanguang et al., "Advanced zinc-air batteries based on high-performance hybrid electrocatalysts," Nature Communications, vol. 4, p. 1805, 2013, doi: 10.1038/ncomms2812.

[108] P. Leung, X. Li, C. Ponce De Len, L. Berlouis, C. T. J. Low, and F. C. Walsh, "Progress in redox flow batteries, remaining challenges and their applications in energy storage," RSC Adv., vol. 2, no. 27, pp. 10125-10156, 2012, doi: 10.1039/c2ra21342g.

[109] G. L. Soloveichik, "Regenerative Fuel Cells for Energy Storage," Proceedings of the IEEE, vol. 102, no. 6, pp. 964-975, 2014, doi: 10.1109/JPROC.2014.2314955.

[110] C. Ponce de León, A. Frías-Ferrer, J. González-García, D. A. Szánto, and F. C. Walsh, "Redox flow cells for energy conversion," Journal of Power Sources, vol. 160, no. 1, pp. 716-732, 9/29/ 2006, doi: http://dx.doi.org/10.1016/j.jpowsour.2006.02.095.

[111] M. R. Mohamed, S. M. Sharkh, and F. C. Walsh, "Redox flow batteries for hybrid electric vehicles: Progress and challenges," ed, 2009, pp. 551-557.

[112] D. Oei, "Chemically regenerative redox fuel cells," Journal of Applied Electrochemistry, vol. 12, no. 1, pp. 41-51, 1982, doi: 10.1007/BF01112063.

[113] S. H. Bergens, C. B. Gorman, and G. M. Whitesides, "A Redox Fuel Cell That Operates with Methane as Fuel at 120°C," Science, vol. 265, no. 5177, pp. 1418-1420, 1994, doi: 10.1126/science.265.5177.1418.

[114] A. Creeth, "Pt-free PEM cathode technology with fundamental durability benefits: FlowCath®," Fuel Cells Bulletin, vol. 2011, no. 4, pp. 12-15, 2011, doi: 10.1016/S1464-2859(11)70126-2.

[115] Z. Xie, Q. Liu, Z. Chang, and X. Zhang, "The developments and challenges of cerium half-cell in zinc–cerium redox flow battery for energy storage," Electrochimica Acta, vol. 90, pp. 695-704, 2/15/ 2013, doi: http://dx.doi.org/10.1016/j.electacta.2012.12.066.

[116] B. Li et al., "Ambipolar zinc-polyiodide electrolyte for a high-energy density aqueous redox flow battery," Nature Communications, Article vol. 6, p. 6303, 02/24/online 2015, doi: 10.1038/ncomms7303http://www.nature.com/articles/ncomms7303#supplementary-information.

[117] M. Wu, M. Liu, G. Long, K. Wan, Z. Liang, and T. S. Zhao, "A novel high-energy-density positive electrolyte with multiple redox couples for redox flow batteries," Applied Energy, vol. 136, pp. 576-581, 12/31/ 2014, doi: http://dx.doi.org/10.1016/j.apenergy.2014.09.076.

[118] S. H. Oh et al., "A metal-free and all-organic redox flow battery with polythiophene as the electroactive species," Journal of Materials Chemistry A, 10.1039/C4TA04730C vol. 2, no. 47, pp. 19994-19998, 2014, doi: 10.1039/C4TA04730C.

[119] L. Sanz, D. Lloyd, E. Magdalena, J. Palma, M. Anderson, and K. Kontturi, "Study and characterization of positive electrolytes for application in the aqueous all-copper redox flow battery," Journal of Power Sources, vol. 278, pp. 175-182, 3/15/ 2015, doi: http://dx.doi.org/10.1016/j.jpowsour.2014.12.034.

[120] L. Sanz, D. Lloyd, E. Magdalena, J. Palma, and K. Kontturi, "Description and performance of a novel aqueous all-copper redox flow battery," Journal of Power Sources, vol. 268, pp. 121-128, 12/5/ 2014, doi: http://dx.doi.org/10.1016/j.jpowsour.2014.06.008.

[121] D. Lloyd, E. Magdalena, L. Sanz, L. Murtomäki, and K. Kontturi, "Preparation of a cost-effective, scalable and energy efficient all-copper redox flow battery," Journal of Power Sources, vol. 292, pp. 87-94, 10/1/ 2015, doi: http://dx.doi.org/10.1016/j.jpowsour.2015.04.176.

[122] P. Leung, "DEVELOPMENT OF A ZINC-CERIUM REDOX FLOW BATTERY," Degree of Doctor of Philosophy PhD, FACULTY OF ENGINEERING & THE ENVIRONMENT SCHOOL OF ENGINEERING SCIENCES, UNIVERSITY OF SOUTHAMPTON United Kingdom, 2011. [Online]. Available: https://eprints.soton.ac.uk/333334/1/PK_Leung_PhD_Development_of_Zn-Ce_redox_flow_battery.pdf

[123] M. C. Wu, T. S. Zhao, H. R. Jiang, Y. K. Zeng, and Y. X. Ren, "High-performance zinc bromine flow battery via improved design of electrolyte and electrode," Journal of Power Sources, vol. 355, pp. 62-68, 2017, doi: 10.1016/j.jpowsour.2017.04.058.

[124] A. Parasuraman, T. M. Lim, C. Menictas, and M. Skyllas-Kazacos, "Review of material research and development for vanadium redox flow battery applications," Electrochimica Acta, vol. 101, pp. 27-40, 7/1/ 2013, doi: http://dx.doi.org/10.1016/j.electacta.2012.09.067.

[125] Á. Cunha, J. Martins, N. Rodrigues, and F. P. Brito, "Vanadium redox flow batteries: a technology review," International Journal of Energy Research, vol. 39, no. 7, pp. 889-918, 2015, doi: 10.1002/er.3260.

[126] W. A. Braff, M. Z. Bazant, and C. R. Buie, "Membrane-less hydrogen bromine flow battery," Nature Communications, Article vol. 4, p. 2346, 08/16/online 2013, doi: 10.1038/ncomms3346.

[127] K. T. Cho, P. Albertus, V. Battaglia, A. Kojic, V. Srinivasan, and A. Z. Weber, "Optimization and Analysis of High-Power Hydrogen/Bromine-Flow Batteries for Grid-Scale Energy Storage," Energy Technology, vol. 1, no. 10, pp. 596-608, 2013, doi: 10.1002/ente.201300108.

[128] C. Bae*, E. P. L. Roberts, M. H. Chakrabarti, and M. Saleem, "All-Chromium Redox Flow Battery for Renewable Energy Storage," International Journal of Green Energy, vol. 8, no. 2, pp. 248-264, 2011/03/09 2011, doi: 10.1080/15435075.2010.549598.

[129] X. Xing, D. Zhang, and Y. Li, "A non-aqueous all-cobalt redox flow battery using 1,10-phenanthrolinecobalt(II) hexafluorophosphate as active species," Journal of Power Sources, vol. 279, pp. 205-209, 4/1/ 2015, doi: http://dx.doi.org/10.1016/j.jpowsour.2015.01.011.

[130] F. C. Walsh et al., "The Development of Zn–Ce Hybrid Redox Flow Batteries for Energy Storage and Their Continuing Challenges," ChemPlusChem, vol. 80, no. 2, pp. 288-311, 2015, doi: 10.1002/cplu.201402103.

[131] P. K. Leung, C. Ponce-de-León, C. T. J. Low, A. A. Shah, and F. C. Walsh, "Characterization of a zinc–cerium flow battery," Journal of Power Sources, vol. 196, no. 11, pp. 5174-5185, 6/1/ 2011, doi: http://dx.doi.org/10.1016/j.jpowsour.2011.01.095.

[132] D. L. a. T. B. Reddy, HANDBOOK OF BATTERIES, Third Edition ed. The McGraw-Hill Companies, 1995.

[133] R. G. A. Wills, J. Collins, D. Stratton-Campbell, C. T. J. Low, D. Pletcher, and F. C. Walsh, "Developments in the soluble lead-acid flow battery," Journal of Applied Electrochemistry, vol. 5, no. 40, pp. 955–965, 2010.

[134] P. E. a. P. L. Nancy Clark, "Development df Zinc/Bromine Batteries for Load-Leveling Applications: Phase 2 Final Report," Sandia National Laboratories, 1999, issue Issued by Sandia National Laboratories, operated for the United States DepaItment of Energy by Sandia Corporation. [Online]. Available: http://prod.sandia.gov/techlib/access-control.cgi/1999/992691.pdf

[135] P. K. Leung, C. Ponce-De-León, F. J. Recio, P. Herrasti, and F. C. Walsh, "Corrosion of the zinc negative electrode of zinc-cerium hybrid redox flow batteries in methanesulfonic acid Batteries," Journal of Applied Electrochemistry, Article vol. 44, no. 9, pp. 1025-1035, 2014, doi: 10.1007/s10800-014-0714-y.

[136] M. Rychcik and M. Skyllas-Kazacos, "Characteristics of a new all-vanadium redox flow battery," Journal of Power Sources, vol. 22, no. 1, pp. 59-67, 1988, doi: 10.1016/0378-7753(88)80005-3.

[137] E. Sum, M. Rychcik, and M. Skyllas-Kazacos, "Investigation of the V(V)/V(IV) system for use in the positive half-cell of a redox battery," Journal of Power Sources, vol. 16, no. 2, pp. 85-95, 1985, doi: 10.1016/0378-7753(85)80082-3.

[138] E. Sum and M. Skyllas-Kazacos, "A study of the V(II)/V(III) redox couple for redox flow cell applications," Journal of Power Sources, vol. 15, no. 2, pp. 179-190, 1985, doi: 10.1016/0378-7753(85)80071-9.

[139] R. Bush and G. Wolf, "Energy Storage Becomes A Virtual Power Plant," Transmission & Distribution World, pp. 8-11, 2009.

[140] X. Wu et al., "Microwave-treated graphite felt as the positive electrode for all-vanadium redox flow battery," Journal of Power Sources, vol. 263, pp. 104-109, 2014, doi: 10.1016/j.jpowsour.2014.04.035.

[141] C. Flox et al., "Active nano-CuPt3 electrocatalyst supported on graphene for enhancing reactions at the cathode in all-vanadium redox flow batteries," vol. 50, ed, 2012, pp. 2372-2374.

[142] K. J. Kim et al., "Novel catalytic effects of Mn 3 O 4 for all vanadium redox flow batteries," Chem. Commun., vol. 48, no. 44, pp. 5455-5457, 2012, doi: 10.1039/c2cc31433a.

[143] Y. Shen, H. Xu, P. Xu, X. Wu, Y. Dong, and L. Lu, "Electrochemical catalytic activity of tungsten trioxide- modified graphite felt toward VO2+/VO2+redox reaction," Electrochimica Acta, vol. 132, pp. 37-41, 2014, doi: 10.1016/j.electacta.2014.03.107.

[144] F. Rahman and M. Skyllas-Kazacos, "Solubility of vanadyl sulfate in concentrated sulfuric acid solutions," Journal of Power Sources, vol. 72, no. 2, pp. 105-110, 1998, doi: 10.1016/S0378-7753(97)02692-X.

[145] F. Rahman and M. Skyllas-Kazacos, "Vanadium redox battery: Positive half-cell electrolyte studies," Journal of Power Sources, vol. 189, no. 2, pp. 1212-1219, 2009, doi: 10.1016/j.jpowsour.2008.12.113.

[146] J. Zhang et al., "Effects of additives on the stability of electrolytes for all-vanadium redox flow batteries," Journal of Applied Electrochemistry, vol. 41, no. 10, pp. 1215-1221, 2011, doi: 10.1007/s10800-011-0312-1.

[147] M. Skyllas-Kazacos, L. Cao, M. Kazacos, N. Kausar, and A. Mousa, "Vanadium Electrolyte Studies for the Vanadium Redox Battery—A Review," vol. 9, ed, 2016, pp. 1521-1543.

[148] E. Valero-Ruiz, M. I. Gonzlez-Snchez, C. Batchelor-Mcauley, and R. G. Compton, "Halogen mediated voltammetric oxidation of biological thiols and disulfides," Analyst, vol. 141, no. 1, pp. 144-149, 2015, doi: 10.1039/c5an01955a.

[149] G. Wang et al., "Several ionic organic compounds as positive electrolyte additives for a vanadium redox flow battery," RSC Adv., vol. 4, no. 108, pp. 63025-63035, 2014, doi: 10.1039/c4ra09108f.

[150] M. Vijayakumar, W. Wang, Z. Nie, V. Sprenkle, and J. Hu, "Elucidating the higher stability of vanadium(V) cations in mixed acid based redox flow battery electrolytes," Journal of Power Sources, vol. 241, pp. 173-177, 2013, doi: 10.1016/j.jpowsour.2013.04.072.

[151] L. Li et al., "A stable vanadium redox-flow battery with high energy density for large-scale energy storage," Advanced Energy Materials, vol. 1, no. 3, pp. 394-400, 2011, doi: 10.1002/aenm.201100008.

[152] C. Flox et al., "Highly electrocatalytic flexible nanofiber for improved vanadium-based redox flow battery cathode electrodes," RSC Adv., vol. 3, no. 30, pp. 12056-12059, 2013, doi: 10.1039/c3ra40463c.

[153] Q. Xu, T. S. Zhao, and P. K. Leung, "Numerical investigations of flow field designs for vanadium redox flow batteries," Applied Energy, vol. 105, pp. 47-56, 5// 2013, doi: http://dx.doi.org/10.1016/j.apenergy.2012.12.041.

[154] M. L. Perry, R. M. Darling, and R. Zaffou, "High power density redox flow battery cells," vol. 53, ed, 2013, pp. 7-16.

[155] D. Schulte, J. Sauer, B. Drillkens, D. U. Schulte, and D. U. Sauer, "Nafion hybrid membranes for use in redox flow batteries," Journal of the Electrochemical Society, vol. 157, no. 9, pp. A989-A992, 2010, doi: 10.1149/1.3456625.

[156] X. Xi, C. Ding, H. Zhang, X. Li, Y. Cheng, and H. Zhang, "Solvent responsive silica composite nanofiltration membrane with controlled pores and improved ion selectivity for vanadium flow battery application," Journal of Power Sources, vol. 274, pp. 1126-1134, 2015, doi: 10.1016/j.jpowsour.2014.10.160.

[157] C. Jia, Y. Cheng, X. Ling, G. Wei, J. Liu, and C. Yan, "Sulfonated Poly(Ether Ether Ketone)/Functionalized Carbon Nanotube Composite Membrane for Vanadium Redox Flow Battery Applications," Electrochimica Acta, vol. 153, pp. 44-48, 2015, doi: 10.1016/j.electacta.2014.11.123.

[158] D. Chen and X. Li, "Sulfonated poly(ether ether ketone) membranes containing pendent carboxylic acid groups and their application in vanadium flow battery," Journal of Power Sources, vol. 247, pp. 629-635, 2014, doi: 10.1016/j.jpowsour.2013.09.006.

[159] W. Dai, Y. Shen, Z. Li, L. Yu, J. Xi, and X. Qiu, "SPEEK/Graphene oxide nanocomposite membranes with superior cyclability for highly efficient vanadium redox flow battery," J. Mater. Chem. A, vol. 2, no. 31, pp. 12423-12432, 2014, doi: 10.1039/c4ta02124j.

[160] Y. Li, X. Li, J. Cao, W. Xu, and H. Zhang, "Composite porous membranes with an ultrathin selective layer for vanadium flow batteries," Chem. Commun., vol. 50, no. 35, pp. 4596-4599, 2014, doi: 10.1039/c3cc49729a.

[161] T. Mohammadi and M. S. Kazacos, "Modification of anion-exchange membranes for vanadium redox flow battery applications," Journal of Power Sources, vol. 63, no. 2, pp. 179-186, 1996, doi: 10.1016/S0378-7753(96)02463-9.

[162] D. Chen, M. A. Hickner, E. Agar, and E. C. Kumbur, "Selective anion exchange membranes for high coulombic efficiency vanadium redox flow batteries," Electrochemistry Communications, vol. 26, pp. 37-40, 2013, doi: 10.1016/j.elecom.2012.10.007.

[163] B. Turker, S. Arroyo Klein, E.-M. Hammer, B. Lenz, and L. Komsiyska, "Modeling a vanadium redox flow battery system for large scale applications," Energy Conversion and Management, vol. 66, pp. 26-32, 2013, doi: 10.1016/j.enconman.2012.09.009.

[164] L. J. Ontiveros and P. E. Mercado, "Modeling of a Vanadium Redox Flow Battery for power system dynamic studies," International Journal of Hydrogen Energy, vol. 39, no. 16, pp. 8720-8727, 2014, doi: 10.1016/j.ijhydene.2013.12.042.

[165] B. Xiong, J. Zhao, K. J. Tseng, M. Skyllas-Kazacos, T. M. Lim, and Y. Zhang, "Thermal hydraulic behavior and efficiency analysis of an all-vanadium redox flow battery," Journal of Power Sources, vol. 242, pp. 314-324, 2013, doi: 10.1016/j.jpowsour.2013.05.092.

[166] K. W. Knehr, E. Agar, C. R. Dennison, A. R. Kalidindi, and E. C. Kumbur, "A Transient Vanadium Flow Battery Model Incorporating Vanadium Crossover and Water Transport through the Membrane," Journal of The Electrochemical Society, vol. 159, no. 9, pp. 1446-1459, 2012.

[167] G. Merei, S. Adler, D. Magnor, M. Leuthold, and D. U. Sauer, "Multi-physics Model for a Vanadium Redox Flow Battery," Energy Procedia, vol. 46, pp. 194-203, 2014, doi: 10.1016/j.egypro.2014.01.173.

[168] F. T. Wandschneider et al., "Model of a vanadium redox flow battery with an anion exchange membrane and a Larminie-correction," Journal of Power Sources, vol. 272, pp. 436-447, 2014, doi: 10.1016/j.jpowsour.2014.08.082.

[169] Z. Wei, J. Zhao, M. Skyllas-Kazacos, and B. Xiong, "Dynamic thermal-hydraulic modeling and stack flow pattern analysis for all-vanadium redox flow battery," Journal of Power Sources, vol. 260, pp. 89-99, 2014, doi: 10.1016/j.jpowsour.2014.02.108.

[170] Y. Ohki, "Redox Flow Battery System for the Stable Supply of Renewable Energy," IEEE Electr. Insul. Mag., vol. 30, no. 6, pp. 48-50, 2014.

[171] A. A. S. Gareth Kear, and Frank C. Walsh, "Development of the all-vanadium redox flow battery for energy storage: a review of technological, financial and policy aspects," INTERNATIONAL JOURNAL OF ENERGY RESEARCH, 2011.

[172] L. Joerissen, J. Garche, C. Fabjan, and G. Tomazic, "Possible use of vanadium redox-flow batteries for energy storage in small grids and stand-alone photovoltaic systems," Journal of Power Sources, vol. 127, no. 1, pp. 98-104, 2004, doi: 10.1016/j.jpowsour.2003.09.066.

[173] M. Zhang, M. Moore, J. Watson, T. A. Zawodzinski, and R. M. Counce, "Capital Cost Sensitivity Analysis of an All-Vanadium Redox-Flow Battery," J. Electrochem. Soc., vol. 159, no. 8, pp. A1183-A1188, 2012, doi: 10.1149/2.041208jes.

[174] W. Wang et al., "A new redox flow battery using Fe/V redox couples in chloride supporting electrolyte," Energy Environ. Sci., vol. 4, no. 10, pp. 4068-4073, 2011, doi: 10.1039/c0ee00765j.

[175] W. Wang et al., "A new Fe/V redox flow battery using a sulfuric/chloric mixed-acid supporting electrolyte," Advanced Energy Materials, vol. 2, no. 4, pp. 487-493, 2012, doi: 10.1002/aenm.201100527.

[176] B. Li et al., "Fe/V redox flow battery electrolyte investigation and optimization," Journal of Power Sources, vol. 229, pp. 1-5, 2013, doi: 10.1016/j.jpowsour.2012.11.119.

[177] L. H. Thaller, "Electrically rechargeable REDOX flow cell," (in English), United States Patent US-PATENT-3,996,064, US-PATENT-APPL-SN-606891, NASA-CASE-LEW-12220-1, **Aug.** 22, **1975**, 1976. [Online]. Available: https://ntrs.nasa.gov/search.jsp?R=19770007638

[178] L. H. Thaller, "Redox flow cell energy storage systems," (in English), United States Patent Appl. 19790016271, Jan 01, 1979, 1979. [Online]. Available: https://ntrs.nasa.gov/search.jsp?R=19790016271

[179] R. F. H. Gahn, N. H. Johnson, J. A., "Cycling Performance of the Iron-Chromium Redox Energy Storage System," Patent 85N27387 Patent Appl. 19850019076, 1985. [Online]. Available: https://ntrs.nasa.gov/search.jsp?R=19850019076

[180] M. Lopezatalaya, G. Codina, Perez, Jr., J. Vazquez, A. Aldaz, and M. A. Climent, "BEHAVIOR OF THE CR(III)/CR(II) REACTION ON GOLD GRAPHITE-ELECTRODES - APPLICATION TO REDOX FLOW STORAGE CELL," J. Power Sources, vol. 35, no. 3, pp. 225-234, 1991.

[181] D. A. Johnson and M. A. Reid, "CHEMICAL AND ELECTROCHEMICAL BEHAVIOR OF THE Cr(III)/Cr(II) HALF-CELL IN THE IRON-CHROMIUM REDOX ENERGY STORAGE SYSTEM," Journal of the Electrochemical Society, vol. 132, no. 5, pp. 1058-1062, 1985.

[182] R. F. H. Gahn, N., "Negative-Electrode Catalysts for Fe/Cr Redox Cells," (in English), United State Patent LEW-14028, Nov 04, 1995, 1987. [Online]. Available: https://ntrs.nasa.gov/search.jsp?R=19870000068

[183] C. H. Bae, E. P. L. Roberts, and R. A. W. Dryfe, "Chromium redox couples for application to redox flow batteries," Electrochimica Acta, vol. 48, no. 3, pp. 279-287, 2002, doi: 10.1016/S0013-4686(02)00649-7.

[184] Y. K. Zeng, T. S. Zhao, X. L. Zhou, J. Zou, and Y. X. Ren, "A hydrogen-ferric ion rebalance cell operating at low hydrogen concentrations for capacity restoration of iron-chromium redox flow batteries," Journal of Power Sources, vol. 352, pp. 77-82, 2017, doi: 10.1016/j.jpowsour.2017.03.125.

[185] R. J. Remick and P. G. P. Ang, "Electrically rechargeable anionically active reduction-oxidation electrical storage-supply system," United States, 1984. [Online]. Available: https://www.osti.gov/biblio/5963537

[186] H. Haller and S. Riedel, "Recent Discoveries of Polyhalogen Anions – from Bromine to Fluorine," Zeitschrift für anorganische und allgemeine Chemie, vol. 640, no. 7, pp. 1281-1291, 2014, doi: 10.1002/zaac.201400085.

[187] P. Zhao, H. Zhang, H. Zhou, and B. Yi, "Nickel foam and carbon felt applications for sodium polysulfide/bromine redox flow battery electrodes," Electrochimica Acta, vol. 51, no. 6, pp. 1091-1098, 2005, doi: 10.1016/j.electacta.2005.06.008.

[188] I. E. L. Stephens, C. Ducati, and D. J. Fray, "Correlating microstructure and activity for polysulfide reduction and oxidation at WS 2 electrocatalysts," Journal of the Electrochemical Society, vol. 160, no. 6, pp. A757-A768, 2013, doi: 10.1149/2.027306jes.

[189] D. P. Scamman, G. W. Reade, and E. P. L. Roberts, "Numerical modelling of a bromide-polysulphide redox flow battery. Part 2: Evaluation of a utility-scale system," Journal of Power Sources, vol. 189, no. 2, pp. 1231-1239, 2009/04/15/ 2009, doi: http://dx.doi.org/10.1016/j.jpowsour.2009.01.076.

[190] D. P. Scamman, G. W. Reade, and E. P. L. Roberts, "Numerical modelling of a bromide–polysulphide redox flow battery: Part 1: Modelling approach and validation for a pilot-scale system," Journal of Power Sources, vol. 189, no. 2, pp. 1220-1230, 2009, doi: 10.1016/j.jpowsour.2009.01.071.

[191] H. Zhou, H. Zhang, P. Zhao, and B. Yi, "A comparative study of carbon felt and activated carbon based electrodes for sodium polysulfide/bromine redox flow battery," Electrochimica Acta, vol. 51, no. 28, pp. 6304-6312, 2006, doi: 10.1016/j.electacta.2006.03.106.

[192] M. Skyllas-Kazacos, "Novel vanadium chloride/polyhalide redox flow battery," Journal of Power Sources, vol. 124, no. 1, pp. 299-302, 2003, doi: 10.1016/S0378-7753(03)00621-9.

[193] M. Skyllas-Kazacos and N. Milne, "Evaluation of iodide and titanium halide redox couple combinations for common electrolyte redox flow cell systems," Journal of Applied Electrochemistry, vol. 41, no. 10, pp. 1233-1243, 2011, doi: 10.1007/s10800-011-0287-y.

[194] J. D. Giner and H. H. Stark, "Redox battery including a bromine positive electrode and a chromium ion negative electrode and method," United States, 1984-09-04, 1984. [Online]. Available: https://www.osti.gov/biblio/5963541

[195] H. Kaneko and K. Nozaki, "Redox battery," (in English), United States Patent US 4362791, 1982. [Online]. Available: https://www.osti.gov/biblio/6532624

[196] W. Kristina, D. Emil, K. Denes, and B. Anders, "Organic Redox Species in Aqueous Flow Batteries: Redox Potentials, Chemical Stability and Solubility," Scientific Reports, vol. 6, no. 1, 2016, doi: 10.1038/srep39101.

[197] M. Yao, H. Senoh, S.-I. Yamazaki, Z. Siroma, T. Sakai, and K. Yasuda, "High-capacity organic positive-electrode material based on a benzoquinone derivative for use in rechargeable lithium batteries," Journal of Power Sources, vol. 195, no. 24, pp. 8336-8340, 2010, doi: 10.1016/j.jpowsour.2010.06.069.

[198] W. Xu et al., "Factors affecting the battery performance of anthraquinone-based organic cathode materials," Journal of Materials Chemistry, vol. 22, no. 9, pp. 4032-4039, 2012, doi: 10.1039/c2jm15764k.

[199] J. R. Ferrell Iii et al., "Exploring the fuel limits of direct oxidation proton exchange membrane fuel cells with platinum based electrocatalysts," Journal of the Electrochemical Society, vol. 159, no. 4, pp. B371-B377, 2012, doi: 10.1149/2.029204jes.

[200] M. Quan, D. Sanchez, M. F. Wasylkiw, and D. K. Smith, "Voltammetry of quinones in unbuffered aqueous solution: reassessing the roles of proton transfer and hydrogen bonding in the aqueous electrochemistry of quinones," Journal of the American Chemical Society, vol. 129, no. 42, p. 12847, 2007, doi: 10.1021/ja0743083.

[201] Y. Xu, Y. Wen, J. Cheng, G. Cao, and Y. Yang, "Study on a single flow acid Cd–chloranil battery," Electrochemistry Communications, vol. 11, no. 7, pp. 1422-1424, 2009, doi: 10.1016/j.elecom.2009.05.021.

[202] Y. Xu, Y.-H. Wen, J. Cheng, G.-P. Cao, and Y.-S. Yang, "A study of tiron in aqueous solutions for redox flow battery application," Electrochimica Acta, vol. 55, no. 3, pp. 715-720, 2010, doi: 10.1016/j.electacta.2009.09.031.

[203] B. Huskinson et al., "A metal-free organic-inorganic aqueous flow battery," Nature, Letter vol. 505, no. 7482, pp. 195-198, 01/09/print 2014, doi: 10.1038/nature12909.
[204] H. Brian et al., "A metal-free organic–inorganic aqueous flow battery," Nature, vol. 505, no. 7482, p. 195, 2014, doi: 10.1038/nature12909.
[205] B. Yang, L. Hoober-Burkhardt, F. Wang, G. Prakash, and Narayanan, Sr., "An Inexpensive Aqueous Flow Battery for Large-Scale Electrical Energy Storage Based on Water-Soluble Organic Redox Couples," J. Electrochem. Soc., vol. 161, no. 9, pp. A1371-A1380, 2014, doi: 10.1149/2.1001409jes.
[206] S. S. Bhogilla, H. Ito, A. Kato, and A. Nakano, "Research and development of a laboratory scale Totalized Hydrogen Energy Utilization System," International Journal of Hydrogen Energy, vol. 41, no. 2, pp. 1224-1236, 2016/01/12/ 2016, doi: https://doi.org/10.1016/j.ijhydene.2015.10.105.
[207] P. J. Bonitatibus, Jr., S. Chakraborty, M. D. Doherty, O. Siclovan, W. D. Jones, and G. L. Soloveichik, "Reversible catalytic dehydrogenation of alcohols for energy storage.(CHEMISTRY)(Report)," vol. 112, no. 6, p. 1687, 2015, doi: 10.1073/pnas.1420199112.
[208] R. H. Crabtree, "Hydrogen storage in liquid organic heterocycles," Energy & Environmental Science, vol. 1, no. 1, pp. 134-138, 2008, doi: 10.1039/b805644g.
[209] C. M. Araujo et al., "Fuel selection for a regenerative organic fuel cell/flow battery: thermodynamic considerations," Energy Environ. Sci., vol. 5, no. 11, pp. 9534-9542, 2012, doi: 10.1039/c2ee22749e.
[210] T. Yamamura, Y. Shiokawa, H. Yamana, and H. Moriyama, "Electrochemical investigation of uranium beta-diketonates for all-uranium redox flow battery," Electrochim. Acta, vol. 48, no. 1, pp. 43-50, 2002, doi: 10.1016/S0013-4686(02)00546-7.
[211] T. Yamamura, K. Shirasaki, Y. Shiokawa, Y. Nakamura, and S. Y. Kim, "Characterization of tetraketone ligands for active materials of all-uranium redox flow battery," Journal of Alloys and Compounds, vol. 374, no. 1, pp. 349-353, 2004, doi: 10.1016/j.jallcom.2003.11.117.
[212] Y. Shiokawa, T. Yamamura, and K. Shirasaki, "Energy Efficiency of an Uranium Redox-Flow Battery Evaluated by the Butler–Volmer Equation," Journal of the Physical Society of Japan, vol. 75, no. Suppl, pp. 137-142, 2006/01/01 2006, doi: 10.1143/JPSJS.75S.137.
[213] K. Hasegawa, A. Kimura, T. Yamamura, and Y. Shiokawa, "Estimation of energy efficiency in neptunium redox flow batteries by the standard rate constants," Journal of Physics and Chemistry of Solids, vol. 66, no. 2, pp. 593-595, 2005, doi: 10.1016/j.jpcs.2004.07.018.
[214] T. Yamamura, N. Watanabe, and Y. Shiokawa, "Energy efficiency of neptunium redox battery in comparison with vanadium battery," Journal of Alloys and Compounds, vol. 408, pp. 1260-1266, 2006, doi: 10.1016/j.jallcom.2005.04.174.
[215] T. Yamamura, N. Watanabe, T. Yano, and Y. Shiokawa, "Electron-transfer kinetics of Np3+/Np4+, NpO2+/NpO22+, V2+/V3+, and VO2+/VO2+ at carbon electrodes," J. Electrochem. Soc., vol. 152, no. 4, pp. A830-A836, 2005, doi: 10.1149/1.1870794.
[216] D. Lloyd, T. Vainikka, and K. Kontturi, "The development of an all copper hybrid redox flow battery using deep eutectic solvents," Electrochimica Acta, vol. 100, pp. 18-23, 2013, doi: 10.1016/j.electacta.2013.03.130.
[217] Q. Liu, A. E. S. Sleightholme, A. A. Shinkle, Y. Li, and L. T. Thompson, "Non-aqueous vanadium acetylacetonate electrolyte for redox flow batteries," Electrochemistry Communications, vol. 11, no. 12, pp. 2312-2315, 2009, doi: 10.1016/j.elecom.2009.10.006.

[218] A. A. Shinkle, A. E. S. Sleightholme, L. D. Griffith, L. T. Thompson, and C. W. Monroe, "Degradation mechanisms in the non-aqueous vanadium acetylacetonate redox flow battery," Journal of Power Sources, vol. 206, pp. 490-496, 2012, doi: 10.1016/j.jpowsour.2010.12.096.

[219] A. A. Shinkle, T. J. Pomaville, A. E. S. Sleightholme, L. T. Thompson, and C. W. Monroe, "Solvents and supporting electrolytes for vanadium acetylacetonate flow batteries," Journal of Power Sources, vol. 248, pp. 1299-1305, 2014, doi: 10.1016/j.jpowsour.2013.10.034.

[220] J. Mun, M. Lee, J. W. Park, D. Oh, D. Lee, and S. G. Doo, "Non-Aqueous Redox Flow Batteries with Nickel and Iron Tris(2,2 '-bipyridine) Complex Electrolyte," Electrochem. Solid State Lett., vol. 15, no. 6, pp. A80-A82, 2012, doi: 10.1149/2.033206esl.

[221] H. Sun, J. W. Park, S. S. Hwang, D. Lee, and M. J. s.-m. a. t. Q. S. I. Lee, "inventor": "$inventor"}" class="style-scope patent-result"></state-modifier>, "Redox flow battery," United States Patent US8481192B2 Patent Appl. 12828551, 2013. [Online]. Available: https://patentimages.storage.googleapis.com/c7/a7/82/68b2e0c4f27ca7/US8481192.pdf

[222] J. W. Park, D. J. Oh, D. Lee, and M. J. Lee, "Organic electrolyte solution and redox flow battery including the same," United State Patent Appl. <state-modifier act="{"type": "OPEN_RESULT", "result": "$result"}" class="style-scope family-viewer">US20130196206A1</state-modifier>, 2012. [Online]. Available: https://patents.google.com/patent/US9257714

[223] J.-y. M. Duk-jin OH, Doo-yeon LEE, Oh-min KWON, Young-gyu KIM, Hyung-tae KIM,, "ORGANIC ELECTROLYTE SOLUTION AND REDOXFLOW BATTERY INCLUDING THE SAME," (in English), United States Patent Appl. 13/888,476, 2014. [Online]. Available: https://patentimages.storage.googleapis.com/2f/22/88/ee7e2759bf941b/US20140099569A1.pdf

[224] Z. Zhang, S. S. Zhang, and SpringerLink, Rechargeable Batteries [electronic resource] : Materials, Technologies and New Trends. Cham, 2015.

[225] W. Wang, W. Xu, L. Cosimbescu, D. Choi, L. Li, and Z. Yang, "Anthraquinone with tailored structure for a nonaqueous metal-organic redox flow battery," Chemical communications (Cambridge, England), vol. 48, no. 53, p. 6669, 2012, doi: 10.1039/c2cc32466k.

[226] R. V. Bugga, W. C. West, A. Kindler, and M. C. Smart, "Lithium-based high energy density flow batteries," ed: Google Patents, 2014.

[227] S.-h. Shin, S.-h. Yun, and S.-h. Moon, "A review of current developments in non-aqueous redox flow batteries: characterization of their membranes for design perspective," RSC Adv., vol. 3, no. 24, pp. 9095-9116, 2013, doi: 10.1039/c3ra00115f.

[228] T. M. Anderson, D. Ingersoll, A. J. Rose, C. L. Staiger, and J. C. Leonard, "Synthesis of an ionic liquid with an iron coordination cation," Dalton Transactions, vol. 39, no. 37, pp. 8609-8612, 2010, doi: 10.1039/c0dt00523a.

[229] H. D. Pratt Iii, A. J. Rose, C. L. Staiger, D. Ingersoll, and T. M. Anderson, "Synthesis and characterization of ionic liquids containing copper, manganese, or zinc coordination cations," Dalton Trans., vol. 40, no. 43, pp. 11396-11401, 2011, doi: 10.1039/c1dt10973a.

[230] M. Duduta et al., "Semi-solid lithium rechargeable flow battery," Advanced Energy Materials, vol. 1, no. 4, pp. 511-516, 2011, doi: 10.1002/aenm.201100152.

[231] S. Hamelet et al., "Non-Aqueous Li-Based Redox Flow Batteries," J. Electrochem. Soc., vol. 159, no. 8, pp. A1360-A1367, 2012, doi: 10.1149/2.071208jes.

[232] Y.-M. Chiang et al., "Metal sulphide electrodes and energy storage devices thereof," United States, [Online]. Available: https://patents.google.com/patent/WO2014121276A2/en

[233] Y.-M. Chiang et al., "Metal sulphide electrodes and energy storage devices thereof," United States, 2014. [Online]. Available: https://patents.google.com/patent/WO2014121276A2/en
[234] Z. Li et al., "Aqueous semi-solid flow cell: demonstration and analysis," Phys. Chem. Chem. Phys., vol. 15, no. 38, pp. 15833-15839, 2013, doi: 10.1039/c3cp53428f.
[235] F. Y. Fan et al., "Polysulfide flow batteries enabled by percolating nanoscale conductor networks," Nano letters, vol. 14, no. 4, p. 2210, 2014, doi: 10.1021/nl500740t.
[236] K. C. Smith, Y. M. Chiang, and W. C. Carter, "Maximizing energetic efficiency in flow batteries utilizing non-newtonian fluids," Journal of the Electrochemical Society, vol. 161, no. 4, pp. A486-A496, 2014, doi: 10.1149/2.011404jes.
[237] L. W. Hruska and R. F. Savinell, "Investigation of Factors Affecting Performance of the Iron-Redox Battery," Journal of the Electrochemical Society, vol. 128, no. 1, pp. 18-25, 1981, doi: 10.1149/1.2127366.
[238] K. Hawthorne, J. Wainright, and R. Savinell, "Studies of Iron-Ligand Complexes for an All-Iron Flow Battery Application," J. Electrochem. Soc., vol. 161, no. 10, pp. A1662-A1671, 2014, doi: 10.1149/2.0761410jes.
[239] R. F. Savinell and J. S. Wainright, "Iron based flow batteries," (in English), 2012. [Online]. Available: https://patents.google.com/patent/WO2012167057A2/en
[240] K. L. Hawthorne, J. S. Wainright, and R. F. Savinell, "Maximizing plating density and efficiency for a negative deposition reaction in a flow battery," Journal of Power Sources, vol. 269, pp. 216-224, 2014, doi: 10.1016/j.jpowsour.2014.06.125.
[241] T. J. Petek, J. S. Wainright, and R. F. Savinell, "Slurry Electrode for An All-Iron Flow Battery for Low Cost Large-Scale Energy Storage," (in English), Conference Proceedings p. 4, 2013.
[242] A. Hazza, D. Pletcher, and R. Wills, "A novel flow battery: A lead acid battery based on an electrolyte with soluble lead(ii &rpar Part I. Preliminary studies," Physical Chemistry Chemical Physics, vol. 6, no. 8, pp. 1773-1778, 2004, doi: 10.1039/b401115e.
[243] D. Pletcher and R. Wills, "A novel flow battery: A lead acid battery based on an electrolyte with soluble lead(ii &rpar Part II. Flow cell studies," Physical Chemistry Chemical Physics, vol. 6, no. 8, pp. 1779-1785, 2004, doi: 10.1039/b401116c.
[244] A. Hazza, D. Pletcher, and R. Wills, "A novel flow battery—A lead acid battery based on an electrolyte with soluble lead(II): IV. The influence of additives," Journal of Power Sources, vol. 149, pp. 103-111, 2005, doi: 10.1016/j.jpowsour.2005.01.049.
[245] D. Pletcher, H. Zhou, G. Kear, C. T. J. Low, F. C. Walsh, and R. G. A. Wills, "A novel flow battery—A lead-acid battery based on an electrolyte with soluble lead(II): Part VI. Studies of the lead dioxide positive electrode," Journal of Power Sources, vol. 180, no. 1, pp. 630-634, 2008, doi: 10.1016/j.jpowsour.2008.02.025.
[246] Y.-H. Wen, C. Gao, J. Cheng, J.-Q. Pan, G.-P. Cao, and Y.-S. Yang, "Effect of Electrolyte on the Performance of Electrodes for an All Lead Flow Battery.," Acta Phys. Chim. Sin., vol. 29, p. 2354−2360., 2013.
[247] J. Collins et al., "A novel flow battery: A lead acid battery based on an electrolyte with soluble lead(II) Part VIII. The cycling of a 10 cm × 10 cm flow cell," Journal of Power Sources, vol. 195, no. 6, pp. 1731-1738, 2010, doi: 10.1016/j.jpowsour.2009.09.044.
[248] D. Pletcher and R. Wills, "A novel flow battery—A lead acid battery based on an electrolyte with soluble lead(II): III. The influence of conditions on battery performance," Journal of Power Sources, vol. 149, pp. 96-102, 2005, doi: 10.1016/j.jpowsour.2005.01.048.

[249] J. Collins et al., "A novel flow battery: A lead acid battery based on an electrolyte with soluble lead(II). Part IX: Electrode and electrolyte conditioning with hydrogen peroxide," Journal of Power Sources, vol. 195, no. 9, pp. 2975-2978, 2010, doi: 10.1016/j.jpowsour.2009.10.109.

[250] C. G. Jie Cheng, Yue-Hua Wen, Jun-Qing Pan, Yan Xu, Gao-Ping Cao, "Performance Improvement of the All-Lead Redox Flow Battery in Fluoroboric Acid Electrolyte," (in English), International Journal of Energy Science (IJES) vol. 3, no. 3, p. 3, 2013.

[251] M. G. Verde, K. J. Carroll, Z. Wang, A. Sathrum, and Y. S. Meng, "Achieving high efficiency and cyclability in inexpensive soluble lead flow batteries," Energy Environ. Sci., vol. 6, no. 5, pp. 1573-1581, 2013, doi: 10.1039/c3ee40631h.

[252] R. Wills, J. Collins, D. Stratton-Campbell, C. Low, D. Pletcher, and F. Walsh, "Developments in the soluble lead-acid flow battery," Journal of Applied Electrochemistry, vol. 40, no. 5, pp. 955-965, 2010, doi: 10.1007/s10800-009-9815-4.

[253] C. P. Zhang, S. M. Sharkh, X. Li, F. C. Walsh, C. N. Zhang, and J. C. Jiang, "The performance of a soluble lead-acid flow battery and its comparison to a static lead-acid battery," Energy Conversion and Management, vol. 52, no. 12, pp. 3391-3398, 2011, doi: 10.1016/j.enconman.2011.07.006.

[254] L. Sanz, D. Lloyd, E. Magdalena, J. Palma, and K. Kontturi, "Description and performance of a novel aqueous all-copper redox flow battery," J. Power Sources, vol. 268, pp. 121-128, 2014, doi: 10.1016/j.jpowsour.2014.06.008.

[255] G. L. Soloveichik, "Electrochemistry: Metal-free energy storage," Nature, News & Views vol. 505, no. 7482, pp. 163-165, 01/09/print 2014, doi: 10.1038/505163a.

[256] P. Jena, "Materials for hydrogen storage: Past, present, and future," Journal of Physical Chemistry Letters, vol. 2, no. 3, pp. 206-211, 2011, doi: 10.1021/jz1015372.

[257] E. M. Gray, C. J. Webb, J. Andrews, B. Shabani, P. J. Tsai, and S. L. I. Chan, "Hydrogen storage for off-grid power supply," International Journal of Hydrogen Energy, vol. 36, no. 1, pp. 654-663, 2011, doi: 10.1016/j.ijhydene.2010.09.051.

[258] Y. Tolmachev, "Hydrogen-halogen electrochemical cells: A review of applications and technologies," Russian Journal of Electrochemistry, vol. 50, no. 4, pp. 301-316, 2014, doi: 10.1134/S1023193513120069.

[259] R. Yeo, J. McBreen, A. Tseung, S. Srinivasan, and J. McElroy, "An electrochemically regenerative hydrogen-chlorine energy storage system: electrode kinetics and cell performance," Journal of Applied Electrochemistry, vol. 10, no. 3, pp. 393-404, 1980, doi: 10.1007/BF00617215.

[260] M. Thomassen, B. Børresen, G. Hagen, and R. Tunold, "H 2 /Cl 2 fuel cell for co-generation of electricity and HCl," Journal of Applied Electrochemistry, vol. 33, no. 1, pp. 9-13, 2003, doi: 10.1023/A:1022942213808.

[261] M. Thomassen, E. Sandnes, B. Børresen, and R. Tunold, "Evaluation of concepts for hydrogen – chlorine fuel cells," Journal of Applied Electrochemistry, vol. 36, no. 7, pp. 813-819, 2006, doi: 10.1007/s10800-006-9140-0.

[262] T. G. Hart, "Gas phase free liquid chlorine electrochemical systems," United States Patent Appl. 744,712, 1978. [Online]. Available: https://patents.google.com/patent/US4086393A/en

[263] W. Glass and G. H. Boyle, "Performance of hydrogen-bromine fuel cells," Adv. Chem. Ser, vol. 47, 1965.

[264] J. F. McElroy and G. G. Patwa, "Electrical energy storage via high efficiency-cost effective hydrogen/halogen regenerative fuel cell systems," American Institute of Chemical Engineers, vol. 76, no. 198, pp. 123-128, 1980.

[265] S. Gross. "Analysis of regenerative fuel cells." Boeing Aerospace Co. (accessed 15/04, 2018).
[266] F. Barbir, T. Molter, and L. Dalton, "Efficiency and weight trade-off analysis of regenerative fuel cells as energy storage for aerospace applications," International Journal of Hydrogen Energy, vol. 30, no. 4, pp. 351-357, 2005, doi: 10.1016/j.ijhydene.2004.08.004.
[267] S. Kamasaki and H. Baba, "Electrochemically regenerative hydrogen-bromine fuel battery system," Mem. Fac. Technol., Tokyo Metrop. Univ, vol. 33, p. 3363−3370, 1983.
[268] S. D. Fritts and R. F. Savinell, "The open circuit voltage of a hydrogen-bromine fuel cell," Proc. - Electrochem Soc, vol. 86, no. 10, p. 73− 85, 1986.
[269] H. Cnobloch and K. Hoehne, "Hydrogen/bromine cells as an energy converter.," vol. 2018, no. 13/04, p. 341−55, 1985.
[270] M. Mastragostino and S. Valcher, "Polymeric salt as bromine complexing agent in a Zn-Br2 model battery," Electrochimica Acta, vol. 28, no. 4, pp. 501-505, 1983/04/01/ 1983, doi: https://doi.org/10.1016/0013-4686(83)85034-8.
[271] K. Cedzynska, "Properties of modified electrolyte for zinc-bromine cells," Electrochimica Acta, vol. 40, no. 8, pp. 971-976, 1995/06/01 1995, doi: http://dx.doi.org/10.1016/0013-4686(94)00372-8.
[272] V. Yufit, B. Hale, M. Matian, P. Mazur, and N. P. Brandon, "Development of a regenerative hydrogen-vanadium fuel cell for energy storage applications," Journal of the Electrochemical Society, vol. 160, no. 6, pp. A856-A861, 2013, doi: 10.1149/2.086306jes.
[273] M. Alon, A. Blum, and E. Peled, "Feasibility study of hydrogen/iron redox flow cell for grid-storage applications," Journal of Power Sources, vol. 240, pp. 417-420, 2013, doi: 10.1016/j.jpowsour.2013.04.032.
[274] V. Pupkevich, V. Glibin, and D. Karamanev, "Phosphorylated polyvinyl alcohol membranes for redox Fe3+/H-2 flow cells," J. Power Sources, vol. 228, pp. 300-307, 2013, doi: 10.1016/j.jpowsour.2012.11.080.
[275] C. Menictas, M. Skyllas-Kazacos, and T. M. Lim, Advances in batteries for medium- and large-scale energy storage. Cambridge, UK ; Waltham, MA, USA, 2014.
[276] P. Alotto, M. Guarnieri, F. Moro, and A. Stella, "Large scale energy storage with redox flow batteries," Compel, vol. 32, no. 5, pp. 1459-1470, 2013, doi: 10.1108/COMPEL-04-2013-0133.
[277] Y. H. Wen, J. Cheng, Y. Xun, P. H. Ma, and Y. S. Yang, "Bifunctional redox flow battery: 2. V(III)/V(II)– -cystine(O) system," Electrochimica Acta, vol. 53, no. 20, pp. 6018-6023, 2008, doi: 10.1016/j.electacta.2008.03.026.
[278] J. Grosse Austing, C. Nunes Kirchner, E.-M. Hammer, L. Komsiyska, and G. Wittstock, "Study of an unitised bidirectional vanadium/air redox flow battery comprising a two-layered cathode," Journal of Power Sources, vol. 273, pp. 1163-1170, 2015, doi: 10.1016/j.jpowsour.2014.09.177.
[279] J. Rugolo, B. Huskinson, and M. J. Aziz, "Model of performance of a regenerative hydrogen chlorine fuel cell for grid-scale electrical energy storage," Journal of the Electrochemical Society, vol. 159, no. 2, pp. B133-B144, 2012, doi: 10.1149/2.030202jes.
[280] J. Pan, Y. Wen, J. Cheng, S. Bai, and Y. Yang, "Evaluation of substrates for zinc negative electrode in acid PbO2-Zn single flow batteries," Chinese Journal of Chemical Engineering, Article vol. 24, no. 4, pp. 529-534, 2016, doi: 10.1016/j.cjche.2016.01.001.
[281] L. Zhang, J. Cheng, Y. s. Yang, Y. h. Wen, X. d. Wang, and G. p. Cao, "Study of zinc electrodes for single flow zinc/nickel battery application," Journal of Power Sources, Article vol. 179, no. 1, pp. 381-387, 2008, doi: 10.1016/j.jpowsour.2007.12.088.

[282] Y. Ito, M. Nyce, R. Plivelich, M. Klein, D. Steingart, and S. Banerjee, "Zinc morphology in zinc-nickel flow assisted batteries and impact on performance," Journal of Power Sources, Article vol. 196, no. 4, pp. 2340-2345, 2011, doi: 10.1016/j.jpowsour.2010.09.065.

[283] M. Guglielmo, "Electric accumulator," (in English), 1**921**. [Online]. Available: https://patents.google.com/patent/US1377722

[284] P. Carr, P. C. Symons, and D. J. Aller, "Operational zinc chlorine battery based on a water store," (in English), United States Patent US 4146680, 1979-03-27, 1979. [Online]. Available: https://www.osti.gov/biblio/6287731

[285] D. R. Martin, "Lecture demonstrations of electrochemical reactions," Journal of Chemical Education, vol. 25, no. 9, p. 495, 1948, doi: 10.1021/ed025p495.

[286] B. L. Wei Wang, Zimin Nie, Xiaoliang, M. V. Wei, Guosheng Li, Ed Thomsen, David Reed, Kerry, a. V. S. Meinhardt, and " Next Generation Aqueous Redox Flow Battery Development." Pacific Northwest National Laboratory Electrochemical Materials and Systems. http://www.sandia.gov/ess/docs/pr_conferences/2014/Wednesday/Session2/06_Wang_Next_Generation_Aqueous.pdf (accessed 28/04/2018, 2018).

[287] L. Bin et al., "Ambipolar zinc-polyiodide electrolyte for a high-energy density aqueous redox flow battery," Nature Communications, vol. 6, no. 1, 2015, doi: 10.1038/ncomms7303.

[288] M. Holland-Cunz, F. Cording, J. Friedl, and U. Stimming, "Redox flow batteries—Concepts and chemistries for cost-effective energy storage," Frontiers in Energy, pp. 1-27, 2018, doi: 10.1007/s11708-018-0552-4.

[289] G. Nikiforidis, R. Cartwright, D. Hodgson, D. Hall, and L. Berlouis, "Factors affecting the performance of the Zn-Ce redox flow battery," Electrochimica Acta, vol. 140, pp. 139-144, 2014, doi: 10.1016/j.electacta.2014.04.150.

[290] Z. Xie, F. Xiong, and D. Zhou, "Study of the Ce 3+ /Ce 4+ redox couple in mixed-acid media (CH 3 SO 3 H and H 2 SO 4) for redox flow battery application," Energy and Fuels, vol. 25, no. 5, pp. 2399-2404, 2011, doi: 10.1021/ef200354b.

[291] S. Gu, K. Gong, E. Z. Yan, and Y. Yan, "A multiple ion-exchange membrane design for redox flow batteries," Energy Environ. Sci., vol. 7, no. 9, pp. 2986-2998, 2014, doi: 10.1039/c4ee00165f.

[292] Russel. "Research Project: Redox Flow Cells Batteries: Zinc-Cerium." https://www.southampton.ac.uk/smmi/research/smmispecific/environmentappliedsolutions/zinc_cerium_redox_flow_battery.page#project_overview (accessed 25/08, 2018).

[293] S. Gu, K. Gong, E. Z. Yan, and Y. Yan, "A multiple ion-exchange membrane design for redox flow batteries," Energy & Environmental Science, vol. 7, pp. 2986-2998, 2014.

[294] G. B. Adams, "Electrolyte is alkali metal ferricyanide salt," 1979.

[295] G. B. Adams, "Electrically rechargeable battery," ed: Google Patents, 1979.

[296] V. E. Systems. "Energy Storage." https://www.viznenergy.com/vizn/ (accessed 18/10, 2018).

[297] S. Biswas et al., "Minimal architecture zinc-bromine battery for low cost electrochemical energy storage," Energy & Environmental Science, 10.1039/C6EE02782B vol. 10, no. 1, pp. 114-120, 2017, doi: 10.1039/C6EE02782B.

[298] Q. Lai, H. Zhang, X. Li, L. Zhang, and Y. Cheng, "A novel single flow zinc-bromine battery with improved energy density.(Report)," Journal of Power Sources, vol. 235, p. 1, 2013.

[299] M. Park, J. Ryu, W. Wang, and J. Cho, "Material design and engineering of next-generation flow-battery technologies," Nature Reviews Materials, Review Article vol. 2, p. 16080, 11/08/online 2016, doi: 10.1038/natrevmats.2016.80.

[300] G. P. Rajarathnam, The Zinc/Bromine Flow Battery [electronic resource] : Materials Challenges and Practical Solutions for Technology Advancement, 1st ed. 2016. ed. Singapore, 2016.

[301] C. Ponce de León and F. C. Walsh, "SECONDARY BATTERIES – ZINC SYSTEMS | Zinc–Bromine A2 - Garche, Jürgen," in Encyclopedia of Electrochemical Power Sources. Amsterdam: Elsevier, 2009, pp. 487-496.

[302] J. J. Paul Denholm, Marissa Hummon, Thomas Jenkin, and David Palchak, Brendan Kirby, Ookie Ma, Mark O'Malley, "The Value of Energy Storage for Grid Applications," United State of America, 2013. Accessed: 05/04/2017. [Online]. Available: http://assets.fiercemarkets.net/public/sites/energy/reports/nrelreport1.pdf

[303] J. M. a. J. Abboud, "Energy Storage," 2002. Accessed: 19/06/2017. [Online]. Available: http://www.ridgeenergystorage.com/ESCWhitepaper.pdf

[304] M. Beaudin, H. Zareipour, A. Schellenberglabe, and W. Rosehart, "Energy storage for mitigating the variability of renewable electricity sources: An updated review," Energy for Sustainable Development, vol. 14, no. 4, pp. 302-314, 12// 2010, doi: http://dx.doi.org/10.1016/j.esd.2010.09.007.

[305] K. W. Knehr, S. Biswas, and D. A. Steingart, "Quantification of the voltage losses in the minimal architecture zinc-bromine battery using GITT and EIS," Journal of the Electrochemical Society, vol. 164, no. 13, pp. A3101-A3108, 2017, doi: 10.1149/2.0821713jes.

[306] E. S. Association. "Zinc-Bromine (ZNBR) Flow Batteries." http://energystorage.org/energy-storage/technologies/zinc-bromine-znbr-flow-batteries (accessed 02/03/2017, 2017).

[307] Q. Lai, H. M. Zhang, X. Li, L. Zhang, and Y. Cheng, "A novel single flow zinc-bromine battery with improved energy density," J. Power Sources, vol. 235, no. C, pp. 1-4, 2013, doi: 10.1016/j.jpowsour.2013.01.193.

[308] J.-D. Jeon, H. S. Yang, J. Shim, H. S. Kim, and J. H. Yang, "Dual function of quaternary ammonium in Zn/Br redox flow battery: Capturing the bromine and lowering the charge transfer resistance," Electrochimica Acta, vol. 127, pp. 397-402, 2014, doi: 10.1016/j.electacta.2014.02.073.

[309] M. Schneider, G. P. Rajarathnam, M. E. Easton, A. F. Masters, T. Maschmeyer, and A. Vassallo, "The influence of novel bromine sequestration agents on zinc/bromine flow battery performance," RSC Adv., vol. 6, no. 112, pp. 110548-110556, 2016, doi: 10.1039/c6ra23446a.

[310] B. Huskinson, M. P. Marshak, M. R. Gerhardt, and M. J. Aziz, "Cycling of a Quinone-Bromide Flow Battery for Large-Scale Electrochemical Energy Storage," ECS Transactions, vol. 61, no. 37, pp. 27-30, September 29, 2014 2014, doi: 10.1149/06137.0027ecst.

[311] S. Er, C. Suh, M. P. Marshak, and A. Aspuru-Guzik, "Computational design of molecules for an all-quinone redox flow battery," Chemical Science, 10.1039/C4SC03030C vol. 6, no. 2, pp. 885-893, 2015, doi: 10.1039/C4SC03030C.

[312] P. Singh and B. Jonshagen, "Zinc□bromine battery for energy storage," Journal of Power Sources, vol. 35, no. 4, pp. 405-410, 1991/09/01 1991, doi: http://dx.doi.org/10.1016/0378-7753(91)80059-7.

[313] E. Energy Storage Association. "Zinc-bromine (ZNBR) Flow Batteries." https://energystorage.org/why-energy-storage/technologies/zinc-bromine-znbr-flow-batteries/ (accessed 26/10/2019, 2019).

[314] S.-C. Yang, "An approximate model for estimating the faradaic efficiency loss in zinc/bromine batteries caused by cell self-discharge," Journal of Power Sources, vol. 50, no. 3, pp. 343-360, 1994/07/01 1994, doi: http://dx.doi.org/10.1016/0378-7753(94)01910-X.

[315] S. L. Chiu and J. R. Selman, "Determination of electrode kinetics by corrosion potential measurements: Zinc corrosion by bromine," Journal of Applied Electrochemistry, journal article vol. 22, no. 1, pp. 28-37, 1992, doi: 10.1007/bf01093008.

[316] M. A. Miller, J. S. Wainright, and R. F. Savinell, "Iron Electrodeposition in a Deep Eutectic Solvent for Flow Batteries," Journal of The Electrochemical Society, vol. 164, no. 4, pp. A796-A803, January 1, 2017 2017, doi: 10.1149/2.1141704jes.

[317] R. A. Antunes, M. C. Lopes de Oliveira, and G. Ett, "Investigation on the corrosion resistance of carbon black–graphite-poly(vinylidene fluoride) composite bipolar plates for polymer electrolyte membrane fuel cells," International Journal of Hydrogen Energy, vol. 36, no. 19, pp. 12474-12485, 2011/09/01/ 2011, doi: https://doi.org/10.1016/j.ijhydene.2011.06.131.

[318] C. M. Hagg and M. Skyllas-Kazacos, "Novel bipolar electrodes for battery applications," Journal of Applied Electrochemistry, journal article vol. 32, no. 10, pp. 1063-1069, October 01 2002, doi: 10.1023/a:1021228304148.

[319] P. J. Lex and J. F. Matthews, "Recent developments in zinc/bromine battery technology at Johnson Controls," Power Sources Symposium, 1992., IEEE 35th International, pp. 88 - 92, 1992.

[320] D. H. Swan, B. Dickinson, M. Arikara, and G. S. Tomazic, "Demonstration of a zinc bromine battery in an electric vehicle," in Proceedings of 9th Annual Battery Conference on Applications and Advances, 11-13 Jan. 1994 1994, pp. 104-109, doi: 10.1109/BCAA.1994.283609.

[321] S. Suresh, T. Kesavan, Y. Munaiah, I. Arulraj, S. Dheenadayalan, and P. Ragupathy, "Zincbromine hybrid flow battery: effect of zinc utilization and performance characteristics," RSC Adv., vol. 4, no. 71, pp. 37947-37953, 2014, doi: 10.1039/c4ra05946h.

[322] A. Heintz and C. Illenberger, "Diffusion coefficients of Br2 in cation exchange membranes," Journal of Membrane Science, vol. 113, no. 2, pp. 175-181, 1996/05/15 1996, doi: http://dx.doi.org/10.1016/0376-7388(95)00026-7.

[323] A. M. V. Gobinath Pillai Rajarathnam, "The Zinc/Bromine Flow Battery Materials Challenges and Practical Solutions for Technology Advancement," pp. 1-18, 2015.

[324] A. M. V. Gobinath Pillai Rajarathnam, The Zinc/Bromine Flow Battery - Materials Challenges and Practical Solutions for Technology Advancement. 2016.

[325] S. Maurya, S.-H. Shin, Y. Kim, and S.-H. Moon, "A review on recent developments of anion exchange membranes for fuel cells and redox flow batteries," RSC Advances, 10.1039/C5RA04741B vol. 5, no. 47, pp. 37206-37230, 2015, doi: 10.1039/C5RA04741B.

[326] S. Gu, K. Gong, E. Z. Yan, and Y. Yan, "A multiple ion-exchange membrane design for redox flow batteries," Energy & Environmental Science, 10.1039/C4EE00165F vol. 7, no. 9, pp. 2986-2998, 2014, doi: 10.1039/C4EE00165F.

[327] C. Arnold and R. A. Assink, "Development of sulfonated polysulfone membranes for redox flow batteries," Journal of Membrane Science, vol. 38, no. 1, pp. 71-83, 1988/07/01 1988, doi: http://dx.doi.org/10.1016/S0376-7388(00)83276-7.

[328] K. R. Hinkle, C. J. Jameson, and S. Murad, "Transport of Vanadium and Oxovanadium Ions Across Zeolite Membranes: A Molecular Dynamics Study," The Journal of Physical Chemistry C, vol. 118, no. 41, pp. 23803-23810, 2014/10/16 2014, doi: 10.1021/jp507155s.

[329] P. N. Ross, "Zinc electrode and rechargeable zinc-air battery," ed: Google Patents, 1989.

[330] M. Jacoby, "Zinc sponge protects rechargeable battery," in C&EN GLOBAL ENTERPRISE, ed: ENERGY STORAGE, 2017, pp. 7–7.

[331] H. Kim, G. Jeong, Y.-u. Kim, J.-h. Kim, C.-m. Park, and H.-j. Sohn, "Metallic anodes for next generation secondary batteries," Chem. Soc. Rev., vol. 42, no. 23, pp. 9011-9034, 2013, doi: 10.1039/c3cs60177c.

[332] S. Higashi, S. Lee, J. Lee, K. Takechi, and Y. Cui, "Avoiding short circuits from zinc metal dendrites in anode by backside-plating configuration," Nature Communications, vol. 7, p. 11801, 2016, doi: 10.1038/ncomms11801.

[333] Y. Liang et al., "Universal quinone electrodes for long cycle life aqueous rechargeable batteries," Nature Materials, vol. 16, no. 8, pp. 841-848, 2017, doi: 10.1038/nmat4919.

[334] P. Tennessen, J. Hall, R. Cole, and P. Kreiner, "Reservoir for multiphase electrolyte flow control," ed: Google Patents, 2016.

[335] K. Oyj, "Albemarle Corporation Files Patent Application for Method for the Synthesis of Quaternary Ammonium Compounds and Compositions Thereof," ed. New Delhi, 2010.

[336] M. Dey, S. S. Dhar, and M. Kalita, "Novel Method of Synthesis of Quaternary Ammonium Tribromides and Investigation of Catalytic Role of Benzyltrimethylammonium Tribromide in Oxidation of Alcohols to Carbonyl Compounds," Synthetic Communications, vol. 43, no. 12, pp. 1734-1742, 2013, doi: 10.1080/00397911.2012.666694.

[337] H. Z. Sommer and L. L. Jackson, "Alkylation of amines. New method for the synthesis of quaternary ammonium compounds from primary and secondary amines," The Journal of Organic Chemistry, vol. 35, no. 5, pp. 1558-1562, 1970, doi: 10.1021/jo00830a064.

[338] M. M. Nakatsuji and T. K. Saha "Zinc-bromine flow batteries in residential electricity supply: Two case studies," Power and Energy Society General Meeting, 2012 IEEE, pp. 1-8, 2012.

[339] K. J. Cathro, K. Cedzynska, D. C. Constable, and P. M. Hoobin, "Selection of quaternary ammonium bromides for use in zinc/bromine cells," Journal of Power Sources, Article vol. 18, no. 4, pp. 349-370, 1986, doi: 10.1016/0378-7753(86)80091-X.

[340] SIGMA-ALDRICH. "SAFETY DATA SHEET." http://www.sigmaaldrich.com/MSDS/MSDS/DisplayMSDSPage.do?country=GB&language=en&productNumber=470864&brand=ALDRICH&PageToGoToURL=http%3A%2F%2Fwww.sigmaaldrich.com%2Fcatalog%2Fproduct%2Faldrich%2F470864%3Flang%3Den (accessed 28/03/2017, 2017).

[341] D. J. Eustace, "Bromine Complexation in Zinc-Bromine Circulating Batteries," Journal of the Electrochemical Society, vol. 127, no. 3, pp. 528-532, 1980, doi: 10.1149/1.2129706.

[342] B. M. Trost and I. Fleming, Comprehensive Organic Synthesis. Elsevier Science, 1991.

[343] G. Bellucci, R. Bianchini, and R. Ambrosetti, "Reaction of tertiary aliphatic amines with halogens. Kinetics and products of the reaction of tribenzylamine with molecular bromine and tribromide ion," Journal of the Chemical Society, Perkin Transactions 2, no. 1, pp. 39-45, 1987, doi: 10.1039/P29870000039.

[344] F. Muñoz and C. Von Sonntag, "The reactions of ozone with tertiary amines including the complexing agents nitrilotriacetic acid (NTA) and ethylenediaminetetraacetic acid (EDTA) in aqueous solution," Journal of the Chemical Society. Perkin Transactions 2, no. 10, pp. 2029-2033, 2000.

[345] A. Fekete, A. K. Malik, A. Kumar, and P. Schmitt-Kopplin, "Amines in the Environment," Critical Reviews in Analytical Chemistry, vol. 40, no. 2, pp. 102-121, 2010, doi: 10.1080/10408340903517495.

[346] Z. Zhao, Q. Li, X. Ji, R. Dimova, R. Lipowsky, and Y. Liu, "Molar mass fractionation in aqueous two-phase polymer solutions of dextran and poly(ethylene glycol)," Journal of Chromatography A, vol. 1452, no. C, pp. 107-115, 2016, doi: 10.1016/j.chroma.2016.04.075.

[347] R. J. Bellows and E. Kantner, "Electrolyte additive for improved battery performance," (in English), 1989-04-04, 1989. [Online]. Available: https://www.osti.gov/biblio/5959922

[348] W. Kautek et al., "In situ investigations of bromine-storing complex formation in a zinc-flow battery at gold electrodes," Journal of the Electrochemical Society, vol. 146, no. 9, pp. 3211-3216, 1999, doi: 10.1149/1.1392456.

[349] A. Degen and M. Kosec, "Effect of pH and impurities on the surface charge of zinc oxide in aqueous solution," Journal of the European Ceramic Society, vol. 20, no. 6, pp. 667-673, 2000, doi: 10.1016/S0955-2219(99)00203-4.

[350] G. Kear, H.-Z. Wú, and M. Jones, "Corrosion of ferrous- and zinc-based materials in CCA, ACQ and CuAz timber preservative aqueous solutions," Materials and Structures, vol. 41, no. 8, pp. 1405-1417, 2008, doi: 10.1617/s11527-007-9338-6.

[351] B. Beverskog and I. Puigdomenech, "Revised pourbaix diagrams for zinc at 25–300 °C," Corrosion Science, vol. 39, no. 1, pp. 107-114, 1997, doi: 10.1016/S0010-938X(97)89246-3.

[352] T. K. A. Hoang, T. N. L. Doan, K. E. K. Sun, and P. Chen, "Corrosion chemistry and protection of zinc & zinc alloys by polymer-containing materials for potential use in rechargeable aqueous batteries," RSC Advances, Article vol. 5, no. 52, pp. 41677-41691, 2015, doi: 10.1039/c5ra00594a.

[353] A. S. Feiner and A. J. McEvoy, "The Nernst equation. (studying chemistry)," Journal of Chemical Education, vol. 71, no. 6, p. 493, 1994, doi: 10.1021/ed071p493.

[354] P. Delahay, M. Pourbaix, and P. Van Rysselberghe, "Potential-pH Diagram of Zinc and Its Applications to the Study of Zinc Corrosion," Journal of the Electrochemical Society, vol. 98, no. 3, pp. 101-105, 1951, doi: 10.1149/1.2778110.

[355] P. K. Leung, T. Martin, A. A. Shah, M. A. Anderson, and J. Palma, "Membrane-less organic-inorganic aqueous flow batteries with improved cell potential," Chemical Communications, vol. 52, no. 99, pp. 14270-14273, 2016, doi: 10.1039/C6CC07692K.

[356] P. K. Leung, T. Martin, A. A. Shah, M. R. Mohamed, M. A. Anderson, and J. Palma, "Membrane-less hybrid flow battery based on low-cost elements," Journal of Power Sources, Article vol. 341, pp. 36-45, 2017, doi: 10.1016/j.jpowsour.2016.11.062.

[357] P. K. Leung, C. Ponce De León, and F. C. Walsh, "An undivided zinc-cerium redox flow battery operating at room temperature (295 K)," Electrochemistry Communications, Article vol. 13, no. 8, pp. 770-773, 2011, doi: 10.1016/j.elecom.2011.04.011.

[358] A. Hazza, D. Pletcher, and R. Wills, "A novel flow battery: A lead acid battery based on an electrolyte with soluble lead(II): Part I. Preliminary studies," Physical Chemistry Chemical Physics, Article vol. 6, no. 8, pp. 1773-1778, 2004, doi: 10.1039/b401115e.

[359] L. Wei, T. S. Zhao, Q. Xu, X. L. Zhou, and Z. H. Zhang, "In-situ investigation of hydrogen evolution behavior in vanadium redox flow batteries," Applied Energy, Article vol. 190, pp. 1112-1118, 2017, doi: 10.1016/j.apenergy.2017.01.039.

[360] H. Liu, Q. Xu, C. Yan, and Y. Qiao, "Corrosion behavior of a positive graphite electrode in vanadium redox flow battery," Electrochimica Acta, Article vol. 56, no. 24, pp. 8783-8790, 2011, doi: 10.1016/j.electacta.2011.07.083.

[361] M. Kazacos and M. Skyllas-Kazacos, "Performance Characteristics of Carbon Plastic Electrodes in the All-Vanadium Redox Cell," Journal of the Electrochemical Society, Article vol. 136, no. 9, pp. 2759-2760, 1989, doi: 10.1149/1.2097588.

[362] S. Zhong, M. Kazacos, R. P. Burford, and M. Skyllas-Kazacos, "Fabrication and activation studies of conducting plastic composite electrodes for redox cells," Journal of Power Sources, Article vol. 36, no. 1, pp. 29-43, 1991, doi: 10.1016/0378-7753(91)80042-V.

[363] H. Z. Peng Qian, Jian Chen, Yuehua Wen, Qingtao Luo, Zonghao Liu , Dongjiang You, Baolian Yi, "A novel electrode-bipolar plate assembly for vanadium redox flow battery applications," Journal of Power Sources, vol. 175, pp. 613–620, 2008.

[364] M. S. Yazici, D. Krassowski, and J. Prakash, "Flexible graphite as battery anode and current collector," Journal of Power Sources, Article vol. 141, no. 1, pp. 171-176, 2005, doi: 10.1016/j.jpowsour.2004.09.009.

[365] R. Y. Wang, D. W. Kirk, and G. X. Zhang, "Effects of deposition conditions on the morphology of zinc deposits from alkaline zincate solutions," Journal of the Electrochemical Society, Article vol. 153, no. 5, pp. C357-C364, 2006, doi: 10.1149/1.2186037.

[366] L. Zhu, H. Zhang, W. Li, and H. Liu, "Great improvement over electrochemical performance of zinc electrodes from sonochemical growth of cerium conversion films on zinc powder," Journal of Alloys and Compounds, vol. 471, no. 1, pp. 481-487, 2009, doi: 10.1016/j.jallcom.2008.03.134.

[367] E. G. Gagnon, "Electrochemical science and technology effect of ten weight percent KOH Electrolyte on the Durability of Zinc/Nickel Oxide Cells Containing Zinc Electrodes with Calcium Hydroxide," Journal of the Electrochemical Society, vol. 138, no. 11, pp. 3173-3176, 1991, doi: 10.1149/1.2085387.

[368] K. I. Popov, M. G. Pavlović, M. D. Spasojević, and V. M. Nakić, "The critical overpotential for zinc dendrite formation," Journal of Applied Electrochemistry, Article vol. 9, no. 4, pp. 533-536, 1979, doi: 10.1007/BF00617566.

[369] D. E. Turney et al., "Rechargeable Zinc Alkaline Anodes for Long-Cycle Energy Storage," Chemistry of Materials, Article vol. 29, no. 11, pp. 4819-4832, 2017, doi: 10.1021/acs.chemmater.7b00754.

[370] M. Chamoun et al., "Hyper-dendritic nanoporous zinc foam anodes," Npg Asia Materials, Original Article vol. 7, p. e178, 04/24/online 2015, doi: 10.1038/am.2015.32 https://www.nature.com/articles/am201532#supplementary-information.

[371] W. M. Wang, J. Wang, and D. Ton, Prospects for Renewable Energy-Chapter 5:Meeting the Challenges of Integration with Storage. Elsevier Inc., 2012, pp. 103-126.

[372] S. Amy L, "RECONSIDERING REGULATORY UNCERTAINTY: MAKING A CASE FOR ENERGY STORAGE," Florida State University Law Review, vol. 41, pp. 697-1173, 2014.

[373] R. M. Darling, K. G. Gallagher, J. A. Kowalski, S. Ha, and F. R. Brushett, "Pathways to low-cost electrochemical energy storage: A comparison of aqueous and nonaqueous flow batteries," Energy and Environmental Science, Article vol. 7, no. 11, pp. 3459-3477, 2014, doi: 10.1039/c4ee02158d.

[374] D. O. Eugene Freeman, and Frank Barnes, "Energy storage for electrical systems in the USA," AIMS Energy, vol. 4, no. 6, pp. 856-875, 2016, doi: 10.3934/energy.2016.6.856.

[375] J. Pan, Y. Wen, J. Cheng, Z. Bai, and Y. Yang, "Zinc deposition and dissolution in sulfuric acid onto a graphiteresin composite electrode as the negative electrode reactions in acidic zinc-based redox flow batteries," Journal of Applied Electrochemistry, Article vol. 43, no. 5, pp. 541-551, 2013, doi: 10.1007/s10800-013-0538-1.

[376] J. Torrent-Burgués, E. Guaus, and F. Sanz, "Initial stages of tin electrodeposition from sulfate baths in the presence of gluconate," Journal of Applied Electrochemistry, Article vol. 32, no. 2, pp. 225-230, 2002, doi: 10.1023/A:1014710500122.

[377] M. Volmer and A. Weber, Zeitschrift fur Physikalische Chemie, p. 277, 1926.

[378] J. Zhu, G. Nakhla, and Y. Cui, "Liquid-solid fluidized bed waste water treatment system for simultaneous carbon, nitrogen and phosphorous removal," ed: Google Patents, 2010.

[379] S. Oka, Fluidized Bed Combustion. 2003, p. 581.
[380] S. P. a. B. F. K. Suksankraisorn, "Prediction of minimum fluidisation velocity from correlations: an observation," Asian Journal Energy Environment, vol. 2, no. 2, p. 10, 2001.
[381] H. T. Bi, N. Ellis, I. A. Abba, and J. R. Grace, "A state-of-the-art review of gas–solid turbulent fluidization," Chemical Engineering Science, vol. 55, no. 21, pp. 4789-4825, 11// 2000, doi: http://dx.doi.org/10.1016/S0009-2509(00)00107-X.
[382] G. Q. Yang, B. Du, and L. S. Fan, "Bubble formation and dynamics in gas–liquid–solid fluidization—A review," Chemical Engineering Science, vol. 62, no. 1–2, pp. 2-27, 1// 2007, doi: http://dx.doi.org/10.1016/j.ces.2006.08.021.
[383] R. Chandran and M. Mansour, "Efficient and cost-effective biomass drying," ed: Google Patents, 2005.
[384] R. Krishna, J. Ellenberger, and D. E. Hennephof, "Analogous description of the hydrodynamics of gas-solid fluidized beds and bubble columns," The Chemical Engineering Journal and the Biochemical Engineering Journal, vol. 53, no. 1, pp. 89-101, 1993/11/01 1993, doi: http://dx.doi.org/10.1016/0923-0467(93)80010-T.
[385] A. Puettmann, E. U. Hartge, and J. Werther, "Application of the flowsheet simulation concept to fluidized bed reactor modeling. Part II—Application to the selective oxidation of n-butane to maleic anhydride in a riser/regenerator system," Chemical Engineering and Processing: Process Intensification, vol. 57–58, pp. 86-95, 7// 2012, doi: http://dx.doi.org/10.1016/j.cep.2011.10.004.
[386] D. Geldart, E. C. Abdullah, and A. Verlinden, "Characterisation of dry powders," Powder Technology, vol. 190, no. 1–2, pp. 70-74, 3/5/ 2009, doi: http://dx.doi.org/10.1016/j.powtec.2008.04.089.
[387] C. G. Philippsen, A. C. F. Vilela, and L. D. Zen, "Fluidized bed modeling applied to the analysis of processes: review and state of the art," Journal of Materials Research and Technology, vol. 4, no. 2, pp. 208-216, 4// 2015, doi: http://dx.doi.org/10.1016/j.jmrt.2014.10.018.
[388] U. Kumar and V. K. Agarwal, "Simulation of 3D gas–solid fluidized bed reactor hydrodynamics," Particulate Science and Technology, vol. 35, no. 1, pp. 1-13, 2017/01/02 2017, doi: 10.1080/02726351.2015.1119227.
[389] D. Chaliampalias et al., "Deposition of zinc coatings with fluidized bed technique," Materials Letters, vol. 61, no. 1, pp. 223-226, 2007, doi: 10.1016/j.matlet.2006.04.036.
[390] M. Horio, F. Scala, Ed. Overview of Fluidization Science and Fluidized Bed Technologies, 'Fluidized-bed Technologies for Near-zero Emission Combustion and Gasification. Woodhead Publishing, 2013.
[391] S. A. M. Mohammed, "HYDRODYNAMIC STUDIES OF BED EXPANSION IN LIQUID SOLID FLUIDIZED BED," Journal of Engineering, no. 3, pp. 5398-5410, 16 September 2010 2010.
[392] G. F. M. H. a. H. H. M. Noor M. Jasem, "EXPERIMENTAL STUDY OF THE EFFECT BED DENSITY ON HEAT TRANSFER COEFFICENTS IN TOWERS WITH GAS SOLID CIRCULATING FLUIDIZED BED," Al-Qadisiya Journal For Engineering Sciences, vol. 2, no. 3, p. 12, 2009.
[393] D. Kunii and O. Levenspiel, "CHAPTER 8 - High-Velocity Fluidization," in Fluidization Engineering (Second Edition). Boston: Butterworth-Heinemann, 1991, pp. 193-210.
[394] S. Zaromb, "Fluidized-bed electrodes and related apparatus and methods," ed: Google Patents, 1980.

[395] A. Mahecha-Botero, J. R. Grace, S. S. E. H. Elnashaie, and C. J. Lim, "Advances in Modeling of Fluidized-Bed Catalytic Reactors: A Comprehensive Review," Chemical Engineering Communications, vol. 196, no. 11, pp. 1375-1405, 2009, doi: 10.1080/00986440902938709.

[396] S. R. McLean and V. I. Nikora, "Characteristics of turbulent unidirectional flow over rough beds: Double-averaging perspective with particular focus on sand dunes and gravel beds," Water Resources Research, vol. 42, no. 10, pp. n/a-n/a, 2006, doi: 10.1029/2005WR004708.

[397] J. A. Gonzalez-Dominguez and R. W. Lew, "Evaluating additives and impurities in zinc electrowinning," JOM, journal article vol. 47, no. 1, pp. 34-37, January 01 1995, doi: 10.1007/bf03221128.

[398] V. Jiricny and J. W. Evans, "Fluidized-bed electrodeposition of zinc," Metallurgical Transactions B, journal article vol. 15, no. 4, pp. 623-631, December 01 1984, doi: 10.1007/bf02657282.

[399] H. Owen and P. H. Schipper, "Process and apparatus for fast fluidized bed regeneration of catalyst in a bubbling bed catalyst regenerator," ed: Google Patents, 1991.

[400] H. Li and D. Li, "Effects of Gas Flow Velocity on Electrical Conductivity of Three-Phase Fluidized-Bed," in 2010 4th International Conference on Bioinformatics and Biomedical Engineering, 18-20 June 2010 2010, pp. 1-4, doi: 10.1109/ICBBE.2010.5517364.

[401] W. M. Gao, L. X. Kong, and P. D. Hodgson, "Numerical simulation of heat and mass transfer in fluidised bed heat treatment furnaces," Journal of Materials Processing Technology, vol. 125–126, pp. 170-178, 9/9/ 2002, doi: http://dx.doi.org/10.1016/S0924-0136(02)00372-2.

[402] T. Huh, G. Savaskan, and J. Evans, "Further studies of a zinc-air cell employing a packed bed anode part II: Regeneration of zinc particles and electrolyte by fluidized bed electrodeposition," Journal of Applied Electrochemistry, vol. 22, no. 10, pp. 916-921, 1992, doi: 10.1007/BF01024139.

[403] R. Othman, A. H. Yahaya, and A. K. Arof, "A zinc–air cell employing a porous zinc electrode fabricated from zinc–graphite-natural biodegradable polymer paste," Journal of Applied Electrochemistry, vol. 32, no. 12, pp. 1347-1353, 2002, doi: 10.1023/A:1022619414787.

[404] T. Huh and J. W. Evans, "Electrical and Electrochemical Behavior of Fluidized Bed Electrodes: I . Potential Transients and Time-Averaged Values," Journal of The Electrochemical Society, vol. 134, no. 2, pp. 308-317, February 1, 1987 1987, doi: 10.1149/1.2100452.

[405] A. M. Langde, D. J. Tidke, and R. L. Sonolikar, "Experimental Investigation of Minimum Fluidization Velocity of Micron Size Particles in Presence of Sound," in 2012 Fifth International Conference on Emerging Trends in Engineering and Technology, 5-7 Nov. 2012 2012, pp. 207-210, doi: 10.1109/ICETET.2012.58.

[406] E. Mehrabi Gohari, M. Sefid, and E. Jahanshahi Javaran, "Numerical simulation of the hydrodynamics of an inverse liquid–solid fluidized bed using combined Lattice Boltzmann and smoothed profile methods," Journal of Dispersion Science and Technology, vol. 38, no. 10, pp. 1471-1482, 2017/10/03 2017, doi: 10.1080/01932691.2016.1253482.

[407] J. F. Claydon. "Hydrodynamic (Fluids in Motion)." http://www.jfccivilengineer.com/index.htm (accessed.

[408] V. E. W. Holder. "Types of flows and benefits." http://www.vewh.vic.gov.au/environmental-water/types-of-flows-and-benefits (accessed.

[409] M. S and F. RO, "Effect of two-fluid model formulation on flow-regime predictions for bubble-column simulations," AIChE J., vol. 53, p. 9, 2007.

[410] R. O. Fox, A. B, and S. WA, "Large-Eddy-Simulation Tools for Multiphase Flows Droplet vaporization model for spray combustion calculations," Annual Review of Fluid Mechanics, vol. 44, no. 1, pp. 47-76, 2012, doi: doi:10.1146/annurev-fluid-120710-101118.

[411] C. S. Jog, Fluid Mechanics Foundations and Applications of Mechanics, 3rd ed. Indian Institute of Science, Bangalore, 2015, p. 589.

[412] X. Li, M. Liu, and Y. Li, "Hydrodynamic behavior of liquid–solid micro-fluidized beds determined from bed expansion," Particuology, vol. 38, pp. 103-112, 2018, doi: 10.1016/j.partic.2017.08.002.

[413] S. V. Ghatage et al., "Stability analysis in solid-liquid fluidized beds: Experimental and computational," Chem. Eng. J., vol. 256, pp. 169-186, 2014, doi: 10.1016/j.cej.2014.06.026.

[414] S. Weber, C. Briens, F. Berruti, E. Chan, and M. Gray, "Agglomerate stability in fluidized beds of glass beads and silica sand," Powder Technology, vol. 165, no. 3, pp. 115-127, 2006, doi: 10.1016/j.powtec.2006.03.006.

[415] N. Gnanasundaram, M. Loganathan, and K. Perumal, "Solid holdup in liquid solid circulating fluidized bed with viscous liquid medium," Alexandria Engineering Journal, vol. 53, no. 4, pp. 959-968, 12// 2014, doi: http://dx.doi.org/10.1016/j.aej.2014.08.001.

[416] P. K. G. "**What is difference between laminar and viscous flow?**" G Pavan Kumar. https://www.quora.com/What-is-difference-between-laminar-and-viscous-flow (accessed 25/08, 2018).

[417] S. M. H. Karimian and G. E. Schneider, "Pressure-based control-volume finite element method for flow at all speeds," AIAA Journal, vol. 33, no. 9, pp. 1611-1618, 1995/09/01 1995, doi: 10.2514/3.12700.

[418] S. M. H. Karimian and G. E. Schneider, "Pressure-based computational method for compressible and incompressible flows," Journal of Thermophysics and Heat Transfer, vol. 8, no. 2, pp. 267-274, 1994/04/01 1994, doi: 10.2514/3.533.

[419] F. A. Morrison. "Compressible Fluids." Michigan Technological University. http://www.chem.mtu.edu/~fmorriso/cm310/compressible_flow.pdf (accessed.

[420] J.-P. B. Thomas B. Gatski, Compressibility, Turbulence and High Speed Flow, 2nd ed. 2013.

[421] S. Jing, Q. Hu, J. Wang, and Y. Jin, "Fluidization of coarse particles in gas–solid conical beds," Chemical Engineering & Processing: Process Intensification, vol. 39, no. 4, pp. 379-387, 2000, doi: 10.1016/S0255-2701(99)00103-8.

[422] E. Ireland, K. Pitt, and R. Smith, "A review of pulsed flow fluidisation; the effects of intermittent gas flow on fluidised gas–solid bed behaviour," Powder Technology, vol. 292, pp. 108-121, 2016, doi: 10.1016/j.powtec.2016.01.018.

[423] I. Nezu and R. Azuma, "Turbulence Characteristics and Interaction between Particles and Fluid in Particle-Laden Open Channel Flows," Journal of Hydraulic Engineering, vol. 130, no. 10, pp. 988-1001, 2004, doi: doi:10.1061/(ASCE)0733-9429(2004)130:10(988).

[424] C. CT, T. TR, and C. JN, "Numerical models for two-phase turbulent flows," Annu. Rev. Fluid Mech., vol. 28, p. 11, 1996.

[425] C. D. Scott and C. W. Hancher, "Use of a tapered fluidized bed as a Continuous bioreactor," Biotechnology and Bioengineering, vol. 18, no. 10, pp. 1393-1403, 1976, doi: 10.1002/bit.260181006.

[426] H. Sutar and C. K. Das, "Mixing and Segregation Characteristics of Binary Granular Material in Tapered Fluidized Bed: A CFD Study," Engineering, vol. 04, no. 04, pp. 215-227, 2012, doi: 10.4236/eng.2012.44029.

[427] M. L. V. de Chiara, M. L. Amodio, F. Scura, L. Spremulli, and G. Colelli, "Design and preliminary test of a fluidised bed photoreactor for ethylene oxidation on mesoporous mixed SiO2/TiO2 nanocomposites under UV-A illumination," 2014, ethylene reduction, fluidised bed photoreactor, postharvest storage, titanium oxide. vol. 45, no. 4, p. 7, 2014-12-21 2014, doi: 10.4081/jae.2014.435.

[428] C.-L. L. a. S.-D. Y. Ming-Yen Wey, "FLUIDIZED BEHAVIOR AND HEAT TRANSFER IN A BUBBLING FLUIDIZED BED INCINERATOR," J. Environ. Eng. Manage, vol. 17, no. 3, pp. 169-175, 2007.

[429] S. S. T. a. K. K. K. S. Suresh P Singh, "Direct prediction of Expanded Bed Height as a function of Reduced Reynolds Number in a Gas Solid Fluidization," International Journal of Current Engineering and Technology, vol. 3, no. 2, pp. 374-377, 2013.

[430] J. Khorshidi and H. Davari, "Experimental Study of Drying Process of COLZA Seeds in Fluidized Bed Dryer by Statistical Methods," Advances in Chemical Engineering and Science, vol. 02, no. 01, pp. 129-135, 2012, doi: 10.4236/aces.2012.21016.

[431] Z. Zhiping, N. Yongjie, and L. Qinggang, "Effect of pressure on minimum fluidization velocity," Journal of Thermal Science, journal article vol. 16, no. 3, pp. 264-269, 2007, doi: 10.1007/s11630-007-0264-2.

[432] B. Paudel and Z.-G. Feng, "Prediction of minimum fluidization velocity for binary mixtures of biomass and inert particles," Powder Technology, vol. 237, pp. 134-140, 3// 2013, doi: http://dx.doi.org/10.1016/j.powtec.2013.01.031.

[433] G. Najafpour, Biochemical Engineering and Biotechnology. Netherlands, 2007.

[434] T. M. a. H. Sato, "Liquid fluidization in conical vessels," The Chemical Engineering Journal, vol. 46, pp. 15-21, August 22, 1990 1991.

[435] RheoSense. "Viscosity of Newtonian and non-Newtonian Fluids." http://www.rheosense.com/applications/viscosity/newtonian-non-newtonian (accessed 20th May, 2016).

[436] S. V. a. S. Kandasamy, "Prediction of Minimum Fluidization Velocity inTwo-Phase and Three-Phase Fluidized Beds: Air/Newtonian and Non-Newtonian Liquids," INTERNATIONAL JOURNALOFCHEMICAL REACTOR ENGINEERING, vol. 8, pp. 1-18, 2010.

[437] F. A. U. O. i. C. Engineering. "Experimental and Theoretical Determination of the Minimum Velocity of Fluidization." Unit Operations Laboratory, Department of Chemical Engineering, University of Florida. http://ww2.che.ufl.edu/unit-ops-lab/experiments/FB/FB-manual.pdf (accessed 1/11, 2018).

[438] M. Taghavivand, K. Choi, and L. Zhang, "Investigation on drying kinetics and tribocharging behaviour of pharmaceutical granules in a fluidized bed dryer," Powder Technology, vol. 316, pp. 171-180, 2017, doi: 10.1016/j.powtec.2016.10.061.

[439] P. G. Carman, "Fluid flow through granular beds," Chemical Engineering Research and Design, vol. 75, no. 1, pp. S32-S46, 1997.

[440] A. K. Johnson, A. L. Yarin, and F. Mashayek, "Packing density and the Kozeny-Carman equation," Neurosurgery, vol. 71, no. 5, p. E1064, 2012, doi: 10.1227/NEU.0b013e31826c57d6.

[441] Y. Gao, X. Li, and H. Ding, "Layer modeling of zinc removal from metallic mixture of waste printed circuit boards by vacuum distillation," Waste Management, vol. 42, no. C, pp. 188-195, 2015, doi: 10.1016/j.wasman.2015.04.023.

[442] A. Rabbani and S. Jamshidi, "Specific surface and porosity relationship for sandstones for prediction of permeability," International Journal of Rock Mechanics and Mining Sciences, vol. 71, no. C, pp. 25-32, 2014, doi: 10.1016/j.ijrmms.2014.06.013.

[443] W.-C. Yang, "Handbook of fluidization and fluid-particle systems (Book Review)," China Particuology, vol. 1, no. 3, pp. 137-137, 2003, doi: 10.1016/S1672-2515(07)60126-2.

[444] M. C. Wu, T. S. Zhao, L. Wei, H. R. Jiang, and R. H. Zhang, "Improved electrolyte for zinc-bromine flow batteries," Journal of Power Sources, vol. 384, pp. 232-239, 2018, doi: 10.1016/j.jpowsour.2018.03.006.

[445] T. Hashimoto, "Electrolyte for zinc bromide battery," (in English), 1993. [Online]. Available: https://patents.google.com/patent/US5188915

[446] F. Wang and L.-S. Fan, "Gas−Solid Fluidization in Mini- and Micro-channels," Industrial & Engineering Chemistry Research, vol. 50, no. 8, pp. 4741-4751, 2011/04/20 2011, doi: 10.1021/ie102245m.

[447] Y. Xiao, D. J. Roberts, G. Zuo, M. Badruzzaman, and G. S. Lehman, "Characterization of microbial populations in pilot-scale fluidized-bed reactors treating perchlorate- and nitrate-laden brine," Water Research, vol. 44, no. 14, pp. 4029-4036, 2010, doi: 10.1016/j.watres.2010.05.006.

[448] A. K. Venkatesan, M. Sharbatmaleki, and J. R. Batista, "Bioregeneration of perchlorate-laden gel-type anion-exchange resin in a fluidized bed reactor," Journal of Hazardous Materials, vol. 177, no. 1, pp. 730-737, 2010, doi: 10.1016/j.jhazmat.2009.12.092.

[449] A. Sahu, T. Conneely, K. Nüsslein, and S. Ergas, "Biological Perchlorate Reduction in Packed Bed Reactors Using Elemental Sulfur," Environmental Science & Technology, vol. 43, no. 12, p. 4466, 2009, doi: 10.1021/es900563f.

[450] P. J. Thomas, G. L. Stansfield, and P. V. Vanitha, "Nanoparticles," Annu. Rep. Prog. Chem., Sect. A: Inorg. Chem., vol. 107, pp. 505-518, 2011, doi: 10.1039/c1ic90030g.

[451] P. Kundu, E. A. Anumol, C. Nethravathi, and N. Ravishankar, "Existing and emerging strategies for the synthesis of nanoscale heterostructures," Phys. Chem. Chem. Phys., vol. 13, no. 43, pp. 19256-19269, 2011, doi: 10.1039/c1cp22343g.

[452] A. Karau, C. Benken, J. Thömmes, and M. R. Kula, "The influence of particle size distribution and operating conditions on the adsorption performance in fluidized beds," Biotechnology and Bioengineering, vol. 55, no. 1, pp. 54-64, 1997, doi: 10.1002/(SICI)1097-0290(19970705)55:1<54::AID-BIT7>3.0.CO;2-W.

[453] Y. A. Hassan and C. Kang, "Pressure Drop in a Pebble Bed Reactor Under High Reynolds Number," Nuclear Technology, vol. 180, no. 2, pp. 159-173, 2012, doi: 10.13182/NT12-A14631.

[454] R. Di Felice, "Hydrodynamics of liquid fluidisation," Chemical Engineering Science, vol. 50, no. 8, pp. 1213-1245, 1995, doi: 10.1016/0009-2509(95)98838-6.

[455] S. Shaul, E. Rabinovich, and H. Kalman, "Typical Fluidization Characteristics for Geldart's Classification Groups," Particulate Science and Technology, vol. 32, no. 2, 2013, doi: 10.1080/02726351.2013.842624.

[456] D. Geldart and A. C. Y. Wong, "Fluidization of powders showing degrees of cohesiveness—I. Bed expansion," Chemical Engineering Science, vol. 39, no. 10, pp. 1481-1488, 1984, doi: 10.1016/0009-2509(84)80006-8.

[457] A. Eich. "Theory and Application of Viscometry with Glass Capillary Viscometers." http://www.chemeurope.com/en/whitepapers/126491/visco-handbook.html (accessed 12/04/2017, 2017).

[458] G. B. Tupper, I. Govender, and A. N. Mainza, "Predicting flows from the Dynamic Ergun Equation," Minerals Engineering, vol. 103-104, pp. 11-13, 2017, doi: 10.1016/j.mineng.2016.07.014.

[459] W. Wong, D. F. Fletcher, D. Traini, H.-K. Chan, and P. M. Young, "The use of computational approaches in inhaler development," Advanced Drug Delivery Reviews, vol. 64, no. 4, pp. 312-322, 2012, doi: 10.1016/j.addr.2011.10.004.

[460] P. Cleary, "Industrial particle flow modelling using discrete element method," Engineering Computations, vol. 26, no. 6, pp. 698-743, 2009, doi: 10.1108/02644400910975487.

[461] A. Tamrakar, D. R. Devarampally, and R. Ramachandran, Chapter 7 - Advanced multiphase hybrid model development of fluidized bed wet granulation processes. 2018, pp. 159-187.
[462] R. Wood, "Simulating fluidized beds accurately using EDEM coupled with ANSYS Fluent," 2017.
[463] Y. Guo and J. S. Curtis, "Discrete Element Method Simulations for Complex Granular Flows," Annu. Rev. Fluid Mech., vol. 47, no. 1, pp. 21-46, 2015, doi: 10.1146/annurev-fluid-010814-014644.
[464] M. Sakai, Y. Yamada, Y. Shigeto, K. Shibata, V. M. Kawasaki, and S. Koshizuka, "Large-scale discrete element modeling in a fluidized bed," International Journal for Numerical Methods in Fluids, vol. 64, no. 10-12, pp. 1319-1335, 2010, doi: 10.1002/fld.2364.
[465] I. ANSYS. "Classification of Multiphase Flow Models." http://www.ansys.org/staticassets/ANSYS/staticassets/resourcelibrary/presentation/brazil-2014ugm-validation-of-filtered-two-fluid-models-for-gasparticle.pdf (accessed.
[466] V. Yarlagadda, G. Lin, P. Y. Chong, and T. Van Nguyen, "High Active Surface Area and Durable Multi-Wall Carbon Nanotube-Based Electrodes for the Bromine Reactions in H2-Br2Fuel Cells," Journal of The Electrochemical Society, vol. 163, no. 1, pp. A5134-A5143, 2015, doi: 10.1149/2.0181601jes.
[467] V. Yarlagadda and T. Van Nguyen, "High Surface Area Carbon Electrodes for the Bromine Reactions in H2-Br2 Fuel Cells," ECS Transactions, vol. 58, no. 36, pp. 25-32, 2014.
[468] E. Agar, C. R. Dennison, K. W. Knehr, and E. C. Kumbur, "Identification of performance limiting electrode using asymmetric cell configuration in vanadium redox flow batteries," Journal of Power Sources, vol. 225, pp. 89-94, 3/1/ 2013, doi: http://dx.doi.org/10.1016/j.jpowsour.2012.10.016.
[469] Ansys, "Solver Numerics in ANSYS Fluent for Single Phase Flows," ed, 2015.
[470] J. F. Richardson, J. H. Harker, and J. R. Backhurst, "CHAPTER 1 - Particulate Solids," in Chemical Engineering (Fifth Edition). Oxford: Butterworth-Heinemann, 2002, pp. 1-94.
[471] D. C. Sau, S. Mohanty, and K. C. Biswal, "Minimum fluidization velocities and maximum bed pressure drops for gas–solid tapered fluidized beds," Chemical Engineering Journal, vol. 132, no. 1, pp. 151-157, 2007/08/01/ 2007, doi: https://doi.org/10.1016/j.cej.2007.01.036.
[472] A. Delebarre, "Revisiting the Wen and Yu Equations for Minimum Fluidization Velocity Prediction," Chemical Engineering Research and Design, vol. 82, no. 5, pp. 587–590, 2004.
[473] W. H. Hui, "A unified coordinates approach to computational fluid dynamics," Journal of Computational and Applied Mathematics, vol. 163, no. 1, pp. 15-28, 2004/02/01/ 2004, doi: https://doi.org/10.1016/j.cam.2003.08.051.
[474] M. Sakai, "How Should the Discrete Element Method Be Applied in Industrial Systems?: A Review," KONA Powder and Particle Journal, vol. 33, no. 0, pp. 169-178, 2016, doi: 10.14356/kona.2016023.
[475] N. G. Deen, M. Van Sint Annaland, M. A. Van der Hoef, and J. A. M. Kuipers, "Review of discrete particle modeling of fluidized beds," Chemical Engineering Science, vol. 62, no. 1–2, pp. 28-44, 1// 2007, doi: http://dx.doi.org/10.1016/j.ces.2006.08.014.
[476] I. J. Eshita, "Turbulence Modeling of Source and Sink Flows," World Academy of Science, Engineering and Technology International Journal of Mechanical and Mechatronics Engineering, vol. 2018, no. 11/02/2018, pp. 830-835, 2014.
[477] H.-W. Nienhuys and A. F. Stappen, "A Delaunay Approach to Interactive Cutting in Triangulated Surfaces," in Algorithmic Foundations of Robotics V, J.-D. Boissonnat, J. Burdick, K. Goldberg, and S. Hutchinson Eds. Berlin, Heidelberg: Springer Berlin Heidelberg, 2004, pp. 113-129.

[478] M. Mezhericher, T. Brosh, and A. Levy, "Modeling of Particle Pneumatic Conveying Using DEM and DPM Methods," Particulate Science and Technology, vol. 29, no. 2, pp. 197-208, 2011, doi: 10.1080/02726351003792914.

[479] N. Behera, V. K. Agarwal, M. G. Jones, and K. C. Williams, "CFD modeling and analysis of dense phase pneumatic conveying of fine particles including particle size distribution," Powder Technology, vol. 244, pp. 30-37, 2013, doi: 10.1016/j.powtec.2013.04.005.

[480] M. S. Gobinath P. Rajarathnam, Xihe Sun, and Anthony M. Vassallo, "The Influence of Supporting Electrolytes on Zinc Half-Cell Performance in Zinc/Bromine Flow Batteries," Journal of The Electrochemical Society, vol. 163, no. 1, pp. A5112-A5117, 2016.

[481] E. Instruments. "UV/ Visible Spectroscopy." (accessed 14/12, 2019).

[482] M. J. K. Thomas, Ultraviolet and visible spectroscopy, 2nd ed. ed. Published on behalf of ACOL University of Greenwich by J. Wiley, 1996.

[483] D. C. Stone. "Molecular Spectroscopy Resources." https://sites.chem.utoronto.ca/chemistry/coursenotes/analsci/molec/uv-vis1.html (accessed 14/12, 2019).

[484] E. Mocellin and T. Goscinska, "Modified carbon electrodes for microscale electrochemistry," Journal of Chemical Education, vol. 75, no. 6, pp. 771-772, 1998, doi: 10.1021/ed075p771.

[485] M. A. T. Gilmartin and J. P. Hart, "Sensing with chemically and biologically modified carbon electrodes. A review," The Analyst, vol. 120, no. 4, pp. 1029-1045, 1995, doi: 10.1039/AN9952001029.

[486] A. V. Abramov et al., "Corrosion resistance of nickel-based alloys in salt and metal melts containing REE," vol. 1886, ed, 2017.

[487] V. Ignat'ev et al., "Investigation of the corrosion resistance of nickel-based alloys in fluoride melts," Atomic Energy, vol. 101, no. 4, pp. 730-738, 2006, doi: 10.1007/s10512-006-0160-y.

[488] V. Konoval, "Corrosion resistance of titanium-chromium diboride and composite material based on it," Refractories and Industrial Ceramics, vol. 51, no. 5, pp. 370-373, 2011, doi: 10.1007/s11148-011-9327-8.

[489] W. H. Smith, "Electroanalytical Chemistry: Basic Principles and Applications (Plambeck, James A.)," Journal of Chemical Education, vol. 61, no. 6, p. A185, 1984, doi: 10.1021/ed061pA185.3.

[490] "Allen J. Bard and Larry R. Faulkner, Electrochemical Methods: Fundamentals and Applications , New York: Wiley, 2001, 2nd ed," Russian Journal of Electrochemistry, vol. 38, no. 12, pp. 1364-1365, 2002, doi: 10.1023/A:1021637209564.

[491] M. A. Brett Christopher and M. Oliveira Brett Ana, Cyclic Linear Voltammetry and Sweep Techniques. Oxford University Press, 1993, pp. 1-1.

[492] K. Polat, M. Aksu, and A. Pekel, "Electroreduction of nitrobenzene to p-aminophenol using voltammetric and semipilot scale preparative electrolysis techniques," J. Appl. Electrochem., vol. 32, no. 2, pp. 217-223, 2002.

[493] R. Wartena, J. Winnick, and P. Pfromm, "Recycling kraft pulping chemicals with molten salt electrolysis," J. Electrochem. Soc., vol. 149, no. 9, pp. D125-D131, 2002, doi: 10.1149/1.1495907.

[494] Z. Hu, P. R. Troyk, and S. F. Cogan, "Comprehensive Cyclic Voltammetry Characterization of AIROF Microelectrodes," in 2005 IEEE Engineering in Medicine and Biology 27th Annual Conference, 17-18 Jan. 2006 2005, pp. 5246-5249, doi: 10.1109/IEMBS.2005.1615662.

[495] N. Elgrishi, K. J. Rountree, B. D. McCarthy, E. S. Rountree, T. T. Eisenhart, and J. L. Dempsey, "A Practical Beginner's Guide to Cyclic Voltammetry," Journal of Chemical Education, vol. 95, no. 2, pp. 194-206, 2018, doi: 10.1021/acs.jchemed.7b00361.

[496] G. A. Mabbott, "An introduction to cyclic voltammetry," Journal of Chemical Education, vol. 60, no. 9, pp. 697-702, 1983, doi: 10.1021/ed060p697.
[497] P. Zuman, "Electrochemistry in non-aqueous solutions: Kosuke Izutsu. Wiley–VCH Verlag GmbH, D-69469 Weinheim, Germany, 2002, ISBN 3-527-30516-5. (Book Review)," vol. 75, ed, 2003, pp. 139-140.
[498] P. T. Kissinger and W. R. Heineman, "Cyclic voltammetry," Journal of Chemical Education, vol. 60, no. 9, p. 702, 1983, doi: 10.1021/ed060p702.
[499] H. Gürsu, M. Gençten, and Y. Şahin, "One-step electrochemical preparation of graphene-coated pencil graphite electrodes by cyclic voltammetry and their application in vanadium redox batteries," Electrochimica Acta, vol. 243, pp. 239-249, 2017, doi: 10.1016/j.electacta.2017.05.065.
[500] M. S. Jagadeesh et al., "The effect of cyclic voltammetry speed on anion intercalation in HOPG," Surface Science, vol. 681, pp. 111-115, 2019, doi: 10.1016/j.susc.2018.11.009.
[501] G. Nikiforidis and W. A. Daoud, "Indium modified graphite electrodes on highly zinc containing methanesulfonate electrolyte for zinc-cerium redox flow battery," Electrochimica Acta, vol. 168, pp. 394-402, 2015, doi: 10.1016/j.electacta.2015.03.118.
[502] K. Q. David P. Trudgeon, Xiaohong Li, Tapas Mallick, Oluwadamilola O. Taiwo, Barun Chakrabarti, Vladimir Yufit, Nigel P. Brandon, David Crevillen-Garcia, Akeel Shah, "Screening of effective electrolyte additives for zinc-based redox flow battery systems," vol. 412, pp. 44-45, 2019.
[503] F. Walsh, "Modern aspects of electrochemistry, volume 27: R.E. White, J.O'M. Bockris and B.E. Conway (eds.) Plenum, New York, 1995, ISBN 0-306-44930-7, xiv + 552 pages, $115 (Book Review)," vol. 402, ed, 1996, pp. 225-226.
[504] N. Pismenskaia, P. Sistat, P. Huguet, V. Nikonenko, and G. Pourcelly, "Chronopotentiometry applied to the study of ion transfer through anion exchange membranes," Journal of Membrane Science, vol. 228, no. 1, pp. 65-76, 2004, doi: 10.1016/j.memsci.2003.09.012.
[505] F. C. Anson, "Chronopotentiometry of Iron(II) and Iron(III) Adsorbed on Platinum Electrodes," Analytical Chemistry, vol. 33, no. 11, pp. 1498-1502, 1961, doi: 10.1021/ac60179a014.
[506] F. C. Anson, "A new technique for the direct study of reactant adsorption at platinum electrodes [2]," Journal of the American Chemical Society, vol. 83, no. 10, pp. 2387-2388, 1961, doi: 10.1021/ja01471a036.
[507] H. B. Herman and A. J. Bard, "Cyclic Chronopotentiometry: Diffusion Controlled Electrode Reaction of a Single Component System," Analytical Chemistry, vol. 35, no. 9, pp. 1121-1125, 1963, doi: 10.1021/ac60202a048.
[508] S. V. Tatwawadi and A. J. Bard, "Chronopotentiometric measurement of adsorption. Riboflavin on a mercury electrode," Analytical Chemistry, vol. 36, no. 1, pp. 2-5, 1964, doi: 10.1021/ac60207a007.
[509] R. W. Murray, "Chronopotentiometric and chronocoulometric measurements of adsorption of lead and mercury(ll) at mercury electrodes," Analytical Chemistry, vol. 38, no. 3, pp. 392-404, 1966, doi: 10.1021/ac60235a006.
[510] V. M. Andre, C. Cepeda, V. V. Harry, M. W. Gary, and L. S. Michael, "Monday, December 4, 2006Poster Session IV7:30 a.m. - 4:30 p.m.(Author abstract)(Report)," Epilepsia, vol. 47, no. s4, p. 289, 2006, doi: 10.1111/j.1528-1167.2006.00001_8.x.
[511] F. G. Wilhelm, N. F. A. van Der Vegt, H. Strathmann, and M. Wessling, "Comparison of bipolar membranes by means of chronopotentiometry," Journal of Membrane Science, vol. 199, no. 1, pp. 177-190, 2002, doi: 10.1016/S0376-7388(01)00696-2.

[512] R. Audinos and G. Pichelin, "Characterization of electrodialysis membranes by chronopotentiometry," Desalination, vol. 68, no. 2-3, pp. 251-263, 1988, doi: 10.1016/0011-9164(88)80059-6.

[513] P. Sistat and G. Pourcelly, "Chronopotentiometric response of an ion-exchange membrane in the underlimiting current-range. Transport phenomena within the diffusion layers," Journal of Membrane Science, vol. 123, no. 1, pp. 121-131, 1997, doi: 10.1016/S0376-7388(96)00210-4.

[514] J. J. Krol, M. Wessling, and H. Strathmann, "Chronopotentiometry and overlimiting ion transport through monopolar ion exchange membranes," Journal of Membrane Science, vol. 162, no. 1, pp. 155-164, 1999, doi: 10.1016/S0376-7388(99)00134-9.

[515] J.-H. Choi and S.-H. Moon, "Pore size characterization of cation-exchange membranes by chronopotentiometry using homologous amine ions," Journal of Membrane Science, vol. 191, no. 1, pp. 225-236, 2001, doi: 10.1016/S0376-7388(01)00513-0.

[516] P. Ray, V. K. Shahi, T. V. Pathak, and G. Ramachandraiah, "Transport phenomenon as a function of counter and co-ions in solution: chronopotentiometric behavior of anion exchange membrane in different aqueous electrolyte solutions," Journal of Membrane Science, vol. 160, no. 2, pp. 243-254, 1999, doi: 10.1016/S0376-7388(99)00088-5.

[517] L. Marder, E. M. Ortega Navarro, V. Pérez-Herranz, A. M. Bernardes, and J. Z. Ferreira, "Evaluation of transition metals transport properties through a cation-exchange membrane by chronopotentiometry," Journal of Membrane Science, vol. 284, no. 1, pp. 267-275, 2006, doi: 10.1016/j.memsci.2006.07.039.

[518] N. J. Evans and B. Sayers, "Recent advances in electrochemical impedance measurement," in Proceedings of 16th Annual International Conference of the IEEE Engineering in Medicine and Biology Society, 3-6 Nov. 1994 1994, vol. 1, p. A72 vol.1, doi: 10.1109/IEMBS.1994.412156.

[519] B. Bullecks, R. Suresh, and R. Rengaswamy, "Rapid impedance measurement using chirp signals for electrochemical system analysis," Computers & Chemical Engineering, vol. 106, no. Supplement C, pp. 421-436, 2017/11/02/ 2017, doi: https://doi.org/10.1016/j.compchemeng.2017.05.018.

[520] D. C. Fair, "The year of the recall: with product recalls and quality issues on the rise, more and more manufacturers are turning to statistical process control," Quality, vol. 47, no. 1, p. 48, 2008.

[521] C. Menictas, M. Skyllas-Kazacos, and T. M. Lim, Advances in Batteries for Medium and Large-Scale Energy Storage: Types and Applications. Elsevier Science, 2014.

[522] K. Wang et al., "Growth of oxygen bubbles during recharge process in zinc-air battery," Journal of Power Sources, vol. 296, pp. 40-45, 2015, doi: 10.1016/j.jpowsour.2015.07.039.

[523] P. Zhang, J. Liang, and F. Zhang, "An Overview of Different Approaches for Battery Lifetime Prediction," vol. 199, ed, 2017, p. <xocs:firstpage xmlns:xocs=""/>.

[524] C. Chen, A. Yuan, H. Zhao, and J. Xu, "Electrochemical behavior of olivine-type LiMnPO.sub.4-based material in a mild aqueous electrolyte.(Report)," Ionics, vol. 18, no. 7, p. 635, 2012, doi: 10.1007/s11581-012-0677-0.

[525] D. Aurbach, B. Markovsky, Y. Talyossef, G. Salitra, H.-J. Kim, and S. Choi, "Studies of cycling behavior, ageing, and interfacial reactions of LiNi0.5Mn1.5O4 and carbon electrodes for lithium-ion 5-V cells," Journal of Power Sources, vol. 162, no. 2, pp. 780-789, 11/22/ 2006, doi: http://dx.doi.org/10.1016/j.jpowsour.2005.07.009.

[526] J. G. Patrick T. Moseley, Electrochemical Energy Storage for Renewable Sources and Grid Balancing, reprint ed. Newnes, 2014, p. 492.

[527] S. M. Haile, "Materials for fuel cells," Materials Today, vol. 6, no. 3, pp. 24-29, 2003, doi: 10.1016/S1369-7021(03)00331-6.

[528] D. Haseltine, "Exploring our energy future," Chemical Engineering Progress, vol. 96, no. 1, p. 75, 2000.
[529] H. R. Jiang, W. Shyy, M. C. Wu, L. Wei, and T. S. Zhao, "Highly active, bi-functional and metal-free B4C-nanoparticle-modified graphite felt electrodes for vanadium redox flow batteries," Journal of Power Sources, Article vol. 365, pp. 34-42, 2017, doi: 10.1016/j.jpowsour.2017.08.075.
[530] L. Wei, T. S. Zhao, G. Zhao, L. An, and L. Zeng, "A high-performance carbon nanoparticle-decorated graphite felt electrode for vanadium redox flow batteries," Applied Energy, Article vol. 176, pp. 74-79, 2016, doi: 10.1016/j.apenergy.2016.05.048.
[531] C. Menictas, M. Skyllas-Kazacos, and T. M. Lim, Advances in batteries for medium- and large-scale energy storage. Oxford: Woodhead Publishing, 2015.
[532] K. Kordesch and J. Daniel-Ivad, Handbook of Batteries, vol. 36, pp. 1168-1185, 2002.
[533] L.-L. M. E.-. LME. "LME ZINC OFFICIAL PRICES, US$ PER TONNE." https://www.lme.com/Metals/Non-ferrous/Zinc#tabIndex=0 (accessed 15/06, 2018).
[534] M. Fleischmanm, L. R. Hill, and G. Sundholm, J. Electroanal. Chem., vol. 157, pp. 359-368, 1983.
[535] X. G. Zhang, Corrosion and Electrochemistry of Zinc, vol. vol. Chapter 1, pp. 1-16, 1996.
[536] D. Crotty, "Zinc alloy plating for the automotive industry," Metal Finishing, Article vol. 94, no. 9, pp. 54-58, 1996, doi: 10.1016/0026-0576(96)82103-9.
[537] E. Budman and R. R. Sizelove, "Zinc alloy plating," J. Met. Finish., vol. 99, pp. 334-339, 2001.
[538] A. E. Saba and A. E. Elsherief, "Continuous electrowinning of zinc," Hydrometallurgy, vol. 54, no. 2–3, pp. 91-106, 1// 2000, doi: http://dx.doi.org/10.1016/S0304-386X(99)00061-4.
[539] E. Budman, "Alkaline noncyanide zinc plating," Metal Finishing, vol. 93, no. 2, pp. 60-63, 1995, doi: 10.1016/0026-0576(95)93303-J.
[540] G. Trejo, R. Ortega B, Y. Meas V, P. Ozil, E. Chainet, and B. Nguyen, "Nucleation and growth of zinc from chloride concentrated solutions," Journal of the Electrochemical Society, Article vol. 145, no. 12, pp. 4090-4097, 1998, doi: 10.1149/1.1838919.
[541] P. Díaz-Arista, Y. Meas, R. Ortega, and G. Trejo, "Electrochemical and AFM study of Zn electrodeposition in the presence of benzylideneacetone in a chloride-based acidic bath," Journal of Applied Electrochemistry, Article vol. 35, no. 2, pp. 217-227, 2005, doi: 10.1007/s10800-004-6304-7.
[542] K. A. Kobe, "Modern electroplating," Journal of Chemical Education, vol. 31, no. 6, p. 335, 1954, doi: 10.1021/ed031p335.3.
[543] D. R. Gabe and M. Clarke, Electroplating. 2013, pp. 12:3-50.
[544] K. M. S. Youssef, C. C. Koch, and P. S. Fedkiw, "Improved corrosion behavior of nanocrystalline zinc produced by pulse-current electrodeposition," Corrosion Science, Article vol. 46, no. 1, pp. 51-64, 2004, doi: 10.1016/S0010-938X(03)00142-2.
[545] K. M. S. Youssef, C. C. Koch, and P. S. Fedkiw, "Influence of Additives and Pulse Electrodeposition Parameters on Production of Nanocrystalline Zinc from Zinc Chloride Electrolytes," Journal of the Electrochemical Society, Article vol. 151, no. 2, pp. C103-C111, 2004, doi: 10.1149/1.1636739.
[546] A. Gomes and M. I. Da Silva Pereira, "Pulsed electrodeposition of Zn in the presence of surfactants," Electrochimica Acta, Article vol. 51, no. 7, pp. 1342-1350, 2006, doi: 10.1016/j.electacta.2005.06.023.
[547] J. Yu, Y. Chen, H. Yang, and Q. Huang, "Influences of organic additives on zinc electrocrystallization from KCl solutions," Journal of the Electrochemical Society, Article vol. 146, no. 5, pp. 1789-1793, 1999, doi: 10.1149/1.1391844.

[548] A. Gomes, A. S. Viana, and M. I. Da Silva Pereira, "Potentiostatic and AFM morphological studies of Zn electrodeposition in the presence of surfactants," Journal of the Electrochemical Society, Article vol. 154, no. 9, pp. D452-D461, 2007, doi: 10.1149/1.2752984.
[549] D. Muñoz-Torrero et al., "Investigation of different anode materials for aluminium rechargeable batteries," Journal of Power Sources, Article vol. 374, pp. 77-83, 2018, doi: 10.1016/j.jpowsour.2017.11.032.
[550] K. Gong, Q. Fang, S. Gu, S. F. Y. Li, and Y. Yan, "Nonaqueous redox-flow batteries: Organic solvents, supporting electrolytes, and redox pairs," Energy and Environmental Science, Review vol. 8, no. 12, pp. 3515-3530, 2015, doi: 10.1039/c5ee02341f.
[551] Y. Zhao et al., "A chemistry and material perspective on lithium redox flow batteries towards high-density electrical energy storage," Chemical Society Reviews, Review vol. 44, no. 22, pp. 7968-7996, 2015, doi: 10.1039/c5cs00289c.
[552] R.-R. S. o. C.-. RSC. "Periodic Table." Royal Society of Chemistry. http://www.rsc.org/periodic-table/element/30/zinc (accessed 15/06, 2018).
[553] Calvert. "Zinc and Cadmium." http://mysite.du.edu/~jcalvert/phys/zinc.htm (accessed 15/06, 2018).
[554] D. W. McComsey, Handbook of Batteries, vol. 8, pp. 184-228, 2002.
[555] J. W. Gallaway et al., "Real-time materials evolution visualized within intact cycling alkaline batteries," Journal of Materials Chemistry A, Article vol. 2, no. 8, pp. 2757-2764, 2014, doi: 10.1039/c3ta15169g.
[556] R. Patrice et al., "Understanding the Second Electron Discharge Plateau in MnO2-Based Alkaline Cells," Journal of the Electrochemical Society, Article vol. 148, no. 5, pp. A448-A455, 2001, doi: 10.1149/1.1362539.
[557] Q. Xu and T. S. Zhao, "Fundamental models for flow batteries," Progress in Energy and Combustion Science, Review vol. 49, pp. 40-58, 2015, doi: 10.1016/j.pecs.2015.02.001.
[558] C. Choi et al., "A review of vanadium electrolytes for vanadium redox flow batteries," Renewable and Sustainable Energy Reviews, Review vol. 69, pp. 263-274, 2017, doi: 10.1016/j.rser.2016.11.188.
[559] K. J. Kim, M. S. Park, Y. J. Kim, J. H. Kim, S. X. Dou, and M. Skyllas-Kazacos, "A technology review of electrodes and reaction mechanisms in vanadium redox flow batteries," Journal of Materials Chemistry A, Article vol. 3, no. 33, pp. 16913-16933, 2015, doi: 10.1039/c5ta02613j.
[560] M. M. Adams, Mench, J. P., Meyers, P. N., Ross, J. T., & Gostick, Q. Liu., "Redox flow batteries: a review," Applied Electrochemistry, vol. 29, no. 41, pp. 1137-1164, 2011.
[561] J. Noack, N. Roznyatovskaya, T. Herr, and P. Fischer, "The Chemistry of Redox-Flow Batteries," Angewandte Chemie - International Edition, Article vol. 54, no. 34, pp. 9776-9809, 2015, doi: 10.1002/anie.201410823.
[562] F. Pan and Q. Wang, "Redox species of redox flow batteries: A review," Molecules, Review vol. 20, no. 11, pp. 20499-20517, 2015, doi: 10.3390/molecules201119711.
[563] A. Khor et al., "Review of zinc-based hybrid flow batteries: From fundamentals to applications," Materials Today Energy, vol. 8, pp. 80-108, 2018/06/01/ 2018, doi: https://doi.org/10.1016/j.mtener.2017.12.012.
[564] Fraunhofer-Gesellschaft. "Energy and environment." Fraunhofer Institute for Chemical Technology. (accessed 23/04, 2016).
[565] J. J. Donghyeon Kim, "Study on Durability and Stability of an Aqueous Electrolyte Solution for Zinc Bromide Hybrid Flow Batteries " Journal of Physics, 2015.

[566] C. Cachet, F. Ganne, G. Maurin, J. Petitjean, V. Vivier, and R. Wiart, "EIS investigation of zinc dissolution in aerated sulfate medium. Part I: bulk zinc," Electrochimica Acta, vol. 47, no. 3, pp. 509-518, 10/31/ 2001, doi: http://dx.doi.org/10.1016/S0013-4686(01)00740-X.

[567] C. Cachet et al., "EIS investigation of zinc dissolution in aerated sulphate medium. Part II: zinc coatings," Electrochimica Acta, vol. 47, no. 21, pp. 3409-3422, 8/15/ 2002, doi: http://dx.doi.org/10.1016/S0013-4686(02)00277-3.

[568] A. M. Alfantazi and D. B. Dreisinger, "An investigation on the effects of orthophenylene diamine and sodium lignin sulfonate on zinc electrowinning from industrial electrolyte," Hydrometallurgy, vol. 69, no. 1–3, pp. 99-107, 4// 2003, doi: http://dx.doi.org/10.1016/S0304-386X(03)00030-6.

[569] D. H. Becking and R. Gustav, "Electrodeposition of zinc," ed: Google Patents, 1967.

[570] Y. Munaiah, S. Suresh, S. Dheenadayalan, V. Pillai, and P. Ragupathy, "Comparative Electrocatalytic Performance of Single-Walled and Multiwalled Carbon Nanotubes for Zinc Bromine Redox Flow Batteries," J. Phys. Chem. C, vol. 118, no. 27, pp. 14795-14804, 2014, doi: 10.1021/jp503287r.

[571] L. Zhang , Q. Lai, J. Zhang, and H. Zhang, "A High-Energy-Density Redox Flow Battery based on Zinc/Polyhalide Chemistry," ChemSusChem, vol. 5, no. 5, pp. 867-869, 2012, doi: 10.1002/cssc.201100530.

[572] P. Kritzer and J. A. Cook, "Nonwovens as separators for alkaline batteries," Journal of the Electrochemical Society, vol. 154, no. 5, pp. A481-A494, 2007, doi: 10.1149/1.2711064.

[573] J. F. Parker, C. N. Chervin, E. S. Nelson, D. R. Rolison, and J. W. Long, "Wiring zinc in three dimensions re-writes battery performancedendrite-free cycling," Energy Environ. Sci., vol. 7, no. 3, pp. 1117-1124, 2014, doi: 10.1039/c3ee43754j.

[574] L. Liu and Z. Yang, "The composite of ZnSn(OH) 6 and Zn–Al layered double hydroxides used as negative material for zinc–nickel alkaline batteries," International Journal of Ionics The Science and Technology of Ionic Motion, vol. 24, no. 7, pp. 2035-2045, 2018, doi: 10.1007/s11581-018-2446-1.

[575] J. McBreen and E. Gannon, "Bismuth oxide as an additive in pasted zinc electrodes," Journal of Power Sources, vol. 15, no. 2, pp. 169-177, 1985, doi: 10.1016/0378-7753(85)80070-7.

[576] J. M. Wang, L. Zhang, C. Zhang, and J. Q. Zhang, "Effects of bismuth ion and tetrabutylammonium bromide on the dendritic growth of zinc in alkaline zincate solutions," Journal of Power Sources, vol. 102, no. 1, pp. 139-143, 2001, doi: 10.1016/S0378-7753(01)00789-3.

[577] C. J. Lan, C. Y. Lee, and T. S. Chin, "Tetra-alkyl ammonium hydroxides as inhibitors of Zn dendrite in Zn-based secondary batteries," Electrochimica Acta, vol. 52, no. 17, pp. 5407-5416, 2007, doi: 10.1016/j.electacta.2007.02.063.

[578] Y. Sharma, M. Aziz, J. Yusof, and K. Kordesch, "Triethanolamine as an additive to the anode to improve the rechargeability of alkaline manganese dioxide batteries," Journal of Power Sources, vol. 94, no. 1, pp. 129-131, 2001, doi: 10.1016/S0378-7753(00)00633-9.

[579] J. Kan, H. Xue, and S. Mu, "Effect of inhibitors on Zn-dendrite formation for zinc-polyaniline secondary battery," Journal of Power Sources, vol. 74, no. 1, pp. 113-116, 1998, doi: 10.1016/S0378-7753(98)00040-8.

[580] S. J. Banik and R. Akolkar, "Suppressing dendrite growth during zinc electrodeposition by PEG-200 additive," Journal of the Electrochemical Society, vol. 160, no. 11, pp. D519-D523, 2013, doi: 10.1149/2.040311jes.

[581] S. Arouete, K. F. Blurton, and H. G. Oswin, "Controlled Current Deposition of Zinc from Alkaline Solution," Journal of The Electrochemical Society, vol. 116, no. 2, p. 166, 1969, doi: 10.1149/1.2411787.

[582] J. McBreen and E. Gannon, "Zinc Electrode Morphology in Alkaline Solutions. II. Study of Alternating Charging Current Modulation on Pasted Zinc Battery Electrodes," Journal of the Electrochemical Society, vol. 130, no. 8, pp. 1641-1645, 1983, doi: 10.1149/1.2120055.

[583] M. H. Katz, T. C. Adler, F. R. McLarnon, and E. J. Cairns, "The effect of pulse charging on the cycle-life performance of zinc/nickel oxide cells," Journal of Power Sources, vol. 22, no. 1, pp. 77-95, 1988, doi: 10.1016/0378-7753(88)80007-7.

9 Appendix

9.1 Engineering Draft of Designed Components Incorporated to the Proposed Zinc-Bromine Battery Cell to be Fabricated.

1. Figure 9.1 and Figure 9.2 are the anode-side and cathode-side endplates. The other cell components were incorporated in between the anode-side and cathode-side endplates. The anode-side and cathode-side of the cell endplates has a measurement of 190mm by 190mm, with a thickness of 20mm. The anode-side endplate has an outer diameter of 30mm and inlet diameter of 15mm to transfer electrolyte from the reservoir tank to the electrode (reactor) and back into the anode-side electrolyte tank. The cathode-side of the battery cell inlet and outlet diameter were 15mm. The cell was designed to enable the electrolyte to pass through the attached fittings coupled to the back of the two endplates (anode and cathode).

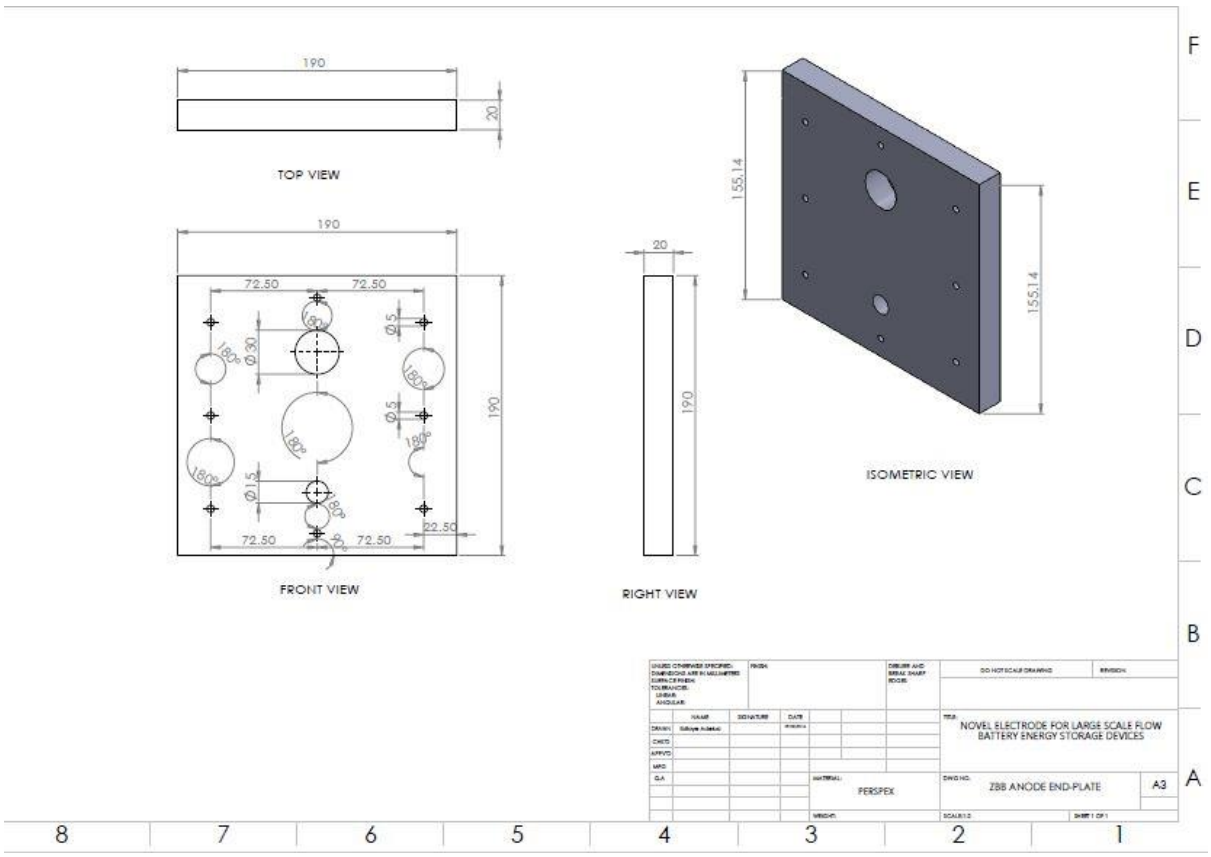

Figure 9. 1: Zinc-Bromine Battery Cell Anode Endplate

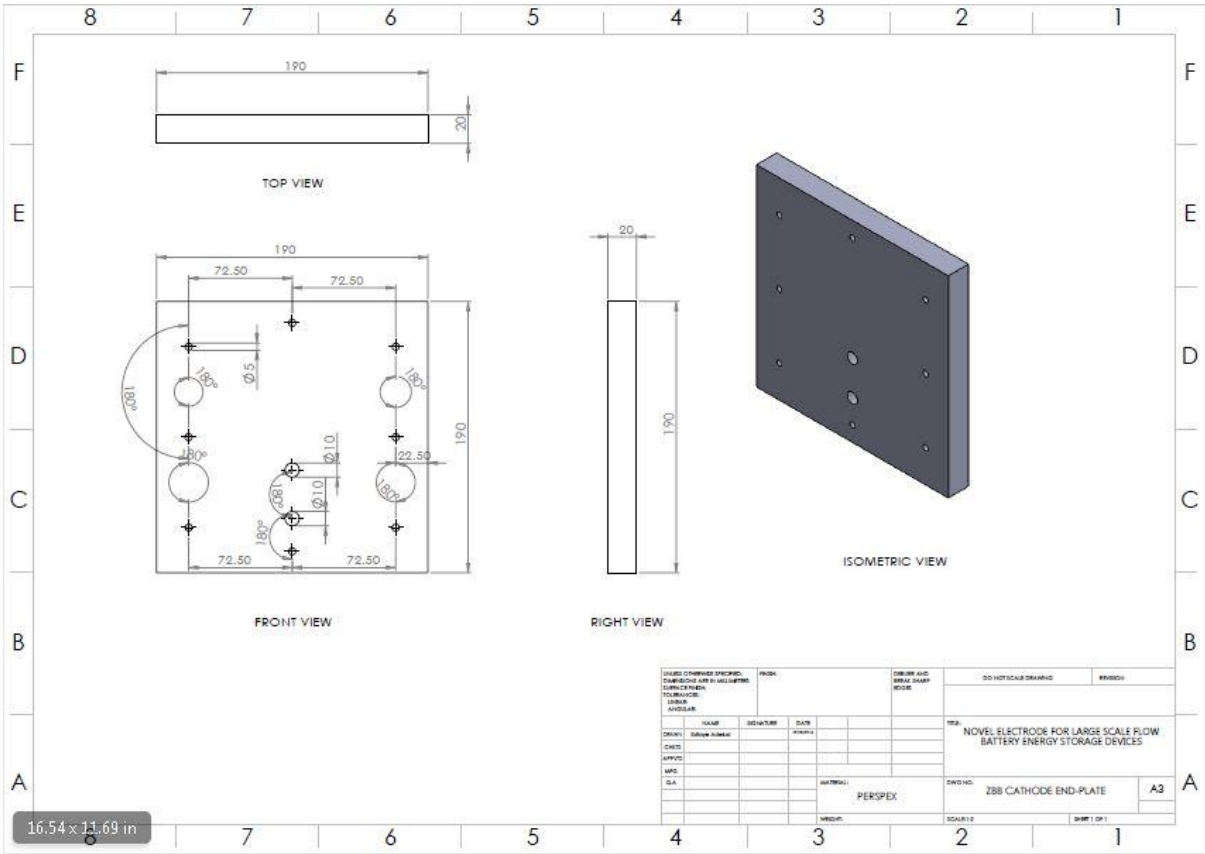

Figure 9. 2: Zinc-Bromine Battery Cell Cathode Endplate

2. Figure 9.3 and 9.4 are the anode gaskets. Two out of all the anode-side three gaskets were presented here in this section. Figure 9.3 is the anode gasket packed in between the anode endplate and the anode reactor electrode feeder. The anode-side and cathode-side gaskets were designed to prevent leakages. The two anode-side gaskets displayed in this section has the same designed measurements.
3. These were the gaskets in between the anode reactor, membrane, anode reactor electrode feeder and the designed anode porous reactor. Figure 9.4 as the anode gasket, is introduced in between the anode reactor and membrane. The battery cell anode gasket placed in between the anode reactor and membrane has the same designed structure as the anode gasket in between the anode reactor feeder and the designed anode porous reactor. The membrane was designed to prevent the cathode-side and anode-side electrolyte from crossing and mixing to destroy the battery cell.

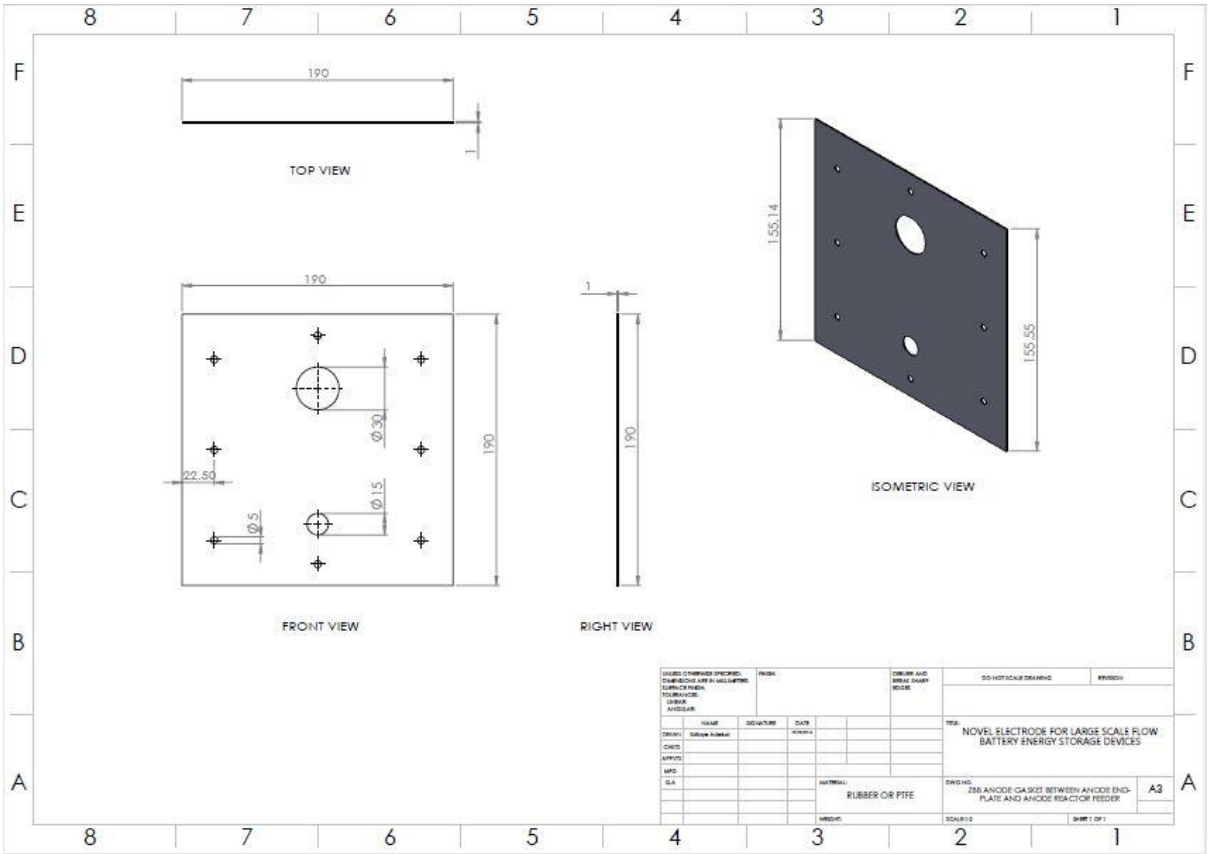

Figure 9. 3: Zinc-Bromine Battery Cell Anode Gasket Between Anode Endplate and Anode Reactor Feeder

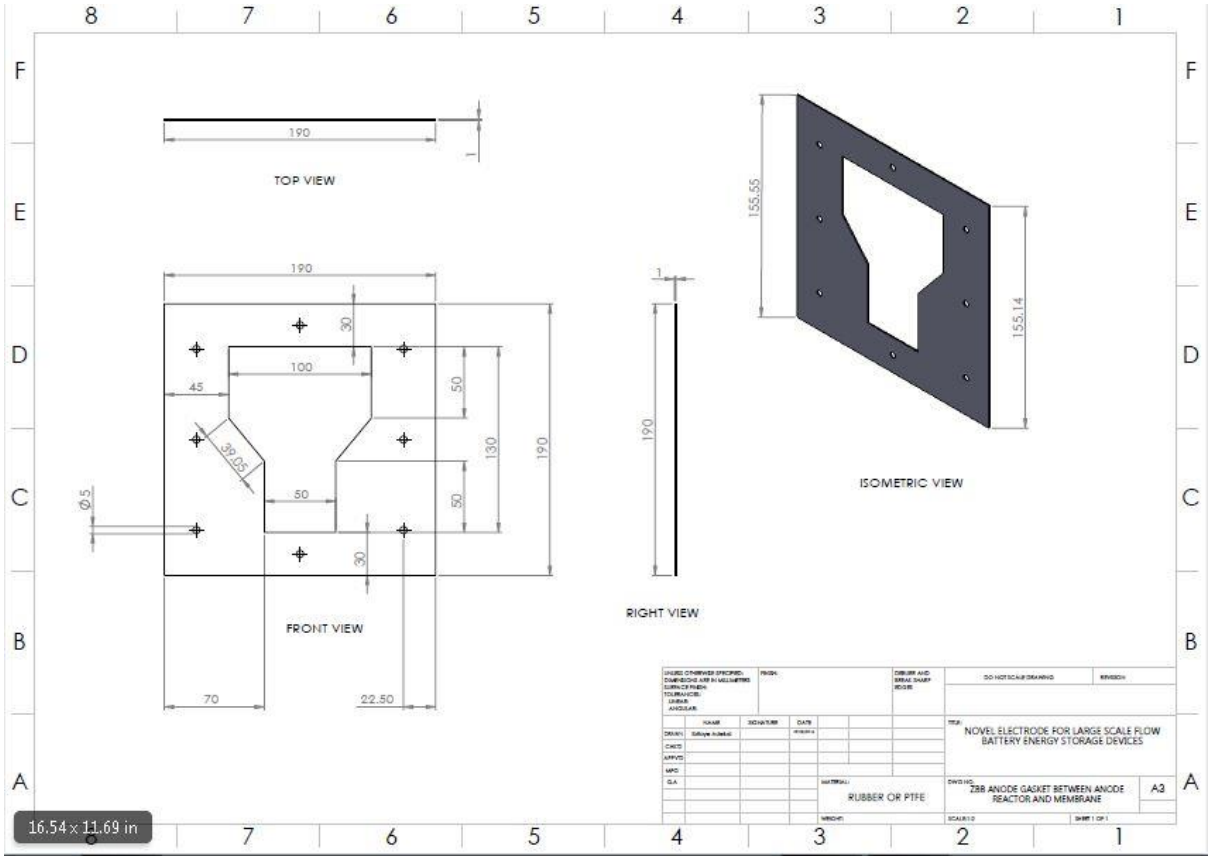

Figure 9. 4: Zinc-Bromine Battery Cell Anode Gasket Between the Anode Reactor and the Membrane

4. Figure 9.5 and Figure 9.6 were the designed cell cathode-side gaskets, positioned individually in between the cathode end-plate and cathode electrode feeder. Three gaskets were initially proposed for the cathode-side cell. These were the battery cell cathode gasket in between the cathode end-plate and cathode reactor feeder, the cathode-side gasket in between the cathode reactor, the membrane and the cathode gasket in between the cathode reactor feeder electrode and cathode reactor (electrode). The cathode-side gasket in between the cathode reactor and membrane, cathode gasket in between the cathode reactor feeder and the cathode reactor (electrode) of the same designed measurement.

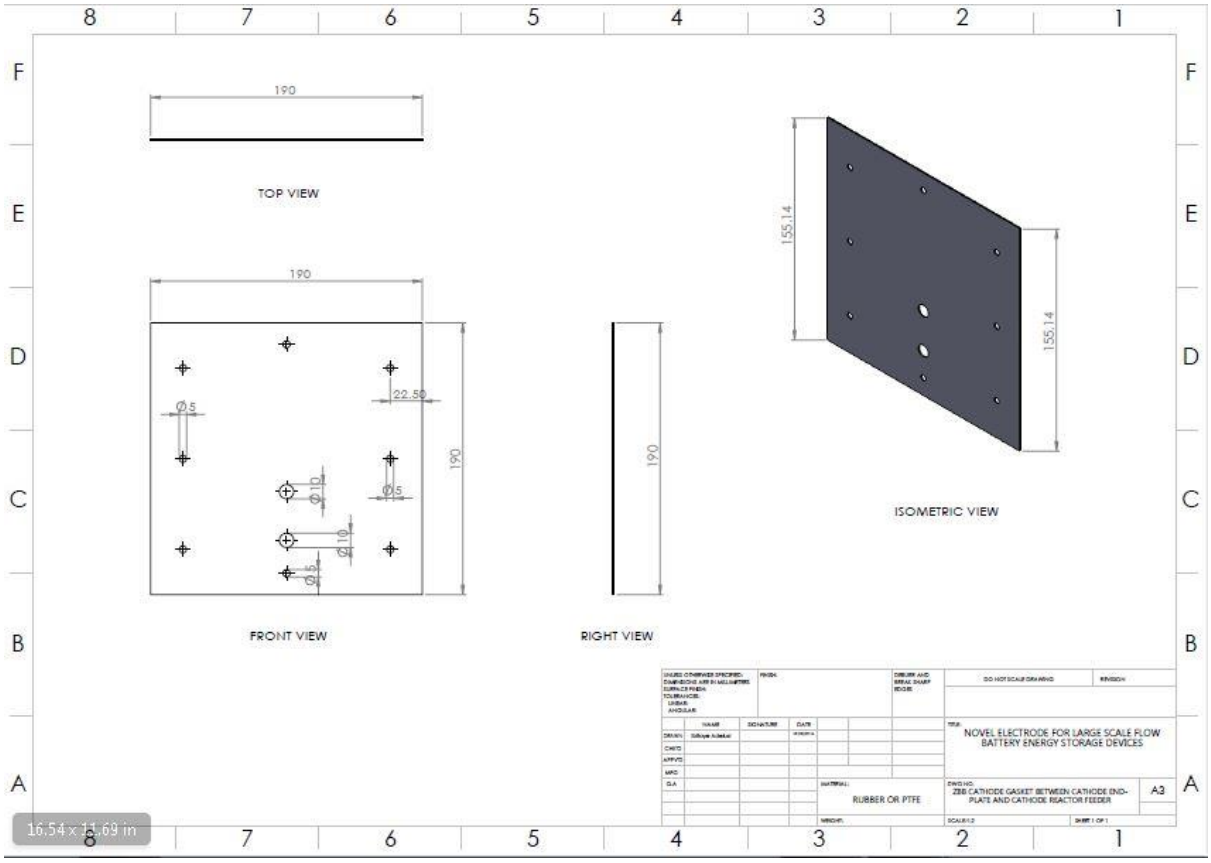

Figure 9. 5: Zinc-Bromine Battery Cell Cathode Gasket Between Cathode Endplate and Cathode Reactor Feeder.

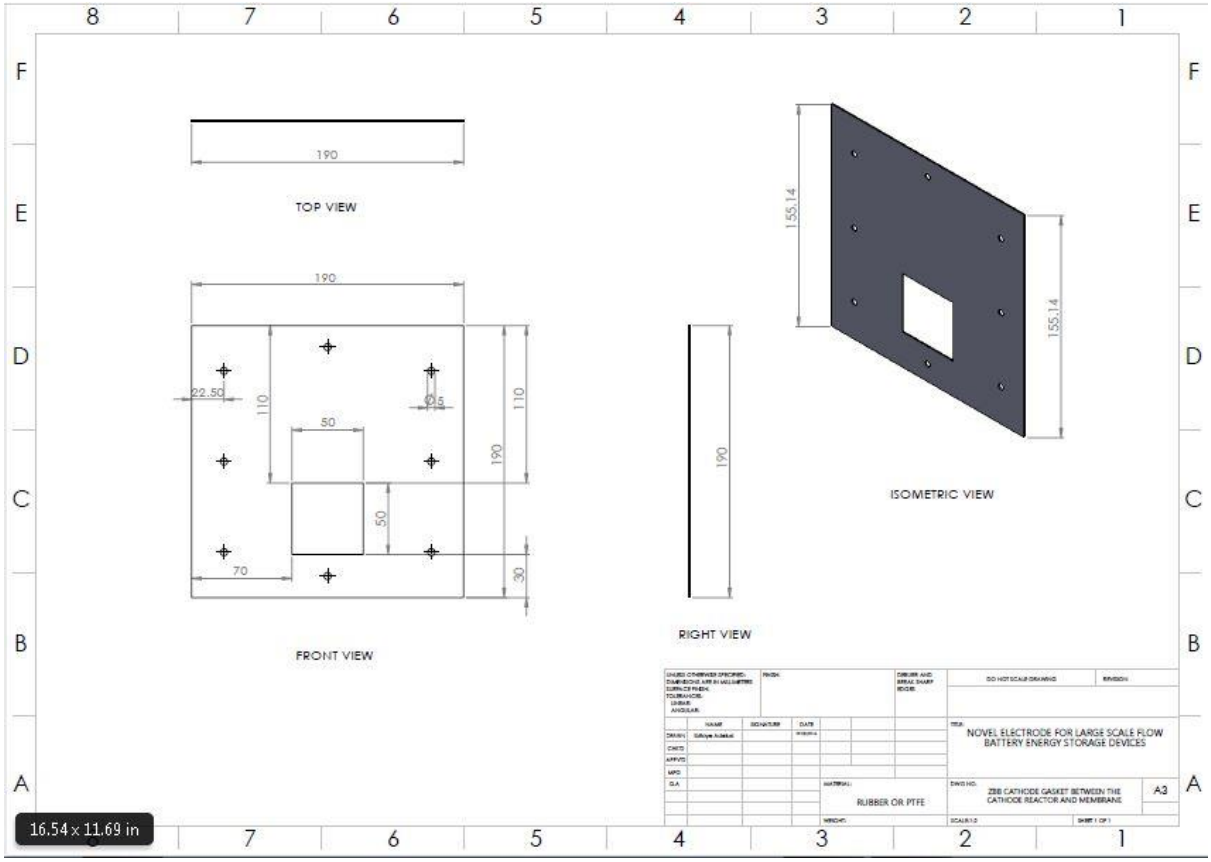

Figure 9. 6: Zinc-Bromine Battery Cell Cathode Gasket Between the Cathode Reactor and Membrane

5. The anode-side and cathode-side feeder electrode designed structure were the same; but has different outlet and inlet diameter as displayed in Figure 9.7 and 9.8. These electrode feeders were designed as the cell current collectors. The anode-side and cathode-side feeder electrodes were different to each other due to the shapes of these two reactors. Figure 9.9 is the cell membrane preventing the anode-side and cathode-side electrolyte from mixing when circulated through the cell stack. The fabricated membrane is 190mm by 190mm with a thickness of 0.15mm.

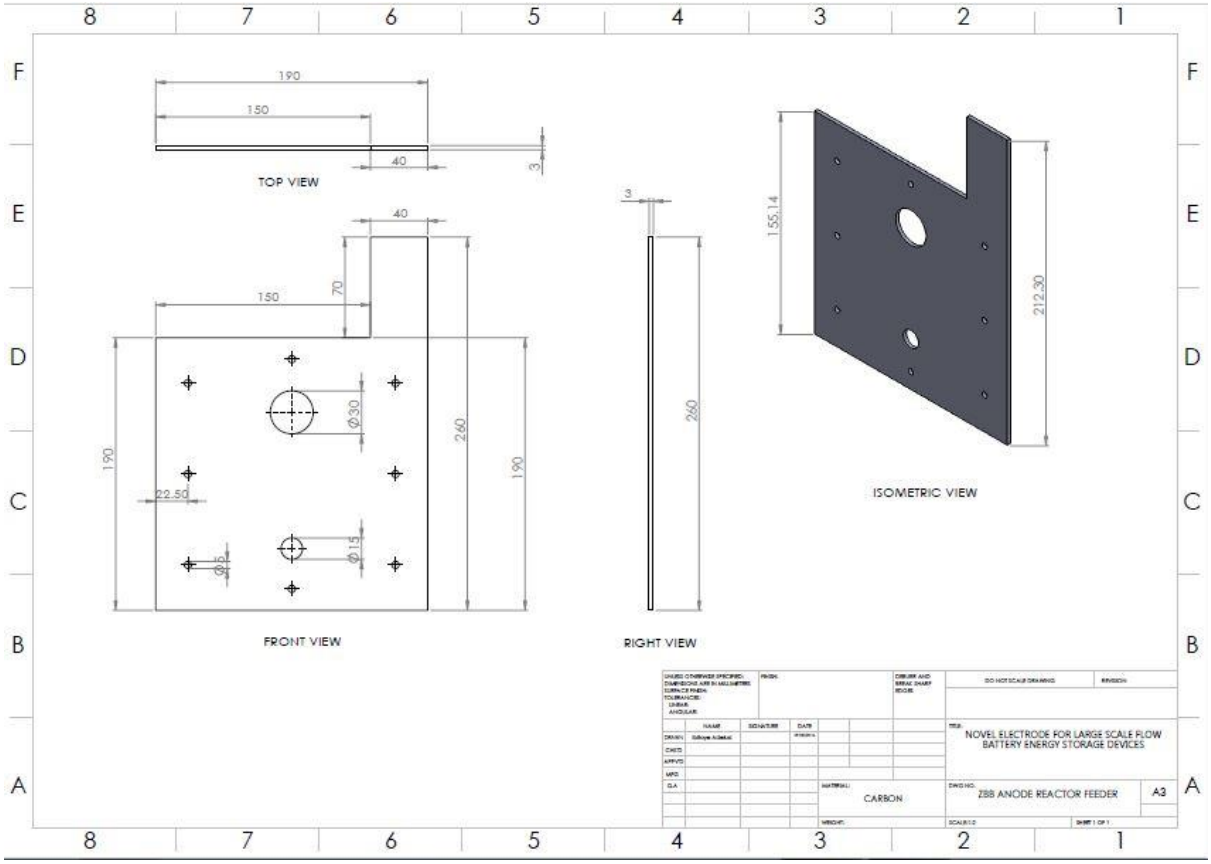

Figure 9. 7: Anode-Side of the Zinc-Bromine Battery Cell Electrode Feeder

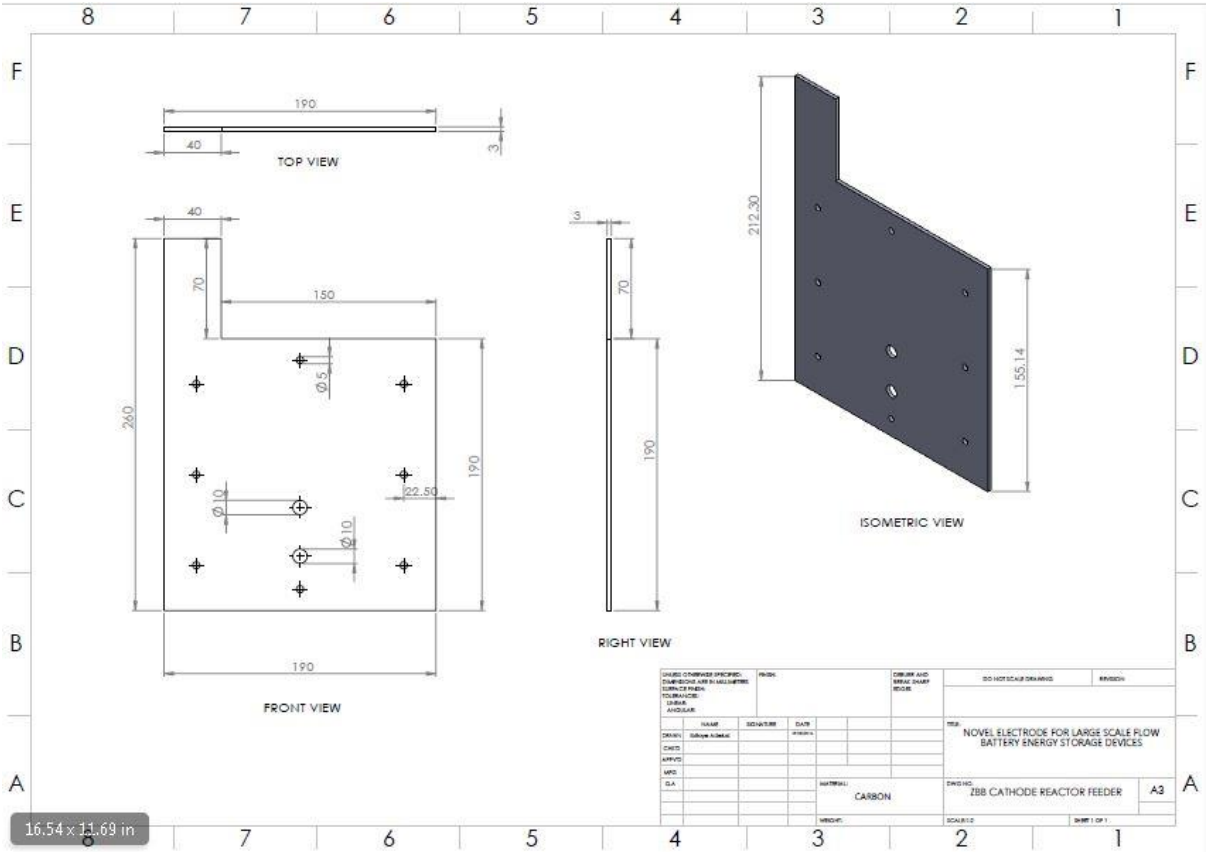

Figure 9. 8: Cathode-Side of the Zinc-Bromine Battery Cell Electrode Feeder

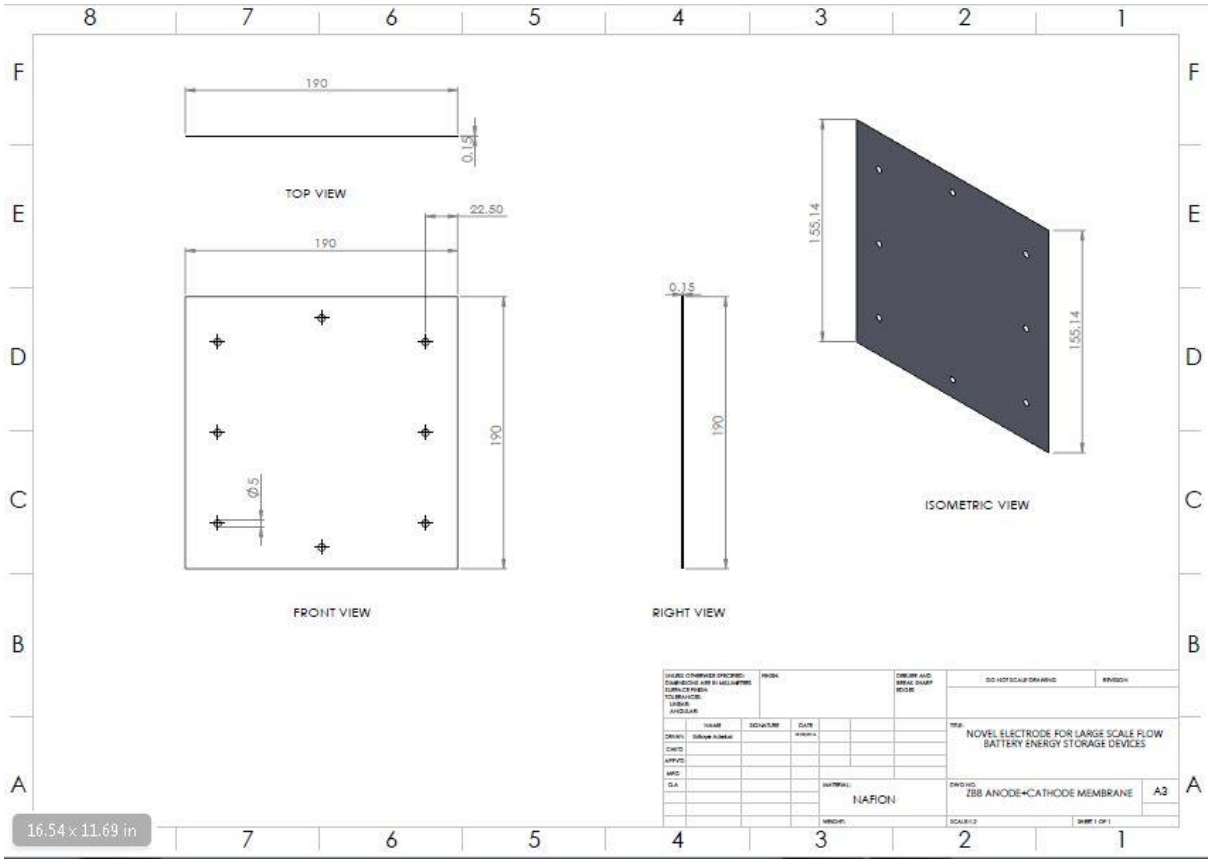

Figure 9. 9: The Zinc-Bromine Battery Cell Membrane

6. The anode-side and cathode-side were made up of two different reactors. The cell anode-side reactor as 100mm by 130mm with 12mm thickness. The cathode-side electrode designed as 50mm by 50mm of 12mm thickness. The anode-side reactor was injected with carbon particles that were charged to form some zinc crystals and plated on the anode feeder electrode. The cathode-side of the cell was not fabricated to incorporate any metallic particles. See Figure 9.10 and Figure 9.11 for the engineering drafts the anode-side reactor and cathode-side reactor measurements.

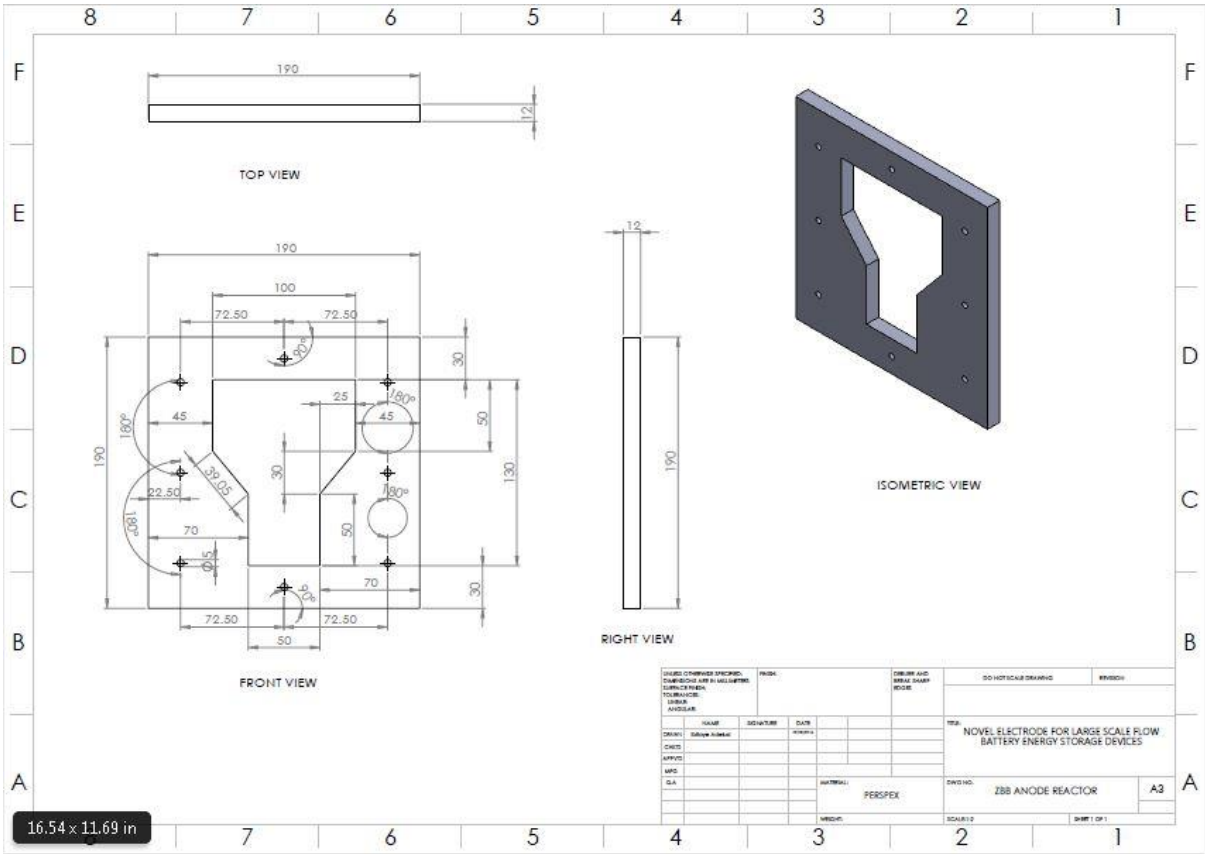

Figure 9. 10: Anode-Side of the Zinc-Bromine Battery Cell Engineering Drafting

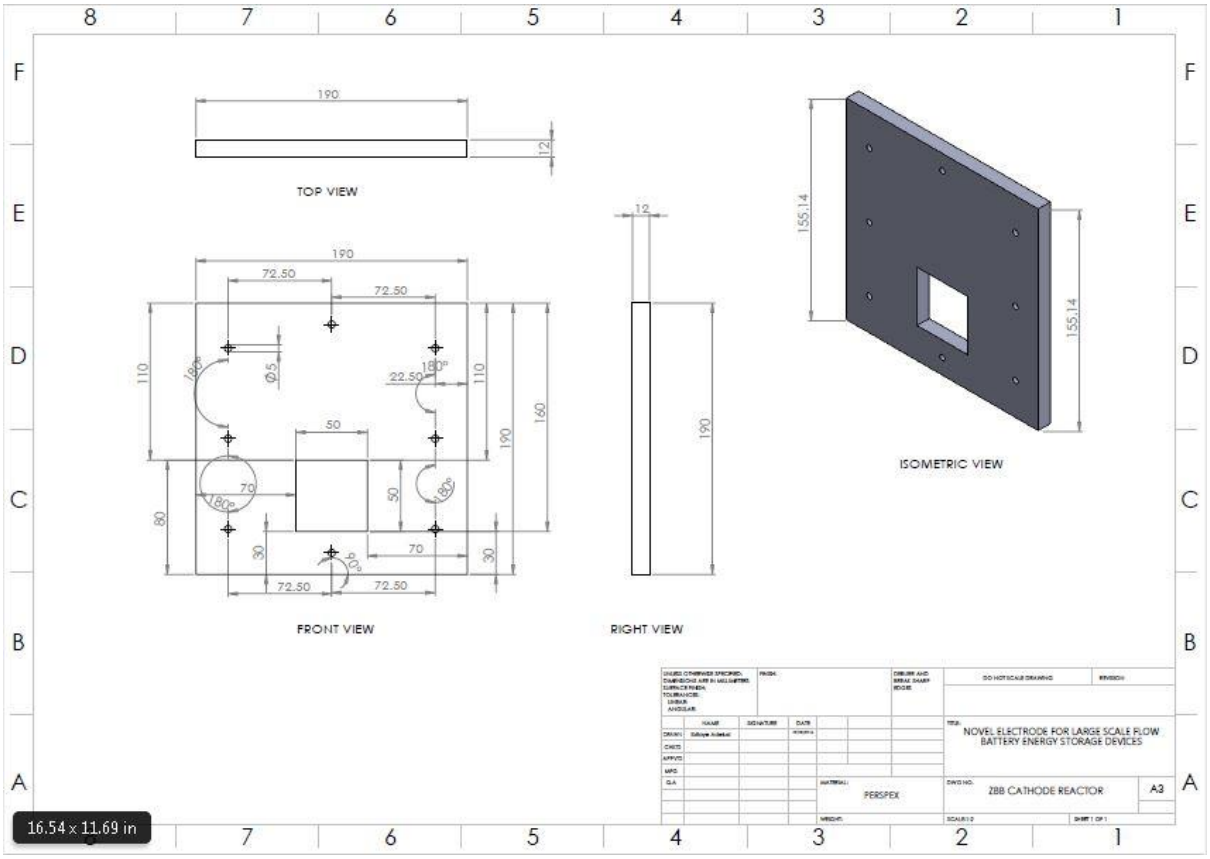

Figure 9. 11: Cathode-Side of the Zinc-Bromine Battery Cell Engineering Drafting

9.1.1 Carbon Vs Nickel Cycle-1 (0.1 Amps Vs -0.1 Amps) @ (3900 Secs and 2000 Secs), (3600 Secs and 1600 Secs) and (2400 secs only to Charge)

Table 9. 1: Cycle-1 to Cycle-3 Cell evaluation: carbon vs nickel charged and discharged experiment-1 @ 0.1 amps for 3900 secs and -0.1 amps (3900 secs and 2000 secs), (3000 secs and 1600 secs), (2400 secs for only to charge) with 3 moles of KBr (535.51 grams), 1 mole of KCl (111.89 grams) as the cathode-side electrolyte and 3 moles of ZnBr2 (675 grams), 1 mole of $ZnCl_2$ (205 grams), and 1 mole of KCl (111.826 grams) as the anode electrolyte solution.

Charged State of Cycle-1		
1	Charged Passed During Charging	0.1A*3900secs = 390C
Discharged State of Cycle-1		
2	Charged Passed During Discharging	-0.1A*2000secs = -200C
3	Charge Efficiency (CE) $\frac{\text{Charged Recovered (Discharge)}}{\text{Charged Input (Charge)}} * 100\%$	$\frac{200}{390} * 100\% = 51.3\%$
4	Energy Efficiency (EE) $\frac{\text{Energy Recovered (Discharge)}}{\text{Energy Input (Charge)}} * 100\%$	$\frac{\text{Charge Recovered} * \text{Average Voltage During Discharge}}{\text{Charge Input} * \text{Average Voltage During Charge}} * 100\%$ $\frac{200 * 0.54}{390 * 2.167} * 100\% = 12.77\%$
Charged State of Cycle-2		
5	Charged Passed During Charging	0.1A*3000secs = 300C
Discharged State of Cycle-2		
6	Charged Passed During Discharging	-0.1A*1600secs = -160C
7	Charge Efficiency (CE) $\frac{\text{Charged Recovered (Discharge)}}{\text{Charged Input (Charge)}} * 100\%$	$\frac{160}{300} * 100\% = 53.3\%$
8	Energy Efficiency (EE) $\frac{\text{Energy Recovered (Discharge)}}{\text{Energy Input (Charge)}} * 100\%$	$\frac{\text{Charge Recovered} * \text{Average Voltage During Discharge}}{\text{Charge Input} * \text{Average Voltage During Charge}} * 100\%$ $\frac{160 * 0.54}{300 * 2.167} * 100\% = 13.29\%$

Charged State of Cycle-3		
9	Charged Passed During Charging	0.1A*2400secs = 240C
CELL INTERRRUPTED @ 13000 SECS DUE TO LEAKAGES		

9.1.2 Nickel Vs Titanium Cycle-1 (0.1 Amps Vs -0.1 Amps) @ (1800 Secs and 900 Secs), (1810 Secs and 900 Secs) and (1705 Secs and 900 Secs)

Table 9. 2: Experimental data of the investigated nickel and titanium electrode for the 3-cycles of charge and discharge at 0.1 amps and -0.1amps for (1800 secs and 900 secs), (1810 secs and 900 secs) and (1705 secs and 900 secs) with 3 moles of KBr (535.51 grams), 1 mole of KCl (111.89 grams) as the cathode-side electrolyte and 3 moles of ZnBr2 (675 grams), 1mole of $ZnCl_2$ (205 grams), and 1 mole of KCl (111.826 grams) as the anode electrolyte solution.

Charged State of Cycle-1		
1	Charged Passed During Charging	0.1A*1800secs = 180C
Discharged State of Cycle-1		
2	Charged Passed During Discharging	-0.1A*900secs = -90C
3	Charge Efficiency (CE) $\frac{\text{Charged Recovered (Discharge)}}{\text{Charged Input (Charge)}} * 100\%$	$\frac{90}{180} * 100\% = 50\%$
4	Energy Efficiency (EE) $\frac{\text{Energy Recovered (Discharge)}}{\text{Energy Input (Charge)}} * 100\%$	$\frac{\text{Charge Recovered} * \text{Average Voltage During Discharge}}{\text{Charge Input} * \text{Average Voltage During Charge}} * 100\%$ $\frac{90 * 1.005}{180 * 2.06} * 100\% = 24.39\%$
Charged State of Cycle-2		
1	Charged Passed During Charging	0.1A*1810secs = 181C
Discharged State of Cycle-2		
2	Charged Passed During Discharging	-0.1A*900secs = -90C

3	Charge Efficiency (CE) $\frac{\text{Charged Recovered (Discharge)}}{\text{Charged Input (Charge)}} * 100\%$	$\frac{90}{181} * 100\% = 49.72\%$
4	Energy Efficiency (EE) $\frac{\text{Energy Recovered (Discharge)}}{\text{Energy Input (Charge)}} * 100\%$	$\frac{\text{Charge Recovered} * \text{Average Voltage During Discharge}}{\text{Charge Input} * \text{Average Voltage During Charge}} * 100\%$ $\frac{90 * 1.005}{181 * 2.06} * 100\% = 24.25\%$
Charged State of Cycle-3		
1	Charged Passed During Charging	0.1A*1705secs = 170.5C
Discharged State of Cycle-3		
2	Charged Passed During Discharging	-0.1A*900secs = -90C
3	Charge Efficiency (CE) $\frac{\text{Charged Recovered (Discharge)}}{\text{Charged Input (Charge)}} * 100\%$	$\frac{90}{170.5} * 100\% = 52.78\%$
4	Energy Efficiency (EE) $\frac{\text{Energy Recovered (Discharge)}}{\text{Energy Input (Charge)}} * 100\%$	$\frac{\text{Charge Recovered} * \text{Average Voltage During Discharge}}{\text{Charge Input} * \text{Average Voltage During Charge}} * 100\%$ $\frac{90 * 1.005}{170.5 * 2.06} * 100\% = 25.75\%$

Table 9. 3: Experimental data of the investigated carbon and nickel electrode for the 3-cycles of charge and discharge at a current rate of 0.1 amps and -0.1 amps for (Cycle-1), (4000 secs and 1900 secs), and (Cycle-2), for (3100 secs and 2000 secs), and (Cycle-3) for (3000 secs and 1900 secs). with 3 moles of KBr (535.51 grams), 1 mole of KCl (111.89 grams) as the cathode-side electrolyte and 3 moles of ZnBr2 (675 grams), 1 mole of $ZnCl_2$ (205 grams), and 1 mole of KCl (111.826 grams) as the anode electrolyte solution.

Charged State of Cycle-1		
1	Charged Passed During Charging	0.1A*4000secs = 400C
Discharged State of Cycle-1		
2	Charged Passed During Discharging	-0.1A*1900secs = -190C

3	Charge Efficiency (CE) $\frac{\text{Charged Recovered (Discharge)}}{\text{Charged Input (Charge)}} * 100\%$	$\frac{90}{180} * 100\% = 47.5\%$
4	Energy Efficiency (EE) $\frac{\text{Energy Recovered (Discharge)}}{\text{Energy Input (Charge)}} * 100\%$	$\frac{\text{Charge Recovered} * \text{Average Voltage During Discharge}}{\text{Charge Input} * \text{Average Voltage During Charge}} * 100\%$ $\frac{190 * 0.5}{400 * 1.7} * 100\% = 13.97\%$
Charged State of Cycle-2		
1	Charged Passed During Charging	-0.1A*3100secs = 310C
Discharged State of Cycle-2		
2	Charged Passed During Discharging	-0.1A*2000secs = -200C
3	Charge Efficiency (CE) $\frac{\text{Charged Recovered (Discharge)}}{\text{Charged Input (Charge)}} * 100\%$	$\frac{200}{310} * 100\% = 64.5\%$
4	Energy Efficiency (EE) $\frac{\text{Energy Recovered (Discharge)}}{\text{Energy Input (Charge)}} * 100\%$	$\frac{\text{Charge Recovered} * \text{Average Voltage During Discharge}}{\text{Charge Input} * \text{Average Voltage During Charge}} * 100\%$ $\frac{200 * 0.5}{310 * 1.7} * 100\% = 18.9\%$
Charged State of Cycle-3		
1	Charged Passed During Charging	0.1A*30005secs = 300C
Discharged State of Cycle-3		
2	Charged Passed During Discharging	-0.1A*1900secs = -190C
3	Charge Efficiency (CE) $\frac{\text{Charged Recovered (Discharge)}}{\text{Charged Input (Charge)}} * 100\%$	$\frac{190}{300} * 100\% = 63.3\%$
4	Energy Efficiency (EE) $\frac{\text{Energy Recovered (Discharge)}}{\text{Energy Input (Charge)}} * 100\%$	$\frac{\text{Charge Recovered} * \text{Average Voltage During Discharge}}{\text{Charge Input} * \text{Average Voltage During Charge}} * 100\%$ $\frac{190 * 0.5}{300 * 1.7} * 100\% = 18.6\%$

Table 9. 4: Experimental data of the investigated nickel and titanium electrode for the 3-cycles of charge and discharge at 0.3 amps and -0.3 amps for (1800 secs and 200 secs), and (2), for (1700 secs and 200 secs), and (3) for (1900 secs and 200 secs) with 3 moles of KBr (535.51 grams), 1 mole of KCl (111.89

grams) as the cathode-side electrolyte and 3 moles of ZnBr2 (675 grams), 1 mole of $ZnCl_2$ (205 grams), and 1 mole of KCl (111.826 grams) as the anode electrolyte solution.

Charged State of Cycle-1		
1	Charged Passed During Charging	0.3A*1800secs = 540C
Discharged State of Cycle-1		
2	Charged Passed During Discharging	-0.3A*200secs = -60C
3	Charge Efficiency (CE) $\frac{\text{Charged Recovered (Discharge)}}{\text{Charged Input (Charge)}} * 100\%$	$\frac{60}{540} * 100\% = 11.11\%$
4	Energy Efficiency (EE) $\frac{\text{Energy Recovered (Discharge)}}{\text{Energy Input (Charge)}} * 100\%$	$\frac{\text{Charge Recovered} * \text{Average Voltage During Discharge}}{\text{Charge Input} * \text{Average Voltage During Charge}} * 100\%$ $\frac{60 * 0.58}{540 * 2.85} * 100\% = 2.26\%$
Charged State of Cycle-2		
1	Charged Passed During Charging	0.3A*1700secs = 510C
Discharged State of Cycle-2		
2	Charged Passed During Discharging	-0.3A*200secs = -60C
3	Charge Efficiency (CE) $\frac{\text{Charged Recovered (Discharge)}}{\text{Charged Input (Charge)}} * 100\%$	$\frac{60}{510} * 100\% = 11.76\%$
4	Energy Efficiency (EE) $\frac{\text{Energy Recovered (Discharge)}}{\text{Energy Input (Charge)}} * 100\%$	$\frac{\text{Charge Recovered} * \text{Average Voltage During Discharge}}{\text{Charge Input} * \text{Average Voltage During Charge}} * 100\%$ $\frac{60 * 0.58}{510 * 2.85} * 100\% = 2.39\%$
Charged State of Cycle-3		
1	Charged Passed During Charging	0.3A*1900secs = 570C
Discharged State of Cycle-3		
2	Charged Passed During Discharging	-0.3A*200secs = -60C
3	Charge Efficiency (CE) $\frac{\text{Charged Recovered (Discharge)}}{\text{Charged Input (Charge)}} * 100\%$	$\frac{60}{570} * 100\% = 10.5\%$
4	Energy Efficiency (EE) $\frac{\text{Energy Recovered (Discharge)}}{\text{Energy Input (Charge)}} * 100\%$	$\frac{\text{Charge Recovered} * \text{Average Voltage During Discharge}}{\text{Charge Input} * \text{Average Voltage During Charge}} * 100\%$

		$\frac{60 * 0.58}{570 * 2.85} * 100\% = 2.14\%$

Table 9. 5: Experimental data of the investigated carbon and nickel electrode for the 3-cycles of charge and discharge at a charge and discharge of 0.4 amps and -0.4 amps for cycle-1, (3900 secs and 1100 secs), and (cycle-2), for (3700 secs and 1300 secs), and (cycle-3) for (3700 secs and 1200 secs) with 3 moles of KBr (535.51 grams), 1 mole of KCl (111.89 grams) as the cathode-side electrolyte and 3 moles of ZnBr2 (675 grams), 1 mole of $ZnCl_2$ (205 grams), and 1 mole of KCl (111.826 grams) as the anode electrolyte solution.

Charged State of Cycle-1		
1	Charged Passed During Charging	0.4A*3900secs = 1560C
Discharged State of Cycle-1		
2	Charged Passed During Discharging	-0.4A*1100secs = -440C
3	Charge Efficiency (CE) $\frac{\text{Charged Recovered (Discharge)}}{\text{Charged Input (Charge)}} * 100\%$	$\frac{440}{1560} * 100\% = 28.20\%$
4	Energy Efficiency (EE) $\frac{\text{Energy Recovered (Discharge)}}{\text{Energy Input (Charge)}} * 100\%$	$\frac{\text{Charge Recovered} * \text{Average Voltage During Discharge}}{\text{Charge Input} * \text{Average Voltage During Charge}} * 100\%$ $\frac{440 * 0.91}{1560 * 2.69} * 100\% = 9.54\%$
Charged State of Cycle-2		
1	Charged Passed During Charging	0.4A*3700secs = 1480C
Discharged State of Cycle-2		
2	Charged Passed During Discharging	-0.4A*1300secs = -520C
3	Charge Efficiency (CE) $\frac{\text{Charged Recovered (Discharge)}}{\text{Charged Input (Charge)}} * 100\%$	$\frac{520}{1480} * 100\% = 35.1\%$
4	Energy Efficiency (EE) $\frac{\text{Energy Recovered (Discharge)}}{\text{Energy Input (Charge)}} * 100\%$	$\frac{\text{Charge Recovered} * \text{Average Voltage During Discharge}}{\text{Charge Input} * \text{Average Voltage During Charge}} * 100\%$ $\frac{520 * 0.91}{1480 * 2.69} * 100\% = 11.88\%$
Charged State of Cycle-3		

1	Charged Passed During Charging	0.4A*3700secs = 1440C
Discharged State of Cycle-3		
2	Charged Passed During Discharging	-0.4A*1200secs = -480C
3	Charge Efficiency (CE) $\frac{\text{Charged Recovered (Discharge)}}{\text{Charged Input (Charge)}} * 100\%$	$\frac{480}{1440} * 100\% = 32.4\%$
4	Energy Efficiency (EE) $\frac{\text{Energy Recovered (Discharge)}}{\text{Energy Input (Charge)}} * 100\%$	$\frac{\text{Charge Recovered} * \text{Average Voltage During Discharge}}{\text{Charge Input} * \text{Average Voltage During Charge}} * 100\%$ $\frac{480 * 0.91}{1440 * 2.69} * 100\% = 11.27\%$

Table 9. 6: Experimental data of the investigated and interrupted 3-cycles of charge and discharge at 0.1 amps and -0.1 amps for cycle-1 (3600 secs, 500 secs), and cycle-2 for (1200 secs) incorporating the carbon and nickel electrode with 3 moles of KBr (535.51 grams), 1 mole of KCl (111.89 grams) as the cathode-side electrolyte and 3 moles of ZnBr2 (675 grams), 1 mole of $ZnCl_2$ (205 grams), and 1 mole of KCl (111.826 grams) as the anode electrolyte solution.

Charged State of Cycle-1		
1	Charged Passed During Charging	0.1A*3600secs = 360C
Discharged State of Cycle-1		
2	Charged Passed During Discharging	-0.1A*500secs = -50C
3	Charge Efficiency (CE) $\frac{\text{Charged Recovered (Discharge)}}{\text{Charged Input (Charge)}} * 100\%$	$\frac{50}{360} * 100\% = 13.9\%$
4	Energy Efficiency (EE) $\frac{\text{Energy Recovered (Discharge)}}{\text{Energy Input (Charge)}} * 100\%$	$\frac{\text{Charge Recovered} * \text{Average Voltage During Discharge}}{\text{Charge Input} * \text{Average Voltage During Charge}} * 100\%$ $\frac{50 * 0.99}{360 * 2.198} * 100\% = 6.25\%$
Charged State of Cycle-2		
1	Charged Passed During Charging	0.1A*1200secs = 120C
Discharged State of Cycle-2 – CELL INTERRUPTED		

Table 9. 7: Experimental data of the investigated titanium and nickel electrode for the 3-cycles of charge and discharge at 0.1 amps and -0.1 amps for cycle-1 @ (1800 secs and 200 secs), cycle-2 @ (1900 secs

and 100 secs) and cycle-3 @ (2000 secs and 300 secs) with 3 moles of KBr (535.51 grams), 1 mole of KCl (111.89 grams) as the cathode-side electrolyte and 3 moles of ZnBr2 (675 grams), 1 mole of $ZnCl_2$ (205 grams), and 1 mole of KCl (111.826 grams) as the anode electrolyte solution.

Charged State of Cycle-1		
1	Charged Passed During Charging	0.1A*1800secs = 180C
Discharged State of Cycle-1		
2	Charged Passed During Discharging	-0.1A*200secs = -20C
3	Charge Efficiency (CE) $\frac{\text{Charged Recovered (Discharge)}}{\text{Charged Input (Charge)}} * 100\%$	$\frac{20}{180} * 100\% = 11.11\%$
4	Energy Efficiency (EE) $\frac{\text{Energy Recovered (Discharge)}}{\text{Energy Input (Charge)}} * 100\%$	$\frac{\text{Charge Recovered} * \text{Average Voltage During Discharge}}{\text{Charge Input} * \text{Average Voltage During Charge}} * 100\%$ $\frac{20 * 0.897}{180 * 2.68} * 100\% = 3.71\%$
Charged State of Cycle-2		
1	Charged Passed During Charging	0.1A*1900secs = 190C
Discharged State of Cycle-2		
2	Charged Passed During Discharging	-0.1A*100secs = -10C
3	Charge Efficiency (CE) $\frac{\text{Charged Recovered (Discharge)}}{\text{Charged Input (Charge)}} * 100\%$	$\frac{10}{190} * 100\% = 5.26\%$
4	Energy Efficiency (EE) $\frac{\text{Energy Recovered (Discharge)}}{\text{Energy Input (Charge)}} * 100\%$	$\frac{\text{Charge Recovered} * \text{Average Voltage During Discharge}}{\text{Charge Input} * \text{Average Voltage During Charge}} * 100\%$ $\frac{10 * 0.897}{190 * 2.68} * 100\% = 1.76\%$
Charged State of Cycle-3		
1	Charged Passed During Charging	0.1A*2000secs = 200C
Discharged State of Cycle-3		
2	Charged Passed During Discharging	-0.1A*300secs = -30C
3	Charge Efficiency (CE)	$\frac{30}{200} * 100\% = 15\%$

	$\frac{\text{Charged Recovered (Discharge)}}{\text{Charged Input (Charge)}} * 100\%$	
4	Energy Efficiency (EE) $\frac{\text{Energy Recovered (Discharge)}}{\text{Energy Input (Charge)}} * 100\%$	$\frac{\text{Charge Recovered} * \text{Average Voltage During Discharge}}{\text{Charge Input} * \text{Average Voltage During Charge}} * 100\%$ $\frac{30 * 0.897}{200 * 2.68} * 100\% = 5.02\%$

Table 9. 8: The Fabricated Cell Bill of Materials

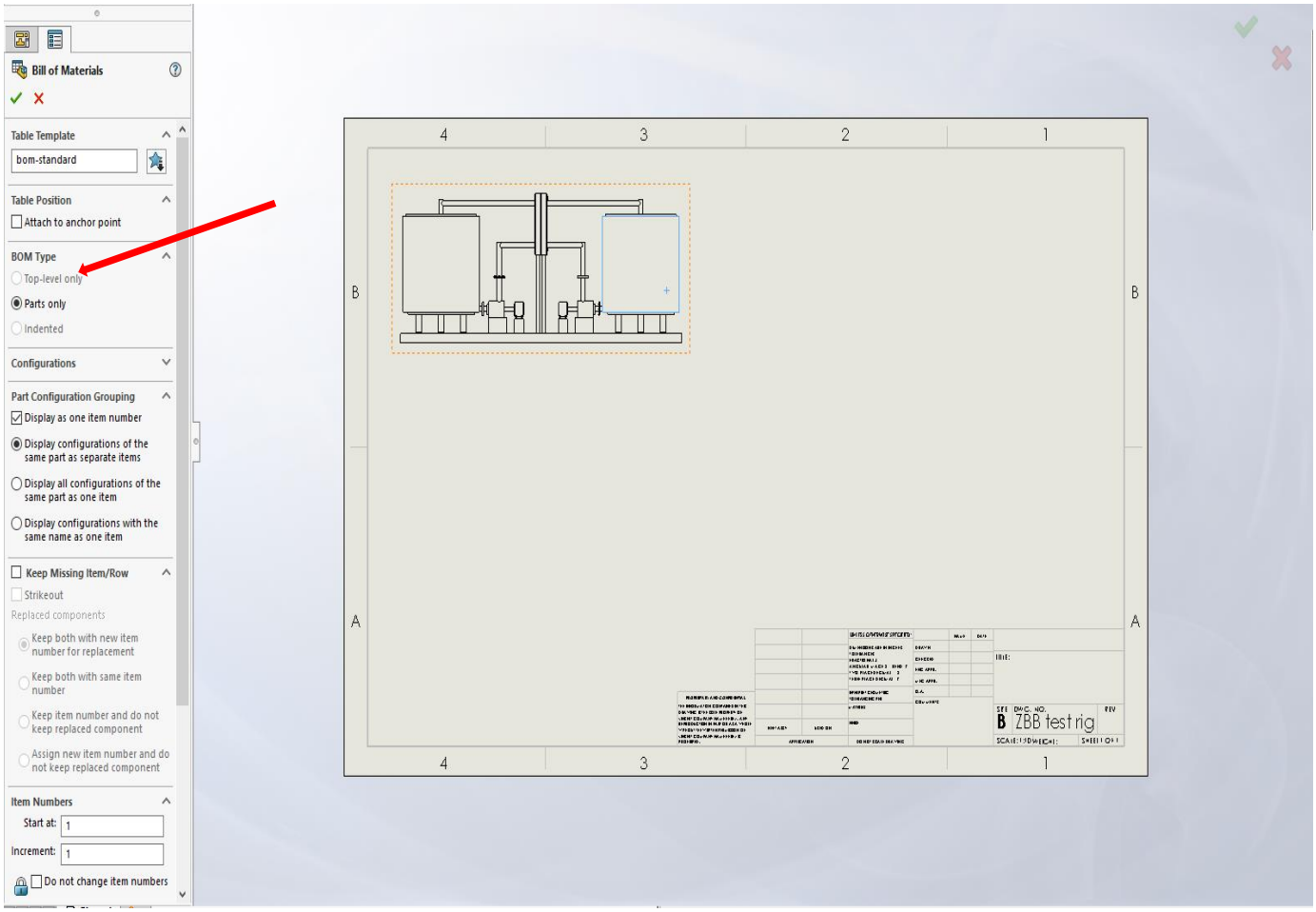

Figure 9. 12: ZBB BOM

10 Attended Conferences and Meetings

- COMSOL Multiphysics Workshop, 2016 in Preston
- Instrumentation Method for Electrochemistry, 2017 Southampton University
- UKES – UK Energy Storage Conferences in University of Newcastle, 2018
- COMSOL Day in Edinburgh 2018
- Energy Lancaster – Energy Storage Systems and Materials – Till Date
- Departmental Review Conferences, 2014 To 2018, Posters Presentations
- Weekly Supervisory Meeting – Supervisors